UNIVERSITY OF NAPLES FEDERICO II

DEPARTMENT OF PHARMACY

PhD program in Pharmaceutical Sciences

The green soul of medicinal chemistry: innovative synthetic approaches towards new anticancer agents

PhD student

Camilla Russo

Coordinator

Prof.

ROSARIA MELI

Tutor

Prof.

MARIATERESA GIUSTINIANO

XXXVI CYCLE (2021-2023)

"Chemistry is the ultimate cult of the new,
and chemical literature captures a history of
innovation and an inclination toward elegance.
There could be no more elegant an endeavour
than to better address issues of pharmaceutical science
within the higher context of environmental stewardship."

From: *"Green Chemistry, a Pharmaceutical Perspective";* Tucker, J. L.; *Organic Process Research and Development,* **2006**, *10*, 315–319.

Table of Contents

List of abbreviations and acronyms

2-Me THF: 2-Methyltetrahydrofuran

3-CR: 3-Component Reaction

4-CR: 4-Component Reaction

AgOTf: Silver triflate

$AlCl_3$: Aluminium chloride

ADP: Adenosine diphosphate

ATP: Adenosine triphosphate

$BF_3 \cdot OEt_2$: Boron trifluoride diethyl etherate

BIR: Baculovirus Inhibitor of apoptosis protein Repeat

CARD: Caspase Recruitment Domain

CD_3OD: Deuterated methanol

$CDCl_3$: Deuterated chloroform

CDK: Cyclin-Dependent Kinase

COS7: CV-1 in Origin with SV40 genes

COSY: Correlated spectroscopy

$Cu(OTf)_2$: Copper triflate

DCM: Dichloromethane

DCM-d_2: Deuterated dichloromethane

DIPEA: *N,N*-Diisopropylethylamine

DMA: *N,N*-Dimethylaniline

DMAP: 4-Dimethylaminopyridine

DMF: Dimethylformamide

DMSO: Dimethyl sulfoxide

DQF-COSY: Double Quantum Filtered Correlated Spectroscopy

EDC HCl: 1-(3-Dimethylaminopropyl)-3-ethylcarbodiimide hydrochloride

EGFR: Epidermal Growth Factor Receptor

EI: Electron Ionisation

$E_{red:}$ Reduction potential

ESI: Electrospray ionisation

Et_3N: Triethylamine

EtOAc: Ethyl Acetate

EtOH: Ethanol

FDA: Food and Drug Administration

GPCR: G Protein-Coupled Receptor

HCl: Hydrochloric acid

HCV: Hepatitis C Virus

HEK: Human Embryonic Kidney

HF: Hydrofluoric acid

HOBt: 1-Hydroxy-benzotriazole

IC_{50}: Half-maximal inhibitory concentration

K_2HPO_4: Potassium hydrogen phosphate

$KMnO_4$: Potassium permanganate

KOTf: Potassium triflate

KSCN: Potassium thiocyanate

$La(OTf)_3$: Lanthanum triflate

LED: Light Emitting Diode

LRR: Leucine-Rich Repeat

M: Molar

MAPK: Mitogen Activated Protein Kinase

MeCN: Acetonitrile

MeCN-d_3: Deuterated acetonitrile

MeOD-d_1: Monodeuterated methanol

MeOH: Methanol

MesAcr: 9-Mesityl-10-methylacridinium

Na_2CO_3: Sodium carbonate

NF-κB: Nuclear Factor kappa B

$NaHCO_3$: Sodium bicarbonate

NaOH: Sodium hydroxide

NMR: Nuclear Magnetic Resonance

NOD: Nucleotide-binding Oligomerisation Domain-containing protein

NOE: Nuclear Overhauser Effect

NOESY: Nuclear Overhauser Effect Spectroscopy

PADAM: Passerini reaction-Amine Deprotection-Acyl Migration

P-3-CR: Passerini 3-Component Reaction

PDGFR: Platelet-Derived Growth Factor Receptor

$Pd(OAc)_2$: Palladium acetate

Ph_2S: Diphenyl sulfide

PIDA: (Diacetoxyiodo)benzene

PYD: Pyrin Domain

RT: Room Temperature

S-3-CR: Strecker 3-Component Reaction

SCE: Saturated Calomel Electrode

$Sm(OTf)_3$: Samarium triflate

T_2O: Tritium oxide

TBATFB: Tetrabutylammonium tetrafluoroborate

TD-DFT: Time-Dependent Density Functional Theory

TEMPO: (2,2,6,6-tetramethylpiperidin1-yl)oxyl

TFA: Trifluoroacetic acid

TFA-*d:* Deuterated trifluoroacetic acid

THF: Tetrahydrofuran

$TiCl_4$: Titanium tetrachloride

TIS: Triisopropylsilane

TMSCN: Cyanotrimethylsilane

$TMSN_3$: Azidotrimethylsilane

TNF: Tumour Necrosis Factor

TOCSY: Total correlation spectroscopy

TPGS-750-M: DL-α-Tocopherol methoxypolyethylene glycol succinate

U-4-CR: Ugi 4-Component Reaction

UK: United Kingdom

US: United States

UT-4-CR: Ugi-Tetrazole 4-Component Reaction

UV: Ultraviolet

VEGFR: Vascular Endothelial Growth Factor Receptor

VIS: Visible

V: Volt

W: Watt

$Yb(OTf)_3$: Ytterbium triflate

$Y(OTf)_3$: Yttrium triflate

$ZnBr_2$: Zinc bromide

Abstract

In the past decades, an increasing awareness of environmental issues has set the stage for the widespread application of the Green Chemistry principles to all fields of Chemical Sciences, both in academia and industry. From a synthetic and pharmaceutical perspective, this has meant looking for novel and more sustainable synthetic approaches to drug-like scaffolds. Whitin this context, multicomponent reactions and visible light photoredox catalysis have both emerged as powerful tools to build up molecules with ease and elegance, while optimising synthetic efficiency, preventing waste generation, and minimising energy consumption.

Capitalising on Prof. Mariateresa Giustiniano's established interest in isocyanide chemistry, this Doctoral Thesis focuses on the development of innovative green synthetic strategies enabling access to a wide and sometimes unexplored chemical space by exploiting either well-known or unconventional reactivities of the *chameleonic* isocyano- functional group, most of the time under visible light irradiation.

After a general introduction to the basic principles of Green Chemistry, isocyanide-based multicomponent reactions, and visible light photoredox catalysis (Chapter 1), Chapter 2 may be described as a methodological one, as it includes our studies aiming to provide innovative synthetic solutions of general utility to the scientific community. In Section 2.1, a novel visible light photocatalytic three-component reaction between *N*-alkyl-*N*-methylanilines, (*N*-isocyanoimino)triphenyl phosphorane, and carboxylic acids, affording pharmaceutically relevant 1,5-disubstituted-1,3,4-oxadiazole derivatives under very mild conditions, is presented. Section 2.2 deals with our commitment to contribute to the flourishing of in water photochemical transformations. It describes a photomicellar catalysed synthesis of amides from *N*-alkyl-*N*-methyl aromatic amines and isocyanides, with particular focus on the study of the localisation of the photocatalyst with respect to the micelles, in order to provide experimental data to drive the identification of the

photocatalyst/surfactant pairing with optimal catalytic efficiency. In line with our interest in exploring isocyanides' unconventional reactivities under visible light irradiation, Section 2.3, Section 2.4, and Section 2.5 report our recent findings about the ability of aromatic isocyanides to harvest the energy of photons, reach an electronically excited state, and promote the formation of radical species from suitable precursors, via single electron transfer oxidation events. After exploiting these observations to perform Ugi and Ugi-like self-catalysed multicomponent reactions (Section 2.3, and Section 2.4) and preliminary assessing the use of aromatic isocyanides as catalytic organic photoactive oxidants in a series of α-amino C(sp^3)-H functionalisations (Section 2.3), our efforts to verify the ability of aromatic isocyanides to promote the generation of both alkyl and acyl radicals from more challenging radical precursors (*i.e.*, Hantzsch esters, potassium alkyltrifluoroborates, and α-oxoacids) are described in Section 2.5. UV-visible absorption and fluorescence experiments, as well as electrochemical measurements of the ground-state redox potentials along with computational calculations of both the ground- and the excited-state redox potentials of a set of nine different aromatic isocyanides provided key insights to drive the rational design of a new generation of isocyanide-based organic photoredox catalysts. As for isocyanides' unconventional reactivities not requiring visible light, in Section 6 a new domino isocyanide insertion/5-*exo*-*dig* cyclisation of readily available Strecker 3-component adducts, elicited by ligation to ytterbium triflate, is reported. Such an approach enabled a fast and easy access to 4-substituted-5-aminoimidazole derivatives, a class of pharmaceutically relevant heterocyclic scaffolds, whose current synthetic strategies are still poorly efficient.

In Chapter 3, the potentialities and the opportunities of applying isocyanides' multifaceted reactivities in the context of medicinal chemistry and drug discovery are further highlighted. Thanks to their high exploratory power, isocyanide-based multicomponent reactions represent a unique tool to rapidly provide diversity and complexity with unprecedent synthetic efficiency, which is particularly relevant for

the construction of molecular libraries for biological evaluations and structure-activity relationship studies. We applied such an approach to the identification of novel small molecule inhibitors acting on emerging anticancer targets. In Section 3.1, based on the increasing evidence of a possible involvement of MICAL2 protein in neo-angiogenesis and metastasis formation in several human cancers, the design, synthesis, biological and computational evaluations of a small library of CCG-1423 analogues (the only MICAL2 small molecule inhibitor known do date) are reported. These studies provided new insights into the structure–activity relationships of CCG-1423, thus paving the way for the discovery of novel MICAL2 inhibitors. Section 3.2 focuses on the identification of a new class of NOD antagonists. NOD1 and NOD2 proteins are pattern recognition receptors whose overactivation has been found to play a role in several inflammatory diseases and human cancer types. We exploited a multicomponent synthetic approach to access a new chemotype, namely 2,3-diaminoindoles, and expand the chemical space of NOD inhibitors. This resulted in the identification of a novel low micromolar NOD1 antagonist, whose direct binding to NOD1, along with characterisation of its binding site, were proved by means of a combination of NMR spectroscopy and computational techniques.

Finally, considering the growing relevance of organic electrosynthesis as a green activation method, Chapter 4 summarises my six-month stay as a visiting PhD student in the Laboratory of Medicinal and Molecular Electrochemistry of Prof. Kevin Lam, University of Greenwich. Besides experiencing first-hand the opportunities and the challenges of synthetic organic electrochemistry, this resulted in the development of a new, practical, mild, and high-yielding hydrogen-free electrochemical method for the reduction of alkene, alkyne, nitro- and azido-compounds. The strategy represents an interesting alternative to classic metal-based catalytic hydrogenations, thus confirming once more the importance of developing innovative and more sustainable synthetic approaches for both organic and medicinal chemistry applications.

Chapter 1

General Introduction

1.1. Towards a Sustainable Development

The massive growing of human and industrial activities over the last century was a milestone for the civilisation and economic development of communities across the world. Countless innovations contributed to significant improvements in the quality of life of industrialised countries, which resulted in an exponential demographic growth: global population doubled between 1960 and 2000[1] and is expected to increase by 47% between 2000 and 2050.[2] The rapid growth in population has required (and still requires) abnormal food production and uncontrolled industrialisation, with consequent resource depletion and spreading pollution. All of this has had inevitable repercussions on the environment, which are more than evident in the current challenges the humanity is facing, *i.e*. ozone layer depletion, acidification and rise of ocean waters, climate changes, and global warming.

Given its importance in modern industry, the chemical sector has obviously played a critical role. The chemical industry traditionally employs highly reactive reagents (usually based on fossil and non-renewable feedstocks) to achieve fast and high-yielding transformations; unfortunately, most of these reagents are also persistent, hazardous, and/or toxic, and pose serious concerns about workers' exposure and release in the environment. Moreover, the chemical processes themselves produce huge amounts of waste (tens of kgs per kg of product[3]), whose handling and disposal are problematic both from a safety and an economic point of view.

In the late 20th century, a general awareness about environmental issues and over-exploitation of natural resources has begun to arise in the form of conferences and political agreements aiming to a "Sustainable Development".[4] The World Commission on Environment and Development was created in 1983 by the United Nations as an independent organisation with the task of evaluating the conflict between globalised economic growth and accelerated ecological degradation, and proposing a long-term agenda of "*actions […], and aspirational goals for the world community*".[5] The resulting ''Brundtland Report" gave the first definition of

sustainable development as "*development that meets the needs of the present without compromising the ability of future generations to meet their own needs."* In 1991 The US (US) Environmental Protection Agency (EPA) launched the "'Alternative Synthetic Routes for Pollution Prevention" program, conceived "*as guidance, by providing a series of approaches to pollution prevention*".[6] It reported a new way to conceive the risk associated with toxic chemicals, highlighting how the best solution to prevent problems with these substances would be not to produce them at all.[7] Since then, the term "Green Chemistry" has begun to appear in different contexts as a general expression to refer to the new way of doing chemistry while trying to limit or eliminate its detrimental impact on the environment and the human health. This culminated in the foundation of the Green Chemistry Institute (GCI, 1997) and in the publication of the textbook "Green Chemistry: Theory and Practice" by Paul Anastas and John C. Warner (1998), a guide on how to work at the molecular level to achieve sustainability.[8] In the following twenty-five years many efforts have been made in this direction and have contributed to advance the field and realise its potential benefits.

1.1.1. Green Chemistry: Principles and Practice

Defined as *"the design of chemical products and processes that minimise or eliminate the use or generation of hazardous substances",*[9] Green Chemistry has been having an enormous impact on all industrial sectors: from agriculture to household products, cosmetic, pharmaceuticals, electronics, energy, and many others. The main reason for its widespread application is the ability of Green Chemistry to combine chemical innovations with environmental and health protection and economic benefits. As James Clark wrote in 1999 "*the green chemistry revolution is providing an enormous number of challenges to those who practice chemistry […]. With these challenges however, there are an equal number of opportunities to discover and apply new chemistry, to improve the economics of*

chemical manufacturing and to enhance the much-tarnished image of chemistry."[10] The core of this new green chemical thinking is the statement "*benign by design*".[11] The Twelve Principles[12] can actually be considered guidelines for a sustainable design of chemical processes and products, taking into account all the aspects of their life cycle: from the choice of raw materials to the efficiency and safety of the transformation, to the toxicity and biodegradability of reagents and products. The main objective is to minimise the environmental and occupational risks which are inherent in chemistry. This requires a new approach based on the use or renewable feedstock and resources, the minimisation of energy consumption, the prevention of pollution and of waste generation, the evaluation of the persistence of chemicals in the environment.

Herein we will shortly present the Twelve Principles (Figure 1.1) as a framework for the discussion, focusing on those among them which are more relevant to our purposes.

Figure 1.1. The Twelve Principles of Green Chemistry.

I. **Waste prevention.** Waste is often the determining factor in the cost, environmental impact, and safety of chemical processes, with an annual spending for its management around $ 1B.[13] This is why "*it is better to prevent waste than to treat or clean up waste after it has been created*." The E-Factor, or Environmental Impact Factor, is a metric introduced in 1992 by Roger Sheldon for quickly assessing the environmental footprint of manufacturing processes.[14] It quantifies the amount of waste generated per kilogram of product, taking into account the chemical yield and including reagents, solvent losses, process aids and, in principle, even the source of energy (as this also leads to waste in the form of carbon dioxide[15]). The ideal E-factor is supposed to be zero, nevertheless E-factors commonly vary over 5 or more orders of magnitude.[16] Several strategies have been developed to address this point, most of them involving simplification, dematerialisation, and closed loop systems.[17,18] On the other hand, the nature of waste should also be considered, as not all types of waste have the same toxicity, hazardousness, persistence, and tendency to bioaccumulation.

II. **Atom Economy.** The concept of Atom Economy (AE), or Atom Efficiency, was first introduced by Barry Trost in 1991.[19] *"Synthetic methods should be designed to maximise the incorporation of all materials used in the process into the final product,"* ideally leaving zero waste. Major benefits of such an approach include more effective use of limited raw materials and decreased waste generation. Calculated as the ratio of the molecular weight of the desired product over the molecular weights of all the reactants used in the reaction, it should be noted that AE does not consider reaction yields and over-stoichiometric quantities of starting materials, as well as solvents and chemicals used in work-up and purification of the reaction mixture. Nevertheless, it is one of the simplest tools to estimate the synthetic efficiency of a reaction before any experiments are performed. Undoubtedly some reactions are inherently more atom economical than others: additions reactions should always be preferred over substitution

reactions, as well as rearrangements, cycloadditions, cross-couplings and multicomponent reactions (see Section 1.2).

III. **Less Hazardous Chemical Synthesis.** "*Wherever practicable, synthetic methods should be designed to use and generate substances that possess little or no toxicity to human health and the environment.*" One of the cornerstones of Green Chemistry is to reduce risk by reducing hazard. Chemical risk is determined by both hazard and exposure, but most of the times it is managed by only limiting exposure to hazardous chemicals, for example by means of adequate protective equipment. The opposite approach, *i.e*. reducing hazard, can be addressed by careful design of alternative synthetic routes allowing to replace or eliminate reagents which are known to be dangerous from a physical (*e.g*., explosivity and corrosivity), global (*e.g*. greenhouse gases and ozone depletion), and toxicological (*e.g*., carcinogenicity) point of view.

IV. **Designing Safer Chemicals.** This is closely related to the third principle and states that "*chemical products should be designed to effect their desired function while minimising their toxicity*." The design of non-toxic chemicals requires collaboration between chemistry, toxicology, genomics, and computational approaches to identify areas of chemical space with reduced hazard potential.[20] Molecular design guidelines relate physicochemical properties including solubility, reactivity, and cell permeability with specific toxicological effects[21] and may help to identify precise structural features which should be avoided as toxicophores.

V. **Safer Solvents and Auxiliaries.** Solvents are probably one of the most challenging areas in Green Chemistry, since they are often used in amounts that largely exceed raw materials, reagents, and products.[22] The vast majority of organic solvents are toxic, flammable, and/or corrosive, and their volatility and solubility pose serious problems concerning pollution, workers' exposure, and water stream contamination. *"The use of auxiliary substances (e.g., solvents, separation agents, etc.) should be made unnecessary wherever possible and*

innocuous when used." The ideal would be not to use any solvent, since "*the best solvent is no solvent*"[3]: many efforts have been made to develop solvent-free reaction systems, as for mechanochemistry,[23] microwave-assisted,[24] and neat reactions. On the other hand, when a solvent cannot be avoided, replacing conventional reaction media with greener alternatives would be desirable. Where possible, water should be the solvent of choice, as it is non-toxic, non-inflammable, abundantly available, and inexpensive (see Section 2.2). Supercritical fluids (SCFs) and ionic liquids have also been gaining increasing attention, as well as solvents derived from renewable biomass (*e.g.* ethyl lactate, glycerol, 2-Me THF).[25]

VI. Design for Energy Efficiency. *"Energy requirements of chemical processes should be recognised for their environmental and economic impacts and should be minimised. If possible, synthetic methods should be conducted at ambient temperature and pressure."* The design of chemical reactions working under mild conditions and/or in short times can lead to significant advantages in terms of energy consumption. It is well known, for example, that reactions requiring long times at elevated temperature under conventional heating can be completed within a few minutes under microwave irradiation, with lower total power consumption.[26] If increasing the energy efficiency of chemical processes is part of the solution, alternative mechanism for energy generation and delivery are also needed. Sonochemistry uses ultra-high frequency waves to cause implosion of air cavities inside the reaction mixture; this converts electric energy into mechanical energy and can lead to dramatic acceleration of the reaction rate.[27] Visible light photoredox catalysis (see Section 1.3) and synthetic organic electrochemistry (see Section 4.1) are other emerging areas which offer unprecedent synthetic opportunities while exploiting alternative energy sources. By generating open-shell species under very mild conditions, they allow for a multitude of transformations not always achievable via traditional pathways and can be exploited as powerful tools to provide unique retrosynthetic disconnections.

VII. **Use of Renewable Feedstocks.** *"A raw material or feedstock should be renewable rather than depleting whenever technically and economically practicable."* Biomass, the material obtainable from living organisms, is the major renewable alternative to petroleum feedstock and fossil resources; it includes wood, crops, agricultural residues, food, and provide a variety of materials such as cellulose, lignin, lactic acid, chitin, and others, which can be converted into valuable chemicals and polymers.[28]

VIII. **Reduce Derivatives.** It is evident that the use of protecting groups and related strategies in chemical syntheses enormously increases the generation of waste, as it requires additional reagents, purification steps, solvents, and energy consumption. "*Unnecessary derivatisation (use of blocking groups, protection/deprotection, temporary modification of physical/chemical processes) should be minimised or avoided, if possible, because such steps require additional reagents and can generate waste."* The switch towards "derivatisation-free" processes requires the development of synthetic strategies endowed with improved chemoselectivity.[29] While sometimes this can be achieved by simply controlling the reaction conditions, there is an urgent need for new inherently chemoselective reactions. Photochemical and electrochemical transformations usually occur with higher selectivity (compared to conventional ones), thanks to (single) electron transfer events involving specific redox-active functionalities. Flow chemistry can reduce derivatisation too, as it allows for a better control of the reaction parameters leading to decreased side-products formation.

IX. **Catalysis.** "*Catalytic reagents (as selective as possible) are superior to stoichiometric reagents."* Catalysis is probably the central core of Green Chemistry as many other principles converge in it: besides avoiding stoichiometric or over-stoichiometric amounts of reagents, catalysis can improve Atom Economy (Principle 2), decrease energy requirements (Principle 6), and increase selectivity (Principle 8) of chemical reactions, thus contributing to an

overall reduction of waste generation (Principle 1). Significant efforts have been devoted to the design of both new homogeneous and heterogeneous systems, with Green Chemistry hot topics including the development of either non-precious metal-based[30] or metal-free[31] catalysts, so to consider their environmental and toxicological implications. Biocatalysis also offers huge opportunities to perform biomimetic transformations under very mild conditions (water as the solvent, atmospheric pressure, and ambient temperature) by means of engineered living organisms or purified enzymes.[32] The latter are generally biodegradable, biocompatible, and renewable, and enzyme-mediated reactions have shown increased chemo-, regio- and stereoselectivity.[33]

X. **Design for Degradation.** The persistence of chemicals in the environment after their use can have serious consequences on the biosphere. *"Chemical products should be designed so that at the end of their function they break down into innocuous degradation products and do not persist in the environment."* The easiest way to achieve this is to consider the biodegradability of chemicals at the design stage: a number of databases about known environmental fate of molecules are available, and structural moieties related to higher persistence (*e.g.*, halogens, quaternary carbons, branched chain, tertiary amines, and polycyclic structures with more than three rings) have been identified. On the other hand, functional groups recognised by ubiquitous enzymes such as esters and amides may facilitate the obtainment of environmental degradable products.[34]

XI. **Real-Time Analysis for Pollution Prevention.** *"Analytical methodologies need to be further developed to allow for real-time, in-process monitoring and control prior to the formation of hazardous substances."* The availability of *in situ* monitoring technologies for reaction control has a crucial role in greening chemistry and preventing accidents: by continuously checking reaction parameters (*i.e.*, temperature, pressure, concentration of reagents and intermediates) it is possible to immediately take actions when problems arise so to prevent the formation of unwanted products (which would complicate the

purification step) or toxic substances. Obviously, these methodologies should be green themselves: Green Analytical Chemistry[2] is an expanding area aiming to the development of analytical procedures that generate less waste and are safer to human health and the environment.[35]

XII. **Inherently Safer Chemistry for Accident Prevention.** Accidents have an enormous cost from a social, economic, and environmental point of view, reason why *"substances and the form of a substance used in a chemical process should be chosen to minimise the potential for chemical accidents, including releases, explosions, and fires."* In 1978 Trevor Kletz introduced the concept of "Inherently Safer Processes" (ISPs[36]) as processes avoiding hazards instead of controlling them, particularly by reducing the use of dangerous materials and the number of hazardous operations. This can be accomplished, for instance, by replacing harmful reagents and by preferring *on-demand* and *on-site* production of hazardous substances, so to limit their storage and transportation.

1.1.2. Pharmaceutical Green Chemistry

While providing revolutionary, life-saving treatments and innovative drugs that allow patients to live longer and healthier lives, the pharmaceutical industry plays a major role in affecting the environment: with E-factor values typically spanning from 25 to 100,[3] it generates more waste than any other oil-refining, bulk, and fine chemical industries, primary contributing to carbon footprint, water stream contamination, and air pollution. The main reason for the higher E-factors of pharmaceutical processes is the molecular complexity of active pharmaceutical ingredients (APIs), usually requiring many steps to have them assembled from commercially available starting materials. The routinary use of stoichiometric reagents (rather than catalysts) and of protecting groups is another contributor to the problem.

A GlaxoSmithKline report of 2007 highlighted how solvents constitute more than 80% of the waste deriving from a typical API manufacture and account for 50% of green-house gas emissions from pharmaceutical industry;[37] solvent selection, recovery, and replacement should then be a priority in drugs' manufacturing. Additionally, APIs have been extensively detected in the environment, due to improper disposal, incomplete metabolisation in the body, waste streams from production sites, and their use in agriculture.[13] Since APIs are biologically active by design, their presence in the environment can pose serious risks for the animal kingdom even at low concentrations.

In light of all this, in 2005 the American Chemical Society (ACS) GCI and several leading global pharmaceutical corporations (including AstraZeneca, Eli Lilly & Company, GlaxoSmithKline, Johnson & Johnson, Merck & Co., Inc., Pfizer, Inc., and Schering–Plough Corporation) instituted the ACS GCI Pharmaceutical Roundtable (ACS GCIPR): a not-for profit organisation with the aim to encourage innovation and enable the implementation of Green Chemistry and Green Engineering into the business of drug discovery, development and production.[38] Since then, pharmaceutical industries have been making considerable efforts to integrate Green Chemistry principles within their activities, from sustainable drug design to innovative green syntheses. Actually, besides reducing environmental impact, more efficient synthetic routes and less hazardous processes also result in cost-effective production of APIs, thus offering strong economic motivations to practice Green Chemistry. It is worth noting, however, that, while most of its principles are directly applicable to pharmaceutical chemistry, some are not: for instance, designing for degradation can be inappropriate for active pharmaceutical ingredients whose biological activities strictly rely on specific chemical features, and that also must prove adequate stability and acceptable shelf life.[39] Some of the current challenges include the development of synthetic strategies maximising Atom Economy and synthetic efficiency, the minimisation of the number of

required chemical steps, the identification of reaction conditions and solvents for improved selectivity and energy efficiency.

Here we discuss three redesigned green syntheses of established generic pharmaceuticals as a matter of example of the successful integration of the Green Chemistry principles into the development and manufacture of APIs.[40]

a) Ibuprofen

Ibuprofen [(*RS*)-2-(4-(2-methylpropyl)phenyl)propanoic acid], one of the most common non-steroidal anti-inflammatory drugs, was first developed and patented by the Boots company in the 1960s.[41] Its traditional synthetic route, known as the Boot's Synthesis (Scheme 1.1a), consisted of six reaction steps with an overall Atom Economy around 40%. This was mostly due to the loss of many of the reactant atoms, leading to the generation of enormous amounts of waste. For example, stoichiometric quantities of $AlCl_3$ were required for the first Friedel–Crafts acylation step of 2-methylpropylbenzene **1.1** and led to corresponding amount of aluminium waste during the subsequent aqueous work-up.

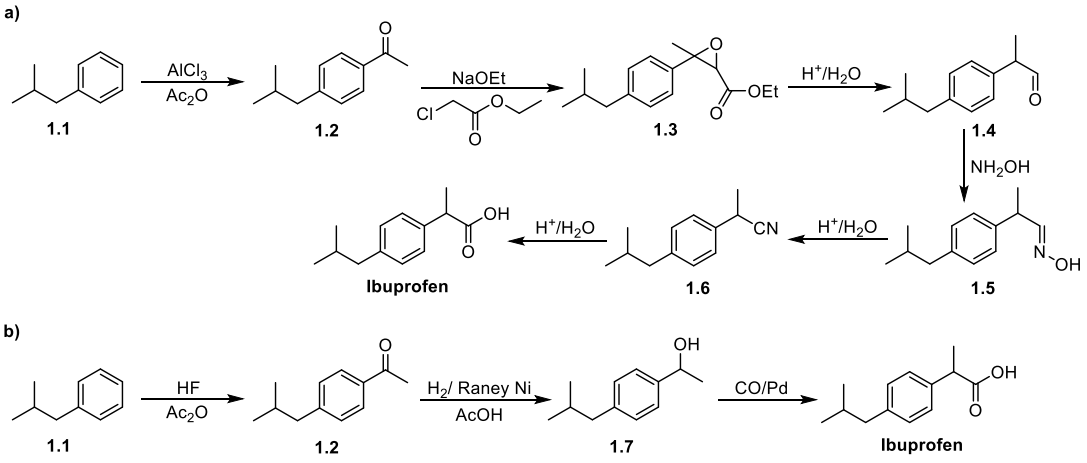

Scheme 1.1. a) Traditional Boot's Synthesis of Ibuprofen; b) Green Synthesis of Ibuprofen.

The Boots−Hoechst−Celanese (BHC) company later developed a new green synthesis[42] (Scheme 1.1b): it consists of only three steps with a final Atom Economy of 77% (which climbs to 99% if considering that the acetic acid generated during the first step can be recovered). $AlCl_3$ was replaced by anhydrous HF as both the Friedel-Crafts catalyst and the solvent, which can be recovered and reused, as well as the Raney nickel and palladium catalysts required for the following hydrogenation and carbonylation step, respectively. This resulted in the elimination of the waste generated, simplification of the product recovery, and reduction of the energy consumption, thus earning the procedure the Presidential Green Chemistry Challenge Award in 1997, as a model of environmental excellence in chemical processing technology.

b) Pregabalin

Pregabalin [(*S*)-(+)-3-aminomethyl-5-methylhexanoic acid)] is an analogue of GABA (γ-aminobutyric acid) extensively used to treat several CNS (central nervous system) diseases, such as epilepsy, neuropathic pain, fibromyalgia, and anxiety. Its first manufacturing process was reported in 1997 by Parke-Davis scientists, who developed a five steps sequence (Scheme 1.2a) suffering from low yield (around 20%) and poor Atom Economy.[43] The final resolution of racemic Pregabalin **1.12**, in particular, was accomplished by means of multistep crystallisation with enantiopure (*S*)-(+)-mandelic acid, and resulted in the generation of huge amount of waste, since the undesired (*R*)-enantiomer could not be recycled. In 2008 researchers at Pfizer proposed an alternative synthetic route[44] (Scheme 1.2b) employing lipolase, a commercially available lipase, to enantioselectively convert *rac*-2-carboxyethyl-3-cyano-5-methylhexanoic acid ethyl ester **1.11** into (*S*)-2-carboxyethyl-3-cyano-5-methylhexanoic acid **1.13** (45% conversion, 98% enantiomeric excess). The following decarboxylation of **1.13** efficiently gave (*S*)-3-cyano-5-methylhexanoic acid ethyl ester **1.14**, a known precursor of Pregabalin. By setting the stereocenter early in the synthetic sequence

and enabling the smooth racemisation and recycle of the unwanted enantiomer **(*R*)-1**, the new strategy contributed to significantly increase the overall process efficiency. The chemoenzymatic route also allowed for a mostly aqueous reaction environment, thus decreasing the need for organic solvents. All this resulted in higher yields of Pregabalin (40–45% after one recycle of **(*R*)-1**) along with substantial reduction of the production of waste (E-factor declined from 86 to 17) compared to the first-generation manufacturing process.

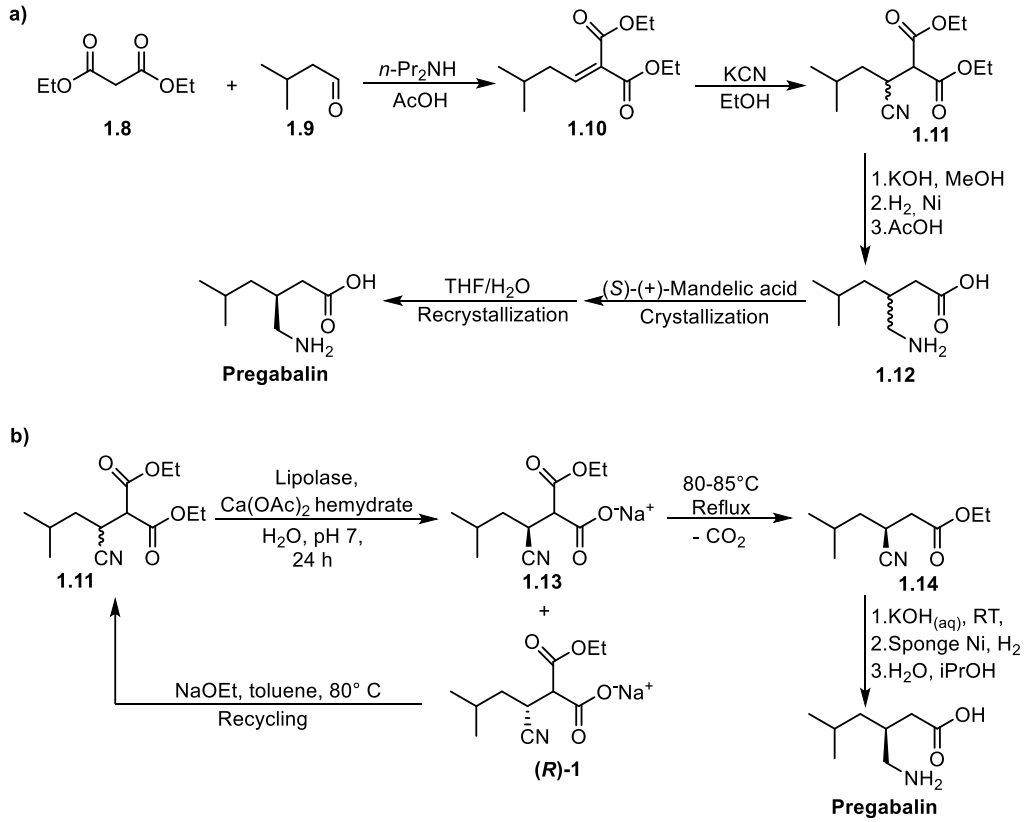

Scheme 1.2. a) Traditional Synthesis of Pregabalin; b) Green Synthesis of Pregabalin.

c) Sertraline

Sertraline [(1*S*,4*S*)-4-(3,4-dichlorophenyl)-*N*-methyl-1,2,3,4-tetrahydronaphthalen-1-amine], is an antidepressant drug of the selective serotonin reuptake inhibitor (SSRI) class. The original Pfizer synthesis[45] (Scheme 1.3a) employed a total of five

different volatile solvents (namely, *n*-hexane, toluene, THF, EtOAc, and EtOH) and titanium tetrachloride ($TiCl_4$, an air-sensitive, corrosive liquid, generating dense HCl fumes when exposed to air) as dehydrating agent for the formation of the imine intermediate **1.16**. The catalytic reduction of **1.16** then provided a 6:1 mixture of *cis* and *trans* amines **1.17** requiring additional purification of the *cis* form and its final resolution by fractional crystallisation with (*R*)-(-)-mandelic acid to finally obtain the desired (1*S*,4*S*)-Sertraline.

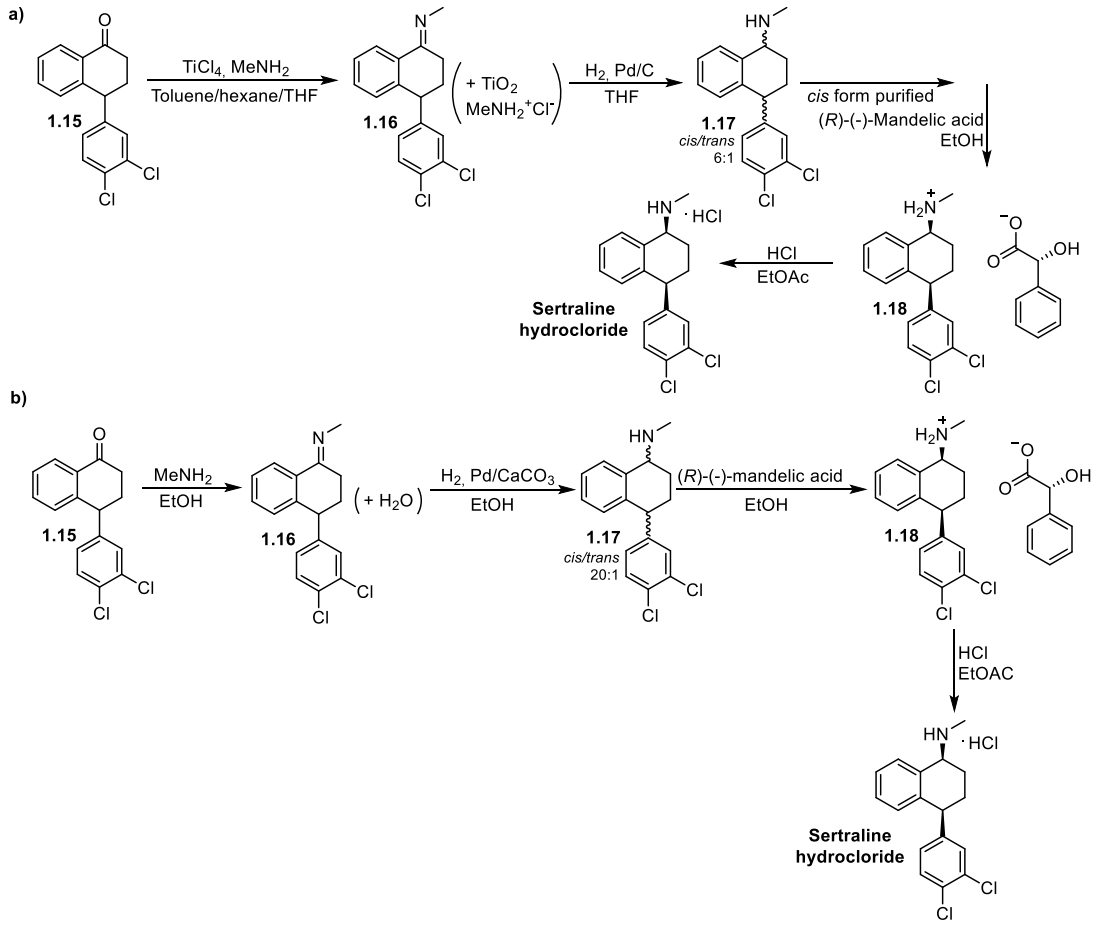

Scheme 1.3. a) Traditional Synthesis of Sertraline; b) Green Synthesis of Sertraline.

This resulted in low yield, hazardous by-products, solid waste, and need for huge amounts of solvents and energy-intensive distillation procedures to recover them.

An alternative approach[46] (Scheme 1.3b) replaced the previous five solvents with just EtOH and EtOAc (both safer from an environmental and health point of view), eliminated the use of $TiCl_4$, and improved the selectivity in the formation of the intermediate *cis* amine (20:1) during the hydrogenative step. Overall, the final yield of Sertraline almost doubled, with decrease of raw material input, improvement of the energy efficiency, and elimination of several toxic waste by-products. The process obtained the US EPA Presidential Green Chemistry Challenge Award in 2002.[47]

1.2. Multicomponent Reactions: an established Green Chemistry tool

Multicomponent reactions (MCRs) are *"reactions that combine at least three reactants in the same pot to generate a product containing all (or almost all) the atoms of the starting materials"*:[48,49] as such, they are atom economic transformations by definition, sometimes considered ideal organic syntheses. This has led MCRs to experience an exponential growth in their usage in recent decades, when they have been emerging as one of the most promising strategies to combine synthetic efficiency with sustainability. Compared to classic multistep approaches, requiring a linear sequence of one-by-one reactions and several intermediate purification steps, an ideal multicomponent synthesis allows the simultaneous addition of all the reactants and reagents in the same pot at the onset of the reaction, and makes them react in a uniquely ordered manner to afford the desired product (Figure 1.2).[50] Interestingly, regardless of the preferred reaction pathway, all mechanisms lead to the same final product, which means the reaction is highly convergent.

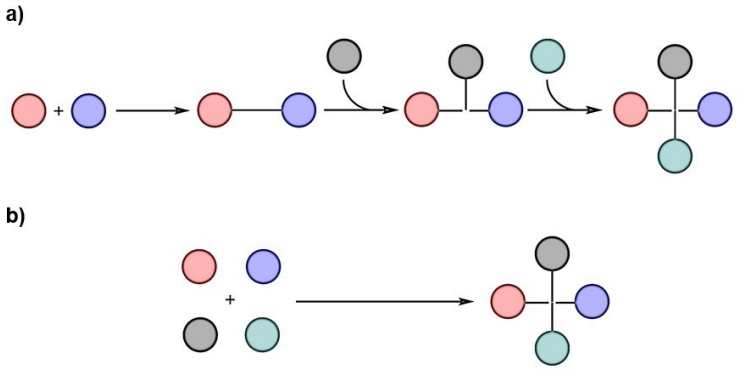

Figure 1.2. a) Multistep linear synthesis *vs* b) Multicomponent reactions.

Typically, a MCR proceeds as a sequence of mono- and bimolecular equilibrium stages pushed ultimately towards the product side by an irreversible, thermodynamically favoured step.[48] As a consequence, the formation of high molecular weight side products is quite limited, while simple small molecules (usually water, alcohols, amines, or common salts) are the only by-products deriving from reactions consisting of sequential condensation/addition stages. This is doubly environmentally beneficial, especially in terms of waste prevention, since both the amount and the hazardousness of the waste generated are minimal.[51] Moreover, most MCRs have an atom economy of at least 80%, which combined with the high yields and excellent selectivity (particularly chemo- and regioselectivity, more challenging stereoselectivity) observed for the majority of MCRs, clearly simplifies the product isolation and purification procedures. It has been found, for example, that MCR products have several features making them particularly suitable for (re)crystallisation rather than chromatographic or distillation techniques. By decreasing the amount of solvents required, this can have significant advantages for industrial applications.

Additionally, most MCRs proceed at ambient temperatures and atmospheric pressure, without any need for exclusion of air or moisture, thus enabling very mild conditions and a substantial reduction of energy requirements.

An additional aspect of MCRs is their unique bond-forming efficiency. Defined as "*the number of bonds which are formed in one sequence*", this concept was introduced in 1996 by Tietze as a criterion to evaluate the quality of MCRs.[52] For a standard MCR it is typically > 1 (its classic value for conventional reactions), since MCRs allow the formation of several bonds in one single operation, usually without isolating any intermediates, changing reaction conditions, and/or adding further reagents. The domino nature of MCRs clearly simplifies operational procedures and, by dramatically shortening the entire synthetic sequence, it is a premise for the overall reduction of waste enabled by these methodologies. Furthermore, it offers route to complex and diverse molecular architectures while saving time and resources. This is particularly relevant considering the advent of High-Throughput Screening (HTS) assays demanding for large number of compounds readily available to be tested. By varying systematically the structural features of the building block starting materials, MCRs allow for a straightforward diversification of the final products and provide access to large libraries of structurally related compounds with ease and elegance. This enables the exploration of a wide chemical space in short times and with unprecedent efficiency.

By virtue of this exceptional complexity-generating and exploratory power, combined with their high productivity and inherent sustainability, MCRs have naturally become a rapidly evolving field of research and have attracted the attention of both academy and industry for a variety of synthetic applications.

1.2.1. A brief history of Multicomponent Reactions

Multicomponent reactions claim a centuries-old history of flourishing developments: the first MCR is generally considered to be the Strecker synthesis of α-amino acids, dating back to 1850.[53] It involves an aldehyde **1.19**, ammonia **1.20**,

and hydrogen cyanide **1.21** to give an α-amino nitrile **1.22**, then hydrolysed to the corresponding α-amino acid **1.23** (Scheme 1.4a).

Later in 1882, Arthur Hantzsch described his multicomponent approach for the synthesis of 1,4-dihydropyridine (DHP) derivatives **1.25**, also known as Hantzsch reaction.[54] It is a four-component reaction (4-CR) between a β-keto ester **1.24** (2 equivalents), an aldehyde **1.19**, and an ammonia donor, reacting in a cyclocondensation to afford the *N*-heterocyclic scaffold (Scheme 1.4b). Importantly, a wide range of calcium channel blockers largely used for the treatment of cardiovascular disease can be prepared according to this procedure, as for Nifedipine, one of the first dihydropyridines to be synthesised at the Bayer AG company, based on the Hantzsch synthesis.

The Biginelli reaction is another elegant transformation.[55] First reported by Pietro Biginelli in 1891,[56] it makes an aldehyde **1.19**, a β-keto ester **1.24**, and urea **1.26** react under acid catalysis to give biologically relevant[57] 3,4-dihydropyrimidin-2(1*H*)-ones **1.27** (DHPMs, Scheme 1.4c).

The Mannich 3-CR[58] (1912) is a particularly useful tool for the synthesis of β-amino carbonyl compounds **1.30**, also known as Mannich bases. This transformation relies on the aminoalkylation of an enolisable carbonyl compound **1.28** with a non-enolisable aldehyde (typically formaldehyde) and ammonia, or any primary or secondary amine **1.29** (Scheme 1.4d). In the case preformed enolates (or modified enolates) are used, the Mannich reaction is usually referred to as the indirect Mannich reaction, and this version is quite popular too.[59]

A further important MCR is the Bucherer-Bergs reaction (BB-4-CR).[60,61] It can be described as an extension of the Strecker 3-CR (S-3-CR) using CO_2 as additional component (Scheme 1.4e). Whereas the S-3-CR is an equilibrium reaction and often delivers the product in unsatisfactory yields, the BB-4-CR is practically irreversible upon addition of CO_2. It is an important method for the obtainment of the hydantoin scaffold **1.33**, which is present in the structures of bioactive

compounds such as antiepileptic drugs including Phenytoin, Fosphenytoin, Mephenytoin, and the anticancer drug Nilutamide.

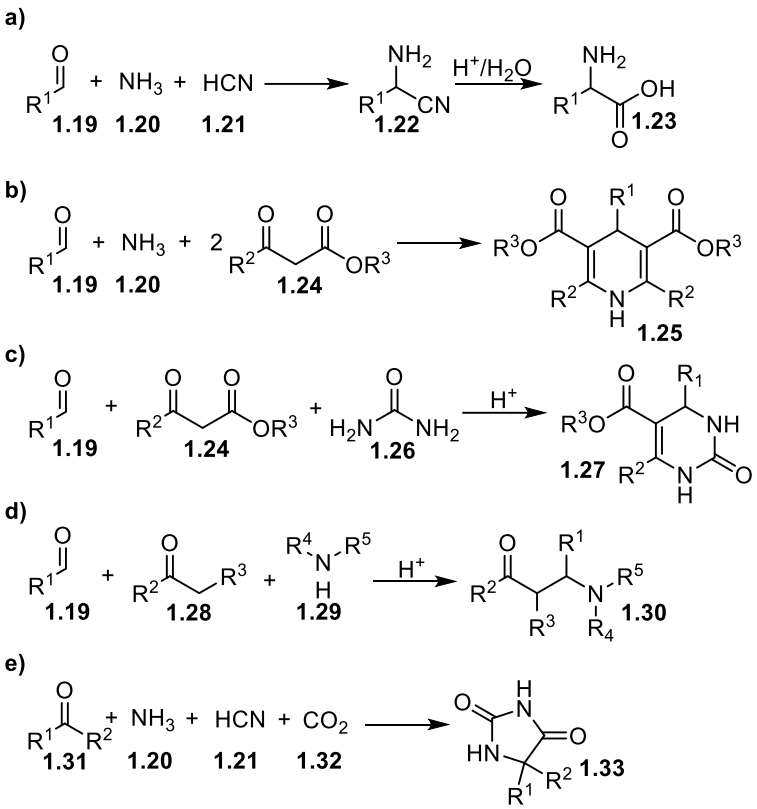

Scheme 1.4. Representative examples of multicomponent reactions.

In 1921, the first MCR involving an isocyanide, *i.e.* the Passerini reaction (P-3-CR), was reported by the Italian chemist Mario Passerini[62] (see Section 1.2.2), followed by the Ugi four-component reaction[63] (U-4-CR, see Section 1.2.2), in 1959: these two transformations opened the doors to the flourishing class of multicomponent reactions usually referred to as IMCRs (Isocyanide-based Multicomponent Reactions) and are often considered the stepping stones for the widespread applications of such chemistry, from chemical biology to process chemistry.

1.2.2. Isocyanide-based Multicomponent Reactions

The history of multicomponent reactions has long been related to that of isocyanides. These are the only stable organic compounds with a formally divalent carbon, able to react with both electrophiles and nucleophiles at the same C atom leading to the formation of the so-called α-adducts. This peculiarity explains their multiple reactivities, which could be considered as transitions from the carbon divalent state to the tetravalent state and vice versa.[64] Originally represented by Nef in their carbenic form[65] (Figure 1.3a), accounting for the ambivalent behaviour of this functional group, a second zwitterionic structure resembling that of carbon monoxide (Figure 1.3a) was proposed in the thirties.[66] The latter explains well the nucleophilicity of isonitriles, and it also justifies the IR stretching band at 2130 cm^{-1} as well as the linear structure of the C–N–C system evidenced by electron diffraction. Nonetheless, it is not able to justify the electrophilicity of the isocyanide carbon atom.[67] More recently, Fleurat-Lessard *et al*. have proved via high level valence bond calculations that the principal structure of isocyanides is the carbenic one, with a statistical weight about twice the zwitterionic form.[68] The second structure, however, imposes linear geometry to these compounds, which is essential to enable an efficient mix between the two forms, thus maximising resonance stabilisation. Finally, the authors suggested that the initial representation proposed by Ivar Ugi (Figure 1.3b), pointing out the π back donation of the nitrogen π lone pair to the carbon vacancy, should be preferred to other depictions.

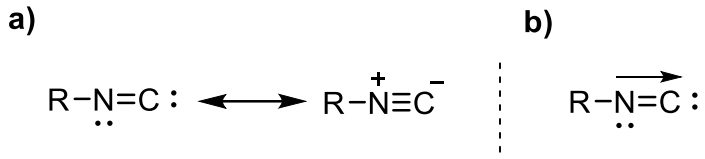

Figure 1.3. a) Carbenic and zwitterionic forms of isocyanides; b) Early representation of isocyanides suggested by Ivar Ugi.

Historically, isocyanides were first synthesised in 1859 by Lieke, who did not recognise them and believed them to be nitriles.[69] However, when trying to hydrolyse the putative nitriles to the corresponding carboxylic acids, he did not obtain the expected products but formamides instead.[48] It was Gautier ten years later who first understood the isomeric relationship between isocyanides and nitriles.[70] Since then, isocyanides have long suffered from a very bad reputation, mainly due to the initial lack of convenient synthetic methods and to their supposed toxicity (probably because of their name resembling that of cyanides). However, an extensive study of isocyanide harmfulness performed at Bayer AG in the 1960s, did not evidence a general toxicity for this class of compounds.[71] Isocyanides' notorious smell also contributed to their poor initial success: Hofmann and Gautier described it as "*highly specific, almost overpowering*", "*horrible*", and "*extremely distressing*", and because of it the first chemists dedicated to the field were forced to work outdoors. It should be noted, however, that if most of volatile isocyanides have a strange, repulsive smell, higher molecular weight isocyanides are usually solid and odourless. Nevertheless, their negative fame has long been the reason why isocyanide chemistry has been investigated poorly and sporadically until 1921, when the first IMCR, namely the Passerini reaction, was reported.[62] The Passerini reaction is a 3-CR involving an oxo-component **1.31** (aldehyde or ketone) an isocyanide **1.34** and a carboxylic acid **1.35** to give α-acyloxy carboxamides **1.36** (Scheme 1.5a). The generally accepted mechanism (Scheme 1.5b) is a concerted one,[49] where the loosely hydrogen-bonded adduct **I**, deriving from the carbonyl compound and the carboxylic acid, reacts with the isocyanide in a single step, through the formation of a three-component cyclic transition state **II**. Overall, this is an α-addition of the carbonyl component (the electrophile) and of the carboxylate (the nucleophile) to the isocyanide to give the intermediate **III**. The α-adduct **III**, which cannot be isolated, then rearranges in an intramolecular transacylation to afford the stable α-acyloxy carboxamide **1.36**.

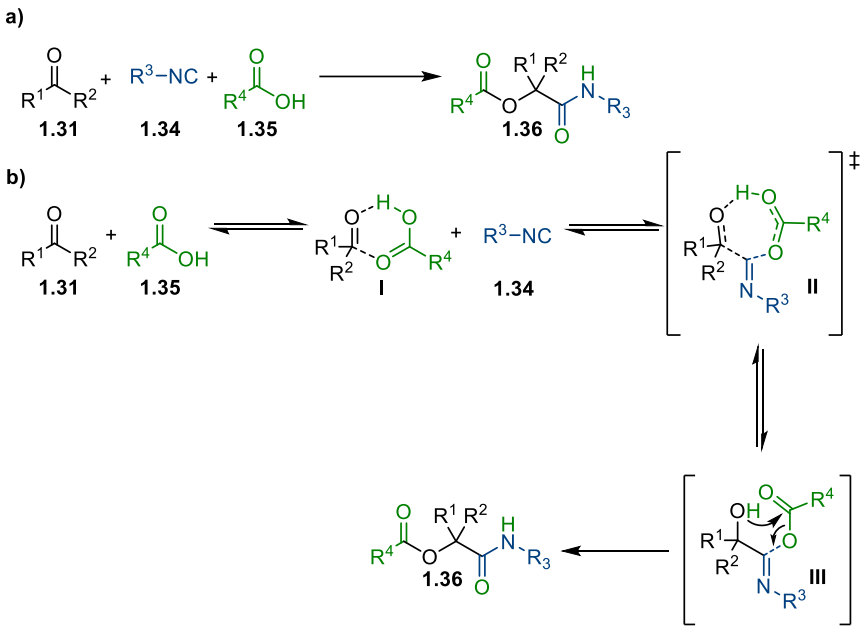

Scheme 1.5. a) Passerini 3-CR; b) Proposed reaction mechanism.

The reaction proceeds faster in low polarity, aprotic solvents (DCM, EtOAc, Et_2O, and THF are the most employed ones), which is in accordance with a non-ionic reaction pathway. The P-3-CR is typically carried out at high concentrations and at room temperature, with reaction times varying from a few hours to several days (in the case of ketones) and a wide tolerance for a variety of functional groups. Despite its synthetic utility, the Passerini 3-CR has long been much less exploited than the Ugi reaction, probably because of esters' lability under physiological conditions, which makes them less attractive than amides from a medicinal chemistry perspective. A renewal of interest in this reaction has thus been achieved by extending its scope from simple α-acyloxy amides to a variety of different products, including heterocycles and peptidomimetics;[72] this has required the use of starting materials specifically functionalised to react in post-condensation modifications and the development of modified Passerini reactions, such as its "truncated" and "interrupted" variants,[73] where water or an intramolecular nucleophile (on either the isocyanide or the carbonyl component) replace the

carboxylic acid, respectively. Substitution of one of the classic components with an alternative one, the so-called Single Reactant Replacement (SRR) approach,[74] has also contributed to the field.

The Ugi reaction was first reported by Ivar Ugi in 1959[63] and could be described as the *aza*-version of the Passerini 3-CR, as it involves an amine as additional reactant: it is therefore a 4-CR between a carbonyl compound **1.31** (aldehyde or ketone), an isocyanide **1.34**, a carboxylic acid **1.35**, and a primary amine **1.37** leading to α-acylamino carboxamides **1.38** (Scheme 1.6a). Worthy of note, the reaction allows for the formation of four new bonds in one single step, with the oxidation of the isocyanide C^{II} atom to the amide C^{IV} atom acting as the driving force for the entire reaction sequence.

From a mechanistic point of view, the U-4-CR begins with the *in situ* formation of the imine **1.39** and its subsequent protonation by the carboxylic acid **1.35**, which gives the corresponding iminium ion **1.40**, endowed with an increased electrophilicity of the C=N bond compared to the imine (an alternative strategy to increase the electrophilicity of the imine is to add a Lewis acid such as $TiCl_4$ or $BF_3 \cdot OEt_2$, being especially the case for electron rich, weakly electrophilic Schiff bases). The exact order of the following events is not univocally accepted[75] as it may proceed either via the addition of the isocyanide **1.34** and the formation of a nitrilium ion **I**, followed by further addition of the carboxylate anion **1.41**[76] (Scheme 1.6b, *path a*), or via the former attack of the carboxylate anion **1.41** to the iminium intermediate **1.40** and subsequent insertion of the isocyanide **1.34**[77] (Scheme 1.6b, *path b*). In both cases the resulting α-adduct **III** is not isolated, as it undergoes an intramolecular acyl migration (first described by Mumm and better known as the Mumm rearrangement[78]) to finally afford the Ugi-product **1.38**. Notably, this is the only irreversible step of the whole sequence, which drives the reaction towards the product side.

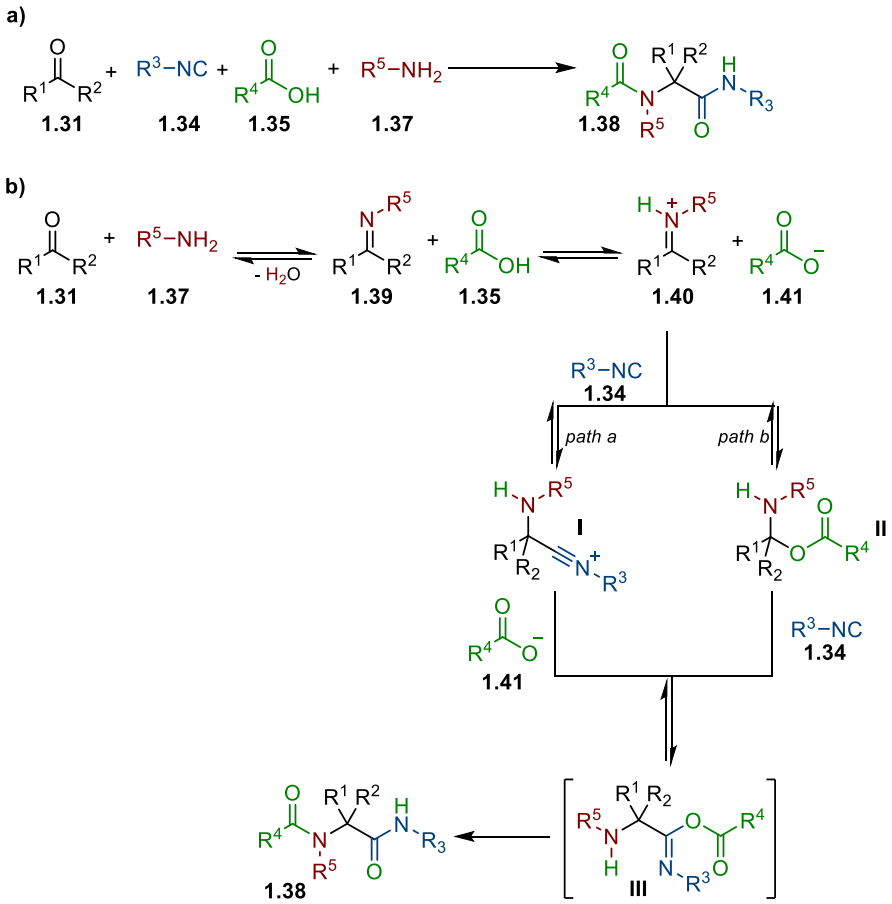

Scheme 1.6. a) Ugi 4-CR; b) Proposed reaction mechanism.

The reaction is favoured by polar protic solvents (typically low-molecular-weight alcohols such as MeOH, EtOH, and trifluoroethanol) at high concentrations (0.5 M - 2 M), while non-polar halogenated solvents usually prevent the solubilisation of the amine, promoting the competitive Passerini reaction to take place. Polar aprotic solvents such as THF, DMF, and dioxane or aqueous media have also proven to be viable alternatives for some applications. While the classic U-4-CR affords peptide-like structures often exhibiting promising pharmacological properties,[79] the possibility to apply "diversification strategies" in terms of both post-Ugi modifications and identification of new MCRs (*e.g.*, by changing one of the starting materials or by combining the Ugi reaction with other transformations) has

incredibly extended the chemical space accessible through this methodology. Over the past decades, the Ugi reaction has become a precious tool to access a variety of molecular architectures: from peptidomimetics to macrocycles, heterocyclic compounds,[80] natural products, and pharmaceutically relevant scaffolds. It was Ugi himself who first adopted his eponymous multicomponent approach for the synthesis of the anaesthetic drug Lidocaine, in 1966.[81] The traditional preparation of such compound relied on a 2-steps sequence making 2,6-dimethyl aniline **1.42** react with chloroacetyl chloride **1.43** and diethylamine **1.45** (Scheme 1.7a).[82] Although both steps worked well and with very good yields, the process generated waste mostly in the form of salts deriving from HCl neutralisation. Ugi was able to obtain Lidocaine in one step starting from 2,6-dimethylphenyl isocyanide **1.46** formaldehyde **1.47**, and diethylamine **1.45**, with water acting as the nucleophilic component (Scheme 1.7b). Notably, the yield was 90% and the AE 100%.

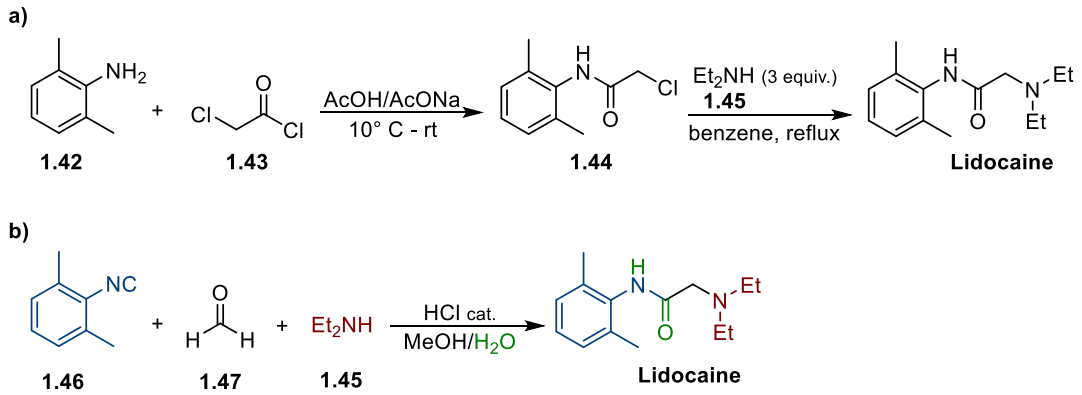

Scheme 1.7. a) Traditional linear synthesis of Lidocaine; b) Ugi's multicomponent synthesis of Lidocaine.

The anti-schistosomiasis drug Praziquantel offers another interesting example. It is usually manufactured in four steps mainly involving substitution reactions plus an intramolecular Pictet–Spengler cyclisation (Scheme 1.8a).[83] This procedure is quite robust, high yielding and not particularly hazardous, nevertheless, the multicomponent approach has several advantages. It consists of only two stages

relying on a Ugi 4-CR, which affords the acylated intermediate **1.56** prior to cyclisation (Scheme 1.8b).[84] The E-factor for this strategy is only 0.7 compared to 3.1 of the previous synthetic route, not even considering the substantial reduction in solvent usage.

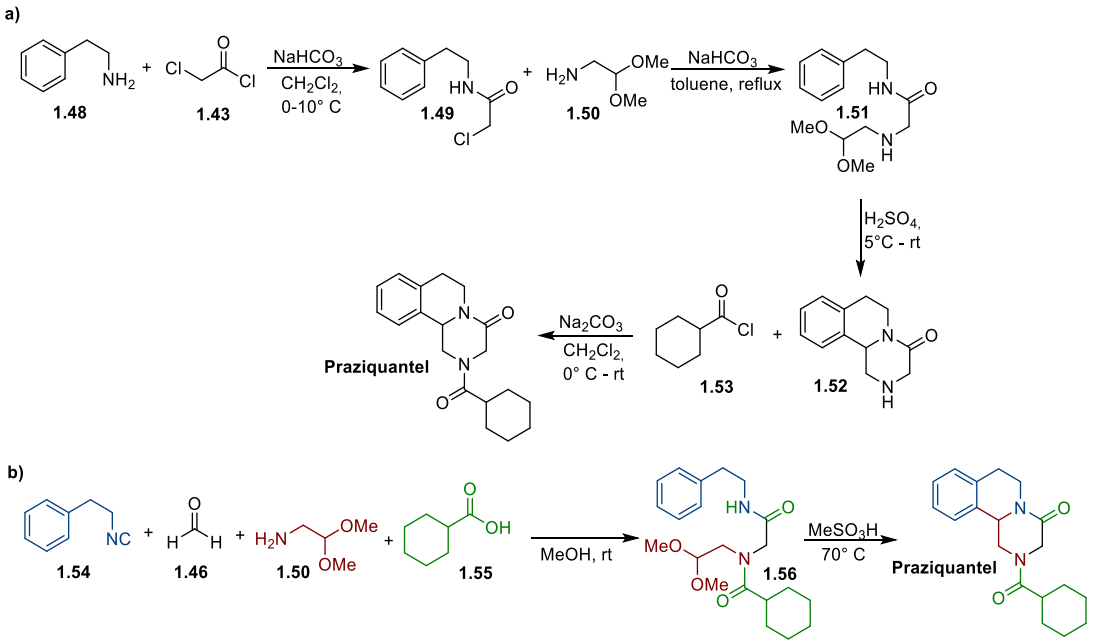

Scheme 1.8. a) Traditional linear synthesis of Praziquantel; b) Domling's multicomponent synthesis of Praziquantel.

In 2016 Orru's group exploited the convertible isocyanide 2-bromo-6-isocyanopyridine **1.57** to efficiently synthesise Carfentanil[85] (a synthetic opioid which is ~100000 times more potent than morphine[86]) via a classic Ugi 4-CR, followed by acidic methanolysis of the so-obtained intermediate **1.61** (Scheme 1.9). This gave Carfentanil in near-quantitative yield.

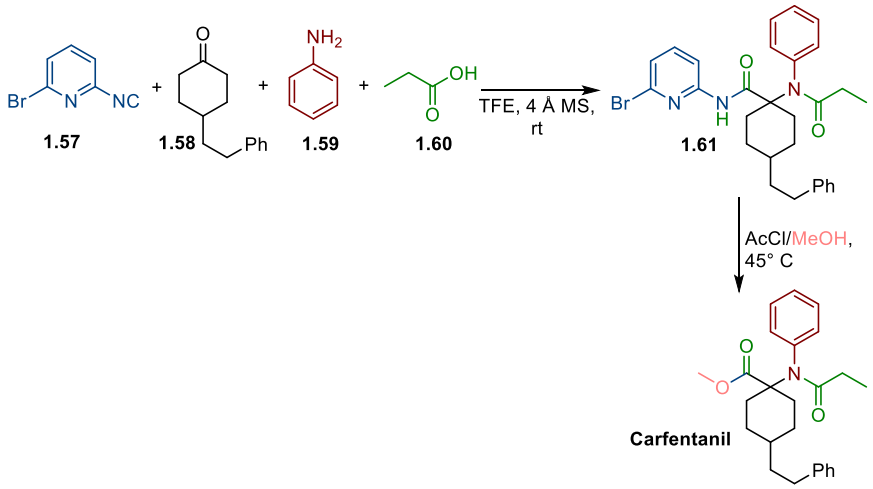

Scheme 1.9. Orru's multicomponent synthesis of Carfentanil.

Finally, the successful combination of a biocatalytic desymmetrisation with a Passerini 3-CR and a Joullié-Ugi 3-CR (exploiting preformed cyclic imines as starting materials) has led to a dramatically shortened and highly concise route to the anti-HCV agent Telaprevir (11 steps instead of 24, Figure 1.4).[87]

All this makes clear how IMCRs deserve a predominant role among all the MCRs described, since they are more versatile and more flexible than the remaining multicomponent approaches. There are virtually no restrictions on the nature of the nucleophiles and electrophiles suitable as starting materials, and this pose no limits to the number of potentially accessible products. For example, cyanates, thiocyanates, azides, phenols, thiols, water, hydrazoic acid, and hydrogen sulfide have replaced the original carboxylic acid;[88] (*Z*)-chloroximes and hydrazonoyl chlorides have been used as precursors of nitrile *N*-oxides and nitrile imines, respectively, to act as the electrophilic group;[89] protected hydrazines, hydroxylamine, diaziridine, urea, sulphonamides have acted as the amine component for the Ugi-4-CR. Despite the large number of examples reported so far, it is reasonable to think that there are many other Passerini and Ugi-related IMCRs lying dormant, waiting to be discovered.

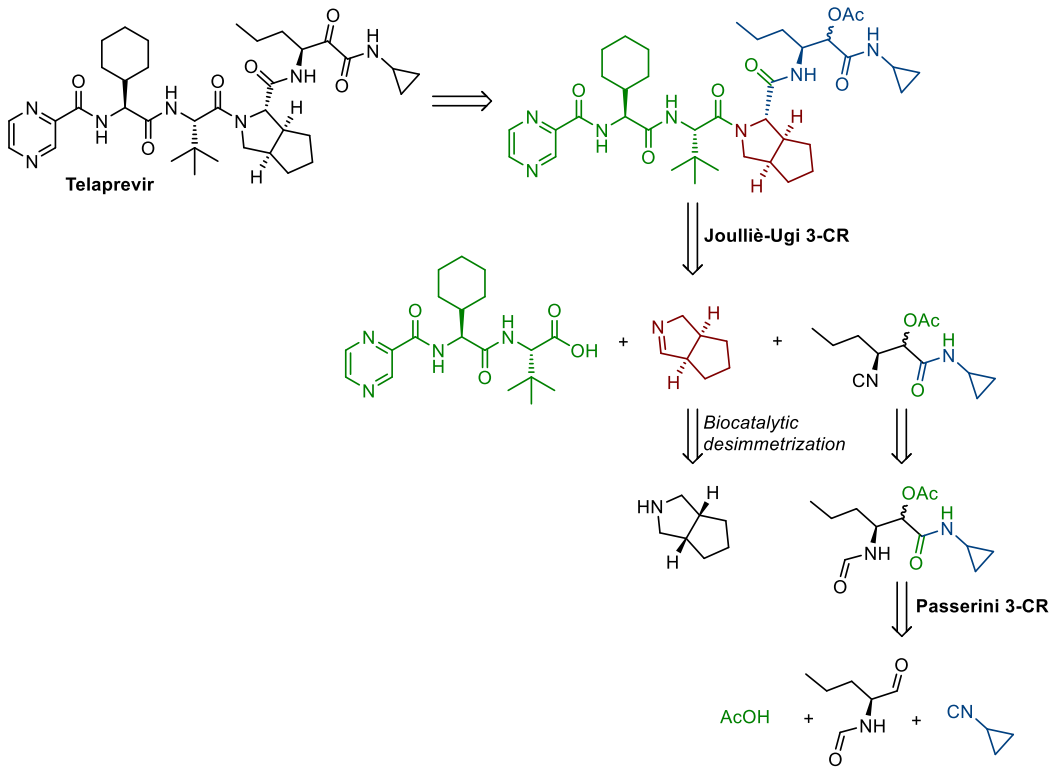

Figure 1.4. Ruijter's biocatalytic/multicomponent approach for the synthesis of Telaprevir.

1.3. Visible Light Photoredox Catalysis for Organic Chemistry

Nature has always inspired chemists to look for synthetic strategies as mild as the ones occurring in the living world; in this regard, photosynthesis is possibly one of the most fascinating natural chemical processes, as it uses sunlight as a source of energy to be stored in the form of chemical bonds, by converting water and carbon dioxide into oxygen and sugars. The Italian chemist Giacomo Ciamician was the first who recognised the potential of using light as a renewable energy source to synthesise molecules. This is what he stated more than a century ago, during his speech to the French Chemical Society: "*For plants, light is the source of energy. Through the intervention of chlorophyll, green plants accumulate solar energy and transform it into chemical energy. […] When oil will have been all burned in our prodigal industries, it may become necessary, even on social grounds, to come to*

exploit solar energy".[90] An intensive work based on the systematic exposition to solar light of an impressive number of different chemicals led him to discover interesting photochemical transformations. These occurred under exceptional mild conditions in what can be considered the first deliberate effort to establish green procedures for chemical syntheses.[91] His visionary intuition actually paved the way to modern photochemistry. As a matter of fact, light offers the ideal form of (renewable) energy: it is free, non-hazardous, environmentally friendly, and photons provide enough energy to achieve the desired transformation without the need for high temperatures or harsh conditions often required by thermal activation.[92] On the other hand, photochemistry has also proved to be able to unlock unique reaction pathways, unavailable under conventional reactivities. This is mainly due to the fact that the chemical behaviour of excited molecules essentially differs from that in the ground state.[93] The development of effective visible light-driven transformations, however, has long been neglected. In fact, considering the equation of photon energy ($E=hc/\gamma$, where h is Planck's constant, c is the speed of light, and γ is the wavelength) and the weak energy of photons in the visible light spectrum postulated by it, photochemical reactions were initially carried out using UV light to excite substrates or reagents. This required special equipment and often caused unselective reactions, which were difficult to predict and control. The situation has changed in recent decades, with the development of light-absorbing chromophores which can be activated by low-energy photons and thus act as photocatalysts (PCs). These are usually polypyridyl complexes of ruthenium (II) and iridium (III), or organic dyes such as Rose Bengal, Eosin Y, triphenylpyrylium or acridinium salts (Figure 1.5), which absorb light in the visible region of the electromagnetic spectrum (at wavelengths where common organic molecules do not absorb) to give photoexcited states whose lifetimes are sufficiently long to engage in bimolecular events with organic molecules, in competition with deactivation pathways.

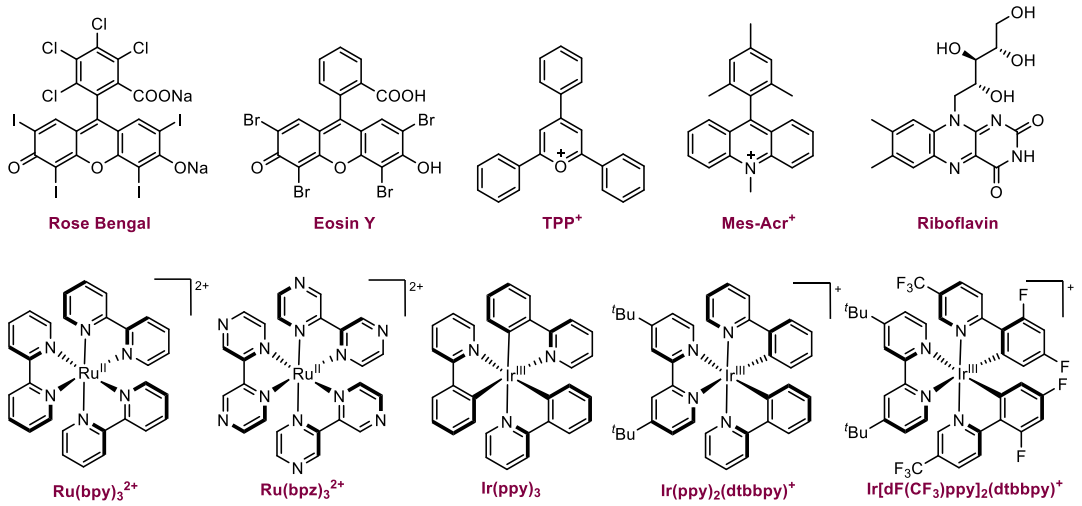

Figure 1.5. Chemical structures of some common photoredox catalysts.

Typically, the absorption of a photon by the singlet ground state PC(S_0), causes the promotion of one of its valence electrons to a higher energetic singlet excited state PC($*S_1^n$), which then relaxes to the lowest vibrational level PC($*S_1^0$) (Figure 1.6). The latter can go back to the singlet ground state via radiative (fluorescence, k_f) or non-radiative (k_{nr}) pathways. Alternatively, it can undergo an efficient intersystem crossing (ISC, k_{isc}, which is a configurational spin flip of the electron) to the triplet state PC($*T_1^n$), followed by internal conversion (k_{IC}) to produce the lowest triplet excited state PC($*T_1^0$). This is reasonably long-lived because its decay to the singlet ground state PC(S_0) is spin-forbidden; it can be deactivated by radiative (phosphorescence, k_p) or non-radiative (kn_r) pathways, or it can in turn activate organic substrates by means of four principal mechanisms: a) single electron transfer; b) proton-coupled electron transfer; c) light-induced atom transfer; d) energy transfer.

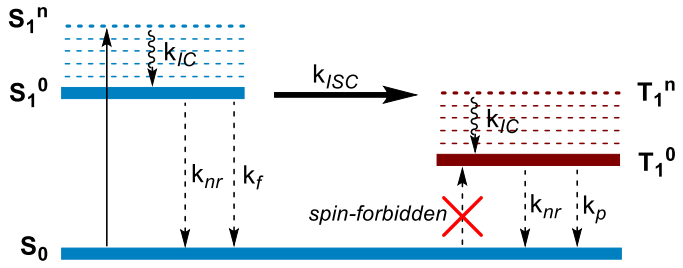

Figure 1.6. Photocatalysts' behaviour under visible light irradiation.

a) Single-Electron Transfer

Single-Electron Transfer (SET) is probably the most common mechanism providing reactive open-shell species under visible light irradiation. Single Electron Transfer photocatalysts are well typified by the complex tris(2,2′-bipyridine)ruthenium (II), or $Ru(bpy)_3^{2+}$: upon absorption of a photon in the visible region, an electron in one of the photocatalyst's metal-centred t_{2g} orbitals is excited to a ligand-centred π^* orbital (Figure 1.7). This transition (known as metal to ligand charge transfer, MLCT) provides a species in which the metal has been oxidised to Ru (III) while the ligand has undergone a single-electron reduction.[94] The initially populated singlet MLCT state rapidly undergoes ISC to give the lowest-energy triplet MLCT state, which is a long-lived species (τ=1100 ns) due to the spin-forbidden transition to the singlet ground state. Importantly, the photoexcited species has a high-energy electron which may be expelled from the π^* orbital, but has also a low-energy hole in the t_{2g} orbital, which is available to accept an electron: as a consequence, the excited photocatalyst is both a better oxidant and a better reductant than the ground state species, and thus can promote single electron oxidations or reductions of suitable substrates, depending on the nature of the latter.

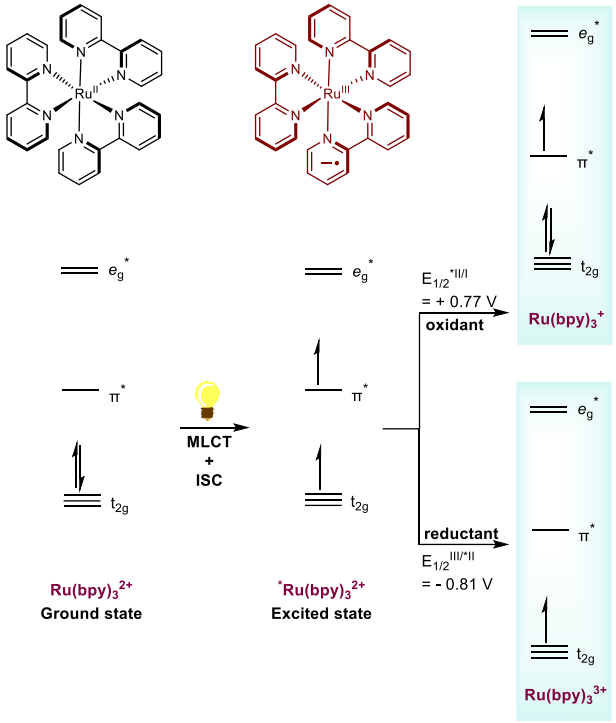

Figure 1.7. Simplified Molecular Orbital depiction of $Ru(bpy)_3^{2+}$ photochemistry.

In a typical oxidative quenching cycle (Figure 1.8), the excited state catalyst PC^* reduces an electron acceptor (A), resulting in a strong oxidant $PC^{\bullet+}$, which can accept an electron from a suitable donor (D) to close the catalytic cycle. Common oxidative quenchers are viologens, polyhalomethanes, dinitro- and dicyanobenzenes, and aryldiazonium salts.[94]

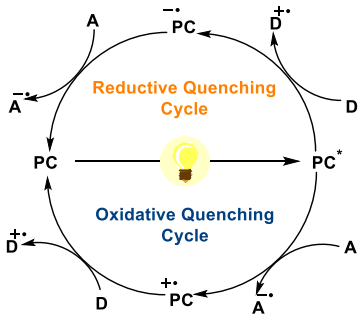

Figure 1.8. SET oxidative and reductive quenching cycles of a common PC.

Conversely, during a reductive quenching cycle (Figure 1.8), the excited state catalyst PC^* serves as an oxidant by accepting an electron from an electron donor (D), and affords the reduced species $PC^{\bullet-}$, with higher reducing ability. This is particularly prone to give an electron to a suitable electron acceptor (A), thus regenerating the ground state PC. Such reductive quenching scenario is typically facilitated by tertiary amines. Photocatalytic processes including both an oxidation and a reduction step without need for any sacrificial oxidant or reductant are defined redox-neutral.[95] Alternatively, the excited photocatalyst can be quenched by a sacrificial electron donor (typically an amine or ascorbic acid) or an electron acceptor (usually oxygen from air or peroxodisulfate) and the reduced or oxidised form can in turn oxidise or reduce a substrate in a ground-state step.[95] Whatever the scenario, the result is the generation of reactive open-shell intermediates, such as radicals and radical ions, ready to undergo organic transformations in a controlled and very mild fashion. This is in contrast to classic chemical approaches to radical species, usually relying on hazardous initiators, toxic reagents, and in many cases, high-temperatures or high-energy UV irradiation.[96] Moreover, the redox potentials at each step of the cycle may be finely tuned via modifications of the ligand backbone of the photocatalyst: while introducing electron-donating substituents increase the reductive strength of the complex, electron-withdrawing groups render the complex more strongly oxidising.[97] This has significantly expanded the repertoire of synthetic transformations that can be accomplished by means of photoredox catalysis.

b) *Proton-Coupled Electron Transfer*

A complementary mechanism to SET is Proton-Coupled Electron Transfer (PCET, Figure 1.9). It consists of redox events in which an electron and a proton are transferred in a concerted elementary step.[98] Differently from hydrogen atom transfer processes, in which the proton and the electron move together from a single donor to a single acceptor, the proton and the electron in a PCET mechanism

can derive from two distinct donors or travel to two different acceptors, and this can significantly increase the thermodynamic feasibility of some transformations. In a typical reductive quenching cycle, the exited state photocatalyst PC^* gets reduced to $PC^{\bullet-}$ by an electron donor, which concurrently loses a proton, while in an oxidative quenching cycle a suitable electron acceptor receives simultaneously an electron from the PC^* (oxidising it to $PC^{\bullet+}$) and a proton from another species (Figure 1.9). In both cases the reaction produces free radical intermediates, which can engage in a variety of organic transformations.

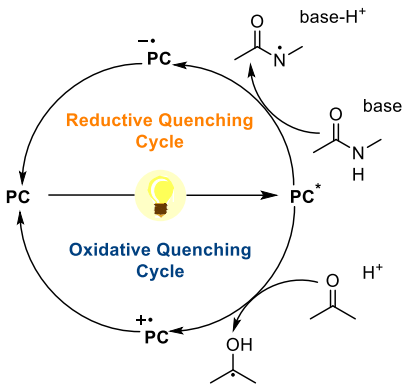

Figure 1.9. PCET oxidative and reductive quenching cycles of a common PC.

c) Light-Induced Atom Transfer

Direct Hydrogen Atom Transfer (*d*-HAT) is the most common Light-Induced Atom Transfer mechanism for the activation of otherwise inert aliphatic C−H bonds.[99] In this process, the energy of photons induces the PC to trigger the homolytic cleavage of C−H bonds in organic molecules, thus generating open shell-species and the reduced form of the PC ($PC^{\bullet}$-H). The mechanism for the PC restoration depends on the synthetic context and can involve a back-HAT event or an electron/proton transfer (ET/PT) sequence towards a chemical species $X^{\bullet}$ specifically included in the reaction mixture to this purpose (*e.g.*, a sacrificial hydrogen acceptor), or transiently formed during the process, also dictating the overall redox balance of the synthetic transformation.[99]

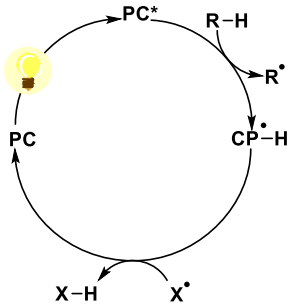

Figure 1.10. *d*-HAT mechanism for the photocatalytic activation of organic substrates.

As shown in Figure 1.11, there are available several classes of PCs$_{HAT}$, including aromatic ketones, xanthene dyes, polyoxometalates such as sodium (NaDT) and tetra-*n*-butylammonium decatungstate (TBADT), uranyl salts, and a metal-oxo porphyrin (Sb-Oxo).

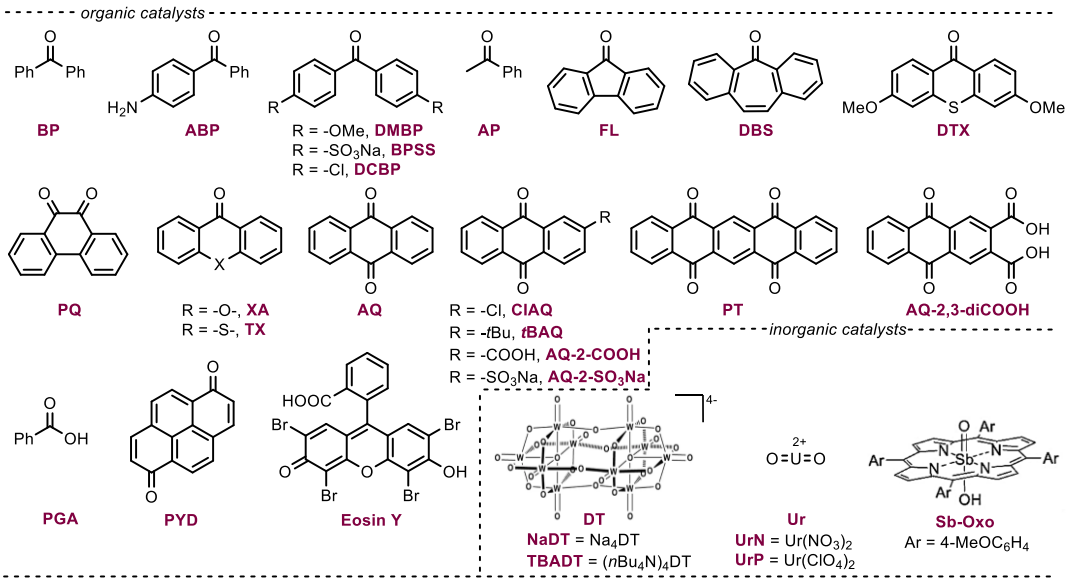

Figure 1.11 Common *d*-HAT photocatalysts.

d) Energy transfer

Energy transfer is still a minor and not exhaustively investigated method for the visible light photocatalytic activation of organic molecules.[100] In this mechanistic

paradigm, a PC^* can transfer its excited state energy to a substrate or reagent that is not able to directly absorb light at the given wavelength: this process is termed triplet−triplet energy transfer (TTET) and couples the decay of the exited PC^* from its triplet state to its ground singlet state with the promotion of another molecule R from its ground singlet state to its lowest-energy triplet state R* (Figure 1.12).

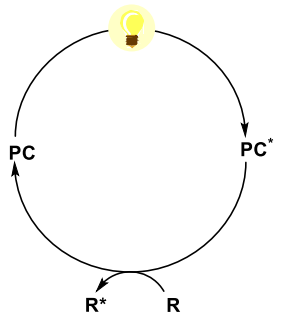

Figure 1.12. Energy transfer mechanism for the photocatalytic activation of organic substrates.

The first application of photoredox catalysis to organic synthesis dates back to forty years ago, when Kellogg demonstrated that the photo-mediated reduction of sulfonium ions to the corresponding alkanes and thioethers, using *N*-substituted 1,4-DHPs as the terminal reductant, could be accelerated by addition of a catalytic amount of $[Ru(bpy)_3]Cl_2$.[101] Despite this early evidence of the opportunities arising from applying photoredox catalysis to organic synthesis, the area remained relatively dormant until the late 2000s, with notable exceptions by Fukuzumi and Tanaka,[102-104] Pac,[105-108] Cano-Yelo and Deronzier,[109-111] and Okada.[112] It has been starting from 2008 that seminal studies from Yoon,[113] MacMillan,[114] and Stephensons'[115] groups have contributed to unearth the potential of this mode of activation as a valuable catalysis platform for organic reactions and have initiated a renewed interest in the field, as evident from the increasing number of publications covering the topic of photoredox catalysis in the last decades (Figure 1.13).

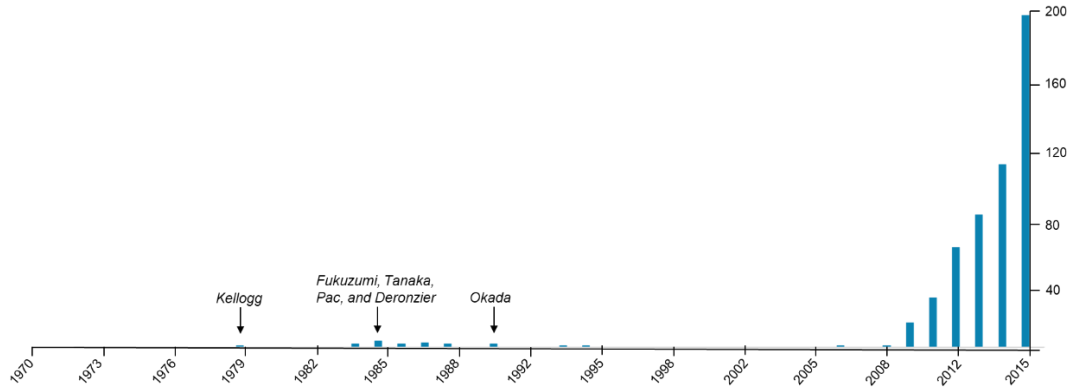

Figure 1.13. Papers published between 1970 and 2015 in the field of organic photoredox catalysis.

Since then, visible light photoredox catalysis has dramatically changed the field of organic synthesis, establishing itself as the election tool for the generation of highly reactive radical intermediates under otherwise unattainable mild conditions. This has provided access to reactivities that are complementary to those of closed-shell, two-electron species, and has contributed to the development of a variety of unconventional strategies for the construction of carbon-carbon and carbon-heteroatom bonds. These strategies often display better chemoselectivity than traditional pathways and broader functional-group compatibility, which makes them particularly suitable for the late-stage editing[116-118] of complex molecular architectures. Introducing small, inert functionalities directly on biorelevant compounds, late in the discovery process, may actually speed up the identification of structure–activity relationships (SARs) and/or address problems associated with on- and off-target effects, metabolism, and pharmacokinetics. Fluoro- and fluoroalkyl- moieties have traditionally been employed due to their resistance toward cytochrome P450-mediated oxidation,[119] while small alkyl functionalities such as the methyl group have been proven to modulate selectivity, improve potency, and prevent enzyme metabolism thanks to both conformational changes and hydrophobic effects (the so-called *magic methyl effect*).[120,121] Whitin this

context, visible light photocatalysis offers unique opportunities to install a wide range of functionalities (from very simple to more complex ones) directly and selectively on drug-like scaffolds, by unlocking site-specific reactivities under very mild reaction conditions.[122] An interesting application is the obtainment of site-selective labelled drugs as diagnostic agents, for mechanistic studies or pharmacokinetic evaluations, as in MacMillan's approach to deuterium- and tritium-labelled nitrogen containing pharmaceuticals, using isotopically labelled water (D_2O or *in situ* formed T_2O) as the source of hydrogen isotope.[123]

Furthermore, the combination of photoredox catalysis with a secondary catalytic system has led to the rise of multicatalytic approaches (*e.g.,* metallo- and organo-photoredox catalysis) enabling the concurrent activation of multiple substrates to achieve challenging chemical transformations.

All this has required a rapid evolution of the light sources employed for photochemical applications, from common compact fluorescent household lightbulbs (CFLs, having broadband emission) to light-emitting diode (LED) arrays, to integrated photoreactors allowing for a finer modulation of both the wavelength and the intensity of light. These two parameters can dramatically affect the efficiency and selectivity of photochemical reactions, and their careful control has proved to be crucial to improve reproducibility of photocatalytic protocols.[124]

One of the main challenges remain the scale-up of photochemical reactions for industrial applications. Photocatalytic methodologies rely on efficient and homogeneous irradiation of the reaction mixture; solvents, reagents, products, and PCs at the point of incident light can all act as filters, reducing the light intensity available for the rest of the reaction mixture.[125] This is especially true for large-scale applications, where photon flux decreases consistently with increasing path length and concentration, according to the Beer-Lambert law ($A = \varepsilon c l$, where A is the absorption, ε is the molar extinction coefficient, c is the concentration, and l is and the optical path length of the light). As a result, incomplete irradiation of reaction solutions occurs in large batch reactors leading to both long reaction times

and poor reaction efficiencies for larger reaction volumes.[96] Continuous flow (micro)reactors are the technology of choice to address this issue.[126] The narrow channel dimensions of flow reactors help to ensure the uniform irradiation of the entire reaction mixture, enabling substantial acceleration and convenient opportunities for the scaling-up of photochemical reactions, compared to batch reactors.

Bibliography

(1) Bloom, D. E.; *Science,* **2011**, *333*, 562–569.

(2) Tobiszewski, M.; Mechlińska, A.; Zygmunt, B.; Namieśnik; *Trends in Analytical Chemistry,* **2009**, *28*, 943–951.

(3) Sheldon, R. A; *Green Chemistry,* **2017**, *19*, 18–43.

(4) De Marco, B. A.; Rechelo, B. S.; Tótoli, E. G.; Kogawa, A. C.; Salgado, H. R. N.; *Saudi Pharmaceutical Journal,* **2019**, *27*, 1–8.

(5) United Nations; *Wayback Machine General Assembly Resolution*, **1983**.

(6) De Vito Stephen C.; Garrett Roger L.; *Designing Safer Chemicals: Green Chemistry for Pollution Prevention*, **1996,** American Chemical Society; Washington DC.

(7) Woodhouse, E. J.; Breyman, S.; *Science, Technology and Human Values* **2005**, *30*, 199–222.

(8) Anastas, P.; Eghbali, N.; *Chemical Society Reviews,* **2010**, *39*, 301–312.

(9) United States Environmental Protection Agency; *Green Chemistry: definition*.

(10) Clark, J. H.; *Green Chemistry,* **1999**, *1*, 1–8.

(11) Zimmerman, J. B.; Anastas, P. T.; Erythropel, H. C.; Leitner, W.; *Science,* **2020**, *367*, 397–400.

(12) Anastas Paul T.; Warner John C.; *Green Chemistry: Theory and Practice*, **1998**, Oxford University Press; New York.

(13) Erythropel, H. C.; Zimmerman, J. B.; de Winter, T. M.; Petitjean, L.; Melnikov, F.; Lam, C. H.; Lounsbury, A. W.; Mellor, K. E.; Janković, N. Z.; Tu, Q.; Pincus, L. N.; Falinski, M. M.; Shi, W.; Coish, P.; Plata, D. L.; Anastas, P. T.; *Green Chemistry* **2018**, *20*, 1929–1961.

(14) Sheldon R. A.; *Chemistry and Industry,* **1992**, *23*, 903–906.

(15) Sheldon, R. A.; *Chemical Communications,* **2008**, *29*, 3352-3365.

(16) Sheldon, R. A.; *ACS Sustainable Chemistry and Engineering*, **2018**, *6*, 32–48.

(17) Zimmerman J. B.; Anastas P. T.; in *Sustainability Science and Engineering*; **2006**, *1*, 201–221; Elsiever; Amsterdam.

(18) Newman, S. G.; Jensen, K. F.; *Green Chemistry,* **2013**, *15*, 1456-1472.

(19) Trost, B.; *Science,* **1991**, *254*, 1471–1477.

(20) Tickner, J. A.; Schifano, J. N.; Blake, A.; Rudisill, C.; Mulvihill, M.; *Environmental Science and Technology,* **2015**, *49*, 742–749.

(21) Voutchkova-Kostal, A. M.; Kostal, J.; Connors, K. A.; Brooks, B. W.; Anastas, P. T.; Zimmerman, J. B.; *Green Chemistry,* **2012**, *14*, 1001-1008.

(22) Slater C. S.; Savelski M. J.; Carole W. A.; Constable D. J. C.; *Green Chemistry in the Pharmaceutical Industry*; **2010**; Wiley-VCH: Weinheim.

(23) James, S. L.; Adams, C. J.; Bolm, C.; Braga, D.; Collier, P.; Friščić, T.; Grepioni, F.; Harris, K. D. M.; Hyett, G.; Jones, W.; Krebs, A.; Mack, J.; Maini, L.; Orpen, A. G.;

Parkin, I. P.; Shearouse, W. C.; Steed, J. W.; Waddell, D. C.; *Chemical Society Reviews,* **2012**, *41*, 413–447.
(24) Kappe, C. O.; Pieber, B.; Dallinger, D.; *Angewandte Chemie International Edition* **2013**, *52*, 1088–1094.
(25) Corrêa A. G.; Paixão M. W.; Schwab R.S.; *Current Organic Synthesis,* **2015**, *12*, 675–695.
(26) Moseley, J. D.; Kappe, C. O.; *Green Chemistry,* **2011**, *13*, 794-806.
(27) Cravotto, G.; Cintas, P.; *Chemical Society Reviews,* **2006**, *35*, 180–196.
(28) Gallezot, P.; *Green Chemistry,* **2007**, *9*, 295-302.
(29) Shenvi, R. A.; O'Malley, D. P.; Baran, P. S.; *Accounts of Chemical Research,* **2009**, *42*, 530–541.
(30) Dunetz, J. R.; Fandrick, D.; Federsel, H.-J; *Organic Process Research and Development,* **2015**, *19*, 1325–1326.
(31) MacMillan, D. W. C.; *Nature,* **2008**, *455*, 304–308.
(32) Sheldon, R. A.; Woodley, J. M.; *Chemical Reviews,* **2018**, *118*, 801–838.
(33) Koeller, K. M.; Wong, C.-H; *Nature,* **2001**, *409*, 232–240.
(34) Boethling, R. S.; Sommer, E.; Di Fiore, D.; *Chemical Reviews,* **2007**, *107*, 2207–2227.
(35) Keith, L. H.; Gron, L. U.; Young, J. L.; *Chemical Reviews,* **2007**, *107*, 2695–2708.
(36) Kletz T. A.; *Chemistry and Industry,* **1978**, *6*, 287–292.
(37) Curzons, A. D.; Jiménez-González, C.; Duncan, A. L.; Constable, D. J. C.; Cunningham, V. L.; *The International Journal of Life Cycle Assess* **2007**, *12*, 272–280.
(38) Constable, D. J. C.; Dunn, P. J.; Hayler, J. D.; Humphrey, G. R.; Leazer, Jr., J. L.; Linderman, R. J.; Lorenz, K.; Manley, J.; Pearlman, B. A.; Wells, A.; Zaks, A.; Zhang, T. Y.; *Green Chemistry,* **2007**, *9*, 411–420.
(39) Tucker, J. L.; *Organic Process Research and Development,* **2006**, *10*, 315–319.
(40) Kar, S.; Sanderson, H.; Roy, K.; Benfenati, E.; Leszczynski, J.; *Chemical Reviews,* **2022**, *122*, 3637–3710.
(41) Stuart, N. J.; Sanders A. S; *United States Patent 3385886*, **1961**.
(42) Cann, M. C.; Connelly, M. E.; *The BHC "Real World Cases in Green Chemistry"*; **2000**, American Chemical Society, Washington DC.
(43) Hoekstra, M. S.; Sobieray, D. M.; Schwindt, M. A.; Mulhern, T. A.; Grote, T. M.; Huckabee, B. K.; Hendrickson, V. S.; Franklin, L. C.; Granger, E. J.; Karrick, G. L.; *Organic Process Research and Development,* **1997**, *1*, 26–38.
(44) Martinez, C. A.; Hu, S.; Dumond, Y.; Tao, J.; Kelleher, P.; Tully, L.; *Organic Process Research and Development,* **2008**, *12*, 392–398.
(45) Adrian G. P.; *United States Patent 5019655A*, **1991**.
(46) Taber, G. P.; Pfisterer, D. M.; Colberg, J. C.; *Organic Process Research and Development***, 2004**, *8*, 385–388.

(47) U.S. Environmental Protection Agency; *Presidential Green Chemistry Challenge: 2002 Greener Synthetic Pathways Award: Pfizer, Inc.: Green Chemistry in the Redesign of the Sertraline Process*., **2022**.
(48) Dömling, A.; Ugi, I.; *Angewandte Chemie International Edition*, **2000**, *39*, 3168–3210.
(49) Alvim, H. G. O.; da Silva Júnior, E. N.; Neto, B. A. D.; *RSC Advances,* **2014**, *4*, 54282–54299.
(50) Dömling, A.; *Chemical Reviews,* **2006**, *106*, 17–89.
(51) Cioc, R. C.; Ruijter, E.; Orru, R. V. A; *Green Chemistry,* **2014**, *16*, 2958–2975.
(52) Tietze, L. F.; *Chemical Reviews,* **1996**, *96*, 115–136.
(53) Strecker, A.; *Liebigs Annalen der Chemie,* **1850**, *75*, 27–45.
(54) Hantzsch, A., *Justus Liebigs Annalen der Chemie,* **1882**, *215*, 1–82.
(55) Tron, G. C.; Minassi, A.; Appendino, G.; *European Journal of Organic Chemistry,* **2011**, *28*, 5541–5550.
(56) Biginelli, P.; *Berichte der deutschen chemischen Gesellschaft,* **1891**, *24*, 1317–1319.
(57) Kappe, C. O.; *European Journal of Medicinal Chemistry,* **2000**, *35*, 1043–1052.
(58) Mannich, C.; Krösche, W.; *Archiv de Pharmazie,* **1912**, *250*, 647–667.
(59) List, B.; *Journal of the American Chemical Society,* **2000**, *122*, 9336–9337.
(60) Bergs, H.; *German Patent 566,094*, **1929**.
(61) Bucherer, T.; Barsch, H.; *Journal für praktische Chemie,* **1934**, *140*, 151.
(62) Passerini, M.; *Gazzetta Chimica Italiana,* **1921**, *51*, 126–129.
(63) Ugi, I.; Meyr, R.; Fetzer, U.; Steinbrückner, C.; *Angewandte Chemie*, **1959**, *71*, 386.
(64) Ugi, I.; *Isonitrile Chemistry*; **1971**, Academic Press Inc.; New York-London.
(65) Nef, J. U.; *Justus Liebigs Annalen der Chemie,* **1892**, *270*, 267–335.
(66) Lindemann, H.; Wiegrebe, L.; *Chemische Berichte* ,**1930**, *63*, 1650–1657.
(67) Giustiniano, M.; Basso, A.; Mercalli, V.; Massarotti, A.; Novellino, E.; Tron, G. C.; Zhu, J.; *Chemical Society Reviews,* **2017**, *46*, 1295–1357.
(68) Ramozzi, R.; Chéron, N.; Braïda, B.; Hiberty, P. C.; Fleurat-Lessard, P.; *New Journal of Chemistry* ,**2012**, *36*, 1137– 1140.
(69) Lieke, W., *Justus Liebigs Annalen der Chemie,* **1859**, *112*, 316–321.
(70) Gautier, A.; *Justus Liebigs Annalen der Chemie,* **1869**, *146*, 119–123.
(71) Ugi, I.; Fetzer, U.; Eholzer, U.; Knupfer, H.; Offermann, K.; *Angewandte Chemie International Edition,* **1965**, *4*, 472–484.
(72) Banfi, L.; Basso, A.; Lambruschini, C.; Moni, L.; Riva, R.; *Chemical Science,* **2021**, *12*, 15445–15472.
(73) Giustiniano, M.; Moni, L.; Sangaletti, L.; Pelliccia, S.; Basso, A.; Novellino, E.; Tron, G. C.; *Synthesis,* **2018**, *50*, 3549–3570.
(74) Ganem, B.; *Accounts of Chemical Research,* **2009**, *42*, 463–472.
(75) Rocha, R. O.; Rodrigues, M. O.; Neto, B. A. D.; *ACS Omega,* **2020**, *5*, 972–979.

(76) Ugi, I.; Offermann, K.; *Angewandte Chemie International Edition,* **1963**, *2*, 624.
(77) Chéron, N.; Ramozzi, R.; Kaïm, L. El; Grimaud, L.; Fleurat-Lessard, P.; *The Journal of Organic Chemistry,* **2012**, *77*, 1361–1366.
(78) Mumm, O.; *Berichte der Deutschen Chemischen Gesellschaft,* **1910**, *43*, 887.
(79) Fouad, M. A.; Abdel-Hamid, H.; Ayoup, M. S.; *RSC Advances,* **2020**, *10*, 42644–42681.
(80) Zhu, J.; *European Journal of Organic Chemistry,* **2003**, 7, 1133–1144.
(81) Ugi, I.; Steinbruckner, C.; *United States Patent 3,247,200*, **1966**.
(82) Loefgren, N. M.; Lundqvist, B. J.; *United States Patent 2441498*, **1948**.
(83) Kim, J. H.; Lee, Y. S.; Park, H.; Kim, C. S.; *Tetrahedron,* **1998**, *54*, 7395–7400.
(84) Cao, H.; Liu, H.; Dömling, A.; *Chemistry – A European Journal,* **2010**, *16*, 12296–12298.
(85) Van der Heijden, G.; Jong, J. A. W.; Ruijter, E.; Orru, R. V. A; *Organic Letters,* **2016**, *18*, 984–987.
(86) Van Daele, P. G. H.; De Bruyn, M. F. L.; Boey, J. M.; Sanczuk, S.; Agten, J. T. M.; Janessen, P. A. J.; *Arzneimittelforschung,* **1976**, *26*, 1521–1531.
(87) Znabet, A.; Polak, M. M.; Janssen, E.; de Kanter, F. J. J.; Turner, N. J.; Orru, R. V. A.; Ruijter, E.; *Chemical Communications,* **2010**, *46*, 7918–7920.
(88) Hooshmand, S. E.; Zhang, W.; *Molecules,* **2023**, *28*, 1642–1658
(89) Giustiniano, M.; Novellino, E.; Tron, G. C.; *Synthesis,* **2016**, *48*, 2721–2731.
(90) Ciamician, G.; *Bulletin de la Société Chimique de France,* **1908**, *3*, 1–27.
(91) Albini, A.; Fagnoni, M; *Green Chemistry,* **2004**, *6*, 1–6.
(92) Crisenza, G. E. M.; Melchiorre, P.; *Nature Communications,* **2020**, *11*, 803–806.
(93) Melchiorre, P.; *Chemical Reviews,* **2022**, *122*, 1483–1484.
(94) Prier, C. K.; Rankic, D. A.; MacMillan, D. W. C.; *Chemical Reviews,* **2013**, *113*, 5322–5363.
(95) Marzo, L.; Pagire, S. K.; Reiser, O.; König, B.; *Angewandte Chemie International Edition,* **2018**, *57*, 10034–10072.
(96) McAtee, R. C.; McClain, E. J.; Stephenson, C. R. J.; *Trends in Chemistry,* **2019**, *1*, 111–125.
(97) Tucker, J. W.; Stephenson, C. R. J.; *The Journal of Organic Chemistry,* **2012**, *77*, 1617–1622.
(98) Gentry, E. C.; Knowles, R. R.; *Accounts of Chemical Research,* **2016**, *49*, 1546–1556.
(99) Capaldo, L.; Ravelli, D.; Fagnoni, M.; *Chemical Reviews,* **2022**, *122*, 1875–1924.
(100) Shaw, M. H.; Twilton, J.; MacMillan, D. W. C.; *The Journal of Organic Chemistry,* **2016**, *81*, 6898–6926.
(101) Hedstrand, D. M.; Kruizinga, W. H.; Kellogg, R. M.; *Tetrahedron Letters,* **1978**, *19*, 1255–1258.
(102) Hironaka, K.; Fukuzumi, S.; Tanaka, T.; *Journal of the Chemical Society, Perkin Transactions 2,* **1984**, *10*, 1705–1709.

(103) Fukuzumi, S.; Koumitsu, S.; Hironaka, K.; Tanaka, T.; *Journal of the American Chemical Society,* **1987**, *109*, 305–316.
(104) Fukuzumi, S.; Mochizuki, S.; Tanaka, T. Tanaka.; *The Journal of Physical Chemistry,* **1990**, *94*, 722–726.
(105) Pac, C.; Ihama, M.; Yasuda, M.; Miyauchi, Y.; Sakurai, H.; *Journal of the American Chemical Society*, **1981**, *103*, 6495–6497.
(106) Pac, C.; Miyauchi, Y.; Ishitani, O.; Ihama, M.; Yasuda, M.; Sakurai, H.; *The Journal of Organic Chemistry,* **1984**, *49*, 26–34.
(107) Ishitani, O.; Pac, C.; Sakurai, H.; *The Journal of Organic Chemistry,* **1983**, *48*, 2941–2942.
(108) Ishitani, O.; Yanagida, S.; Takamuku, S.; Pac, C.; *The Journal of Organic Chemistry,* **1987**, *52*, 2790–2796.
(109) Cano-Yelo, H.; Deronzier, A. Cano-Yelo, H.; *Tetrahedron Letters,* **1984**, *25*, 5517–5520.
(110) Cano-Yelo, H.; Deronzier, A.; *Journal of the Chemical Society, Perkin Transactions 2,* **1984**, *6*, 1093–1098.
(111) Cano-Yelo, H.; Deronzier, A. Cano-Yelo, H.; *Journal of Photochemistry and Photobiology,* **1987**, *37*, 315–321.
(112) Okada, K.; Okamoto, K.; Morita, N.; Okubo, K.; Oda, M.; *Journal of the American Chemical Society,* **1991**, *113*, 9401–9402.
(113) Ischay, M. A.; Anzovino, M. E.; Du, J.; Yoon, T. P.; *Journal of the American Chemical Society,* **2008**, *130*, 12886–12887.
(114) Nicewicz, D. A.; MacMillan, D. W. C.; *Science,* **2008**, *322*, 77–80.
(115) Narayanam, J. M. R.; Tucker, J. W.; Stephenson, C. R. J.; *Journal of the American Chemical Society,* **2009**, *131*, 8756–8757
(116) Moir, M.; Danon, J. J.; Reekie, T. A.; Kassiou, M.; *Expert Opinion in Drug Discovery,* **2019**, *14*, 1137–1149.
(117) Cernak, T.; Dykstra, K. D.; Tyagarajan, S.; Vachal, P.; Krska, S. W.; *Chemical Society Reviews,* **2016**, *45*, 546–576.
(118) Wencel-Delord, J.; Glorius, F.; *Nature Chemistry,* **2013**, *5*, 369–375.
(119) Müller, K.; Faeh, C.; Diederich, F.; *Science,* **2007**, *317*, 1881–1886.
(120) Barreiro, E. J.; Kümmerle, A. E.; Fraga, C. A. M.; *Chemical Reviews,* **2011**, *111*, 5215–5246.
(121) Schönherr, H.; Cernak, T.; *Angewandte Chemie International Edition,* **2013**, *52*, 12256–12267.
(122) Cannalire, R.; Pelliccia, S.; Sancineto, L.; Novellino, E.; Tron, G. C.; Giustiniano, M.; *Chemical Society Reviews,* **2021**, *50*, 766–897.
(123) Loh, Y. Y.; Nagao, K.; Hoover, A. J.; Hesk, D.; Rivera, N. R.; Colletti, S. L.; Davies, I. W.; MacMillan, D. W. C.; *Science,* **2017**, *358*, 1182–1187.
(124) Le, C. C.; Wismer, M. K.; Shi, Z.-C.; Zhang, R.; Conway, D. V.; Li, G.; Vachal, P.; Davies, I. W.; MacMillan, D. W. C.; *ACS Central Science,* **2017**, *3*, 647–653.

(125) Reischauer, S.; Pieber, B.; *iScience*, **2021**, *24*, 102209.
(126) Plutschack, M. B.; Pieber, B.; Gilmore, K.; Seeberger, P. H.; *Chemical Reviews,* **2017**, *117*, 11796–11893.

Chapter 2

Development of green synthetic strategies: exploring unconventional (photo)reactivities of the isocyano-functional group

Medicinal chemistry continuously demands for new chemical entities (NCEs) exhibiting key pharmacophoric points to selectively interact with specific biological targets. This requires novel synthetic strategies to be efficiently developed in order to access complex and diverse molecular architectures with ease and in short times, while reaching unexplored regions of chemical space. Hopefully, these strategies should meet current sustainability criteria in affording versatile and direct routes to drug-like scaffolds that also minimise their environmental impact in terms of waste generation, atom economy, and energy consumption.

In this chapter, we will describe our efforts in exploiting the peculiar electronic properties of the isocyano-functional group to develop innovative synthetic solutions for the construction of drug-like small molecules.

Starting from a successful combination of the well-known advantages of IMCRs with the innate green features of photoredox catalysis for the obtainment of pharmaceutically relevant 1,5-disubstituted-1,3,4-oxadiazole derivatives (Section 2.1), we moved to investigate the opportunity of performing in water photo-induced transformations by exploiting micellar catalysis as a valuable alternative to commonly employed organic solvents (Section 2.2). While looking for new isocyanide-based photochemical reactions proceeding via Electron Donor-Acceptor (EDA) complexes formation (and thus not requiring any photocatalyst), we serendipitously came across a totally unknown photocatalytic activity of aromatic isocyanides in the α-amino C(sp^3)-H functionalisation. These findings were exploited either in self-catalysed reactions of isocyanides with water and aromatic tertiary amines, giving amide products under very mild conditions, or in the cross-dehydrogenative coupling of the latter with a range of different nucleophiles such as in Michael addition, Mannich-, Strecker-, *aza*-Henry-, and Kabachnik-Fields-type reactions (Section 2.3). Visible light-driven metal-free self-catalysed Ugi and Ugi-like multicomponent reactions leading to multifunctional molecular architectures were also developed (Section 2.4). Moreover, the possibility to tune

optical and redox properties of aryl isocyanides by properly substituting their aromatic moieties was further evaluated in the attempt to oxidise substrates other than aromatic tertiary amines, endowed with more challenging redox potentials (Section 2.5).

Apart from the potentialities and the challenges of bringing isocyanides into play in visible light-promoted two- or multicomponent processes (that we have also recently highlighted in two review articles[1,2]), isocyanides' (non-photo) unconventional reactivities offer additional opportunities to explore a wider chemical space. In this regard, the possibility to exploit isocyanides as polarised triple bonds upon Lewis acid activation led us to smoothly synthesise 4-substituted-5-aminoimidazole derivatives from Strecker multicomponent adducts via an ytterbium-promoted isocyanide insertion/5-*exo*-*dig* cyclisation (Section 2.6).

2.1. Visible light photocatalytic Ugi/*aza*-Wittig cascade towards 2-aminomethyl-1,3,4-oxadiazole derivatives

The 1,3,4-oxadiazole core is a structural motif frequently occurring in drug-like scaffolds, wherein it has been introduced for several purposes:

- it can be a key pharmacophoric unit, either contributing to ligand binding or providing appropriate orientation for substituents;[3]
- it can behave as bioisosteric replacement for carbonyl frameworks such as esters, amides, carbamates, and hydroxamic esters;[4,5]
- it can modulate chemical-physical properties by affecting lipophilicity and water-solubility of oxadiazole-containing molecules.[6]

Both 1,2,4- and 1,3,4-oxadiazole heterocyclic systems have been found to be effective bioisosteres of the amide bond, as they retain its geometry and have both planarity and dipole moment similar to those of the amide functionality, despite they lack its H-bond donating ability (Figure 2.1).

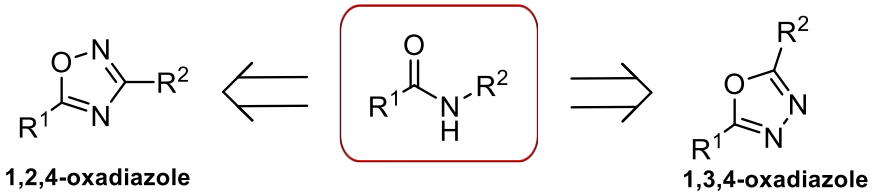

Figure 2.1. 1,2,4- and 1,3,4-oxadiazoles as bioisosteric replacements of the amide bond.

This bioisosteric replacement introduces structural rigidity, which may result in compounds with improved potency, selectivity, and pharmacokinetic properties, especially in terms of metabolic stability, membrane permeability, and CNS penetration.[7] Yudin's group, for example, has shown how the incorporation of a 1,3,4-oxadiazole ring into peptide macrocycles increases cell membrane penetration compared to amide congeners.[8]

The 1,2,4- and 1,3,4-regioisomers are geometrically virtually identical, thus providing the same space orientation to possible substituents and showing similar overall molecular shapes. Nevertheless, the 1,3,4-isomer often displays superior physicochemical and pharmacological properties compared to its isomeric partner, including reduced lipophilicity, improved aqueous solubility, and better metabolic stability.[6,9] This can be principally ascribed to its greater dipole moment, which affects the molecular charge distributions, and to the higher H-bond acceptor strength of the two nitrogen atoms within the 1,3,4-regioisomer. Furthermore, the 1,3,4-oxadiazole core is shared by a wide range of biologically active compounds: from the antihypertensive Nesapidil, to the antibiotic Furamizole, to the antiretroviral drug Raltegravir, and the anticancer agent Zibotentan (Figure 2.2). It thus deserves the status of privileged structure in medicinal chemistry.[10,11]

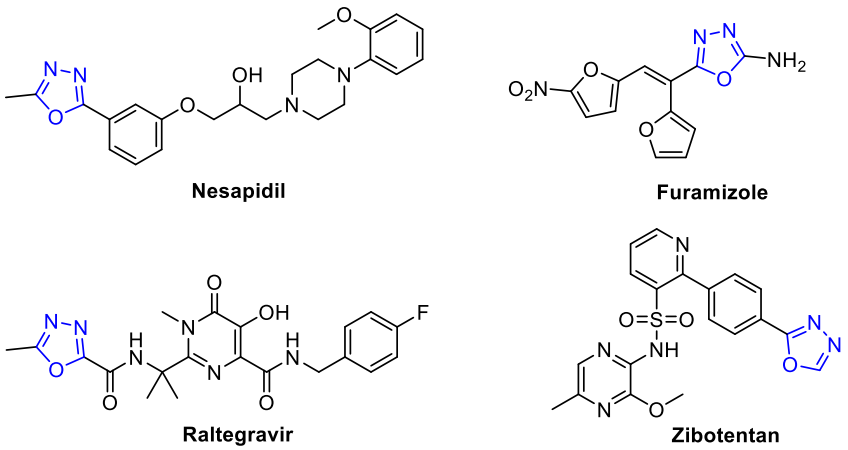

Figure 2.2. Examples of biologically active compounds incorporating the 1,3,4-oxadiazole core.

This explains the high number of protocols that have been reported in the literature for the synthesis of 1,3,4-oxadiazole derivatives.[11] Most of them are multi-step in nature, and generally exploit 1,2-diacylhydrazines as common building blocks to be cyclised under a variety of conditions, often requiring strong acidic pHs and elevated temperatures. Milder conditions have been achieved via the generation of phosphonium intermediates, whose oxophilicity can be exploited to initiate the cyclodehydration process.[12] The Huisgen reaction is an alternative route: it exploits the reaction of 5-substituted 1*H*-tetrazoles with electrophiles (such as carboxylic acid, anhydrides, or acyl chlorides), followed by extrusion of nitrogen and formation of a 1,5-dipole (*i.e.*, a nitrilimine) which subsequently cyclises to the desired 1,3,4-oxadiazole.[13] Several multicomponent approaches have also been reported. In 2010 Ramazani developed a one-pot Ugi 4-CR/*aza*-Wittig sequence affording 2,5-disubstituted-1,3,4-oxadiazoles at ambient temperature and without the need for any catalyst or activation[14] (Scheme 2.1a): it involved an aromatic aldehyde **2.1**, a secondary amine **2.2**, a carboxylic acid **2.3** and (*N*-isocyanoimino)triphenylphosphorane **2.4** as the key functionalised isocyanide allowing for the intramolecular *aza*-Wittig cyclisation.[15]

Van der Eiken's lab described the copper-catalysed three component coupling of pre-formed 2-substituted-1,3,4-oxadiazoles **2.7** with aldehydes **2.6** and secondary amines **2.2**[16] (Scheme 2.1b), while, more recently, Dömling developed a robust Ugi-tetrazole/Huisgen sequence[17] relying on the 4-CR of an aldehyde **2.6**, a secondary amine **2.2**, azidotrimethylsilane **2.8** and the cleavable 1,1,3,3-tetramethylbutyl isocyanide **2.9**, followed by acidic removal of the isocyanide alkyl moiety and treatment of the resulting 5-substituted-1*H*-tetrazole with an acyl chloride **2.11** at 120°C (Scheme 2.1c). Despite these strategies are valuable tools to build large and diverse libraries of 2,5-disubstituted 1,3,4-oxadiazole derivatives, all of them are limited to strongly nucleophilic secondary aliphatic amines.

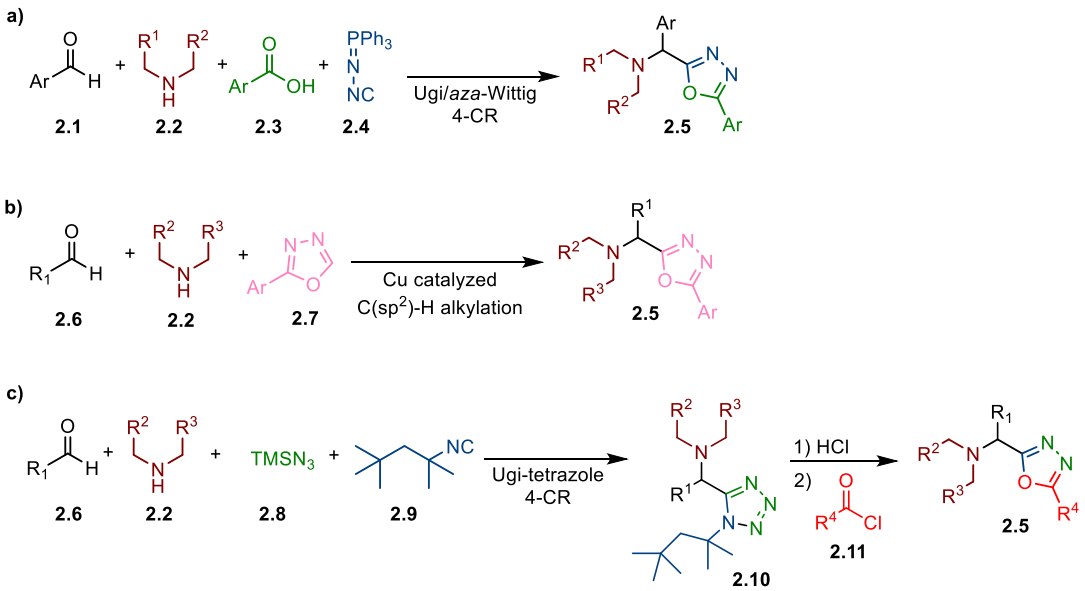

Scheme 2.1. Previous multicomponent approaches to 1,3,4-oxadiazoles.

In order to expand the substrate scope of the existing methodologies to 1,3,4-oxadiazoles incorporating aromatic amines, we reasoned that such a task could be accomplished by harnessing a photoredox catalytic *in situ* oxidation of an *N*-metyl-*N*-alkylaniline **2.12**, followed by a radical/polar crossover interception of the so-

formed iminium ion with (*N*-isocyanoimino)triphenylphosphorane **2.4** and a carboxylic acid **2.13**.[18]

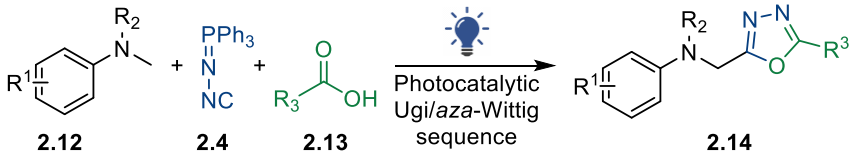

Scheme 2.2. One-pot multicomponent photocatalytic Ugi/*aza*-Wittig domino sequence developed.

Optimisation of the reaction conditions

To verify the feasibility of such a photocatalytic multicomponent approach, we reacted *N,N*-dimethylaniline (DMA) **2.15**, (*N*-isocyanoimino)triphenylphosphorane **2.4**, and *m*-toluic acid **2.16** as model substrates, in the presence of $[Ir(ppy)_2bpy]PF_6$ as the photocatalyst, in MeCN, under irradiation with 30W blue LED (wavelength: 450 – 455 nm), at room temperature (Table 2.1, Entry 1). After 20 hours, the desired product **2.17** was recovered in a modest 25% yield, probably due to unproductive degradation pathways of the isocyanide **2.4**. Increasing the isocyanide amount to 2 equivalents led to an improved 32% yield (Entry 2). While the addition of 3 Å molecular sieves provided some beneficial effects (Entry 3), working at higher concentration of the starting materials (1.0 M rather than 0.1 M) led to a decreased 23% yield (Entry 4). A screening of different metal-based and organic photocatalysts, such as *fac*-$Ir(ppy)_3$ and Eosin Y, did not furnish better outcomes, even when the amounts of the isocyanide and PC were further increased (Entry 5-6). During this survey for the optimal reaction conditions, we noticed that the product yield was decreased by the formation of a two-component monosubstituted 1,3,4-oxadiazole via the *aza*-Wittig background reaction between isocyanide and *m*-toluic acid,[19] probably due to a not efficient oxidation of DMA to the corresponding iminium ion. This observation prompted us to opt for a stronger oxidising PC, such as $Ru(bpy)_3(PF_6)_2$ (E_{red} Ru(II)*/Ru(I) = + 0.77 V *vs* SCE,

compared to $[Ir(ppy)_2bpy]PF_6$ (E_{red} Ir(III)*/Ir(II) = + 0.68 V *vs* SCE), and *fac*-$Ir(ppy)_3$ (E_{red} Ir(III)*/Ir(II) = + 0.31 V *vs* SCE)).[20] Accordingly, when the reaction was performed in the presence of $Ru(bpy)_3(PF_6)_2$, the yield increased to 50% (Entry 9). Longer reaction times (Entry 10) and DMA equivalents doubling (Entry 11) only led to slight improvements, while the use of $[Ru(bpy)_3]Cl_2 \bullet 6\ H_2O$ as the photocatalyst provided an optimum 67% yield (Entry 12).

Entry	2.15 (equiv.)	2.4 (equiv.)	PC (mol%)	2.17 Yield (%)
1	2	1	$[Ir(ppy)_2bpy]PF_6$ 1%	25[a]
2	1	2	$[Ir(ppy)_2bpy]PF_6$ 1%	32[a]
3[b]	1	2	$[Ir(ppy)_2bpy]PF_6$ 1%	36[a]
4[b,c]	1	2	$[Ir(ppy)_2bpy]PF_6$ 1%	23[d]
5[b]	1	2	*fac*-$Ir(ppy)_3$ 1%	27[d]
6[b]	1	2	Eosin Y 1%	18[d]
7[b]	1	2.5	Eosin Y 1%	12[d]
8[b]	1	2	Eosin Y 5%	6[a]
9[b]	1	2	$Ru(bpy)_3(PF_6)_2$ 2%	50[a]
10[b,e]	1	2	$Ru(bpy)_3(PF_6)_2$ 2%	57[a]
11[b]	2	2	$Ru(bpy)_3(PF_6)_2$ 2%	53[a]
12[b]	2	2	$[Ru(bpy)_3]Cl_2 \bullet 6\ H_2O$ 2%	67[a]

Conditions: reaction performed on a 0.08 mmol scale of **2.16**, in dry MeCN (0.1 M), under 30W blue LED irradiation (450 – 455 nm), RT, 20 h.
[a] Isolated yield
[b] 3 Å molecular sieves added
[c] Reaction performed at higher concentration (1.0 M)
[d] NMR yield (determined by using 1,3,5-trimethoxybenzene (TMB) as internal standard)
[e] Reaction time: 48 h

Table 2.1. Optimisation of the reaction conditions for the photocatalytic Ugi/*aza*-Wittig sequence.

Substrate scope

With the optimum conditions in hand, we investigated the robustness of the protocol by reacting (*N*-isocyanoimino)triphenylphosphorane **2.4** with a series of

differently substituted *N*-methyl-*N*-alkyl aromatic amines **2.12** and carboxylic acids **2.13** (Figure 2.3).

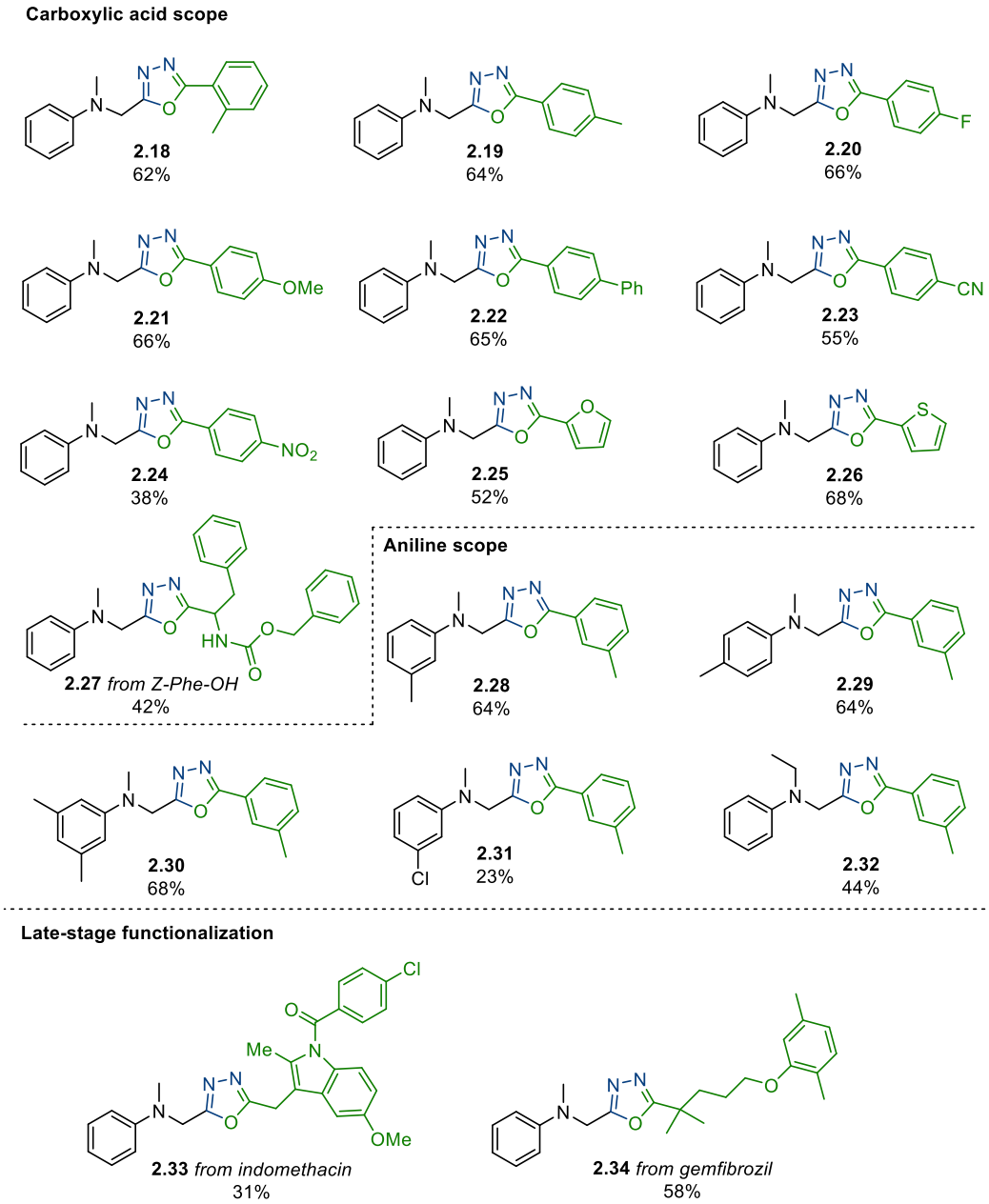

Figure 2.3. Substrate scope for the photocatalytic Ugi/*aza*-Wittig sequence.

Both aromatic (**2.18-2.24**) and heteroaromatic carboxylic acids (**2.25, 2.26**), as well as aliphatic ones (**2.27**), proved to be competent starting materials, with a good tolerance for a variety of functional groups including methyl- (**2.18**), even in the *ortho* position (**2.19**), halogens (**2.20**), ether (**2.21**), cyano- (**2.23**), nitro- (**2.24**), and carbamate (**2.27**) functionalities. Similarly, the scope of the aniline proved that the substitution pattern (*meta*- or *para*-methyl, **2.28** and **2.29**, respectively) did not affect the reaction efficiency. However, while electron-rich *N*,*N*-dimethylaniline derivatives were found to be suitable starting materials (**2.30**), the presence of an electron-withdrawing substituent, such as a chlorine at the *meta* position, led to a modest 26% yield (**2.31**). Interestingly, regioselectivity for methyl- oxidation was observed when *N*-ethyl-*N*-methylaniline was used as the starting amine component (**2.32**). Finally, to further explore the potential of the mild developed conditions, late-stage functionalisation of complex carboxylic acids such as indomethacin and gemfibrozil was also attempted: they gave the corresponding 1,3,4-oxadiazole derivatives **2.33** and **2.34** in 31 and 58% yield, respectively.

Two-step one-pot protocol for the synthesis of non-symmetrical diacylhydrazines

To expand the synthetic potential of the developed transformation, a tandem two-step one-pot conversion of DMA **2.15**, (*N*-isocyanoimino)triphenylphosphorane **2.4**, and *m*-toluic acid **2.16** to non-symmetrical 1,2-diacylhydrazine **2.35** was further attempted. To this end, HCl 6 N (1:1 *v/v* final concentration with respect to the solvent) was added *in situ* to the 1,3,4-oxadiazole **2.17** formed according to standard conditions: after stirring for 20 hours at room temperature, the acid hydrolysis of the heterocyclic core provided facile and expeditious access to the desired product **2.35** (Scheme 2.3). Worthy of note, a representative synthesis of similar scaffolds has been reported in three steps with an overall yield around 29%.[21] To our knowledge, our protocol stands for the first photocatalytic multicomponent strategy leading to such valuable scaffolds.[22-24]

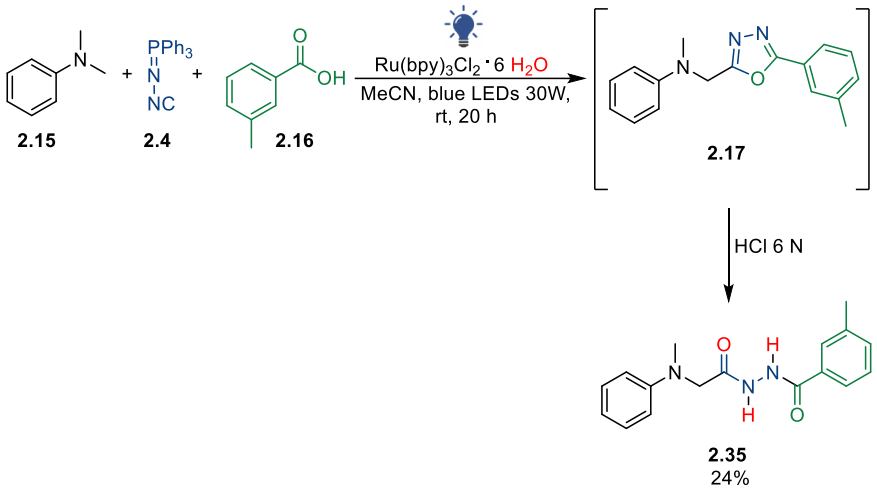

Scheme 2.3. Tandem two-step one-pot photocatalytic synthesis of non-symmetrical 1,2-diacylhydrazines.

Proposed reaction mechanism

A plausible mechanism for the developed visible light photocatalytic Ugi/*aza*-Wittig cascade is depicted in Scheme 2.4. Under visible light irradiation, the photocatalyst $[Ru(bpy)_3]Cl_2 \bullet 6\ H_2O$ undergoes a MLCT and populates the excited state Ru (II)*. The latter is quenched by the aniline derivative **2.12**, affording the reduced ruthenium complex Ru (I) and the corresponding aniline radical cation **I**. Regeneration of the photocatalyst in the presence of molecular oxygen provides a superoxide radical anion, which triggers the formation of the iminium ion **II** upon hydrogen atom abstraction from **I**, thus leading to a radical/polar crossover. Hence, the iminium ion **II** is attacked by (*N*-isocyanoimino)triphenylphosphorane **2.4** to generate the nitrilium ion **III**, which in turn undergoes addition of the carboxylic acid **2.13** to give the α-adduct **IV**. The latter can engage in a domino intramolecular *aza*-Wittig reaction finally affording the desired 1,3,4-oxadiazole derivative **2.14** with loss of triphenylphosphine oxide ($POPh_3$).

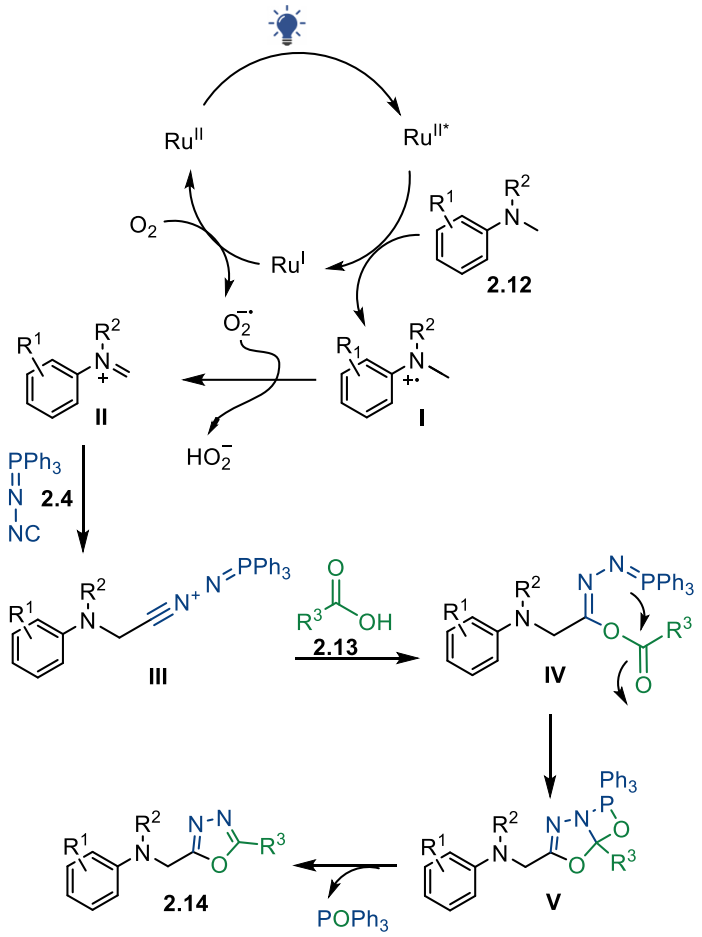

Scheme 2.4. Proposed reaction mechanism for the developed photocatalytic Ugi/*aza*-Wittig sequence.

2.2. Photomicellar catalysed synthesis of amides from isocyanides and *N*-alkyl-*N*-methyl aromatic amines

As previously discussed (see Sections 1.1.1 and 1.1.2), solvent minimisation, replacement, and selection play a critical role in greening chemistry. Several selection guides have been elaborated by leading pharmaceutical companies and institutions in order to help chemists with the choice of the "greenest" solvent for specific applications:[25,26] they take into account different criteria, including safety, occupational health, environmental impact, quality (risk of impurities in the final

drug), industrial constraints (*e.g.*, boiling point, freezing temperature, density, recyclability), and costs. Despite some differences exist, reflecting cultures and policies of the respective parent institutions, all these guides share one common point: water is the best possible reaction medium for organic syntheses. It is inflammable, incombustible, non-toxic, cheap, readily available, polar, and easy to separate from nonpolar immiscible organic solvents. In addition, water is unique for its exclusive ability to trigger new reactivities relying on unconventional reaction pathways. Since Breslow reported his seminal results about hydrophobic acceleration of Diels-Alder reaction in the 1980s,[27] many transformations originally developed in organic solvents have been successfully performed in aqueous media, sometimes with substantial improvements, such as faster reaction rates and greater selectivity.[28] While most of the time these reactions take place "on water",[29] and no real solvation of the reaction components occurs, performing reactions truly "in water" is especially challenging, as it requires the substrates to solubilise in the aqueous medium.[30] Professor Lipshutz's group has given a key contribution to the field by developing non-ionic surfactants that in water spontaneously self-assemble into micellar form.[31] With critical micelle concentrations (CMCs) typically on the order of 10^{-3}-10^{-4} M,[32] these micellar arrays are able to act as "nanoreactors" mimicking enzymes' hydrophobic pockets, which provide suitable reaction vessels for lipophilic substrates and catalysts. By overcoming the need for large amounts of organic solvents while preserving both efficiency and selectivity in promoting organic transformations, micellar catalysis has thus been established as a huge opportunity to perform reactions in water. While a plethora of key synthetic transformations[33] (including condensations, oxidations, deprotections, multicomponent reactions, C-C and C-heteroatom bond-forming processes, and even metal-catalysed cross-couplings[34]) have been carried out under micellar catalytic conditions, very few reports about visible light-promoted synthetic methodologies in water are available so far. We have recently highlighted in a review article the opportunities and the challenges of merging

water as a reaction medium with the innate green properties of visible light photoredox catalysis.[35] This has often required either the development of water soluble photocatalysts[36,37] (in the case of polar substrates such as amino acids, peptides, and proteins) or the design of specific micellar photocatalytic systems. In 2018 Lipshutz reported the synthesis of an amphoteric polyethylene glycol ubiquinol succinate (PQS)-attached photocatalyst **PQS-[Ir]**[38] able to self-aggregate in water into nanomicelles, whereas the covalently bound Ir complex promoted, upon visible light excitation, different representative reactions, including difunctionalisation of alkenes **2.36** and sulfonylation of enol acetates **2.39** (Scheme 2.5). Notwithstanding the obvious and exclusive advantages offered by this micellar photocatalytic system, the need to covalently functionalise the surfactant in order to introduce the active photocatalytic moiety could limit a broad application of such an approach. This observation is even more relevant when considering new chemical transformations, for which screening of different photocatalysts endowed with different redox potentials, as well as of different surfactants, is usually required to achieve optimum reaction conditions. To this end, the desirable commercial availability of a wide range of surfactants covalently modified with different photoredox active catalysts would expedite the spreading of micellar systems as reaction media in visible light-triggered transformations.

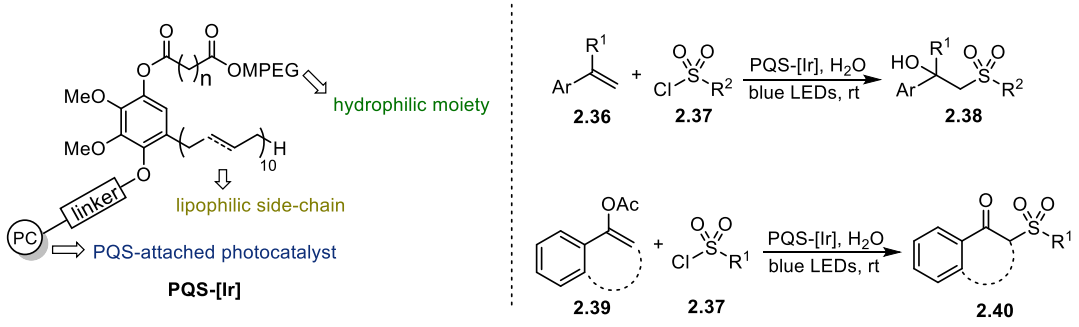

Scheme 2.5. Lipshutz's PQS-attached photocatalyst and representative reactions promoted by it.

In the meantime, with the hope that such an array of photoactive micelles will be soon available, we wondered if the switch from organic solvents to aqueous micellar solutions could be feasible, at least for those transformations involving water either as a cosolvent or a substrate.[39] Following our interests in isocyanide-based visible light-phototriggered processes, we chose as the model reaction a photoredox catalysed synthesis of amides **2.42** from isocyanides **2.41** and *N*-methyl-*N*-alkyl aromatic amines **2.12**, reported by Rueping *et al.* in 2013 (Scheme 2.6).[40]

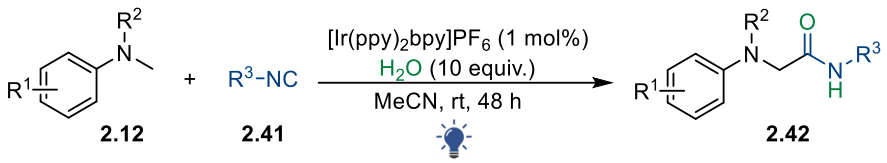

Scheme 2.6. Rueping's visible light photocatalytic synthesis of amides from isocyanides and *N*-methyl-*N*-alkyl aromatic amines.

Optimisation of the reaction conditions

The original conditions[40] made isocyanides and *N*-methyl-*N*-alkyl aromatic amines react in the presence of 10 equivalents of water and $[Ir(ppy)_2bpy]PF_6$ as the photocatalyst, in MeCN, at room temperature, under blue LED irradiation for 48 h. In a preliminary test reaction involving *N,N*-dimethylaniline **2.15** and *p*-toluenesulfonylmethyl isocyanide (TosMIC) **2.43** we tried to replace MeCN with a 2% aqueous solution of the non-ionic surfactant TPGS-750-M (Table 2.2, Entry 2): this gave the desired product **2.44** in a fair 30% yield, proving that a water-based solvent system could be feasible for this transformation (as a reference, **2.44** was obtained in 70% yield when the reaction was performed in MeCN according to literature conditions, Entry 1). Optimisation was carried out by performing the reaction in the presence of different micellar media (Figure 2.4) and photoredox catalysts, and by changing temperature, light source potency, and equivalents of the starting materials.

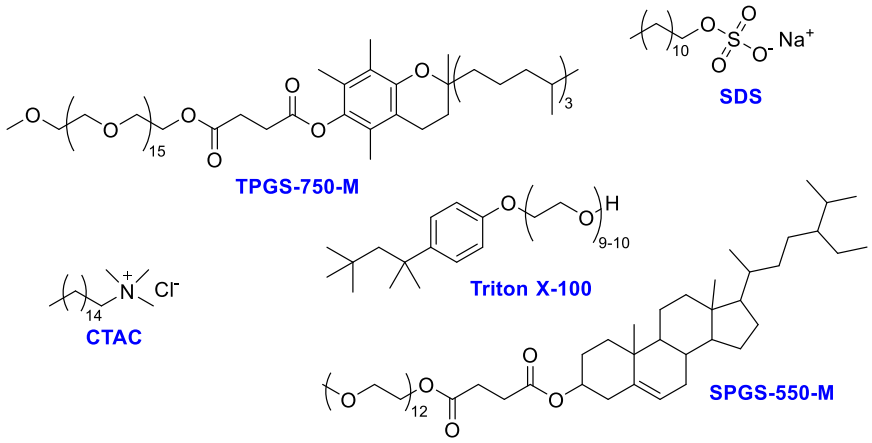

Figure 2.4. Structures of the surfactants tested.

Irradiation with 30W blue LED (wavelength: 450 – 455 nm) slightly increased the yield to 40% (Entry 3), and the beneficial effect of the micellar medium was made clear when performing the reaction in pure water (Entry 4). An increase of the reaction temperature to ~50 °C (fan switched off) led to detrimental results both in TPGS-750-M and in pure water (Entries 5 and 6), as well as the addition of Na_2CO_3 as a base (Entry 7). Interestingly, doubling the DMA amount while decreasing the isocyanide **2.43** (1 instead of 1.5 equivalents) led to a good 68% yield (Entry 8), while reducing **2.15** to 1.5 equivalents was detrimental (Entry 9). Again, the micellar medium was shown to be key for the success of the reaction under the new conditions (Entry 10). A further screening of both metal-based and organic photocatalysts did not produce better results (Entries 11−16), whereas a survey of different micellar media (Entries 17−24) resulted in the identification of a 2% aqueous solution of the anionic surfactant sodium dodecyl sulfate (SDS) as the best solvent system (Entry 24), affording the desired **2.44** in a good 75% yield, which was comparable to the yield obtained in MeCN (Entry 1). When these reaction conditions were applied to a ten-fold mmol scale (3 mmol), they were still found able to provide the desired product, although in a moderate 20% yield. Finally, further attempts to use an organic photocatalyst (Entry 25), as well as reducing the catalyst loading (Entry 26) were unproductive.

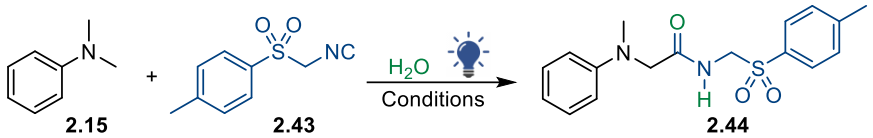

Entry	2.15 (equiv.)	2.43 (equiv.)	PC (mol%)	Solvent (0.15 M)	T	W	2.44 Yield (%)
1	1	1.5	$[Ir(ppy)_2bpy]PF_6$ (1)	MeCN	RT	16	70
2	1	1.5	$[Ir(ppy)_2bpy]PF_6$ (1)	2% TPGS-750-M	RT	16	30[b]
3	1	1.5	$[Ir(ppy)_2bpy]PF_6$ (1)	2% TPGS-750-M	RT	30	40[b]
4	1	1.5	$[Ir(ppy)_2bpy]PF_6$ (1)	H_2O	50°C	30	20[b]
5	1	1.5	$[Ir(ppy)_2bpy]PF_6$ (1)	2% TPGS-750-M	50°C	30	15[b]
6	1	1.5	$[Ir(ppy)_2bpy]PF_6$ (1)	H_2O	RT	30	12[b]
7[a]	1	1.5	$[Ir(ppy)_2bpy]PF_6$ (1)	2% TPGS-750-M	RT	30	ND
8	2	1	$[Ir(ppy)_2bpy]PF_6$ (1)	2% TPGS-750-M	RT	30	68 (50[b])
9	1.5	1	$[Ir(ppy)_2bpy]PF_6$ (1)	2% TPGS-750-M	RT	30	38[b]
10	2	1	$[Ir(ppy)_2bpy]PF_6$ (1)	H_2O	RT	30	22[b]
11	2	1	*fac*-$Ir(ppy)_3$ (1)	2% TPGS-750-M	RT	30	25[b]
12	2	1	$Ru(bpy)_3(PF_6)_2$ (1)	2% TPGS-750-M	RT	30	6.5[b]
13	2	1	Rose Bengal (1)	2% TPGS-750-M	RT	30	20[b]
14	2	1	Eosin Y (1)	2% TPGS-750-M	RT	30	17[b]
15	2	1	$[Mes\text{-}Acr]BF_4$ (1)	2% TPGS-750-M	RT	30	7[b]
16	2	1	Eosin Y (5)	2% TPGS-750-M	RT	30	20[b]
17	2	1	$[Ir(ppy)_2bpy]PF_6$ (1)	1% TPGS-750-M	RT	30	12[b]
18	2	1	$[Ir(ppy)_2bpy]PF_6$ (1)	2% SPGS-550-M	RT	30	33[b]
19	2	1	$[Ir(ppy)_2bpy]PF_6$ (1)	5% TPGS-750-M	RT	30	32[b]
20	2	1	$[Ir(ppy)_2bpy]PF_6$ (1)	2% Triton X-100	RT	30	31[b]
21	2	1	Eosin Y (5)	2% Triton X-100	RT	30	30[b]
22	2	1	$[Ir(ppy)_2bpy]PF_6$ (1)	2% CTAC	RT	30	15[b]
23	2	1	Eosin Y (5)	2% CTAC	RT	30	30[b]
24	2	1	$[Ir(ppy)_2bpy]PF_6$ (1)	2% SDS	RT	30	75 (64[b])
25	2	1	Eosin Y (5)	2% SDS	RT	30	18[b]
26	2	1	$[Ir(ppy)_2bpy]PF_6$ (0.5)	2% SDS	RT	30	25[b]

Conditions: reaction performed on a 0.08 mmol scale, under 30W blue LED irradiation (450 – 455 nm), 48 h.
[a] In the presence of Na_2CO_3 (1 equiv.)
[b] NMR yield (determined by using TMB as internal standard)

Table 2.2. Optimisation of the reaction conditions for the photomicellar catalysed synthesis of amides from isocyanides and *N*-alkyl- *N*-methyl aromatic amines.

Substrate scope, sunlight induced reaction, and recycling of the micellar medium

With the aim to prove the generality of the in water protocol, the substrate scope was investigated by reacting *N,N*-dimethylaniline **2.15** with both aliphatic and

aromatic isocyanides, which gave good yields regardless the presence of either electron-withdrawing or electron-donating substituents (**2.45**-**2.52**, Figure 2.5, yields in parentheses refer to the reaction performed in MeCN as reported in ref. 40).

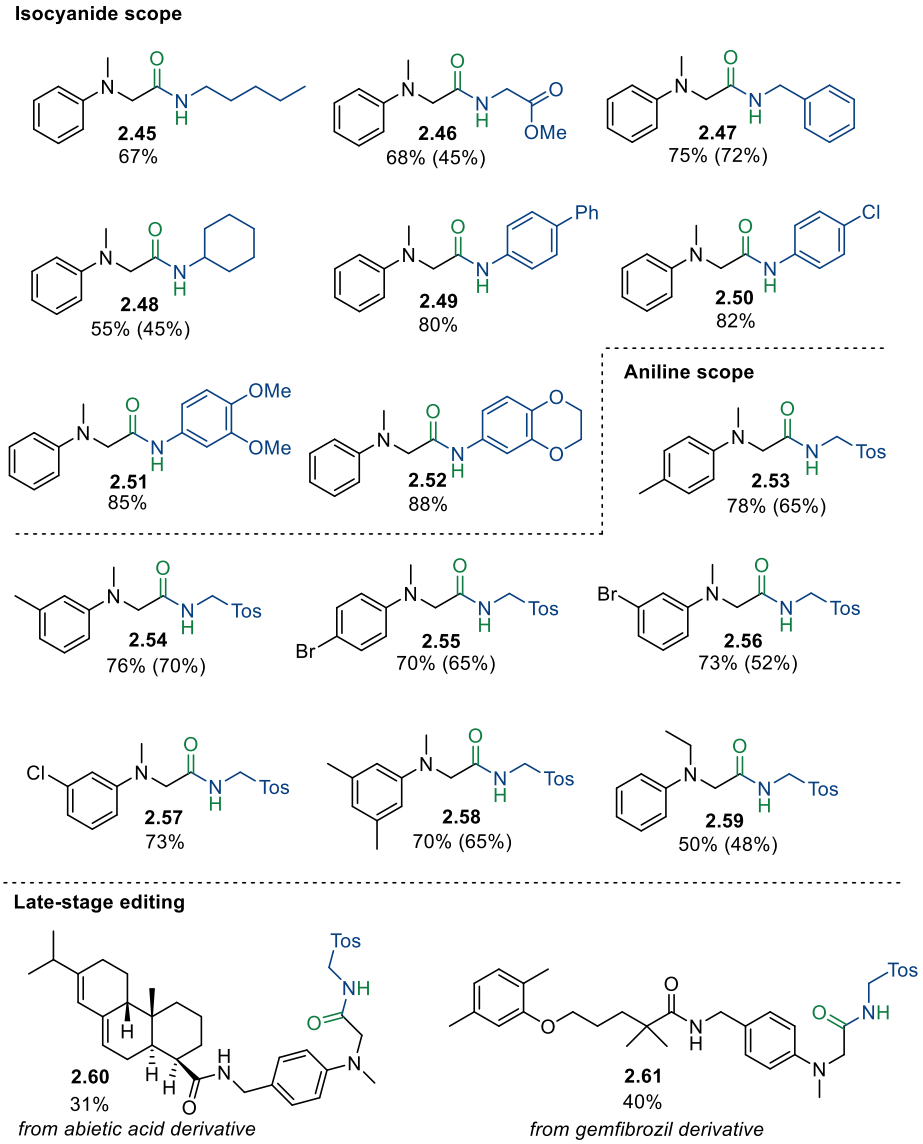

Figure 2.5. Substrate scope for the photomicellar catalysed synthesis of amides from isocyanides and *N*-methyl-*N*-alkyl aromatic amines.

Similarly, the aromatic amine scope was good, with yields close to or higher than those obtained in MeCN for both electron-rich (**2.53**, **2.54**, **2.58**) and electron-poor (**2.55**–**2.57**) anilines. Finally, non-symmetrical *N*-ethyl-*N*-methylaniline regioselectively afforded amide **2.59** in a good 50% yield. Noteworthy, the mild reaction conditions enabled a good functional groups tolerance, as further highlighted in the late-stage functionalisation of abietic acid and gemfibrozil-derived *N,N*-dimethylanilines, which gave **2.60** and **2.61** in 31 and 40% yield, respectively.

The robustness of the protocol was further proved by performing the reaction under sunlight irradiation, which led to the target compound **2.44** in a good 60% yield (Scheme 2.7a). Moreover, recycling of the micellar aqueous medium by introducing all the components to the aqueous mixture deriving from the previous reaction, after extraction with EtOAc, was found to be efficient up to three times, with no or slight change in the yields (Scheme 2.7b).

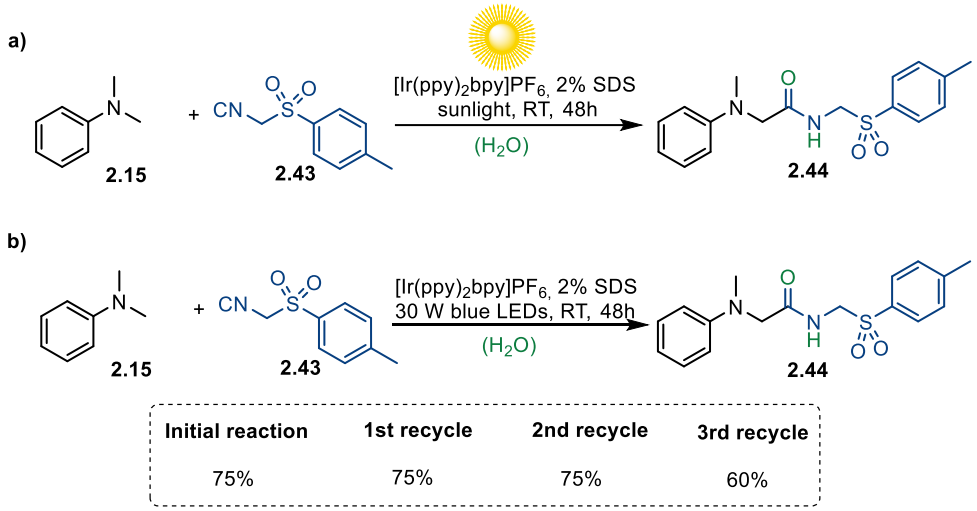

Scheme 2.7. a) Sunlight induced reaction; b) Recycling of the micellar aqueous medium.

NMR studies of photocatalyst/surfactant interactions

In order to investigate whether a rational approach for selecting the best performing photocatalyst/surfactant pairs could be feasible, the interactions occurring between the photocatalyst and SDS and cetyltrimethylammonium chloride (CTAC) 2% aqueous solutions (*i.e.*, the most and the least efficient micellar systems) were studied at the atomic level via solution NMR techniques.[41] These NMR studies were conducted in collaboration with Dr. F. Santoro, Dr. D. Brancaccio, and Prof. A. Carotenuto from University of Naples Federico II. At first, 1D ^{1}H NMR spectra of $[Ir(ppy)_2bpy]PF_6$ in pure water and in micellar aqueous media were recorded: while the spectrum of the catalyst in pure water showed low intensity and broad signals (Figure 2.6a), probably due to its poor solubility and consequent aggregation phenomena, both the proton spectra acquired in SDS and CTAC 2% aqueous solutions showed narrow and well-resolved signals (Figure 2.6b and 2.6c), being similar to each other and to that obtained in organic solvents (*e.g.*, DCM-d_2).[42]

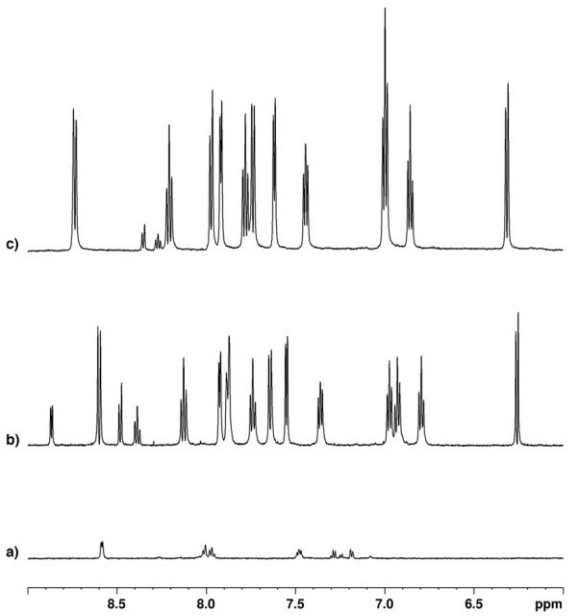

Figure 2.6. ^{1}H NMR spectra of $[Ir(ppy)_2bpy]PF_6$ in pure water (a), and 2% aqueous SDS (b) and CATC (c) solutions.

Complete assignment of the proton signals of $[Ir(ppy)_2bpy]PF_6$ in the presence of micelles was achieved via analysis of 2D $^1H-^1H$ COSY, TOCSY, and NOESY spectra and it is reported in Table 2.3.

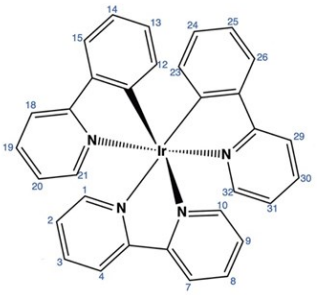

Atom	SDS (ppm)	CTAC (ppm)
H1	7.92	7.92
H2	7.36	7.39
H3	8.12	8.16
H4	8.6	8.68
H7	8.6	8.68
H8	8.12	8.16
H9	7.36	7.39
H10	7.92	7.92
H12	6.25	6.26
H13	6.79	6.80
H14	6.92	6.95
H15	7.64	7.68
H18	7.88	7.87
H19	7.74	7.73
H20	6.97	6.95
H21	7.55	7.57
H23	6.25	6.26
H24	6.79	6.80
H25	6.92	6.95
H26	7.64	7.68
H29	7.88	7.87
H30	7.74	7.73
H31	6.97	6.95
H32	7.55	7.57

Table 2.3. NMR resonance assignments of $[Ir(ppy)_2bpy]PF_6$ in SDS and CTAC 2% aqueous solutions.

Furthermore, the localisation of $[Ir(ppy)_2bpy]PF_6$ with respect to the surface and the interior of SDS and CTAC micelles was studied using 16-doxyl stearic acid (16-doxyl) and Mn^{2+} as paramagnetic probes. It is well-known that unpaired electrons could lead to dramatically accelerated longitudinal and transverse relaxation rates of protons in spatial proximity via highly efficient spin and electron relaxation.[43] Therefore, these paramagnetic probes were expected to cause the broadening and decrease in the resonance intensities of the NMR signals either for molecules outside the micelles (Mn^{2+}) or deeply buried inside them (16-doxyl).[44,45] To our knowledge, this is the first application of such probes to the characterisation of a (photo)micellar reaction environment. Accordingly, ^1H NMR spectra of $[Ir(ppy)_2bpy]PF_6$, in SDS and CTAC solutions in the presence of increasing concentrations of the spin-labels, with all the other conditions kept constant, were recorded (Figure 2.7). In SDS solution all the signals of the photocatalyst decreased in intensities after the addition of both Mn^{2+} and 16-doxyl at the highest concentrations (Figure 2.7f-h and 2.7g′-h′, on the left): this suggested that the catalyst is, on average, positioned on the micelle surface and can flip from the outer to inner part of it so that it can feel both the external (Mn^{2+}) and internal (16-doxyl) paramagnetic effects. In CTAC solution, instead, a generalised reduction of the signals' intensity was observed upon the addition of 16-doxyl (Figure 2.7d′-h′, on the right), while the addition of Mn^{2+} reduced the signal intensity of 30% at most (Figure 2.7b−h, on the right). These findings revealed that $[Ir(ppy)_2bpy]PF_6$ tends to be deeply inserted in CTAC micelles, probably because of the electronic repulsion between the positively charged metal centre of the photocatalyst and the CTAC quaternary ammonium head. To further investigate the catalyst/micelle relative orientation, we acquired NOESY spectra of $[Ir(ppy)_2bpy]PF_6$ together with (not deuterated) SDS and CTAC 2% solutions (Figure 2.8): as shown in Figure 2.8a, NOE cross-peaks corresponding to intermolecular contacts were observed in the $[Ir(ppy)_2bpy]PF_6$/CTAC system only for the main chain CH_2 of CTAC with all

the catalyst protons, thus confirming that [Ir(ppy)$_2$bpy]PF$_6$ is deeply buried inside these micelles.

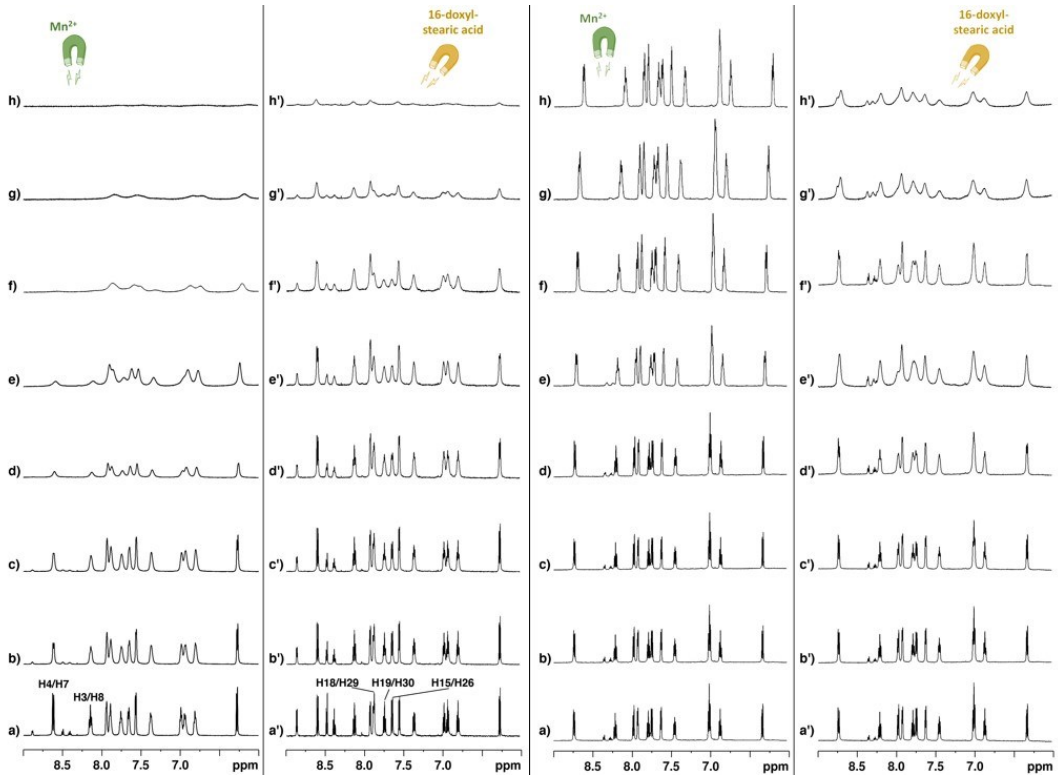

Figure 2.7. ^{1}H NMR spectra of [Ir(ppy)$_2$bpy]PF$_6$, in SDS (left) and CTAC (right) 2% solution (a,a′) and in the presence of 0.1 mM (b,b′), 0.2 mM (c,c′), 0.5 mM (d,d′), 1.0 mM (e,e′), 2.0 mM (f,f′), 3.0 mM (g,g′), and 5.0 mM (h,h′) of Mn^{2+} and 16-doxyl-stearic acid probes.

Considering the [Ir(ppy)$_2$bpy]PF$_6$/SDS system (Figure 2.8b), cross-peaks suggestive of intermolecular contacts were observed between the catalyst and different proton signals of SDS (αCH$_2$, βCH$_2$, and main chain CH$_2$), thus confirming that the catalyst is positioned on the micelle surface in the presence of SDS micelles. More in detail, catalyst's H3/H8 and H20/H31 interact selectively with SDS αCH$_2$ and H4/H7, whereas H1/H10, H18/H29, H15, H26, H21/H3, and H12/H23 interact with SDS α and βCH$_2$, as reported in Figure 2.8b. The main chain

CH_2 of SDS interacts with all the catalyst protons, indicating a degree of movement freedom.

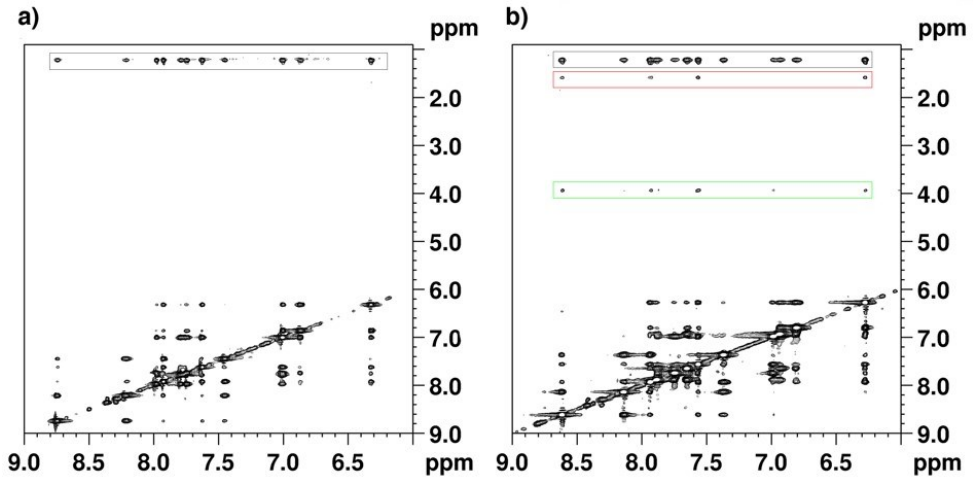

Figure 2.8. $^1H-^1H$ 2D NOESY spectra of $[Ir(ppy)_2bpy]PF_6$ in CTAC (a) and (b) SDS 2% solutions. Different signal strips are evidenced as boxes: black, main chain CH_2; green, αCH_2; red, βCH_2.

Paramagnetic probes and NOE results are consistent and allowed us to establish the average relative disposition of the $[Ir(ppy)_2bpy]PF_6$/SDS system, as reported in Figure 2.9. In this model the 2,2′-bipyridine moiety is positioned mostly outside, whereas the 2-phenylpyridinates are located inside the micelles.

Overall, such studies revealed a *reverse polarity principle*, according to which a negatively charged surfactant such as SDS could provide the localisation of a positively charged photocatalyst on the micelles' surface, while a cationic surfactant such as CTAC would cause a burying of the photocatalyst deeply inside the micelles, probably preventing its interaction with light. According to the experimental results, the photocatalyst should be positioned on the micelles' surface and almost be free to move inside and outside them to provide optimal catalytic efficiency: the latter condition may be enabled by selecting opposite charged photocatalyst/surfactant pairs, as in the case of $[Ir(ppy)_2bpy]PF_6$ and SDS.

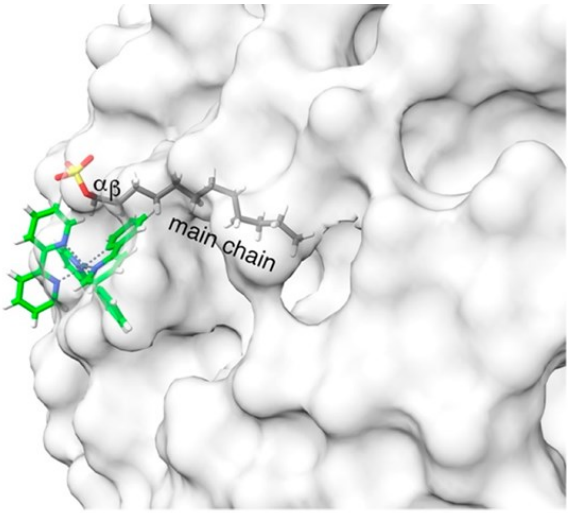

Figure 2.9. Graphic representation of $[Ir(ppy)_2bpy]PF_6$ bound with SDS micelles. Catalyst atoms are reported with the following colour codes: carbon, green; hydrogen, white; nitrogen, blue. The micelle is reported as a gray surface. For the sake of clarity, only one SDS molecule is shown (colour code: carbon, gray; hydrogen, white; oxygen, red; sulfur, yellow).

2.3. Visible light photocatalytic activity of isocyanides: *proof-of-concept* and application to the α-amino C(sp^3)-H functionalisation

While isocyanides' *chameleonic electronic properties* and unique reactivity features have been widely exploited in isocyanide-based multicomponent reactions (nucleophile/carbene reactivity, Figure 2.10a) and in Lewis acid catalysed migratory insertions into nucleophiles[46-49] (electrophile reactivity, Figure 2.10b) less has been explored about isocyanide somophile behaviour (Figure 2.10c), which results from the presence of a lone pair on the (carbenic) carbon atom of isocyanides, making them excellent *geminal acceptors* in reactions involving the formation of open-shell species.

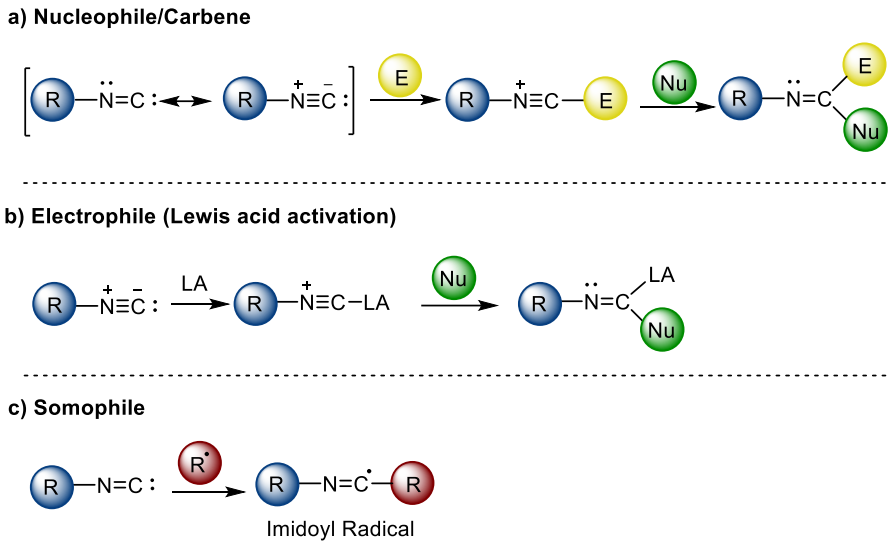

Figure 2.10. Multiple reactivity modes of isocyanides.

In recent years, the impressive progresses of visible light photoredox catalysis in the mild generation of both carbon and heteroatom-centred radicals have contributed to shed new light on isocyanides' somophile reactivity, as proved by the increasing number of transformations involving the addition of photo-generated radical species to the isocyanide carbon atom, followed by intra-molecular cyclisation of 2-isocyanobiphenyls and related analogues,[50] or two- (or multi)component reactions leading to amides, ketoamides, and other interesting molecular scaffolds.[51-53] More in detail, the addition of radical species to the isocyanide carbon atom affords imidoyl radical intermediates, which are considered very attractive chemical species.[54,55] Reported for the first time by Shono in 1964[56] and described sometimes as isoelectronic equivalents of acyl radicals, imidoyl radicals have proven to be extremely versatile synthetic intermediates, as they can undergo different fates depending on the reaction conditions and the species involved.[57] Most common reaction pathways include (Figure 2.11):

- oxidation to nitrilium ions;
- α-fragmentation (α-FGM) to give back the isocyanide and the radical species;
- β-fragmentation (β-FGM) to nitriles;

- intra- and intermolecular addition to unsaturated systems of alkenes and alkynes, as well as cyclisation onto aromatic rings (*e.g.*, phenyl ring at the *ortho*- position of 2-isocyanobiphenyl, Figure 2.11b).

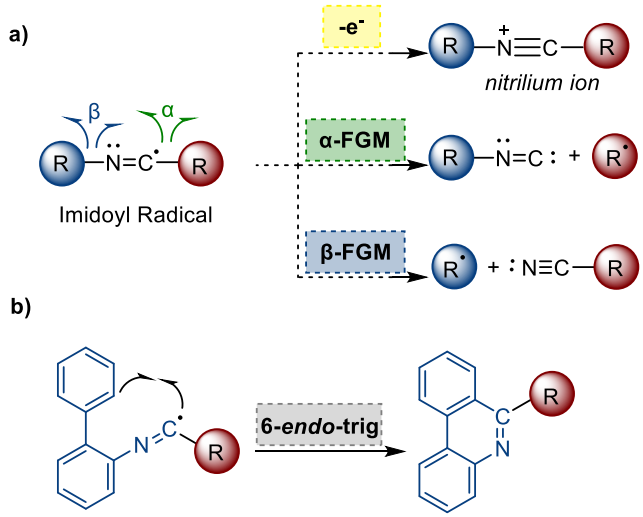

Figure 2.11. Possible fates of imidoyl radicals.

They have therefore been used in a plethora of transformations including cyclisations, annulations, and cascade reactions leading to the construction of various nitrogen-containing heterocycles (*e.g.*, indoles, phenanthridines, pyrrolidines, quinolines, quinoxalines, and fused polycyclic derivatives). While most of the current literature is based on these reactivity profiles, mainly triggered by either metal-based or organic visible light photocatalysts, processes involving the formation of imidoyl radical anions have been marginally reported, the latter being considered unstable radical species.[58] In 2018 Wang *et al.* developed an interesting photoinduced synthesis of C6-(vinyl sulfone)phenanthridine derivatives **2.65** via the three-component reaction of sulfinic acids **2.62**, alkynes **2.63**, and isocyanides **2.64**;[59] the reaction involved for the first time the generation of an isocyanide radical anion **II**, as the consequence of a photoinduced SET between the

arylsulfinate anion and *o*-isocyanobiaryls, following the formation of an EDA complex (Scheme 2.8).

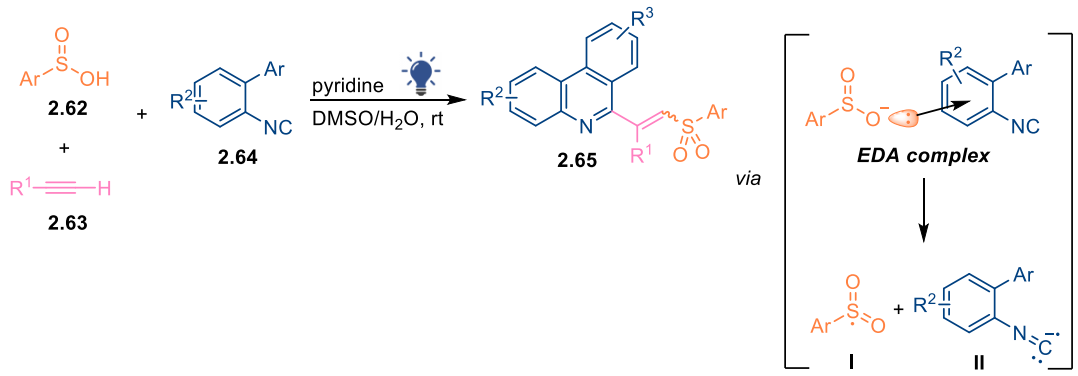

Scheme 2.8. Wang's photoinduced synthesis of C6-(vinyl sulfone)phenanthridines, reporting for the first time the formation of an isocyanide radical anion.

Fascinated by this poorly investigated radical species, we wondered whether the exploitation of such isocyanide radical anion could lead to the development of new synthetic transformations proceeding via the formation of EDA complexes.[60] In this regard, it is worth noting that while the origins of visible light photoredox catalysis are undeniably tied to the use of precious metal complexes (only available in limited amounts), the ground state association between an electron-rich donor (D) and an electron-poor acceptor (A), can produce a new molecular aggregate able to absorb light in the visible region (even when the two precursors do not), thus enabling an electron transfer event without the need for any external photocatalyst.[61,62] This inherent green feature of photochemical reactions involving EDA complexes has recently attracted considerable interest from the scientific community, and countless contributions have been reported, expanding the potential of visible light-driven radical synthetic chemistry. Notable achievements include biaryl coupling,[63] intramolecular cyclisation,[64] and catalytic asymmetric alkylation protocols.[65,66]

Keeping in mind the previously reported EDA complex formation between arylsulfinate anions and *o*-isocyanobiaryls (Scheme 2.8), we therefore tried to replace the arylsulfinate anion by screening a series of possible electron donors endowed with different redox potentials (*i.e.*, carboxylic and boronic acids, *N,N*-dimethylaniline).[67] Interestingly, the test reaction of 4-isocyanobiphenyl **2.66** with DMA **2.15**, in the presence of 10 equivalents of water, in MeCN, at room temperature, under irradiation with 30W blue LED (wavelength: 450 – 455 nm), and open to air led to the formation of the amide **2.67** in 20% yield (Scheme 2.9).

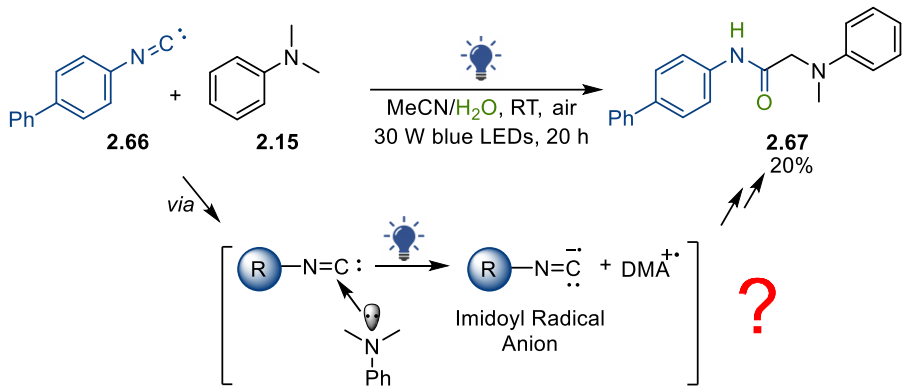

Scheme 2.9. Test reaction between 4-isocyanobiphenyl and DMA.

2.3.1. Aromatic isocyanides: direct photoexcitation

Mechanistic investigations

Intrigued by this preliminary result and in order to gain information useful to optimise the reaction conditions, the UV-VIS absorption spectra of **2.66**, DMA, and a mixture of both were recorded to verify the formation of the expected EDA complex (we sincerely thank Prof. J. Amato for UV-VIS spectroscopic measurements and fluorescence experiments). Surprisingly, no bathochromic shift was observed for the mixture (Figure 2.12a), which led to exclude any EDA complex formation. Nevertheless, we noticed that the absorption spectrum of **2.66** was characterised by two bands with λ_{max} at 265 and 360 nm (Figure 2.12b).

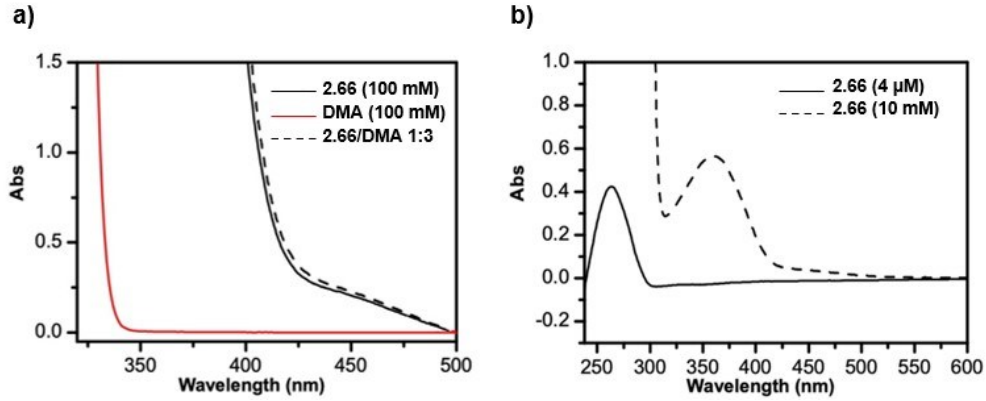

Figure 2.12. a) UV-VIS spectra of 4-isocyanobiphenyl alone, DMA alone and a 1:3 mixture of both at 25 °C; b) UV-VIS spectra of 4-isocyanobiphenyl at 25 °C.

This observation prompted us to propose a mechanistic hypothesis entailing a catalytic role of the aromatic isocyanide upon its direct photoexcitation with visible light (Scheme 2.10). More in detail, upon light absorption, **2.66** can reach an electronically excited state **2.66***, and thus act as photocatalyst: a SET from DMA to **2.66*** leads to the formation of the imidoyl radical anion **2.66**$^{\bullet-}$ and the radical cation of dimethylaniline DMA$^{\bullet+}$. Molecular oxygen then regenerates the ground state isocyanide, while forming a superoxide radical anion $O_2^{\bullet-}$, which in turn can abstract a hydrogen atom from DMA$^{\bullet+}$, leading to the formation of the corresponding iminium ion DMA^{+}. The latter is then intercepted by the ground-state isocyanide **2.66** to afford the nitrilium ion **I**, which, after the addition of water, finally gives the amide **2.67**. The overall reaction mechanism therefore proceeds via a radical/polar crossover pathway.

Stern-Volmer fluorescence quenching of **2.66** in the presence of increasing amounts of DMA (Figure 2.13) and formation of the ^{18}O-labeled product when performing the reaction in the presence of $H_2{}^{18}O$, as detected by means of high-resolution mass spectrometry (HRMS) analysis of the crude reaction mixture (see Experimental Section), further supported this mechanistic hypothesis.

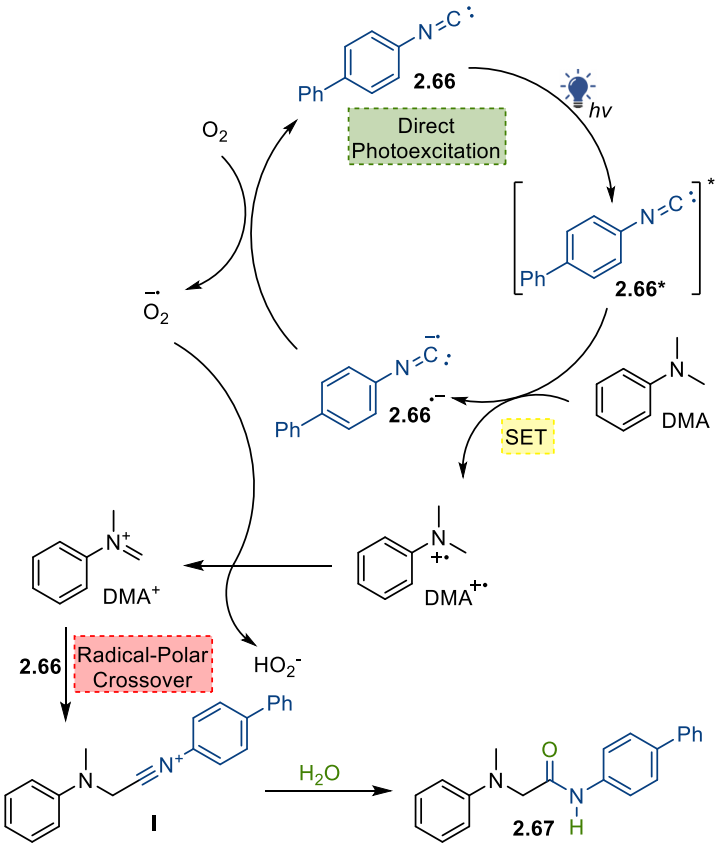

Scheme 2.10. Proposed reaction mechanism for the visible light self-catalysed reaction of aromatic isocyanides with *N,N*-dimethylaniline derivatives.

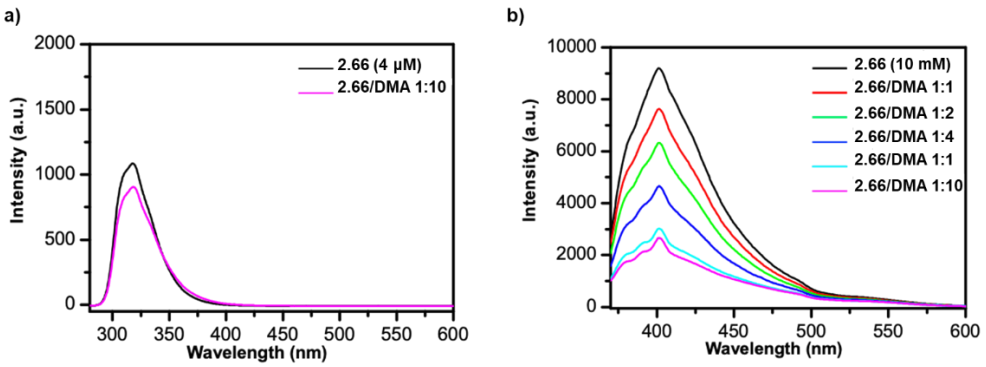

Figure 2.13. a) Fluorescence spectra of 4-isocyanobiphenyl in the absence and presence of DMA at 25 °C and an excitation wavelength of 265 nm; b) Stern−Volmer fluorescence quenching of 4-isocyanobiphenyl with increasing amounts of DMA at 25 °C and an excitation wavelength of 360 nm.

Optimisation of the reaction conditions

The collected mechanistic information provided rational bases to identify optimum reaction conditions. Changing the ratio of **2.66**/DMA, as well as reaction times or the light source (18 W black light, wavelength: 365 nm) did not improve the yield of amide **2.67** (Table 2.4, Entries 2-4). Hence, we wondered if the poor yield of **2.67** could be ascribed to a very short half-life of the imidoyl radical anion **2.66**$^{\bullet-}$, which would lead to a back-electron transfer (BET) event to isocyanide **2.66** and DMA, thus preventing the quantitative oxidation of DMA to DMA^{+}. In light of these considerations, we reasoned that the use of a σ-electron acceptor, such as a Lewis acid, could promote the stabilisation of the imidoyl radical anion and prevent unproductive BETs. Actually, the reaction performed in the presence of 30 mol% loading of $Yb(OTf)_3$ afforded the amide **2.67** in 95% isolated yield (Entry 5). While the irradiation with black light did not change the yield (Entry 6), no product was obtained when the light was carefully excluded (Entry 7), proving the photocatalytic nature of the transformation. Other Lewis acids such as silver, lanthanum, and copper triflates, as well as other transition metals and different ytterbium sources showed to have either no or poorer catalytic activity (Entries 8-16). A further survey of the minimum amount of $Yb(OTf)_3$ required to get optimum yields revealed that a 10 mol% loading was effective with a reaction time of 20 hours (Entries 17-20). Further attempts to scale up the reaction to 0.25 and 0.8 mmol afforded 41 and 23% yields, respectively, with a recovery of about 50% of the starting isocyanide. Interestingly, the use of 30W blue LED was crucial for the transformation, as performing the reaction under irradiation with 1W blue LED afforded only traces of **2.67** (Entry 21).

In order to elucidate the role of $Yb(OTf)_3$ and to exclude a mechanistic pathway involving a Ligand-to-Metal-Charge Transfer (LMCT), we also recorded the UV-VIS absorption spectrum of **2.66** in the presence of the metal catalyst. While no charge-transfer bands were observed, fluorescence experiments revealed a possible static quenching due to the formation of a ground-state Yb-isocyanide complex.

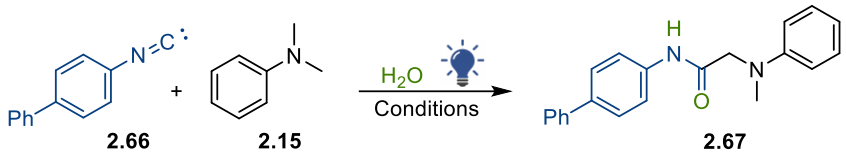

2.66 2.15 2.67

Entry	2.15 (equiv.)	Light source	LA (equiv.)	Time	2.67 Yield[a] (%)
1	0.7	Blue LED 30W	-	20 h	20
2	2	Blue LED 30W	-	20 h	14
3	2	Blue LED 30W	-	48 h	21
4	2	Black light 18W	-	20 h	14
5	2	Blue LED 30W	$Yb(OTf)_3$ (0.3)	20 h	99 (95)[b]
6	2	Black light 18W	$Yb(OTf)_3$ (0.3)	20 h	99
7	2	None	$Yb(OTf)_3$ (0.3)	20 h	Traces
8	2	Blue LED 30W	AgOTf (0.3)	20 h	14
9	2	Blue LED 30W	$La(OTf)_3$ (0.3)	20 h	7
10	2	Blue LED 30W	$Cu(OTf)_2$ (0.3)	20 h	14
11	2	Blue LED 30W	$Cu(OAc)_2 \cdot H_2O$ (0.3)	20 h	14
12	2	Blue LED 30W	$CuCl_2$ (0.3)	20 h	21
13	2	Blue LED 30W	$Pd(OAc)_2$ (0.3)	20 h	Traces
14	2	Blue LED 30W	$Ni(OTf)_2$ (0.3)	20 h	Traces
15	2	Blue LED 30W	$Yb(OAc)_3 \cdot 4\,H_2O$ (0.3)	20 h	13
16	2	Blue LED 30W	$YbCl_3 \cdot 6\,H_2O$ (0.3)	20 h	35
17	2	Blue LED 30W	$Yb(OTf)_3$ (0.01)	20 h	52
18	2	Blue LED 30W	$Yb(OTf)_3$ (0.05)	20 h	76
19	2	Blue LED 30W	$Yb(OTf)_3$ (0.1)	20 h	99 (91)[b]
20	2	Blue LED 30W	$Yb(OTf)_3$ (0.05)	48 h	94
21	2	Blue LED 1W	$Yb(OTf)_3$ (0.1)	20 h	Traces

Conditions: reaction performed on a 0.08 mmol scale of **2.66**, with 10 equivalents of water, in MeCN (0.1 M), RT.
[a] NMR yield (determined by using TMB as internal standard)
[b] Isolated yield

Table 2.4. Optimisation of the reaction conditions for the visible light self-catalysed reaction of aromatic isocyanides with *N,N*-dimethylaniline derivatives.

This hypothesis was further supported by an *on/off effect* observed with the addition of ammonium hydroxide, which was able to disrupt the Yb-isocyanide complex and completely restore the fluorescence behaviour of **2.66** (Figure 2.14).

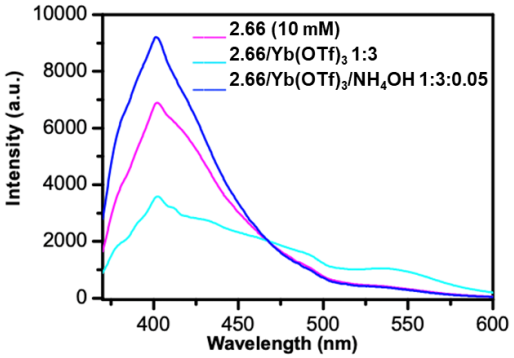

Figure 2.14. Superimposition of the fluorescence spectra (360 nm excitation wavelength) of isocyanide **2.66** in the absence and presence of $Yb(OTf)_3$, and upon addition of ammonium hydroxide.

Substrate scope

With the optimised conditions in hand, the substrate scope of both aromatic isocyanides and *N,N*-dimethylaniline derivatives was investigated. As shown in Figure 2.15 both electron-poor (**2.68**, **2.69**) and electron rich aromatic isocyanides (**2.70-2.72**) gave excellent yields, with the *para* and *meta*-substitution patterns not affecting the formation of the desired products. Interestingly, even *ortho*-isocyanobiphenyl, usually reacting intramolecularly when involved in the formation of imidoyl radical intermediates, gave the linear amide **2.75** in 94% yield, thus supporting the radical/polar crossover mechanistic hypothesis. As for the amine partners, both electron-poor (**2.76**) and electron-rich (**2.77-2.79**) *N,N*-dimethylanilines proved to be competent starting materials, as well as cyclic tertiary aromatic amines (**2.80**, **2.81**). On another hand, heteroaromatic dimethylanilines such as *N,N*-dimethyl aminopyridine, along with *N*-methyldiphenyl amine, secondary anilines, tertiary aliphatic amines, and amides, were all unsuccessful substrates. These results, however, are consistent with previously reported reactions.[68,69]

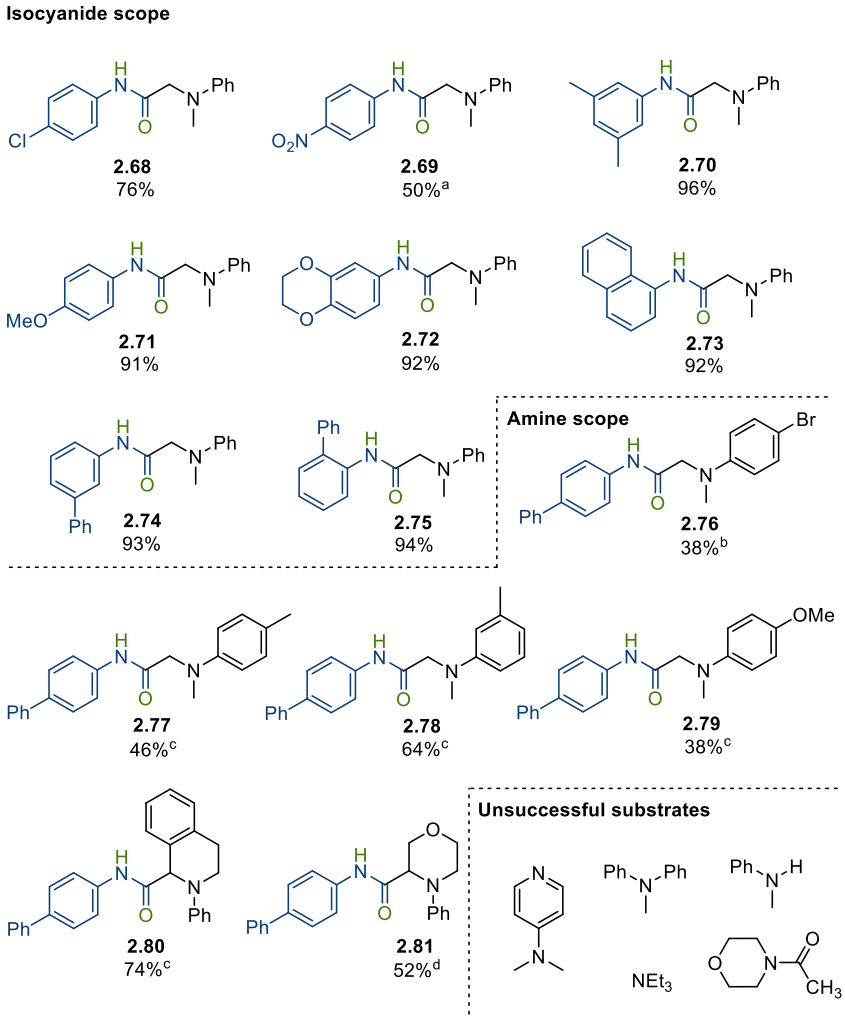

[a] Reaction performed without $Yb(OTf)_3$; [b] 5 days; [c] 48 h; [d] 72 h

Figure 2.15. Substrate scope for the visible light self-catalysed reaction of aromatic isocyanides with *N,N*-dimethylaniline derivatives.

2.3.2. Aliphatic isocyanides: EDA complex formation with tertiary aromatic amines

Mechanistic investigations and optimisation of the reaction conditions

With the aim to further expand the isocyanide scope to aliphatic ones and to prove the ability of aromatic isocyanides to act as photocatalysts, a test reaction involving cyclohexyl isocyanide **2.82**, *N,N*-dimethylaniline **2.15**, a catalytic 20 mol% loading

of isocyanide **2.66** and 10 mol% of $Yb(OTf)_3$ was performed, and the desired amide **2.83** was collected in 16% yield after 20 h (Table 2.5, Entry 1). A short survey of the best performing reaction conditions surprisingly revealed that optimum results were obtained in the absence of both **2.66** and $Yb(OTf)_3$ (Entry 6).

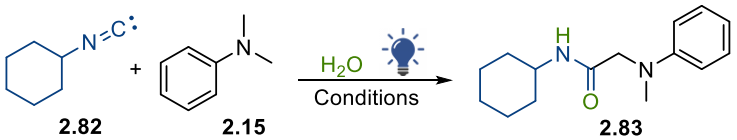

2.82 **2.15** **2.83**

Entry	2.15 (equiv.)	PC (equiv.)	LA (equiv.)	Time	2.83 Yield[a] (%)
1	2	**2.66** (0.2)	$Yb(OTf)_3$ (0.1)	20 h	16
2	2	**2.66** (0.2)	$Yb(OTf)_3$ (0.1)	48 h	32
3	2	**2.66** (0.2)	$Yb(OTf)_3$ (0.1)	72 h	34
4	0.7	**2.66** (0.2)	$Yb(OTf)_3$ (0.1)	48 h	21
5	2	-	$Yb(OTf)_3$ (0.1)	48 h	18
6	2	-	-	72 h	53

Conditions: reaction performed on a 0.08 mmol scale of **2.82**, with 10 equivalents of water, in MeCN (0.1 M), under 30W blue LED irradiation (450 – 455 nm), RT.
[a] Isolated yield

Table 2.5. Optimisation of the reaction conditions for the visible light-promoted reaction of aliphatic isocyanides with *N,N*-dimethylaniline derivatives.

To shed light on the nature of this unexpected outcome, UV−VIS absorption spectra of DMA alone and in combination with the aliphatic non-volatile 1-adamantyl isocyanide **2.84** were therefore recorded. As evident from Figure 2.16, such experiments showed a charge-transfer band due to the formation of an EDA complex between DMA and **2.84**, thus suggesting the mechanistic hypothesis reported in Scheme 2.11.

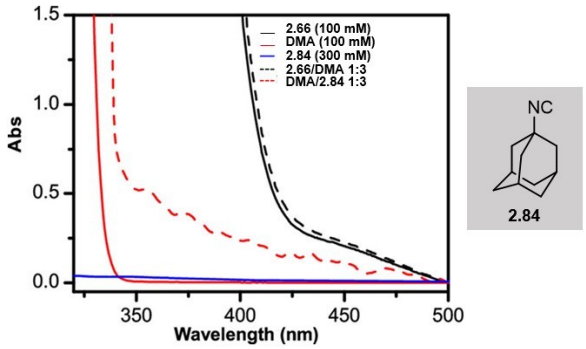

Figure 2.16. UV–VIS absorption spectra of 1-adamanthyl isocyanide alone, DMA alone, and a mixture of both at 25°C. For comparison, spectra of 4-isocyanobiphenyl alone and upon addition of DMA are also reported.

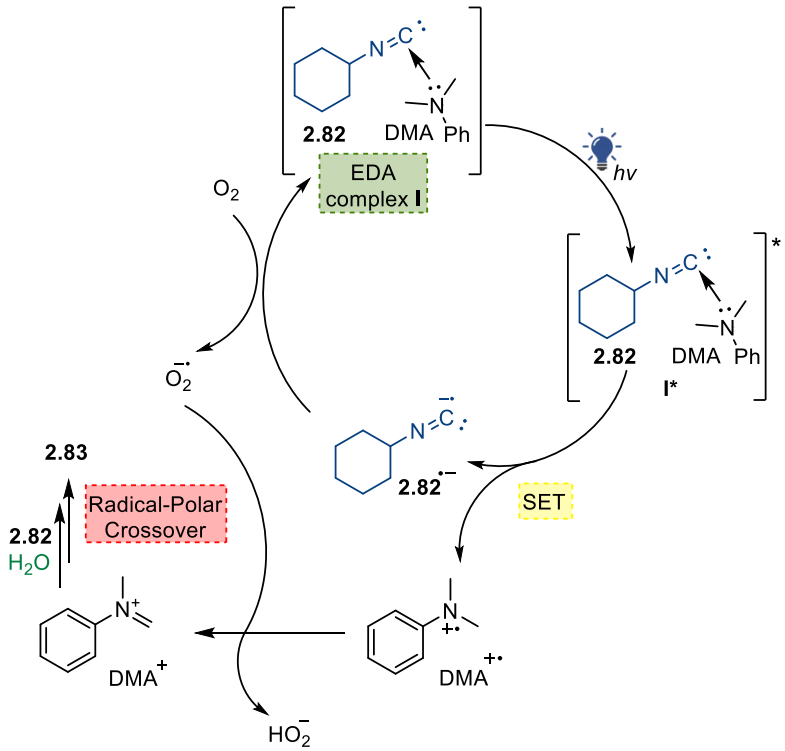

Scheme 2.11. Proposed reaction mechanism for the visible light-promoted reaction of aliphatic isocyanides with *N,N*-dimethylanilines via EDA complex formation.

More in detail, visible light excitation of the EDA complex **I** triggers a SET from DMA (the donor) to the isocyanide **2.82** (the acceptor), thus forming the radical cation $DMA^{\bullet+}$ and the isocyanide radical anion $\mathbf{2.82}^{\bullet-}$. The latter can be oxidised

back to **2.82** by molecular oxygen, which leads to a superoxide radical anion $O_2^{\bullet-}$ responsible for hydrogen atom abstraction from $DMA^{\bullet+}$, eventually affording the iminium ion DMA^+. The latter undergoes the sequential additions of the isocyanide **2.82** and water to finally afford the amide product **2.83**. As stated above, overall, the reaction proceeds via a radical-polar crossover mechanism.

Aliphatic isocyanides: substrate scope

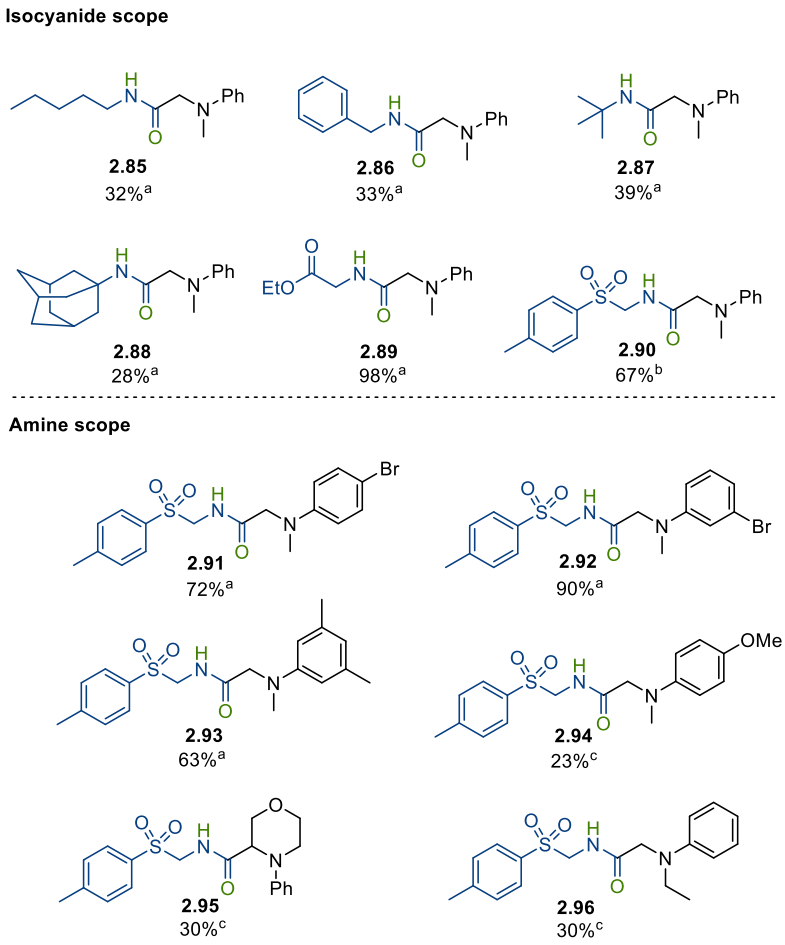

Figure 2.17. Substrate scope for the visible light-promoted reaction of aliphatic isocyanides with *N,N*-dimethylaniline derivatives via EDA complex formation.

Regarding the generality of the transformation, it proved to be efficient with electron-rich primary, secondary, and bulky tertiary aliphatic isocyanides (Figure 2.17, **2.85**−**2.88**), working particularly well in the case of isocyanides bearing electron-withdrawing groups (**2.89**, **2.90**). When *p*-toluenesulfonylmethyl isocyanide was reacted with different *N,N*-dimethylanilines, excellent yields were observed in the presence of electron-withdrawing substituents, regardless of the *para*- or *meta*- substitution pattern (72% and 90% for **2.91** and **2.92**, respectively), while electron-donor substituents (**2.93**, **2.94**) as well as cyclic tertiary aromatic amines (**2.95**) led to yields from good to moderate (23-63%). Interestingly, non-symmetrical *N*-ethyl-*N*-methylaniline was selectively oxidised at the methyl group giving the regioisomer **2.96** in a moderate 30% yield.

2.3.3. (Photo)catalytic role of aromatic isocyanides: proof-of-concept

While unearthing EDA complexes formation between aliphatic isocyanides and tertiary aromatic amines contributed to explain the mechanism underlying the formation of amide derivatives **2.83**, **2.85-2.96**, on the other hand, the need for proving the possible catalytic role of aromatic isocyanides remained unfulfilled. Accordingly, in order to investigate whether this unexplored photocatalytic reactivity of aromatic isocyanides could be harnessed at a more general level, a range of both carbon and hetero-atom (pro)nucleophiles, such as diethyl malonate **2.98** (Mannich-type reaction[70]), cyanotrimethylsilane **2.99** (TMSCN, Strecker-type reaction[71]), nitromethane **2.100** (*aza*-Henry reaction[72]), malononitrile **2.101**,[70] and dimethyl phosphite **2.102** (Kabachnik-Fields-type reaction[73]), were reacted with *N*-phenyl-1,2,3,4-tetrahydroisoquinoline **2.97** in the presence of a 20 mol% loading of the isocyanide **2.66** as the photocatalyst (Scheme 2.12). Here, the resonance-stabilised carbanions (Michael donors, Nu^- in Scheme 2.12) were formed upon deprotonation by the *in situ* formed hydroperoxide anion HO_2^-, without requiring the addition of any further base.

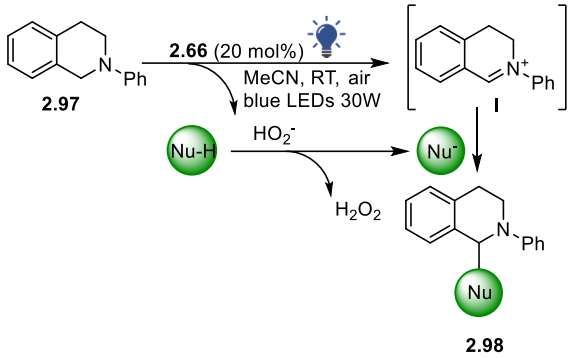

Scheme 2.12. General mechanism for the Michael-type addition promoted by isocyanide **2.66** as the photocatalyst.

Amine	(Pro)Nucleophile	Product (yield)[a]	Reaction
	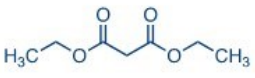 **2.98**	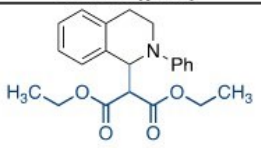 **2.103** 94% (40%)	Mannich
	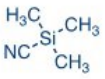 **2.99**	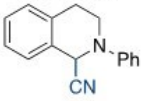 **2.104** 98% (75%)	Strecker
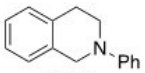 **2.97**	CH_3NO_2 **2.100**	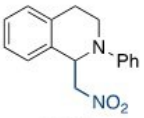 **2.105** 69% (57%)	*aza*-Henry
	 **2.101**	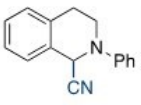 **2.104** 36% 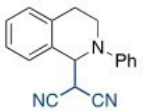 **2.106** 27%	Michael addition
	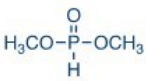 **2.102**	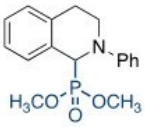 **2.107** 92% (63%)	Phosphonylation

[a] NMR yield (determined by using TMB as internal standard); in parentheses isolated yield

Table 2.6. Michael-type additions promoted by isocyanide **2.66** as the photocatalyst.

As shown in Table 2.6, all the (pro)nucleophiles gave the corresponding cross-dehydrogenative coupling adducts in good to excellent yields, contrary to the reaction between *N*-phenyl-1,2,3,4-tetrahydroisoquinoline **2.97** and diethyl malonate **2.99** in the absence of **2.66,** which barely afforded a 4% yield of product. TMSCN **2.100** and nitromethane **2.101** led to the Strecker and *aza*-Henry products **2.104** and **2.105** in 98 and 69% yields, respectively. Malononitrile **2.102** showed to be effective as a Michael donor under standard reaction conditions, leading to a mixture of α-aminonitrile **2.104** and adduct **2.106**, in accordance with previous reports in the literature.[68,69] Dimethyl phosphite also afforded the phosphonylated product **2.107** in an excellent 92% yield.

As a whole, these experimental data provided the *proof-of-concept* for a potential exploitation of aromatic isocyanides as a new class of highly tuneable organic photocatalysts. Actually, the addition of electron-withdrawing or electron-donor groups on their aromatic moiety, as well as the ring expansion to polycyclic scaffolds, might reasonably allow for a fine modulation of their redox and optical properties, thus eventually expanding the substrate scope to a broader range of $C(sp^3)$−H bonds (see Section 2.5).

2.4. Visible light photocatalytic metal-free multicomponent Ugi-like chemistry

Before delving deeper into exploring the opportunities and the challenges of using aromatic isocyanides as organic visible light photocatalysts, we wondered if the newly discovered (photo)reactivities of isocyanides (direct photoexcitation for aromatic ones and EDA complexes formation with tertiary aromatic amines in the case of aliphatic isonitriles) could not only be preserved in the presence of different nucleophiles but also combined with isocyanides' established ability to be engaged in multicomponent processes. We therefore investigated the feasibility of a series of visible light triggered Ugi-like multicomponent reactions under unprecedented metal-free reaction conditions (Figure 2.18a). While most of these transformations

usually require the use of either an iridium or ruthenium based photocatalyst,[40,74,75] the possibility to exploit isocyanides as self-catalysing agents would, in fact, allow to avoid precious metals while benefiting from the innate green properties of MCRs, thus combining multiple green chemistry features to afford new and efficient synthetic methodologies for drug-like scaffolds.[76]

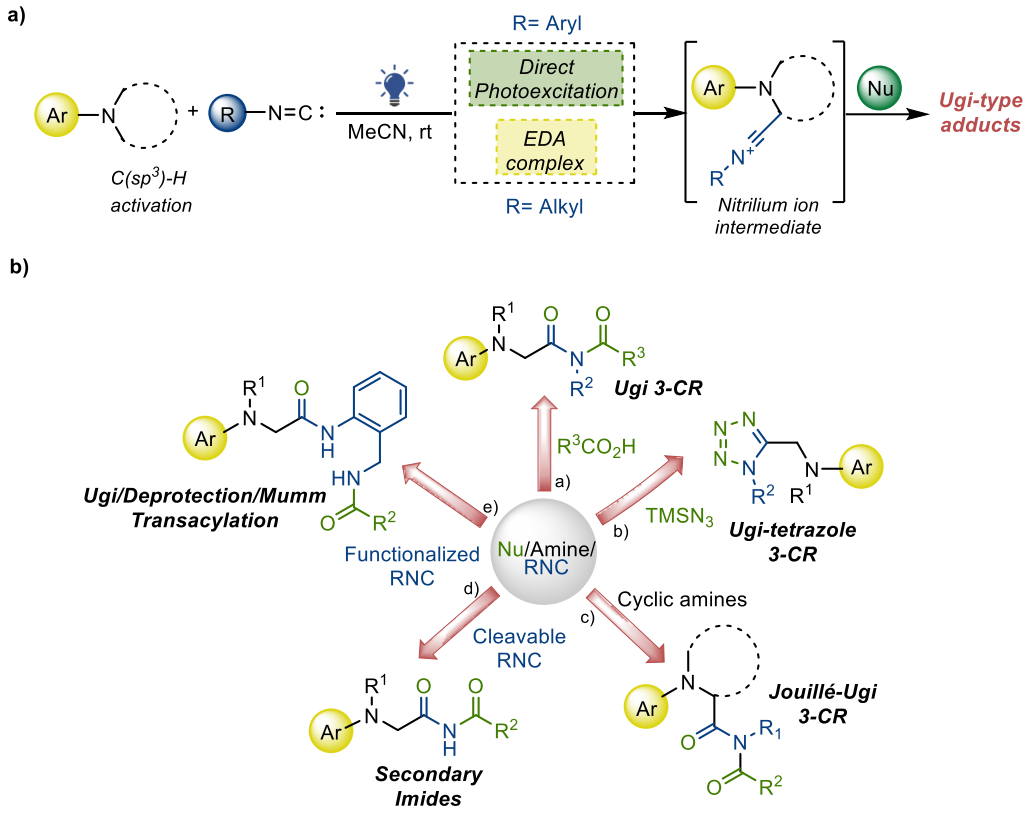

Figure 2.18. a) Mechanistic bases for photo-triggered metal-free Ugi-like multicomponent reactions; b) Collection of transformations investigated herein.

To this end, depending on either the selected nucleophiles or the use of functionalised starting materials, we developed a small collection of different transformations leading to multifunctional molecular architectures, not always accessible via classic MCRs.[77] More in detail, they included (Figure 2.18b):

a) Ugi 3-CR (nucleophiles: both aliphatic and aromatic carboxylic acids);

b) Ugi-tetrazole 3-CR (nucleophile: azidotrimethylsilane $TMSN_3$);

c) Jouillè-Ugi 3-CR (cyclic tertiary aromatic amines as starting materials);

d) Synthesis of secondary imides by using 2,4-dimethoxybenzyl isocyanide as a cleavable one (to our knowledge, reported herein for the first time);

e) A one-pot domino Ugi 3-CR/deprotection/Mumm transacylation sequence leading to densely functionalised bis-amide derivatives.

2.4.1. Ugi 3-CR

In order to verify the feasibility of a visible light-induced metal-free Ugi-like 3-CR, *N,N*-dimethylaniline **2.15**, cyclohexyl isocyanide **2.82**, and *m*-toluic acid **2.16** were dissolved in MeCN and reacted overnight, at room temperature, under 30W blue LED irradiation (wavelength: 450 – 455 nm). To our delight this afforded the expected Ugi-like product **2.108** in an excellent 99% yield (Table 2.7, Entry 1).

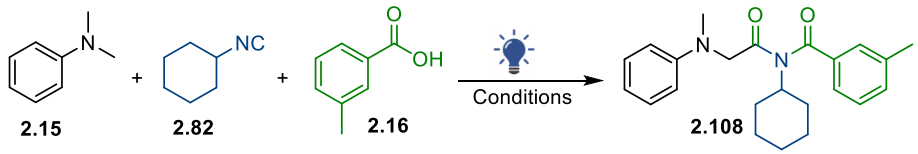

Entry	2.15 (equiv.)	2.82 (equiv.)	2.16 (equiv.)	Light source	Time	2.108 Yield[a] (%)
1	2	1	2	Blue LED 30W	72 h	99
2	2	1	1.5	Blue LED 30W	72 h	99
3	2	1	1	Blue LED 30W	72 h	82[b]
4	2	1	1.5	Blue LED 30W	48 h	83[b]
5[c]	2	1	1.5	Blue LED 30W	72 h	83[b]
6	2	1	1.5	None	72 h	Traces

Conditions: reaction performed on a 0.08 mmol scale of **2.82**, in dry MeCN (0.1 M), RT, open to air, in the presence of 3Å MS.
[a] Isolated yield
[b] NMR yield (determined by using TMB as internal standard)
[c] No MS

Table 2.7. Optimisation of the reaction conditions for the visible light-promoted metal-free Ugi 3-CR.

Decreasing the equivalents of **2.16** to 1.5 and 1 gave 99 and 82% yields, respectively (Entries 2-3), while shorter reaction times (Entry 4) as well as the absence of molecular sieves (Entry 5) proved to be detrimental. Finally, only traces of product **2.108** were collected when performing the reaction in the dark, thus confirming the photocatalytic nature of the transformation (Entry 6).

In order to evaluate the substrate scope and the robustness of the developed metal-free visible light-triggered Ugi-like 3-CR, the optimised reaction conditions (Table 2.7, Entry 2) were applied to different aliphatic and aromatic isocyanides (Figure 2.19, **2.109-2.112**), as well as carboxylic acids (**2.111-2.116**), affording the desired Ugi adducts with yields spanning from 53% to 99%.

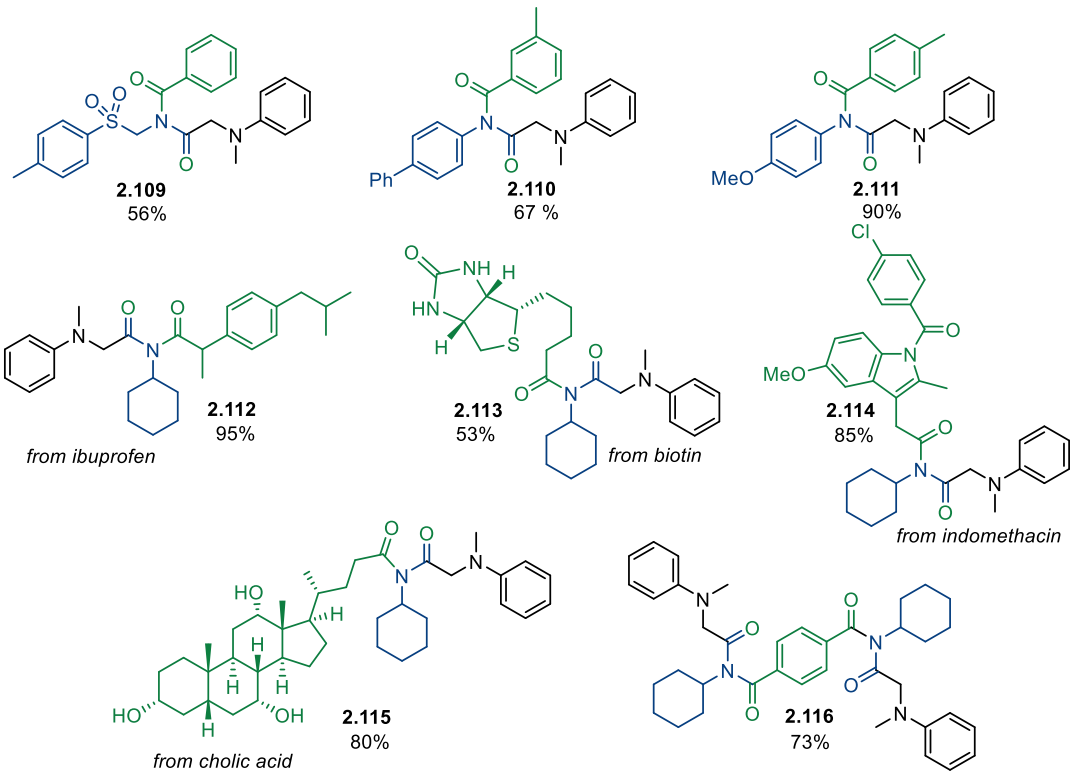

Figure 2.19. Substrate scope for the visible light-promoted metal-free Ugi-like 3-CR.

The mildness of the protocol also proved to be suitable for the late-stage editing of drugs and natural compounds, including ibuprofen, biotin, indomethacin, and

cholic acid (**2.112-2.115**). Interestingly, the use of difunctionalised starting material, such as the terephthalic acid, led to the dimeric derivative **2.116** in a good 73% yield.

2.4.2. Ugi-tetrazole 3-CR

Prompted by the good yields and the excellent substrate scope shown by the Ugi 3-CR, we wondered if replacing the carboxylic acid component with a different nucleophile such as $TMSN_3$, which is known to react with the *in situ* formed nitrilium ion as a 1,3-dipole in a [3+2] cycloaddition reaction,[78] could be tolerated under the required photocatalytic conditions so to smoothly afford 1,5-disubstituted tetrazole derivatives. This could be of particular interest for medicinal chemistry applications, considering the occurrence of the tetrazole motif in a wide range of biologically active compounds, spanning from sartan antihypertensive drugs to antimicrobial agents, and anti-ashma medications (Figure 2.20), wherein the tetrazole core frequently appears as bioisosteric replacement of carboxylic acid and amide moieties, exhibiting increased lipophilicity,[79] and enhanced metabolic stability.[80]

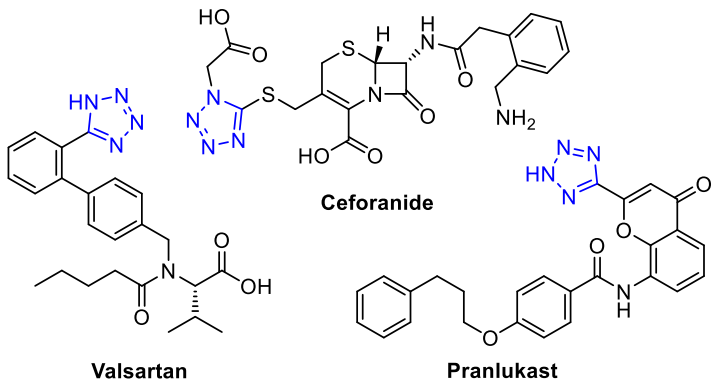

Figure 2.20. Examples of biologically active compounds containing a tetrazole motif.

We therefore reacted DMA **2.15**, cyclohexyl isocyanide **2.82**, and $TMSN_3$ **2.8** under standard conditions as for the Ugi 3-CR (Table 2.8, Entry 1), obtaining the desired tetrazole **2.117** in 60% yield. Increasing the equivalents of isocyanide **2.82** and $TMSN_3$ **2.8** to 3, while reducing the amount of aniline led to 86% yield (Entry 2). Attempts to decrease the amount or eliminate the organic solvent, gave either a modest 30% yield or just a few traces of the product (Entries 3-4), while a further test reaction with 2 equivalents of both the isocyanide **2.82** and $TMSN_3$ **2.8**, in MeCN, revealed this stoichiometry to be already sufficient to afford an excellent 92% yield (Entry 5). Also in this case, light was found to be essential to promote the transformation, as no product was detected when the reaction was performed in the dark (Entry 6).

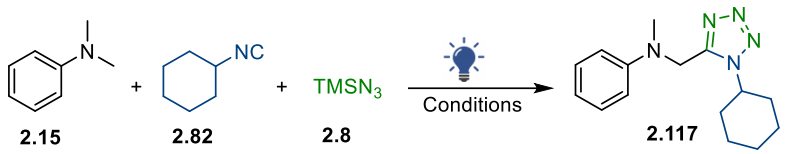

2.15 **2.82** **2.8** **2.117**

Entry	2.15 (equiv.)	2.82 (equiv.)	2.8 (equiv.)	Light source	Solvent (0.15 M)	2.117 Yield[a] (%)
1	2	1	1.5	Blue LED 30W	MeCN[b]	60[c]
2	1	3	3	Blue LED 30W	MeCN[b]	86
3	1	3	3	Blue LED 30W	MeCN:H_2O 1:1	30[c]
4	1	3	3	Blue LED 30W	TPGS-750M 2%	Traces
5	1	3	2	Blue LED 30W	MeCN[b]	92[c]
6	1	3	3	None	MeCN[b]	ND

Conditions: reaction performed on a 0.08 mmol scale, RT, open to air, 48 h.
[a] Isolated yield
[b] 3Å MS
[c] NMR yield (determined by using TMB as internal standard)

Table 2.8. Optimisation of the reaction conditions for the visible light-promoted metal-free Ugi-tetrazole 3-CR.

The optimised reaction conditions proved to be effective with both primary, secondary, and tertiary aliphatic isocyanides, as well as with aromatic ones (Figure 2.21). Similarly, both electron-poor (**2.121**) and electron-rich (**2.122**) aromatic

tertiary amines resulted competent substrates in giving the corresponding tetrazole derivatives.

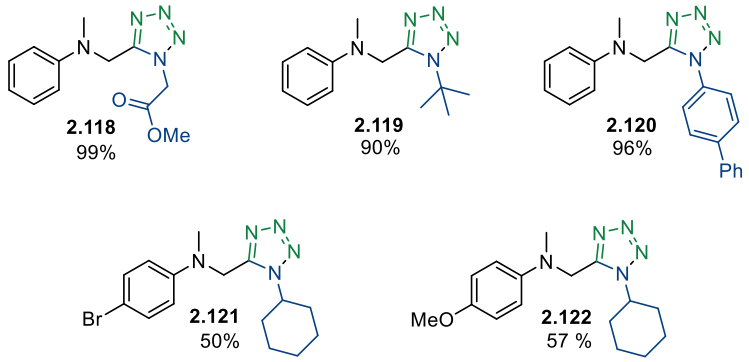

Figure 2.21. Substrate scope for the visible light-promoted metal-free Ugi-tetrazole 3-CR.

2.4.3. Joulliè-Ugi 3-CR

Reported for the first time in 1982, the Joulliè-Ugi 3-CR[81] involves a cyclic imine **2.123**, an isocyanide **2.41**, and a carboxylic acid **2.13** to give an acyl derivative of a secondary cyclic amine **2.124** (Scheme 2.13a). It is therefore considered a very useful synthetic tool to provide access to conformationally constrained peptidomimetics and antibacterial depsipeptides.[82]

We reasoned that a visible light-promoted and metal-free version of such a transformation could probably be accomplished by exploiting the isocyanide-mediated oxidation of a tertiary cyclic aromatic amines **2.125**, which would lead to the iminium ion **I** further reacting with the isocyanide **2.41** and a carboxylic acid **2.13** to finally afford constrained imide derivatives **2.126** (Scheme 2.13b).

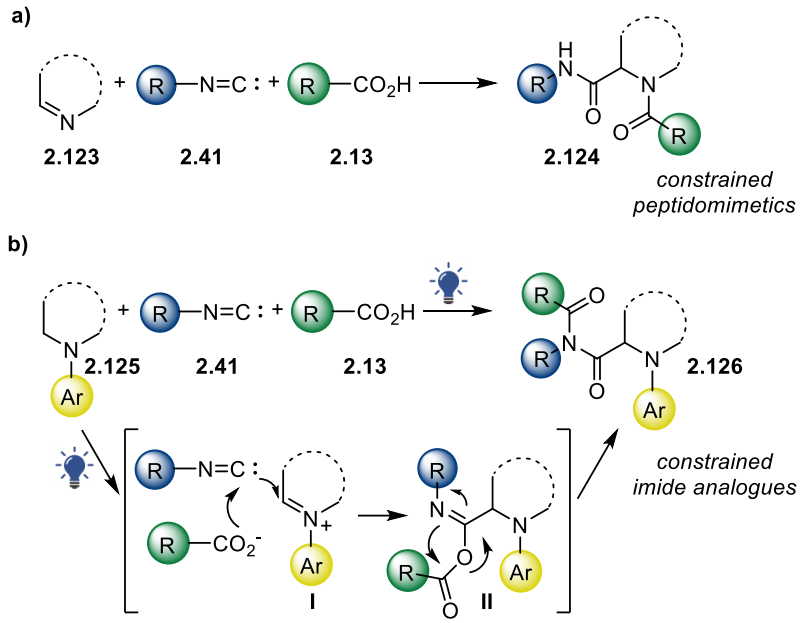

Scheme 2.13. a) Traditional Joullié-Ugi 3-CR; b) Metal-free visible light photocatalytic Joullié-Ugi 3-CR developed herein.

By applying standard conditions as for the Ugi 3-CR (Table 2.7, Entry 2) a small library of imide derivatives was rapidly synthesised with a good substrate scope: different cyclic tertiary aromatic amines such as *N*-phenyl-tetrahydroisoquinoline (Figure 2.22, **2.127**-**2.129**), *N*-phenylpyrrolidine (**2.130**-**2.131**), and *N*-phenylpiperidine (**2.132**) were found to be suitable starting materials, as well as both aromatic (**2.127**, **2.131**-**2.132**) and aliphatic carboxylic acids (**2.128**-**2.130**). Interestingly, both aromatic (**2.127**-**2.128**, **2.11**-**2.132**) and aliphatic isocyanides (**2.129**-**2.130**) afforded the desired products in good or excellent yields, thus confirming the successful exploitation of the self-catalytic activity of isocyanides either via direct photoexcitation (in the case of aromatic substrates) or through the formation of an EDA complex (in the case of aliphatic isocyanides).

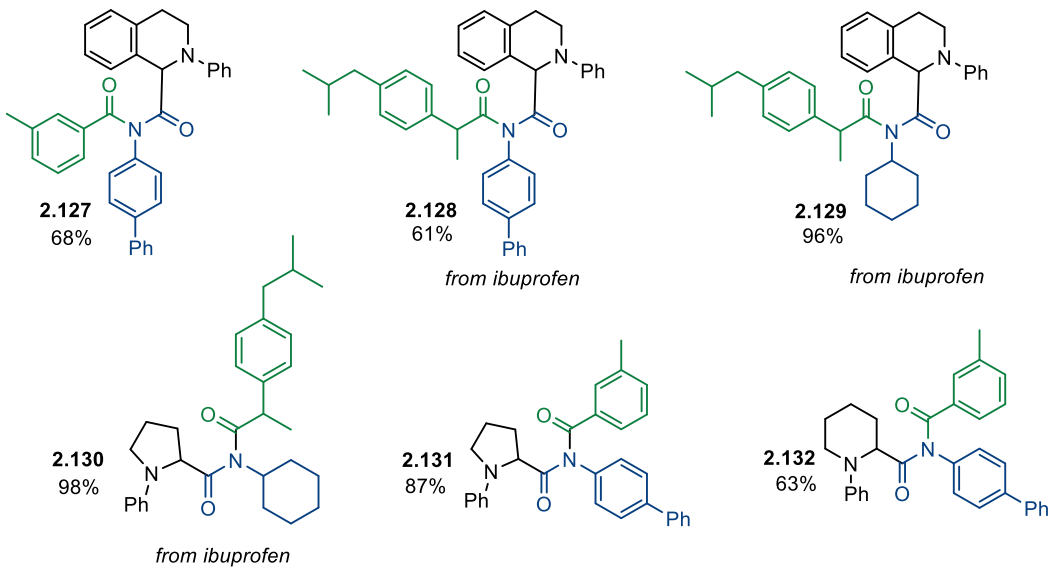

Figure 2.22. Substrate scope for the metal-free visible light photocatalytic Joullié-Ugi 3-CR.

2.4.4. Synthesis of secondary imides by using 2,4-dimethoxybenzyl isocyanide as a cleavable one

To further explore the advantages of the metal-free visible light photocatalytic protocol developed, we carried out some post-condensation modifications. This is a very useful approach to enable two-step one-pot multicomponent processes: after performing the MCR, the conditions are changed without any intermediate purification in order to trigger a new transformation exploiting the functional groups introduced during the previous step. At first, we applied this strategy to the synthesis of secondary imides by using 2,4-dimethoxybenzyl isocyanide **2.133** as a cleavable one. Accordingly, the Ugi 3-CR involving such a substrate was performed under standard conditions to afford tertiary imides with general structure **2.134** (Scheme 2.14a); after the photocatalytic step, these intermediates were converted *in situ* into secondary linear imides **2.135** by simply evaporating the solvent and adding a 1:1 DCM/TFA mixture. This easily led to the secondary imide products after stirring for 4 hours at 50°C. To our knowledge, isocyanide **2.133** was

here reported as a cleavable one for the first time; it proved to be superior to other well-known cleavable isocyanides such as the Walborsky reagent,[83] as, when 1,1,3,3-tetramethylbutyl isocyanide **2.9** was reacted with DMA and *m*-toluic acid to give the corresponding Ugi 3-CR adduct and then stirred in DCM/TFA to attempt the removal of the isocyanide alkyl moiety, the desired secondary imide was recovered only in traces. On the contrary, **2.133** afforded the expected secondary imides **2.136** and **2.137** in 40% and 36% yields, respectively, when reacted with *m*-toluic acid and *N,N*-dimethylaniline or *N,N*,3,5-tetramethylaniline according to our newly developed two-step one-pot protocol (Scheme 2.14b). It should be noted that the moderate 38% average yield corresponds to a 62% theoretical yield for each step (*i.e.*, the MCR and the TFA-promoted cleavage of the 2,4-dimethoxybenzyl moiety).

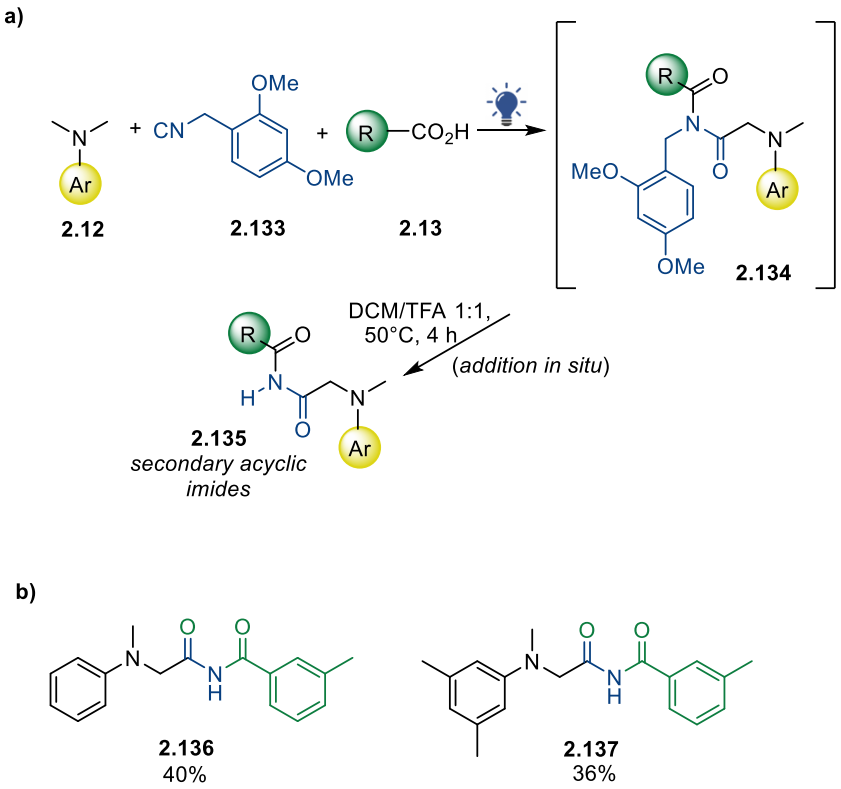

Scheme 2.14. Synthesis of secondary imides via the use of 2,4-dimethoxybenzyl isocyanide as a cleavable one.

2.4.5. One-pot domino Ugi 3-CR/deprotection/Mumm transacylation sequence

The second post-condensation modification we developed consisted of a one-pot domino Ugi 3-CR/deprotection/Mumm transacylation sequence, leading to densely functionalised bis-amide derivatives. This transformation is reminiscent of both the PADAM protocol (Passerini reaction/Amine Deprotection/Acyl Migration) reported by Prof. L. Banfi in 2000,[84] and the split-Ugi reaction described by Prof. G. B. Giovenzana and Prof. G. C. Tron in 2006.[85] The first one relied on the use of *N*-Boc-α-aminoaldehydes **2.138** as starting materials to be reacted with isocyanides **2.41** and carboxylic acids **2.13** in a Passerini reaction, followed by one-pot Boc deprotection and acyl migration to afford peptide-like structures **2.140** containing an α-hydroxy-β-amino acid unit or, after oxidation, an α-oxo-β-amino acid unit (Scheme 2.15a). The second transformation, instead, exploited bis secondary diamines **2.141** as substitutes of primary amines in the Ugi 4-CR: while one of the two secondary amine groups reacted with the carbonyl compound **2.142** to afford the iminium ion (then intercepted by the isocyanide and the carboxylate moiety), the second amine group could take part in the final transacylation step (a "remote" Mumm rearrangement), allowing for an enlargement of the conventional Ugi 4-CR products backbone (Scheme 2.15b). In analogy with these two transformations, we speculated that performing our photo-induced Ugi 3-CR with the use of the isocyanide **2.143**, bearing a Boc-protected amino group tethered at the *ortho*-position, would afford a tertiary imide **2.144**, which could undergo a base-promoted Mumm transacylation after the acidic cleavage of the Boc-protecting group (Scheme 2.15c). As in the PADAM protocol the reaction required the TFA-mediated deprotection of the nucleophilic primary amine, but, like the split-Ugi reaction, the final step relied on the transacylation of a nitrogen atom. It is worth noting that, while the original Ugi 4-CR gives both a tertiary and a secondary amide bond and the split-Ugi reaction affords two tertiary amide bonds, our protocol provided access to peptidomimetic structures **2.145** incorporating two

secondary amide bonds. According to Figure 2.23, electron-donor substituents on the amine aromatic ring seemed to be able to afford better yields (**2.147**) than electron-withdrawing ones (**2.148**). Again, the average 51% yield of the three-step one-pot protocol stands for a medium 80% theoretical yield for each step, while keeping all the advantages of avoiding multiple purifications, longer times, and the use of coupling reagents, otherwise required for multistep syntheses.

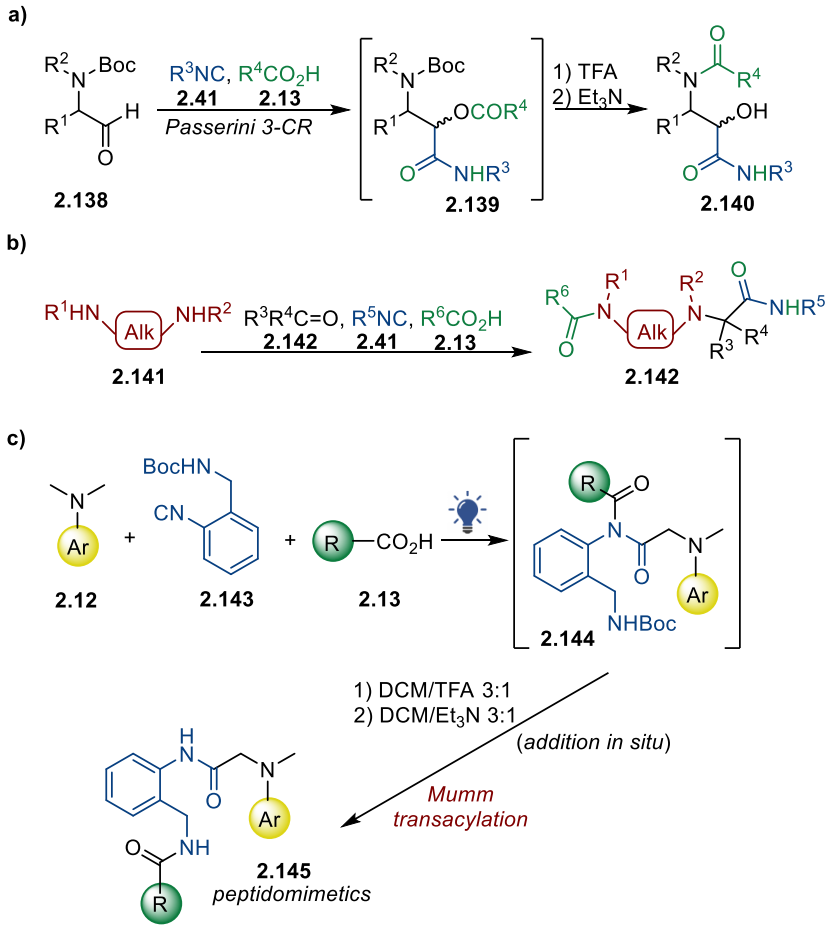

Scheme 2.15. a) PADAM protocol; b) Split-Ugi 4-CR; c) Three-step one-pot Ugi 3-CR/deprotection/Mumm transacylation sequence.

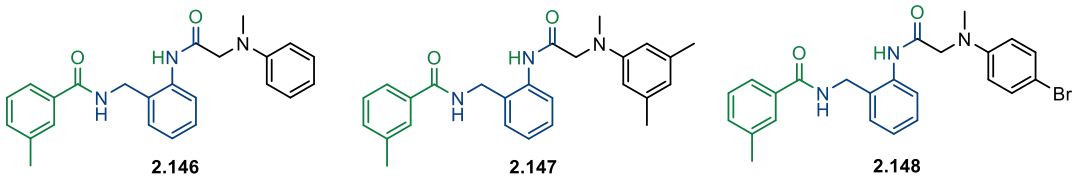

Figure 2.23. Bis-amide derivatives synthesised according to the Ugi 3-CR/deprotection/Mumm transacylation sequence.

2.5. Isocyanides as catalytic electron acceptors in the visible light-promoted oxidative formation of benzyl and acyl radicals

After proving the ability of aromatic isocyanides to harvest the energy of photons and act as catalytic organic photoactive oxidants when reacting with tertiary aromatic amines (both in self-catalysed reactions and in a range of α-amino C(sp^3)-H functionalisations involving other nucleophiles, Figure 2.25a) we wondered if proper modifications of the isocyanide aromatic moiety might allow to modulate their optical and redox properties to promote the photooxidation of more challenging substrates (*i.e.*, with higher redox potentials).[86] In theory, the addition of electron-withdrawing substituents on the isocyanide aromatic ring should, indeed, stabilise the isocyanide radical anion generated upon oxidation of a suitable partner, thus resulting in a higher redox potential for the excited state isocyanide. With this in mind, a library of nine aromatic isocyanides bearing either electron-donor or electron-withdrawing groups of various strengths, namely methoxy-, trifluoromethyl-, nitrile, and nitro- functionalities on either biphenyl- (Figure 2.24, **2.66**, **2.149**-**2.152**) or phenyl- moieties (**2.153**-**2.156**), was designed and synthesised in order to obtain photocatalysts with different chromophores and redox properties. On this basis, we undertook a theoretical and experimental study on the feasibility of photo-induced electron transfer (PET) events involving this set of isocyanides and a selection of chemical species endowed with different redox potentials and known to generate both alkyl- and acyl- radicals under photooxidative reaction conditions.

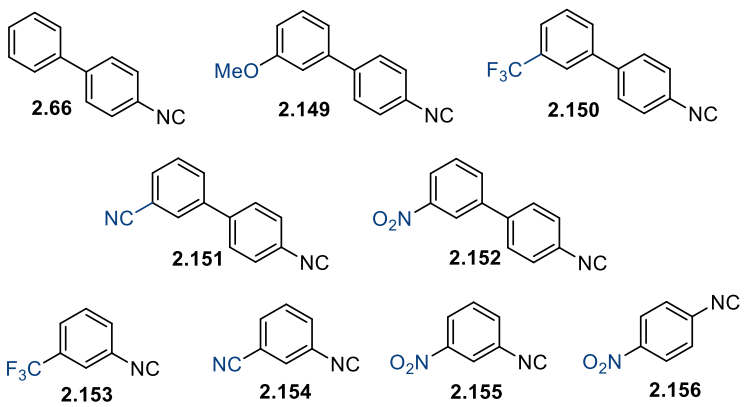

Figure 2.24. Library of aromatic isocyanides synthesised.

The investigated species, listed in order of increasing redox potential, included Hantzsch esters (E_{red} +1.0 V *vs* SCE, on average), carboxylic acids (carboxylate anion E_{red} +1.5 V *vs* SCE, on average) potassium alkyltrifluoroborates (E_{red} +1.8 V *vs* SCE, on average), and α-ketoacids (carboxylate anion, E_{red} +2.0 V *vs* SCE, on average), whose oxidative fragmentation, often requiring a metal-based photocatalyst, results in the generation of the corresponding open-shell species (Figure 2.25b).[87] To preliminarily assess the thermodynamic feasibility of these isocyanide-promoted PETs, electrochemical measurements of the ground-state redox potentials of the nine synthesised isocyanides, along with computational calculations of both their ground- and excited-state redox potentials were performed (see Section 2.5.1), and the resulting data drove the selection of a limited number of isocyanides (**2.153-2.155**) to be preferentially employed in the subsequent experimental studies. While carboxylic acids did not afford any product on a preparative scale, albeit the adduct of the corresponding alkyl radical with a radical quencher such as TEMPO [(2,2,6,6-tetramethylpiperidin1-yl)oxyl] was detected by HRMS, Hantzsch esters, potassium alkyltrifluoroborates, and α-oxoacids resulted in hydroperoxide, alcohol, and aldehyde derivatives (see Sections 2.5.2, 2.5.3 and 2.5.4, respectively), when irradiated under 30W blue LED in the presence of catalytic amounts (generally 20 mol%) of an aromatic isocyanide.

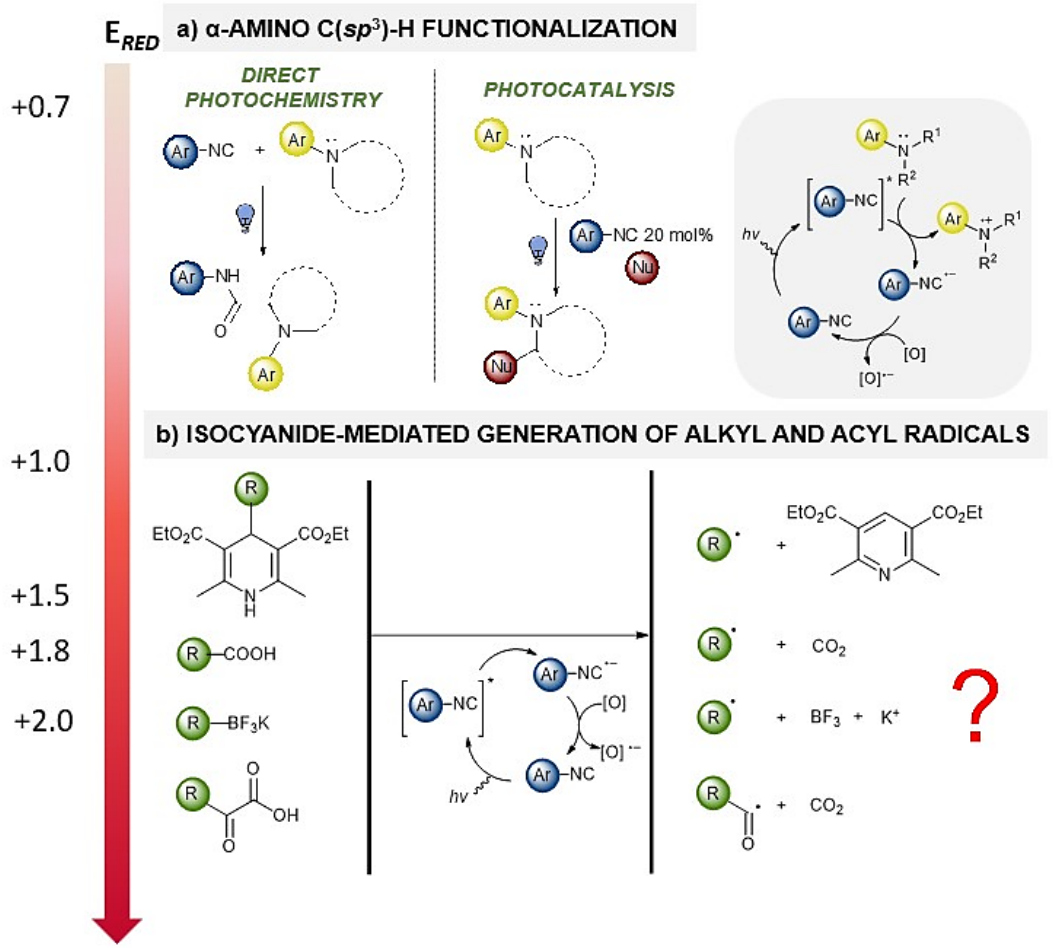

Figure 2.25. Isocyanides as photoactive catalytic single electron oxidants in (a) the α-amino C(sp^3)-H functionalisation, (b) the oxidative formation of alkyl and acyl radicals.

Further synthetic applications involved tandem one-pot multicomponent reactions, late-stage functionalisation, and isotopic labelling. The results obtained, together with additional spectroscopic studies such as Stern–Volmer fluorescence quenching analyses, provided key knowledge about the (re)activity of aromatic isocyanides as organic catalytic single electron oxidants under visible light irradiation, which may represent a green alternative to common oxidants such as halosuccinimides (*N*-chloro-, *N*-bromo-, and *N*-iodo-succinimide), Selectfluor®, persulfates, peroxides and peresters, halocarbons such as bromotrichloromethane, hypervalent iodine reagents, and transition metals.[87]

2.5.1. Theoretical and electrochemical studies

Theoretical and electrochemical studies were performed in collaboration with Dr. G. Donati and Prof. L. Marinelli from University of Naples Federico II, and Dr. F. Giustiniano and Prof. R. J. Whitby from University of Southampton, respectively. At first, the ability of aryl isocyanides to promote a SET oxidation upon visible light irradiation was investigated through a theoretical approach by computing the redox potentials of compounds **2.66**, **2.149-2.156** in both their ground ($E°_{red}$) and excited ($E°*_{red}$) electronic states: Density Functional Theory (DFT) was used for all the ground-state calculations, while its time-dependent version[88,89] (TD-DFT) was employed for computing excited state properties. The theoretical model was further corroborated by Cyclic Voltammetry (CV) measurements of the ground-state redox potentials ($E°_{1/2}$) of the nine synthesised isocyanides, which yielded redox potentials values within 0.1–0.3 V of those obtained by calculation.

Ar-NC	$E°_{red}$ (V *vs* SCE) calculated	$E°*_{red}$ (V *vs* SCE) calculated	$E°_{1/2}$ (V *vs* SCE) Measured	$E°_{1/2}$ residuals (V, measured - calculated)
2.66	- 2.11	+1.63	-2.23	-0.12
2.149	-2.13	+1.79	-2.22	-0.09
2.150	-1.98	+1.80	-2.16[a]	-0.18
2.151	-1.69	+1.89	-2.01	-0.33
2.152	-0.86	+1.93	-1.10	-0.24
2.153	-2.11	+2.73	-2.29[a]	-0.18
2.154	-1.87	+2.56	-1.98[a]	-0.11
2.155	-0.71	+2.24	-0.96	-0.25
2.156	-0.66	+2.24	-0.95	-0.29

[a] E_{pc}

Table 2.9. Redox potentials of isocyanides **2.66**, **2.149-2.156** (V *vs* SCE) calculated and measured via CV.

The measurements were performed in a MeCN/TBATFB/Ag-AgCl electrochemical system, in the absence of air and water, and referenced to the ferrocene/ferrocenium redox couple to obtain the standard redox potentials,

reported here *vs* SCE. Table 2.9 summarises the results of both the theoretical calculations and CV measurements.

Reduction potentials in the ground state

The calculated reduction potentials in the ground state were in very good agreement with those measured by cyclic voltammetry, as corroborated by the linear correlation found between the calculated and measured reduction potentials, showing an R^2 value of 0.989 (Figure 2.26). More in detail, the isocyanide compounds appeared to cluster in two different $E°_{red}$ regions: isocyanides **2.66**, **2.149**, and **2.153** had poorer and similar oxidising properties, with calculated $E°_{red}$ values in the range between -2.13 and -2.11 V, followed by compounds **2.150**, **2.151**, **2.154**. On the other side, compounds **2.152**, **2.155**, and **2.156** showed larger $E°_{red}$, spanning between computed values of -0.86 and -0.66 V *vs* SCE.

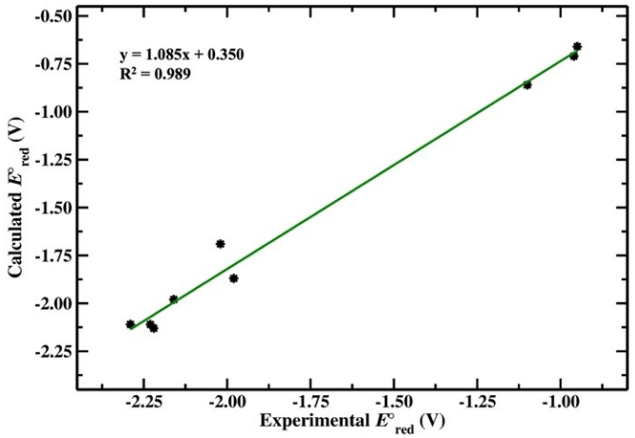

Figure 2.26. Linear correlation plot for the calculated and experimental ground state redox potentials (V *vs* SCE) in MeCN.

As firstly demonstrated by Maccoll in 1949,[90] the frontier molecular orbital energies and the redox potentials can be linearly correlated, where the reduction potentials are related to the energy of the Lowest Unoccupied Molecular Orbitals (LUMOs), while the oxidation potentials correlate with the Highest Occupied

Molecular Orbitals (HOMOs). In Figure 2.27 the calculated $E°_{red}$ were reported as function of the LUMO energies for all the isocyanide compounds. A well-defined linear correlation was detected, where the largest $E°_{red}$ correspond to lowest LUMO energies and vice versa: this means that a lower energy of the LUMOs is correlated to an easier capability of the isocyanide to accept an electron, resulting in better oxidising properties for compounds **2.152**, **2.155**, and **2.156**.

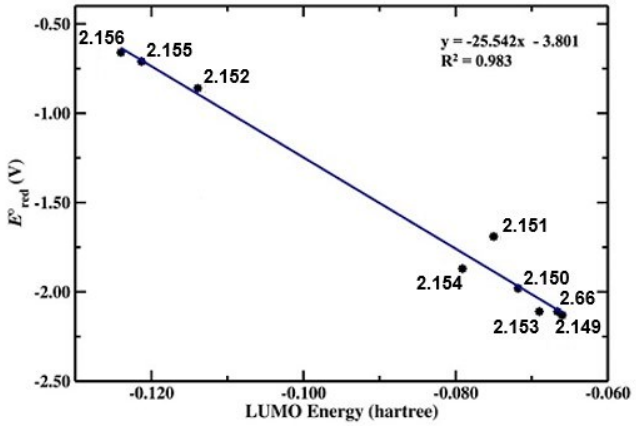

Figure 2.27. Correlation plot for the LUMO energies and the calculated ground state redox potentials (V *vs* SCE) in MeCN.

It is clear that the decrease in LUMO energies depends on both the nature of the functional groups and on the aromatic scaffold (biphenyl or phenyl moieties): as expected, electron-withdrawing substituents, (especially the nitro group, *i.e.*, **2.152**, **2.155**, and **2.156**), were found to have the largest capability of decreasing the LUMO energies, resulting in higher redox potentials. Figure 2.28 shows isodensity surfaces of the HOMOs (left panels) and LUMOs (right panels) of the nine ground state isocyanides **2.66**, **2.149**-**2.156**.

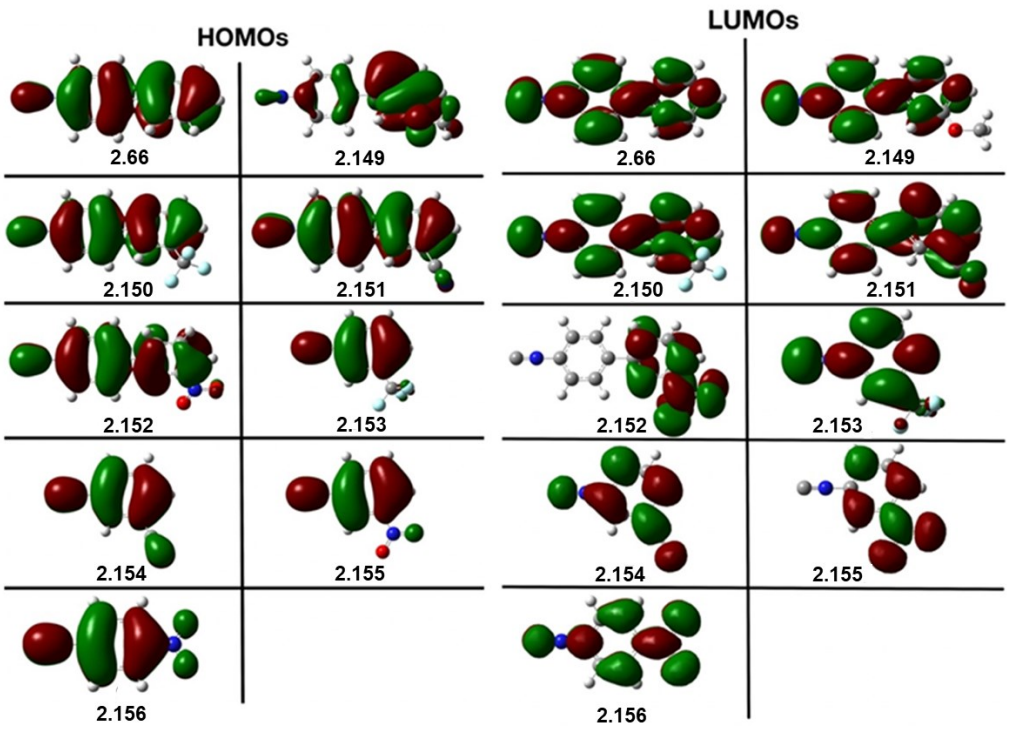

Figure 2.28. Isodensity surfaces evaluated for compounds **2.66**, **2.149-2.156** of their HOMOs (left panels) and LUMOs (right panels).

While in the LUMO isosurface plots of compounds **2.152**, **2.155**, and **2.156** the electronic density is withdrawn by the nitro group from the isocyanide moiety, lowering their LUMO energies and thus favouring the gain of an electron upon reduction, the LUMO isosurfaces do not significantly change between the unsubstituted (**2.66**), methoxy- (**2.149**) and trifluoromethyl- (**2.150**) substituted biphenyl compounds. The cyano-substituted compounds show a larger isodensity delocalisation over the previous ones, resulting in both lower LUMO energies and slightly better redox potentials for both the biphenyl (**2.151**) and phenyl (**2.154)** derivatives.

Reduction potentials in the excited state

As stated above, the excited state reduction potentials ($E°^*_{red}$) were computed by TD-DFT calculations and are reported in Table 2.9 for all the previously examined

compounds. Upon excitation, the ability of isocyanides to act as oxidising agents importantly increases in all the cases, although to a different extent, demonstrating an overall capability of these isocyanides to act as photo-oxidants. Regarding biphenyl compounds (**2.66**, **2.149**-**2.152**), Table 2.10 reports the inter-ring dihedral angles reaching values closer to planar configuration (±180° C), and the inter-ring bond distances (CC), undergoing a shortening. Conversely, isocyanide bond distances (NC) increase and the bond between the isocyanide nitrogen atom and the carbon atom of the aromatic ring (NC_{Ar}) becomes shorter for all biphenyls (in a less extent for **2.152**). These results suggest that the structural reorganisation due to the electronic excitation, in terms of larger co-planarity and charge delocalisation can improve the isocyanides' oxidising abilities. For phenyl compounds **2.153**-**2.156**, an increase in the isocyanide bond length (NC) is observed, suggesting a weakening of the bond, with the most affecting compounds not carrying the nitro substituents, whose N-C bonds remain almost unchanged. The N-C_{Ar} bond distance undergoes a shortening for all isocyanides except than for **2.155** and **2.156**, where only the C-R bond distance is the most perturbed, undergoing a decrease of ~0.1 Å. Overall, the phenyl compounds show the largest $E°^*_{red}$: in the phenyl rings, the effect of the substituents in influencing the electronic and nuclear properties in the excited state is, actually, emphasised with respect to the biphenyls, due to the absence of the conjugation that has a mitigating effect. This results in an improvement of their oxidising properties. The nitro-, trifluoromethyl- and cyano-substituents cause the biggest changes in the excited electronic state, given their electron-withdrawing nature and larger capability in affecting the electronic reorganisation upon excitation. As a result, compounds **2.154** and **2.155** were selected as the most promising photocatalysts for the following experimental studies.

Ar-NC	NC S_0	NC S_1	NC_{Ar} S_0	NC_{Ar} S_1	CR S_0	CR S_1	CC S_0	CC S_1	Dihedral S_0	Dihedral S_1
2.66	1.176	1.190	1.388	1.356	–	–	1.485	1.420	141.26	177.32
2.149	1.176	1.188	1.388	1.362	1.367	1.336	1.486	1.439	141.28	171.89
2.150	1.176	1.189	1.388	1.356	1.503	1.504	1.485	1.417	140.84	179.82
2.151	1.176	1.188	1.388	1.356	1.435	1.433	1.485	1.418	140.32	-180.00
2.152	1.182	1.181	1.383	1.367	1.476	1.420	1.483	1.448	-141.73	-159.34
2.153	1.176	1.190	1.387	1.351	1.505	1.483	–	–	–	–
2.154	1.176	1.187	1.388	1.355	1.435	1.404	–	–	–	–
2.155	1.176	1.176	1.386	1.387	1.471	1.368	–	–	–	–
2.156	1.176	1.177	1.384	1.381	1.468	1.362	–	–	–	–

Table 2.10. Structural parameters of isocyanides **2.66**, **2.149-2.156** in the ground and excited electronic states. All bond distances are in Å, the biphenyls inter-ring dihedral angle are in degrees. NC: isocyanide bond. NC_{Ar}: isocyanide nitrogen- aromatic carbon bond; CC: inter-ring carbon-carbon bond; CR: aromatic carbon-functional group atom bond.

2.5.2. Synthetic studies involving Hantzsch esters

4-Alkyl-1,4-dihydropyridines (DHPs, also known as Hantzsch esters) have been conveniently exploited as alkyl radical precursors[91-93] thanks to a smooth oxidative fragmentation to form a fully aromatic pyridine (E_{red} = +1.0 V *vs* SCE, on average). Furthermore, they are bench-stable solids, easily synthesised from widely available aliphatic aldehydes. In order to evaluate the feasibility of an isocyanide-mediated PET event, Hantzsch ester **2.157** was selected as a model substrate. Following the mechanistic hypothesis in Scheme 2.16 we supposed, indeed, that the latter might undergo a SET oxidation promoted by the electronically excited isocyanide, affording the benzyl radical **I**, which in the presence of a H-donor such as triisopropylsilane (TIS) would give 4-phenyltoluene **2.159**.

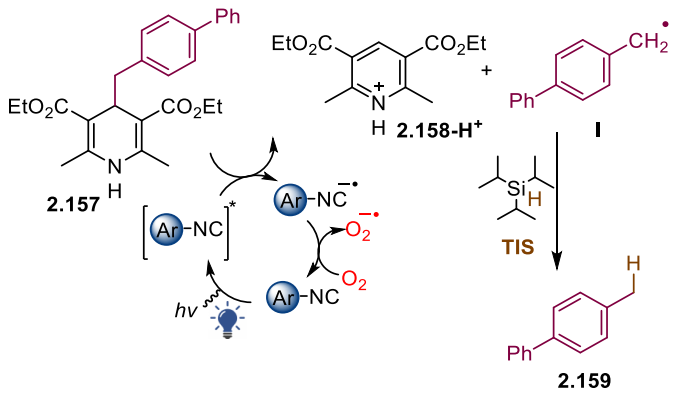

Scheme 2.16. Initial mechanistic design for the isocyanide-promoted SET photooxidation of Hantzsch esters.

Nevertheless, when a test reaction of **2.157** in the presence of a 20 mol% loading of isocyanide **2.155** and 1 equivalent of TIS was performed in MeCN, under 30W blue LED irradiation (wavelength: 450 – 455 nm), at room temperature, overnight, the hydroperoxide **2.160** was obtained in 47% yield (Table 2.11, Entry 1). Of note, the reaction was carried out open to air in order to enable the regeneration of the isocyanide ground state via oxidation of the isocyanide radical anion mediated by molecular oxygen. The use of TIS as an additive proved to be beneficial to the reaction, since its absence led to a poor outcome (Entry 2), as well as the use of Hantzsch ester (HE, diethyl 1,4-dihydro-2,6-dimethyl-3,5 pyridinedicarboxylate) as H-donor (Entry 3), a different light source (Entries 4 and 5), or the use of isocyanide **2.154** as the photocatalyst (Entry 6). Interestingly, the hydroperoxide **2.160** formed in a moderate 29% yield even in the absence of any photocatalyst (Entry 7), albeit *m*-nitro-phenyl isocyanide **2.155** proved to be able to promote its formation in 58% yield after 48 h (Entry 8).

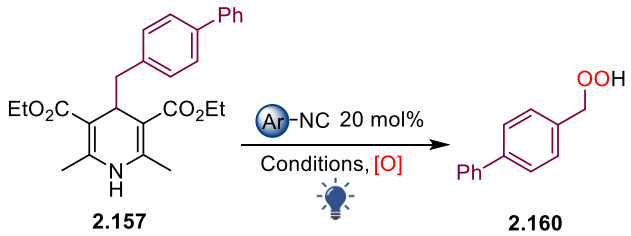

2.157 2.160

Entry	H-donor (1 equiv.)	Catalyst	Light source	Time	2.160 Yield[a] (%)
1	TIS	**2.155**	Blue LED 30W	20 h	47
2	None	**2.155**	Blue LED 30W	20 h	38
3	HE	**2.155**	Blue LED 30W	20 h	16[b]
4	None	**2.155**	Blue LED 1W	20 h	5
5	None	None	Blue LED 1W	20 h	4
6	TIS	**2.154**	Blue LED 30W	20 h	37
7	TIS	None	Blue LED 30W	20 h	29[b]
8	TIS	**2.155**	Blue LED 30W	48 h	58

Conditions: reaction performed on a 0.08 mmol scale in dry MeCN, RT, open to air.
[a] Isolated yield
[b] NMR yield (determined by using TMB as internal standard)

Table 2.11. Optimisation of the reaction conditions for the isocyanide-promoted SET photooxidation of Hantzsch esters.

On the other hand, as for substrates other than benzylic ones, a test reaction involving a Hantzsch ester bearing an *n*-undecyl alkyl chain did not afford the hydroperoxide derivative (probably due to the low stability of the corresponding primary alkyl radical) even if the oxidised pyridine derivative was detected in 35% yield. These results prompted us to investigate the UV-VIS absorption properties of both **2.157** and **2.155** (Figure 2.29). While it was not possible to measure a significant fluorescence band for the isocyanide **2.155**, probably due to the nitro functional group acting as an intramolecular fluorescence quencher,[94,95] the absorption bands in the visible light region for both **2.155** and **2.157**, along with a fluorescence peak (irradiation wavelength = 343 nm) for **2.157** provided experimental data to support the mechanistic hypotheses depicted in Scheme 2.17 (*path a* in the absence of **2.155**, and either *path b* or *path c* in the presence of a catalytic amount of **2.155**).

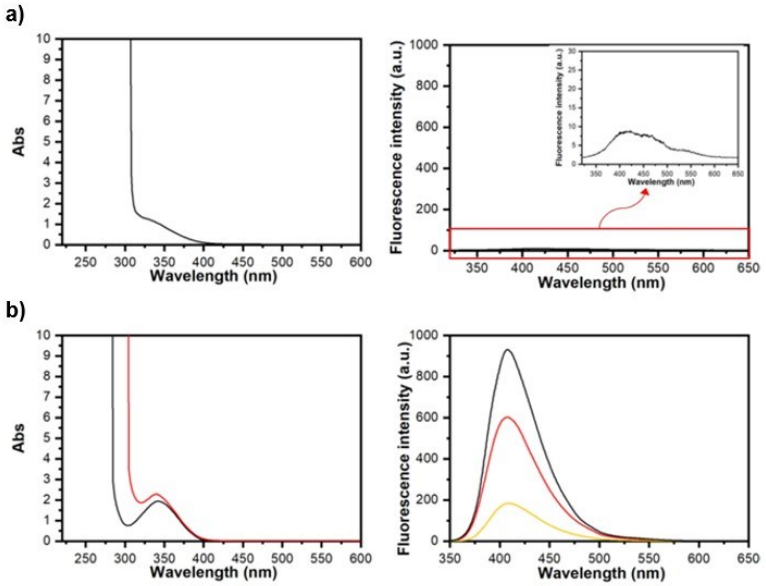

Figure 2.29. UV-VIS absorption and fluorescence spectra for (a) **2.155**, and (b) **2.157** in the absence (black line) and presence of increasing amounts of **2.155** (10 and 50 equiv., red and yellow lines, respectively).

According to *path a*, the Hantzsch ester **2.157** is able to absorb a photon and reach an electronically excited state **2.157***, which is then quenched by molecular oxygen to give the benzyl radical **I**, a superoxide radical anion **II**, and the pyridinium cation **2.158-H**$^+$. Deprotonation of the latter by the superoxide radical anion **II** provides a hydroperoxide radical **III**, which is in turn able to quench the benzyl radical **I** in a radical-radical coupling, to finally afford the hydroperoxide **2.160**. The latter mechanistic aspect was further corroborated by the dramatic drop of the yield to 15% and 7% when the reaction was performed in the presence of 1,4-benzoquinone (3 and 10 equivalents, respectively) as a superoxide radical anion scavenger. In the presence of **2.155**, instead, the formation of **2.160** could hinge on the photocatalytic activity of the isocyanide (*path b*), reaching an excited state upon visible light irradiation and promoting a SET oxidation of **2.157**: this would result in the pyridinium ion **2.158-H**$^+$, the benzyl radical **I**, and the isocyanide radical anion, then oxidised back by molecular oxygen to regenerate the ground state isocyanide, while giving a superoxide radical anion **II**. Abstraction of a proton

from **2.158–H**$^+$ by the latter, then leads to the formation of the hydroperoxide radical **III**, whose radical-radical coupling with **I** results in the generation of **2.160**.

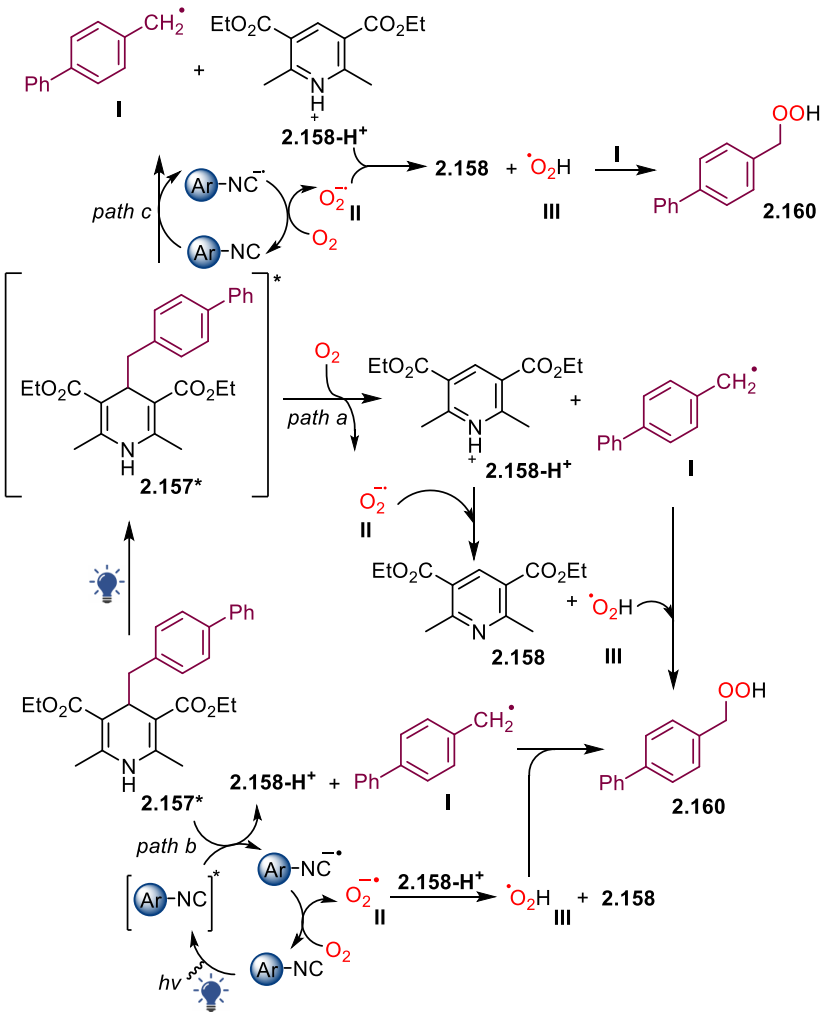

Scheme 2.17. Possible mechanistic pathways for the isocyanide-promoted formation of hydroperoxide derivatives from Hantzsch esters under visible light irradiation.

Alternatively, as shown in *path c*, the isocyanide might also be able to act as a catalytic sacrificial electron-acceptor. Following this mechanistic hypothesis, it would promote the oxidative fragmentation of the excited Hantzsch ester **2.157*** to **I** and **2.158-H**$^+$, and then provide a superoxide radical anion **II** upon reduction of molecular oxygen by the so-formed isocyanide radical anion. Protonation of **II** to

the hydroperoxide radical **III** and coupling of the latter with the benzyl radical **I** would finally afford the hydroperoxide derivative **2.160**. This mechanistic path was supported by Stern–Volmer quenching experiments (Figure 2.19b, right panel) where **2.155** was found to be able to completely quench the fluorescence peak of **2.157***.

2.5.3. Synthetic studies involving potassium alkyltrifluoroborates

The exploitation of potassium alkyltrifluoroborates as alkyl radical precursors has been pioneered by Prof. G. Molander in 2014 in a photoredox/nickel dual catalytic formation of $C(sp^2)$-$C(sp^3)$ bonds.[96] This first seminal report set the stage for a wide range of processes involving catalytic single-electron oxidative fragmentation of alkyltrifluoroborates.[97-99] Besides iridium and ruthenium polypyridyl complexes, it has been shown that organophotocatalysts such as MesAcr ($E_{1/2}$ PC^*/PC^- +2.06 V *vs* SCE), 4CzIPN ($E_{1/2}$ PC^*/PC^- +1.35 V *vs* SCE), and Eosin Y ($E_{1/2}$ PC^*/PC^- +0.83 V *vs* SCE) could be harnessed to promote the generation of alkyl radical species from alkyltrifluoroborates. Prompted by the preliminary results achieved with Hantzsch ester **2.157**, and considering the desirable features of alkyltrifluoroborates such as commercially availability, convenient synthesis on a multi-gram scale, good functional group tolerance, and reasonable oxidation potential, we engaged in the investigation of a PET promoted by aryl isocyanides. To this end, potassium ([1,1'-biphenyl]-4-ylmethyl)trifluoroborate **2.161** was synthesised and irradiated with 30W blue LED in a MeCN/H_2O 8:2 solvent mixture, in the presence of isocyanide **2.155** (20 mol%) and TIS as a H-donor, at room temperature for 20 h. Again, the expected product, 4-phenyltoluene **2.159**, was not observed while alcohol derivative **2.162** was isolated in 65% yield (Table 2.12, Entry 1). The use of TIS as an additive proved to be beneficial (Entry 2), albeit a further increase to 2 equivalents led to poorer results (Entry 3). The screening of different solvents (Entries 4–7), as well as HE as the H-donor (Entry 8), isocyanide **2.154** as

photoactive single-electron oxidant (Entry 9), and longer reaction times (Entry 10) did not produce better outcomes.

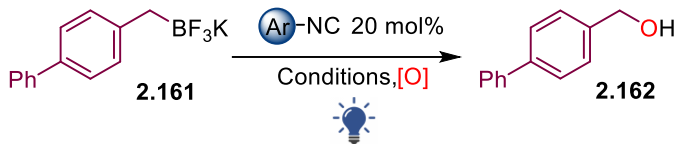

Entry	H-donor (equiv.)	Catalyst	Solvent (0.15 M)	Time	2.162 Yield[a] (%)
1	TIS (1)	**2.155**	MeCN/H_2O 8:2	20 h	65
2	None	**2.155**	MeCN/H_2O 8:2	20 h	50
3	TIS (2)	**2.155**	MeCN/H_2O 8:2	20 h	52
4	TIS (1)	**2.155**	MeCN/H_2O 3:1	20 h	25[b]
5	TIS (1)	**2.155**	MeCN/H_2O 9:1	20 h	45[b]
6	TIS (1)	**2.155**	MeOH	20 h	60
7	TIS (1)	**2.155**	$_i$PrOH	20 h	49
8	TIS (1)	**2.155**	MeCN/H_2O 8:2	20 h	58
9	TIS (1)	**2.154**	MeCN/H_2O 8:2	20 h	32
10	TIS (1)	**2.155**	MeCN/H_2O 8:2	48 h	42
11	TIS (1)	None	MeCN/H_2O 8:2	20 h	ND

Conditions: reaction performed on a 0.08 mmol scale, under 30W blue LED irradiation (450 – 455 nm), RT, open to air.
[a] Isolated yield
[b] NMR yield (determined by using TMB as internal standard)

Table 2.12. Optimisation of the reaction conditions for the isocyanide-promoted SET photooxidation of potassium alkyltrifluoroborates.

Differently from HEs, the presence of an aryl isocyanide was mandatory to promote the formation of the alcohol derivative **2.162**, as no product was detected when the reaction was performed in the absence of **2.155** (Entry 11). Alkyl trifluoroborates other than benzylic ones failed to afford the corresponding alcohols, with most of the starting material recovered.

Based on these results, a mechanistic hypothesis for the formation of **2.162**, was reported in Scheme 2.18: the electronically excited isocyanide is able to promote a SET oxidation of potassium alkyltrifluoroborate **2.160**, further undergoing a fragmentation to benzyl radical **I**, boron trifluoride (BF_3), and a potassium ion (K^+).

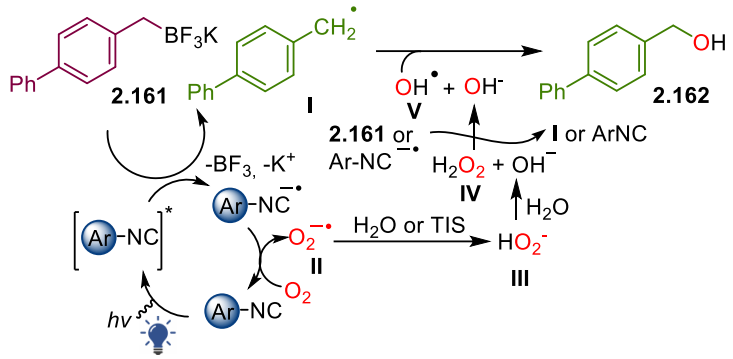

Scheme 2.18. Mechanistic hypothesis for the isocyanide-promoted formation of alcohol derivatives from potassium alkyltrifuoroborates, under visible light irradiation.

Regeneration of the ground state isocyanide by molecular oxygen forms a superoxide radical anion **II**, which abstracts a hydrogen atom from either TIS or H_2O to give the hydroperoxide anion **III**, then protonated by excess water to hydrogen peroxide **IV**. Further SET reduction of the latter leads to the hydroxyl radical **V**, which can undergo a radical-radical coupling with **I** to finally give the alcohol derivative **2.162**. In theory, the reduction of **IV** could be promoted either by the isocyanide radical anion or by **2.161**, in a chain formation of **I**. However, any attempts of forming **2.162** by reacting **2.161** in hydrogen peroxide (either 3% or 30%, both in absence and in the presence of light) led to exclude the latter hypothesis, while the comparison between the redox potential of hydrogen peroxide ($E°_{red}$ +0.24 V *vs* SCE) and the redox couple **2.155**/**2.155**$^{\bullet-}$ ($E°_{red}$ = 0.71 V *vs* SCE) further supported the role of the isocyanide radical anion as single electron donor.

2.5.4. Synthetic studies involving α-ketoacids

The first report about the use of α-ketoacids as acyl radical precursors dates back to 1972, when Prof. Minisci reported a silver catalysed decarboxylative homolytic acylation of pyridine and pyrazine derivatives.[100] With the advent of the visible

light photoredox catalysis era, α-ketoacids have been widely exploited in a range of synthetic applications including the decarboxylative/oxidative synthesis of amides,[101] the hydroacylation of dialkylazodicarboxylates,[102] the direct synthesis of ketones,[103] and decarboxylative ynonylation reactions,[104] to cite a few.[105] While most of these synthetic protocols require the use of metal-based photocatalysts, we wondered whether an aromatic isocyanide such as **2.153–2.155** could promote the oxidative decarboxylation of phenylglyoxylic acid **2.163** to the corresponding acyl radical **I**, which could then undergo a hydrogen atom abstraction to give the aldehyde derivative **2.164** (Scheme 2.19).

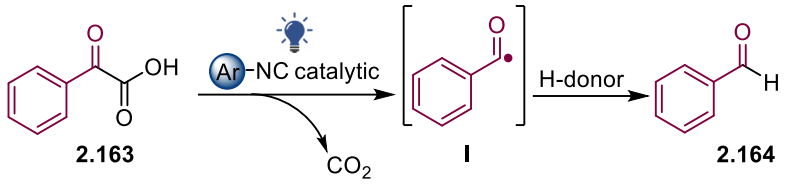

Scheme 2.19. Initial mechanistic design for the isocyanide-promoted photooxidative decarboxylation of α-ketoacids to aldehydes.

To this end, different H-donors, solvents, and reaction times were evaluated (Table 2.13) by monitoring the residual **2.163** via NMR spectroscopy. A 60% conversion was observed in the presence of isocyanide **2.154** (20 mol%), TIS (1equiv.), and K_2HPO_4 (1.2 equiv.), in a MeCN/H_2O 3:1 solvent mixture (0.25M), at room temperature, under irradiation with 30W blue LED for 72h (Entry 15).

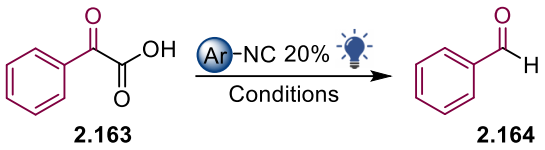

2.163 **2.164**

Entry	H-donor (equiv.)	Catalyst	Solvent (0.25 M)	Time	Residual **2.163**[a] (%)
1	TIS (1)	**2.153**	MeCN/H_2O 1:1	20 h	80
2	TIS (1)	**2.154**	MeCN/H_2O 1:1	20 h	86
3	TIS (1)	**2.155**	MeCN/H_2O 1:1	20 h	85
4[b]	TIS (1)	**2.154**	MeCN/H_2O 1:1	20 h	85
5	Hantzsch ester (1)	**2.154**	MeCN/H_2O 1:1	20 h	72
6	Ascorbic acid (1)	**2.154**	MeCN/H_2O 1:1	20 h	91
7	TFA (1)	**2.154**	MeCN/H_2O 1:1	20 h	68
8	TIS (10)	**2.154**	MeCN/H_2O 1:1	20 h	92
9	TIS (5)	**2.154**	MeCN/H_2O 1:1	20 h	78
10	TIS (2)	**2.154**	MeCN/H_2O 1:1	48 h	88
11	TIS (1)	**2.154**	MeCN/H_2O 3:1	20 h	65
12	TIS (1)	**2.154**	MeCN/H_2O 1:3	20 h	75
13	TIS (0.8)	**2.154**	MeCN/H_2O 3:1	20 h	68
14	TIS (1)	**2.154**	MeCN/H_2O 3:1	48 h	48
15	TIS (1)	**2.154**	MeCN/H_2O 3:1	72 h	40
16	TIS (1)	**2.154**	MeCN/H_2O 3:1	4 d	40

Conditions: reaction performed on a 0.08 mmol scale, in the presence of 1.2 equivalents of K_2HPO_4 as the base, under 30W blue LED irradiation (450 – 455 nm), RT.
[a] Determined by NMR (TMB as internal standard)
[b] In the dark

Table 2.13. Optimisation of the reaction conditions for the isocyanide-promoted photooxidative decarboxylation of α-ketoacids to aldehydes.

The application of the optimum reaction conditions to 2-([1,1'-biphenyl]-4-yl)-2-oxo-acetic acid **2.165** enabled the isolation of the aldehyde **2.166** in 82% yield (Table 2.14, Entry 1). Interestingly, similar results were obtained in the absence of **2.154**, albeit with lower yield (Entry 2), while TIS, as well as light irradiation (Entries 3-5), proved to be essential to promote the reaction.

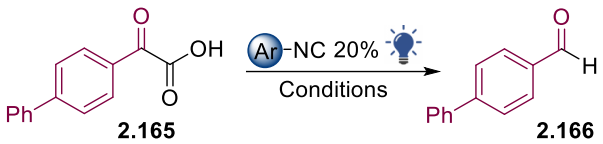

Entry	H-donor (1 equiv.)	Catalyst	2.166 Yield[a] (%)
1	TIS	**2.154**	82
2	TIS	None	71
3	None	**2.154**	58
4[b]	TIS	**2.154**	10
5[b]	TIS	None	8

Conditions: reaction performed on a 0.08 mmol scale, in a 3:1 MeCN/H_2O (0.25 M) mixture, in the presence of 1.2 equivalents of K_2HPO_4 as the base, under 30W blue LED irradiation (450 – 455 nm), RT, 72 h.
[a] NMR yield (determined by using TMB as internal standard)
[b] In the dark

Table 2.14. Further optimisation of the reaction conditions for the isocyanide-promoted photooxidative decarboxylation of α-ketoacids to aldehydes.

The generality of the transformation, along with the beneficial effect of the aryl isocyanide **2.154**, were further evaluated by converting a small set of α-ketoacids bearing both electron-donor and electron-withdrawing groups into the corresponding aldehydes **2.167-2.170** (Figure 2.30a, yields in parentheses refer to the reaction performed in the absence of **2.154**). Furthermore, the mild reaction conditions enabled the *in situ* interception of the aldehydes in a variety of tandem one-pot multicomponent transformations, such as the P-3-CR, the S-3-CR, and the Ugi-tetrazole 4-CR (UT-4-CR, see the Experimental Section for further details on the optimisation of the reaction conditions). Interestingly, the presence of isocyanide **2.154** exerted a more pronounced influence on the yields of the multicomponent products, as shown for the Passerini 3-CR adduct **2.171** (58% yield in the presence of a 20 mol% loading of **2.154**; 26% yield in the absence of **2.154**).

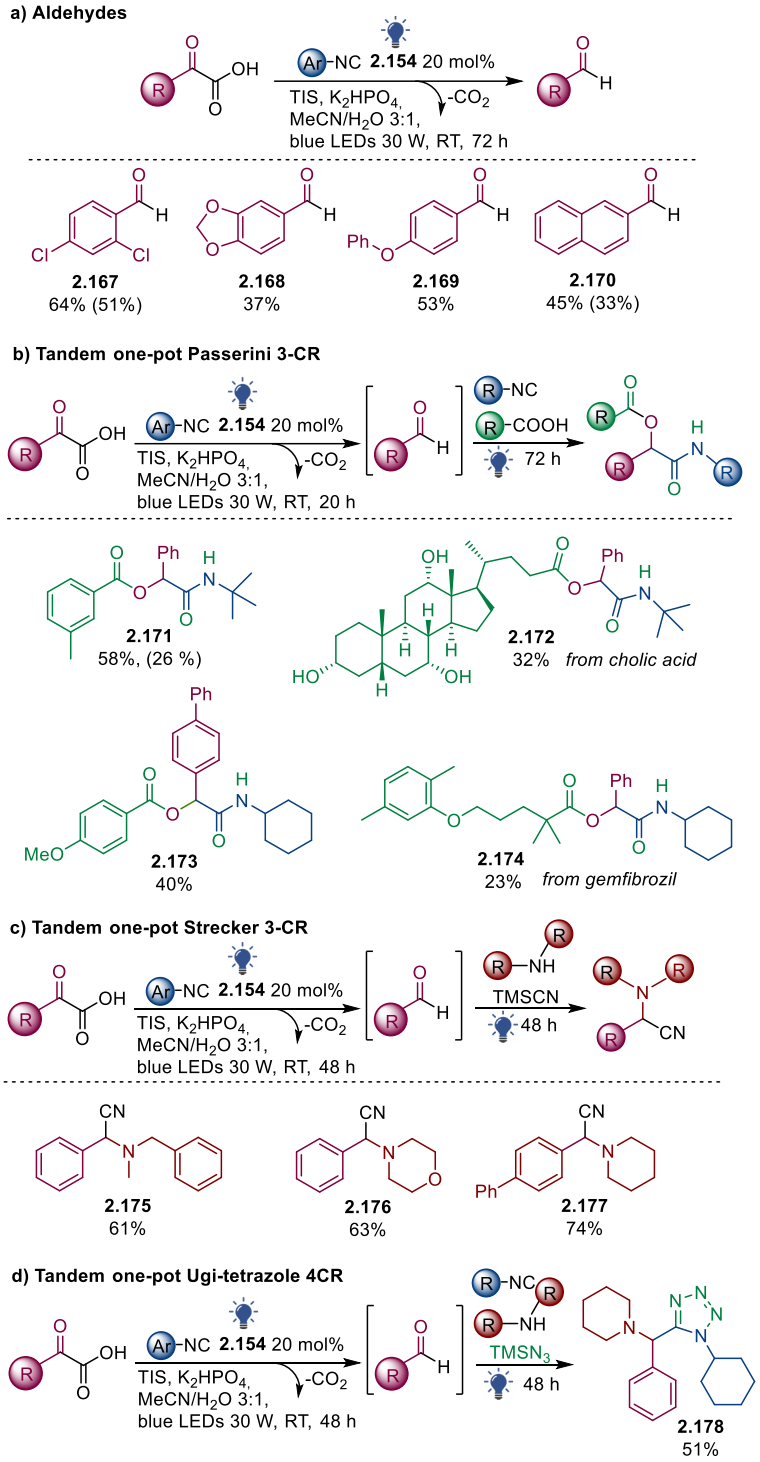

Figure 2.30. Isocyanide-promoted photooxidative decarboxylation of α-ketoacids to aldehydes and tandem MCRs.

Examples **2.172** and **2.174** involved the late-stage functionalisation of cholic acid and gemfibrozil to afford the ester derivatives in 32% and 23% yields, respectively (Figure 2.30b). Overall, the moderate yields of the P-3-CR could be ascribed to a slow reaction rate in the solvent system required for the photocatalytic step (MeCN/H_2O 3:1), as comparison with a P-3-CR starting from benzaldehyde and performed in the same solvent mixture led to the same identical 58% yield for products **2.171** (see also the Experimental Section). The P-3-CR is, indeed, known to be favoured in apolar aprotic solvents. A small library of α-aminonitriles **2.175**-**2.177** was obtained by adding to the aldehyde formed *in situ* either a linear or a cyclic secondary aliphatic amine and TMSCN (Figure 2.30c), while the tetrazole **2.178** was formed upon addition of piperidine, cyclohexyl isocyanide, and $TMSN_3$ in an Ugi-tetrazole 4-CR (Figure 2.30d). Worthy of note, the yields obtained from the tandem decarboxylative aldehyde formation/MCR were comparable to those obtained starting directly from the aldehydes (*e.g.*, S-3-CR for product **2.175**: 85% NMR yield starting from benzaldehyde and 73% NMR yield with the tandem one-pot method starting from α-ketoacids; UT-4-CR for product **2.178**: 63% NMR yield starting from benzaldehyde and 80% NMR yield with the tandem one-pot method starting from α-ketoacids; see also the Experimental Section). To our knowledge, this is the first synthetic methodology where the α-ketoacid carbonyl C(sp^2) ends up in a C(sp^3) without requiring net-reducing conditions.

In order to provide experimental data supporting a working mechanistic hypothesis for the formation of aldehydes derivatives, UV-VIS absorption and fluorescence measurements were performed for both 3-isocyanobenzonitrile **2.154** (Figure 2.31a) and phenylglyoxylic acid **2.163** (Figure 2.31b).

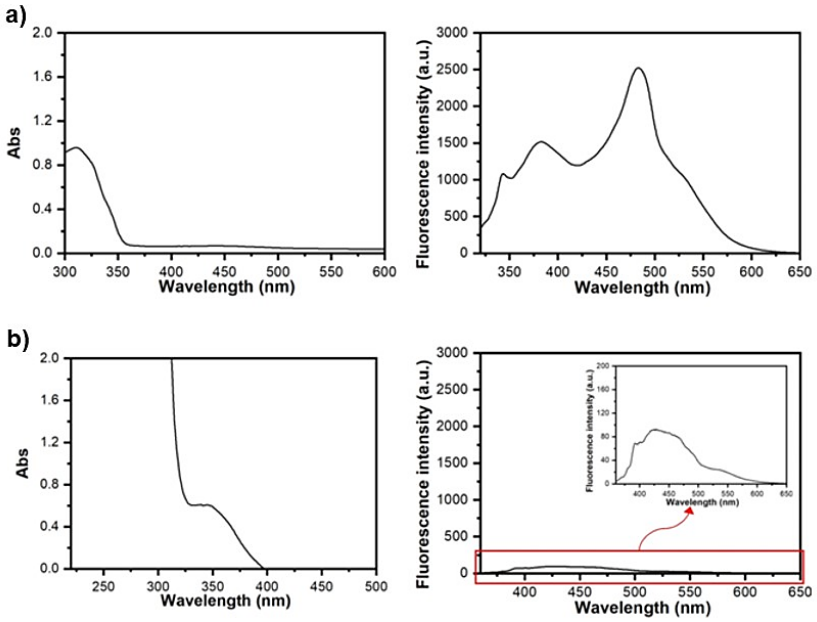

Figure 2.31. UV-VIS absorption and fluorescence spectra of (a) 3-isocyanobenzonitrile and (b) phenylglyoxylic acid.

Based on such experiments, it is reasonable to propose the formation of the aldehyde derivatives in the absence of a catalytic aryl isocyanide as due to the ability of phenylglyoxylic acid **2.163** to absorb a photon and reach an electronically excited state (Scheme 2.20, *path a*). The latter can then be quenched by molecular oxygen to form the acyl radical **I** and the superoxide radical anion **II**, followed by hydrogen atom abstraction to give the aldehyde **2.164**. In the presence of the aryl isocyanide, instead, two mechanistic pathways could possibly lead to the observed increase in the yield of **2.164**, where the isocyanide could act either as a photoactive single electron oxidant (Scheme 2.20, *path b*) or as a *sacrificial catalytic single electron acceptor* (Scheme 2.20, *path c*).

Path b was further supported by Stern–Volmer fluorescence quenching of **2.154** by adding increasing amounts of **2.163** (Figure 2.31).

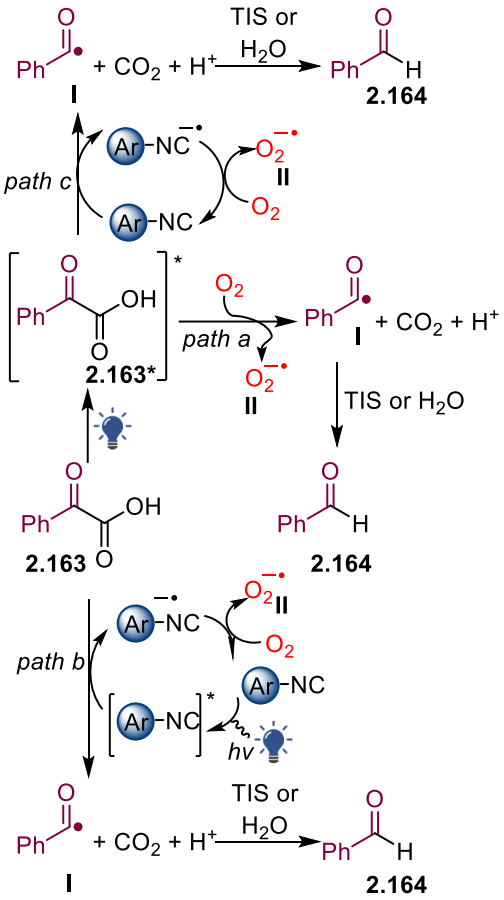

Scheme 2.20. Possible mechanistic pathways for the isocyanide-promoted photooxidative decarboxylation of α-ketoacids to aldehydes.

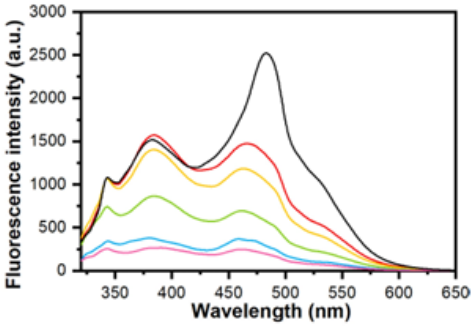

Figure 2.31. Stern–Volmer quenching of 3-isocyanobenzonitrile (black line) via addition of increasing amounts of phenylglyoxylic acid (0.1, 0.2, 0.4, 0.8 and 1.0 equivalents: red, yellow, green, cyano, and magenta lines, respectively).

Additionally, the hydrogen atom source was identified via formation of the labelled aldehyde **2.166–D** (87% yield, 98% deuterium incorporation) when water was replaced with deuterium oxide (D_2O, Scheme 2.21a).[106]

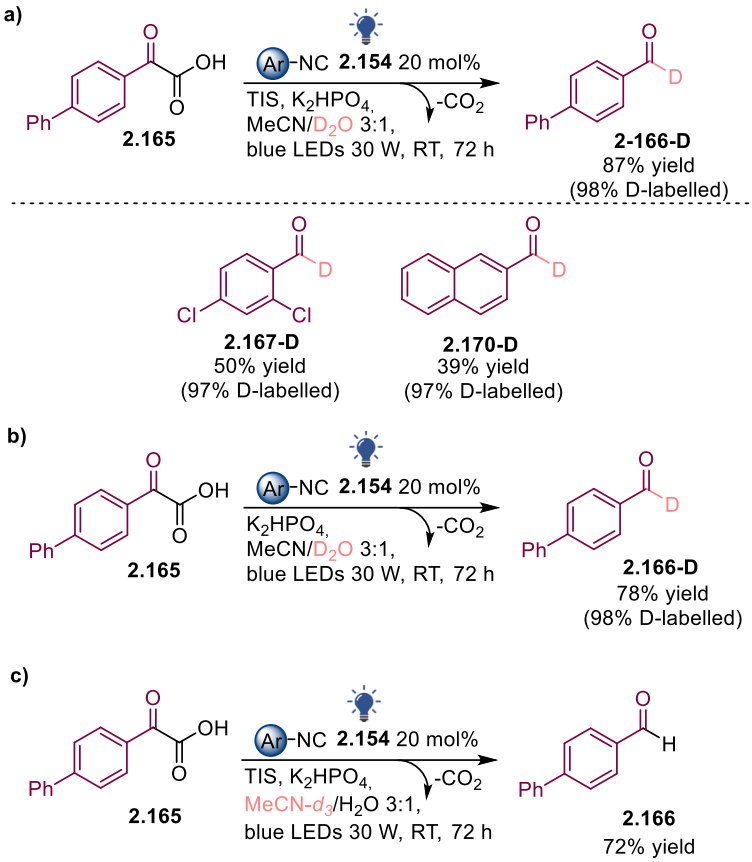

Scheme 2.21. Deuterium labelling experiments and isocyanide-promoted photooxidative decarboxylation of α-ketoacids to deuterated aldehydes.

On one hand, this led to exclude the role of TIS as hydrogen atom donor; on the other hand, a test reaction performed in the absence of TIS afforded a decreased yield (78%) while not changing the isotopic labelling (98%, Scheme 2.21b), thus excluding its role as a deuterium atom transfer catalyst. This observation was further corroborated by comparing the ^1H NMR spectra of TIS in MeCN alone and after the addition of D_2O and irradiation under 30W blue LED for 20 h, which

showed no signs of Si-H/Si-D exchange (see the Experimental Section). Moreover, when the reaction was performed in the presence of deuterated acetonitrile (MeCN-d_3, Scheme 2.21c), the non-deuterated product **2.166** was obtained in 72% yield, while no **2.166–D** was observed.

The optimal conditions for deuterium labelling were further applied to the synthesis of deuterated derivatives **2.167-D** and **2.170-D,** which both exhibited excellent deuterium incorporation (Scheme 2.21a).

Site selective deuteration of C-H bonds into bioactive compounds has been emerging as a valuable tool to improve pharmacokinetic parameters of drugs by either slowing down their metabolic cleavage[107] or preventing their metabolism-mediated toxicity; in some cases, it has also been proven to stabilise chemically unstable stereoisomers, as shown for thalidomide.[108] Furthermore, deuterated compounds find wide applications as structural labels in a variety of analytical techniques and are key to mechanistic investigations based on the measurement of kinetic isotope effects (KIEs).[109] For instance, deuterium labelled drugs can help in the elucidation of their mechanism of action and in the development of PET tracers. Since FDA approved deutetrabenazine in 2017 to treat choreas associated with Huntington's disease, a good number of derivatives have reached clinical trials. Notwithstanding their therapeutic value, deuterium labelled drugs are currently obtained via poor synthetic approaches such as conventional multistep routes starting from expensive deuterated reagents or isotope exchange, including reductive deuteration in the presence of D_2 gas. Prompted by the urgent need of identifying a straightforward, green, and direct access to deuterated drug-like compounds, we wondered if the developed SET oxidation/D-abstraction sequence affording D-labelled aldehydes could be exploited in tandem one-pot multicomponent reactions. To this end, the P-3-CR (Scheme 2.22a), the S-3-CR (Scheme 2.22b), and the UT-4-CR (Scheme 2.22c) were selected as model MCRs. After the visible light triggered formation of aldehydes **2.166–D** and **2.164–D**, the corresponding reactants (*tert*-butyl isocyanide and *m*-toluic acid for the P-3-CR, *N*-

benzylmethylamine and TMSCN for the S-3-CR, and cyclohexyl isocyanide, piperidine, and $TMSN_3$ for the UT-4-CR) were added *in situ* and reacted at room temperature for 48–72 h, leading to the formation of C(sp^3)-D bonds as in products **2.179–D**, **2.175–D**, and **2.178–D**. The deuterium labelled multicomponent adducts were obtained in good yields and percentages of deuterium incorporation. To our knowledge, this is the first report about a one-pot multicomponent conversion of a C(sp^2)-C(sp^2) bond into a C(sp^3)-D bond. Moreover, the protocol offers a direct and simple route to access complex deuterated molecular architectures with ease-of-use and versatility, thus representing a valuable alternative to traditional multistep approaches.

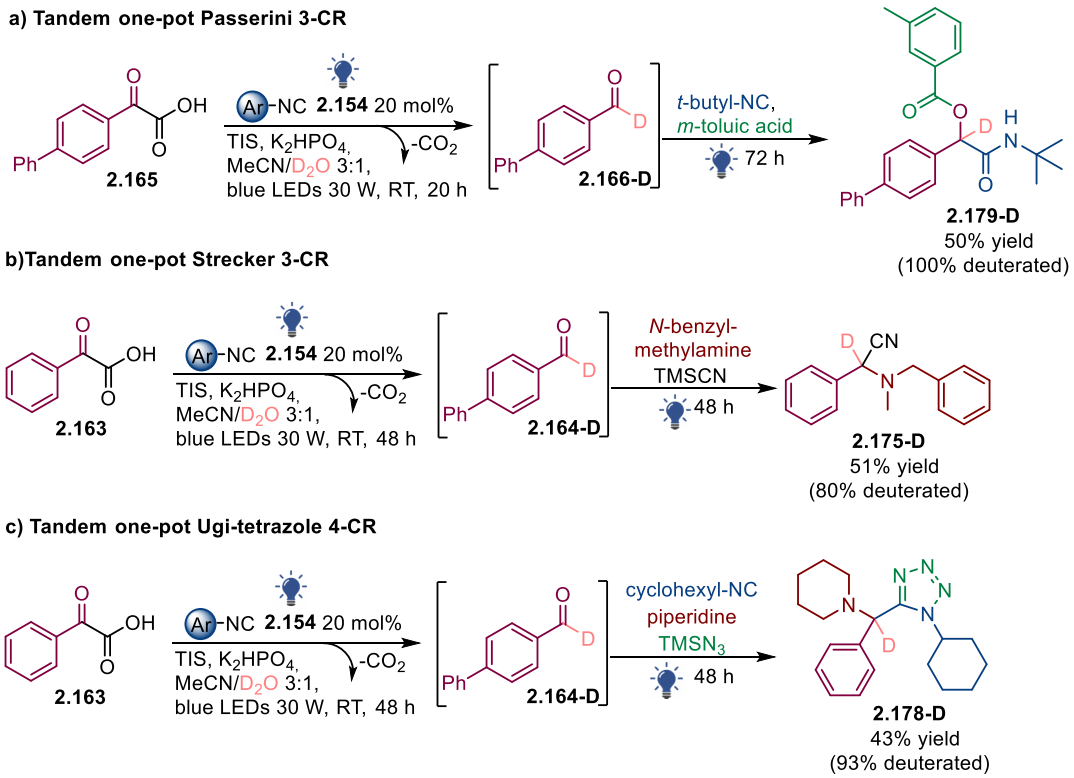

Scheme 2.22. Tandem one-pot isocyanide-promoted PET oxidation/D- abstraction/MCRs to D-labelled derivatives.

2.6. Domino synthesis of 5-aminoimidazoles from Strecker multicomponent adducts via ytterbium-promoted isocyanide insertion/5-*exo-dig* cyclisation

Besides carbene-like and somophile reactivities, a non-negligible part of isocyanides' chemistry relies on their ability to efficiently form metal complexes, thus setting the stage for a well-developed isocyanide organometallic chemistry field.[110] In a synthetic perspective, the possibility to exploit migratory insertions upon ligation to transition metals has recently received much attention, with most of the reported applications consisting of palladium-promoted imidoylative cross-couplings,[111] where isocyanides undergo 1,1-migratory insertion into either σ- or π-bonds (Scheme 2.23). Interesting transformations have also been reported under base metals catalysis.[112]

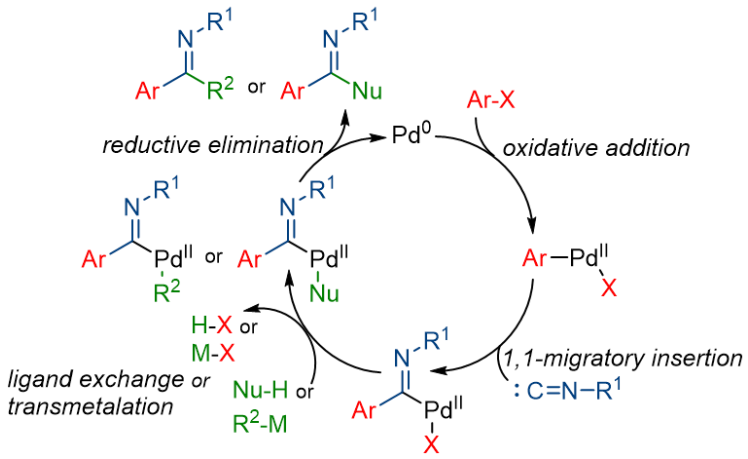

Scheme 2.23. Typical catalytic cycle for redox-neutral Pd-catalysed isocyanide 1,1-migratory insertion reactions.

These insertion pathways take advantage of the ability of isocyanides to act as strong two-electron donors and allow to modulate their reactivity depending on the nature of the coordinated metals. More in detail, coordination to electron-rich π-electron releasing elements (low-valent, Groups 6 and 7) enhances the isocyano-

nitrogen nucleophilicity, thus enabling *N*-alkylation to provide aminocarbyne species, in the presence of an electrophile (Figure 2.32).[113] σ-electron acceptors (Lewis acids, including Cu, Zn, Ag and lanthanides) as the metal centre, instead, confer a strong electrophilic character to the carbon atom of the isocyanide and make it susceptible to nucleophilic attack.

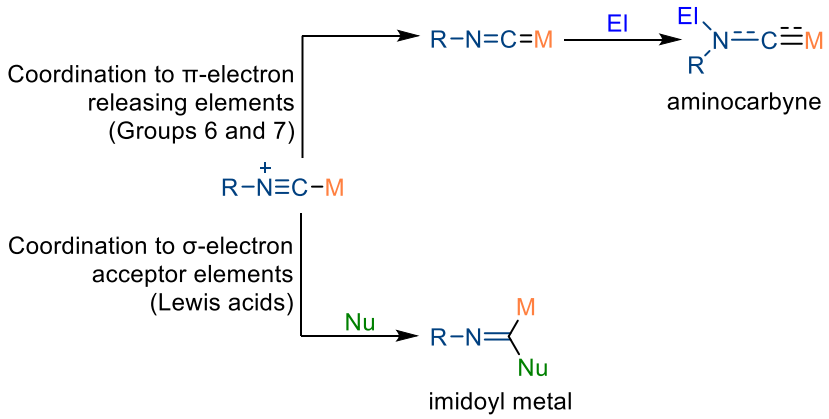

Figure 2.32. Isocyanides' reactivities upon ligation to metals.

In the presence of a nucleophile containing an electrophilic site, the nitrogen and the divalent carbon atom can therefore behave as nucleophilic and electrophilic centres, respectively, enabling the isocyanide to react *formally* as a polarised triple bond (Figure 2.33).

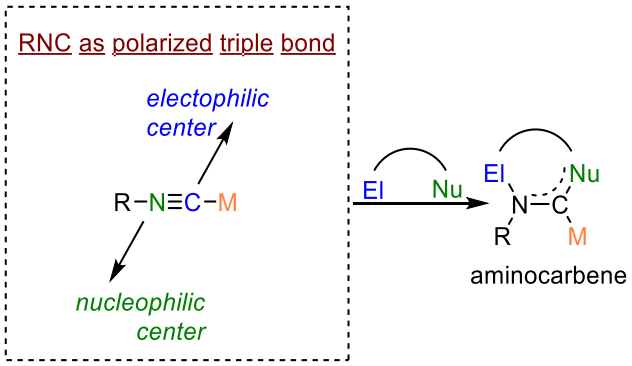

Figure 2.33. Isocyanide as polarised triple bond.

Accordingly, a sequence of nucleophilic addition to the ligated isocyano carbon atom followed by an intramolecular *N*-alkylation can take place, affording heterocyclic aminocarbene species.[114]

Prof. Zhu exploited such an approach to synthesise imidazoles and imidazolium salts **2.181** from isocyanides **2.41** and secondary propargylamines **2.180**, in the presence of an $Yb(OTf)_3$/AgOTf/KOTf multiple catalytic system, where $Yb(OTf)_3$ promoted the insertion of the isonitrile to the NH bond of the amine, AgOTf catalysed the 5-*exo-dig* cyclisation of the resulting amidine to the tethered triple bond, and KOTf promoted the salt metathesis, thereby providing at the same time the counterion to the imidazolium (Scheme 2.24a).[46] Interestingly, when primary propargylamines were employed, 5-*exo-dig* or 6-*endo-dig* cyclisation could alternatively take place, depending on the catalyst loading, leading to the formation of either imidazoles **2.182** or 1,6-dihydropyrimidines **2.183** (Scheme 2.24b).[48]

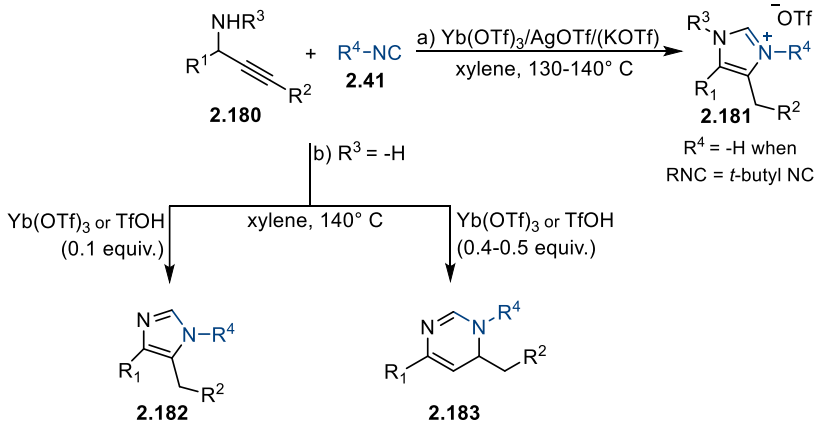

Scheme 2.24. Zhu's syntheses of imidazoles, imidazolium salts, and 6-dihydropyrimidines by reacting isocyanides as polarised triple bonds.

Inspired by such a transformation, we wondered whether readily available Strecker 3-component adducts of general structure **2.185** could be suitable amphoteric substrates for the Lewis acid-promoted heteroannulation of isocyanides **2.41** to 5-aminoimidazoles **2.186**.[115] Herein, both the isocyanide and the cyanide groups

would be engaged as polarised triple bonds in a domino sequence of (1) insertion of the isocyanide to the N–H bond of the amine and (2) 5-*exo-dig* cyclisation of the resulting amidine **I** onto the tethered nitrile (*path a,* Scheme 2.25). Alternatively, protodemetallation of the intermediate amidine **I** could take place, followed by Lewis acid activation of the nitrile group to facilitate the addition (*path b,* Scheme 2.25). A similar strategy may appear even more interesting if considering the poor availability of synthetic procedures to get 4-substituted-5-aminoimidazole derivatives,[116-118] notwithstanding the potential of this scaffold as useful intermediate for the synthesis of bioactive compounds.[119-121]

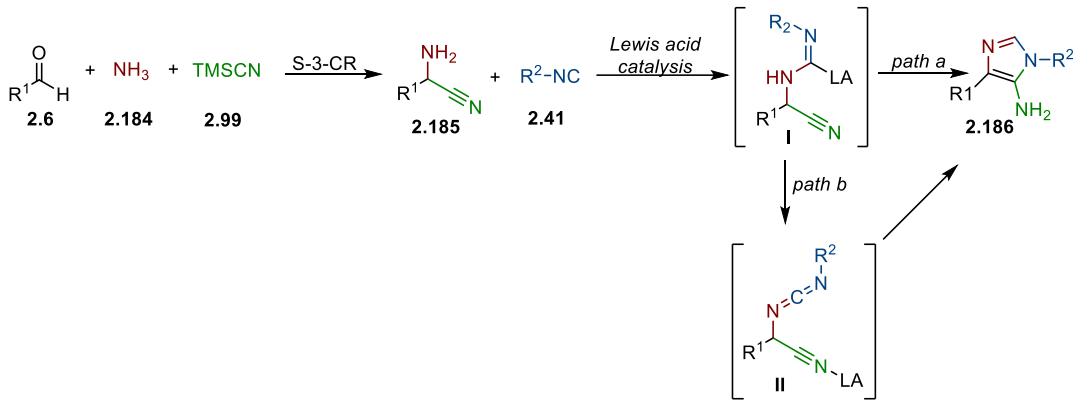

Scheme 2.25. Initial mechanistic design for the Lewis acid-promoted heteroannulation between isocyanides and Strecker adducts.

Optimisation of the reaction conditions

To initially assess the feasibility of our approach, Strecker adduct **2.187** and *tert*-butyl isocyanide **2.188** were selected as model substrates and reacted in the presence of 0.6 equivalents of $Yb(OTf)_3$ as the Lewis acid, in toluene, at 110 °C for 30 min. The desired 5-aminoimidazole **2.189** was recovered in a modest 45% yield (Table 2.15, Entry 1). Optimisation of the reaction conditions was therefore performed by changing the loading and the nature of the Lewis acid, temperature, heating method, solvent, and reaction time.

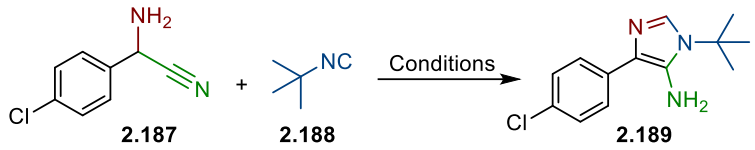

Entry	Catalyst (equiv.)	Temperature	Solvent	Time	2.189 Yield[a] (%)
1	$Yb(OTf)_3$ (0.6)	110° C	Toluene (0.2 M)	30 min	45[b]
2	$Yb(OTf)_3$ (0.4)	110° C	Toluene (0.2 M)	90 min	22
3	$Yb(OTf)_3$ (0.4)	130° C (MW)	Toluene (0.2 M)	10 min	35
4	$Yb(OTf)_3$/AgOTf (0.4/0.2)	110° C	Toluene (0.2 M)	90 min	17
5	$Pd(OAc)_2$ (0.4)	110° C	Toluene (0.2 M)	24 h	11
6	$Cu(OTf)_2$ (0.5)	110° C	Toluene (0.2 M)	90 min	ND
7	$ZnBr_2$ (0.5)	110° C	Toluene (0.2 M)	30 min	ND
8	$Sm(OTf)_3$ (0.5)	130° C (MW)	Toluene (0.2 M)	10 min	31
9	$La(OTf)_3$ (0.5)	130° C (MW)	Toluene (0.2 M)	10 min	3
10	$Y(OTf)_3$ (0.5)	130° C (MW)	Toluene (0.2 M)	10 min	29
11	$Yb(OTf)_3$ (0.6)	130° C (MW)	Toluene (0.6 M)	10 min	46[b]
12	$Yb(OTf)_3$ (0.5)	130° C (MW)	Toluene (0.6 M)	10 min	35
13	$Yb(OTf)_3$ (1)	RT	Toluene (0.6 M)	10 min	36
14	$Yb(OTf)_3$ (0.6)	130° C (MW)	Toluene (0.6 M)	10 min	ND
15	$Yb(OTf)_3$ (0.6)	130° C (MW)	1,4-dioxane (0.6 M)	10 min	7
16	$Yb(OTf)_3$ (0.6)	130° C (MW)	DMF (0.6 M)	10 min	ND
17	$Yb(OTf)_3$ (0.6)	130° C (MW)	DMSO (0.6 M)	10 min	ND
18	$Yb(OTf)_3$ (0.6)	130° C (MW)	DME (0.6 M)	10 min	58
19	$Yb(OTf)_3$ (0.6)	130° C (MW)	THF (0.6 M)	10 min	30
20	$Yb(OTf)_3$ (0.6)	130° C (MW)	2-Me THF (0.6 M)	10 min	77[b]

Conditions: reaction performed on a 0.3 mmol scale of **2.187**, in the presence of 2 equivalents **2.188**.
[a] NMR yield (determined by using TMB as internal standard)
[b] Isolated yield

Table 2.15. Optimisation of the reaction conditions for the Lewis acid-promoted heteroannulation between Strecker adducts and isocyanides.

Decreasing the equivalents of $Yb(OTf)_3$ to 0.4 while heating the mixture for 90 min halved the yield to 22% (Entry 2). Similarly, shorter reaction times under microwave (MW) irradiation were detrimental (Entry 3), as well as the addition of AgOTf, which led to a poor 17% yield (Entry 4). Different metal catalysts, such as $Pd(OAc)_2$, $Cu(OTf)_2$, $ZnBr_2$, $Y(OTf)_3$ (Entries 5–7, 10), including other lanthanides such as $Sm(OTf)_3$ and $La(OTf)_3$ (Entries 8–9) were not effective, while increasing

the loading of $Yb(OTf)_3$ to 0.6 equivalents and performing the reaction at higher concentration, at 130 °C, under MW irradiation gave product **2.189** in 46% yield (Entry 11). A further increase in the Lewis acid amount, as well as its decrease, did not improve reaction yields (Entries 12 and 13). On the other hand, heating proved to be essential to promote the transformation (Entry 14). Finally, a screening of different solvents (Entries 15–20) revealed that 2-Me THF was the most suitable one, affording the desired product in a good 77% isolated yield (Entry 20).

Substrate scope

With the optimised conditions in hand, the generality of the transformation was evaluated by reacting a range of differently substituted S-3-CR adducts with *tert*-butyl isocyanide. While the absence of any substituent on their aromatic ring did not change the yield (Figure 2.34, **2.190**), a halogen atom such as chlorine or fluorine at the *ortho*- (**2.191**, **2.192**) or *meta*-position (**2.193**) slightly decreased the yields to 46%–56%. The presence of two chlorine atoms, in both *meta*- and *para*-position led to a satisfying 54% yield (**2.194**), while the electron-withdrawing $–CF_3$ group at the *para*- position gave a moderate 31% yield (**2.195**). Electron-donor substituents were well tolerated (**2.196**–**2.198**), as well as polycyclic aromatic moieties (**2.199**, **2.200**). It is worth noting that such reaction yields were referred to a double domino process, *i.e.*, the insertion of the isocyanide to the N–H bond of the amine and the 5-*exo*-*dig* cyclisation of the resulting amidine onto the tethered nitrile. On the other hand, α-aminonitriles bearing aliphatic substituents as well as other secondary and tertiary aliphatic isocyanides such as cyclohexyl- and 1,1,3,3-tetramethylbutyl isocyanide failed to give the desired products (**2.201**–**2.204**). This is probably to be ascribed to well-known over-insertion/polymerisation issues of isocyanides affecting metal-catalysed cross-couplings).[122-124]

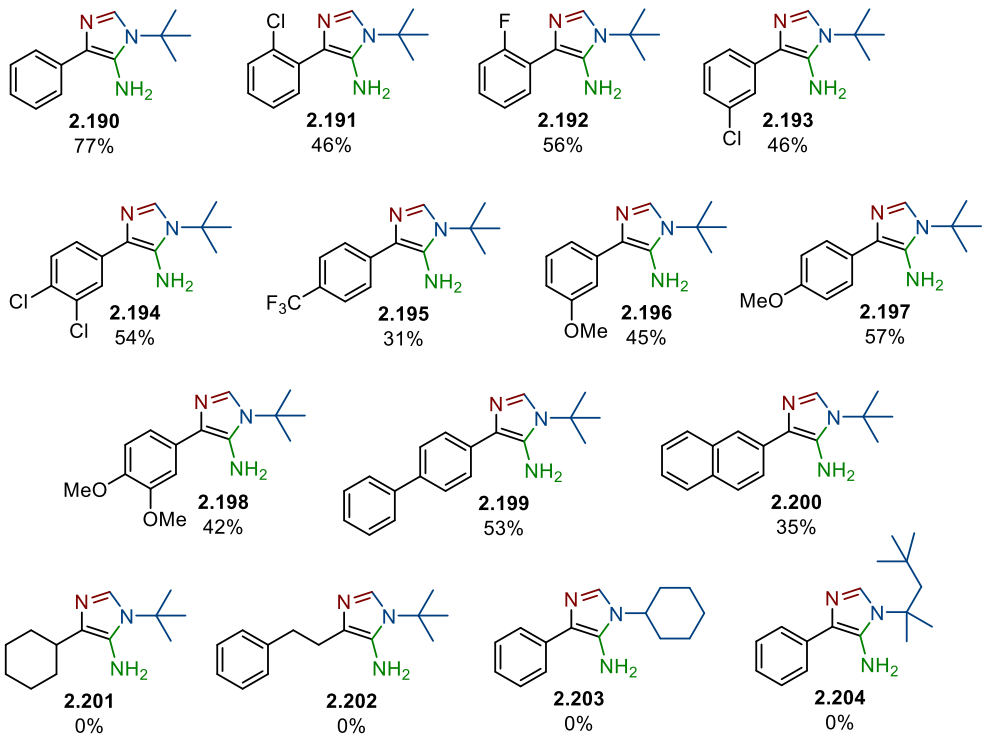

Figure 2.34. Substrate scope for Lewis acid-promoted heteroannulation between Strecker adducts and isocyanides.

Albeit the limitation in the isocyanide scope, the newly developed route to 4-subsituted-5-aminoimidazole derivatives offers a unique opportunity to gain access to such an elusive class of compounds in short times under MW irradiation, thus highlighting how the exploitation of isocyanides' unconventional reactivities could be an invaluable asset in the enrichment of the accessible chemical space.

Bibliography

(1) Russo, C.; Brunelli, F.; Cesare Tron, G.; Giustiniano, M.; *Chemistry – A European Journal* **2023**, *29*.
(2) Russo, C.; Brunelli, F.; Tron, G. C.; Giustiniano, M.; *European Journal of Organic Chemistry,* **2023**, *26.*
(3) Ohmoto, K.; Yamamoto, T.; Horiuchi, T.; Imanishi, H.; Odagaki, Y.; Kawabata, K.; Sekioka, T.; Hirota, Y.; Matsuoka, S.; Nakai, H.; Toda, M.; Cheronis, J. C.; Spruce, L. W.; Gyorkos, A.; Wieczorek, M.; *Journal of Medicinal Chemistry,* **2000**, *43*, 4927–4929.
(4) Warmus, J. S.; Flamme, C.; Zhang, L. Y.; Barrett, S.; Bridges, A.; Chen, H.; Gowan, R.; Kaufman, M.; Sebolt-Leopold, J.; Leopold, W.; Merriman, R.; Ohren, J.; Pavlovsky, A.; Przybranowski, S.; Tecle, H.; Valik, H.; Whitehead, C.; Zhang, E.; *Bioorganic and Medicinal Chemistry Letters,* **2008**, *18*, 6171–6174.
(5) McBriar, M. D.; Clader, J. W.; Chu, I.; Del Vecchio, R. A.; Favreau, L.; Greenlee, W. J.; Hyde, L. A.; Nomeir, A. A.; Parker, E. M.; Pissarnitski, D. A.; Song, L.; Zhang, L.; Zhao, Z.; *Bioorganic and Medicinal Chemistry Letters,* **2008**, *18*, 215–219.
(6) Boström, J.; Hogner, A.; Llinàs, A.; Wellner, E.; Plowright, A. T.; *Journal of Medicinal Chemistry,* **2012**, *55*, 1817–1830.
(7) Sun, S.; Jia, Q.; Zhang, Z.; *Bioorganic and Medicinal Chemistry Letters,* **2019**, *29*, 2535–2550.
(8) Frost, J. R.; Scully, C. C. G.; Yudin, A. K.; *Nature Chemistry,* **2016**, *8*, 1105–1111.
(9) Goldberg, K.; Groombridge, S.; Hudson, J.; Leach, A. G.; MacFaul, P. A.; Pickup, A.; Poultney, R.; Scott, J. S.; Svensson, P. H.; Sweeney, J.; *Medicinal Chemistry Communications,* **2012**, *3*, 600–604.
(10) Li, Z.; Zhan, P.; Liu, X.; *Mini-Reviews in Medicinal Chemistry,* **2011**, *11*, 1130–1142.
(11) Jakopin, Z.; Dolenc, M.; *Current Organic Chemistry,* **2008**, *12*, 850–898.
(12) Rajapakse, H. A.; Zhu, H.; Young, M. B.; Mott, B. T.; *Tetrahedron Letters,* **2006**, *47*, 4827–4830.
(13) Huisgen, R.; Sauer, J.; Sturm, H. J.; *Angewandte Chemie,* **1958**, *70*, 272–273.
(14) Ramazani, A.; Rezaei, A.; *Organic Letters,* **2010**, *12*, 2852–2855.
(15) Palacios, F.; Aparicio, D.; Rubiales, G.; Alonso, C.; De Los Santos, J.; *Current Organic Chemistry,* **2009**, *13*, 810–828.
(16) Vachhani, D. D.; Sharma, A.; Van der Eycken, E.; *Angewandte Chemie International Edition,* **2013**, *52*, 2547–2550.
(17) Wang, Q.; Mgimpatsang, K. C.; Konstantinidou, M.; Shishkina, S. V.; Dömling, A.; *Organic Letters,* **2019**, *21*, 7320–7323.
(18) Russo, C.; Cannalire, R.; Luciano, P.; Brunelli, F.; Tron, G. C.; Giustiniano, M.; *Synthesis,* **2021**, *53*, 4419–4427.
(19) Souldozi, A.; Ramazani, A.; *Tetrahedron Letters,* **2007**, *48*, 1549–1551.

(20) Reckenthäler, M.; Griesbeck, A. G.; *Advanced Synthesis and Catalysis,* **2013**, *355*, 2727–2744.
(21) Komaraiah, A.; Sailu, B.; Reddy, P. S. N.; *Synthetic Communications,* **2007**, *38*, 114–121.
(22) Zarei, M.; Nakhli, M. E.; *Research on Chemical Intermediates* **2017**, *43*, 1909–1918.
(23) Zareef M.; Iqbal R.; Mirza B.; Khan M. K.; Manan A.; Asim F.; Khan S. W.; *Arkivoc,* **2008**, *2*, 141–152.
(24) Cui, Z.; Huang, J.; Li, Y.; Ling, Y.; Yang, X.; Chen, F.; *Chinese Journal of Chemistry,* **2008**, *26*, 916–922.
(25) Prat, D.; Hayler, J.; Wells, A.; *Green Chemistry,* **2014**, *16*, 4546–4551.
(26) Prat, D.; Wells, A.; Hayler, J.; Sneddon, H.; McElroy, C. R.; Abou-Shehada, S.; Dunn, P. J.; *Green Chemistry* **2016**, *18*, 288–296.
(27) Rideout, D. C.; Breslow, R.; *Journal of the American Chemical Society,* **1980**, *102*, 7816–7817.
(28) Cortes-Clerget, M.; Yu, J.; Kincaid, J. R. A.; Walde, P.; Gallou, F.; Lipshutz, B. H.; *Chemical Science,* **2021**, *12*, 4237–4266.
(29) Narayan, S.; Muldoon, J.; Finn, M. G.; Fokin, V. V.; Kolb, H. C.; Sharpless, K. B.; *Angewandte Chemie International Edition,* **2005**, *44*, 3275–3279.
(30) Lipshutz, B. H.; Ghorai, S.; Cortes-Clerget, M.; *Chemistry – A European Journal,* **2018**, *24*, 6672–6695.
(31) Lipshutz, B. H.; Ghorai, S.; *Green Chemistry,* **2014**, *16*, 3660–3679.
(32) Myers, D.; *Surfactant Science and Technology*; **2005**, John Wiley & Sons, Inc., Hoboken.
(33) La Sorella, G.; Strukul, G.; Scarso, A.; *Green Chemistry,* **2015**, *17*, 644–683.
(34) Handa, S.; Wang, Y.; Gallou, F.; Lipshutz, B. H.; *Science,* **2015**, *349*, 1087–1091.
(35) Russo, C.; Brunelli, F.; Tron, G. C.; Giustiniano, M.; *The Journal of Organic Chemistry,* **2023**, *88*, 6284–6293.
(36) De Bruijn, A. D.; Roelfes, G.; *Chemistry – A European Journal,* **2018**, *24*, 12728–12733.
(37) Nguyen, T.-T. H.; O'Brien, C. J.; Tran, M. L. N.; Olson, S. H.; Settineri, N. S.; Prusiner, S. B.; Paras, N. A.; Conrad, J.; *Organic Letters,* **2021**, *23*, 3823–3827.
(38) Bu, M.; Cai, C.; Gallou, F.; Lipshutz, B. H.; *Green Chemistry,* **2018**, *20*, 1233–1237.
(39) Cannalire, R.; Santoro, F.; Russo, C.; Graziani, G.; Tron, G. C.; Carotenuto, A.; Brancaccio, D.; Giustiniano, M.; *ACS Organic and Inorganic Au;* **2022**, *2*, 66–74.
(40) Rueping, M.; Vila, C.; *Organic Letters,* **2013**, *15*, 2092–2095.
(41) Schönhoff, M.; *Current Opinion in Colloid and Interface Science,* **2013**, *18*, 201–213.

(42) Schneider, G. E.; Bolink, H. J.; Constable, E. C.; Ertl, C. D.; Housecroft, C. E.; Pertegàs, A.; Zampese, J. A.; Kanitz, A.; Kessler, F.; Meier, S. B.; *Dalton Transactions,* **2014**, *43*, 1961–1964.
(43) Saviello, M. R.; Malfi, S.; Campiglia, P.; Cavalli, A.; Grieco, P.; Novellino, E.; Carotenuto, A.; *Biochemistry,* **2010**, *49*, 1477–1485.
(44) Brown, L. R.; Bösch, C.; Wüthrich, K.; *Biochimica et Biophysica Acta (BBA) – Biomembranes,* **1981**, *642*, 296–312.
(45) Lindberg, M.; Jarvet, J.; Langel, Ü.; Gräslund, A.; *Biochemistry,* **2001**, *40*, 3141–3149.
(46) Tong, S.; Wang, Q.; Wang, M.; Zhu, J.; *Angewandte Chemie,* **2015**, *127*, 1309–1313.
(47) Tong, S.; Zhao, S.; He, Q.; Wang, Q.; Wang, M.; Zhu, J.; *Angewandte Chemie International Edition,* **2017**, *56*, 6599–6603.
(48) Tong, S.; Wang, Q.; Wang, M.; Zhu, J.; *Chemistry – A European Journal,* **2016**, *22*, 8332–8338.
(49) Wang, W.; Liu, T.; Ding, C.-H.; Xu, B.; *Organic Chemistry Frontiers,* **2021**, *8*, 3525–3542.
(50) Zhang, B.; Studer, A.; *Chemical Society Reviews,* **2015**, *44*, 3505–3521.
(51) Huang, W.; Wang, Y.; Weng, Y.; Shrestha, M.; Qu, J.; Chen, Y.; *Organic Letters* **2020**, *22*, 3245–3250.
(52) Lv, Y.; Bao, P.; Yue, H.; Li, J.-S.; Wei, W.; *Green Chemistry,* **2019**, *21*, 6051–6055.
(53) Bao, W.-H.; Wu, C.; Wang, J.-T.; Xia, W.; Chen, P.; Tang, Z.; Xu, X.; He, W.-M.; *Organic and Biomolecular Chemistry,* **2018**, *16*, 8403–8407.
(54) Lei, J.; Huang, J.; Zhu, Q.; *Organic and Biomolecular Chemistry,* **2016**, *14*, 2593–2602.
(55) Sharma, S.; Pandey, A. P.; Sharma, A.; *Advanced Synthesis and Catalysis,* **2020**, *362*, 5196–5218.
(56) Shono, T.; Kimura, M.; Ito, Y.; Nishida, K.; Oda, R.; *Bulletin of the Chemical Society of Japan,* **1964**, *37*, 635–637.
(57) Minozzi, M.; Nanni, D.; Spagnolo, P.; *Current Organic Chemistry,* **2007**, *11*, 1366–1384.
(58) Giles, J. R. M.; Roberts, B. P.; *Journal of the Chemical Society, Perkin Transactions 2,* **1983**, 6, 743–755.
(59) Li, Y.; Miao, T.; Li, P.; Wang, L.; *Organic Letters,* **2018**, *20*, 1735–1739.
(60) Crisenza, G. E. M.; Mazzarella, D.; Melchiorre, P.; *Journal of the American Chemical Society,* **2020**, *142*, 5461–5476.
(61) Foster, R.; *The Journal of Physical Chemistry,* **1980**, *84*, 2135–2141.
(62) Lima, C. G. S.; De M. Lima, T.; Duarte, M.; Jurberg, I. D.; Paixão, M. W.; *ACS Catalysis,* **2016**, *6*, 1389–1407.
(63) Tobisu, M.; Furukawa, T.; Chatani, N.; *Chemistry Letters,* **2013**, *42*, 1203–1205.

(64) Davies, J.; Booth, S. G.; Essafi, S.; Dryfe, R. A. W.; Leonori, D.; *Angewandte Chemie International Edition,* **2015**, *54*, 14017–14021.
(65) Arceo, E.; Jurberg, I. D.; Álvarez-Fernández, A.; Melchiorre, P.; *Nature Chemistry,* **2013**, *5*, 750–756.
(66) Cao, Z.-Y.; Ghosh, T.; Melchiorre, P.; *Nature Communications,* **2018**, *9*, 3274–3283.
(67) Russo, C.; Amato, J.; Tron, G. C.; Giustiniano, M.; *The Journal of Organic Chemistry,* **2021**, *86*, 18117–18127.
(68) Tsang, A. S. -K.; Hashmi, A. S. K.; Comba, P.; Kerscher, M.; Chan, B.; Todd, M. H.; *Chemistry – A European Journal,* **2017**, *23*, 9313–9318.
(69) Andrade-Sampedro, P.; Correa, A.; Matxain, J. M.; *The Journal of Organic Chemistry,* **2020**, *85*, 13133–13140.
(70) Hari, D. P.; König, B.; *Organic Letters,* **2011**, *13*, 3852–3855.
(71) Rueping, M.; Zhu, S.; Koenigs, R. M.; *Chemical Communications,* **2011**, *47*, 12709.
(72) Condie, A. G.; González-Gómez, J. C.; Stephenson, C. R. J.; *Journal of the American Chemical Society,* **2010**, *132*, 1464–1465.
(73) Rueping, M.; Zhu, S.; Koenigs, R. M.; *Chemical Communications,* **2011**, *47*, 8679–8681.
(74) Yagishita, F.; Nagamori, T.; Shimokawa, S.; Hoshi, K.; Yoshida, Y.; Imada, Y.; Kawamura, Y.; *Tetrahedron Letters,* **2020**, *61*, 151782.
(75) Chen, Y.; Feng, G.; *Organic and Biomolecular Chemistry,* **2015**, *13*, 4260–4265.
(76) Coppola, G. A.; Pillitteri, S.; Van der Eycken, E. V.; You, S.-L.; Sharma, U. K.; *Chemical Society Reviews,* **2022**, *51*, 2313–2382.
(77) Russo, C.; Graziani, G.; Cannalire, R.; Tron, G. C.; Giustiniano, M.; *Green Chemistry,* **2022**, *24*, 3993–4003.
(78) Neochoritis, C. G.; Zhao, T.; Dömling, A.; *Chemical Reviews,* **2019**, *119*, 1970–2042.
(79) Kubo, K.; Kohara, Y.; Yoshimura, Y.; Inada, Y.; Shibouta, Y.; Furukawa, Y.; Kato, T.; Nishikawa, K.; Naka, T.; *Journal of Medicinal Chemistry,* **1993**, *36*, 2343–2349.
(80) Holland, G. F.; Pereira, J. N.; *Journal of Medicinal Chemistry,* **1967**, *10*, 149–154.
(81) Nutt, R. F.; Joullie, M. M.; *Journal of the American Chemical Society,* **1982**, *104*, 5852–5853.
(82) Gazzotti, S.; Rainoldi, G.; Silvani, A.; *Expert Opinion on Drug Discovery,* **2019**, *14*, 639–652.
(83) Giustiniano, M.; Basso, A.; Mercalli, V.; Massarotti, A.; Novellino, E.; Tron, G. C.; Zhu, J.; *Chemical Society Reviews,* **2017**, *46*, 1295–1357.
(84) Banfi, L.; Guanti, G.; Riva, R.; *Chemical Communications,* **2000**, *11*, 985–986.
(85) Giovenzana, G. B.; Tron, G. C.; Di Paola, S.; Menegotto, I. G.; Pirali, T. A; *Angewandte Chemie International Edition,* **2006**, *45*, 1099–1102.

(86) Russo, C.; Donati, G.; Giustiniano, F.; Amato, J.; Marinelli, L.; Whitby, R. J.; Giustiniano, M.; *Chemistry – A European Journal* **2023**, *29,* e2023018.
(87) Reed, N. L.; Yoon, T. P.; *Chemical Society Reviews,* **2021**, *50*, 2954–2967.
(88) Casida M.E.; *Recent Advances in Density Functional Methods (Part I)*; **1995**, World Scientific Publishing, Singapore.
(89) Liang, W.; Fischer, S. A.; Frisch, M. J.; Li, X.; *Journal of Chemical Theory and Computation,* **2011**, *7*, 3540–3547.
(90) Maccoll, A.; *Nature,* **1949**, *163*, 178–179.
(91) Bieszczad, B.; Perego, L. A.; Melchiorre, P.; *Angewandte Chemie International Edition,* **2019**, *58*, 16878–16883.
(92) Gandolfo, E.; Tang, X.; Raha Roy, S.; Melchiorre, P.; *Angewandte Chemie International Edition,* **2019**, *58*, 16854–16858.
(93) Wang, P.-Z.; Chen, J.-R.; Xiao, W.-J.; *Organic and Biomolecular Chemistry,* **2019**, *17*, 6936–6951.
(94) Poronik, Y. M.; Sadowski, B.; Szychta, K.; Quina, F. H.; Vullev, V. I.; Gryko, D. T.; *Journal of Materials Chemistry C,* **2022**, *10*, 2870–2904.
(95) Chen, M.; Chen, D.; Chou, P.; *ChemPlusChem,* **2021**, *86*, 11–27.
(96) Tellis, J. C.; Primer, D. N.; Molander, G. A.; *Science,* **2014**, *345*, 433–436.
(97) Duan, K.; Yan, X.; Liu, Y.; Li, Z.; *Advanced Synthesis and Catalysis,* **2018**, *360*, 2781–2795.
(98) Matsui, J. K.; Lang, S. B.; Heitz, D. R.; Molander, G. A.; *ACS Catalysis,* **2017**, *7*, 2563–2575.
(99) Molander, G. A.; Sandrock, D. L.; *Current Opinion in Drug Discovery and Development,* **2009**, *12*, 811–823.
(100) Caronna, T.; Fronza, G.; Minisci, F.; Porta, O.; *Journal of the Chemical Society, Perkin Transactions 2,* **1972**, *14*, 2035–2038.
(101) Liu, J.; Liu, Q.; Yi, H.; Qin, C.; Bai, R.; Qi, X.; Lan, Y.; Lei, A.; *Angewandte Chemie International Edition,* **2014**, *53*, 502–506.
(102) Papadopoulos, G. N.; Limnios, D.; Kokotos, C. G.; *Chemistry – A European Journal,* **2014**, *20*, 13811–13814.
(103) Chu, L.; Lipshultz, J. M.; MacMillan, D. W. C.; *Angewandte Chemie International Edition,* **2015**, *54*, 7929–7933.
(104) Tan, H.; Li, H.; Ji, W.; Wang, L.; *Angewandte Chemie International Edition,* **2015**, *54*, 8374–8377.
(105) For an exhaustive review about acyl-transfer reactions involving α-keto acids see: Penteado, F.; Lopes, E. F.; Alves, D.; Perin, G.; Jacob, R. G.; Lenardão, E. J.; *Chemical Reviews,* **2019**, *119*, 7113–7278.
(106) Hu, C.-H.; Li, Y.; *The Journal of Organic Chemistry,* **2023**, *88*, 6401–6406.
(107) Wiberg, K. B.; *Chemical Reviews,* **1955**, *55*, 713–743.
(108) Pirali, T.; Serafini, M.; Cargnin, S.; Genazzani, A. A.; *Journal of Medicinal Chemistry,* **2019**, *62*, 5276–5297.

(109) Simmons, E. M.; Hartwig, J. F.; *Angewandte Chemie International Edition,* **2012**, *51*, 3066–3072.
(110) Singleton, E.; Oosthuizen, H. E.; *Advances in Organometallic Chemistry*, **1983**, *22* 209–310.
(111) Collet, J. W.; Roose, T. R.; Weijers, B.; Maes, B. U. W.; Ruijter, E.; Orru, R. V. A.; *Molecules,* **2020**, *25*, 4906–4957.
(112) Collet, J. W.; Roose, T. R.; Ruijter, E.; Maes, B. U. W.; Orru, R. V. A.; *Angewandte Chemie International Edition,* **2020**, *59*, 540–558.
(113) Pombeiro, A. J. L.; Guedes da Silva, M. F. C.; Michelin, R. A.; *Coordination Chemistry Reviews,* **2001**, *218*, 43–74.
(114) Michelin, R. A.; Pombeiro, A. J. L.; Guedes da Silva, M. F. C.; *Coordination Chemistry Reviews,* **2001**, *218*, 75–112.
(115) Cannalire, R.; Russo, C.; Luciano, P.; Cerra, B.; Gioiello, A.; Brunelli, F.; Tron, G. C.; Giustiniano, M.; *Molecular Diversity,* **2023**, *27*, 511–515.
(116) Wang, X.; Fu, J.; Mo, J.; Tian, Y.; Liu, C.; Tang, H.; Sun, Z.; Pan, Y.; *Advanced Synthesis and Catalysis,* **2021**, *363*, 2762–2766.
(117) Soh, C. H.; Chui, W. K.; Lam, Y.; *Journal of Combinatorial Chemistry,* **2006**, *8*, 464–468.
(118) Bell, C. E.; Shaw, A. Y.; De Moliner, F.; Hulme, C.; *Tetrahedron,* **2014**, *70*, 54–59.
(119) Svec, R. L.; Furiassi, L.; Skibinski, C. G.; Fan, T. M.; Riggins, G. J.; Hergenrother, P. J.; *ACS Chemical Biology,* **2018**, *13*, 3206–3216.
(120) Hergenrother P. J.; Fan T. M.; Svec R. L.; *Patent WO 2020033880*, **2020**.
(121) Hergenrother P. J.; Fan T. M.; Svec R. L.; *US Patent 20210002286*, **2021**.
(122) Millich, F.; *Chemical Reviews,* **1972**, *72*, 101–113.
(123) Wu, Z.-Q.; Ono, R. J.; Chen, Z.; Bielawski, C. W.; *Journal of the American Chemical Society,* **2010**, *132*, 14000–14001.
(124) Xue, Y.-X.; Zhu, Y.-Y.; Gao, L.-M.; He, X.-Y.; Liu, N.; Zhang, W.-Y.; Yin, J.; Ding, Y.; Zhou, H.; Wu, Z.-Q.; *Journal of the American Chemical Society,* **2014**, *136*, 4706–4713.

Experimental Section

General methods

Commercially available reagents and solvents were used without further purification.

Photochemical reactions were carried out using a PhotoRedOx Box (EvoluChem^{TM}) equipped with 30W blue LED (EvoluChem^{TM}, model: HCK1012-01-008, wavelength 450 nm, LED: CREE XPE). A holder suitable for 4 mL scintillation vials (45 x 14.7 mm) was fitted within the box so to allow a fixed distance of the samples from the light source.

Reactions requiring MW heating were performed by employing a microwave reactor Biotage Initiator 2.0, version 2.3, build 6250.

All reactions were routinely checked by thin-layer chromatography (TLC) on 5x20 cm plates with a layer thickness of 0.25 mm (silica gel 60 F_{254}), and monitored by using UV, $KMnO_4$, and/or ninhydrin as the revelation method. Preparative TLC separations were performed on 20x20 cm glass plates with a layer thickness of 0.50 mm (silica gel 60 F_{254}), employing the reported eluents. Column chromatography purifications were carried out on silica gel 60 (70–230 mesh ASTM) using the reported eluents.

All NMR spectra were recorded on Bruker Avance NEO 400, 600 or 700 MHz instruments. Experiments for structure elucidation were performed in the reported deuterated solvents, at 25° C, with a RT-DR-BF/1H-5-mm-OZ SmartProbe. Chemical shifts (δ) are reported in part per million (ppm) relative to the residual solvent peak; coupling constants (*J*), are reported in hertz (Hz).

High-resolution ESI-MS spectra were performed on a Thermo LTQ Orbitrap XL mass spectrometer. The spectra were recorded by infusion into the ESI source using MeOH as the solvent.

UV-VIS spectra were acquired on a Jasco J-730 UV-VIS spectrophotometer (Jasco, Japan) equipped with an ETCS-761 Peltier temperature controller. All spectra were recorded at 25° C and 100 nm/min scan speed, using sealed quartz cuvettes with a path length of 1 cm.

Fluorescence measurements were performed on a Jasco FP-8300 spectrofluorometer equipped with a PCT-818 Peltier temperature controller system (Jasco). All spectra were acquired at 25° C, using sealed quartz cuvettes with a path length of 1 cm, 100 nm/min scan speed, and 5 nm excitation and emission slit widths.

Cyclic voltammograms were recorded on a Metrohm Autolab PGSTAT101, using a glassy carbon working electrode and a SCE reference electrode, with a scan rate of 0.1 V/s.

2.1.

General procedure for the synthesis of 1,5-disubstituted-1,3,4-oxadiazole derivatives 2.17–2.34 via visible light photocatalytic Ugi/*aza*-Wittig cascade

The carboxylic acid **2.13** (0.08 mmol, 1 equiv.), (*N*-isocyanoimino)triphenylphosphorane **2.4** (0.16 mmol, 2 equiv.), the aniline derivative **2.12** (0.16 mmol, 2 equiv.), and $[Ru(bpy)_3]Cl_2 \cdot 6\ H_2O$ (0.0016 mmol, 2 mol%) were added to a 4 mL colourless glass vial equipped with a magnetic stir bar. The reaction components were dissolved in 800 µL of anhydrous MeCN (0.1 M) and 3 Å activated molecular sieves (80 mg) were added to the resulting mixture, which was stirred open to air in a PhotoRedOx Box, under 30W blue LED irradiation, at room temperature, for 20 h. After completion of the reaction, as monitored by TLC (DCM/EtOAc 9:1), the solvent was removed under vacuum and the crude mixture was purified as specified for each compound.

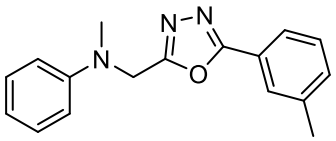

N-Methyl-*N*-{[5-(*m*-tolyl)-1,3,4-oxadiazol-2-yl]methyl}aniline (**2.17**). The crude material was purified by silica gel chromatography (*n*-hexane/EtOAc 97:3) to give the product as a yellow amorphous solid (14.9 mg, 67% yield). ^{1}H NMR (400 MHz, $CDCl_3$) δ 7.81 (s, 1H), 7.77 (d, J = 7.3 Hz, 1H), 7.39-7.27 (m, 4H), 6.95-6.90 (m, 2H), 6.81 (t, J = 7.3 Hz, 1H), 4.76 (s, 2H), 3.14 (s, 3H), 2.41 (s, 3H); ^{13}C {^{1}H} NMR (176 MHz, $CDCl_3$) δ 165.4, 163.8, 148.5, 138.9, 132.6, 129.3, 128.9, 127.5, 124.1, 123.6, 118.3, 113.3, 47.8, 39.0, 21.3; HRMS (ESI) *m/z:* calcd $[M + H]^+$ for $C_{17}H_{18}N_3O^+$ 280.1444; found $[M + H]^+$ 280.1446.

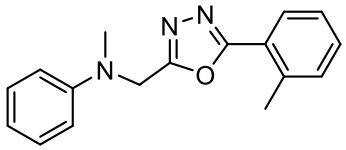

N-Methyl-*N*-{[5-(*o*-tolyl)-1,3,4-oxadiazol-2-yl]methyl}aniline (**2.18**) The crude material was purified by column chromatography (*n*-hexane/EtOAc 96:4) to give the product as an off-white amorphous solid (13.9 mg, 62% yield). ^{1}H NMR (700 MHz, $CDCl_3$) δ 7.80 (d, J = 7.8 Hz, 1H), 7.34 (t, J = 7.5 Hz, 1H), 7.26–7.20 (m, 4H), 6.87 (d, J = 8.4 Hz, 2H), 6.76 (t, J = 7.3 Hz, 1H), 4.74 (s, 2H), 3.09 (s, 3H), 2.55 (s, 3H); ^{13}C {^{1}H} NMR (176 MHz, $CDCl_3$) δ 165.5, 163.4, 148.4, 138.4, 131.7, 131.3, 129.3, 129.0, 126.1, 122.8, 118.3, 113.3, 47.6, 39.0, 22.0; HRMS (ESI) *m/z:* calcd $[M + H]^+$ for $C_{17}H_{18}N_3O^+$ 280.1444; found $[M + H]^+$ 280.1444.

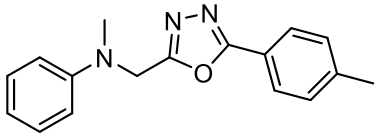

N-Methyl-*N*-{[5-(*p*-tolyl)-1,3,4-oxadiazol-2-yl]methyl}aniline (**2.19**). The crude material was purified by column chromatography (*n*-hexane/EtOAc 96:4) to give

the product as an off-white amorphous solid (14.4 mg, 64% yield). ^{1}H NMR (700 MHz, $CDCl_3$) δ 7.81–7.77 (m, 2H), 7.22–7.17 (m, 4H), 6.86–6.82 (m, 2H), 6.73 (t, J = 7.3 Hz, 1H), 4.68 (s, 2H), 3.06 (s, 3H), 2.33 (s, 3H); ^{13}C {^{1}H} NMR (176 MHz, $CDCl_3$) δ 165.4, 163.6, 148.5, 142.3, 129.7, 129.3, 126.9, 121.0, 118.3, 113.3, 47.7, 39.0, 21.6; HRMS (ESI) *m/z:* calcd $[M + H]^+$ for $C_{17}H_{18}N_3O^+$ 280.1444; found $[M + H]^+$ 280.1445.

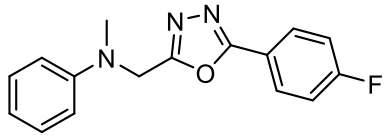

N-{[5-(4-Fluorophenyl)-1,3,4-oxadiazol-2-yl]methyl}-*N*-methyl aniline (**2.20**). The crude material was purified by column chromatography (*n*-hexane/EtOAc 97:3) to give the product as a colourless sticky solid (15.0 mg, 66% yield). ^{1}H NMR (400 MHz, $CDCl_3$) δ 7.98–7.91 (m, 2H), 7.27–7.22 (m, 2H), 7.16–7.09 (m, 2H), 6.87 (d, J = 8.1 Hz, 2H), 6.78 (t, J = 7.3 Hz, 1H), 4.72 (s, 2H), 3.09 (s, 3H); ^{13}C {^{1}H} NMR (100 MHz, $CDCl_3$) δ 164.9 (d, $J_{C\text{-}F}$ = 220 Hz), 164.4, 163.6, 148.5, 129.4, 129.2 (d, $J_{C\text{-}F}$ = 10.0 Hz), 120.0 (d, $J_{C\text{-}F}$ = 3.0 Hz), 118.4, 116.4 (d, $J_{C\text{-}F}$ = 20.0 Hz), 113.3, 47.7, 39.0; HRMS (ESI) *m/z:* calcd $[M + H]^+$ for $C_{16}H_{14}FN_3O^+$ 284.1194; found $[M + H]^+$ 284.1194.

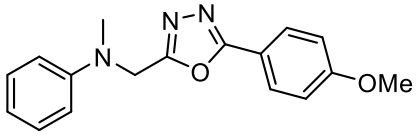

N-{[5-(4-Methoxyphenyl)-1,3,4-oxadiazol-2-yl]methyl}-*N*-methyl aniline (**2.21**). The crude material was purified by column chromatography (*n*-hexane/EtOAc 90:10) to give the product as pale-yellow amorphous solid (15.6 mg, 66% yield). ^{1}H NMR (700 MHz, $CDCl_3$) δ 7.93–7-88 (m, 2H), 7.30–7-25 (m, 2H), 7.00–6.95 (m, 2H), 6.93–6.88 (m, 2H), 6.81 (t, J = 7.3 Hz, 1H), 4.74 (s, 2H), 3.86 (s, 3H), 3.13 (s, 3H); ^{13}C {^{1}H} NMR (176 MHz, $CDCl_3$) δ 165.2, 163.4, 162.4, 148.5,

129.3, 128.7, 118.2, 116.2, 114.4, 113.3, 55.5, 47.7, 38.9; HRMS (ESI) *m/z:* calcd $[M + H]^+$ for $C_{17}H_{18}N_3O_2^+$ 296.1394; found $[M + H]^+$ 296.1391.

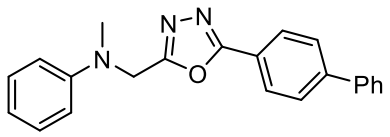

N-{[5-(1,1′-Biphenyl-4-yl)-1,3,4-oxadiazol-2-yl]methyl}-*N*-methyl aniline (**2.22**). The crude material was purified by column chromatography (*n*-hexane/EtOAc 95:5) to give the product as an off-white solid (17.9 mg, 65% yield). ^{1}H NMR (700 MHz, $CDCl_3$) δ 8.10–8.00 (m, 2H), 7.73–7.68 (m, 2H), 7.65–7.60 (m, 2H), 7.50–7.45 (m, 2H), 7.41 (d, J = 7.4 Hz, 1H), 7.32–7.28 (m, 2H), 6.97–6.92 (m, 2H), 6.83 (t, J = 7.3 Hz, 1H), 4.79 (s, 2H), 3.16 (s, 3H); ^{13}C {^{1}H} NMR (100 MHz, $CDCl_3$) δ 165.1, 163.9, 148.5, 144.6, 139.8, 122.4, 129.0, 128.2, 127.7, 127.4, 127.2, 122.5, 118.4, 113.4, 47.8, 39.0; HRMS (ESI) *m/z:* calcd $[M + H]^+$ for $C_{22}H_{20}N_3O^+$ 342.1601; found $[M + H]^+$ 342.1600.

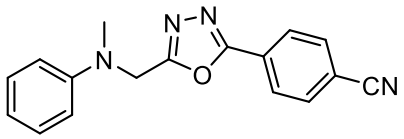

4-(5-{[Methyl(phenyl)amino]methyl}-1,3,4-oxadiazol-2-yl)benzo nitrile (**2.23**). The crude material was purified by column chromatography (*n*-hexane/EtOAc 93:7) to give the product as a colourless sticky solid (12.8 mg, 55% yield). ^{1}H NMR (700 MHz, $CDCl_3$) δ 8.10–8.00 (m, 2H), 7.76–7.71 (m, 2H), 7.25–7.20 (m, 2H), 6.89–6.83 (m, 2H), 6.78 (t, J = 7.3 Hz, 1H), 4.75 (s, 2H), 3.10 (s, 3H); ^{13}C {^{1}H} NMR (176 MHz, $CDCl_3$) δ 164.8, 163.7, 148.3, 132.8, 129.4, 127.6, 127.4, 118.6, 117.8, 115.3, 113.3, 47.8, 39.1; HRMS (ESI) *m/z:* calcd $[M + H]^+$ for $C_{17}H_{15}N_4O^+$ 291.1240; found $[M + H]^+$ 291.1240.

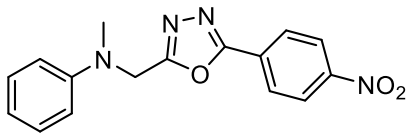

N-Methyl-*N*-{[5-(4-nitrophenyl)-1,3,4-oxadiazol-2-yl]methyl}aniline (**2.24**). The crude material was purified by column chromatography (*n*-hexane/EtOAc 90:10) to give the product as a yellow amorphous solid (9.5 mg, 38% yield). ^{1}H NMR (400 MHz, $CDCl_3$) δ 8.33–8.28 (m, 2H), 8.15–8.10 (m, 2H), 7.25–7.20 (m, 2H), 6.88–6.83 (m, 2H), 6.79 (t, J = 7.3 Hz, 1H), 4.76 (s, 2H), 3.10 (s, 3H); ^{13}C {^{1}H} NMR (100 MHz, $CDCl_3$) δ 165.0 163.5, 149.6, 148.3, 129.4, 129.2, 127.9, 124.4, 118.6, 113.4, 47.8, 39.1; HRMS (ESI) *m/z:* calcd $[M + H]^+$ for $C_{16}H_{15}N_4O_3^+$ 311.1139; found $[M + H]^+$ 311.1134.

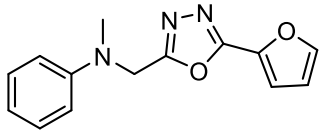

N-{[5-(2-Furyl)-1,3,4-oxadiazol-2-yl]methyl}-*N*-methylaniline (**2.25**). The crude material was purified by column chromatography (*n*-hexane/EtOAc 95:5) to give the product as a brownish amorphous solid (10.6 mg, 52% yield). ^{1}H NMR (400 MHz, $CDCl_3$) δ 7.60 (d, J = 1.2 Hz, 1H), 7.29–7.23 (m, 2H), 7.10 (d, J = 3.5 Hz, 1H), 6.90–6.85 (m, 2H), 6.80 (t, J = 7.3 Hz, 1H), 6.56 (dd, J_a = 3.5, J_b =1.8 Hz, 1H), 4.74 (s, 2H), 3.12 (s, 3H); ^{13}C {^{1}H} NMR (100 MHz, $CDCl_3$) δ 163.2, 158.1, 148.4, 145.7, 139.3, 129.3, 118.4, 114.2, 113.3, 112.1, 47.6, 39.0; HRMS (ESI) *m/z:* calcd $[M + H]^+$ for $C_{14}H_{14}N_3O_2^+$ 256.1081; found $[M + H]^+$ 256.1079.

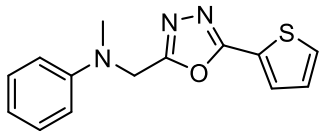

N-Methyl-*N*-{[5-(2-thienyl)-1,3,4-oxadiazol-2-yl]methyl}aniline (**2.26**). The crude material was purified by column chromatography (*n*-hexane/EtOAc 96:4) to give

the product as an off-white amorphous solid (14.8 mg, 68% yield). ^{1}H NMR (400 MHz, $CDCl_3$) δ 7.64 (dd, J_a = 3.7, J_b = 1.1 Hz, 1H), 7.49 (dd, J_a = 5.0, J_b =1.1 Hz, 1H), 7.25–7.20 (m, 2H), 7.10 (dd, J_a = 5.0, J_b = 3.8 Hz, 1H), 6.90–6.95 (m, 2H), 6.78 (t, J = 7.3 Hz, 1H), 4.70 (s, 2H), 3.09 (s, 3H); ^{13}C {^{1}H} NMR (100 MHz, $CDCl_3$) δ 163.3, 161.4, 148.5, 130.3, 129.9, 129.3, 128.1, 118.4, 113.4, 47.7, 39.0; HRMS (ESI) *m/z:* calcd $[M + H]^+$ for $C_{14}H_{14}N_3OS^+$ 272.0852; found $[M + H]^+$ 272.0851.

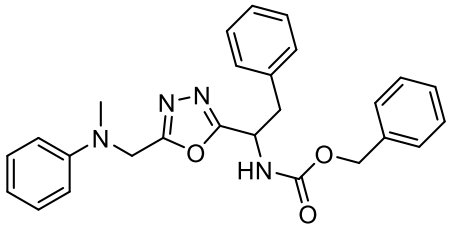

Benzyl[1-(5-{[methyl(phenyl)amino]methyl}-1,3,4-oxadiazol-2yl)-2-phenylethyl] carbamate (**2.27**). The crude material was purified by preparative TLC (*n*-hexane/Et_2O 20:80) to give the product as an off-white amorphous solid (14.9 mg, 42% yield). ^{1}H NMR (700 MHz, DMSO-d_6) δ 8.15 (d, J = 8.0 Hz, 1H), 7.35–7.30 (m, 3H), 7.27–7.21 (m, 2H), 7.21–7.17 (m, 5H), 7.15–7.10 (m, 2H), 6.83–6.78 (m, 2H), 6.71 (t, J = 7.1 Hz, 1H), 5.05–4.98 (m, 3H), 4.79 (s, 2H), 3.18 – 3.11 (m, 1H), 3.09 (d, J = 9.4 Hz, 1H), 2.98 (s, 3H); ^{13}C {^{1}H} NMR (176 MHz, DMSO-d_6) δ 166.8, 164.6, 156.0, 148.8, 137.2, 137.1, 129.6, 129.4, 128.8, 128.7, 117.8, 113.3, 66.0, 49.2, 46.8, 39.6, 38.0; HRMS (ESI) *m/z:* calcd $[M + H]^+$ for $C_{26}H_{27}N_4O_3^+$ 443.2078; found $[M + H]^+$ 443.2070.

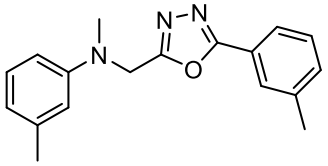

N,3-Dimethyl-*N*-{[5-(*m*-tolyl)-1,3,4-oxadiazol-2-yl]methyl}aniline (**2.28**). The crude material was purified by column chromatography (*n*-hexane/EtOAc 97:3) to

give the product as a yellow amorphous solid (15.0 mg, 64% yield). ^{1}H NMR (400 MHz, $CDCl_3$) δ 7.82 (s, 1H), 7.77 (d, J = 7.3 Hz, 1H), 7.40–7.30 (m, 2H), 7.17 (dd, J_a = 9.0, J_b = 7.5 Hz, 1H), 6.76 – 6.70 (m, 2H), 6.64 (d, J = 7.4 Hz, 1H), 4.74 (s, 2H), 3.12 (s, 3H), 2.41 (s, 3H), 2.33 (s, 3H); ^{13}C {^{1}H} NMR (100 MHz, $CDCl_3$) δ 165.4, 163.9, 148.6, 139.1, 138.9, 132.6, 129.2, 128.9, 127.5, 124.1, 123.6, 119.3, 114.1, 110.6, 47.8, 39.0, 21.9, 21.3; HRMS (ESI) *m/z:* calcd $[M + H]^+$ for $C_{18}H_{20}N_3O^+$ 294.1601; found $[M + H]^+$ 294.1610.

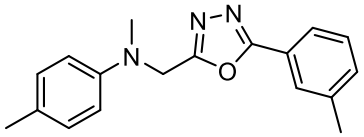

N,4-Dimethyl-*N*-{[5-(*m*-tolyl)-1,3,4-oxadiazol-2-yl]methyl}aniline (**2.29**). The crude material was purified by column chromatography (*n*-hexane/EtOAc 97:3) to give the product as an orange amorphous solid (15.0 mg, 64% yield). ^{1}H NMR (400 MHz, $CDCl_3$) δ 7 7.81 (s, 1H), 7.77 (d, J = 7.3 Hz, 1H), 7.40–7.30 (m, 2H), 7.12–7.05 (m, 2H), 6.87–6.82 (m, 2H), 4.72 (s, 2H), 3.10 (s, 3H), 2.40 (s, 3H), 2.24 (s, 3H); ^{13}C {^{1}H} NMR (100 MHz, $CDCl_3$) δ 165.4, 164.0, 146.5, 138.9, 132.6, 129.9, 128.9, 127.8, 127.5, 124.1, 123.6, 113.8, 48.1, 39.2, 21.3, 20.3; HRMS (ESI) *m/z:* calcd $[M + H]^+$ for $C_{18}H_{20}N_3O^+$ 294.1601; found $[M + H]^+$ 294.1597.

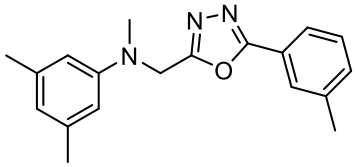

N,3,5-Trimethyl-*N*-{[5-(*m*-tolyl)-1,3,4-oxadiazol-2-yl]methyl}aniline (**2.30**). The crude material was purified by preparative TLC (DCM/EtOAc 90:10) to give the product as an off-white amorphous solid (16.7 mg, 68% yield). ^{1}H NMR (400 MHz, $CDCl_3$) δ 7.82 (s, 1H), 7.78 (d, J = 7.4 Hz, 1H), 7.39–7.30 (m, 2H), 6.55 (s, 2H), 6.48 (s, 1H), 4.73 (s, 2H), 3.11 (s, 3H), 2.41 (s, 3H), 2.29 (s, 6H); ^{13}C {^{1}H} NMR (100 MHz, $CDCl_3$) δ 165.3, 164.0, 148.7, 138.9, 138.89, 132.6, 128.9,127.5,

123.7, 120.4, 111.4, 47.8, 39.0, 21.7, 21.3; HRMS (ESI) *m/z:* calcd $[M + H]^+$ for $C_{19}H_{22}N_3O^+$ 308.1757; found $[M + H]^+$ 308.1755.

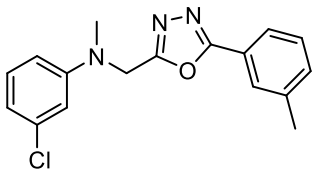

3-Chloro-*N*-methyl-*N*-{[5-(*m*-tolyl)-1,3,4-oxadiazol-2-yl]methyl}aniline (**2.31**). The crude material was purified by column chromatography (*n*-hexane/EtOAc 96:4) to give the product as a colourless sticky solid (6.6 mg, 23% yield). ^{1}H NMR (400 MHz, $CDCl_3$) δ 7.82 (s, 1H), 7.77 (d, J = 7.3 Hz, 1H), 7.38–7.32 (m, 2H), 7.17 (t, J = 8.1 Hz, 1H), 6.87 (t, J = 2.2 Hz, 1H), 6.80.6.75 (m, 2H), 4.75 (s, 2H), 3.13 (s, 3H), 2.42 (s, 3H); ^{13}C {^{1}H} NMR (100 MHz, $CDCl_3$) δ 165.5, 163.3, 149.6, 139.0, 135.2, 132.7, 130.3, 129.0, 127.5, 124.1, 123.5, 118.1, 113.2, 111.3, 47.5, 39.0, 21.3; HRMS (ESI) *m/z:* calcd $[M + H]^+$ for $C_{17}H_{17}ClN_3O^+$ 314.1055; found $[M + H]^+$ 314.1055.

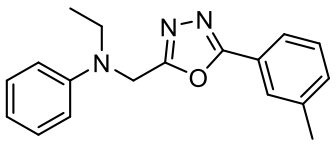

N-Ethyl-*N*-{[5-(*m*-tolyl)-1,3,4-oxadiazol-2-yl]methyl}aniline (**2.32**). The crude material was purified by preparative TLC (DCM/EtOAc 90:10) to give the product as an orange sticky solid (10.3 mg, 44% yield). ^{1}H NMR (400 MHz, $CDCl_3$) δ 7.82 (s, 1H), 7.77 (d, J = 7.3 Hz, 1H), 7.39–7.30 (m, 2H), 7.28–7.23 (m, 2H), 6.93–6.88 (m, 2H), 6.78 (t, J = 7.2 Hz, 1H), 4.73 (s, 2H), 3.57 (q, J = 7.1 Hz, 2H), 2.41 (s, 3H), 1.27 (t, J = 7.1 Hz, 3H); ^{13}C {^{1}H} NMR (100 MHz, $CDCl_3$) δ 165.4, 164.3, 147.4, 138.9, 132.6, 129.4, 128.9, 127.4, 124.1, 123.6, 117.8, 113.1, 45.6, 45.3, 21.3, 12.2; HRMS (ESI) *m/z:* calcd $[M + H]^+$ for $C_{18}H_{20}N_3O^+$ 294.1601; found $[M + H]^+$ 294.1601.

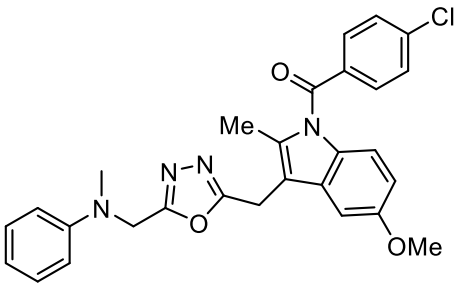

(4-Chlorophenyl){5-methoxy-2-methyl-3-[(5-{[methyl(phenyl)amino]methyl}-1,3,4-oxadiazol-2-yl)methyl]-1H-indol-1-yl}methanone (**2.33**). The crude material was purified by preparative TLC (DCM/EtOAc 90:10) to give the product as a yellow oil (12.5 mg, 31% yield). ^{1}H NMR (400 MHz, $CDCl_3$) δ 7.68–7.61 (m, 2H), 7.50–7.44 (m, 2H), 7.24–7.17 (m, 2H), 6.94 (d, J = 2.5 Hz, 1H), 6.84 (d, J = 9.0 Hz, 1H), 6.81–6.74 (m, 3H), 6.67 (dd, J_a = 9.0, J_b = 2.5 Hz, 1H), 4.61 (s, 2H), 4.19 (s, 2H), 3.78 (s, 3H), 3.02 (s, 3H), 2.37 (d, J = 8.1 Hz, 3H); ^{13}C {^{1}H} NMR (100 MHz, $CDCl_3$) δ 168.3, 165.2, 164.4, 156.2, 148.4, 139.5, 136.1, 133.7, 131.2, 130.8, 130.0, 129.3, 129.2, 118.3, 115.0, 113.2, 112.1, 111.8, 100.9, 55.7, 47.6, 38.8, 20.9, 13.2; HRMS (ESI) *m/z:* calcd $[M + H]^+$ for $C_{28}H_{26}ClN_4O_3^+$ 501.1688; found $[M + H]^+$ 501.1690.

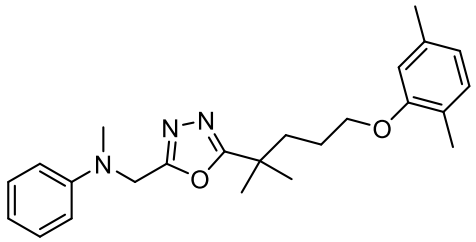

N-({5-[5-(2,5-Dimethylphenoxy)-2-methylpentan-2-yl]-1,3,4-oxadiazol-2-yl}methyl)-*N*-methylaniline (**2.34**). The crude material was purified by preparative TLC (DCM/EtOAc 95:5) to give the product as a pinkish oil (18.3 mg, 58% yield). ^{1}H NMR (400 MHz, $CDCl_3$) δ 7.20–7.26 (m, 2H), 7.00 (d, J = 7.4 Hz, 1H), 6.87–6.82 (m, 2H), 6.79 (t, J = 7.3 Hz, 1H), 6.66 (d, J = 7.4 Hz, 1H), 6.55 (s, 1H), 4.63 (s, 2H), 3.79 (t, J = 6.1 Hz, 2H), 3.04 (s, 3H), 2.31 (s, 3H), 2.16 (s, 3H), 1.85–1.78 (m, 2H), 1.63–1.57 (s, 2H), 1.38 (s, 6H); ^{13}C {^{1}H} NMR (100 MHz, $CDCl_3$) δ

172.8, 164.0, 156.8, 148.6, 136.5, 130.3, 129.2, 123.5, 120.8, 118.4, 113.5, 111.9, 67.4, 47.7, 38.9, 37.9, 35.6, 26.0, 24.8, 21.4, 15.8; HRMS (ESI) *m/z:* calcd $[M + H]^+$ for $C_{24}H_{32}N_3O_2^+$ 394.2489; found $[M + H]^+$ 394.2489.

Procedure for the tandem two-step one-pot photocatalytic synthesis of 3-methyl-*N′*-(*N*-methyl-*N*-phenylglycyl)benzohydrazide 2.35

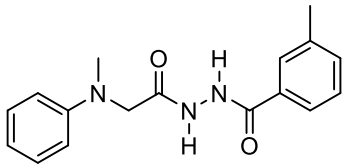

m-Toluic acid **2.16** (0.08 mmol, 1 equiv.), (*N*-isocyanoimino)triphenylphosphorane **2.4** (0.16 mmol, 2 equiv.), *N,N*-dimethylaniline **2.15** (0.16 mmol, 2 equiv.), and $[Ru(bpy)_3]Cl_2 \cdot 6\ H_2O$ (0.0016 mmol, 2 mol%) were added to a 4 mL colourless glass vial equipped with a magnetic stir bar. The reaction components were dissolved in 800 μL of anhydrous MeCN (0.1 M) and 3 Å activated molecular sieves (80 mg) were added to the resulting mixture, which was stirred open to air in a PhotoRedOx Box, under 30W blue LED irradiation, at room temperature, for 20 h. Then HCl 6 N (800 μL) was added and the mixture was stirred at room temperature for additional 20 h. After completion of the reaction, as monitored by TLC (DCM/EtOAc 8:2), the solvent was removed under vacuum and the crude mixture was purified by preparative TLC (DCM/EtOAc 8:2) to give the product as a dark yellow sticky solid (5.7 mg, 24% yield). ^{1}H NMR (400 MHz, DMSO-d_6) δ 10.29 (s, -N*H*), 10.02 (s, -N*H*), 7.69 (s, 1H), 7.67–7.62 (m, 1H), 7.39–7.33 (m, 2H), 7.20–7.15 (m, 2H), 6.77–6.70 (m, 2H), 6.65 (d, J = 7.3 Hz, 1H), 4.05 (s, 2H), 3.02 (s, 3H), 2.35 (s, 3H); ^{13}C {^{1}H} NMR (100 MHz, DMSO-d_6) δ 169.8, 166.0, 149.7, 138.2, 132.9, 132.8, 129.3, 128.8, 128.5, 125.0, 116.8, 112.6, 54.5, 21.4; HRMS (ESI) *m/z:* calcd $[M + H]^+$ for $C_{17}H_{20}N_3O_2^+$ 298.1550; found $[M + H]^+$ 298.1547.

2.2.

Starting materials

Procedure for the synthesis of (1*R*,4*aR*,4*bR*,10*aR*)-*N*-(4-(dimethylamino)benzyl)-7-isopropyl-1,4a-dimethyl-1,2,3,4,4a,4b,5,6,10,10a-decahydrophenanthrene-1-carboxamide

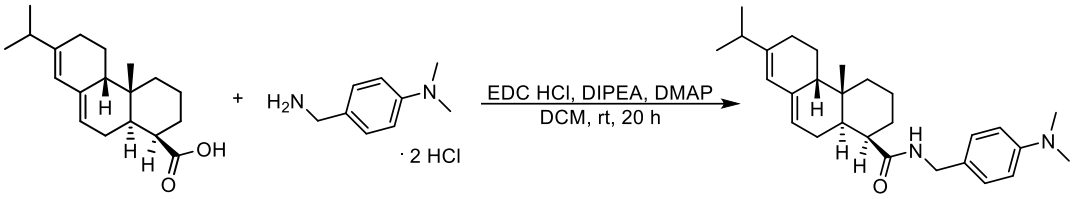

The title compound was prepared by reacting 4-(dimethylamino)benzylamine dihydrochloride (1.5 mmol, 1 equiv.) with abietic acid (1.6 mmol, 1.1 equiv.) in the presence of EDC HCl (1.6 mmol, 1.1 equiv.), DIPEA (7.5 mmol, 5 equiv.), and DMAP (0.075 mmol, 5 mol%) in DCM (10 mL, 0.15 M) at room temperature overnight. The crude material was purified by column chromatography (*n*-hexane/EtOAc 90:10 to 85:15) to give the product as an amorphous solid (131.0 mg, 20% yield). ^{1}H NMR (700 MHz, DMSO-d_6) δ 7.89 (t, J = 5.7 Hz, 1H), 7.05−7.00 (m, 2H), 6.68−6.63 (m, 2H), 5.71 (s, 1H), 5.30 (d, J = 5.1 Hz, 1H), 4.18−4.08 (m, 2H), 2.85 (s, 6H), 2.25−2.16 (m, 1H), 2.10−1.36 (m, 12H), 1.17 (s, 3H), 1.15−1.08 (m, 2H), 0.97 (dd, J_a = 6.8, J_b = 1.5 Hz, 6H), 0.76 (s, 3H); ^{13}C {^{1}H} NMR (176 MHz, DMSO-d_6) δ 177.7, 149.9, 144.7, 135.3, 128.4, 128.3, 122.9, 121.2, 112.8, 50.9, 45.8, 45.1, 42.4, 40.8, 38.2, 37.6, 34.7, 34.6, 27.4, 25.3, 22.4, 21.8, 21.2, 18.4, 17.4; HRMS (ESI) *m/z:* calcd $[M + H]^+$ for $C_{29}H_{43}N_2O^+$ 435.3369; found $[M + H]^+$ 435.3381.

Procedure for the synthesis of *N*-(4-(dimethylamino)benzyl)-5-(2,5-dimethylphenoxy)-2,2-dimethylpentanamide

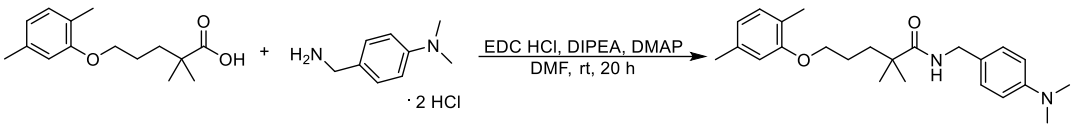

The title compound was prepared by reacting 4-(dimethylamino)benzylamine dihydrochloride (1.5 mmol, 1 equiv.) with gemfibrozil (1.6 mmol, 1.1 equiv.) in the presence of EDC HCl (1.6 mmol, 1.1 equiv.), DIPEA (7.5 mmol, 5 equiv.), and DMAP (0.075 mmol, 5 mol%) in DMF (2.5 mL, 0.6 M) at room temperature overnight. The crude material was diluted with brine and the product extracted with EtOAc (x5). The organic phase was further washed with brine solution (x5), dried over sodium sulfate, filtered, and evaporated under reduced pressure. The resulting mixture was purified by column chromatography (*n*-hexane/EtOAc 90:10 to 80:20) to give the product as an amorphous solid (93 mg, 16% yield). ^{1}H NMR (700 MHz, $CDCl_3$) δ 7.17−7.13 (m, 2H), 6.99 (d, J = 7.4 Hz, 1H), 6.73−6.68 (m, 2H), 6.66 (d, J = 7.5 Hz, 1H), 6.61 (s, 1H), 5.80 (brs, -N*H*), 4.34 (d, J = 5.3 Hz, 2H), 3.91 (t, J = 6.1 Hz, 2H), 2.94 (s, 6H), 2.30 (s, 3H), 2.15 (s, 3H), 1.80−1.73 (m, 2H), 1.72−1.69 (m, 2H), 1.22 (s, 6H). ^{13}C {^{1}H} NMR (176 MHz, $CDCl_3$) δ 177.1, 156.9, 136.5, 130.3, 128.9, 123.5, 120.7, 112.0, 68.0, 43.3, 41.9, 37.6, 25.6, 25.1, 21.4, 15.8. HRMS (ESI) *m/z:* calcd $[M + H]^+$ for $C_{24}H_{35}N_2O_2^+$ 383.5555; found $[M + H]^+$ 383.5572.

General procedure for the photomicellar catalysed synthesis of amide derivatives 2.44-2.61

The isocyanide **2.41** (0.3 mmol, 1 equiv.), the aniline derivative **2.12** (0.6 mmol, 2 equiv.), and $[Ir(ppy)_2bpy]PF_6$ (0.003 mmol, 1 mol%), were added to a 4 mL colourless glass vial equipped with a magnetic stir bar. Then 2 mL of the micellar solution (2% weight/ volume concentration, 0.15 M) were added into the reaction

vial, and the resulting mixture was stirred open to air in a PhotoRedOx Box, under 30W blue LED irradiation, at room temperature, for 48 h. After completion of the reaction, as monitored by TLC, the reaction mixture was extracted with EtOAc (x3), the collected organic layers were washed with brine (x1), dried over dry Na_2SO_4, filtered, and evaporated to dryness to give a reaction crude which was purified as specified for each compound.

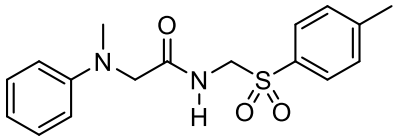

2-(Methyl(phenyl)amino)-*N*-(tosylmethyl)acetamide (**2.44**).[1] The crude material was purified by trituration with *n*-hexane/EtOAc (2:1) or column chromatography (*n*-hexane/EtOAc 8:2 to 5:5) to give the product as a white amorphous solid (74.8 mg, 75% yield). ^{1}H NMR (400 MHz, $CDCl_3$) δ 7.72 (d, J = 8.3 Hz, 2H), 7.37−7.26 (m, 5H), 6.89 (t, J = 7.3 Hz, -N*H*), 6.68 (d, J = 7.9 Hz, 2H), 4.69 (d, J = 6.9 Hz, 2H), 3.75 (s, 2H), 2.99 (s, 3H), 2.46 (s, 3H); ^{13}C {^{1}H} NMR (100 MHz, $CDCl_3$) δ 170.3, 149.0, 145.6, 133.8, 130.0, 129.5, 128.8, 119.3, 113.4, 59.8, 58.6, 40.1, 21.8; HRMS (ESI) *m/z:* calcd $[M + H]^+$ for $C_{17}H_{21}N_2O_3S^+$ 333.1267; found $[M + H]^+$ 333.1279.

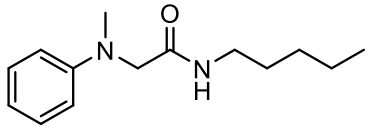

2-(Methyl(phenyl)amino)-*N*-pentylacetamide (**2.45**).[2] The crude material was purified by column chromatography (*n*-hexane/EtOAc 8:2 to 6:4) to give the product as a colourless oil (47.1 mg, 67% yield). ^{1}H NMR (400 MHz, $CDCl_3$) δ 7.31−7.23 (m, 2H), 6.84 (t, J = 7.3 Hz, 1H), 6.77−6−70 (m, 2H), 6.56 (brs, -N*H*), 3.85 (s, 2H), 3.27 (q, J = 9.4 Hz, 2H), 3.00 (s, 3H), 1.49−1.41 (m, 2H), 1.34−1.16 (m, 4H), 0.85 (t, J = 7.2 Hz, 3H); ^{13}C {^{1}H} NMR (100 MHz, $CDCl_3$) δ 170.2,

149.3, 129.4, 118.6, 113.1, 59.0, 39.7, 39.2, 29.3, 29.0, 22.3, 14.0; HRMS (ESI) *m/z:* calcd $[M + H]^+$ for $C_{14}H_{23}N_2O^+$ 235.1805; found $[M + H]^+$ 235.1808.

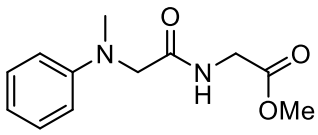

Methyl *N*-methyl-*N*-phenylglycylglycinate (**2.46**).[1] The crude material was purified by column chromatography (*n*-hexane/EtOAc 8:2 to 6:4) to give the product as a colourless oil (48.2 mg, 68% yield). ^{1}H NMR (400 MHz, $CDCl_3$) δ 7.31−7.25 (m, 2H), 7.05 (brs, -N*H*), 6.85 (t, J = 7.3 Hz, 1H), 6.81− 6.75 (m, 2H), 4.07 (d, J = 5.8 Hz, 2H), 3.91 (s, 2H), 3.73 (s, 3H), 3.04 (s, 3H); ^{13}C {^{1}H} NMR (100 MHz, $CDCl_3$) δ 171.1, 170.0, 149.3, 129.4, 118.9, 113.4, 58.8, 52.4, 40.8, 39.8; HRMS (ESI) *m/z:* calcd $[M + H]^+$ for $C_{17}H_{17}N_2O_3^+$ 237.1234; found $[M + H]^+$ 237.1243.

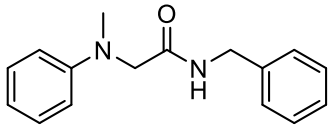

N-Benzyl-2-(methyl(phenyl)amino)acetamide (**2.47**).[1] The crude material was purified by column chromatography (*n*-hexane/EtOAc 8:2 to 6:4) to give the product as a colourless oil (57.2 mg, 75% yield). ^{1}H NMR (400 MHz, $CDCl_3$) δ 7.32−7.23 (m, 5H), 7.22−7.17 (m, 2H), 6.91 (brs, -N*H*), 6.84 (t, J = 7.3 Hz, 1H), 6.77−6.71 (m, 2H), 4.49 (d, J = 6.0 Hz, 2H), 3.92 (s, 2H), 3.00 (s, 3H); ^{13}C {^{1}H} NMR (100 MHz, $CDCl_3$) δ 170.4, 149.3, 138.0, 129.4, 128.7, 127.5, 127.5, 118.8, 113.3, 59.0, 43.1, 39.9; HRMS (ESI) *m/z:* calcd $[M + H]^+$ for $C_{16}H_{19}N_2O^+$ 255.1492; found $[M + H]^+$ 255.1504.

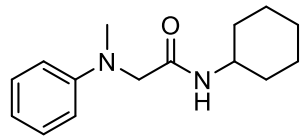

N-Cyclohexyl-2-(methyl(phenyl)amino)acetamide (**2.48**).[1] The crude material was purified by column chromatography (*n*-hexane/EtOAc 8:2 to 6:4) to give the product as a colourless oil (40.6 mg, 55% yield). ^{1}H NMR (400 MHz, $CDCl_3$) δ 7.31−7.23 (m, 2H), 6.84 (t, J = 7.3 Hz, 1H), 6.77−6−71 (m, 2H), 6.45 (brs, -N*H*), 3.86−3−81 (m, 3H), 2.99 (s, 3H), 1.90−1.80 (m, 2H), 1.72−1.53 (m, 4H), 1.40−1.34 (m, 2H), 1.17−0.99 (m, 2H); ^{13}C {^{1}H} NMR (100 MHz, $CDCl_3$) δ 169.3, 150.1, 129.4, 118.7, 113.3, 59.2, 47.8, 39.7, 33.0, 25.4, 24.8; HRMS (ESI) *m/z:* calcd $[M + H]^+$ for $C_{15}H_{23}N_2O^+$ 247.1805; found $[M + H]^+$ 247.1815.

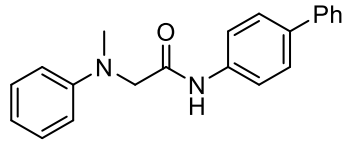

N-([1,1′-Biphenyl]-4-yl)-2-(methyl(phenyl)amino)acetamide (**2.49**). The crude material (reaction performed with 3 equivalents of *N,N*-dimethylaniline; reaction time: 72 h) was purified by column chromatography (*n*-hexane/EtOAc 8:2 to 6:4) to give the product as a pale-brown solid (75.9 mg, 80% yield). ^{1}H NMR (400 MHz, $CDCl_3$) δ 8.47 (brs, -N*H*), 7.63−7.58 (m, 2H), 7.58−7.53 (m, 4H), 7.45−7.40 (m, 2H), 7.36−7.29 (m, 2H), 6.91 (t, J = 7.3 Hz, 1H), 6.88−6.84 (m, 2H), 3.98 (s, 4H), 3.10 (s, 3H); ^{13}C {^{1}H} NMR (100 MHz, $CDCl_3$) δ 168.8, 149.5, 140.5, 137.5, 136.5, 129.6, 128.8, 127.6, 127.2, 126.9, 120.2, 119.5, 113.8, 60.1, 40.1; HRMS (ESI) *m/z:* calcd $[M + H]^+$ for $C_{21}H_{21}N_2O^+$ 317.1648; found $[M + H]^+$ 317.1662.

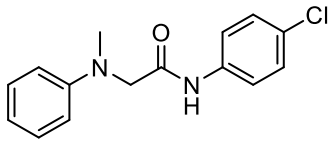

N-(4-Chlorophenyl)-2-(methyl(phenyl)amino)acetamide (**2.50**).[3] The crude material was purified by column chromatography (*n*-hexane/EtOAc 8:2 to 6:4) to give the product as a whitish solid; (67.6 mg, 82% yield). ^{1}H NMR (400 MHz, $CDCl_3$) δ 8.43 (brs, -N*H*), 7.52−7.44 (m, 2H), 7.35−7.26 (m, 4H), 6.91 (t, J = 7.3 Hz, 1H), 6.85−6.80 (m, 2H), 3.95 (s, 2H), 3.08 (s, 3H); ^{13}C {^{1}H} NMR (100 MHz, $CDCl_3$) δ 168.9, 149.6, 135.9, 129.4, 129.7, 129.2, 121.3, 119.7, 113.9, 60.2, 40.3; HRMS (ESI) *m/z:* calcd $[M + H]^+$ for $C_{15}H_{16}ClN_2O^+$ 275.0946; found $[M + H]^+$ 275.0955.

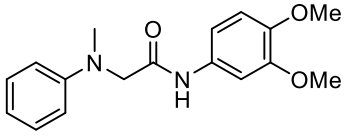

N-(3,4-Dimethoxyphenyl)-2-(methyl(phenyl)amino)acetamide (**2.51**). The crude material (reaction performed with 3 equivalents of *N,N*-dimethylaniline and $[Ir(ppy)_2bpy]PF_6$ 2 mol%; reaction time: 72 h) was purified by column chromatography (*n*-hexane/EtOAc 8:2 to 6:4) to give the product as a yellow solid; (76.6 mg, 85% yield). ^{1}H NMR (400 MHz, $CDCl_3$) δ 8.33 (brs, -N*H*), 7.35−7.28 (m, 3H), 6.93−6.87 (m, 2H), 6.86−6.82 (m, 2H), 6.79 (d, J = 8.6 Hz, 1H), 3.95 (s, 2H), 3.89 (s, 3H), 3.85 (s, 3H), 3.08 (s, 3H); ^{13}C {^{1}H} NMR (100 MHz, $CDCl_3$) 168.6, 149.7, 149.2, 146.2, 131.0, 129.6, 119.5, 113.9, 112.0, 111.4, 104.9, 60.2, 56.2, 56.1, 40.2; HRMS (ESI) *m/z:* calcd $[M + H]^+$ for $C_{17}H_{21}N_2O_3^+$ 301.1547; found $[M + H]^+$ 301.1556.

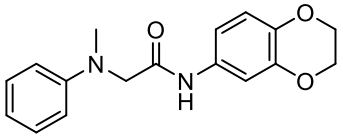

N-(2,3-Dihydrobenzo[*b*][1,4]dioxin-6-yl)-2-(methyl(phenyl)amino)acetamide (**2.52**). The crude material (reaction performed with 3 equivalents of *N,N*-dimethylaniline, $[Ir(ppy)_2bpy]PF_6$ 2 mol%; reaction time: 72 h) was purified by column chromatography (*n*-hexane/EtOAc 8:2 to 6:4) to give the product as a yellow solid; (78.8 mg, 88% yield). ^{1}H NMR (400 MHz, $CDCl_3$) δ 8.26 (brs, -N*H*), 7.33−7.27 (m, 2H), 7.17 (d, J = 2.5 Hz, 1H), 6.92−6.85 (m, 2H), 6.84−6.76 (m, 3H), 4.25−4.20 (m, 4H), 3.93 (s, 2H), 3.06 (s, 3H); ^{13}C {^{1}H} NMR (100 MHz, $CDCl_3$) δ 168.5, 149.6, 143.6, 140.8, 131.0, 129.6, 119.4, 117.3, 113.8, 113.7, 109.9, 64.5, 64.4, 60.0, 40.2; HRMS (ESI) *m/z:* calcd $[M + H]^+$ for $C_{17}H_{19}N_2O_3^+$ 299.1390; found $[M + H]^+$ 299.1399.

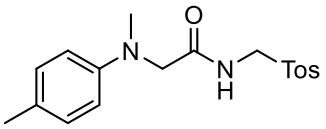

2-(Methyl(*p*-tolyl)amino)-*N*-(tosylmethyl)acetamide (**2.53**).[1] The crude material was purified by column chromatography (*n*-hexane/EtOAc 8:2 to 6:4) to give the product as a whitish solid; (81.0 mg, 78% yield). ^{1}H NMR (700 MHz, $CDCl_3$) δ 7.75−7.70 (m, 2H), 7.38 (brs, -N*H*), 7.36−7.32 (m, 2H), 7.12−7.07 (m, 2H), 6.65−6.55 (m, 2H), 4.69 (d, J = 6.8 Hz, 2H), 3.70 (s, 2H), 2.95 (s, 3H), 2.46 (s, 3H), 2.29 (s, 3H); ^{13}C {^{1}H} NMR (100 MHz, $CDCl_3$) δ 170.5, 147.0, 145.6, 133.8, 130.0, 129.9, 128.9, 128.8, 113.8, 59.8, 58.9, 40.4, 21.8, 20.3; HRMS (ESI) *m/z:* calcd $[M + H]^+$ for $C_{18}H_{23}N_2O_3S^+$ 347.1424; found $[M + H]^+$ 347.1435.

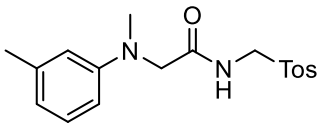

2-(Methyl(*m*-tolyl)amino)-*N*-(tosylmethyl)acetamide (**2.54**).[1] The crude material was purified by column chromatography (*n*-hexane/EtOAc 8:2 to 6:4) to give the product as a whitish solid; (79.0 mg, 76% yield). ^{1}H NMR (700 MHz, $CDCl_3$) δ 7.75−7.70 (m, 2H), 7.36−7.29 (m, 3H), 7.17 (t, J = 7.8 Hz, -N*H*), 6.71 (d, J = 7.1 Hz, 1H), 6.52 (s, 1H), 6.48 (d, J = 8.1 Hz, 1H), 4.68 (d, J = 6.8 Hz, 2H), 3.74 (s, 2H), 2.97 (s, 3H), 2.45 (s, 3H), 2.34 (s, 3H); ^{13}C {^{1}H} NMR (100 MHz, $CDCl_3$) δ 170.4, 149.1, 145.5, 139.4, 133.8, 130.0, 129.3, 128.8, 120.2, 114.2, 110.6, 59.9, 58.6, 40.1, 21.8, 21.8; HRMS (ESI) *m/z:* calcd $[M + H]^+$ for $C_{18}H_{23}N_2O_3S^+$ 347.1424; found $[M + H]^+$ 347.1437.

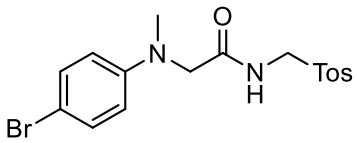

2-((4-Bromophenyl)(methyl)amino)-*N*-(tosylmethyl) acetamide (**2.55**).[4] The crude material was purified by column chromatography (*n*-hexane/EtOAc 8:2 to 6:4) to give the product as a whitish solid; (86.4 mg, 70% yield). ^{1}H NMR (700 MHz, $CDCl_3$) δ 7.76−7.72 (m, 2H), 7.40−7.30 (m, 4H), 7.18 (s, 2H), 6.55−6.50 (m, 2H), 4.69 (d, J = 6.8 Hz, 2H), 3.74 (s, 2H), 2.98 (s, 3H), 2.47 (s, 3H); ^{13}C {^{1}H} NMR (100 MHz, $CDCl_3$) δ 169.8, 147.9, 145.7, 133.7, 132.2, 130.1, 130.0, 128.8, 128.8, 115.0, 111.5, 59.8, 58.4, 40.2, 21.8; HRMS (ESI) *m/z:* calcd $[M + H]^+$ for $C_{17}H_{20}BrN_2O_3S^+$ 411.0373; found $[M + H]^+$ 411.0387.

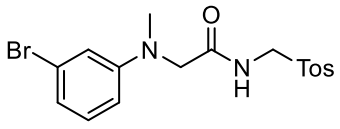

2-((3-Bromophenyl)(methyl)amino)-*N*-(tosylmethyl) acetamide (**2.56**).[1] The crude material was purified by trituration with *n*-hexane/EtOAc (2:1) to give the product

as a whitish solid; (90.1 mg, 73% yield). ^{1}H NMR (700 MHz, $CDCl_3$) δ 7.75− 7.70 (m, 2H), 7.38−7.33 (m, 2H), 7.17 (t, J = 6.6 Hz, -N*H*), 7.13 (t, J = 8.1 Hz, 1H), 7.00 (d, J = 7.8 Hz, 1H), 6.82 (s, 1H), 6.57 (dd, J_a = 8.3, J_b = 2.2 Hz, 1H), 4.68 (d, J = 6.8 Hz, 2H), 3.76 (s, 2H), 2.98 (s, 3H), 2.46 (s, 3H); ^{13}C {^{1}H} NMR (176 MHz, $CDCl_3$) δ 169.6, 150.2, 145.7, 133.7, 130.7, 130.1, 128.8, 123.7, 122.0, 116.6, 111.9, 59.8, 58.0, 39.9, 21.8; HRMS (ESI) *m/z:* calcd $[M + H]^+$ for $C_{17}H_{20}BrN_2O_3S^+$ 411.0373; found $[M + H]^+$ 411.0389.

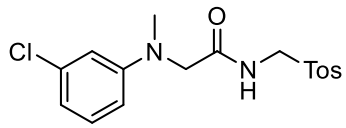

2-((3-Chlorophenyl)(methyl)amino)-*N*-(tosylmethyl)acetamide (**2.57**). The crude material was purified by trituration with *n*-hexane/EtOAc (2:1) to give the product as a pale-brown solid; (80.3 mg, 73% yield). ^{1}H NMR (700 MHz, $CDCl_3$) δ 7.75− 7.70 (m, 2H), 7.38−7.33 (m, 2H), 7.19 (t, J = 8.1 Hz, 1H), 7.14 (t, J = 6.5 Hz, -N*H*), 6.86 (dd, J_a = 7.9, J_b = 1.0 Hz, 1H), 6.65 (t, J = 2.0 Hz, 1H), 6.53 (dd, J_a = 8.4, J_b = 2.4 Hz, 1H), 4.69 (d, J = 6.8 Hz, 2H), 3.76 (s, 2H), 2.99 (s, 3H), 2.46 (s, 3H); ^{13}C {^{1}H} NMR (176 MHz, $CDCl_3$) δ 169.6, 150.0, 145.7, 135.4, 133.7, 130.5, 130.0, 128.8, 119.1, 113.3, 111.4, 59.8, 58.1, 40.0, 21.8; HRMS (ESI) *m/z:* calcd $[M + H]^+$ for $C_{17}H_{20}ClN_2O_3S^+$ 367.0878; found $[M + H]^+$ 367.0893.

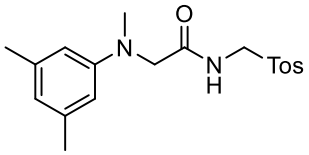

2-((3,5-Dimethylphenyl)(methyl)amino)-*N*-(tosylmethyl) acetamide (**2.58**).[1] The crude material was purified by trituration with *n*-hexane/EtOAc (2:1) to give the product as a whitish solid; (75.7 mg, 70% yield). ^{1}H NMR (700 MHz, $CDCl_3$) δ 7.74− 7.69 (m, 2H), 7.34−7.29 (m, 2H), 6.55 (s, 1H), 6.33 (s, 2H), 4.68 (d, J = 6.9 Hz, 2H), 3.73 (s, 2H), 2.95 (s, 3H), 2.45 (s, 3H), 2.30 (s, 6H); ^{13}C {^{1}H} NMR (100

MHz, $CDCl_3$) δ 169.5, 148.2, 144.5, 138.2, 132.9, 128.9, 127.8, 120.2, 110.4, 58.8, 57.6, 39.0, 20.8, 20.7; HRMS (ESI) *m/z:* calcd $[M + H]^+$ for $C_{19}H_{25}N_2O_3S^+$ 361.1580; found $[M + H]^+$ 361.1592.

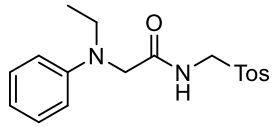

2-(Ethyl(phenyl)amino)-*N*-(tosylmethyl)acetamide (**2.59**).[1] The crude material was purified by column chromatography (*n*-hexane/EtOAc 8:2 to 6:4) to give the product as a white solid; (52.0 mg, 50% yield). ^{1}H NMR (400 MHz, $CDCl_3$) δ 7. 7.73−7.68 (m, 2H), 7.36−7.26 (m, 5H), 6.88 (*t*, J = 7.3 Hz, 1H), 6.70−6.65 (m, 2H), 4.67 (d, *J* = 6.9 Hz, 2H), 3.75 (s, 2H), 3.43 (q, *J* = 7.1 Hz, 2H), 2.47 (s, 3H), 1.19 (t, *J* = 7.1 Hz, 3H); ^{13}C {^{1}H} NMR (100 MHz, $CDCl_3$) δ 170.5, 147.4, 145.5, 133.9, 129.9, 129.6, 128.8, 119.0, 113.7, 59.9, 55.4, 46.5, 21.8, 11.5; HRMS (ESI) *m/z:* calcd $[M + H]^+$ for $C_{18}H_{23}N_2O_3S^+$ 347.4525; found $[M + H]^+$ 347.4534.

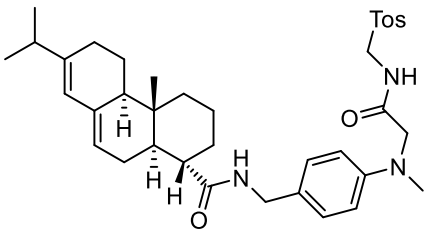

(1*R*,4*aR*,4*bR*,10*aR*)-7-Isopropyl-1,4a-dimethyl-*N*-(4-(methyl(2-oxo-2((tosylmethyl)amino)ethyl)amino)benzyl)-1,2,3,4,4*a*,4*b*,5,6,10,10*a*-decahydrophenanthrene-1-carboxamide (**2.60**). The crude material [reaction performed on a 0.15 mmol scale of isocyanide] was purified by column chromatography (*n*-hexane/EtOAc 8:2 to 5:5) to give the product as a white solid; (30.0 mg, 31% yield). ^{1}H NMR (400 MHz, $CDCl_3$) δ 7.75−7.70 (m, 2H), 7.36−7.31 (m, 2H), 7.20−7.15 (m, 2H), 6.65−6.60 (m, 2H), 5.94 (t, *J* = 5.0 Hz, -N*H*), 5.74 (s, 1H), 5.32 (d, *J* = 4.5 Hz, 1H), 4.68 (d, *J* = 6.9 Hz, 2H), 4.38 (d, *J* = 5.6 Hz, 1H), 4.31 (d, *J* = 5.1 Hz, 1H), 3.74 (s, 2H), 2.98 (s, 3H), 2.46 (s, 3H), 2.21 (s, 1H), 2.10−1.79 (m, 10H), 1.62−1.50 (m,

2H), 1.27−1.22 (m, 5H), 1.00 (dd, J_a = 6.8, J_b = 3.3 Hz, 6H), 0.82 (s, 3H); ^{13}C {^{1}H} NMR (100 MHz, $CDCl_3$) δ 178.2, 170.1, 148.4, 145.6, 145.3, 135.6, 133.8, 130.0, 129.4, 129.2, 128.8, 122.4, 120.4, 113.6, 59.9, 58.5, 51.0, 46.4, 45.7, 43.3, 40.1, 38.3, 37.7, 34.9, 34.7, 27.4, 25.4, 22.5, 21.8, 21.4, 20.8, 18.3, 17.1, 14.1; HRMS (ESI) *m/z:* calcd $[M + H]^+$ for $C_{38}H_{52}N_3O_4S^+$ 646.3673; found $[M + H]^+$ 646.3701.

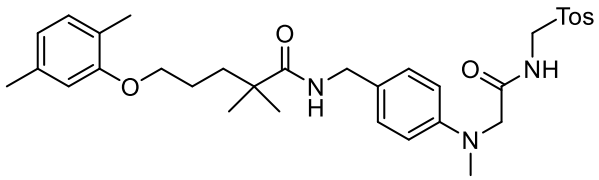

5-(2,5-Dimethylphenoxy)-2,2-dimethyl-N-(4-(methyl(2-oxo-2-((tosylmethyl)amino)ethyl)amino)benzyl)pentanamide (**2.61**). The crude material [reaction performed on a 0.12 mmol scale of isocyanide] was purified by column chromatography (*n*-hexane/EtOAc 8:2 to 5:5) to give the product as a colourless oil; (28.5 mg, 40% yield). ^{1}H NMR (400 MHz, $CDCl_3$) δ 7.73−7.68 (m, 2H), 7.36−7.27 (m, 3H), 7.20−7.15 (m, 2H), 6.99 (d, J = 7.4 Hz, 1H), 6.65−6.60 (m, 4H), 5.92 (t, J = 5.0 Hz, 1H), 4.66 (d, J = 6.9 Hz, 2H), 4.36 (d, J = 5.5 Hz, 2H), 3.91 (t, J = 5.7 Hz, 2H), 3.73 (s, 2H), 2.96 (s, 3H), 2.45 (s, 3H), 2.30 (s, 3H), 2.14 (s, 3H), 1.80−1.67 (m, 2H), 1.22 (s, 6H); ^{13}C {^{1}H} NMR (100 MHz, $CDCl_3$) δ 177.3, 170.1, 156.9, 148.4, 145.6, 136.5, 133.8, 130.3, 130.0, 129.3, 129.1, 128.8, 123.5, 120.8, 113.6, 112.1, 68.0, 59.9, 58.4, 43.0, 41.9, 40.1, 37.5, 25.6, 25.2, 21.8, 21.4, 15.8; HRMS (ESI) *m/z:* calcd $[M + H]^+$ for $C_{33}H_{44}N_3O_5S^+$ 594.2996; found $[M + H]^+$ 594.3016.

NMR spectroscopy studies of photocatalyst/surfactant interactions

The samples for NMR spectroscopy were prepared by dissolving the appropriate amount of $[Ir(ppy)_2bpy]PF_6$ in 540 µL of CTAC and SDS (either deuterated or not) 2% aqueous solutions and 60 µL of D_2O (pH 5.0) to obtain a concentration 1.5 mM of $[Ir(ppy)_2bpy]PF_6$. NMR experiments were recorded on a Bruker Avance NEO

600 MHz spectrometer equipped with a z-gradient 5 mm triple-resonance probe head. For interaction studies between the micelles $[Ir(ppy)_2bpy]PF_6$, DQF-COSY, TOCSY, and NOESY spectra were recorded in the phase-sensitive mode using the method from States. TOCSY experiments were acquired with a mixing time of 80 ms and a data block size of 4096 addresses in t_2 and 256 equidistant t_1 values. NOESY experiments were run with a mixing time of 500 ms. The proton, DQF-COSY, TOCSY, and NOESY spectra were processed and analysed with the Bruker TOPSPIN 4.1.1 software packages.

2.3.

General procedure for synthesis of amide derivatives 2.67-2.81 via the visible light self-catalysed reaction of aromatic isocyanides with *N,N*-dimethylanilines

The isocyanide (0.08, 1 equiv. mmol) and $Yb(OTf)_3$ (0.008 mmol, 0.1 equiv.) were added to a 4 mL colourless screw-cap glass vial equipped with a magnetic stir bar. 800 μL of dry MeCN (0.1 M), 14.4 μL of microfiltered water (0.8 mmol, 10 equiv.), and the aniline derivative (0.16 mmol, 2 equiv.) were then added into the reaction vial via a syringe. The resulting mixture was stirred open to air in a Photoredox box (EvoluChem), under 30W blue LED irradiation, at room temperature, until completion of the reaction, as monitored by TLC (specific reaction times are available for each compound). Then, the solvent was removed under vacuum and the crude mixture was purified by column chromatography.

Compounds **2.67**, **2.68**, and **2.72** structurally correspond to **2.49**, **2.50**, and **2.52**, respectively. We have decided to assign them different notations in order to differentiate the respective synthetic pathways.

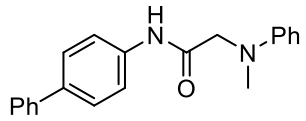

N-([1,1′-Biphenyl]-4-yl)-2-(methyl(phenyl)amino)acetamide (**2.67**). The crude material (reaction time: 20 h) was purified by column chromatography (*n*-hexane/EtOAc 97:3) to give the product as a light pink solid (23.0 mg, 91% yield; 62.6 mg, 23% yield when the reaction was performed on a 0.8 mmol scale, with a recovery of 51% of the starting isocyanide (reaction time: 5dd); 41% NMR yield when the reaction was performed on a 0.25 mmol scale, with 50% of unreacted 4-isocyanobiphenyl (reaction time: 5dd)). For NMR characterisation data see compound **2.49**; HRMS (ESI) *m/z*: calcd $[M + H]^+$ for $C_{21}H_{21}N_2O^+$ 317.1648; found [M + H]+ 317.1650.

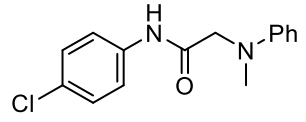

N-(4-Chlorophenyl)-2-(methyl(phenyl)amino)acetamide (**2.68**).[3] The crude material (reaction time: 20 h) was purified by column chromatography (*n*-hexane/EtOAc 97:3) to give the product as a whitish solid (16.7 mg, 76% yield). For NMR characterisation data see compound **2.50**; HRMS (ESI) m/z: calcd $[M + H]^+$ for $C_{15}H_{16}ClN_2O^+$ 275.0946; found $[M + H]^+$ 275.0943.

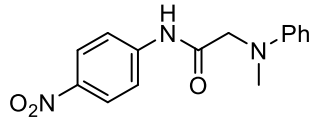

2-(Methyl(phenyl)amino)-N-(4-nitrophenyl)acetamide (**2.69**). The crude material (reaction performed without $Yb(OTf)_3$; reaction time: 5 days) was purified by column chromatography (*n*-hexane/EtOAc 94:6) to give the product as a yellow amorphous solid (11.5 mg, 50% yield). ^1H NMR (700 MHz, $CDCl_3$) δ 8.78 (brs, −N*H*), 8.21−8.20 (m, 2H), 7.73−7.72 (m, 2H), 7.32 (dd, J_a = 8.7, J_b = 7.4 Hz, 2H),

6.93 (t, J = 7.3 Hz, 1H), 6.84 (d, J = 8.1 Hz, 2H), 3.99 (s, 2H), 3.10 (s, 3H); ^{13}C {^{1}H} NMR (176 MHz, $CDCl_3$) δ 169.5, 149.3, 143.8, 142.9, 129.7, 125.1, 120.0, 119.3, 114.0, 60.3, 40.4; HRMS (ESI) *m/z*: calcd $[M + H]^+$ for $C_{15}H_{16}N_3O_3^+$ 286.1186; found $[M + H]^+$ 286.1185.

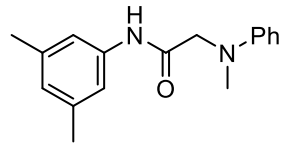

N-(3,5-Dimethylphenyl)-2-(methyl(phenyl)amino)acetamide (**2.70**). The crude material (reaction time: 20 h) was purified by column chromatography (*n*-hexane/EtOAc 97:3) to give the product as a brownish solid (20.7 mg, 96% yield). ^{1}H NMR (700 MHz, $CDCl_3$) δ 8.32 (brs, −N*H*), 7.32−7.29 (m, 2H), 7.16 (s, 2H), 6.90 (t, J = 7.3 Hz, 1H), 6.83 (d, J = 8.0 Hz, 2H), 6.77 (s, 1H), 3.94 (s, 2H), 3.07 (s, 3H), 2.29 (s, 6H); ^{13}C {^{1}H} NMR (101 MHz, $CDCl_3$) δ 168.5, 149.5, 138.8, 137.1, 129.5, 126.3, 119.4, 117.6, 113.7, 60.1, 40.0, 21.3; HRMS (ESI) *m/z*: calcd $[M + H]^+$ for $C_{17}H_{21}N_2O^+$ 269.1648; found [M + H]+ 269.1647.

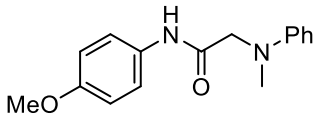

N-(4-Methoxyphenyl)-2-(methyl(phenyl)amino)acetamide (**2.71**).[5] The crude material (reaction time: 20 h) was purified by column chromatography (*n*-hexane/EtOAc 95:5) to give the product as a brown solid (19.6 mg, 91% yield). ^{1}H NMR (700 MHz, $CDCl_3$) δ 8.32 (brs, −N*H*), 7.43−7.41 (m, 2H), 7.32−7.29 (m, 2H), 6.89 (t, J = 7.4 Hz, 1H), 6.86−6.83 (m, 4H), 3.95 (s, 2H), 3.78 (s, 3H), 3.08 (s, 3H); ^{13}C {^{1}H} NMR (101 MHz, $CDCl_3$) δ 168.5, 156.7, 149.5, 130.4, 129.5, 121.8, 119.3, 114.2, 113.7, 59.9, 55.5, 40.1; HRMS (ESI) *m/z*: calcd $[M + H]^+$ for $C_{16}H_{19}N_2O_2^+$ 271.1441; found $[M + H]^+$ 271.1439

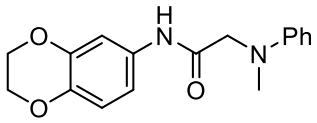

N-(2,3-Dihydrobenzo[*b*][1,4]dioxin-6-yl)-2-(methyl(phenyl)amino)-acetamide (**2.72**). The crude material (reaction time: 20 h) was purified by column chromatography (*n*-hexane/EtOAc 85:15) to give the product as a brownish solid (22.0 mg, 92% yield). For NMR characterisation data see compound **2.52**; HRMS (ESI) *m/z*: calcd $[M + H]^+$ for $C_{17}H_{19}N_2O_3^+$ 299.1390; found $[M + H]^+$ 299.1390.

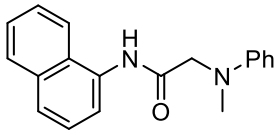

2-(Methyl(phenyl)amino)-*N*-(naphthalen-1-yl)acetamide (**2.73**). The crude material (reaction time: 20 h) was purified by column chromatography (*n*-hexane/EtOAc 96:4) to give the product as a brown solid (21.3 mg, 92% yield). ^{1}H NMR (400 MHz, $CDCl_3$) δ 8.96 (brs, −N*H*), 8.08 (d, J = 7.5 Hz, 1H), 7.84 (d, J = 8.1 Hz, 1H), 7.68 (d, J = 8.2 Hz, 1H), 7.49 (t, J = 7.9 Hz, 1H), 7.45−7.42 (m, 2H), 7.38−7.34 (m, 3H), 6.97−6.92 (m, 3H), 4.12 (s, 2H), 3.21 (s, 3H); ^{13}C {^{1}H} NMR (101 MHz, $CDCl_3$) δ 168.9, 149.3, 134.1, 131.7, 129.7, 128.8, 126.6, 126.4, 126.0, 125.8, 125.6, 120.0, 120.0, 119.6, 113.9, 59.9, 40.4; HRMS (ESI) *m/z*: calcd $[M + H]^+$ for $C_{19}H_{19}N_2O^+$ 291.1492; found $[M + H]^+$ 291.1489.

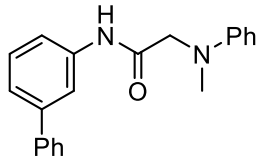

N-([1,1′-Biphenyl]-3-yl)-2-(methyl(phenyl)amino)acetamide (**2.74**). The crude material (reaction time: 20 h) was purified by column chromatography (*n*-hexane/EtOAc 98:2) to give the product as a reddish solid (23.5 mg, 93% yield). ^{1}H NMR (400 MHz, $CDCl_3$) δ 8.50 (brs, −N*H*), 7.73−7.72 (m, 1H), 7.59−7.55 (m,

3H), 7.44−7.40 (m, 3H), 7.38−7.29 (m, 5H), 6.91 (t, J = 7.3 Hz, 1H), 6.86 (d, J = 8.0 Hz, 2H), 3.98 (s, 2H), 3.10 (s, 3H); ^{13}C {^{1}H} NMR (101 MHz, $CDCl_3$) δ 168.8, 149.5, 142.2, 140.6, 137.7, 129.6, 129.4, 128.7, 127.5, 127.2, 123.4, 119.5, 118.8, 118.7, 113.8, 60.2, 40.1; HRMS (ESI) *m/z*: calcd $[M + H]^+$ for $C_{21}H_{21}N_2O^+$ 317.1648; found $[M + H]^+$ 317.1648.

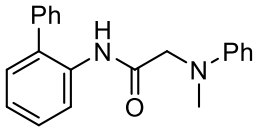

N-([1,1′-Biphenyl]-2-yl)-2-(methyl(phenyl)amino)acetamide (**2.75**). The crude material (reaction time: 20 h) was purified by column chromatography (*n*-hexane/EtOAc 98:2) to give the product as a reddish sticky solid (23.8 mg, 94% yield). ^{1}H NMR (400 MHz, $CDCl_3$) δ 8.65 (brs, −N*H*), 8.46 (d, J = 8.1 Hz, 1H), 7.33−7.29 (m, 1H), 7.18−7.04 (m, 7H), 7.00−6.98 (m, 2H), 6.77 (t, J = 7.3 Hz, 1H), 6.48 (d, J = 8.0 Hz, 2H), 3.74 (s, 2H), 2.58 (s, 3H); ^{13}C {^{1}H} NMR (101 MHz, $CDCl_3$) δ 168.6, 148.7, 137.6, 134.6, 131.9, 129.8, 129.2, 129.0, 128.8, 128.5, 127.6, 124.1, 119.9, 118.8, 113.2, 59.6, 39.4; HRMS (ESI) *m/z*: calcd $[M + H]^+$ for $C_{21}H_{21}N_2O^+$ 317.1648; found $[M + H]^+$ 317.1646.

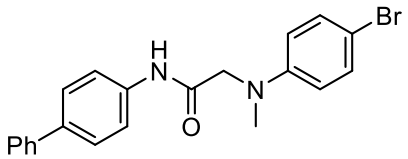

N-([1,1′-Biphenyl]-4-yl)-2-((4-bromophenyl)(methyl)amino) acetamide (**2.76**). The crude material (reaction time: 5 days) was purified by column chromatography (*n*-hexane/EtOAc 95:5) to give the product as an off-white solid (12.1 mg, 38% yield). ^{1}H NMR (700 MHz, $CDCl_3$) δ 8.31 (brs, −N*H*), 7.59−7.55 (m, 6H), 7.43 (t, J = 7.7 Hz, 2H), 7.40−7.38 (m, 2H), 7.33 (t, J = 7.4 Hz, 1H), 6.71 (d, J = 9.0 Hz, 2H), 3.96 (s, 2H), 3.09 (s, 3H); ^{13}C {^{1}H} NMR (176 MHz, $CDCl_3$) δ 168.2, 148.4, 140.4, 137.7, 136.3, 132.3, 128.8, 127.7, 127.2, 126.9, 120.2, 115.3, 111.8, 59.9, 40.3;

HRMS (ESI) *m/z*: calcd $[M + H]^+$ for $C_{21}H_{20}BrN_2O^+$ 395.0754; found $[M + H]^+$ 395.0753.

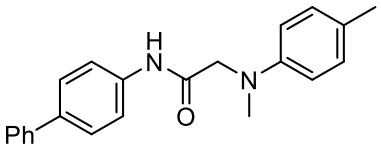

N-([1,1′-Biphenyl]-4-yl)-2-(methyl(*p*-tolyl)amino)acetamide (**2.77**). The crude material (reaction time: 48 h) was purified by column chromatography (*n*-hexane/EtOAc 97:3) and preparative TLC (100% DCM) to give the product as a light pink solid (12.1 mg, 46% yield). ^{1}H NMR (700 MHz, $CDCl_3$) δ 8.57 (brs, −N*H*), 7.61 (d, J = 8.6 Hz, 2H), 7.57−7.55 (m, 4H), 7.42 (t, J = 7.7 Hz, 2H), 7.33 (t, J = 7.4 Hz, 1H), 7.12 (d, J = 8.4 Hz, 2H), 6.77 (d, J = 8.5 Hz, 2H), 3.93 (s, 2H), 3.06 (s, 3H), 2.29 (s, 3H); ^{13}C {^{1}H} NMR (176 MHz, $CDCl_3$) δ 169.0, 147.4, 140.5, 137.4, 136.6, 130.0, 129.0, 128.8, 127.6, 127.2, 126.9, 120.2, 114.1, 60.5, 40.4, 20.3; HRMS (ESI) *m/z*: calcd $[M + H]^+$ for $C_{22}H_{23}N_2O^+$ 331.1805; found $[M + H]^+$ 331.1806.

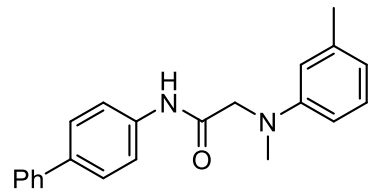

N-([1,1′-Biphenyl]-4-yl)-2-(methyl(*m*-tolyl)amino)acetamide (**2.78**). The crude material (reaction time: 48 h) was purified by column chromatography (*n*-hexane/EtOAc 98:2) to give the product as a light pink solid (16.9 mg, 64% yield). ^{1}H NMR (700 MHz, $CDCl_3$) δ 8.51 (brs, −N*H*), 7.62−7.61 (d, 2H), 7.57−7.56 (m, 4H), 7.43 (t, J = 7.7 Hz, 2H), 7.33 (t, J = 7.4 Hz, 1H), 7.22− 7.19 (m, 1H), 6.74 (d, J = 7.5 Hz, 1H), 6.67−6.66 (m, 2H), 3.97 (s, 2H), 3.08 (s, 3H), 2.35 (s, 3H); ^{13}C {^{1}H} NMR (176 MHz, $CDCl_3$) δ 168.9, 149.6, 140.5, 139.5, 137.5, 136.5, 129.4,

128.8, 127.7, 127.2, 126.9, 120.4, 120.2, 114.6, 111.0, 60.2, 40.1, 21.8; HRMS (ESI) *m/z*: calcd $[M + H]^+$ for $C_{22}H_{23}N_2O^+$ 331.1805; found $[M + H]^+$ 331.1806.

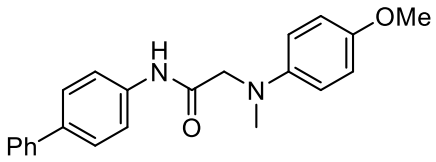

N-([1,1′-Biphenyl]-4-yl)-2-((4-methoxyphenyl)(methyl)-amino)acetamide (**2.79**). The crude material (reaction performed with 3 equivalents of 4-methoxy-*N,N*-dimethylaniline; reaction time: 48 h) was purified by column chromatography (*n*-hexane/EtOAc 95:5) to give the product as a dark green solid (10.5 mg, 38% yield). ^{1}H NMR (700 MHz, $CDCl_3$) δ 8.71 (brs, −N*H*), 7.63−7.62 (m, 2H), 7.57−7.56 (m, 4H), 7.43 (t, J = 7.7 Hz, 2H), 7.33 (t, J = 7.4 Hz, 1H), 6.89−6.88 (m, 2H), 6.84−6.82 (m, 2H), 3.88 (s, 2H), 3.78 (s, 3H), 3.02 (s, 3H); ^{13}C {^{1}H} NMR (176 MHz, $CDCl_3$) δ 169.0, 153.6, 144.0, 140.5, 137.4, 136.6, 128.8, 127.6, 127.1, 126.9, 120.1, 115.9, 114.9, 61.0, 55.7, 41.0; HRMS (ESI) *m/z*: calcd $[M + H]^+$ for $C_{22}H_{23}N_2O_2^+$ 347.1754; found $[M + H]^+$ 347.1750.

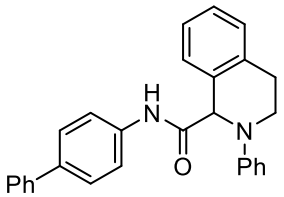

N-([1,1′-Biphenyl]-4-yl)-2-phenyl-1,2,3,4-tetrahydroisoquinoline-1-carboxamide (**2.80**). The crude material (reaction time: 48 h) was purified by column chromatography (*n*-hexane/EtOAc 98:2) to give the product as an off-white solid (24.0 mg, 74% yield). ^{1}H NMR (400 MHz, $CDCl_3$) δ 8.89 (brs, −N*H*), 7.69 (d, J = 7.2 Hz, 1H), 7.60−7.52 (m, 6H), 7.43 (t, J = 7.6 Hz, 2H), 7.39−7.27 (m, 5H), 7.21 (d, J = 7.1 Hz, 1H), 7.06 (d, J = 8.2 Hz, 2H), 6.98 (t, J = 7.3 Hz, 1H), 5.13 (s, 1H), 4.00−3.95 (m, 1H), 3.47−3.41 (m, 1H), 3.19−3.03 (m, 2H); ^{13}C {^{1}H} NMR (101 MHz, $CDCl_3$) δ 170.6, 149.4, 140.5, 137.3, 136.8, 134.5, 132.1, 129.6, 129.1,

128.7, 127.8, 127.7, 127.5, 127.1, 126.8 (3 C), 120.4, 120.1, 115.3, 66.4, 45.4, 28.8; HRMS (ESI) *m/z*: calcd $[M + H]^+$ for $C_{28}H_{25}N_2O^+$ 405.1961; found $[M + H]^+$ 405.1957.

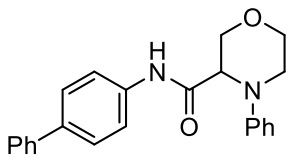

N-([1,1′-Biphenyl]-4-yl)-4-phenylmorpholine-3-carboxamide (**2.81**). The crude material (reaction time: 72 h) was purified by column chromatography (*n*-hexane/EtOAc 95:5) to give the product as a light purple solid (15.0 mg, 52% yield). ^{1}H NMR (700 MHz, $CDCl_3$) δ 8.17 (brs, −N*H*), 7.53 (d, J = 7.3 Hz, 2H), 7.50 (d, J = 8.5 Hz, 2H), 7.44 (d, J = 8.6 Hz, 2H), 7.41 (t, J = 7.7 Hz, 2H), 7.36−7.30 (m, 3H), 7.07 (d, J = 8.1 Hz, 2H), 7.00 (t, J = 7.3 Hz, 1H), 4.20−4.19 (m, 1H), 4.16−4.15 (m, 1H), 4.10−4.09 (m, 1H), 3.96−3.89 (m, 2H), 3.53−3.50 (m, 1H), 3.32−3.29 (m, 1H); ^{13}C {^{1}H} NMR (176 MHz, $CDCl_3$) δ 168.5, 149.6, 140.4, 137.5, 136.5, 129.9, 128.8, 127.6, 127.2, 126.9, 122.2, 120.2, 117.7, 67.7, 66.5, 62.0, 49.0; HRMS (ESI) *m/z*: calcd $[M + H]^+$ for $C_{23}H_{23}N_2O_2^+$ 359.1754; found $[M + H]^+$ 319.1754.

General procedure for the synthesis of amide derivatives 2.83, 2.85-2.96 via the visible light-promoted reaction of aliphatic isocyanides with *N,N*-dimethylanilines

The isocyanide (0.08 mmol, 1 equiv.), the aniline derivative (0.16 mmol, 2 equiv.), 800 μL of dry MeCN (0.1 M), and 14.4 μL of microfiltered water (0.8 mmol, 10 equiv.), were added to a 4 mL colourless screw-cap glass vial equipped with a magnetic stir bar. The resulting mixture was stirred open to air in a Photoredox box (EvoluChem), under 30W blue LED irradiation, at room temperature, until completion of the reaction, as monitored by TLC (specific reaction times are

available for each compound). Then, the solvent was removed under vacuum and the crude mixture was purified by column chromatography.

Compounds **2.83**, **2.85**, **2.86**, **2.90**, **2.91**, **2.92**, **2.93**, and **2.96** structurally correspond to **2.48**, **2.45**, **2.47**, **2.44**, **2.55**, **2.56**, **2.58**, and **2.59**, respectively. We have decided to assign them different notations in order to differentiate the respective synthetic pathways.

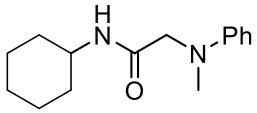

N-Cyclohexyl-2-(methyl(phenyl)amino)acetamide (**2.83**).[1] The crude material (reaction time: 72 h) was purified by column chromatography (*n*-hexane/EtOAc 9:1) to give the product as an off-white solid (10.4 mg, 53% yield). For NMR characterisation data see compound **2.48**; HRMS (ESI) *m/z*: calcd $[M + H]^+$ for $C_{15}H_{23}N_2O^+$ 247.1805; found $[M + H]^+$ 247.1804.

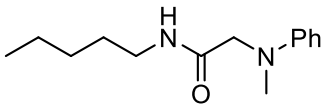

2-(Methyl(phenyl)amino)-*N*-pentylacetamide (**2.85**).[2] The crude material (reaction time: 48 h) was purified by column chromatography (*n*-hexane/EtOAc 9:1) to give the product as an off white amorphous solid (6.0 mg, 32% yield). For NMR characterisation data see compound **2.45**; HRMS (ESI) *m/z*: calcd $[M + H]^+$ for $C_{14}H_{23}N_2O^+$ 235.180; found $[M + H]^+$ 235.1808.

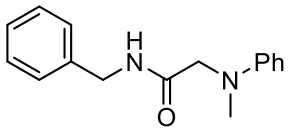

N-Benzyl-2-(methyl(phenyl)amino)acetamide (**2.86**).[1] The crude material (reaction time: 48 h) was purified by column chromatography (*n*-hexane/EtOAc 9:1) to give the product as a brownish solid (6.7 mg, 33% yield). For NMR characterisation data see compound **2.47**; HRMS (ESI) *m/z*: calcd $[M + H]^+$ for $C_{16}H_{19}N_2O^+$ 255.1492; found $[M + H]^+$ 255.1496.

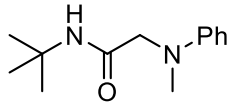

N-((Methyl(phenyl)amino)methyl)pivalamide (**2.87**).[1] The crude material (reaction time: 48 h) was purified by column chromatography (*n*-hexane/EtOAc 96:4) to give the product as an off white amorphous solid (6.9 mg, 39% yield). ^{1}H NMR (400 MHz, $CDCl_3$) δ 7.29−7.25 (m, 2H), 6.85 (t, J = 7.3 Hz, 1H), 6.74 (d, J = 8.0 Hz, 2H), 6.38 (brs, −N*H*), 3.73 (s, 2H), 2.98 (s, 3H), 1.33 (s, 9H); ^{13}C {^{1}H} NMR (176 MHz, $CDCl_3$) δ 169.6, 149.5, 129.3, 118.7, 113.4, 59.9, 50.9, 39.8, 28.7; HRMS (ESI) *m/z*: calcd $[M + H]^+$ for $C_{13}H_{21}N_2O^+$ 221.1648; found $[M + H]^+$ 221.1654.

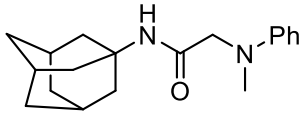

N-((3*s*,5*s*,7*s*)-Adamantan-1-yl)-2-(methyl(phenyl)amino) acetamide (**2.88**). The crude material (reaction time: 48 h) was purified by column chromatography (*n*-hexane/EtOAc 9:1) to give the product as an off-white solid (6.7 mg, 28% yield). ^{1}H NMR (400 MHz, $CDCl_3$) δ 7.29−7.25 (m, 3H), 6.84 (t, J = 7.3 Hz, 1H), 6.74 (d, J = 8.0 Hz, 2H), 6.25 (brs, −N*H*), 3.71 (s, 2H), 2.98 (s, 3H), 2.06 (s, 3H), 1.96 (d, J = 2.8 Hz, 6H), 1.67−1.65 (m, 6H); ^{13}C {^{1}H} NMR (101 MHz, $CDCl_3$) δ 169.2,

149.5, 129.3, 118.7, 113.4, 59.9, 51.6, 41.6, 39.7, 36.3, 29.4; HRMS (ESI) *m/z*: calcd $[M + H]^+$ for $C_{19}H_{27}N_2O^+$ 299.2118; found $[M + H]^+$ 299.2117.

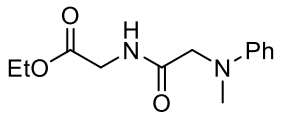

Ethyl *N*-Methyl-*N*-phenylglycylglycinate (**2.89**).[1] The crude material (reaction time: 48 h) was purified by column chromatography (*n*-hexane/EtOAc 85:15) to give the product as a yellow solid (19.6 mg, 98% yield). ^{1}H NMR (400 MHz, $CDCl_3$) δ 7.30− 7.26 (m, 2H), 7.05 (brt, −N*H*), 6.85 (t, J = 7.3 Hz, 1H), 6.78 (d, J = 8.1 Hz, 2H), 4.18 (q, J = 7.1 Hz, 2H), 4.06 (d, J = 5.7 Hz, 2H), 3.91 (s, 2H), 3.04 (s, 3H), 1.26 (t, J = 7.1 Hz, 3H); ^{13}C {^{1}H} NMR (101 MHz, $CDCl_3$) δ 171.0, 169.5, 149.4, 129.4, 118.8, 113.4, 61.5, 58.8, 41.0, 39.7, 14.1; HRMS (ESI) *m/z*: calcd $[M + H]^+$ for $C_{13}H_{19}N_2O_3^+$ 251.1390; found $[M + H]^+$ 251.1391.

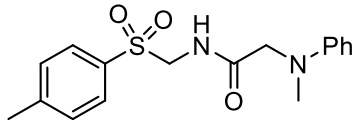

2-(Methyl(phenyl)amino)-*N*-(tosylmethyl)acetamide (**2.90**).[1] The crude material (reaction time: 20 h) was purified by column chromatography (*n*-hexane/EtOAc 85:15) to give the product as a white solid (17.8 mg, 67% yield). For NMR characterisation data see compound **2.44**; HRMS (ESI) *m/z*: calcd $[M + H]^+$ for $C_{17}H_{21}N_2O_3S^+$ 333.1267; found $[M + H]^+$ 333.1267.

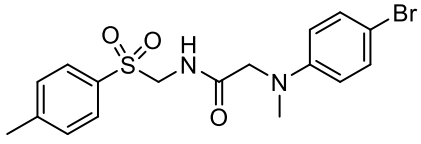

2-((4-Bromophenyl)(methyl)amino)-*N*-(tosylmethyl)acetamide (**2.91**).[6] The crude material (reaction time: 48 h) was purified by column chromatography (*n*-hexane/EtOAc 7:3) to give the product as an off-white solid (23.7 mg, 72% yield).

For NMR characterisation data see compound **2.55**; HRMS (ESI) *m/z*: calcd [M + H]$^+$ for $C_{17}H_{20}BrN_2O_3S^+$ 411.0373; found [M + H]$^+$ 411.0373.

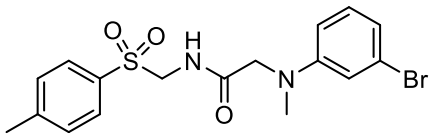

2-((3-Bromophenyl)(methyl)amino)-N-(tosylmethyl)acetamide (**2.92**).[1] The crude material (reaction time: 48 h) was purified by column chromatography (*n*-hexane/EtOAc 75:25) to give the product as a beige solid (29.5 mg, 90% yield). For NMR characterisation data see compound **2.56**; HRMS (ESI) *m/z*: calcd [M + H]$^+$ for $C_{17}H_{20}BrN_2O_3S^+$ 411.0373; found [M + H]$^+$ 411.0377.

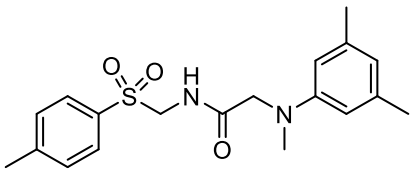

2-((3,5-Dimethylphenyl)(methyl)amino)-*N*-(tosylmethyl)-acetamide (**2.93**).[1] The crude material (reaction time: 48 h) was purified by column chromatography (*n*-hexane/EtOAc 8:2) to give the product as a beige sticky solid (18.1 mg, 63% yield). For NMR characterisation data see compound **2.58**; HRMS (ESI) *m/z*: calcd [M + H]$^+$ for $C_{19}H_{25}N_2O_3S^+$ 361.1580; found [M + H]$^+$ 361.1579.

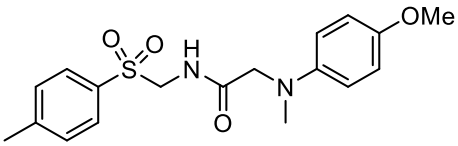

2-((4-Methoxyphenyl)(methyl)amino)-*N*-(tosylmethyl)acetamide (**2.94**).[5] The crude material (reaction time: 72 h) was purified by column chromatography (*n*-hexane/EtOAc 75:25) to give the product as a brownish sticky solid (6.8 mg, 23% yield). ^{1}H NMR (700 MHz, $CDCl_3$) δ 7.72 (d, J = 8.1 Hz, 2H), 7.53 (brt, −N*H*), 7.33 (d, J = 8.1 Hz, 2H), 6.85 (d, J = 9.0 Hz, 2H), 6.67 (d, J = 9.0 Hz, 2H), 4.70 (d,

J = 6.9 Hz, 2H), 3.78 (s, 3H), 3.65 (s, 2H), 2.91 (s, 3H), 2.45 (s, 3H); ^{13}C {^{1}H} NMR (176 MHz, $CDCl_3$) δ 170.5, 153.6, 145.6, 143.7, 133.8, 130.0, 128.8, 115.7, 114.8, 59.9, 59.6, 55.7, 41.1, 21.8; HRMS (ESI) *m/z*: calcd $[M + H]^+$ for $C_{18}H_{23}N_2O_4S^+$ 363.1373; found $[M + H]^+$ 363.1375.

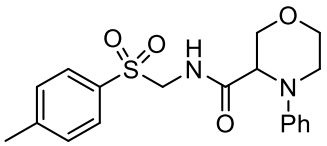

4-Phenyl-*N*-(tosylmethyl)morpholine-3-carboxamide (**2.95**). The crude material (reaction time: 72 h) was purified by column chromatography (*n*-hexane/EtOAc 75:25) to give the product as a white solid (9.0 mg, 30% yield). ^{1}H NMR (700 MHz, $CDCl_3$) δ 7.59 (d, *J* = 8.1 Hz, 2H), 7.33 (t, *J* = 7.8 Hz, 2H), 7.27 (d, *J* = 8.0 Hz, 2H), 7.02−6.99 (m, 2H), 6.91 (d, *J* = 8.3 Hz, 2H), 4.73−4.69 (m, 1H), 4.47−4.44 (m, 1H), 3.96−3.94 (m, 1H), 3.90−3.88 (m, 2H), 3.82−3.78 (m, 2H), 3.43−3.40 (m, 1H), 3.24−3. 21 (m, 1H), 2.43 (s, 3H); ^{13}C {^{1}H} NMR (176 MHz, $CDCl_3$) δ 170.1, 149.2, 145.4, 133.9, 129.9, 129.8, 128.7, 121.9, 117.1, 67.7, 66.5, 60.6, 59.9, 48.1, 21.8; HRMS (ESI) *m/z*: calcd $[M + H]^+$ for $C_{19}H_{23}N_2O_4S^+$ 375.1373; found $[M + H]^+$ 375.1375.

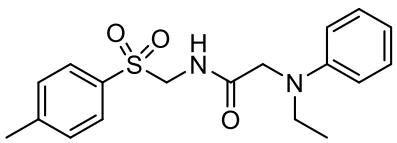

2-(Ethyl(phenyl)amino)-N-(tosylmethyl)acetamide (**2.96**).[1] The crude material (reaction time: 72 h) was purified by column chromatography (*n*-hexane/EtOAc 85:15) to give the product as a beige amorphous solid (8.3 mg, 30% yield). For NMR characterisation data see compound **2.59**; HRMS (ESI) *m/z*: calcd $[M + H]^+$ for $C_{18}H_{23}N_2O_3S^+$ 347.1424; found $[M + H]^+$ 347.1426.

General procedure for the synthesis of compounds 2.103, 2.104, and 2.107 via Michael-type additions promoted by 4-isocyanobiphenyl as the photocatalyst

The pro-nucleophile (0.08 mmol, 1 equiv.), *N*-phenyl-1,2,3,4-tetrahydroisoquinoline (0.16 mmol, 2 equiv.), and 800 μL of dry MeCN (0.1 M) were added to a 4 mL colourless screw-cap glass vial equipped with a magnetic stir bar. Then, 4-isocyanobiphenyl (0.016 mmol, 20% mol) was added to the resulting mixture, which was stirred open to air in a Photoredox box (EvoluChem), under 30W blue LED irradiation, at room temperature, for 20 h. After completion of the reaction, as monitored by TLC, the solvent was removed under vacuum and the crude mixture was purified by column chromatography.

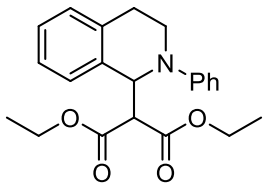

Diethyl 2-(2-phenyl-1,2,3,4-tetrahydroisoquinolin-1-yl)malonate (**2.103**).[7] The crude material was purified by column chromatography (*n*-hexane + Et_3N 0.1% *v/v*) to give the product as a yellowish sticky solid (11.7 mg, 40% isolated yield; NMR yield: 94%). ^1H NMR (400 MHz, $CDCl_3$) δ 7.30−7.08 (m, 6H), 6.98 (d, J = 8.1 Hz, 2H), 6.75 (t, J = 7.3 Hz, 1H), 5.72 (d, J = 9.1 Hz, 1H), 4.16−3.95 (m, 4H), 3.89 (d, J = 9.2 Hz, 1H), 3.71−3.62 (m, 2H), 3.11−3.03 (m, 1H), 2.91−2.85 (m, 1H), 1.17 (t, J = 7.1 Hz, 3H), 1.09 (t, J = 7.1 Hz, 3H); ^{13}C {^1H} NMR (176 MHz, $CDCl_3$) δ 168.0, 167.2, 148.9, 136.0, 134.83, 129.1, 128.9, 127.5, 127.2, 126.0, 118.5, 115.1, 61.6, 59.6, 57.9, 42.3, 26.1, 13.9, 13.9; HRMS (ESI) *m/z*: calcd $[M + H]^+$ for $C_{22}H_{26}NO_4^+$ 368.1856; found $[M + H]^+$ 368.1856.

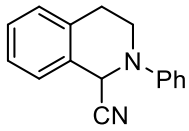

2-Phenyl-1,2,3,4-tetrahydroisoquinoline-1-carbonitrile (**2.104**).[8] The crude material was purified by column chromatography *n*-hexane + Et_3N 0.05% *v/v*) to give the product as a yellowish solid (14.0 mg, 75% isolated yield; NMR yield: 98%). ^1H NMR (700 MHz, $CDCl_3$) δ 7.39−7.36 (m, 2H), 7.34−7.27 (m, 3H), 7.25 (d, J = 7.5 Hz, 1H), 7.10 (d, J = 8.0 Hz, 2H), 7.03 (t, J = 7.3 Hz, 1H), 5.53 (s, 1H), 3.80−3.77 (m, 1H), 3.52−3.48 (m, 1H), 3.20−3.15 (m, 1H), 3.00−2.97 (m, 1H); ^{13}C {^1H} NMR (176 MHz, $CDCl_3$) δ 148.4, 134.6, 129.6, 129.4, 128.8, 127.1, 126.9, 121.9, 117.8, 117.6, 53.3, 44.2, 28.6. HRMS (ESI) *m/z*: calcd $[M + H]^+$ for $C_{16}H_{15}N_2^+$ 235.1230; found $[M + H]^+$ 235.1232.

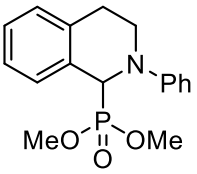

Dimethyl (2-Phenyl-1,2,3,4-tetrahydroisoquinolin-1-yl) phosphonate (**2.107**).[8] The crude material was purified by column chromatography (*n*-hexane/EtOAc 85:15) to give the product as a yellow sticky solid (16.1 mg, 63% yield). ^1H NMR (700 MHz, $CDCl_3$) δ 7.39−7.37 (m, 2H), 7.30−7.28 (m, 2H), 7.24−7.18 (m, 2H), 7.00 (d, J = 7.7 Hz, 2H), 6.84 (t, J = 7.0 Hz, 1H), 5.23 (d, J = 20.3 Hz, 1H), 4.06−4.02 (m, 1H), 3.69 (d, J = 10.5 Hz, 3H), 3.67 (d, J = 10.5 Hz, 3H), 3.67−3.65 (m, 1H), 3.11−3.01 (m, 2H); ^{13}C {^1H} NMR (176 MHz, $CDCl_3$) δ 149.2 (d, $J_{C–P}$ = 6.3 Hz), 136.4 (d, $J_{C–P}$ = 6.0 Hz), 130.4, 129.3, 128.8 (d, $J_{C–P}$ = 2.5 Hz), 127.9 (d, $J_{C–P}$ = 4.9 Hz), 127.5 (d, $J_{C–P}$ = 3.7 Hz), 126.0 (d, $J_{C–P}$ = 2.5 Hz), 118.7, 114.8, 58.8 (d, $J_{C–P}$ = 160.0 Hz), 53.9 (d, $J_{C–P}$ = 6.9 Hz), 52.9 (d, $J_{C–P}$ = 7.6 Hz), 43.6, 26.7; HRMS (ESI) *m/z*: calcd $[M + K]^+$ for $C_{17}H_{20}KNO_3P^+$ 356.0812; found $[M + K]^+$ 356.0813.

Procedure for the synthesis of compound 2.105 via Michael-type addition promoted by 4-isocyanobiphenyl as the photocatalyst

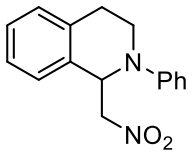

1-(Nitromethyl)-2-phenyl-1,2,3,4-tetrahydroisoquinoline (**2.105**).[9] *N*-phenyl-1,2,3,4-tetrahydroisoquinoline (0.08 mmol, 1 equiv.), nitromethane (130 µL, 2.4 mmol, 30 equiv.), and 800 µL of dry MeCN (0.1 M) were added to a 4 mL colourless screw-cap glass vial equipped with a magnetic stir bar. Then, 4-isocyanobiphenyl (0.016 mmol, 20% mol) was added to the resulting mixture, which was stirred open to air in a Photoredox box (EvoluChem), under 30W blue LED irradiation, at room temperature, for 20 h. After completion of the reaction, as monitored by TLC, the solvent and the excess of nitromethane were removed under vacuum and the crude mixture was purified by preparative TLC (*n*-hexane/THF 8:2) to give the product as a yellow amorphous solid (12,2 mg, 57% isolated yield; NMR yield: 69%). ^{1}H NMR (700 MHz, $CDCl_3$) δ 7.29−7.25 (m, 3H), 7.22−7.19 (m, 2H), 7.14 (d, J = 7.5 Hz, 1H), 6.98 (d, J = 8.3 Hz, 2H), 6.85 (t, J = 7.3 Hz, 1H), 5.55 (t, J = 7.2 Hz, 1H), 4.88 (dd, J_a = 11.9, J_b = 7.8 Hz, 1H), 4.57 (dd, J_a = 11.9, J_b = 6.7 Hz, 1H), 3.69−3.61 (m, 2H), 3.11−3.07 (m, 1H), 2.82−2.78 (m, 1H); ^{13}C {^{1}H} NMR (176 MHz, $CDCl_3$) δ 148.4, 135.3, 132.9, 129.5, 129.2, 128.1, 127.0, 126.7, 119.4, 115.1, 78.8, 58.2, 42.1, 26.5; HRMS (ESI) *m/z*: calcd [M + H]+ for $C_{16}H_{17}N_2O_2^+$ 269.1285; found $[M + H]^+$ 269.1285.

Procedure for the synthesis of compound 2.106 via Michael-type addition promoted by 4-isocyanobiphenyl as the photocatalyst

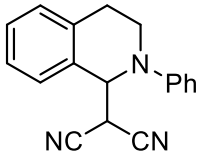

2-(2-Phenyl-1,2,3,4-tetrahydroisoquinolin-1-yl)malononitrile (**2.106**).[7] *N*-phenyl-1,2,3,4-tetrahydroisoquinoline (0.08 mmol, 1 equiv.), malononitrile (26.6 μL, 0.48 mmol, 6 equiv.), and 800 μL of dry MeCN (0.1 M) were added to a 4 mL colourless screw-cap glass vial equipped with a magnetic stir bar. Then, 4-isocyanobiphenyl (0.016 mmol, 20% mol) was added to the resulting mixture, which was stirred open flask in a Photoredox box (EvoluChem), under 30W blue LED irradiation, at room temperature, for 20 h. After completion of the reaction, as monitored by TLC, the solvent and the excess of malononitrile were removed under vacuum and the crude ^{1}H NMR spectrum in the presence of TMB as internal standard was registered (NMR yield: 27%).

HRMS spectrum of the reaction performed in the presence of $H_2{}^{18}O$

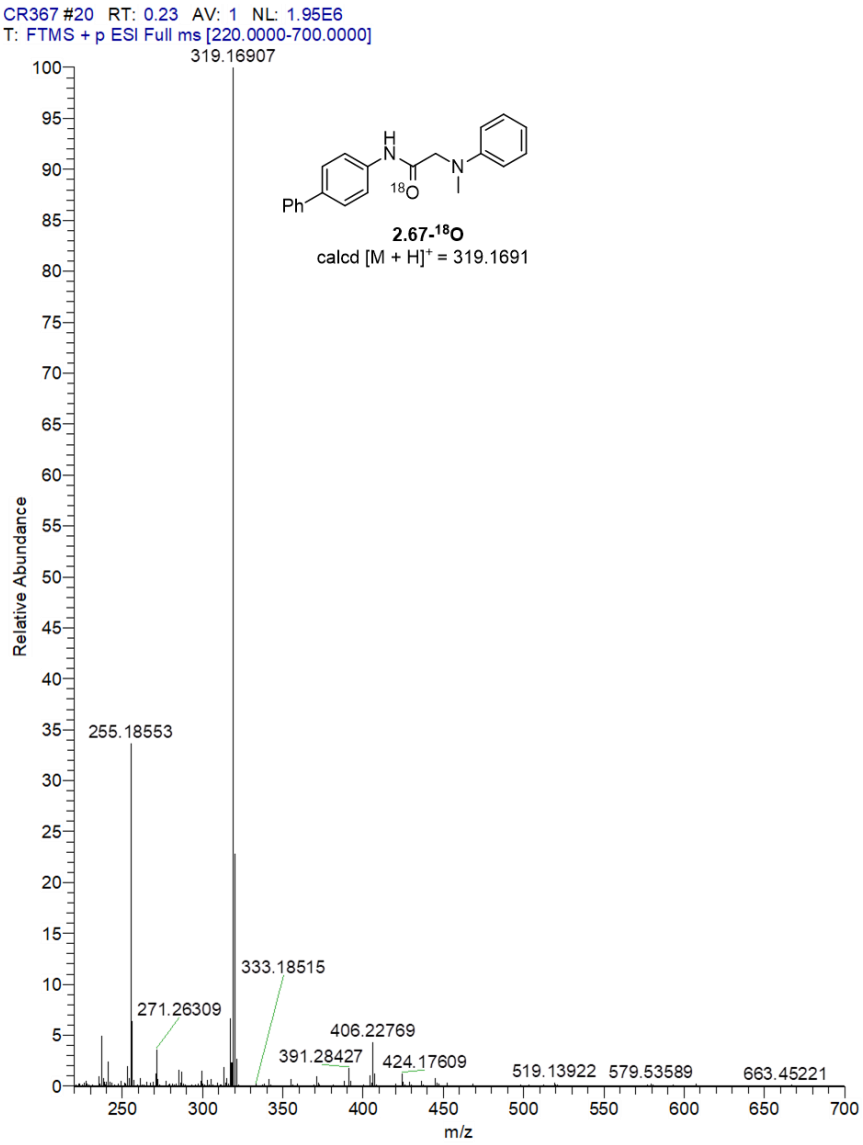

Absorption measurements

UV-VIS absorption spectra were acquired on a Jasco V-730 Spectrophotometer (JASCO Inc., Tokyo, Japan) equipped with an ETCS-761 Peltier temperature controller. All spectra were recorded at 25° C and 100 nm/min scan speed, using a

sealed quartz cuvette with a path length of 1 cm. Spectra of pure 4-isocyanobiphenyl **2.66** in MeCN and 10 equiv. of H_2O were collected in the 250–600 nm wavelength range. Spectra of *N,N*-dimethylaniline **2.15** alone and in combination with isocyanide **2.66** or **2.84** were recorded in the 300–600 nm wavelength range.

Fluorescence experiments

Fluorescence measurements were performed on a Jasco FP-8300 spectrofluorometer equipped with a PCT-818 Peltier temperature controller system (Jasco), using a sealed quartz cuvette with a path length of 1 cm. A 100 nm/min scan speed and 5 nm excitation and emission slit widths were used. Spectra of 4-isocyanobiphenyl **2.66** were recorded at 25 °C in the 275–600 nm and 370–600 nm wavelength range upon excitation at 265 and 360 nm, respectively. Stern-Volmer fluorescence quenching experiments were carried out by stepwise addition of *N,N*-dimethylaniline **2.15** to the cell containing a fixed concentration of 4-isocyanobiphenyl **2.66** (10 mM in MeCN + 10 equiv. of H_2O). Spectra were recorded using the following parameters: 360 nm excitation wavelength, 370–600 nm emission range. The same parameters were also used to record fluorescence spectra of 4-isocyanobiphenyl **2.66** in the absence and presence of $Yb(OTf)_3$, and upon addition of ammonium hydroxide.

2.4.

Starting materials

Procedure for the synthesis of *tert*-butyl (2-isocyanobenzyl)carbamate 2.143

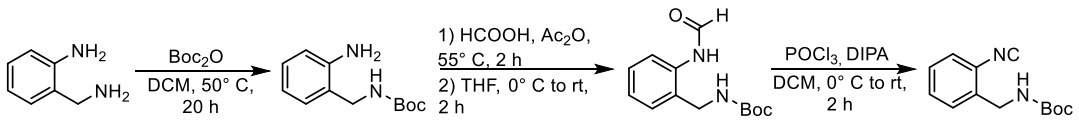

Step 1: In a 50 mL round bottom flask equipped with a magnetic stir bar, 2-aminobenzylamine (4.1 mmol, 1 equiv.) was dissolved in DCM (16.4 mL, 0.25 M) and di-*tert*-butyl dicarbonate (4.1 mmol, 1 equiv.) was added to the solution. The resulting mixture was stirred at 50° C overnight, until completion of the reaction, as monitored by TLC. Then the solvent was removed under vacuum and the crude mixture was purified by column chromatography (*n*-hexane/EtOAc 97:3) to afford *tert*-butyl (2-aminobenzyl)carbamate as a white solid (829.5 mg, 91% yield).

Step 2: In a 50 mL two-necked round bottom flask, a mixture of formic acid (362.0 µL, 9.6 mmol, 2.7 equiv.) and acetic anhydride (771.2 µL, 8.2 mmol, 2.3 equiv.,) was stirred at 55°C for 2 h. After the reaction was cooled at room temperature, the crude mixture was added dropwise to a solution of *tert*-butyl (2-aminobenzyl)carbamate (3.5 mmol, 1 equiv.) in THF (5.8 mL, 0.6 M), at 0° C. The resulting mixture was stirred at room temperature for additional 2 h, until completion of the reaction, as monitored by TLC. Then the reaction was cooled to 0° C and a saturated aqueous solution of $NaHCO_3$ was added slowly under vigorous stirring, until neutral pH was reached. EtOAc was added, and the two phases were separated; the aqueous layer was further extracted with EtOAc (x2), then the combined organic extracts were washed with brine, dried over sodium sulfate, and concentrated under reduced pressure to give *tert*-butyl (2-

formamidobenzyl)carbamate in quantitative yield. The crude material was used in the next step without further purification.

Step 3: In a 100 ml round bottom flask equipped whit a magnetic stir bar, *tert*-butyl (2-formamidobenzyl)carbamate (3.5 mmol, 1 equiv.) was dissolved in DCM (50 mL, 0.07 M), and diisopropylamine (3.0 mL, 21 mmol, 6 equiv.) was added to the solution. After cooling to 0°C, phosphorus oxychloride (687 µL, 7.3 mmol, 2.1 equiv.) was added dropwise to the reaction mixture, which was stirred at room temperature for 2 h. After completion of the reaction, as monitored by TLC, the mixture was cooled to 0° C and a saturated aqueous solution of $NaHCO_3$ was added slowly under vigorous stirring, until pH ~ 9. Then DCM was added, and the two phases were separated; the organic layer was further washed with saturated aqueous solution of $NaHCO_3$ (x2), and brine (x1), dried over sodium sulfate, and concentrated under vacuum. The crude mixture was purified by column chromatography (*n*-hexane/EtOAc 95:5) to afford *tert*-butyl (2-isocyanobenzyl)carbamate **2.143** as a yellow solid (510.5 mg, 63% yield).

General procedure for the synthesis of imide derivatives 2.108-2.112, 2.114, and 2.127-2.132 via the visible light-promoted metal-free Ugi 3-CR and Joullié-Ugi 3-CR

The isocyanide (0.08 mmol, 1 equiv.), the carboxylic acid component (0.12 mmol, 1.5 equiv.), the aniline derivative (0.16 mmol, 2 equiv.) and 800 µL of dry MeCN (0.1 M) were added to a 4 mL colourless screw-cap glass vial equipped with a magnetic stir bar; 80 mg of 3 Å activated molecular sieves were then added to the resulting mixture, which was stirred open to air in a PhotoRedOx Box (EvoluChem™), under 30W blue LED irradiation, at room temperature, until completion of the reaction, as monitored by TLC (specific reaction times are available for each compound). Then the solvent was removed under vacuum and the crude mixture was purified by column chromatography.

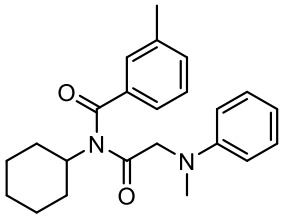

N-Cyclohexyl-3-methyl-*N*-(*N*-methyl-*N*-phenylglycyl)benzamide (**2.108**). The crude material (reaction time: 72 h) was purified by column chromatography (*n*-hexane/EtOAc 99:1) to give the product as a pale yellow amorphous solid (28.9 mg, 99% yield, also when performed on a 0.8 mmol scale). ^{1}H NMR (400 MHz, $CDCl_3$) δ 7.33 (d, J = 7.6 Hz, 1H), 7.28 (d, J = 7.6 Hz, 1H), 7.22–7.19 (m, 2H), 7.16–7.12 (m, 2H), 6.77 (t, J = 7.3 Hz, 1H), 6.42 (d, J = 8.1 Hz, 2H), 4.03–3.95 (m, 1H), 3.86 (s, 2H), 2.62 (s, 3H), 2.22 (s, 3H), 1.95–1.86 (m, 2H), 1.76–1.72 (m, 4H), 1.58–1.55 (m, 1H), 1.23–1.11 (m, 3H); ^{13}C {^{1}H} NMR (101 MHz, $CDCl_3$) δ 174.1, 173.4, 148.3, 138.5, 134.8, 133.6, 129.9, 128.9, 128.3, 126.2, 118.6, 113.2, 58.6, 58.2, 39.9, 30.0, 26.23, 25.2, 21.2; HRMS (ESI) *m/z*: calcd $[M + H]^+$ for $C_{23}H_{29}N_2O_2^+$ 365.2224; found $[M + H]^+$ 365.2225.

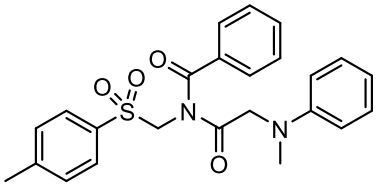

N-(*N*-methyl-*N*-phenylglycyl)-*N*-(tosylmethyl)benzamide (**2.109**).[6] The crude material (reaction time: 20 h) was purified by column chromatography (*n*-hexane/EtOAc 93:7) to give the product as a yellow amorphous solid (19.6 mg, 56% yield). ^{1}H NMR (700 MHz, $CDCl_3$) δ 7.76 (d, J = 8.2 Hz, 2H), 7.57 (t, J = 7.4 Hz, 1H), 7.54 (d, J = 7.3 Hz, 2H), 7.42 (t, J = 7.8 Hz, 2H), 7.33 (d, J = 8.0 Hz, 2H), 7.17 – 7.15 (m, 2H), 6.77 (t, J = 7.3 Hz, 1H), 6.46 (d, J = 8.2 Hz, 2H), 5.09 (s, 2H), 4.13 (s, 2H), 2.72 (s, 3H), 2.44 (s, 3H); ^{13}C {^{1}H} NMR (176 MHz, $CDCl_3$) δ 173.1, 171.7, 148.4, 145.6, 134.4, 133.3, 132.6, 129.9, 129.2, 129.2, 129.0, 129.0, 118.3,

112.8, 65.1, 57.5, 40.01, 21.8; HRMS (ESI) *m/z:* calcd $[M + H]^+$ for $C_{24}H_{25}N_2O_4S^+$ 437.1530; found $[M + H]^+$ 437.1532

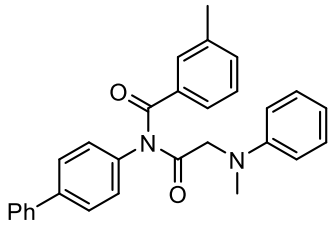

N-([1,1′-Biphenyl]-4-yl)-3-methyl-*N*-(*N*-methyl-*N*-phenylglycyl)benzamide (**2.110**). The crude material (reaction time: 72 h) was purified by column chromatography (*n*-hexane/EtOAc 98:2) to give the product as a reddish sticky solid (23.4 mg, 67% yield). ^{1}H NMR (700 MHz, $CDCl_3$) δ 7.51–7.49 (m, 4H), 7.40 (t, J = 7.7 Hz, 2H), 7.33 (t, J = 7.4 Hz, 1H), 7.30–7.28 (m, 2H), 7.25 (d, J = 8.8 Hz, 1H), 7.18–7.17 (m, 2H), 7.14 (d, J = 8.4 Hz, 2H), 7.09–7.07 (m, 1H), 6.85 (t, J = 7.3 Hz, 1H), 6.70 (d, J = 8.2 Hz, 2H), 4.44 (s, 2H), 2.90 (s, 3H), 2.16 (s, 3H); ^{13}C {^{1}H} NMR (176 MHz, $CDCl_3$) δ 176.0, 172.1 148.6, 140.4, 140.0, 138.0, 137.6, 133.4, 133.0, 130.7, 129.3, 128.8, 128.1, 128.0, 127.6, 127.5, 127.2, 127.1, 118.1, 112.7, 58.4, 40.6, 21.2; HRMS (ESI) *m/z*: calcd $[M + H]^+$ for $C_{29}H_{27}N_2O_2^+$ 435.2067; found $[M + H]^+$ 435.2053.

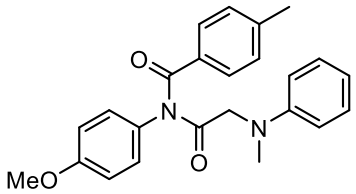

N-(4-Methoxyphenyl)-4-methyl-*N*-(*N*-methyl-N-phenylglycyl)benzamide (**2.111**). The crude material (reaction time: 72 h) was purified by column chromatography (*n*-hexane/EtOAc 98:2) to give the product as a reddish sticky solid (27.9 mg, 90% yield). ^{1}H NMR (700 MHz, $CDCl_3$) δ 7.25 (d, J = 8.2 Hz, 2H), 7.23–7.20 (m, 2H), 6.94–6.92 (m, 4H), 6.77 (t, J = 7.3 Hz, 1H), 6.75 (d, J = 8.9 Hz, 2H), 6.64 (d, J = 8.2 Hz, 2H), 4.37 (s, 2H), 3.68 (s, 3H), 2.87 (s, 3H), 2.24 (s, 3H); ^{13}C {^{1}H} NMR

(176 MHz, $CDCl_3$) δ 176.0, 172.1, 158.7, 148.7, 143.2, 131.2, 130.6, 130.0, 129.2, 128.9, 128.6, 117.8, 114.7, 112.6, 58.4, 55.4, 40.5, 21.6; HRMS (ESI) *m/z*: calcd $[M + H]^+$ for $C_{24}H_{25}N_2O_3^+$ 389.1860; found $[M + H]^+$ 389.1852.

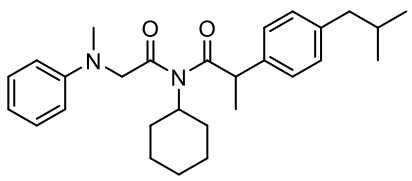

N-Cyclohexyl-2-(4-isobutylphenyl)-*N*-(*N*-methyl-*N*-phenylglycyl)propanamide (**2.112**). The crude material (reaction time: 48 h) was purified by column chromatography (*n*-hexane/EtOAc 99.5:0.5) to give the product as a pale-yellow sticky solid (33.0 mg, 95% yield). ^1H NMR (700 MHz, $CDCl_3$) δ 7.17 (d, J = 8.0 Hz, 2H), 7.15–7.12 (m, 4H), 6.67 (t, J = 7.3 Hz, 1H), 6.53 (d, J = 8.2 Hz, 2H), 4.38 (d, J = 18.0 Hz, 1H), 4.30 (d, J = 18.0 Hz, 1H), 4.01 (q, J = 6.8 Hz, 1H), 3.70–3.66 (m, 1H), 3.00 (s, 3H), 2.46 (d, J = 7.2 Hz, 2H), 2.21–2.15 (m, 1H), 1.85–1.79 (m, 2H), 1.77–1.75 (m, 1H), 1.63–1.61 (m, 1H), 1.49–1.48 (m, 5H), 1.18–1.12 (m, 1H), 1.03–0.97 (m, 1H), 0.87 (d, J = 6.7 Hz, 6H), 0.85–0.79 (m, 1H), 0.74–0.73 (m, 1H); ^{13}C $\{^1H\}$ NMR (176 MHz, $CDCl_3$) δ 178.8, 175.9, 148.9, 141.0, 137.7, 129.9, 129.1, 127.2, 116.9, 112.0, 59.2, 58.7, 46.9, 45.0, 39.8, 30.6, 30.3, 29.0, 26.8, 26.4, 25.0, 22.3, 22.2, 20.3; HRMS (ESI) *m/z*: calcd $[M + H]^+$ for $C_{28}H_{39}N_2O_2^+$ 435.3007; found $[M + H]^+$ 435.3020.

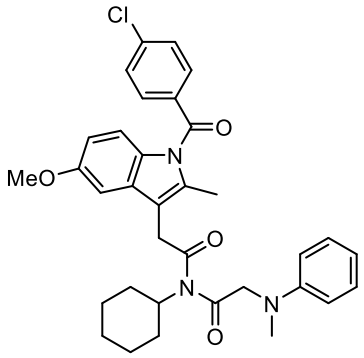

2-(1-(4-Chlorobenzoyl)-5-methoxy-2-methyl-1*H*-indol-3-yl)-*N*-cyclohexyl-*N*-(*N*-methyl-*N*-phenylglycyl)acetamide (**2.114**). The crude material (reaction time: 72 h) was purified by column chromatography (*n*-hexane/EtOAc 96:4) to give the product as a yellowish solid (40.0 mg, 85% yield). ^{1}H NMR (700 MHz, $CDCl_3$) δ 7.65 (d, J = 8.4 Hz, 2H), 7.47 (d, J = 8.4 Hz, 2H), 7.17–7.15 (m, 2H), 6.93 (d, J = 2.4 Hz, 1H), 6.82 (d, J = 9.0 Hz, 1H), 6.71 (t, J = 7.3 Hz, 1H), 6.68 (dd, J_a = 9.0, J_b = 2.5 Hz, 1H), 6.59 (d, J = 8.3 Hz, 2H), 4.39 (s, 2H), 3.96 (s, 2H), 3.79 (s, 3H), 3.72–3.69 (m, 1H), 3.02 (s, 3H), 2.41 (s, 3H), 2.21–2.16 (m, 2H), 1.77–1.75 (m, 2H), 1.62–1.50 (m, 3H), 1.15–1.08 (m, 3H); ^{13}C {^{1}H} NMR (176 MHz, $CDCl_3$) δ 175.5, 175.0, 168.2, 156.1, 148.8, 139.5, 135.9, 133.7, 131.2, 130.8, 130.4, 129.2 (4C), 117.3, 115.1, 112.4, 112.1, 111.7, 101.2, 59.3, 59.1, 55.7, 39.7, 34.6, 30.1, 26.6, 24.9, 13.5; HRMS (ESI) *m/z*: calcd $[M + H]^+$ for $C_{34}H_{37}ClN_3O_4^+$ 586.2467; found $[M + H]^+$ 586.2487.

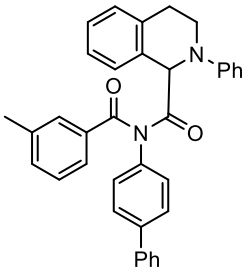

N-([1,1′-Biphenyl]-4-yl)-*N*-(3-methylbenzoyl)-2-phenyl-1,2,3,4-tetrahydroisoquinoline-1-carboxamide (**2.127**). The crude material (reaction time: 48 h) was purified by column chromatography (*n*-hexane/EtOAc 98.5:1.5) to give

the product as a yellowish amorphous solid (28.4 mg, 68% yield). ^{1}H NMR (700 MHz, $CDCl_3$) δ 7.49–7.48 (m, 3H), 7.45 (d, J = 8.5 Hz, 2H), 7.39 (t, J = 7.7 Hz, 2H), 7.31 (t, J = 7.4 Hz, 1H), 7.30 (s, 1H), 7.28–7.27 (m, 1H), 7.25–7.22 (m, 2H), 7.21–7.18 (m, 4H), 7.12 (t, J = 7.6 Hz, 1H), 6.98 (d, J = 8.5 Hz, 2H), 6.85 (t, J = 7.3 Hz, 1H), 6.79 (d, J = 8.1 Hz, 2H), 6.13 (s, 1H), 3.75–3.71 (m, 1H), 3.60–3.57 (m, 1H), 2.95–2.89 (m, 2H), 2.24 (s, 3H); ^{13}C {^{1}H} NMR (176 MHz, $CDCl_3$) δ 176.2, 171.9, 148.1, 140.2, 140.0, 138.3, 138.0, 135.4, 133.8, 133.1, 132.1, 130.5, 129.1, 128.8, 128.7, 128.6 (2C), 127.9, 127.8, 127.7, 127.6, 127.0, 126.8, 126.2, 119.8, 116.2, 61.5, 44.6, 26.9, 21.2; HRMS (ESI) *m/z*: calcd $[M + H]^+$ for $C_{36}H_{31}N_2O_2^+$ 523.2381; found $[M + H]^+$ 523.2374.

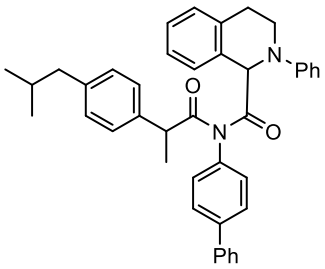

N-([1,1′-Biphenyl]-4-yl)-*N*-(2-(4-isobutylphenyl)propanoyl)-2-phenyl-1,2,3,4-tetrahydroisoquinoline-1-carboxamide (**2.128**). The crude material (reaction time: 72 h) was purified by column chromatography (*n*-hexane/EtOAc 99:1) to give the product as an off-white solid (29.1 mg, 61% yield; 1:0.6 diastereomeric mixture). ^{1}H NMR (700 MHz, $CDCl_3$; major diastereomer) δ 7.52–7.50 (m, 2H), 7.45–7.40 (m, 4H), 7.38–7.35 (m, 1H), 7.33–7.31 (m, 2H), 7.28–7.27 (m, 1H), 7.15 (d, J = 7.6 Hz, 2H), 7.01 (d, J = 8.0 Hz, 4H), 6.97–6.94 (m, 1H), 6.89 (d, J = 8.0 Hz, 2H), 6.87 (t, J = 7.3 Hz, 1H), 6.79–6.74 (m, 1H), 6.66–6.63 (m, 1H), 6.53 (m, 1H), 3.80–3.73 (m, 2H), 3.57–3.51 (m, 1H), 3.03–2.99 (m, 1H), 2.95–2.86 (m, 2H), 2.47 (d, J = 7.2 Hz, 2H), 1.92–1.84 (m, 1H), 1.50 (d, J = 6.9 Hz, 3H), 0.92 (d, J = 6.6 Hz, 6H); ^{13}C {^{1}H} NMR (176 MHz, $CDCl_3$; major diastereomer) δ 177.5, 177.4; 149.1, 141.7, 140.8, 140.0, 137.4, 137.1, 136.0, 132.5, 129.4, 129.3, 129.2, 128.9, 128.2, 127.9, 127.9, 127.8, 127.7, 127.6, 127.2, 126.3, 118.6, 114.9, 62.4, 45.7, 45.1, 43.5, 30.3,

27.9, 22.4, 19.9; HRMS (ESI) *m/z*: calcd $[M + H]^+$ for $C_{41}H_{41}N_2O_2^+$ 593.3163; found $[M + H]^+$ 593.3153.

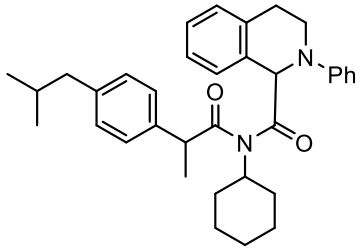

N-Cyclohexyl-*N*-(2-(4-isobutylphenyl)propanoyl)-2-phenyl-1,2,3,4 tetrahydroisoquinoline-1-carboxamide (**2.129**). The crude material (reaction time: 72 h) was purified by column chromatography (*n*-hexane/EtOAc 99.5:0.5) to give the product as an off-white amorphous solid (40.2 mg, 96% yield; 1:1 diastereomeric mixture). ^{1}H NMR (700 MHz, $CDCl_3$) δ 7.35–7.34 (m, 1H), 7.31–7.28 (m, 3H), 7.27–7.22 (m, 4H), 7.21–7.18 (m, 1H), 7.16–7.13 (m, 4H), 7.10–7.07 (m, 3H), 7.03–7.02 (m, 4H), 6.99–6.96 (m, 4H), 6.86 (t, J = 7.2 Hz, 1H), 6.81 (t, J = 7.2 Hz, 1H), 6.24–6.23 (m, 2H), 3.86 (q, J = 6.7 Hz, 1H), 3.82 (q, J = 6.8 Hz, 1H), 3.75–3.71 (m, 1H), 3.70–3.67 (m, 1H), 3.64–3.50 (m, 4H), 3.04–3.00 (m, 1H), 2.97–2.85 (m, 3H), 2.45–2.43 (m, 4H), 1.93–1.87 (m, 1H), 1.86–1.80 (m, 2H), 1.75–1.68 (m, 2H), 1.63–1.61 (m, 2H), 1.51 (d, J = 6.8 Hz, 3H), 1.41–1.36 (m, 8H), 1.05–0.99 (m, 2H), 0.95–0.89 (m, 4H), 0.88–0.86 (m, 12H), 0.76–0.74 (m, 2H), 0.64–0.58 (m, 1H), 0.53–0.51 (m, 1H); ^{13}C {^{1}H} NMR (176 MHz, $CDCl_3$) δ 178.8, 178.0, 177.7, 149.2, 148.7, 140.7, 140.7, 137.8, 137.6, 135.7, 135.4, 132.9, 132.3, 129.6, 129.5, 129.3, 129.3, 128.4, 128.4, 127.9, 127.8, 127.8, 127.6, 127.4, 127.3, 126.3, 126.3, 119.2, 118.8, 115.7, 115.1, 63.5, 63.5, 58.9, 58.5, 46.7, 46.6, 45.0, 45.0, 30.9, 30.4, 30.2, 29.7, 29.4, 27.8, 27.2, 26.6, 26.6, 26.3, 26.3, 25.0, 22.3, 22.3, 20.5, 20.2; HRMS (ESI) *m/z*: calcd $[M + H]^+$ for $C_{35}H_{43}N_2O_2^+$ 523.3320; found $[M + H]^+$ 523.3312.

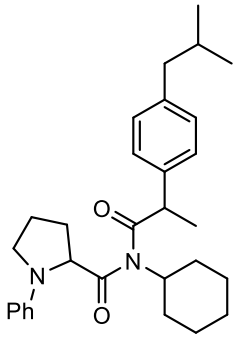

N-Cyclohexyl-*N*-(2-(4-isobutylphenyl)propanoyl)-1-phenylpyrrolidine-2-carboxamide (**2.130**). The crude material (reaction time: 72 h) was purified by column chromatography (*n*-hexane/EtOAc 98:2) to give the product as a colourless sticky solid (36.1 mg, 98% yield, 1:1 diastereomeric mixture). ^{1}H NMR(700 MHz, $CDCl_3$) δ 7.28 (d, J = 8.0 Hz, 2H), 7.21–7.18 (m, 6H), 7.13 (d, J = 8.0 Hz, 2H), 7.01 (t, J = 7.9 Hz, 2H), 6.67 (t, J = 7.3 Hz, 1H), 6.60 (t, J = 7.3 Hz, 1H), 6.55 (d, J = 8.0 Hz, 2H), 6.29 (d, J = 8.0 Hz, 2H), 4.90 (m, 1H), 4.61 (dd, J_a = 8.7, J_b = 2.0 Hz, 1H), 4.16 (q, J = 6.7 Hz, 1H), 4.05 (q, J = 6.8 Hz, 1H), 3.82–3.78 (m, 1H), 3.76–3.72 (m, 1H), 3.59–3.54 (m, 2H), 3.43–3.37 (m, 2H), 2.52–2.50 (m, 2H), 2.47 (d, J = 7.2 Hz, 2H), 2.44–2.38 (m, 1H), 2.31–2.13 (m, 6H), 2.05–1.83 (m, 8H), 1.81–1.76 (m, 2H), 1.70–1.66 (m, 3H), 1.54–1.52 (m, 9H), 1.23–1.14 (m, 2H), 1.07–0.99 (m, 2H), 0.97–0.90 (m, 9H), 0.88 (d, J = 6.6 Hz, 6H); ^{13}C {^{1}H} NMR (176 MHz, $CDCl_3$) δ 180.3, 179.2, 179.1, 179.0, 146.6, 146.3, 141.2, 140.9, 137.8, 137.7, 130.0, 129.7, 129.1, 129.0, 127.5, 127.3, 116.3, 116.1, 112.0, 111.8, 63.2, 62.9, 58.8, 58.6, 48.8, 48.4, 47.2, 46.9, 45.1, 45.0, 31.8, 31.3, 31.0, 30.5, 30.3, 30.2, 29.4, 28.4, 26.9, 26.8, 26.5, 26.5, 25.0, 23.2, 23.1, 22.4, 22.2, 20.5, 20.1; HRMS (ESI) *m/z*: calcd $[M+ H]^+$ for $C_{30}H_{41}N_2O_2^+$ 461.3163; found $[M + H]^+$ 461.3153.

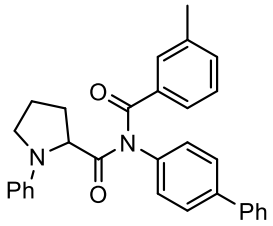

N-([1,1′-Biphenyl]-4-yl)-*N*-(3-methylbenzoyl)-1-phenylpyrrolidine-2-carboxamide (**2.131**). The crude material (reaction time: 72 h) was purified by column chromatography (*n*-hexane/EtOAc 98.5:1.5) to give the product as an orange amorphous solid (31.9 mg, 87% yield). ^{1}H NMR (700 MHz, $CDCl_3$) δ 7.53–7.51 (m, 4H), 7.42–7.37 (m, 4H), 7.33 (t, J = 7.4 Hz, 1H), 7.24 (t, J = 7.9 Hz, 2H), 7.20–7.19 (m, 3H), 7.12 (t, J = 7.6 Hz, 1H), 6.75 (t, J = 7.3 Hz, 1H), 6.64 (d, J = 8.0 Hz, 2H), 4.86 (dd, J_a = 8.5, J_b = 3.7 Hz, 1H), 3.55–3.52 (m, 1H), 3.41–3.38 (m, 1H), 2.55–2.51 (m, 1H), 2.47–2.41 (m, 1H), 2.27–2.25 (m, 1H), 2.23 (s, 3H), 2.07–2.02 (m, 1H); ^{13}C NMR {^{1}H} (176 MHz, $CDCl_3$) δ 178.8, 172.4, 146.8, 140.69, 139.9, 138.2, 137.8, 133.7, 133.3, 130.4, 129.2, 128.8, 128.2, 128.1, 128.0, 127.7, 127.1, 126.8, 117.1, 112.4, 62.7, 49.1, 31.3, 23.7, 21.2; HRMS (ESI) *m/z*: calcd $[M + H]^+$ for $C_{31}H_{29}N_2O_2^+$ 461.2224; found $[M + H]^+$ 461.2214.

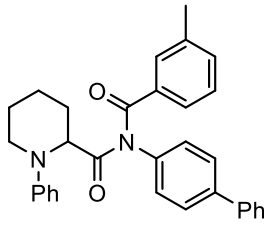

N-([1,1′-Biphenyl]-4-yl)-*N*-(3-methylbenzoyl)-1-phenylpiperidine-2-carboxamide (**2.132**). The crude material (reaction time: 48 h) was purified by column chromatography (*n*-hexane/EtOAc 98:2) to give the product as a yellowish amorphous solid (24.0 mg, 63% yield). ^{1}H NMR (700 MHz, $CDCl_3$) δ 7.51–7.50 (m, 2H), 7.49–7.48 (m, 2H), 7.40 (t, J = 7.7 Hz, 2H), 7.33 (t, J = 7.4 Hz, 1H), 7.28 (s, 1H), 7.24–7.21 (m, 3H), 7.18 (d, J = 7.5 Hz, 1H), 7.11 (t, J = 7.6 Hz, 1H), 6.98–6.96 (m, 2H), 6.88 (t, J = 7.3 Hz, 1H), 6.85 (d, J = 8.2 Hz, 2H), 5.10–5.09 (m, 1H),

3.46–3.42 (m, 1H), 3.37–3.35 (m, 1H), 2.37–2.35 (m, 1H), 2.23 (s, 3H), 1.99–1.94 (m, 1H), 1.87–1.82 (m, 1H), 1.80–1.78 (m, 1H), 1.75–1.72 (m, 1H), 1.64–1.57 (m, 1H); ^{13}C {^{1}H} NMR (176 MHz, $CDCl_3$) δ 176.8, 172.0, 149.6, 140.5, 140.0, 138.2, 138.1, 134.0, 133.0, 130.2, 129.1, 128.8, 128.0, 128.0, 127.9, 127.6, 127.0, 126.6, 119.9, 116.7, 58.2, 45.8, 25.8, 24.6, 21.2, 19.9; HRMS (ESI) *m/z*: calcd $[M + H]^+$ for $C_{32}H_{31}N_2O_2^+$ 475.2381; found $[M + H]^+$ 475.2396.

General procedure for the synthesis of imide derivatives 2.113 and 2.115 via the visible light-promoted metal-free Ugi 3-CR

The isocyanide (0.08 mmol, 1 equiv.), the carboxylic acid component (0.16 mmol, 2 equiv.), the aniline derivative (0.16 mmol, 2 equiv.) and 800 μL of a 9:1 MeCN/H_2O mixture (0.1 M) were added to a 4 mL colourless screw-cap glass vial equipped with a magnetic stir bar. The resulting mixture was stirred open to air in a PhotoRedOx Box (EvoluChem™), under 30W blue LED irradiation, at room temperature, for 72 h. After completion of the reaction, as monitored by TLC, the solvent was removed under vacuum and the crude mixture was purified by column chromatography.

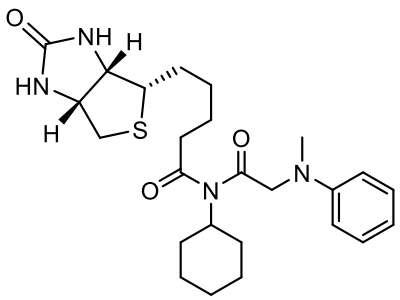

N-Cyclohexyl-*N*-(*N*-methyl-*N*-phenylglycyl)-5-((3*aS*,4*S*,6*aR*)-2-oxohexahydro-1*H*-thieno[3,4-d]imidazol-4-yl)pentanamide (**2.113**). The crude material was purified by column chromatography (DCM/MeOH 98:2) to give the product as an off-white amorphous solid (20.0 mg, 53% yield). ^{1}H NMR (700 MHz, $CDCl_3$) δ 7.21 (t, *J* =

7.9 Hz, 2H), 6.72 (t, J = 7.2 Hz, 1H), 6.64 (d, J = 8.2 Hz, 2H), 5.88 (brs, -N*H*), 5.37 (brs, -N*H*), 4.49–4.47 (m, 1H), 4.35 (s, 2H), 4.29–4.28 (m, 1H), 3.68–3.65 (m, 1H), 3.16–3.13 (m, 1H), 3.01 (s, 3H), 2.89 (dd, J_a = 12.8, J_b 5.0 Hz, 1H), 2.72 (d, J = 12.8 Hz, 1H), 2.54 (t, J = 7.4 Hz, 2H), 2.18–2.12 (m, 2H), 1.82–1.80 (m, 2H), 1.76–1.65 (m, 4H), 1.64–1.60 (m, 3H), 1.51–1.42 (m, 2H), 1.22–1.20 (m, 2H), 1.16–1.10 (m, 1H); ^{13}C {^{1}H} NMR (176 MHz, $CDCl_3$) δ 177.3, 175.4, 163.7, 148.9, 129.2, 117.2, 112.2, 62.0, 60.1, 59.3, 58.7, 55.4, 40.6, 39.8, 37.3, 30.2, 28.5, 28.4, 26.6, 25.0, 24.9; HRMS (ESI) *m/z*: calcd $[M + H]^+$ for $C_{25}H_{37}N_4O_3S^+$ 473.2581; found $[M + H]^+$ 473.2584.

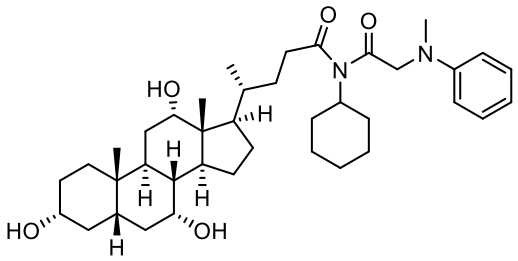

(*R*)-*N*-Cyclohexyl-*N*-(*N*-methyl-*N*-phenylglycyl)-4-((3*R*,5*S*,7*R*,8*R*,9*S*,10*S*,12*S*,13*R*,14*S*,17*R*)-3,7,12-trihydroxy-10,13-dimethylhexadecahydro-1*H*-cyclopenta[*a*]phenanthren-17-yl)pentanamide (**2.115**). The crude material was purified by column chromatography (DCM/MeOH 97:3) to give the product as an off-white amorphous solid (41.0 mg, 80% yield). ^{1}H NMR (700 MHz, $CDCl_3$) δ 7.20 (t, J = 7.9 Hz, 2H), 6.71 (t, J = 7.2 Hz, 1H), 6.63 (d, J = 8.3 Hz, 2H), 4.35 (s, 2H), 3.96 (s, 1H), 3.85 (s, 1H), 3.68–3.65 (m, 1H), 3.48–3.43 (m, 1H), 3.01 (s, 3H), 2.59–2.55 (m, 2H), 2.46–2.41 (m, 1H), 2.27–2.13 (m, 4H), 1.95–1.88 (m, 3H), 1.83–1.78 (m, 5H), 1.76–1.66 (m, 4H), 1.64–1.60 (m, 4H), 1.56–1.50 (m, 3H), 1.45–1.39 (m, 4H), 1.33–1.27 (m, 2H), 1.23–1.20 (m, 2H), 1.16–1.09 (m, 2H), 1.01 (d, J = 6.1 Hz, 3H), 1.00–0.95 (m, 1H), 0.89 (s, 3H), 0.68 (s, 3H); ^{13}C {^{1}H} NMR (176 MHz, $CDCl_3$) δ 178.2, 175.5, 148.9, 129.1, 117.1, 112.1, 73.1, 71.9, 68.5, 59.4, 58.8, 47.1, 46.5, 41.7, 41.5, 39.8, 39.6, 39.5, 35.4, 35.3, 34.8, 34.7, 34.7, 31.2,

30.4, 30.2, 30.2, 29.7, 28.2, 27.6, 26.7, 26.4, 25.1, 23.3, 22.5, 17.6, 12.5; HRMS (ESI) *m/z*: calcd $[M + H]^+$ for $C_{39}H_{61}N_2O_5^+$ 637.4575; found $[M + H]^+$ 637.4570.

General procedure for the synthesis of imide derivative 2.116 via the visible light-promoted metal-free Ugi 3-CR

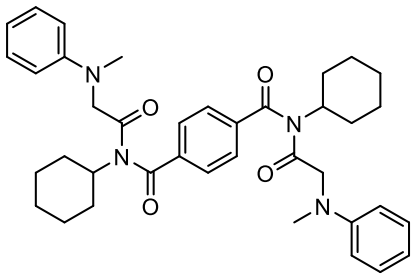

N^1,N^4-Dicyclohexyl-N^1,N^4-bis(*N*-methyl-*N*-phenylglycyl)terephthalamide (**2.116**). Terephthalic acid (0.08 mmol, 1 equiv.), cyclohexyl isocyanide (0.16 mmol, 2 equiv.), *N,N*-dimethylaniline (30.4 µL, 0.24 mmol, 3 equiv.), and 800 µL of dry MeCN (0.1 M) were added to a 4 mL colourless screw-cap glass vial equipped with a magnetic stir bar; 80 mg of 3 Å activated molecular sieves were then added to the resulting mixture, which was stirred open to air in a PhotoRedOx Box (EvoluChem™), under 30W blue LED irradiation, at room temperature, for 72 h. After completion of the reaction, as monitored by TLC, the solvent was removed under vacuum and the crude mixture was purified by column chromatography (*n*-hexane/EtOAc 97:3), to give the product as a yellow amorphous solid (36.4 mg, 73% yield). ^{1}H NMR (700 MHz, $CDCl_3$) δ 7.32 (s, 4H), 7.12 (t, J = 7.9 Hz, 4H), 6.80 (t, J = 7.2 Hz, 2H), 6.40 (d, J = 8.2 Hz, 4H), 3.96–3.93 (m, 2H), 3.81 (s, 4H), 2.55 (s, 6H), 1.90–1.84 (m, 4H), 1.78–1.76 (m, 4H), 1.70–1.68 (m, 4H), 1.60–1.58 (m, 2H), 1.24–1.19 (m, 4H), 1.13–1.08 (m, 2H); ^{13}C {^{1}H} NMR (176 MHz, $CDCl_3$) δ 173.7, 171.6, 148.0, 137.9, 129.0, 128.6, 119.4, 113.6, 58.3, 58.3, 40.0, 30.0, 26.3, 25.2; HRMS (ESI) *m/z*: calcd $[M + H]^+$ for $C_{38}H_{47}N_4O_4^+$ 623.3592; found $[M + H]^+$ 623.3578.

General procedure for the synthesis of tetrazole derivatives 2.117 and 2.122 via the visible light-promoted metal-free Ugi-tetrazole 3-CR

The aniline derivative (0.3 mmol, 1 equiv.), the isocyanide (0.6 mmol, 2 equiv.), azidotrimethylsilane (0.6 mmol, 2 equiv.), and 2.0 mL of dry MeCN (0.15 M) were added to a 4 mL colourless screw-cap glass vial equipped with a magnetic stir bar. The resulting mixture was stirred open to air in a PhotoRedOx Box (EvoluChem™), under 30W blue LED irradiation, at room temperature, for 48 h. After completion of the reaction, as monitored by TLC, the solvent was removed under vacuum and the crude mixture was purified by column chromatography.

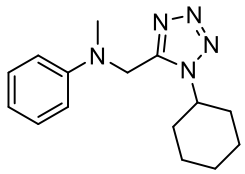

N-((1-Cyclohexyl-1*H*-tetrazol-5-yl)methyl)-*N*-methylaniline (**2.117**). The crude material was purified by column chromatography (*n*-hexane/EtOAc 92:8) to give the product as a beige solid (70.2 mg, 86% yield). ^{1}H NMR (700 MHz, $CDCl_3$) δ 7.29–7.27 (m, 2H), 6.89–6.86 (m, 3H), 4.75 (s, 2H), 4.20–4.16 (m, 1H), 2.88 (s, 3H), 1.95–1.90 (m, 2H), 1.86–1.81 (m, 4H), 1.68–1.66 (m, 1H), 1.28–1.15 (m, 3H); ^{13}C {^{1}H} NMR (176 MHz, $CDCl_3$) δ 151.3, 149.2, 129.5, 119.6, 114.8, 58.3, 46.6, 38.9, 32.9, 25.3, 24.7; HRMS (ESI) *m/z*: calcd $[M + H]^+$ for $C_{15}H_{22}N_5^+$ 272.1870; found $[M + H]^+$ 272.1866.

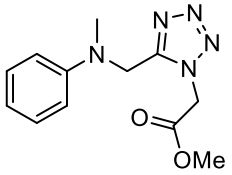

Methyl 2-(5-((methyl(phenyl)amino)methyl)-1*H*-tetrazol-1-yl)acetate (**2.118**).[10] The crude material was purified by column chromatography (*n*-hexane/EtOAc

88:12) to give the product as a pale-yellow solid (77.7 mg, 99% yield). ^{1}H NMR (700 MHz, $CDCl_3$) δ 7.26 – 7.24 (m, 2H), 6.87 (t, J = 7.3 Hz, 1H), 6.79 (d, J = 8.1 Hz, 2H), 5.10 (s, 2H), 4.78 (s, 2H), 3.66 (s, 3H), 2.88 (s, 3H); ^{13}C {^{1}H} NMR (176 MHz, $CDCl_3$) δ 165.9, 153.6, 148.8, 129.6, 120.0, 114.6, 53.0, 48.5, 48.0, 40.1; HRMS (ESI) *m/z:* calcd $[M + H]^+$ for $C_{12}H_{16}N_5O_2^+$ 262.1299; found $[M + H]^+$ 262.1305.

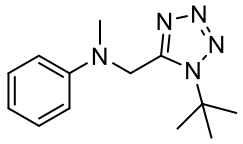

N-((1-(*tert*-Butyl)-1*H*-tetrazol-5-yl)methyl)-*N*-methylaniline (**2.119**). The crude material was purified by column chromatography (*n*-hexane/EtOAc 95 :5) to give the product as an off-white solid (66.0 mg, 90% yield). ^{1}H NMR (700 MHz, $CDCl_3$) δ 7.29–7.27 (m, 2H), 6.87–6.85 (m, 3H), 4.76 (s, 2H), 2.92 (s, 3H), 1.74 (s, 9H); ^{13}C {^{1}H} NMR (176 MHz, $CDCl_3$) δ 151.7, 149.4, 129.4, 119.3, 114.7, 61.5, 47.7, 39.4, 29.4; HRMS (ESI) *m/z*: calcd $[M + H]^+$ for $C_{13}H_{20}N_5^+$ 246.1714; found $[M + H]^+$ 247.1724.

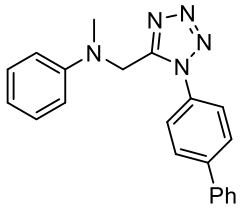

N-((1-([1,1′-Biphenyl]-4-yl)-1*H*-tetrazol-5-yl)methyl)-*N*-methylaniline (**2.120**). The crude material was purified by column chromatography (*n*-hexane/EtOAc 96:4) to give the product as a brownish solid (26.2 mg, 96% yield; reaction per formed on a 0.08 mmol scale). ^{1}H NMR (700 MHz, $CDCl_3$) δ 7.71 (d, J = 8.4 Hz, 2H), 7.61 (d, J = 7.2 Hz, 2H), 7.51 (t, J = 7.7 Hz, 2H), 7.45–7.43 (m, 3H), 7.16–7.14 (m, 2H), 6.78 (t, J = 7.3 Hz, 1H), 6.63 (d, J = 8.3 Hz, 2H), 4.79 (s, 2H), 2.86 (s, 3H); ^{13}C{^{1}H} NMR (176 MHz, $CDCl_3$) δ 153.0, 148.4, 143.7, 139.2, 132.7,

129.3, 129.1, 128.4, 128.3, 127.3, 125.6, 118.9, 114.1, 46.6, 39.1; HRMS (ESI) *m/z*: calcd $[M + H]^+$ for $C_{21}H_{20}N_5^+$ 342.1714; found $[M + H]^+$ 342.1706.

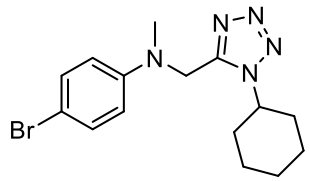

4-Bromo-*N*-((1-cyclohexyl-1*H*-tetrazol-5-yl)methyl)-*N*-methyl aniline (**2.121**). The crude material (reaction performed with 3 equivalents of cyclohexyl isocyanide and azidotrimethylsilane) was purified by column chromatography (*n*-hexane/EtOAc 9:1) to give the product as a white solid (52.5 mg, 50% yield;). ^{1}H NMR (700 MHz, $CDCl_3$) δ 7.37–7.35 (m, 2H), 6.76–6.74 (m, 2H), 4.72 (s, 2H), 4.16–4.12 (m, 1H), 2.90 (s, 3H), 1.99–1.93 (m, 2H), 1.90–1.88 (m, 2H), 1.85–1.83 (m, 2H), 1.72–1.70 (m, 1H), 1.31–1.19 (m, 3H); ^{13}C $\{^1$H$\}$ NMR (176 MHz, $CDCl_3$) δ 151.0, 148.1, 132.2, 116.1, 111.6, 58.4, 46.5, 39.1, 32.9, 25.3, 24.7; HRMS (ESI) *m/z*: calcd $[M + H]^+$ for $C_{15}H_{21}BrN_5^+$ 350.0975; found $[M + H]^+$ 350.0987.

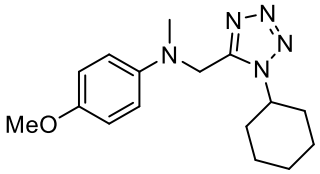

N-((1-Cyclohexyl-1*H*-tetrazol-5-yl)methyl)-4-methoxy-*N*-methylaniline (**2.122**). The crude material was purified by column chromatography (*n*-hexane/EtOAc 85:15) to give the product as a brownish solid (51.2 mg, 57% yield). ^{1}H NMR (700 MHz, $CDCl_3$) δ 6.89 (d, J = 8.7 Hz, 2H), 6.85 (d, J = 8.8 Hz, 2H), 4.59 (s, 2H), 4.25–4.22 (m, 1H), 3.77 (s, 3H), 2.78 (s, 3H), 1.97–1.92 (m, 2H), 1.89–1.87 (m, 2H), 1.84–1.82 (m, 2H), 1.69 (m, 1H), 0.89–0.87 (m, 3H); ^{13}C $\{^1$H$\}$ NMR (176 MHz, $CDCl_3$) δ 154.2, 151.1, 143.9, 118.3, 114.8, 58.4, 55.6, 48.2, 40.4, 32.9, 25.4, 24.8; HRMS (ESI) *m/z*: calcd [M + H]+ for $C_{16}H_{24}N_5O^+$ 302.1975; found $[M + H]^+$ 30 2.1984.

General procedure for the synthesis of secondary linear imides 2.136 and 2.137 via the use of 2,4-dimethoxybenzyl isocyanide as a cleavable one

2,4-Dimethoxybenzyl isocyanide **2.133** (0.08 mmol, 1 equiv.), *m*-toluic acid **2.16** (0.12 mmol, 1.5 equiv.), the aniline derivative (0.16 mmol, 2 equiv.) and 800 µL of dry MeCN (0.1 M) were added to a 4 mL colourless screw-cap glass vial equipped with a magnetic stir bar; 80 mg of 3 Å activated molecular sieves were then added to the resulting mixture, which was stirred open to air in a PhotoRedOx Box (EvoluChem™), under 30W blue LED irradiation, at room temperature, for 48 h. After completion of the reaction, as monitored by TLC, the crude mixture was transferred into a 10 ml round bottom flask and the solvent was removed under vacuum; a 1:1 DCM/TFA mixture (0.1 M, 400 µL of dry DCM and 400 µL of TFA) was then added at 0 °C, and the resulting mixture was stirred at 50° C for 4 h. After completion of the reaction, as monitored by TLC, the solvent was removed under vacuum, by adding *n*-hexane several times in order to remove the residual TFA, and the crude mixture was purified by column chromatography.

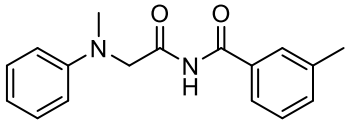

3-Methyl-*N*-(*N*-methyl-*N*-phenylglycyl)benzamide (**2.136**). The crude material was purified by column chromatography (*n*-hexane/EtOAc 96:4) to give the product as a colourless sticky solid (9.1 mg, 40% yield). ^{1}H NMR (700 MHz, $CDCl_3$) δ 9.14 (brs, -N*H*), 7.54 (s, 1H), 7.51 (d, J = 7.7 Hz, 1H), 7.39 (d, J = 7.6 Hz, 1H), 7.33 (t, J = 7.6 Hz, 1H), 7.30–7.27 (m, 2H), 6.83 (t, J = 7.3 Hz, 1H), 6.78 (d, J = 8.1 Hz, 2H), 4.47 (s, 2H), 3.11 (s, 3H), 2.38 (s, 3H); ^{13}C {^{1}H} NMR (176 MHz, $CDCl_3$) δ 171.8, 165.4, 148.8, 139.1, 134.1, 132.5, 129.5, 128.9, 128.4, 124.7, 118.4, 112.9, 58.7, 39.8, 21.3; HRMS (ESI) *m/z*: calcd $[M + H]^+$ for $C_{17}H_{19}N_2O_2^+$ 283.1442; found $[M + H]^+$ 283.1434.

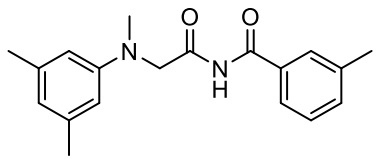

N-(*N*-(3,5-Dimethylphenyl)-*N*-methylglycyl)-3-methylbenzamide (**2.137**). The crude material was purified by column chromatography (*n*-hexane/EtOAc 94 :6) to give the product as a pinkish solid (9.0 mg, 36% yield). ^{1}H NMR (700 MHz, $CDCl_3$) δ 9.26 (brs, -N*H*), 7.51 (s, 1H), 7.49 (d, J = 7.8 Hz, 1H), 7.39 (d, J = 7.5 Hz, 1H), 7.32 (t, J = 7.6 Hz, 1H), 6.51 (s, 1H), 6.42 (s, 2H), 4.37 (s, 2H), 3.07 (s, 3H), 2.37 (s, 3H), 2.28 (s, 6H); ^{13}C {^{1}H} NMR (176 MHz, $CDCl_3$) δ 171.5, 165.3, 148.9, 139.2, 139.0, 134.0, 132.6, 128.9, 128.4, 124.7, 120.7, 111.1, 58.9, 40.0, 21.8, 21.3; HRMS (ESI) *m/z*: calcd $[M + H]^+$ for $C_{19}H_{23}N_2O_2^+$ 311.1754; found $[M + H]^+$ 311.1746.

General procedure for the synthesis of bis-amide derivatives 2.146-2.148 via the Ugi 3-CR/deprotection/Mumm transacylation sequence

Tert-butyl (2-isocyanobenzyl)carbamate **2.143** (0.08 mmol, 1 equiv.), *m*-toluic acid **2.16** (0.12 mmol, 1.5 equiv.), the aniline derivative (0.16 mmol, 2 equiv.) and 800 µL of dry MeCN (0.1 M) were added to a 4 mL colourless screw-cap glass vial equipped with a magnetic stir bar; 80 mg of 3 Å activated molecular sieves were then added to the resulting mixture, which was stirred open to air in a PhotoRedOx Box (EvoluChem™), under 30W blue LED irradiation, at room temperature, for 48–72 h. After completion of the reaction, as monitored by TLC, the crude mixture was transferred into a 10 ml round bottom flask and the solvent was removed under vacuum; a 3:1 DCM/TFA mixture (0.1 M, 600 µL of dry DCM and 200 µL of TFA) was then added at 0° C, and the resulting mixture was stirred at room temperature for 1 h until completion of the reaction, as monitored by TLC. After evaporating TFA under a nitrogen positive flow, a 3:1 DCM/Et_3N mixture (0.1 M, 600 µL of dry DCM and 200 µL of Et_3N) was added dropwise at 0 °C, and the resulting

mixture was stirred at room temperature for 1 h until completion of the reaction, as monitored by TLC. Then the solvent was removed under vacuum and the crude mixture was purified by column chromatography.

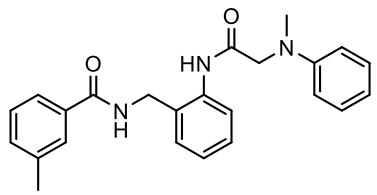

3-Methyl-*N*-(2-(2-(methyl(phenyl)amino)acetamido)benzyl)benzamide (**2.146**). The crude material was purified by column chromatography (*n*-hexane/EtOAc 75:25) to give the product as a pale-yellow amorphous solid (15.3 mg, 49% yield; 1:0.9 mixture of rotamers). ^{1}H NMR (700 MHz, $CDCl_3$; major rotamer) δ 9.55 (brs, -N*H*), 7.79 (d, J = 8.0 Hz, 1H), 7.50 (s, 1H), 7.46 (d, J = 7.4 Hz, 1H), 7.32–7.26 (m, 1H), 7.24–7.20 (m, 4H), 7.16–7.10 (m, 2H), 6.78–6.77 (m, 3H), 6.73 (brt, -N*H*), 4.34 (d, J = 5.9 Hz, 2H), 4.09 (s, 2H), 3.18 (s, 3H), 2.36 (s, 3H); ^{13}C {^{1}H} NMR (176 MHz, $CDCl_3$; major rotamer) δ 171.8, 166.6, 149.1, 138.4, 136.5, 134.7, 132.5, 130.4, 129.6, 129.5, 128.9, 128.7, 128.5, 125.5, 124.6, 124.0, 118.3, 113.3, 58.9, 40.7, 39.9, 21.5; HRMS (ESI) *m/z*: calcd $[M + H]^+$ for $C_{24}H_{26}N_3O_2^+$ 388.2020; found $[M + H]^+$ 388.2012.

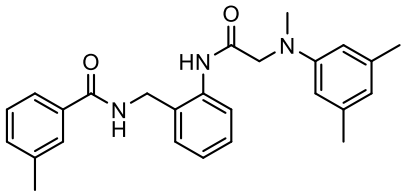

N-(2-(2-((3,5-Dimethylphenyl)(methyl)amino)acetamido)benzyl)3-methyl benzamide (**2.147**). The crude material was purified by column chromatography (*n*-hexane/EtOAc 87:13) to give the product as a beige solid (22.9 mg, 69% yield; 1:0.6 mixture of rotamers). ^{1}H NMR (700 MHz, $CDCl_3$; major rotamer) δ 9.35 (brs, -N*H*), 7.73 (d, J = 8.0 Hz, 1H), 7.51 (s, 1H), 7.45 (d, J = 7.4 Hz, 1H), 7.37–7.31

(m, 4H), 7.17–7.15 (m, 1H), 6.77 (brt, -N*H*), 6.45 (s, 1H), 6.41 (s, 2H), 4.40 (d, *J* = 5.7 Hz, 2H), 4.04 (s, 2H), 3.13 (s, 3H), 2.36 (s, 3H), 2.23 (s, 6H); ^{13}C {^{1}H} NMR (176 MHz, $CDCl_3$; major rotamer) δ 170.5, 167.7, 149.3, 138.9, 138.4, 135.6, 133.7, 132.4, 130.8, 130.7, 128.9, 128.4, 127.7, 126.0, 124.7, 124.0, 120.6, 111.2, 59.2, 40.8, 40.4, 21.7, 21.3; HRMS (ESI) *m/z*: calcd $[M + H]^+$ for $C_{26}H_{30}N_3O_2^+$ 416.2333; found $[M + H]^+$ 416.2325.

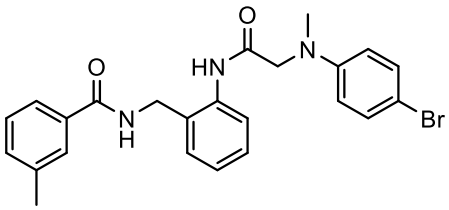

N-(2-(2-((4-Bromophenyl)(methyl)amino)acetamido)benzyl)-3-methylbenzamide (**2.148**). The crude material was purified by column chromatography (*n*-hexane/EtOAc 80:20) to give the product as an off-white amorphous solid (12.8 mg, 34% yield; 1:0.6 mixture of rotamers). ^{1}H NMR (700 MHz, $CDCl_3$; major rotamer) δ 9.86 (brs, -N*H*), 7.46 (s, 1H), 7.44 (d, *J* = 7.6 Hz, 1H), 7.37 (d, *J* = 7.2 Hz, 1H), 7.36–7.65 (m, 4H), 7.24–7.22 (m, 2H), 7.14–7.11 (m, 1H), 6.66 (brt, J = 5.6Hz, -N*H*), 6.61–6.60 (m, 2H), 4.33 (d, *J* =6.1Hz, 2H), 4.10 (s,2H), 3.18 (s,3H), 2.37 (s,3H); ^{13}C {^{1}H} NMR (176 MHz, $CDCl_3$) δ 169.5, 167.9, 148.1, 138.5, 135.9, 133.2, 132.7, 131.8, 130.7, 129.2, 129.0, 128.5, 127.7, 125.4, 124.5, 124.0, 114.5, 111.0, 58.6, 40.8, 40.4, 21.4; HRMS (ESI) *m/z*: calcd $[M + H]^+$ for $C_{24}H_{25}BrN_3O_2^+$ 466.1125; found $[M + H]^+$ 466.1122.

2.5.

Optimisation of the reaction conditions for the tandem one-pot Passerini 3-CR

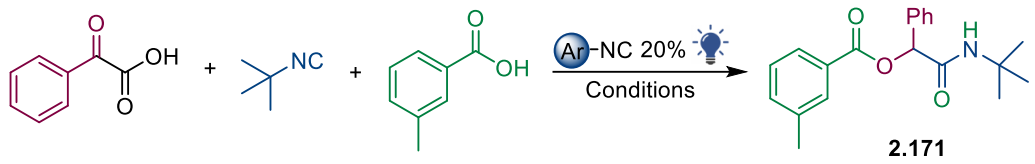

2.171

Entry	Phenylglyoxylic acid (equiv.)	*tert*-butyl NC (equiv.)	*m*-toluic acid (equiv.)	Solvent (0.25 M)	2.171 Yield[a] (%)
1	1	1 + 1 (after 20 h)	2 + 1 (after 48 h)	MeCN/H_2O 3:1	30
2	1	2	3	MeCN/H_2O 3:1	27
3	1	2	3	H_2O	Traces
4	1	2 (after 48 h)	3 (after 48 h)	MeCN/H_2O 3:1	56
5	1	2 (after 20 h)	3 (after 20 h)	MeCN/H_2O 3:1	70 (58)[b]

Conditions: reaction performed on a 0.08 mmol scale, in the presence of **2.154** (20 mol%), TIS (1 equiv.), and K_2HPO_4 (1.2 equiv.) as the base, under 30W blue LED irradiation, RT, 4 days.
[a] NMR yield (determined by using TMB as internal standard)
[b] Isolated yield

Optimisation of the reaction conditions for the tandem one-pot Strecker 3-CR

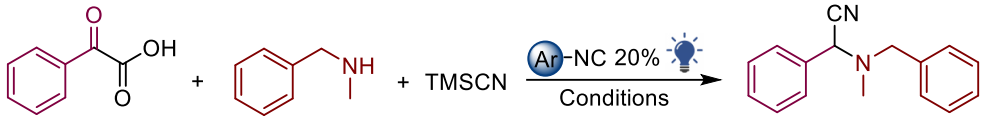

2.175

Entry	Phenylglyoxylic acid (equiv.)	*N*-benzylmethylamine (equiv.)	TMSCN (equiv.)	Time	2.175 Yield[a] (%)
1	1	1	2	20 h	Traces
2	1	1 (after 20 h)	2 (after 20 h)	3 d	58
3	1	1 (after 48 h)	2 (after 48 h)	4 d	73 (61)[b]

Conditions: reaction performed on a 0.08 mmol scale, in the presence of **2.154** (20 mol%), TIS (1 equiv.), and K_2HPO_4 (1.2 equiv.) as the base, in a 3:1 MeCN/H_2O solvent system (0.25 M) under 30W blue LED irradiation, RT.
[a] NMR yield (determined by using TMB as internal standard)
[b] Isolated yield

Optimisation of the reaction conditions for the tandem one-pot Ugi-tetrazole 4-CR

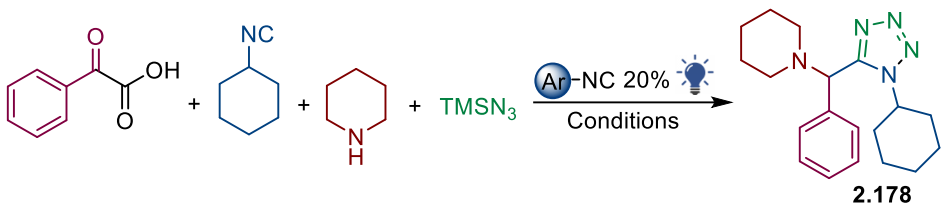

Entry	Phenylglyoxylic acid (equiv.)	Cyclohexyl NC (equiv.)	Piperidine (equiv.)	$TMSN_3$ (equiv.)	Time	2.178 Yield[a] (%)
1	1	2 (after 20 h)	1.5 (after 20 h)	2 (after 20 h)	3 d	33
2	1	3 (after 20 h)	1.5 (after 20 h)	3 (after 20 h)	3 d	72
3	1	2 (after 48 h)	1.5 (after 48 h)	2 (after 48 h)	4 d	80 (51)[b]

Conditions: reaction performed on a 0.08 mmol scale, in the presence of **2.154** (20 mol%), TIS (1 equiv.), and K_2HPO_4 (1.2 equiv.) as the base, in a 3:1 $MeCN/H_2O$ solvent system (0.25 M) under 30W blue LED irradiation, RT.
[a] NMR yield (determined by using TMB as internal standard)
[b] Isolated yield

Starting materials

Procedure for the synthesis of diethyl 4-([1,1'-biphenyl]-4-ylmethyl)-2,6-dimethyl-1,4-dihydropyridine-3,5-dicarboxylate 2.157

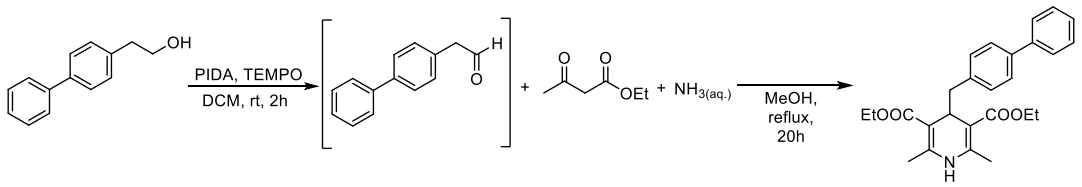

Step 1:[11] In a 50 mL round-bottom flask equipped with a magnetic stir bar 2-([1,1'-biphenyl]-4-yl)ethan-1-ol (1 mmol, 1 equiv.) was dissolved in DCM (1 mL, 1 M), and PIDA (1.1 mmol, 1.1equiv.) and TEMPO (0.1 mmol, 10 mol%) were then added. The mixture was stirred at room temperature for 2 h, until completion of the reaction, as monitored by TLC. Then the solvent was removed under a positive

flow of nitrogen and the crude reaction mixture was used in the following step without purification.

Step 2: The crude 2-([1,1'-biphenyl]-4-yl)acetaldehyde (1 mmol, 1 equiv.) was dissolved in MeOH (670 µL, 1.5 M), and ethyl acetoacetate (255.2µL, 2 mmol, 2 equiv.) and aqueous NH_4OH (NH_3 30–33% in water, 10 mmol, 10 equiv.) were added. The resulting mixture was stirred at reflux overnight, then the solvent was removed under vacuum and the crude material was purified by column chromatography (*n*-hexane/EtOAc 96:4) to give diethyl 4-([1,1'-biphenyl]-4-ylmethyl)-2,6-dimethyl-1,4-dihydropyridine-3,5-dicarboxylate **2.157** as a beige solid (213.8 mg, 51% yield). ^{1}HNMR (400 MHz, $CDCl_3$) δ 7.58–7.55 (m, 2H), 7.44–7.40 (m, 4H), 7.33–7.30 (m, 1H), 7.12–7.10 (m, 2H), 5.26 (brs, -N*H*), 4.22 (t, *J* = 5.5Hz, 1H), 4.13–3.99 (m, 4H), 2.62 (d, *J* = 5.6Hz, 2H), 2.20 (s, 6H), 1.23 (t, *J* = 7.1Hz, 6H); ^{13}C{^{1}H} NMR (101MHz, $CDCl_3$) δ 167.8, 145.3, 141.3, 138.6, 138.5, 130.5, 128.7, 127.0, 126.9, 126.0, 102.1, 59.6, 42.1, 35.6, 19.3, 14.4.; HRMS (ESI) *m/z*: calcd $[M + H]^+$ for $C_{26}H_{30}NO_4^+$ 420.2170; found $[M + H]^+$ 420.2169.

Procedure for the synthesis of potassium ([1,1'-biphenyl]-4-ylmethyl)trifluoroborate 2.161

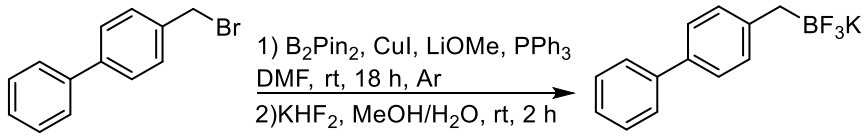

Synthesised according to a literature procedure.[12] 4-(Bromomethyl)-1,1'-biphenyl (2 mmol, 1 equiv.), CuI (0.2 mmol, 10 mol%), LiOMe (4 mmol, 2 equiv.), PPh_3 (0.26 mmol, 13 mol%), and bis(pinacolato)diboron (3 mmol, 1.5 equiv.) were added to a 100 mL Schlenk tube equipped with a magnetic stir bar, and the vessel was evacuated and filled with argon three times. Dry DMF (8 mL, 0.25 M) was then added by syringe under argon atmosphere. The resulting mixture was stirred

vigorously at 25° C for 18 h. The reaction mixture was diluted with EtOAc and filtered through silica gel. Then the mixture was washed with brine (x3). The organic layer was dried over sodium sulfate, filtered, concentrated to near dryness, then diluted with MeOH (8 mL) and cooled to 0 °C. Saturated aqueous solution of KHF_2 (5 mL, 10 mmol) was added dropwise and the resulting suspension was stirred for 2 h and then concentrated to dryness. The residue, a white solid, was extracted with hot acetone (3 x 6 mL), and the combined filtered extracts were concentrated to near dryness. Cold ether was added, and the resultant precipitate was collected and dried to afford potassium ([1,1'-biphenyl]-4-ylmethyl)trifluoroborate **2.161** as a white solid (274.5 mg, 50% yield). Characterisation data were in agreement with literature reports.[13]

General procedure for the synthesis of *α*-ketoacids

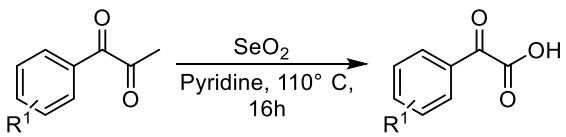

Synthesised according to a literature procedure.[14] To a 25 mL dry round bottom flask equipped with a magnetic stir bar the aryl ketone (1 equiv.) and selenium dioxide (2 equiv.) were added, followed by anhydrous pyridine (0.25 M). The reaction mixture was stirred at 110° C for 16 h. After completion of the reaction, as monitored by TLC, the solution containing precipitated selenium was filtered and the residue was washed with EtOAc. The filtrate was treated with 1 M aqueous NaOH and the aqueous layer was separated. This procedure was repeated three times, then the aqueous layers were combined and acidified with 1 M aqueous HCl (until pH ~ 1.5). Thus, the aqueous mixture was extracted with EtOAc (x3), and the combined organic layers were washed with brine, dried over sodium sulfate, and concentrated under vacuum to provide a solid, which was washed three times with *n*-hexane and then dried to afford the desired α-ketoacid.

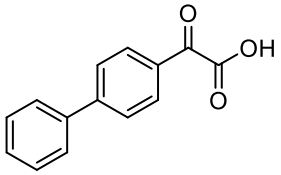

2-([1,1'-biphenyl]-4-yl)-2-oxoacetic acid. The title compound was prepared according to the reported general procedure starting from 4-acethylbiphenyl (3 mmol), and obtained as an off-white solid (448.0 mg, 66% yield). Characterisation data are in agreement with literature reports.[15]

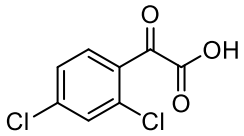

2-(2,4-dichlorophenyl)-2-oxoacetic acid. The title compound was prepared according to the reported general procedure starting from 2',4'-dichloroactetophenone (2.7 mmol), and obtained as a reddish solid (474.0 mg, 80% yield). Characterisation data are in agreement with literature reports.[16]

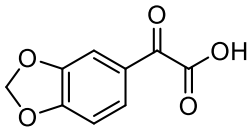

2-(benzo[d][1,3]dioxol-5-yl)-2-oxoacetic acid. The title compound was prepared according to the reported general procedure starting from 3',4'-(methylenedioxy)acetophenone (2.4 mmol), and obtained as an off-white solid (368.1 mg, 79% yield). Characterisation data are in agreement with literature reports.[15]

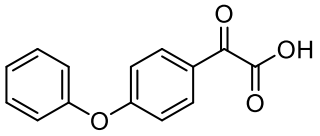

2-oxo-2-(4-phenoxyphenyl)acetic acid. The title compound was prepared according to the reported general procedure starting from 4'-phenoxyacetophenone (2.4 mmol), and obtained as a yellowish oil (470. 8 mg, 81% yield). Characterisation data are in agreement with literature reports.[17]

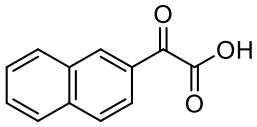

2-(naphthalen-2-yl)-2-oxoacetic acid. The title compound was prepared according to the reported general procedure starting from 2-acetonaphtone (2.9 mmol), and obtained as a yellow solid (494.5 mg, 85% yield). Characterisation data are in agreement with literature reports.[15]

Synthesis and characterisation data of isocyanides 2.66, 2.149-2.156

General procedure A for the synthesis of isocyanides 2.66, 2.154–2.156

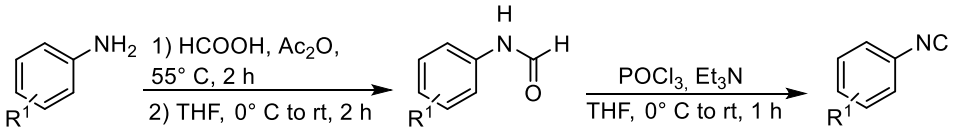

Synthesised according to a literature procedure.[18] *Step* 1: In a 50 mL two-necked round bottom flask, a mixture of formic acid (2.7 equiv.) and acetic anhydride (2.3 equiv.) was stirred at 55° C for 2 h. After the reaction was cooled at room temperature, the crude mixture was added dropwise to a solution of the starting aniline (1 equiv.) in THF (0.6 M), at 0° C. The resulting mixture was stirred at room temperature for 2 h, until completion of the reaction, as monitored by TLC.

Then the reaction was cooled to 0° C and a saturated aqueous solution of $NaHCO_3$ was added slowly under vigorous stirring, until neutral pH was reached. EtOAc was added, and the two phases were separated; the aqueous layer was further extracted with EtOAc (x2), then the combined organic extracts were washed with brine, dried over sodium sulfate, filtered, and concentrated under vacuum to give the resulting formamide in quantitative yield. The crude material was used in the next step without further purification.

Step 2: In a 100 ml round bottom flask equipped whit a magnetic stir bar, the formamide was dissolved in THF (0.6 M), and Et_3N (6.7 equiv.) was added to the solution. After cooling to 0°C, phosphorus oxychloride (1.7 equiv.) was added dropwise under argon atmosphere to the reaction mixture, which was stirred at room temperature for 1 h. After completion of the reaction, as monitored by TLC, the mixture was cooled to 0° C and a saturated aqueous solution of Na_2CO_3 was added slowly under vigorous stirring, until pH ~ 9. Then DCM was added, and the two phases were separated; the aqueous layer was further extracted with DCM (x2), then the combined organic extracts were washed with brine, dried over sodium sulfate, filtered, concentrated under vacuum, and the crude mixture was purified by column chromatography.

General procedure B for the synthesis of isocyanides 2.149-2.151

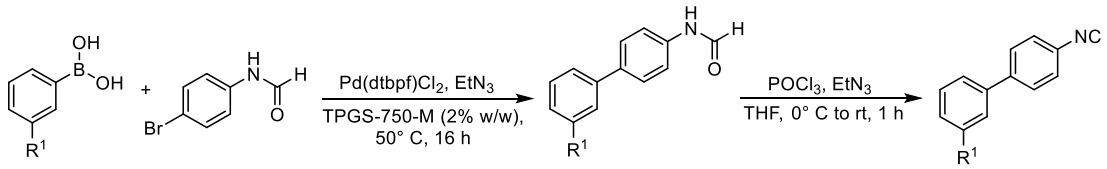

N-Biaryl formamides were prepared via Suzuki−Miyaura cross-couplings of arylboronic acids with *N*-(4-bromophenyl)formamide, following an in water protocol reported by Lipshutz,[19] and then dehydrated according to standard methods[18] to afford the desired isocyanides.

Step 1: *N*-(4-bromophenyl)formamide (1 equiv.), the arylboronic acid (1.5 equiv.) and Pd(dtbpf)Cl_2 (2 mol%), were added under argon to a 50 mL round bottom flask equipped with a magnetic stir bar. Aqueous TPGS-750-M (2% w/w, 0.5 M) and Et_3N (3 equiv.) were then added via syringe while vigorously stirring. The reaction mixture was stirred overnight at 50° C. Upon completion of the reaction, as monitored by TLC, the crude mixture was diluted with brine and extracted with EtOAc (x3). The organic extracts were dried over sodium sulfate, filtered, concentrated under vacuum, and the crude product was purified by column chromatography (*n*-hexane/EtOAc 70:30 or 50:50).

Step 2: The *N*-biaryl formamide intermediate was dissolved in THF (0.6 M), and Et_3N (6.7 equiv.) was added to the solution. After cooling to 0°C, phosphorus oxychloride (1.7 equiv.) was added dropwise under argon atmosphere to the reaction mixture, which was stirred at room temperature for 1 h. After completion of the reaction, as monitored by TLC, the mixture was cooled to 0° C and a saturated aqueous solution of Na_2CO_3 was added slowly under vigorous stirring, until pH ~ 9. Then DCM was added, and the two phases were separated; the aqueous layer was further extracted with DCM (x2), then the combined organic extracts were washed with brine, dried over sodium sulfate, filtered, and concentrated under vacuum. The crude mixture was purified by silica gel chromatography.

Procedure C for the synthesis of isocyanide 2.152

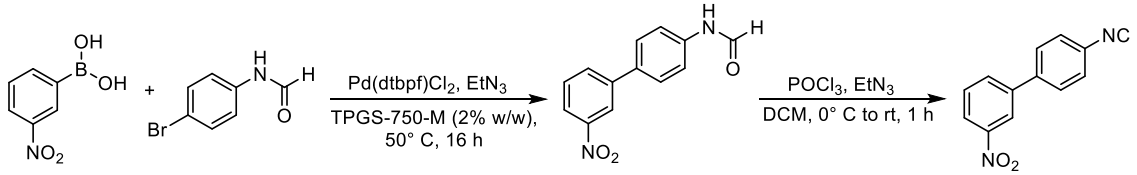

N-(3'-nitro-[1,1'-biphenyl]-4-yl)formamide was prepared via Suzuki−Miyaura cross-couplings of (3-nitrophenyl)boronic acid with *N*-(4-bromophenyl)formamide,

following an in water protocol reported by Lipshutz,[19] and then dehydrated according to the method developed by Dömling *et al*.[20] to afford the desired 4'-isocyano-3-nitro-1,1'-biphenyl **2.152**.

Step 1: *N*-(4-bromophenyl)formamide (1.3 mmol, 1 equiv.), (3-nitrophenyl)boronic acid (1.9 mmol, 1.5 equiv.) and Pd(dtbpf)Cl_2 (2 mol%) were added under argon to a 50 mL round bottom flask equipped with a magnetic stir bar. 2.6 mL of aqueous TPGS-750-M (2% w/w, 0.5 M) and Et_3N (0.73 mmol, 3 equiv.) were then added via syringe while vigorously stirring. The reaction mixture was stirred overnight at 50° C. Upon completion of the reaction, as monitored by TLC, the crude mixture was diluted with brine and extracted with EtOAc (x3). The organic extracts were dried over sodium sulfate, filtered, and concentrated under vacuum, and the crude product was purified by column chromatography (30:70 *n*-hexane/EtOAc) to give *N*-(3'-nitro-[1,1'-biphenyl]-4-yl)formamide as a brownish solid (211.3 mg, 87% yield).

Step 2: The intermediate *N*-(3'-nitro-[1,1'-biphenyl]-4-yl)formamide (1.1 mmol, 1 equiv.) was suspended in DCM (550 μL, 2 M), and Et_3N (5.5 mmol, 5 equiv.) was added to the suspension. After cooling to 0°C, phosphorus oxychloride (1.1 mmol, equiv.) was added dropwise under argon atmosphere to the reaction mixture, which was stirred at room temperature for 1 h. After completion of the reaction, as monitored by TLC, the crude mixture was transferred into a column pre-packed with dry 100-200 mesh size silica, and the isocyanide was eluted with Et_2O.

Procedure D for the synthesis of isocyanide 2.153

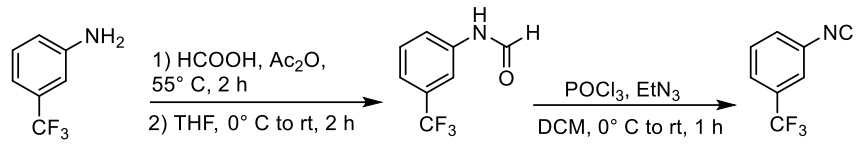

N-(3-(Trifluoromethyl)phenyl)formamide was prepared according to the standard procedure[18] and then dehydrated following the method developed by Dömling *et al.*[20] to afford the desired 1-isocyano-3-(trifluoromethyl)benzene **2.153**.

Step 1: In a 50 mL two-necked round bottom flask, a mixture of formic acid (8.4 mmol, 2.7 equiv.) and acetic anhydride (7.1 mmol, 2.3 equiv.) was stirred at 55°C for 2 h. After the reaction was cooled at room temperature, the crude mixture was added dropwise to a solution of the starting 3-(trifluoromethyl)aniline (3.1 mmol, 1 equiv.) in THF (5.2 mL, 0.6 M) at 0° C. The resulting mixture was stirred at room temperature for 2 h, until completion of the reaction, as monitored by TLC. Then the reaction was cooled to 0° C and a saturated aqueous solution of $NaHCO_3$ was added slowly under vigorous stirring, until neutral pH was reached. EtOAc was added, and the two phases were separated; the aqueous layer was further extracted with EtOAc (x2), then the combined organic extracts were washed with brine, dried over sodium sulfate, filtered, and concentrated under vacuum to give the resulting formamide in quantitative yield. The crude material was used in the next step without further purification.

Step 2: In a 100 ml round bottom flask equipped whit a magnetic stir bar *N*-(3-(trifluoromethyl)phenyl)formamide (3.1 mmol, 1 equiv.) was suspended in DCM (1.6 mL, 2 M), and Et_3N (15.5 mmol, 5 equiv.) was added to the suspension. After cooling to 0°C, phosphorus oxychloride (3.1 mmol, 1 equiv.) was added dropwise under argon atmosphere to the reaction mixture, which was stirred at room temperature for 1 h. After completion of the reaction, as monitored by TLC, the crude mixture was transferred into a column pre-packed with dry 100-200 mesh size silica, and the isocyanide was eluted with Et_2O.

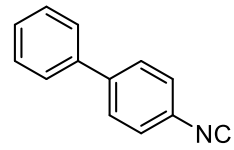

4-Isocyano-1,1'-biphenyl (**2.66**). The title compound was prepared according to general procedure A starting from 4-aminobiphenyl (5.9 mmol). The crude material was purified by column chromatography (*n*-hexane/EtOAc 95:5) to give the product as an orange solid (1.0 g, 95% yield over two steps). Characterisation data are in agreement with literature reports.[18]

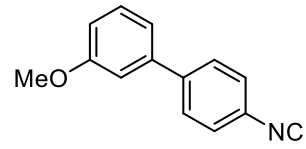

4'-Isocyano-3-methoxy-1,1'-biphenyl (**2.149**). The title compound was prepared according to general procedure B starting from *N*-(4-bromophenyl)formamide (1.0 mmol) and (3-methoxyphenyl)boronic acid (1.5 mmol). The crude material was purified by column chromatography (*n*-hexane/EtOAc 90:10) to give the product as a green solid (161.1 mg, 77% yield over two steps). ^{1}H NMR (400 MHz, $CDCl_3$) δ 7.61–7.58 (m, 2H), 7.45–7.40 (m, 2H),7.38 (t, J = 8.0 Hz, 1H), 7.15–7.13 (m, 1H), 7.08–7.07 (m, 1H), 6.95–6.93 (m, 1H), 3.87 (s, 3H); ^{13}C {^{1}H} NMR (101 MHz, $CDCl_3$) δ 164.6, 160.1, 142.3, 140.9, 130.1, 128.1, 126.8, 125.7 (t, J = 11.2 Hz, Ar-N*C*), 119.6, 113.5, 113.0, 55.4; HRMS (ESI) *m/z*: calcd $[M + H]^+$ for $C_{14}H_{12}NO^+$ 210.0913; found $[M + H]^+$ 210.0908.

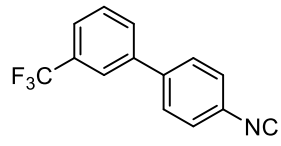

4'-Isocyano-3-(trifluoromethyl)-1,1'-biphenyl (**2.150**). The title compound was prepared according to general procedure B starting from *N*-(4-bromophenyl)formamide (1.7 mmol) and (3-(trifluoromethyl)phenyl)boronic acid

(2.6 mmol). The crude material was purified by column chromatography (*n*-hexane/EtOAc 90:10) to give the product as a green solid (281.6 mg, 67% yield over two step). ^{1}H NMR (700 MHz, $CDCl_3$) δ 7.80 (s, 1H), 7.74 (d, J = 7.7 Hz, 1H), 7.66 (d, J = 7.7 Hz, 1H), 7.64–7.57 (m, 3H), 7.49 (d, J = 8.4 Hz, 2H); ^{13}C {^{1}H} NMR (101 MHz, $CDCl_3$) δ 165.3, 140.9, 140.2, 131.5 (q, $J_{C\text{-}F}$ = 32.4Hz), 130.4, 129.6, 128.2, 127.0, 126.3 (t, J = 11.6Hz, Ar-N*C*), 124.9 (q, $J_{C\text{-}F}$ = 3.6 Hz), 124.0 (q, $J_{C\text{-}F}$ = 273.2 Hz); 123.9 (q, $J_{C\text{-}F}$ = 3.6 Hz); HRMS (ESI) *m/z*: calcd [M + H]$^+$ for $C_{14}H_9F_3N^+$ 248.0682; found [M + H]$^+$ 248.0675.

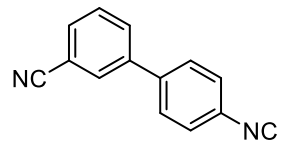

4'-Isocyano-[1,1'-biphenyl]-3-carbonitrile (**2.151**). The title compound was prepared according to general procedure B starting from *N*-(4-bromophenyl)formamide (1.2 mmol) and (3-cyanophenyl)boronic acid (1.8 mmol). The crude material was purified by column chromatography (*n*-hexane/EtOAc 95:5) to give the product as a beige solid (206.7 mg, 81% yield over two steps). ^{1}H NMR (400 MHz, $CDCl_3$) δ 7.84 (s, 1H), 7.79 (d, J = 7.5 Hz, 1H), 7.69 (d, J = 7.2 Hz, 1H), 7.60–7.58 (m, 3H), 7.51–7.49 (m, 2H); ^{13}C {^{1}H} NMR (101 MHz, $CDCl_3$) δ 165.6, 140.6, 140.0, 131.6, 131.4, 130.7, 129.9, 128.1, 127.2, 126.6 (t, J = 13.2Hz, Ar-N*C*), 118.4, 113.4; HRMS (ESI) *m/z*: calcd [M + H]$^+$ for $C_{14}H_9N_2^+$ 205.0760; found [M + H]$^+$ 205.0757.

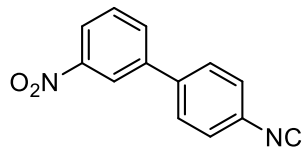

4'-Isocyano-3-nitro-1,1'-biphenyl (**2.152**). The title compound was prepared according to general procedure C to give the product as a brownish solid (128.2 mg, 44% yield over two steps). ^{1}H NMR (600 MHz, $CDCl_3$) δ 8.43 (s,1H), 8.27–

8.25 (m, 1H), 7.90–7.88(m, 1H), 7.67–7.64 (m, 3H), 7.52 (d, J = 8.0 Hz, 2H); ^{13}C {^{1}H} NMR (101 MHz, $CDCl_3$) δ 165.8, 148.8, 141.0, 139.8, 133.0, 130.1, 128.3, 127.2, 126.7 (t, J = 11.9 Hz, Ar-N*C*), 123.0, 122.0; HRMS (ESI) *m/z*: calcd [M + H]$^+$ for $C_{13}H_9N_2O_2^+$ 225.0659; found [M + H]$^+$ 225.0653.

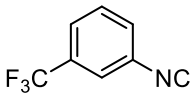

1-Isocyano-3-(trifluoromethyl)benzene (**2.153**). The title compound was prepared according to general procedure D to give the product as a brown sticky solid (164.8 mg, 31% yield over two steps). Characterisation data are in agreement with literature reports.[21]

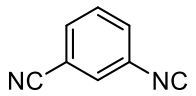

3-Isocyanobenzonitrile (**2.154**). The title compound was prepared according to general procedure A starting from 3-aminobenzonitrile (4.2 mmol). The crude material was purified by column chromatography (*n*-hexane/EtOAc 95:5) to give the product as a pale-yellow solid (476.3 mg, 88% yield). Characterisation data are in agreement with literature reports.[22]

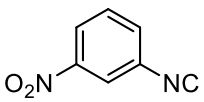

1-Isocyano-3-nitrobenzene (**2.155**). The title compound was prepared according to general procedure A starting from 3-nitroaniline (7.2 mmol). The crude material was purified by column chromatography (*n*-hexane/EtOAc 90:10) to give the product as a brownish solid (853.0 mg, 80% yield). Characterisation data are in agreement with literature reports.[23]

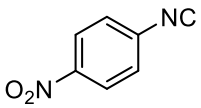

1-Isocyano-4-nitrobenzene (**2.156**). The title compound was prepared according to general procedure A starting from 4-nitroaniline (7.2 mmol). The crude material was purified by column chromatography (*n*-hexane/EtOAc 90:10) to give the product as a brownish solid (906.5 mg, 85% yield). Characterisation data are in agreement with literature reports.[23]

General procedure for the synthetic studies involving Hantzsch esters

In a 4 mL colourless screw-cap glass vial equipped with a magnetic stir bar diethyl 4-([1,1'-biphenyl]-4-ylmethyl)-2,6-dimethyl-1,4-dihydropyridine-3,5-dicarboxylate **2.157** (0.08 mmol, 1 equiv.) was dissolved in dry MeCN (530 μL, 0.15 M), and the selected H-donor (HE or TIS, 0.08 mmol, 1 equiv.) and isocyanide (0.016 mmol, 20 mol%) were then added. The resulting mixture was stirred open to air in a PhotoRedOx Box (EvoluChem™), under 30W or 1W blue LED irradiation, at room temperature, for 20-48 h. Then the crude material was diluted with EtOAc and washed with an aqueous 1 M HCl solution (x3). The aqueous layers were further extracted with EtOAc (x2), then the combined organic extracts were washed with brine, dried over sodium sulfate, filtered, and concentrated under vacuum. The crude material was purified by column chromatography.

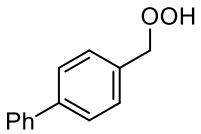

4-(Hydroperoxymethyl)-1,1'-biphenyl (**2.160**). The title compound was prepared according to the reported general procedure, employing 1-isocyano-3-nitrobenzene **2.155**, TIS as the H-donor, and 30W blue LED as the light source, with a reaction time of 48h. The crude material was purified by column chromatography (*n*-

hexane/EtOAc 99:1) to give the product as a pale-yellow solid (9.3mg, 58% yield). ^{1}H NMR (400 MHz, $CDCl_3$) δ 8.02 (brs, -OO*H*), 7.63–7.58 (m, 4H), 7.49–7.43 (m, 4H), 7.39–7.34 (m, 1H), 5.06 (s, 2H); ^{13}C {^{1}H} NMR (101 MHz, $CDCl_3$) δ 141.6, 140.7, 134.7, 129.5, 128.8, 127.5, 127.4, 127.2,79.0; HRMS (ESI) *m/z*: calcd $[M + H]^+$ for $C_{13}H_{13}O_2^+$ 201.0910; found $[M + H]^+$ 201.0902; *m/z* of the corresponding aldehyde was also present: calcd $[M + H]^+$ for $C_{13}H_{11}O^+$ 183.0805; found $[M + H]^+$ 183.0805.

General procedure for the synthetic studies involving potassium alkyltrifluoroborates

In a 4 mL colourless screw-cap glass vial equipped with a magnetic stir bar potassium ([1,1'-biphenyl]-4-ylmethyl)trifluoroborate **2.161** (0.08 mmol, 1 equiv.) was dissolved in a MeCN/H_2O mixture (9:1, 8:2 or 3:1, 530µL, 0.15 M) and the selected H-donor (HE or TIS, 0.08 mmol, 1 equiv.) and isocyanide (0.016 mmol, 20 mol%) were then added. The resulting mixture was stirred open flask in a PhotoRedOx Box (EvoluChem™), under 30W blue LED irradiation, at room temperature, for 20-48 h. Then the solvent was removed under vacuum and the crude material was purified by column chromatography.

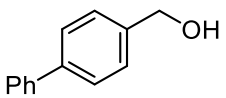

[1,1'-Biphenyl]-4-ylmethanol (**2.162**). The title compound was prepared according to the reported general procedure, employing 1-isocyano-3-nitrobenzene **2.155**, TIS as the H-donor, and an 8:2 MeCN/H_2O mixture as the solvent system, with a reaction time of 20 h. The crude material was purified by column chromatography (*n*-hexane/EtOAc 98:2) to give the product as a pale-yellow solid (9.6 mg, 65% yield). ^{1}H NMR (400 MHz, $CDCl_3$) δ 7.62–7.59 (m, 4H), 7.48–7.43 (m, 4H), 7.37 (t, J = 7.3 Hz, 1H), 4.74 (s, 2H;), 1.95 (brs, -O*H*); ^{13}C {^{1}H} NMR (101 MHz,

$CDCl_3$) δ 141.0, 140.8, 140.0, 128.9, 127.6, 127.4, 127.2, 65.2; HRMS (ESI) *m/z* $[M + Na]^+$ calcd for $C_{13}H_{12}NaO^+$ 207.0780, found $[M + H]^+$ 207.0777.

Synthetic studies involving α-ketoacids

General procedure for the synthesis of aldehyde derivatives 2.166-2.170

In a 4 mL colourless screw-cap glass vial equipped with a magnetic stir bar the α-ketoacid (0.08 mmol, 1 equiv.) was dissolved in a 3:1 MeCN/H_2O mixture (320 μL, 0.25 M,) and K_2HPO_4 (0.096 mmol, 1.2 equiv.), TIS (0.08 mmol, 1equiv.) and 3-isocyanobenzonitrile **2.154** (0.016 mmol, 20 mol%) were then added. The resulting mixture was stirred in a PhotoRedOxBox (EvoluChem™), under 30W blue LED irradiation, at room temperature, for 72 h. Then the solvent was removed under vacuum and the crude material was purified by column chromatography.

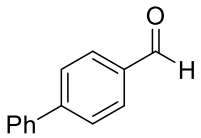

[1,1'-Biphenyl]-4-carbaldehyde (**2.166**).[24] The crude material was purified by column chromatography (*n*-hexane/EtOAc 99:1) to give the product as a colourless oil (12.0 mg, 82% yield). ^1H NMR (400 MHz, $CDCl_3$) δ 10.06 (s, 1H), 7.98–7.93 (m, 2H), 7.78–7.74 (m, 2H), 7.66–7.62 (m, 2H), 7.52–7.46 (m, 2H), 7.45–7.40 (m, 1H); ^{13}C {^1H} NMR (101 MHz, $CDCl_3$) δ 192.0, 147.3, 139.8, 135.3, 130.4, 129.1, 128.6, 127.8, 127.5; HRMS (ESI) *m/z:* calcd $[M + H]^+$ for $C_{13}H_{11}O^+$ 183.0804; found $[M + H]^+$ 183.0798.

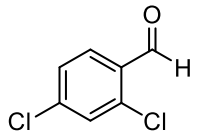

2,4-Dichlorobenzaldehyde (**2.167**).[24] The crude material was purified by column chromatography (*n*-hexane/EtOAc 99.5:0.5 to give the product as a colourless oil (9.0 mg, 64% yield). ^{1}H NMR (400 MHz, $CDCl_3$) δ 10.38 (s, 1H), 7.83 (d, J = 8.4 Hz, 1H), 7.44 (s, 1H), 7.33 (d, J = 8.4 Hz, 1H); ^{13}C {^{1}H} NMR (101 MHz, $CDCl_3$) δ 188.5, 141.2, 138.6, 131.0, 130.5, 130.4, 128.0; HRMS (ESI) *m/z*: calcd $[M + H]^+$ for $C_7H_5Cl_2O^+$ 176.9683; found $[M + H]^+$ 176.9677.

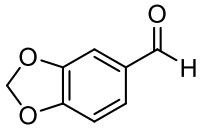

Benzo[*d*][1,3]dioxole-5-carbaldehyde (**2.168**).[25] The crude material was purified by column chromatography (*n*-hexane/EtOAc 99:1) to give the product as a colourless oil (4.5 mg, 37% yield). ^{1}H NMR (400 MHz, $CDCl_3$) δ 9.81 (s, 1H), 7.41 (dd, J_a = 7.9, J_b = 1.7 Hz, 1H), 7.33 (d, J = 1.4 Hz, 1H), 6.93 (d, J = 8.3 Hz, 1H), 6.07 (s, 2H); ^{13}C {^{1}H} NMR (101 MHz, $CDCl_3$) δ 190.2, 153.0, 148.6, 131.8, 128.6, 108.3, 106.8, 102.0; HRMS (ESI) *m/z*: calcd $[M + H]^+$ for $C_8H_7O_3^+$ 151.0390; found 151.0386.

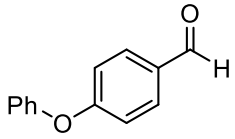

4-Phenoxybenzaldehyde (**2.169**).[26] The crude material was purified by column chromatography (*n*-hexane/EtOAc 99.5:0.5) to give the product as a colourless oil (8.4 mg, 53% yield). ^{1}H NMR ($CDCl_3$, 400 MHz) δ 9.92 (s, 1H), 7.89 – 7.80 (m, 2H), 7.46 – 7.38 (m, 2H), 7.30 – 7.18 (m, 1H), 7.13 – 7.03 (m, 4H); ^{13}C {^{1}H} NMR (101 MHz, $CDCl_3$) δ 190.8, 163.3, 155.1, 132.0, 131.3, 130.2, 125.0, 120.4, 117.6;

HRMS (ESI) *m/z*: calcd $[M + H]^+$ for $C_{13}H_{11}O_2^+$ 199.0754; found $[M + H]^+$ 199.0746.

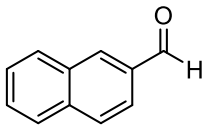

2-Naphthaldehyde (**2.170**).[24] The crude material was purified by column chromatography (*n*-hexane/EtOAc 99.5:0.5) to give the product as a colourless oil (5.6 mg, 45% yield). ^{1}H NMR ($CDCl_3$, 400 MHz) δ 10.13 (s, 1H), 8.28 (s, 1H), 7.99–7.84 (m, 4H), 7.65–7.53 (m, 2H); ^{13}C {^{1}H} NMR (101 MHz, $CDCl_3$) *δ* 192.2, 136.5, 134.6, 134.1, 132.7, 129.6, 129.14, 129.10, 128.1, 127.1, 122.8; HRMS (ESI) *m/z*: calcd $[M + H]^+$ for $C_{11}H_9O^+$ 157.0648; found $[M + H]^+$ 157.0642.

General procedure for the tandem one-pot Passerini 3-CR

In a 4 mL colourless screw-cap glass vial equipped with a magnetic stir bar the α-ketoacid (0.08 mmol, 1 equiv.) was dissolved in a 3:1 MeCN/H_2O mixture (320μL, 0.25 M) and K_2HPO_4 (0.096 mmol, 1.2 equiv.), TIS (0.08 mmol, 1 equiv.) and 3-isocyanobenzonitrile **2.154** (0.016 mmol, 20 mol%) were then added. The resulting mixture was stirred in a PhotoRedOx Box (EvoluChem™), under 30W blue LED irradiation, at room temperature, for 20 h. Then the selected isocyanide (0.16 mmol, 2 equiv.) and carboxylic acid (0.24 mmol, 3 equiv.) were added in situ, and the resulting mixture was stirred under 30W blue LED irradiation, at room temperature, for additional 72 h. The crude material was diluted with EtOAc and washed with a saturated aqueous solution of $NaHCO_3$ (x3). The aqueous layers were further extracted with EtOAc (x2), then the combined organic extracts were washed with brine, dried over sodium sulfate, filtered, and concentrated under vacuum. The crude material was purified by column chromatography.

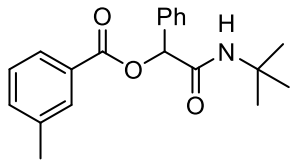

2-(*Tert*-butylamino)-2-oxo-1-phenylethyl-3-methylbenzoate (**2.171**). The crude material was purified by column chromatography (*n*-hexane/EtOAc 96:4) to give the product as a white solid (15.1 mg, 58% yield). ^{1}H NMR (400 MHz, $CDCl_3$) δ 7.89–7.88 (m, 2H), 7.54–7.52 (m, 2H), 7.43–7.33 (m, 5H), 6.21 (s, 1H), 6.00 (brs - N*H*), 2.42 (s, 3H), 1.37 (s, 9H); ^{13}C {^{1}H} NMR (101 MHz, $CDCl_3$) δ 167.4, 165.1, 138.5, 136.0, 134.4, 130.3, 128.9, 128.8, 128.5, 127.5, 126.9, 76.0, 51.6, 28.7, 21.3; HRMS (ESI) *m/z*: calcd $[M + H]^+$ for $C_{20}H_{24}NO_3^+$ 326.1751; found $[M + H]^+$ 326.1737.

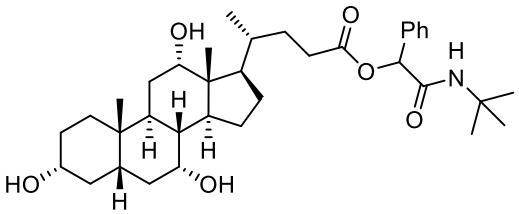

2-(*Tert*-butylamino)-2-oxo-1-phenylethyl(4*R*)-4-((3*R*,5*S*,7*R*,8*R*,9*S*,10*S*,12*S*,13*R*, 14*S*,17*R*)-3,7,12-trihydroxy-10,13-dimethylhexadecahydro-1*H*-cyclopenta[*a*] phenanthren-17-yl)pentanoate (**2.172**). The crude material was purified by column chromatography (DCM/MeOH 98:2) to give the product as a pale-yellow solid (15.1 mg, 32% yield). ^{1}H NMR (400 MHz, $CDCl_3$) δ 7.41–7.33 (m, 5H), 5.96 (s, 1H), 5.92 (brs, -N*H*), 3.96 (brs, -O*H*), 3.84 (brs, -O*H*), 3.48–3.41 (m, 1H), 2.53–2.32 (m,1H), 2.24–2.16 (m, 2H), 1.96–1.51 (m, 10H), 1.44–1.32 (m, 14H),1.30–1.18 (m, 4H), 1.14–1.06 (m, 1H), 1.00–0.94 (m, 4H), 0.92–0.85 (m, 6H), 0.64 (s, 3H); ^{13}C {^{1}H} NMR (101 MHz, $CDCl_3$, mix of rotamers) δ 172.4, 172.3, 167.5, 167.4, 136.1, 136.1, 128.8, 128.8, 128.7, 127.5, 127.4, 75.5, 75.5, 73.0, 72.0, 68.4, 51.5, 46.9, 46.5, 41.9, 41.4, 39.6, 39.5, 35.2, 35.1, 35.0, 34.7, 34.6, 31.6, 31.2, 31.2, 30.8, 30.7, 30.4, 29.9, 29.7, 28.7, 28.3, 27.5, 27.4, 26.6, 23.2, 22.7, 22.5, 17.3, 14.1,

12.5; HRMS (ESI) *m/z*: calcd $[M + H]^+$ for $C_{36}H_{56}NO_6^+$ 598.4103; found $[M + H]^+$ 598.4083.

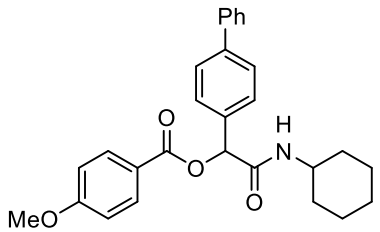

1-([1,1'-Biphenyl]-4-yl)-2-(cyclohexylamino)-2-oxoethyl-4-methoxybenzoate (**2.173**). The crude material was purified by column chromatography (*n*-hexane/EtOAc 90:10) to give the product as a white solid (14.1 mg, 40% yield). ^{1}H NMR (400 MHz, $CDCl_3$) δ 8.07 (d, J = 8.8 Hz, 2H), 7.62–7.56 (m, 6H),7.43 (t, J = 7.6 Hz, 2H),7.37–7.3 (m, 1H), 6.97 (d, J = 8.8 Hz, 2H), 6.33 (s, 1H), 6.11 (brd, J = 8.1Hz, -N*H*), 3.91–3.80 (m, 4H), 1.97–1.90 (m, 2H), 1.72–1.66 (m, 2H), 1.43–1.32 (m, 2H), 1.22–1.13 (m, 4H); ^{13}C {^{1}H} NMR (101 MHz, $CDCl_3$) δ 167.5, 164.6, 164.0, 141.8, 140.6, 135.0, 131.9, 128.8, 127.8, 127.5 (3C), 127.2, 121.6, 114.0, 75.4, 55.5, 48.2, 33.0, 32.9, 25.5, 24.7, 24.7; HRMS (ESI) *m/z*: calcd $[M + H]^+$ for $C_{28}H_{30}NO_4^+$ 444.2169; found $[M + H]^+$ 444.2154.

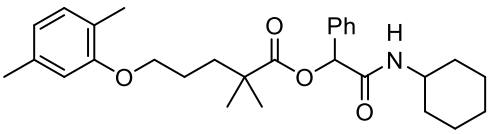

2-(Cyclohexylamino)-2-oxo-1-phenylethyl-5-(2,5-dimethylphenoxy)-2,2 dimethylpentanoate (**2.174**). The crude material was purified by column chromatography (*n*-hexane/EtOAc 97:3) to give the product as a colourless sticky solid (8.6 mg, 23% yield). ^{1}H NMR (400 MHz, $CDCl_3$) δ 7.43–7.41 (m, 2H), 7.37–7.33 (m, 3H), 6.99 (d, J = 7.4 Hz, 1H), 6.66 (d, J = 7.4 Hz, 1H), 6.58 (s, 1H), 6.05 (s, 1H), 5.95 (brd, J = 7.7 Hz, -N*H*), 3.91–3.78 (m, 3H), 2.30 (s, 3H), 2.14 (s, 3H), 1.94–1.58 (m, 6H), 1.43–1.26 (m, 9H), 1.16–1.05 (m, 2H), 0.93–0.82 (m, 3H); ^{13}C {^{1}H} NMR (101 MHz, $CDCl_3$) δ 175.8, 167.4, 161.6, 136.5, 135.9, 130.3, 128.8,

128.7, 127.2, 123.5, 120.8, 112.0, 75.3, 67.8, 48.0, 42.2, 37.1, 32.9, 32.9, 29.7, 25.4, 25.3, 25.1, 25.0, 24.6, 21.4, 15.8; HRMS (ESI) *m/z*: calcd $[M + H]^+$ for $C_{29}H_{40}NO_4^+$ 466.2952; found $[M + H]^+$ 466.2934.

General procedure for the tandem one-pot Strecker 3-CR

In a 4 mL colourless screw-cap glass vial equipped with a magnetic stir bar the α-ketoacid (0.08mmol, 1 equiv.) was dissolved in a 3:1 MeCN/H_2O mixture (320 μL, 0.25 M) and K_2HPO_4 (0.096 mmol, 1.2 equiv.), TIS (0.08 mmol, 1 equiv.) and 3-isocyanobenzonitrile **2.154** (0.016 mmol, 20 mol%) were then added. The resulting mixture was stirred in a PhotoRedOx Box (EvoluChem™), under 30W blue LED irradiation, at room temperature, for 48 h. Then a secondary amine (0.08 mmol,1 equiv.) and TMSCN (0.16 mmol, 2 equiv.) were added in situ, and the resulting mixture was stirred under 30W blue LED irradiation, at room temperature, for additional 48 h. The crude material was diluted with EtOAc and washed with a saturated aqueous solution of $NaHCO_3$ (x3). The aqueous layers were further extracted with EtOAc (x2), then the combined organic extracts were washed with brine, dried over sodium sulfate, filtered, and concentrated under vacuum. The crude material was purified by column chromatography.

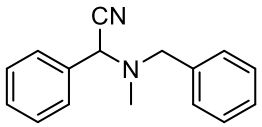

2-(Benzyl(methyl)amino)-2-phenylacetonitrile (**2.175**).[27] The crude material was purified by column chromatography (*n*-hexane/EtOAc 99:1) to give the product as a colourless oil (11.5 mg, 61% yield). ^{1}H NMR (400 MHz, $CDCl_3$) δ 7.58–7.51 (m, 2H), δ 7.45–7.26 (m, 8H), 4.90 (s, 1H), 3.84 (d, J = 13.1 Hz, 1H), 3.57 (d, J = 13.1 Hz, 1H), 2.27 (s, 3H). ^{13}C {^{1}H} NMR (101 MHz, $CDCl_3$) δ 137.5, 133.8, 129.1,

128.9, 128.9, 128.8, 127.9, 127.9, 115.3, 60.3, 59.4, 38.4; HRMS (ESI) *m/z*: $[M + H]^+$ calcd for $C_{16}H_{17}N_2^+$ 237.1386; found 237.1379.

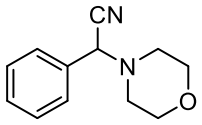

2-Morpholino-2-phenylacetonitrile (**2.176**).[28] The crude material was purified by column chromatography (*n*-hexane/EtOAc 97:3) to give the product as a white solid (10.2 mg, 63% yield). ^{1}H NMR (400 MHz, $CDCl_3$) δ 7.54 (d, 2H, J = 7.3 Hz, 1H), 7.36–7.44 (m, 3H), 4.82 (s, 1H), 3.68–3.78 (m, 4H), 2.54–2.62 (m, 4H); ^{13}C {^{1}H} NMR (101 MHz, $CDCl_3$) δ 130.6, 128.5, 127.9,127.2, 116.0, 66.0, 62.5, 48.8; HRMS (ESI) *m/z*: $[M + H]^+$ calcd for $C_{12}H_{15}N_2O^+$ 203.1179; found 203.1171.

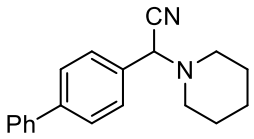

2-([1,1'-Biphenyl]-4-yl)-2-(piperidin-1-yl)acetonitrile (**2.177**). The crude material was purified by column chromatography (*n*-hexane/EtOAc 99:1) to give the product as a pale-yellow solid (16.4 mg, 74% yield). ^{1}H NMR (400 MHz, $CDCl_3$) δ 7.65–7.57 (m, 6H), 7.45 (t, J = 7.6 Hz, 2H), 7.39–7.35 (m, 1H), 4.86 (s, 1H), 2.61–2.51 (m, 4H), 1.67–1.59 (m, 4H), 1.53–1.49 (m, 2H); ^{13}C {^{1}H} NMR (101 MHz, $CDCl_3$) δ 141.7, 140.3 (2C), 128.9, 128.3, 127.6, 127.4, 127.1, 115.6, 62.8, 51.0, 25.8, 23.9; HRMS (ESI) *m/z*: calcd $[M + H]^+$ for $C_{19}H_{21}N_2^+$ 277.1699; found $[M + H]^+$ 277.1691.

Procedure for the tandem one-pot Ugi-tetrazole 4-CR

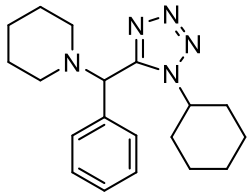

1-((1 cyclohexyl-1*H*-tetrazol-5-yl)(phenyl)methyl)piperidine (**2.178**). In a 4 mL colourless screw-capglass vial equipped with a magnetic stir bar phenylglyoxylic acid **2.163** (0.08 mmol, 1 equiv.) was dissolved in a 9:1 MeCN/H_2O mixture (320 µL, 0.25 M) and K_2HPO_4 (0.096 mmol, 1.2 equiv.), TIS (0.08 mmol, 1 equiv.) and 3-isocyanobenzonitrile **2.154** (0.016 mmol, 20 mol%) were then added. The resulting mixture was stirred in a PhotoRedOx Box (EvoluChem™), under 30W blue LED irradiation, at room temperature, for 48 h. Then cyclohexyl isocyanide (0.16 mmol, 2 equiv.), $TMSN_3$ (0.16 mmol, 2 equiv.) and piperidine (0.12 mmol, 1.5 equiv.) were added in situ, and the resulting mixture was stirred under 30W blue LED irradiation, at room temperature, for additional 48 h. Then the solvent was removed under vacuum and the crude material was purified by column chromatography (*n*-hexane/EtOAc 97:3) to give the product as a colourless oil (13.2 mg, 51% yield). ^{1}H NMR (400 MHz, $CDCl_3$) δ 7.43 (d, J = 7.6 Hz, 2H),7.36–7.26 (m, 3H), 5.00 (s, 1H), 4.68 (m, 1H), 2.60–2.53 (m, 2H), 2.29–2.21 (m, 2H), 2.01–1.72 (m, 7H), 1.63–1.44 (m, 6H), 1.38–1.25 (m, 3H); ^{13}C {^{1}H} NMR (101 MHz, $CDCl_3$) δ 153.7, 135.7, 128.6, 128.5, 128.3, 65.7, 58.0, 52.6, 32.8, 32.8, 26.1, 25.6, 25.4, 24.9, 24.2; HRMS (ESI) *m/z*: calcd $[M + H]^+$ for $C_{19}H_{28}N_5^+$ 326.2340; found $[M + H]^+$ 326.2327.

Procedure for the Passerini 3-CR starting from benzaldehyde

In a 4 mL colourless screw-cap glass vial equipped with a magnetic stir bar benzaldehyde (0.08 mmol, 1 equiv.), *tert*-butyl isocyanide (0.08 mmol, 1 equiv.)

and *m*-toluic acid (0.08 mmol, 1 equiv.) were dissolved in a 3:1 MeCN/H_2O mixture (320 μL, 0.25 M). The reaction was stirred at room temperature for 72 h, then the solvent was removed under vacuum and the yield determined by NMR analysis of the crude reaction mixture after adding TMB as internal standard (58% NMR yield).

Procedure for the Strecker 3-CR starting from benzaldehyde

In a 4 mL colourless screw-cap glass vial equipped with a magnetic stir bar benzaldehyde (0.08 mmol, 1 equiv.), *N*-benzylmethylamine (0.08 mmol, 1 equiv.) and TMSCN (0.16 mmol, 2 equiv.) were dissolved in a 3:1 MeCN/H_2O mixture (320 μL, 0.25 M). The reaction was stirred at room temperature for 48 h, then the solvent was removed under vacuum and the yield determined by NMR analysis of the crude reaction mixture after adding TMB as internal standard (85% NMR yield).

Procedure for the Ugi-tetrazole 4-CR starting from benzaldehyde

In a 4 mL colourless screw-cap glass vial equipped with a magnetic stir bar benzaldehyde (0.08 mmol, 1 equiv.), cyclohexyl isocyanide (0.08 mmol, 1 equiv.), $TMSN_3$ (0.08 mmol, 1 equiv.) and piperidine (0.08 mmol, 1 equiv.) were dissolved in 9:1 MeCN/H_2O mixture (320 μL, 0.25 M). The reaction was stirred at room temperature for 48 h, then the solvent was removed under vacuum and the yield determined by NMR analysis of the crude reaction mixture after adding TMB as internal standard (63% NMR yield).

Deuterium labelling experiments

General procedure for the synthesis of aldehyde derivatives 2.166-D, 2.167-D and 2.170-D

In a 4 mL colourless screw-cap glass vial equipped with a magnetic stir bar the α-ketoacid (0.08 mmol, 1 equiv.) was dissolved in a 3:1 MeCN/D_2O mixture (320 μL, 0.25 M,) and K_2HPO_4 (0.096 mmol, 1.2 equiv.), TIS (0.08 mmol, 1equiv.) and 3-isocyanobenzonitrile **2.154** (0.016 mmol, 20 mol%) were then added. The resulting mixture was stirred in a PhotoRedOxBox (EvoluChem™), under 30W blue LED irradiation, at room temperature, for 72 h. Then the solvent was removed under vacuum and the crude material was purified by column chromatography.

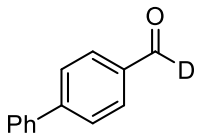

[1,1'-Biphenyl]-4-carbaldehyde-*d* (**2.166**-D).[29] The crude material was purified by column chromatography (*n*-hexane/EtOAc 99:1) to give the product as a colourless oil (12.8 mg, 87% yield, 98% deuterium incorporation) ^{1}H NMR (400 MHz, $CDCl_3$) δ 8.02 – 7.88 (m, 2H), 7.73 (d, J = 7.2 Hz, 2H), 7.62 (d, J = 7.6 Hz, 2H), 7.46 (t, J = 7.6 Hz, 2H), 7.40 (dd, J_a = 7.6, J_a = 6.4 Hz, 1H); ^{13}C {^{1}H} NMR (101 MHz, $CDCl_3$) δ 191.7 (t, J = 26.5 Hz), 147.2, 139.7, 135.1 (t, J = 3.5 Hz), 130.3, 129.1, 128.5, 127.7, 127.4; HRMS (ESI) *m/z*: calcd $[M + H]^+$ for $C_{13}H_{10}DO^+$ 184.0876; found $[M + H]^+$ 184.0862.

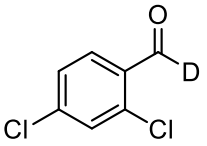

2,4-Dichlorobenzaldehyde-*d* (**2.167-D**). The crude material was purified by column chromatography (*n*-hexane/EtOAc 99.5:0.5) to give the product as a colourless oil (7.0 mg, 50% yield, 97% deuterium incorporation). ^{1}H NMR (400 MHz, $CDCl_3$) δ 7.88 (d, J = 8.4 Hz, 1H), 7.49 (d, J = 1.9 Hz, 1H), 7.38 (dd, J_a = 8.4, J_b =1.9 Hz, 2H); ^{13}C {^{1}H} NMR (101 MHz, $CDCl_3$) δ 188.2 (t, J = 26.5 Hz), 141.1, 138.6, 130.9 (t, J = 3.5 Hz), 130.5, 130.3, 128.0; HRMS *m/z*: calcd $[M + H]^+$ for $C_7H_4DCl_2O^+$ 175.9775; found $[M + H]^+$ 175.9771.

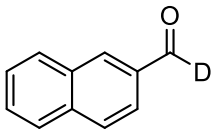

2-Naphthaldehyde-*d* (**2.170-D**).[29] The crude material was purified by column chromatography (*n*-hexane/EtOAc 99.5:0.5) to give the product as a colourless oil (4.9 mg, 39% yield, 97% deuterium incorporation). ^{1}H NMR (400 MHz, $CDCl_3$) δ 8.31 (s, 1H), 8.03 – 7.85 (m, 4H), 7.72–7.50 (m, 2H); ^{13}C {^{1}H} NMR (101 MHz, $CDCl_3$) δ 192.1 (t, J = 26.5 Hz), 136.5, 134.7, 134.1 (t, J = 3.5 Hz), 132.7, 129.6, 129.2, 129.1, 128.2, 127.2, 122.8; HRMS (ESI) *m/z*: calcd $[M + H]^+$ for $C_{11}H_8DO^+$ 158.0711; found $[M + H]^+$ 158.0704.

Procedure for the tandem one-pot Passerini 3-CR to D-labelled derivative 2.179-D

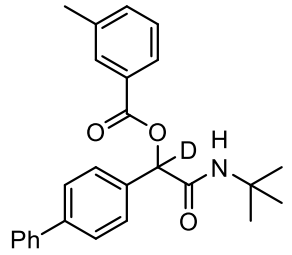

1-([1,1'-Biphenyl]-4-yl)-2-(tert-butylamino)-2-oxoethyl-1-*d*-3-methylbenzoate (**2.179-D**). In a 4 mL colourless screw-cap glass vial equipped with a magnetic stir bar 2-([1,1'-biphenyl]-4-yl)-2 oxoacetic acid **2.165** (0.08 mmol, 1 equiv.) was dissolved in a 3:1 MeCN/D_2O mixture (320 μL, 0.25 M) and K_2HPO_4 (0.096 mmol, 1.2 equiv.), TIS (0.08 mmol, 1 equiv.) and 3-isocyanobenzonitrile **2.154** (0.016 mmol, 20 mol%) were then added. The resulting mixture was stirred in a PhotoRedOx Box (EvoluChem™), under 30W blue LED irradiation, at room temperature, for 20 h. Then *tert*-butyl isocyanide (0.16 mmol, 2 equiv.) and *m*-toluic acid (0.24 mmol, 3 equiv.) were added in situ, and the resulting mixture was stirred under 30W blue LED irradiation, at room temperature, for additional 72 h. The crude material was diluted with EtOAc and washed with a saturated aqueous solution of $NaHCO_3$ (x3). The aqueous layers were further extracted with EtOAc (x2), then the combined organic extracts were washed with brine, dried over sodium sulfate, filtered, and concentrated under vacuum. The crude material was purified by column chromatography (*n*-hexane/EtOAc 96:4) to give the product as a yellow solid (16.1 mg, 50% yield, 100% deuterium incorporation). ^{1}H NMR (400 MHz, $CDCl_3$) δ 7.91–7.90 (m, 2H), 7.63–7.57 (m, 6H), 7.46–7.33 (m, 5H), 6.07 (brs, -N*H*), 2.43 (s, 3H), 1.39 (s, 9H); ^{13}C {^{1}H} NMR (101 MHz, $CDCl_3$) δ 167.4, 165.1, 141.8, 140.6, 138.6, 134.9, 134.4, 130.3, 129.3, 128.8, 128.6, 127.9, 127.6, 127.5, 127.2, 126.9, 75.5 (t, J = 23.2 Hz), 51.6, 28.7, 21.3; HRMS (ESI) *m/z*: calcd $[M + H]^+$ for $C_{26}H_{27}DNO_3^+$ 403.2127; found $[M + H]^+$ 403.2115.

Procedure for the tandem one-pot Strecker 3-CR to D-labelled derivative 2.175-D

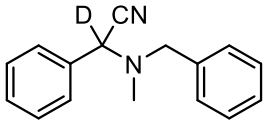

2-(Benzyl(methyl)amino)-2-phenylacetonitrile-*d* (**2.175-D**). In a 4 mL colourless screw-cap glass vial equipped with a magnetic stir bar phenylglyoxylic acid **2.163** (0.08 mmol, 1 equiv.) was dissolved in a 3:1 MeCN/D_2O mixture (320 μL, 0.25 M) and K_2HPO_4 (0.096 mmol, 1.2 equiv.), TIS (0.08 mmol, 1 equiv.) and 3-isocyanobenzonitrile **2.154** (0.016 mmol, 20 mol%) were then added. The resulting mixture was stirred in a PhotoRedOx Box (EvoluChem™), under 30W blue LED irradiation, at room temperature, for 48 h. Then *N*-benzylmethylamine (0.08 mmol, 1 equiv.) and TMSCN (0.16 mmol, 2equiv.) were added in situ, and the resulting mixture was stirred under 30W blue LED irradiation, at room temperature, for additional 48 h. The crude material was diluted with EtOAc and washed with a saturated aqueous solution of $NaHCO_3$ (x3). The aqueous layers were further extracted with EtOAc (x2), then the combined organic extracts were washed with brine, dried over sodium sulfate, filtered, and concentrated under vacuum. The crude material was purified by column chromatography (*n*-hexane/EtOAc 99.5:0.5) to give the product as a colourless oil (9.6 mg, 51% yield, 80% deuterium incorporation). ^{1}H NMR (400 MHz, $CDCl_3$) δ 7.55–7.52 (m, 2H), 7.42–7.28 (m, 8H), 3.83 (d, J = 13.1 Hz, 1H), 3.56 (d, J = 13.1 Hz, 1H), 2.26 (s, 3H); ^{13}C {^{1}H} NMR (101 MHz, $CDCl_3$) δ 137.5, 133.8, 128.9, 128.8, 128.8, 128.7, 127.7, 127.7, 115.2, 59.8 (t, J = 22.2 Hz), 59.3, 38.3; HRMS (ESI) *m/z*: calcd $[M + H]^+$ for $C_{16}H_{16}DN_2^+$ 238.1450; found $[M + H]^+$ 238.1440.

Procedure for the tandem one-pot Ugi-tetrazole 4-CR to D-labelled derivative 2.178-D

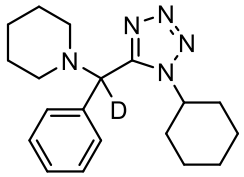

1-((1 Cyclohexyl-1*H*-tetrazol-5-yl)(phenyl)methyl-*d*)piperidine (**2.178-D**). In a 4 mL colourless screw-capglass vial equipped with a magnetic stir bar phenylglyoxylic acid **2.163** (0.08 mmol, 1 equiv.) was dissolved in a 9:1 MeCN/D_2O mixture (320 μL, 0.25 M) and K_2HPO_4 (0.096 mmol, 1.2 equiv.), TIS (0.08 mmol, 1 equiv.) and 3-isocyanobenzonitrile **2.154** (0.016 mmol, 20 mol%) were then added. The resulting mixture was stirred in a PhotoRedOx Box (EvoluChem™), under 30W blue LED irradiation, at room temperature, for 48 h. Then cyclohexyl isocyanide (0.16 mmol, 2 equiv.), $TMSN_3$ (0.16 mmol, 2 equiv.) and piperidine (0.12 mmol, 1.5 equiv.) were added in situ, and the resulting mixture was stirred under 30W blue LED irradiation, at room temperature, for additional 48 h. Then the solvent was removed under vacuum and the crude material was purified by column chromatography (*n*-hexane/EtOAc 98:2) to give the product as a colourless oil (11.2 mg, 42% yield, 93% deuterium incorporation). ^{1}H NMR (400 MHz, $CDCl_3$) *δ*7.44–7.42 (m, 2H), 7.36–7.26 (m, 3H), 4.71–4.63 (m, 1H), 2.61–2.53 (m, 2H), 2.30–2.23 (m, 2H), 1.99–1.72 (m, 7H), 1.66–1.29(m, 9H); ^{13}C {^{1}H} NMR (101 MHz, $CDCl_3$) *δ* 153.5, 135.5, 128.6, 128.6, 128.3, 65.2 (t, *J* = 19.8 Hz), 58.0, 52.5, 32.8, 32.8, 26.1, 25.6, 25.4, 24.9, 24.2; HRMS (ESI) *m/z*: calcd $[M + H]^+$ for $C_{19}H_{27}DN^+$ 327.2402; found $[M + H]^+$ 327.2389.

Procedure for the Passerini 3-CR starting from[1,1'-biphenyl]-4 carbaldehyde-*d* 2.166-D

In a 4 mL colourless screw-cap glass vial equipped with a magnetic stir bar [1,1'-biphenyl]-4-carbaldehyde-*d* **2.166-D** (0.08 mmol, 1 equiv.), *tert*-butyl isocyanide (0.08 mmol, 1 equiv.) and *m*-toluic acid (0.08 mmol, 1 equiv.) were dissolved in a 3:1 MeCN/H_2O mixture (320 µL, 0.25 M). The reaction was stirred at room temperature for 72 h, then the crude material was diluted with EtOAc and washed with a saturated aqueous solution of $NaHCO_3$ (x3). The aqueous layers were further extracted with EtOAc (x2), then the combined organic extracts were washed with brine, dried over sodium sulfate, filtered, and concentrated under vacuum. The crude material was purified by column chromatography (*n*-hexane/EtOAc 96:4) to give the product as a yellow solid (17.4 mg, 54%yield).

NMR investigations about the role of TIS

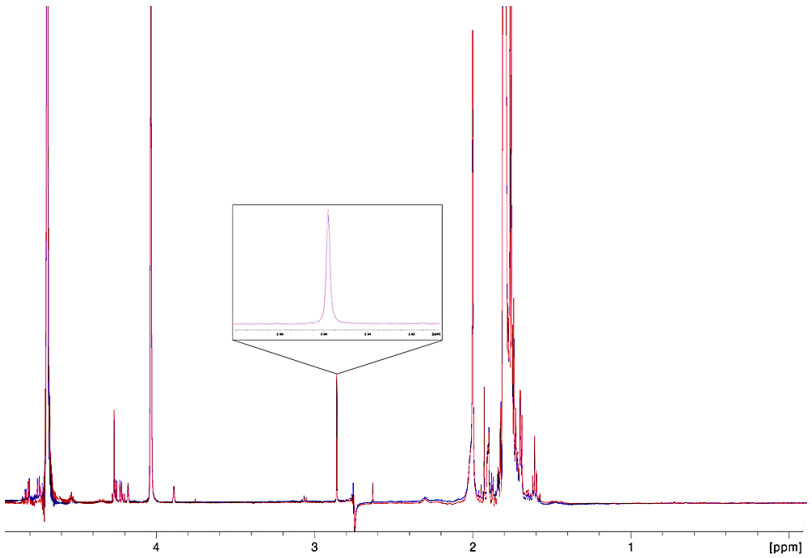

Superimposition of ^1H NMR spectra of TIS in MeCN alone, and after the addition of D_2O and irradiation under 30W blue LED for 20 h. Any Si-*H*/Si-*D* exchange (zoom of the Si-*H* in the box) could be observed, thus excluding a possible role of TIS as a deuterium atom transfer catalyst.

For details about computational studies, cyclic voltammetry, UV-VIS and fluoresce measurements see: Russo, C.; Donati, G.; Giustiniano, F.; Amato, J.; Marinelli, L.; Whitby, R. J.; Giustiniano, M.; *Chemistry – A European Journal* **2023**, *29,* e2023018, Supporting Information.

2.6.

Starting materials

General procedure for the synthesis of Strecker 3-CR adducts

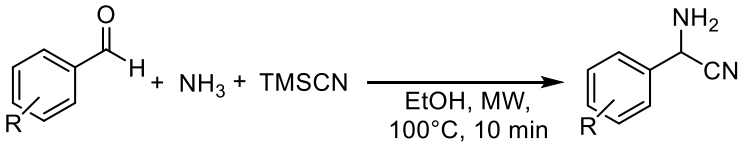

Into a 20 mL MW reactor vessel equipped with a magnetic stirrer, the aldehyde compound (5.5 mmol, 1 equiv.) was dissolved in a 2 M solution of ammonia in EtOH (11.0 mmol, 2 equiv.) and cooled to 0°C. TMSCN (5.5 mmol, 1 equiv.) was then added, the vessel was closed, and the reaction mixture was heated by MW irradiation using the following parameters: T = 100 °C, time = 10 min, cooling off. After cooling the reaction mixture to 0° C with an ice bath, $NaHCO_3$ sat. sol. was added, then the aqueous mixture was acidified to pH = 4 with 2 N HCl, and impurities were extracted with EtOAc (x3; until complete decolouration of the aqueous phase). The resulting aqueous mixture was basified to pH = 8-9 with sat. sol. Na_2CO_3 and extracted with EtOAc (x3). The combined organic extracts were dried over sodium sulfate, filtered, and concentrated under vacuum to give a crude mixture which was purified by trituration with *n*-hexane.

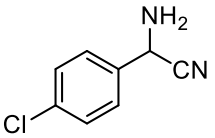

2-Amino-2-(4-chlorophenyl)acetonitrile. The title compound was prepared according to the reported general procedure starting from 4-chlorobenzaldehyde, and obtained as a yellow solid (687.2 mg, 75% yield). Characterisation data are in agreement with literature reports.[34]

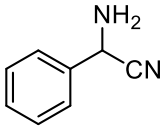

2-Amino-2-phenylacetonitrile. The title compound was prepared according to the reported general procedure starting from benzaldehyde, and obtained as a white solid (508.8 mg, 70% yield). Characterisation data are in agreement with literature reports.[34]

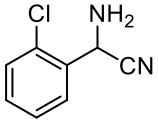

2-Amino-2-(2-chlorophenyl)acetonitrile. The title compound was prepared according to the reported general procedure starting from 2-chlorobenzaldehyde, and obtained as a yellow solid (430.6 mg, 47% yield). Characterisation data are in agreement with literature reports.[34]

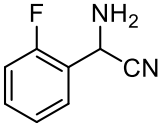

2-Amino-2-(2-fluorophenyl)acetonitrile. The title compound was prepared according to the reported general procedure starting from 2-fluorobenzaldehyde,

and obtained as a yellowish oil (371.5 mg, 45% yield). Characterisation data are in agreement with literature reports.[35]

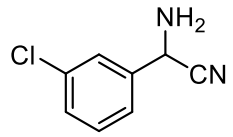

2-(3-Chlorophenyl)acetonitrile. The title compound was prepared according to the reported general procedure starting from 3-chlorobenzaldehyde, and obtained as a yellow solid (421.5 mg, 46% yield). Characterisation data are in agreement with literature reports.[34]

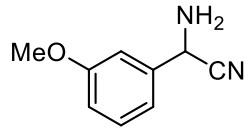

2-Amino-2-(3-methoxyphenyl)acetonitrile. The title compound was prepared according to the reported general procedure starting from 3-methoxybenzaldehyde, and obtained as a brownish solid (267.6 mg, 30% yield). Characterisation data are in agreement with literature reports.[36]

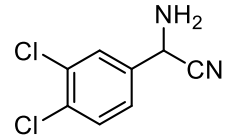

2-Amino-2-(3,4-dichlorophenyl)acetonitrile. The title compound was prepared according to the reported general procedure starting from 3,4-dichlorobenzaldehyde, and obtained as a yellow solid (552.8 mg, 50% yield). Characterisation data are in agreement with literature reports.[37]

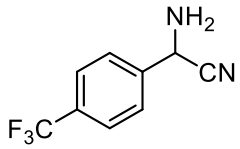

2-Amino-2-(4-(trifluoromethyl)phenyl)acetonitrile. The title compound was prepared according to the reported general procedure starting from 4-(trifluoromethyl)benzaldehyde, and obtained as an orange oil (451.3 mg, 41% yield). Characterisation data are in agreement with literature reports.[35]

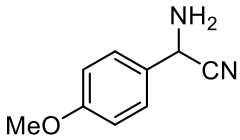

2-Amino-2-(4-methoxyphenyl)acetonitrile. The title compound was prepared according to the reported general procedure starting from 4-methoxybenzaldehyde, and obtained as a yellow solid (401.4 mg, 45% yield). Characterisation data are in agreement with literature reports.[34]

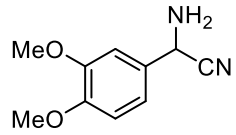

2-Amino-2-(3,4-dimethoxyphenyl)acetonitrile. The title compound was prepared according to the reported general procedure starting from 4-methoxybenzaldehyde, and obtained as a yellow solid (179.6, 17% yield). Characterisation data are in agreement with literature reports.[38]

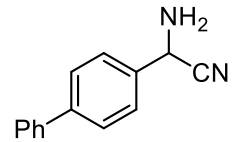

2-([1,1'-Biphenyl]-4-yl)-2-aminoacetonitrile. The title compound was prepared according to the reported general procedure starting from biphenyl-4-

carboxaldehyde, and obtained as a yellow solid (532.3 mg, 47% yield). ^{1}H NMR (700 MHz, $CDCl_3$) δ 7.67–7.64 (m, 2H), 7.63–7.58 (m, 4H), 7.48–7.44 (m, 2H), 7.38 (t, J = 7.4 Hz, 1H), 4.97 (s, 1H), 1.99 (s, 2H); ^{13}C NMR {^{1}H} (176 MHz, $CDCl_3$) δ 142.1, 140.2, 135.2, 128.9, 127.8, 127.2, 127.1, 120.9, 47.1; HRMS (ESI) *m/z*: calcd $[M + H]^+$ for $C_{14}H_{13}N_2^+$ (oxidised form) 207.0917; found$[M + H]^+$ 207.0917.

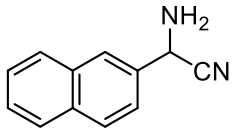

2-Amino-2-(naphthalen-2-yl)acetonitrile. The title compound was prepared according to the reported general procedure starting from 2-naphthaldehyde, and obtained as a white solid (370.8 mg, 37% yield). Characterisation data are in agreement with literature reports.[34]

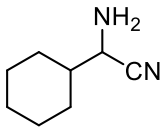

2-Amino-2-cyclohexylacetonitrile. The title compound was prepared according to the reported general procedure starting from cyclohexanecarbaldehyde, and obtained as a colourless oil (304.0 mg, 40% yield). Characterisation data are in agreement with literature reports.[34]

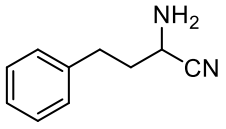

2-Amino-4-phenylbutanenitrile. The title compound was prepared according to the reported general procedure starting from 3-phenylpropanal, and obtained as a yellowish oil (176.2 mg, 20% yield). Characterisation data are in agreement with literature reports.[39]

General procedure for the synthesis of 4-substituted-5-aminoimidazole derivatives 2.189-2.200

The appropriate starting 2-aminoacetonitrile (0.3 mmol, 1 equiv.) was dissolved in dry 2-MeTHF (0.2 M) into a MW reactor vessel (0.5-2 mL size) equipped with a magnetic stirrer. Then, $Yb(OTf)_3$ (0.18 mmol, 0.6 equiv.) and *tert*-butyl isocyanide (0.6 mmol, 2 equiv.) were added, the vessel was closed and heated by MW irradiation using the following parameters: T = 130 °C, time = 10 min., cooling off. After cooling, the reaction mixture was diluted with EtOAc, the organic phase was washed with $NaHCO_3$ (x2), dried over sodium sulfate, filtered, and concentrated under vacuum to afford a dark reaction crude which was purified by column chromatography.

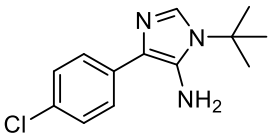

1-(*Tert*-butyl)-4-(4-chlorophenyl)-1*H*-imidazol-5-amine (**2.189**). The crude material was purified by column chromatography (DCM/MeOH 98:2) to give the product as a brown sticky solid (57.7 mg, 77% yield). ^{1}H NMR (700 MHz, CD_3OD) δ 7.67–7.62 (m, 2H), 7.47 (s, 1H), 7.37–7.33 (m, 2H), 1.71 (s, 9H); ^{13}C {^{1}H} NMR (176 MHz, CD_3OD) δ 133.7, 133.1, 130.8), 129.6, 128.1, 127.2, 125.9, 56.00, 28.3; HRMS (ESI) *m/z*: calcd $[M + H]^+$ for $C_{13}H_{17}ClN_3^+$ 250.1106; found $[M + H]^+$ 250.1106.

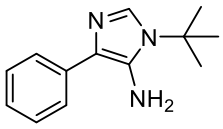

1-(*Tert*-butyl)-4-phenyl-1*H*-imidazol-5-amine (**2.190**). The crude material was purified by column chromatography (DCM/MeOH 98:2) to give the product as a

brown sticky solid (50.0 mg, 77% yield). ^{1}H NMR (700 MHz, CD_3OD) δ 7.66–7.62 (m, 2H), 7.47 (s, 1H), 7.40–7.35 (m, 2H), 7.19 (t, J = 7.4 Hz, 1H), 1.72 (s, 9H); ^{13}C {^{1}H} NMR (176 MHz, CD_3OD) δ 134.9, 132.7, 129.3, 128.1, 126.9, 125.9,125.4, 55.9, 28.4; HRMS (ESI) *m/z*: calcd $[M + H]^+$ for $C_{13}H_{18}N_3^+$ 216.1495; found $[M + H]^+$ 216.1496.

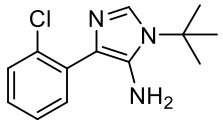

1-(*Tert*-butyl)-4-(2-chlorophenyl)-1*H*-imidazol-5-amine (**2.191**). The crude material was purified by column chromatography (DCM/MeOH 98:2) to give the product as a brown sticky solid (35.5 mg, 46% yield). ^{1}H NMR (700 MHz, CD_3OD) δ 7.49 (s, 1H), 7.46 (d, J = 7.9 Hz, 1H), 7.43 (d, J = 7.5 Hz, 1H), 7.33 (t, J = 7.4 Hz, 1H), 7.30 (d, J = 7.7 Hz, 1H), 1.71 (s, 9H); ^{13}C NMR (176 MHz, CD_3OD) δ 133.5 (2C), 133.0, 132.0, 129.5, 129.3, 128.4, 126.5, 125.3, 56.1, 28.3; HRMS (ESI) *m/z*: calcd $[M + H]^+$ for $C_{13}H_{17}ClN_3^+$ 250.1106; found $[M + H]^+$ 250.1111.

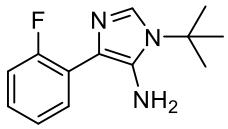

1-(*Tert*-butyl)-4-(2-fluorophenyl)-1*H*-imidazol-5-amine (**2.192**). The crude material was purified by column chromatography (DCM/MeOH 98:2) to give the product as a brown sticky solid (39.1 mg, 56% yield). ^{1}H NMR (700 MHz, CD_3OD) δ 7.55–7.50 (m, 2H), 7.29 (d, J = 7.1 Hz, 1H), 7.21 (t, J = 7.5 Hz, 1H), 7.15 (dd, J_a = 11.0, J_b = 8.3 Hz, 1H), 1.71 (s, 9H); ^{13}C NMR (176 MHz, CD_3OD) δ 159.2 (d, $J_{C\text{-}F}$ = 246.4), 134.1, 130.5 (d, $J_{C\text{-}F}$ = 4.1 Hz), 130.1, 127.9 (d, $J_{C\text{-}F}$ = 8.3 Hz), 124.1 (d, $J_{C\text{-}F}$ = 3.5 Hz), 122.2 (d, $J_{C\text{-}F}$ = 15.1 Hz), 121.6, 115.2 (d, $J_{C\text{-}F}$ = 22.9 Hz), 56.09, 28.3; HRMS (ESI) *m/z*: calcd $[M + H]^+$ for $C_{13}H_{17}FN_3^+$ 234.1401; found $[M + H]^+$ 234.1404.

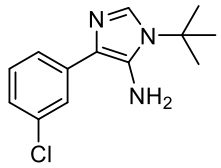

1-(*Tert*-butyl)-4-(3-chlorophenyl)-1*H*-imidazol-5-amine (**2.193**). The crude material was purified by column chromatography (DCM/MeOH 98:2) to give the product as a brown sticky solid (34.6 mg, 46% yield). ^{1}H NMR (700 MHz, CD_3OD) δ 7.70 (t, J = 1.8 Hz, 1H), 7.61–7.59 (m, 1H), 7.47 (s, 1H), 7.34 (t, J = 7.9 Hz, 1H), 7.17 (ddd, J_a = 8.0, J_b = 2.1, J_c = 0.9 Hz, 1H), 1.71 (s, 9H); ^{13}C {^{1}H} NMR (176 MHz, CD_3OD) δ 137.0, 134.1, 133.5, 129.7, 129.5, 125.5, 125.4, 125.0, 123.8, 56.0, 28.3; HRMS (ESI) *m/z*: calcd $[M + H]^+$ for $C_{13}H_{17}ClN_3^+$ 250.1106; found $[M + H]^+$ 250.1104.

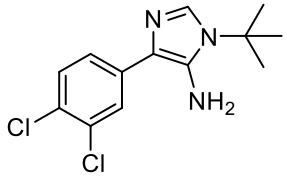

1-(*Tert*-butyl)-4-(3,4-dichlorophenyl)-1*H*-imidazol-5-amine (**2.194**). The crude material was purified by column chromatography (*n*-hexane/EtOAc 80:20) to give the product as a brown sticky solid (46.3 mg, 54% yield). ^{1}H NMR (700 MHz, CD_3OD) δ 7.86 (d, J = 2.0 Hz, 1H), 7.62 (dd, J_a = 8.4, J_b = 2.0 Hz, 1H), 7.50–7.45 (m, 2H), 1.71 (s, 9H); ^{13}C {^{1}H} NMR (176 MHz, CD_3OD) δ 134.9, 132.7, 129.3, 128.1, 126.9, 125.9,125.4, 55.9, 28.4; HRMS (ESI) *m/z*: calcd $[M + H]^+$ for $C_{13}H_{16}Cl_2N_3^+$ 284.0716; found $[M + H]^+$ 284.0717.

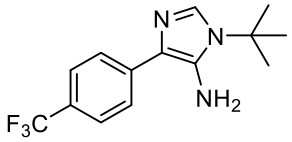

1-(*Tert*-butyl)-4-(4-(trifluoromethyl)phenyl)-1*H*-imidazol-5-amine (**2.195**). The crude material was purified by column chromatography (DCM/MeOH 98:2) to

give the product as a brown sticky solid (26.7 mg, 31% yield). ^{1}H NMR (700 MHz, CD_3OD) δ 7.87–7.83 (m, 2H), 7.67–7.62 (m, 2H), 7.50 (s, 1H), 1.72 (s, 9H); ^{13}C NMR (176 MHz, CD_3OD) δ 139.0, 134.4, 130.0, 126.6 (q, $J_{C\text{-}F}$ = 32.4 Hz), 125.7-125.5 (m), 124.92 (dd, $J_{aC\text{-}F}$ = 7.2, $J_{bC\text{-}F}$ 3.4 Hz), 124.2 (q, $J_{C\text{-}F}$ = 260.0 Hz), 122.3, 56.1, 28.3; HRMS (ESI) *m/z*: calcd $[M + H]^+$ for $C_{14}H_{17}F_3N_3^+$ 284.1369; found $[M + H]^+$ 284.1366.

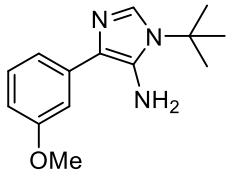

1-(*Tert*-butyl)-4-(3,4-dimethoxyphenyl)-1*H*-imidazol-5-amine (**2.196**). The crude material was purified by column chromatography (DCM/MeOH 98:2) to give the product as a brown sticky solid (33.4 mg, 45% yield) ^{1}H NMR (700 MHz, CD_3OD) δ 7.36 (s, 1H), 7.19–7.16 (t, J = 7.0 Hz, 1H), 7.13–7.10 (m, 2H), 6.68–6.65 (m, 1H), 3.72 (s, 3H), 1.61 (s, 9H); ^{13}C $\{^{1}H\}$ NMR (176 MHz, CD_3OD) δ 160.0, 151.3, 136.2, 132.9, 129.2, 129.1, 126.5, 118.2, 111.3, 111.2, 56.0, 54.2; HRMS (ESI) *m/z*: calcd $[M + H]^+$ for $C_{14}H_{20}N_3O^+$ 246.1601; found $[M + H]^+$ 246.1598.

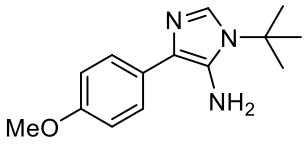

1-(*Tert*-butyl)-4-(4-methoxyphenyl)-1*H*-imidazol-5-amine (**2.197**). The crude material was purified by column chromatography (DCM/MeOH 98:2) to give the product as a brown sticky solid (42.3 mg, 57% yield). ^{1}H NMR (700 MHz, CD_3OD) δ 7.57–7.53 (m, 2H), 7.45 (s, 1H), 6.97–6.93 (m, 2H), 3.81 (s, 3H), 1.71 (s, 9H); ^{13}C $\{^{1}H\}$ NMR (176 MHz, CD_3OD) δ 158.1, 131.7, 129.0, 127.4, 127.3, 113.6, 55.9, 54.3, 28.4; HRMS (ESI) *m/z*: calcd $[M + H]^+$ for $C_{14}H_{20}N_3O^+$ 246.1601; found $[M + H]^+$ 246.1601.

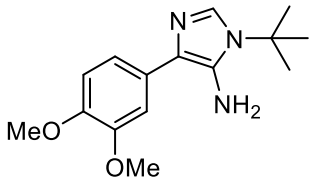

1-(*Tert*-butyl)-4-(3,4-dimethoxyphenyl)-1*H*-imidazol-5-amine (**2.198**). The crude material was purified by column chromatography (DCM/MeOH 97:3) to give the product as a brown sticky solid (34.5 mg, 42% yield). ^{1}H NMR (700 MHz, CD_3OD) δ 7.46 (s, 1H), 7.28 (s, 1H), 7.19 (dd, J_a = 8.2, J_b =1.5 Hz, 1H), 6.98 (d, J = 8.3 Hz, 1H), 3.88 (s, 3H), 3.84 (s, 3H), 1.71 (s, 9H); ^{13}C {^{1}H} NMR (176 MHz, CD_3OD) δ 149.1, 147.4, 132.0, 129.1, 128.2, 127.2, 118.4, 111.8, 110.4, 55.9, 55.2, 55.0, 28.4; HRMS (ESI) *m/z*: calcd $[M + H]^+$ for $C_{15}H_{22}N_3O_2^+$ 276.1707; found $[M + H]^+$ 276.1709.

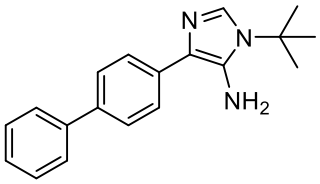

4-([1,1'-Biphenyl]-4-yl)-1-(*tert*-butyl)-1*H*-imidazol-5-amine (**2.199**). The crude material was purified by column chromatography (DCM/MeOH 98:2) to give the product as a brown sticky solid (46.0 mg, 53% yield). ^{1}H NMR (700 MHz, CD_3OD) δ 7.75–7.73 (m, 2H), 7.66–7.62 (m, 4H), 7.48 (s, 1H), 7.45–7.40 (m, 2H), 7.32 (d, J = 7.4 Hz, 1H), 1.72 (s, 9H); ^{13}C {^{1}H} NMR (176 MHz, CD_3OD) δ 140.8, 138.2, 134.0, 133.0, 129.5, 128.4,126.7, 126.6, 126.5, 126.3, 126.2, 56.0, 28.4; HRMS (ESI) *m/z*: calcd $[M + H]^+$ for $C_{19}H_{22}N_3^+$ 292.1808; found $[M + H]^+$ 292.1809.

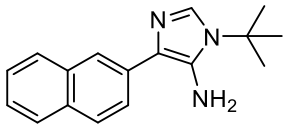

1-(*Tert*-butyl)-4-(naphthalen-2-yl)-1*H*-imidazol-5-amine (**2.200**). The crude material was purified by column chromatography (DCM/MeOH 98:2) to give the product as a brown sticky solid (27.5 mg, 35% yield). ^{1}H NMR (700 MHz, CD_3OD) δ 8.08 (s, 1H), 7.88–7.84 (m, 3H), 7.81 (d, J = 8.0 Hz, 1H), 7.52 (s, 1H), 7.45 (t, J = 7.1 Hz, 1H), 7.41 (t, J = 7.3 Hz, 1H), 1.74 (s, 9H); ^{13}C {^{1}H} NMR (176 MHz, CD_3OD) δ 133.9, 133.2, 132.5, 131.9, 129.5, 127.6, 127.4, 127.2, 126.8, 125.6, 124.9, 124.8, 123.6, 56.0, 28.4; HRMS (ESI) *m/z*: calcd $[M + H]^+$ for $C_{17}H_{20}N_3^+$ 266.1652; found $[M + H]^+$ 266.1653.

References

(1) Rueping, M.; Vila, C.; *Organic Letters,* **2013**, *15*, 2092–2095.

(2) Guerrero, I.; San Segundo, M.; Correa, A.; *Chemical Communications,* **2018**, *54*, 1627–1630.

(3) Zhou, H.; Lu, P.; Gu, X.; Li, P.; *Organic Letters,* **2013**, *15*, 5646–5649.

(4) Ye, X.; Xie, C.; Huang, R.; Liu, J.; *Synlett,* **2012**, *23*, 409–412.

(5) Youssef, A. I.; Farag, H. H.; F. Abdelkader, M. A.; Elgendy, M. A.; *Indian Journal of Chemistry, Sect. B: Organic Chemistry Including Medicinal Chemistry,* **1976**, *14B*, 279–281.

(6) Ye, X.; Xie, C.; Pan, Y.; Han, L.; Xie, T.; *Organic Letters,* **2010**, *12*, 4240–4243.

(7) Hari, D. P.; König, B.; *Organic Letters,* **2011**, *13*, 3852–3855.

(8) Rueping, M.; Zhu, S.; Koenigs, R. M.; *Chemical Communications,* **2011**, *47*, 8679.

(9) Condie, A. G.; González-Gómez, J. C.; Stephenson, C. R. J.; *Journal of the American Chemical Society,* **2010**, *132*, 1464–1465.

(10) Li, D.; Lei, J.; *Tetrahedron Letters,* **2020**, *61*, 152345.

(11) De Mico, A.; Margarita, R.; Parlanti, L.; Vescovi, A.; Piancatelli, G. A.; *The Journal of Organic Chemistry,* **1997**, *62*, 6974–6977.

(12) Zhou, S.; Lv, K.; Fu, R.; Zhu, C.; Bao, X.; *ACS Catalysis,* **2021**, *11*, 5026–5034.

(13) Liu, W.; Liu, P.; Lv, L.; Li, C.; *Angewandte Chemie International Edition,* **2018**, *57*, 13499–13503.

(14) Zhao, W.-W.; Shao, Y.-C.; Wang, A.-N.; Huang, J.-L.; He, C.-Y.; Cui, B.-D.; Wan, N.-W.; Chen, Y.-Z.; Han, W.-Y.; *Organic Letters,* **2021**, *23*, 9256–9261.

(15) Xie, S.; Li, D.; Huang, H.; Zhang, F.; Chen, Y.; *Journal of the American Chemical Society,* **2019**, *141*, 16237–16242.
(16) Li, P.-G.; Zhu, H.; Fan, M.; Yan, C.; Shi, K.; Chi, X.-W.; Zou, L.-H.; *Organic and Biomolecular Chemistry,* **2019**, *17*, 5902–5907.
(17) Wadhwa, K.; Yang, C.; West, P. R.; Deming, K. C.; Chemburkar, S. R.; Reddy, R. E.; *Synthetic Communications,* **2008**, *38*, 4434–4444.
(18) Dewanji, A.; Mück-Lichtenfeld, C.; Bergander, K.; Daniliuc, C. G.; Studer, A.; *Chemistry – A European Journal,* **2015**, *21*, 12295–12298.
(19) Lipshutz, B. H.; Petersen, T. B.; Abela, A. R.; *Organic Letters,* **2008**, *10*, 1333–1336.
(20) Patil, P.; Ahmadian-Moghaddam, M.; Dömling, A.; *Green Chemistry,* **2020**, *22*, 6902–6911.
(21) Polisar, J. G.; Norton, J. R.; *Tetrahedron,* **2012**, *68*, 10236–10240.
(22) Mayr, A.; Mao, L.-F.; *Inorganic Chemistry,* **1998**, *37*, 5776–5780.
(23) Wang, X.; Wang, Q.-G.; Luo, Q.-L.; *Synthesis,* **2014**, *47*, 49–54.
(24) Zhao, G.; Wang, Y.; Wang, C.; Lei, H.; Yi, B.; Tong, R.; *Green Chemistry,* **2022**, *24*, 4041–4049.
(25) Tobita, F.; Yasukawa, T.; Yamashita, Y.; Kobayashi, S.; *Catalysis Science and Technology,* **2022**, *12*, 1043–1048.
(26) Li, H.; Sibley, C. D.; Kharel, Y.; Huang, T.; Brown, A. M.; Wonilowicz, L. G.; Bevan, D. R.; Lynch, K. R.; Santos, W. L.; *Bioorganic and Medicinal Chemistry,* **2021**, *30*, 115941.
(27) Liu, L.; Liu, Y.; Shen, X.; Zhang, X.; Deng, S.; Chen, Y.; *The Journal of Organic Chemistry,* **2022**, *87*, 6321–6329.
(28) Ghogare, R.; *Organic Communications,* **2020**, *13*, 103–113.
(29) Dong, J.; Wang, X.; Wang, Z.; Song, H.; Liu, Y.; Wang, Q.; *Chemical Science,* **2020**, *11*, 1026–1031.
(30) Becke, A. D.; *Journal of Chemical Physics,* **1993**, *98*, 5648–5652.
(31) Lee, C.; Yang, W.; Parr, R. G.; *Physical Review B,* **1988**, *37*, 785–789.
(32) Gussoni, M.; Ramos, M. N.; Castiglioni, C.; Zerbi, G.; *Chemical Physics Letters,* **1989**, *160*, 200–205.
(33) Frisch, M. J.; Trucks, G. W.; Schlegel, H. B.; Scuseria, G. E.; Robb M. A.; *Gaussian 16, Revision A.03*, **2016**, Gaussian Inc., Wallingford.
(34) Li, Q.-H.; Li, Z.-F.; Tao, J.; Li, W.-F.; Ren, L.-Q.; Li, Q.; Peng, Y.-G.; Liu, T.-L.; *Organic Letters,* **2019**, *21*, 8429–8433.
(35) Vukelić, S.; Ushakov, D. B.; Gilmore, K.; Koksch, B.; Seeberger, P. H.; *European Journal of Organic Chemistry,* **2015**, *2015*, 3036–3039.
(36) Wang, M.-X.; Lin, S.-J.; *The Journal of Organic Chemistry,* **2002**, *67*, 6542–6545.
(37) Rebbaa, A.; Lettan R. B.; *Patent WO2015031109*, **2015**.
(38) Kehayova, P. D.; Bokinsky, G. E.; Huber, J. D.; Jain, A.; *Organic Letters,* **1999**, *1*, 187–188.

(39) Vukelić, S.; Koksch, B.; Seeberger, P. H.; Gilmore, K.; *Chemistry – A European Journal,* **2016**, *22*, 13451–13454.

Chapter 3

Isocyanide-based Multicomponent Reactions as valuable allies in the medicinal chemist's quest for new anticancer agents

Cancer treatment is one of the most pressing therapeutic needs of our time, with more than 18 million cancer cases reported around the world in 2020, and nearly 10 million deaths[1] (second leading cause of mortality after cardiovascular disease). Although substantial efforts in anticancer drug discovery and development have led to the approval of several effective drugs for the treatment of malignancies, this global burden is still expected to grow, as incidence and mortality continue to increase, largely due to worsening in risk factors such as aging, overweight status, and smoking.[2,3] Moreover, the success with existing therapies is often limited due to their high toxicity and lack of tumour selectivity.[4] The majority of classical chemotherapeutics act on all rapidly proliferating cells without any discrimination between healthy and cancerous ones, thus leading to well-known unwanted side effects. By selectively targeting molecular entities that play a role in cancer development, progression, and metastasis, molecular targeted therapy interferes with cell pathways which are specific for tumorigenesis, and it is now considered a first-line approach to treat various types of human cancers.[5] At present, hundreds of different biological targets have been identified, including receptor proteins (*e.g.*, EGFR, VEGFR, PDGFR), signal transduction proteins (*e.g.*, tyrosine kinases), proteins involved in the synthesis of mRNA threads participating in neoplastic transformation, structural, functional, and cell cycle control (*e.g.*, CDKs) proteins.[6] As molecular targets for anticancer therapies are discovered with increasing frequency, there are growing possibilities of developing new anticancer agents. In this chapter we will describe our efforts in designing and synthesising NCEs potentially active on emerging anticancer targets such as MICAL2,[7] a cytoskeleton dynamics regulator which is strongly expressed in several cancer types, and NOD1 and NOD2,[8] two pattern recognition receptors (PRR) involved in the innate immune response, whose overactivation is implied in a wide range of human inflammatory disorders and malignancies. In both cases IMCRs were used as precious tools to rapidly access diverse but structurally related compounds to be biologically evaluated for SARs investigations.

3.1. Enriching the Arsenal of Pharmacological Tools against MICAL2

Molecule Interacting with CasL 2 (MICAL 2) is a multidomain nucleocytoplasmic protein belonging to the MICAL family of proteins, which in *Homo sapiens* consists of three members (MICAL1, MICAL2, and MICAL3) and two MICAL-like homologs (MICAL-L1 and MICAL-L2) expressed in specific neuronal and non-neuronal tissues during development as well as in adulthood. MICAL1, MICAL2, and MICAL3 work as redox enzymes exerting a dynamic control over polymerisation of actin, as they catalyse a NADPH-dependent F-actin depolymerising reaction, associated to their *N*-terminal FAD-containing domain.[7] Being actin one of the most abundant proteins in eukaryotic cells, involved in a variety of functions ranging from cell shape, adhesion, and motility to proliferation, differentiation, and survival, MICAL proteins take part in key physiological activities such as cytoskeleton remodelling, vesicle trafficking, axon guidance, autophagy and phagocytosis, and angiogenesis.[9] The variety of their functions is reflected in the multidomain structural organisation of these proteins, which is quite conserved among the three members of the family and consists of the already cited *N*-terminal flavoprotein monooxygenase domain (MO), a calponin homology (CH) and a LIM domain, with modulatory roles, and a less conserved *C*-terminal region.[7] In both MICAL1 and MICAL3 the latter contains a Pro-rich motif (P) for the interaction with the Src Homology 3 (SH3) domain of CasL,[10] a Glu-rich region (E) of unknown function, and a Rab binding domain (RBD), while these sequences are missing in MICAL2, where the LIM domain is at the *C*-terminus of the protein and well separated from the CH domain (Figure 3.1). Additional nuclear localisation signals (NLSs) are present in both MICAL2 and MICAL3, with the former being found to partially localise in the nucleus of HEK293T, COS7 and HeLa cells, where it regulates the nuclear actin levels and modulates the transcription of genes (mainly involved in cell differentiation and motility) under

the control of the serum response factor (SRF)/myocardin-related transcription factor-A (MRTF-A) complex.[7,11]

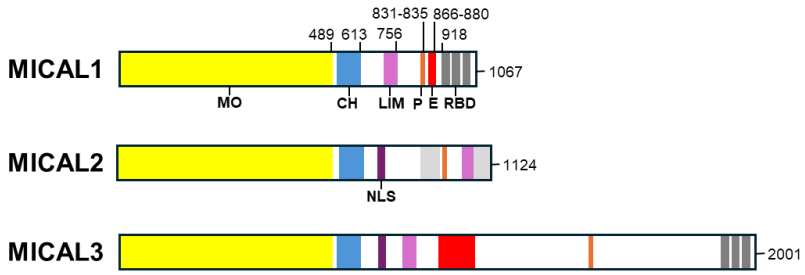

Figure 3.1. Domain organisation in MICAL proteins (colour code: MO, yellow; CH, cyan; LIM, fuchsia; P, orange; E, red; RBD, dark grey).

Although MICAL2 role in many human diseases is far from being clear, it is known to exert significant impacts on multiple cancer types: MICAL2 isoforms found in prostate cancer cells have indicated its contribution to tumour progression,[12] while increased expression of the protein was associated with the epithelial to mesenchymal transition that leads to metastasis formation in gastric and renal tumours.[13] Moreover, MICAL2 is involved in bladder cancer pathogenesis,[14] in breast cancer cell migration,[15] and in chemoresistance and increased mortality in endometrial cancer patients.[16] It has therefore been emerging as a promising target against cancer cell motility, migration, and metastasis. Drugs targeting these mechanisms are usually referred to as migrastatics[17] and are nowadays considered a complementary tool to antiproliferative agents for the treatment of solid cancers. In addition, MICAL2 has been found to be overexpressed in neo-angiogenic endothelial cells (ECs) of many human solid tumours (gastric, kidney and breast carcinoma, glioblastoma, and cardiac myxoma), thus playing a role in angiogenesis and vascular development.[18] For example, knock-down (KD) of MICAL2 gene has resulted in reduced ECs viability and functional properties, interfering with their responses to VEGF stimulation. The anti-angiogenic approach to treat cancer, initially proposed by Judah

Folkman,[19] aims to inhibit tumour growth by preventing the maturation of a functional vessel network, compromising the existing tumour-associated vasculature, and hindering new vessel formation. Within this context, MICAL2 emerges as an interesting target not only for migrastatic but also for anti-angiogenic therapies. Nevertheless, to date only one small-molecule inhibitor, namely CCG-1423, has been described.[11] In this regard, the treatment of human dermal microvascular ECs (HMEC-1) with 10 μM CCG-1423, has been proven to significantly reduce cell proliferation and the covered area in wound healing assay (WHA, one of the most common bioassays for evaluating the therapeutic impact on cell migration, thanks to its simplicity in experimental setup and data processing).[20] Furthermore, CCG-1423 has been found to completely suppress cell motility response to TNF-α, as no statistically significant differences between cells treated with CCG-1423 before and after exposure to TNF-α have been observed.[18] On this basis, with the aim to enlarge the arsenal of pharmacological tools available against MICAL2, we took CCG-1423 as a model to construct a small library of analogues to be biologically evaluated on different MICAL2-expressing HMEC-1 and renal adenocarcinoma (786-O) cell lines. The collected data, together with molecular modelling studies, provided the first SARs of CCG-1423, thus offering new insights for the development of potential anticancer agents acting as MICAL2 inhibitors.

Design and synthesis

Based on the chemical structure of CCG-1423, a library of rigidified analogues **3.1**-**3.12** (Figure 3.2) was designed and synthesised so to maintain the 3,5-bis(trifluoromethyl)phenyl- and 4-chlorophenyl- moieties of the *lead compound* (or to feature aromatic rings able to mimic them), while presenting variability in the linker. More in detail, compounds **3.1**-**3.6** retained the 3,5-bis(trifluoromethyl)phenyl- moiety, while the 4-chlorophenyl- portion was included in an indole or benzimidazole nucleus, with a linker of variable length, featuring

one (**3.1** and **3.2**) or two (**3.3**-**3.6**) amido functions inserted to connect the pharmacophoric aromatic units and confer some adaptability to the whole molecule. Derivatives **3.7**-**3.10** were fitted with an *N*-carboxypyrrolidine (**3.7** and **3.8**), or *N*-carboxypiperidine (**3.9** and **3.10**) central core linking the 3,5-bis(trifluoromethyl)benzamide and the 4-chlorophenyl- moieties; in compounds **3.7**-**3.8** the stereochemistry at 3-position of the pyrrolidine was also investigated, while in derivatives **3.9** and **3.10**, the relative position of the two aryl portions was examined. Finally, compounds **3.11** and **3.12** were endowed with open-chain linkers bearing ester, amido-, and oxyimino- functions and supporting a *n*-pentane group in place of the methyl- group of CCG-1423, in order to explore the chemical space around the central position.

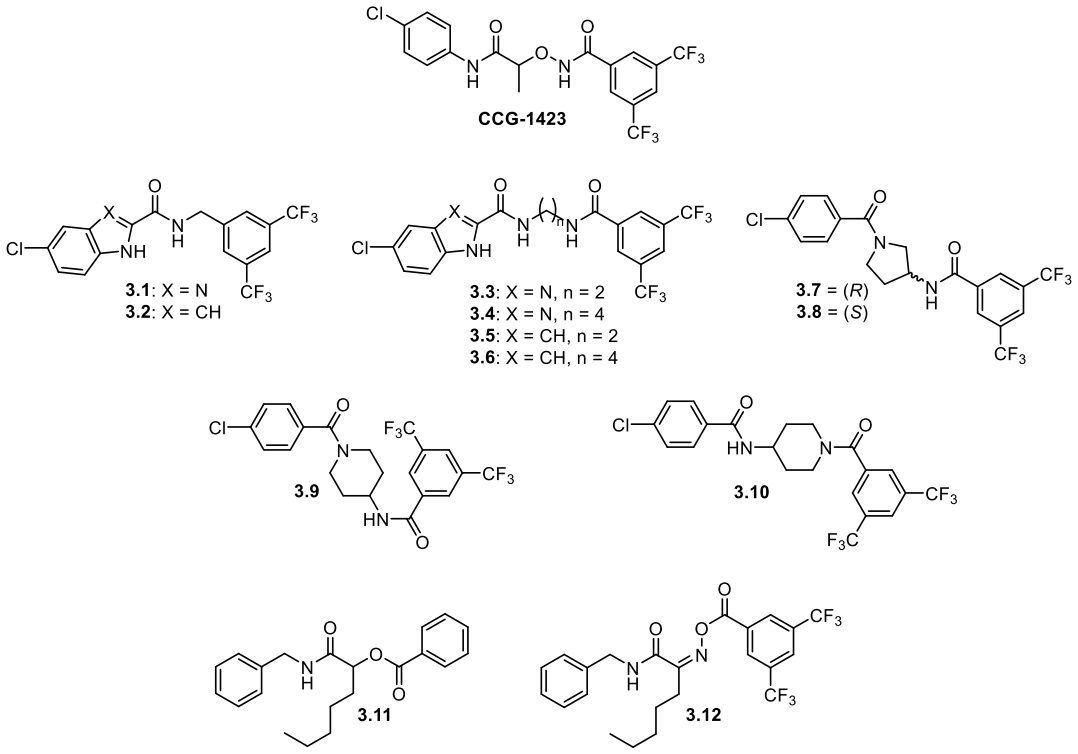

Figure 3.2 Chemical structures of CCG-1423 and of its newly synthesised analogues.

While compounds **3.1**-**3.6** were synthesised by the group of Prof. S. Taliani, from University of Pisa, we contributed to the library with compounds **3.7**-**3.12**. Derivatives **3.7**-**3.10** were obtained in two or three reaction steps, via simple sequences of acylation and coupling reactions, starting from commercially available enantiopure (*R*)- and (*S*)-3-aminopyrrolidines **3.14** and **3.15** (Scheme 3.1a, **3.7** and **3.8**, respectively) or 4-amino-1-Boc-piperidine **3.19** (Scheme 3.1b, **3.9** and **3.10**, an intermediate *N*-deprotection step was required in this case).

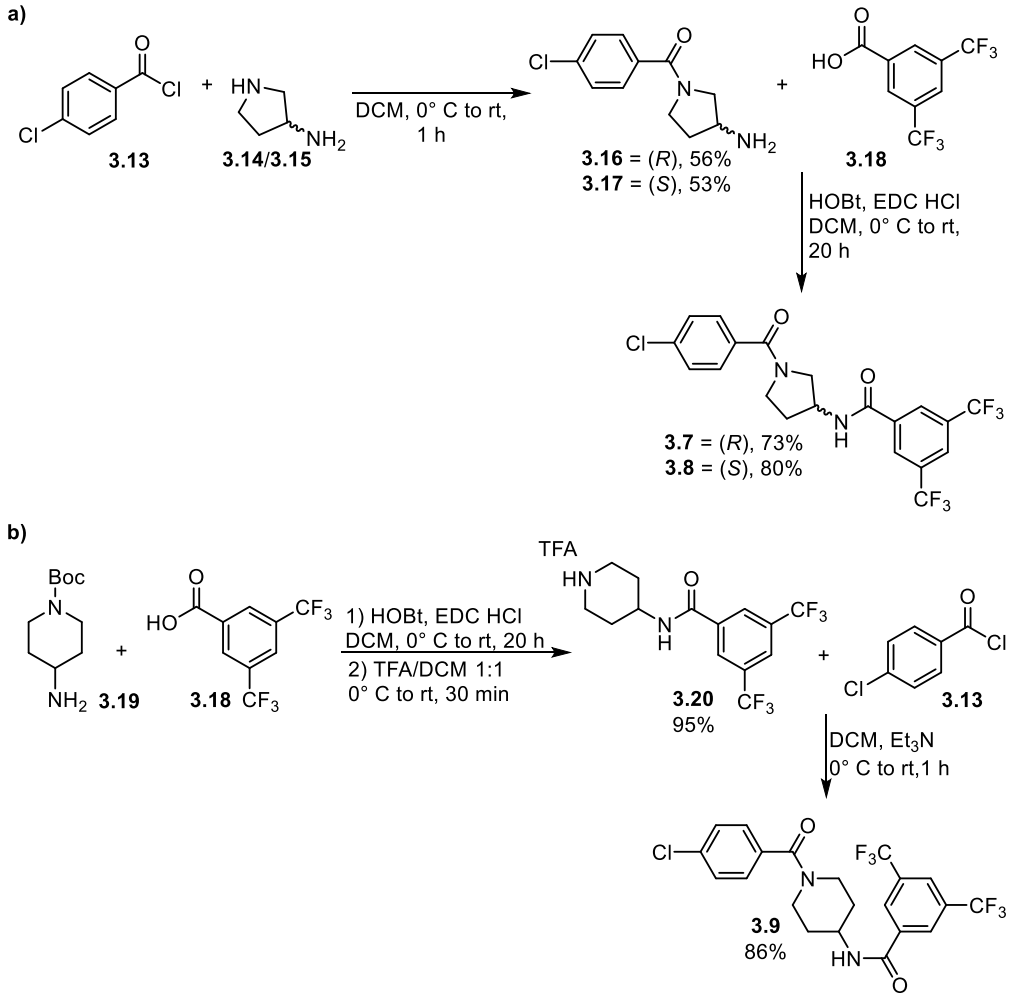

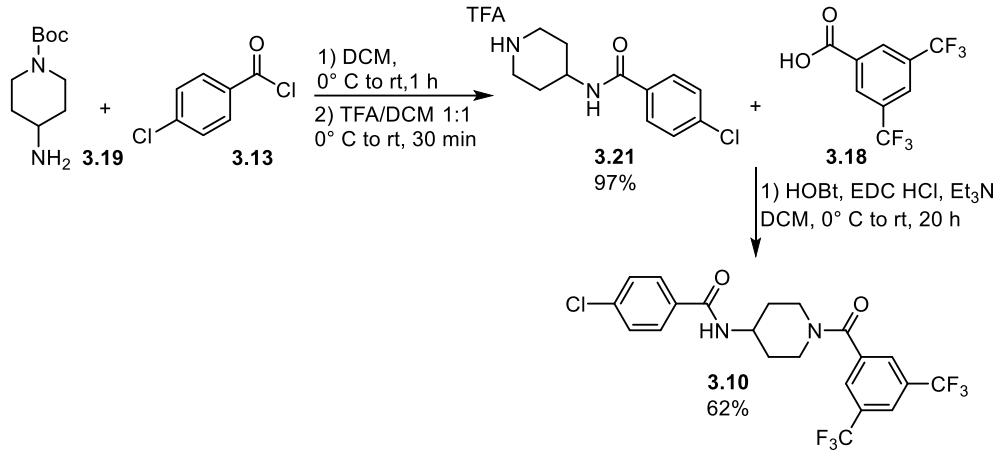

Scheme 3.1. Syntheses of compounds (a) **3.7**-**3.8**, (b) **3.9**-**3.10**.

On the other hand, compounds **3.11** and **3.12** were readily synthesised in a one-pot green fashion via a Passerini 3-CR involving *n*-hexanal **3.22**, benzyl isocyanide **3.23**, and benzoic acid **3.24** (Scheme 3.2a) and a Passerini-like 3-CR[21] combining *Z*-chlorooxime **3.25**, benzyl isocyanide **3.23**, and 3,5-bis(trifluoromethyl)benzoic acid **3.18** (Scheme 3.2b), respectively.

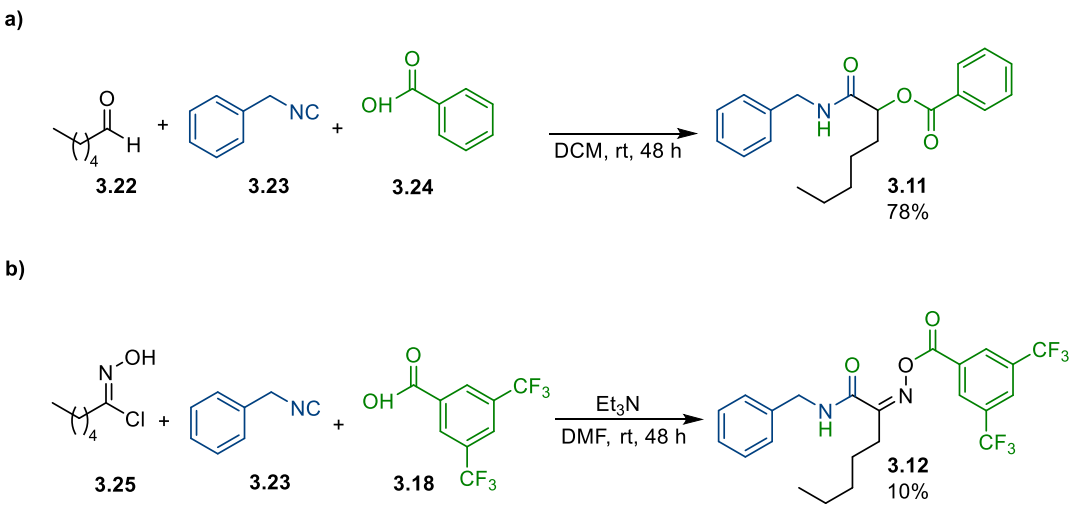

Scheme 3.2. One-pot syntheses of compounds (a) **3.11** and (b) **3.12**.

Such a multicomponent approach allowed to obtain the target compounds in just one reaction step and avoiding any coupling reagent, protection/deprotection, and intermediate purification, thus significantly decreasing the time and the resources required for the synthetic process. This is even more relevant considering that the *lead compound* CCG-1423 is usually synthesised via a seven-steps synthetic pathway with a 14% overall yield.[22]

Protein expression and biological assays

Prof. D. Angeloni's group, from Scuola Superiore Sant'Anna in Pisa, was in charge of biological evaluations. Despite several attempts to express high levels of MICAL2 protein (MO and CH domains) using different strains of *Escherichia coli* and cell growth conditions, it was not possible to obtain an appreciable overexpression of $MICAL2_{1\text{-}629}$ for biophysical assays. Since full-length MICAL2 is not commercially available, we decided to directly test our compounds in cell-based analyses, opting for a simple viability assay based on Trypan blue exclusion[23] and cell counting, and a WHA to evaluate possible effects on cell motility. The antiproliferative activity of compounds **3.1**-**3.12** was tested incubating human dermal microvascular endothelial cells (HMECs-1) and renal adenocarcinoma cells (786-O) with each newly synthesised compound, while WHA was carried out only on HMECs-1. All tested compounds did not show any relevant effect in these biological assays, except for **3.3**, **3.6**, and **3.12**. More in detail, compound **3.3** at a 10 μM concentration determined 35% reduction of vital human HMECs-1, compared to control, after 72 hours (Figure 3.3a); on the other hand, it did not cause any effect on 2D motility in a 6 hours WHA, suggesting a specific effect on cell viability but not on adhesion or motility. Similarly, when tested on 786-O wild type (WT) cells, **3.3** caused a 30% reduction of parental cell number at 96 hours (Figure 3.3b) and, importantly, had no effect on 786-O cells in which MICAL2 had been knocked down (786-O KD cells), suggesting a somehow MICAL2 dependent effect (Figure 3.3c).

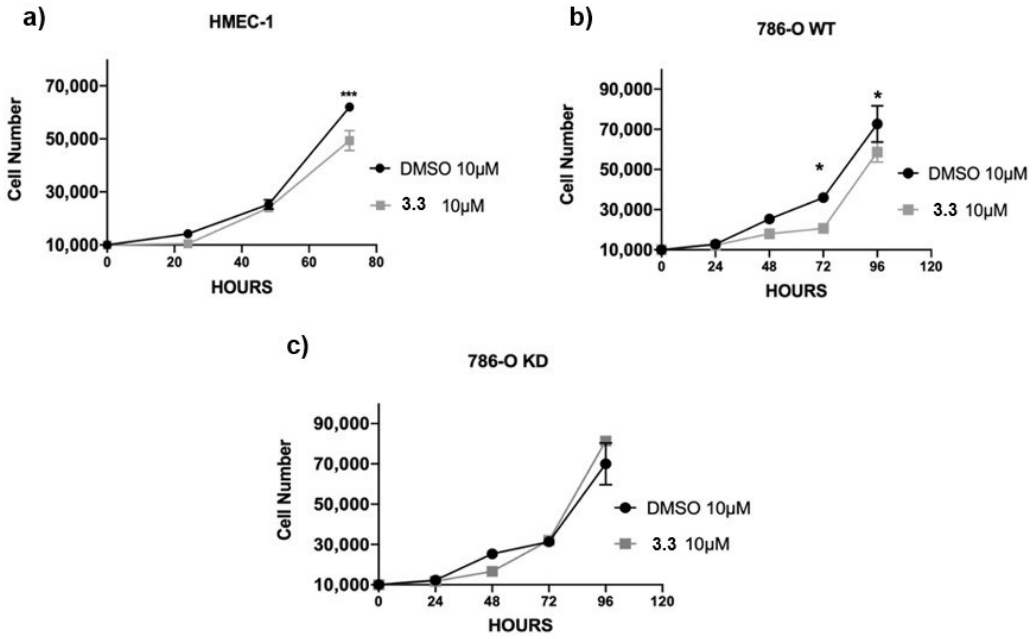

Figure 3.3. Results of cell viability assays for compound **3.3** 10 μM on (a) HMECs-1, (b) 786-O WT, and (c) 786-O KD cells.

Within the same chemical subclass, compound **3.6** induced a 25% reduction of vital HMECs-1 at 72 hours, at a 5 μM concentration (Figure 3.4), while it had no effect on 2D motility.

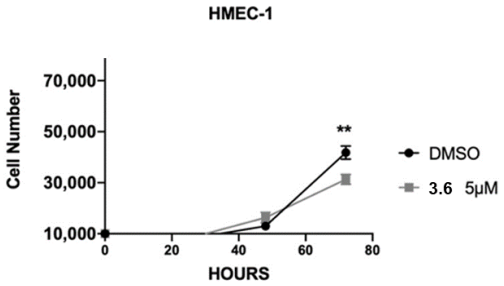

Figure 3.4. Results of cell viability assays for compound **3.6** 5 μM on HMECs-1.

On the contrary, compound **3.12** elicited no effect on HMECs-1 number up to 72 hours, but it caused 40% reduction of performance in a 6-hour WHA performed on HMECs-1 after 48 hours of exposure to 10 μM concentration of the drug. Importantly, no significant differences, compared to the control, were observed for

HMECs-1 KD (Figure 3.5). This suggests that the observed biological effects were mediated by MICAL2 protein, via a direct or indirect interaction of the tested compounds with the protein.

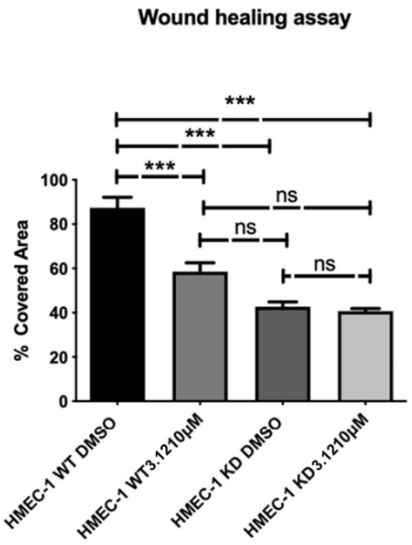

Figure 3.5. Results of WHA for compound **3.12** 10 μM on HMECs-1 WT and HMECs-1 KD.

Interestingly, the effects of **3.3** and **3.12** on cell function were not the same, although both typical of MICAL2 inhibition. Even if we cannot fully explain this observation as few information are available on MICAL2 multiple functions and on how they are regulated by small molecules binding, in principle it is possible that a biased signalling exists for structurally different compounds upon MICAL2 binding.

Molecular modelling

Neither the X-ray structure of human MICAL2 alone or in combination with inhibitors, nor the exact binding site of CCG-1423 are available to date. Thus, a receptor-based approach was not feasible. However, starting from CCG-1423, the group of Prof. L. Marinelli (University of Naples Federico II) investigated a plausible 3D superposition between the known inhibitor and each new analogue. To

note, the (*S)*-CCG-1423 isomer was considered, as it exhibited a slightly higher inhibitory effect in the case of MRTF-A.[22] First of all, in absence of the binding conformation of CCG-1423 into its target protein, a conformational analysis was accomplished with the aid of Macromodel (Schrodinger package, MaestroVersion 12.2.012, Release 2019-4). The resulting pool of 171 conformers was divided into 10 clusters on the base of the atomic Root-Mean-Square Deviation (RMSD), and evaluated according to their potential energy (Table 3.1). Five clusters (1, 2, 8, 9, and 10) were characterised by a high average potential energy (21 kJ/mol) and/or contained conformers with one or both amide bonds in *cis* conformation, thus they were discarded. The other clusters included lower energy conformers with no geometry distortions.

Cluster	**1**	**2**	**3**	**4**	**5**	**6**	**7**	**8**	**9**	**10**
N° conformers	15	15	15	47	21	9	30	2	9	8
Average energy (kJ/mol)	22.7	22.5	20.7	17.2	16.2	15.9	21.0	24.9	20.9	20.7

Table 3.1. Number of conformers and average energy for each conformational analysis cluster.

In particular, cluster 4 was the most populated (47 conformers) and contained the lowest-energy minimum conformation which was selected for further analysis. Specifically, this conformer was processed with the Phase module of Schrödinger suite, that found ten points potentially important for the binding (Figure 3.6): three hydrophobic groups (green spheres), three hydrogen bond receptor groups (pink spheres), two aromatic rings (orange circles), and two hydrogen bond donors (light blue spheres).

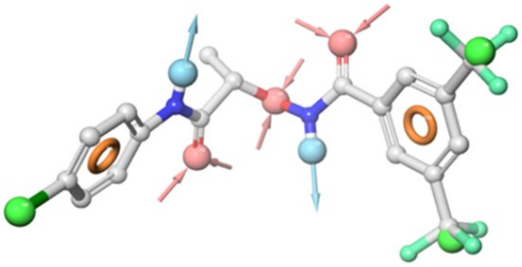

Figure 3.6. Ball and stick 3D representation of the lowest-energy minimum conformation of CCG-1423 ((*S*)-stereoisomer).

The Phase module was used again in order to find the best superimposition between each newly synthesised ligand and CCG-1423, by identifying for each compound the best conformer to maximise the match with the chosen points of CCG-1423 (Figure 3.7). Looking at these results, along with the *in cell* data, it is possible to assert that, among the subclass **3.1**-**3.6**, compounds **3.1** and **3.2** both had linkers too short compared to CCG-1423, while derivatives **3.3** and **3.6** gave the best superimposition, actually corresponding to higher inhibition of cell proliferation. Substitution of the CONHOCH(CH_3)CONH bridge of CCG-1423 with groups such as *N*-carboxypyrrolidine (**3.7** and **3.8**) or *N*-carboxypiperidine (**3.9** and **3.10**) completely abolished the compounds activity: this might be due either to the different orientation of the 4-chlorophenyl ring imposed by the novel linker, or to its bulkiness with respect to the central bridge of CCG-1423. Finally, **3.11** showed poor pharmacophoric similarity with the *lead compound* (and poor biological activity), while **3.12** exerted the highest effect on cell motility despite its alignment with the chosen points of CCG-1423 was only partial. Although a full SARs rationalisation is not feasible at the moment, due to the lack of any tests on the isolated protein and any information on the MICAL2 exact site of binding, the collected data clearly point out that the linker between the 3,5-bis(trifluoromethyl)phenyl- and the 4-chlorophenyl- moieties not only plays the role of spacer but it is probably important for the interaction with the protein. Synthesis of other compounds, along with the availability of the synthetic protein

for in vitro assays, will be necessary to add new pieces to the complex story of MICAL2 inhibitors recognition and binding.

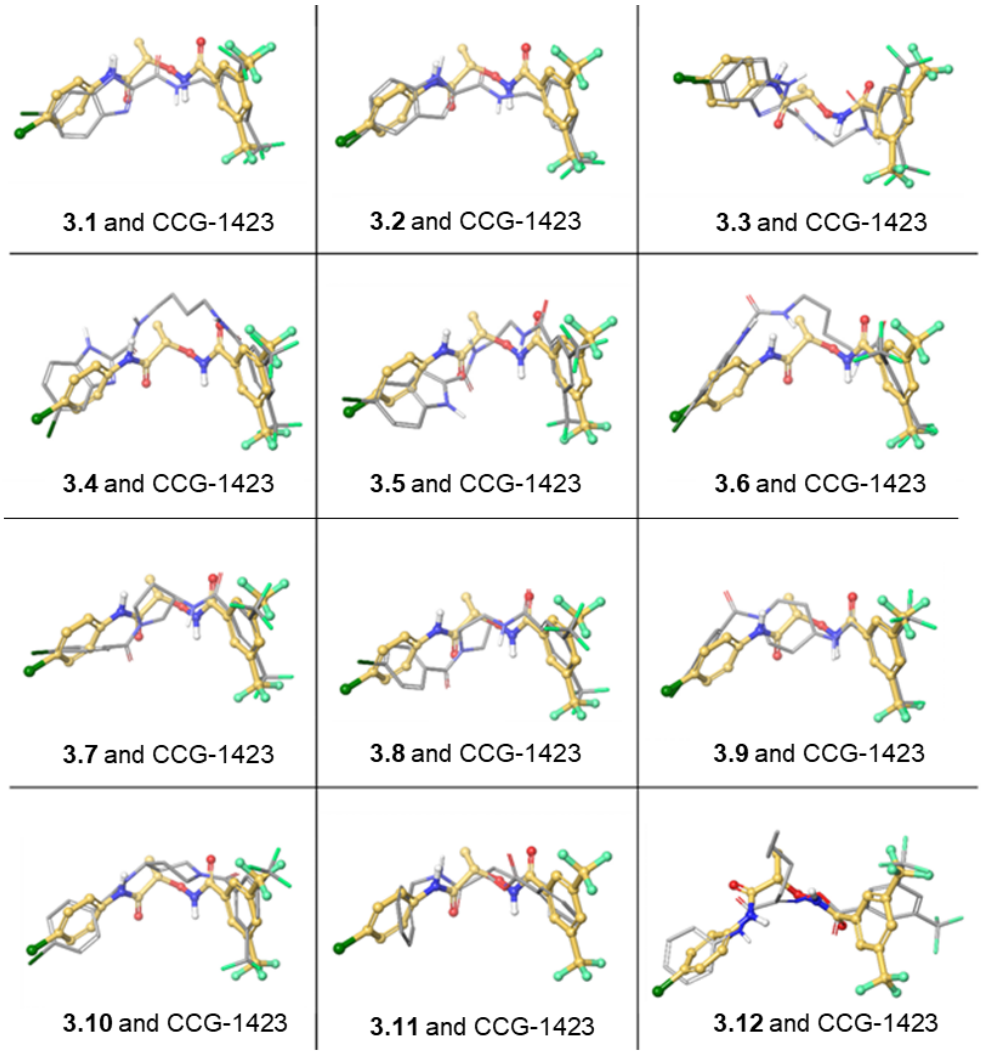

Figure 3.7. Best alignment of compounds **3.1**-**3.12** on the lowest-energy minimum conformation of CCG-1423.

3.2. Discovery of 2,3-diaminoindole derivatives as a novel class of NOD antagonists

NOD1 and NOD2 are the best characterised members of the NOD-like Receptor (NLR) family of proteins,[8] a group including more than twenty PRRs able to regulate cell pathways underpinning the innate immune response to cellular injury and stress,[24] and mostly located in the cytosol of epithelial cells of the gastrointestinal tract,[25] mesothelial,[26] and immune cells (monocytes/ macrophages, dendritic cells, and lymphocytes).[27-29] These proteins share a common structural organisation consisting of three separate domains[30] (Figure 3.8): a *C*-terminal LRR region, involved in the recognition and binding of specific PAMPs/DAMPs (Pathogen-Associated Molecular Patterns/Damage-Associated Molecular Patterns); a central NACHT domain with nucleotide triphosphatase activity, directing self-oligomerisation processes of the activated receptor, and an *N*-terminal effector sequence, which can be a BIR, CARD or PYD domain, depending on the subfamily (NLRA, NLRB, NLRC, and NLRP). NOD1 and NOD2 work as intracellular sensors of bacterial peptidoglycan derivatives (*γ*-D-glutamyl-*meso*-diaminopimelic acid, iE-DAP, and muramyl dipeptide, MDP, respectively) and play a key role in host defence against infections by inducing the expression of inflammatory cytokines, chemokines, and anti-microbial peptides via downstream activation of NF-κB and MAPK pathways.[31,32] On the other hand, several studies have demonstrated a genetic association between single nucleotide polymorphisms in *CARD4* or *CARD15* genes (codifying for NOD1 and NOD2, respectively) and increased susceptibility to asthma,[33] inflammatory bowel diseases,[34,35] and other auto-inflammatory granulomatous pathologies such as Blau's syndrome and early-onset sarcoidosis.[36] Moreover, these proteins seem to be involved in systemic inflammatory conditions such as type 1 and type 2 diabetes[37,38] and atherosclerosis,[39] and CNS degenerative diseases such as multiple sclerosis.[40] Additionally, overexpression of either NOD1 or NOD2 has been related to the

onset and progression of triple negative breast cancer,[41] while NOD1 upregulation has been found to promote colorectal, cervical, and ovarian carcinogenesis and to foster metastases formation in colon[42] and prostate cancer.[43]

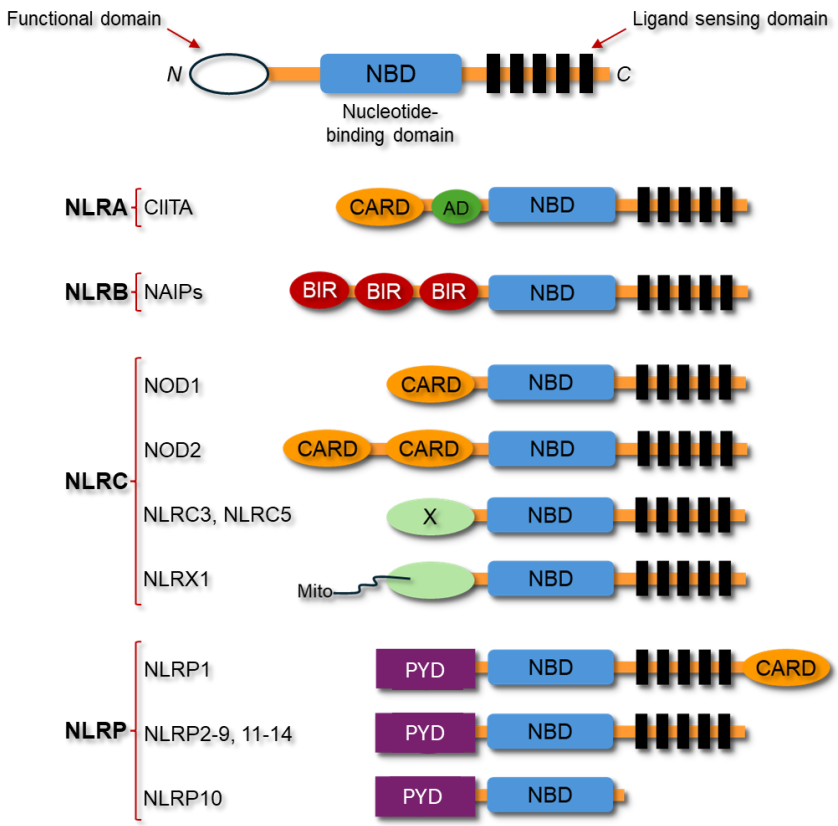

Figure 3.8. Domain organisation in NLRs proteins.

Therefore, there is ample evidence that a selective inhibition of NOD1 and NOD2 signalling might be exploited in the treatment of many acute and chronic diseases, including cancer. A wide range of chemotypes spanning from natural compounds, such as curcumin and parthenolide, to synthetic ones, including tetrahydroisoquinolines, indolines, 2-aminobenzimidazoles,[44] purine derivatives,[45] benzimidazole diamides,[46] and benzofused five-membered sultams[47] are known to act as NOD antagonists downregulating the NF-κB and MAPK pathways (Figure 3.9). Liu *et al.* have also reported that 1,4-benzodiazepine-2,5-diones[48] and

quinazolinones[49] (Figure 3.9) targeting both NOD1 and NOD2 are able to sensitise *in vivo* Lewis lung carcinoma and B16 tumour-bearing mice to paclitaxel treatment, via inhibition of NF-κB and MAPK.

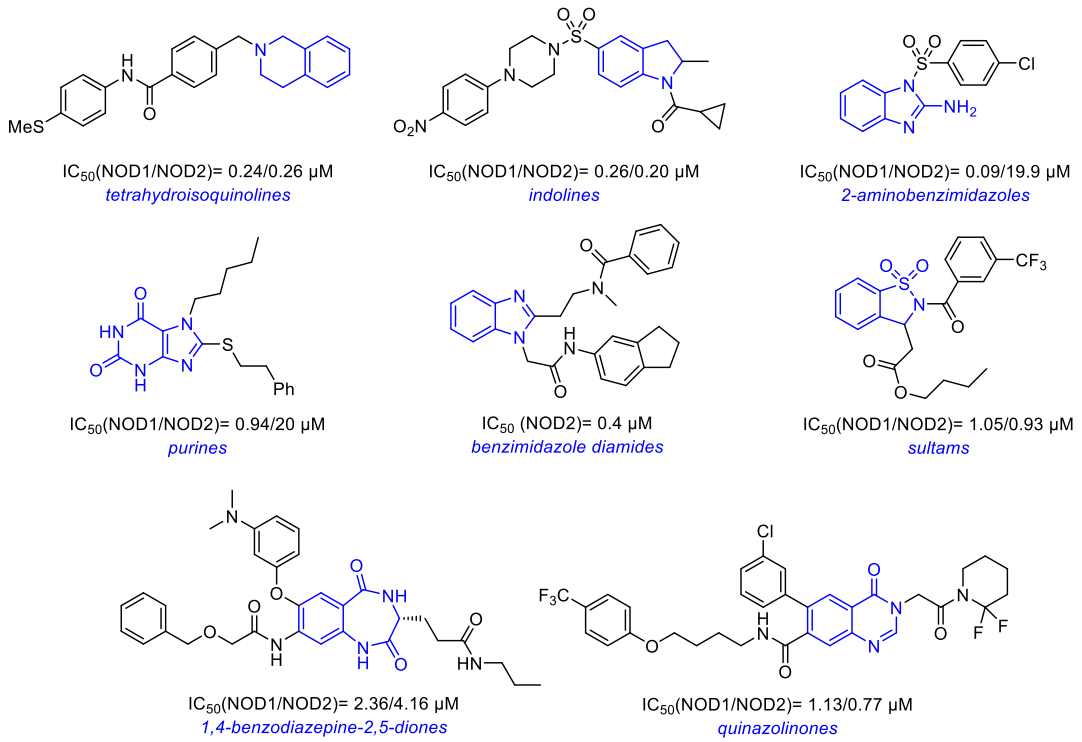

Figure 3.9. Representative NOD antagonists reported in the literature.

Among these compounds, Noditinib-1[50] (**3.13** in Figure 3.10), belonging to the 2-aminobenzimidazole class, has been recognised as a reference NLR antagonist for its ability to selectively inhibit NOD1-dependent NF-κB activation.[44] Considering the structural similarity to **3.13** of 2,3-diamino substituted indole derivatives **3.14**, we wondered if similar compounds might act as selective NOD1 antagonists, thus furnishing new pharmacological tools to study the molecular pathways involving NOD1 overactivation in both inflammatory processes and cancer progression. Replacing the benzimidazole core of **3.13** with a 2,3-diaminoindole scaffold could

actually provide different SARs and optimisation opportunities, not to mention the ease of synthesis and diversification of such a class of compounds.

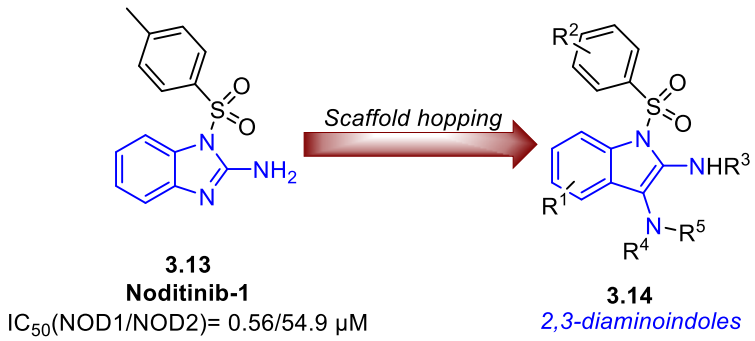

Figure 3.10. Scaffold hopping from 2-aminobenzimidazole (Noditinib-1) to multi-functionalised 2,3-diaminoindoles.

While 2,3-diaminoindoles have long been considered an elusive scaffold, due to major challenges and harsh conditions associated with their synthesis,[51] our laboratory recently developed a one-pot multicomponent approach providing a convenient and straightforward route[52] to 2,3-diamino substitute indole derivatives. It consists of an interrupted Ugi 3-CR leading to 2,3-diaminoindoles of general structure **3.14**, containing five points of diversity which can be introduced in just one operationally simple step. An in-house library of twenty-one 2,3-diaminoindoles was synthesised according to this strategy and pharmacologically screened with the aim to gain new insights into the SARs of NOD antagonists. Reporter-gene assays in NOD1- and NOD2-overexpressing HEK-Blue cell lines were used to test the new compounds, with major focus on their NOD1-antagonist activity in conjunction with counter-screening for NOD2-antagonist activity, as described in previous reports.[53,54] The results of this initial screening provided key information to guide the design and synthesis of a second focused library of eight additional compounds. The latter included **3.44**, which was identified as a low-micromolar and moderately selective NOD1 antagonist. Importantly, both the reference compound Noditinib-1 and our *hit compound* **3.44**, were additionally

studied through protein-based NMR experiments, fluoresce titration assays, and molecular modelling studies which provided, for the first time, *proof-of-evidence* of their direct binding to NOD1. These studies also enabled the identification of the NOD1 binding site of **3.44**, thus paving the way for a future structure-based rational design of potent and selective antagonists.

Synthesis of the in-house library of 2,3-diaminoindole derivatives

Compounds **3.18-3.38** were smoothly synthesised via the previously mentioned interrupted Ugi 3-CR developed in our laboratory, by reacting equimolar amounts of a sulfonyl amino arylaldehyde **3.15**, an isocyanide **3.16**, and a secondary amine **3.17** in DCM, at room temperature, for 2-72 hours (Scheme 3.3).

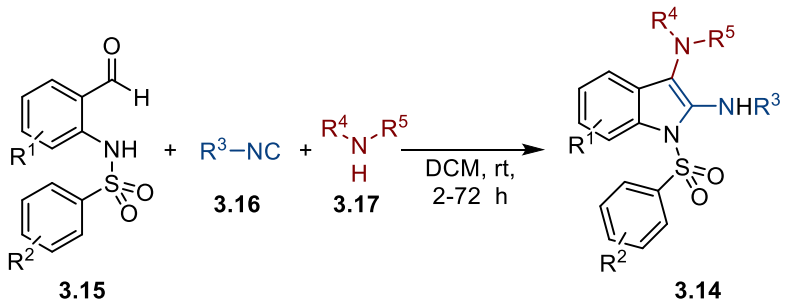

Scheme 3.3. Interrupted Ugi 3-CR leading to multi-functionalised 2,3-diaminoindole derivatives.

The multicomponent protocol exhibited an extraordinary atom economy (only one molecule of water is lost during the process) and a high bond forming efficiency, since two new C-N bonds and one C-C bond could be formed concomitantly during the one-pot process. The success of the transformation lies in the presence of the amphoteric sulfonylamino group, sequentially acting as a Brønsted acids and as a nucleophile. According to the above reported reaction conditions, eight different *ortho*-sulfonylamino aryl aldehydes, seven either aromatic or aliphatic isocyanides, and five linear or cyclic secondary amines were combined to get a library of 21 multi-functionalised 2,3-diaminoindoles **3.18-3.38** as shown in Table 3.2.

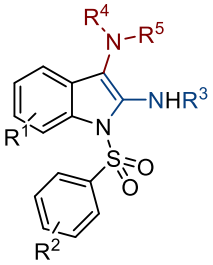

Compound	-R^1	-R^2	-R^3	-R^4R^5	Yield (%)
3.18	H	4-Me	*tert*-Butyl	$(Ethyl)_2$	85
3.19	H	4-Me	*tert*-Butyl	Morpholine	92
3.20	H	4-Me	*tert*-Butyl	Piperidine	66
3.21	H	4-Me	Benzyl	*N*-Methyl-piperazine	67
3.22	6-Cl	4-Me	β-Naphthyl	*N*-Methyl-propargyl	50
3.23	H	4-Me	*n*-Pentyl	Morpholine	72
3.24	H	4-Me	*n*-Pentyl	Piperidine	51
3.25	6-Cl	4-Me	*tert*-Butyl	Piperidine	86
3.26	6-Cl	4-Me	*n*-Pentyl	Morpholine	69
3.27	H	4-NO_2	*tert*-Butyl	Morpholine	85
3.28	H	4-OMe	*tert*-Butyl	Morpholine	46
3.29	4-Me	4-Me	*tert*-Butyl	$(Ethyl)_2$	73
3.30	5-Cl	4-Me	*tert*-Butyl	Piperidine	61
3.31	5-Cl	4-Me	*tert*-Butyl	Morpholine	70
3.32	Naphthyl	4-Me	Cyclohexyl	*N*-Methyl-piperazine	44
3.33	H	4-Me	*tert*-Butyl	*N*-Methyl-benzyl	82
3.34	H	4-Me	Cyclohexyl	$(Benzyl)_2$	53
3.35	5-Cl	4-Me	Cyclopropyl	Morpholine	70
3.36	H	4-Me	Butyl linker (dimeric compound)	Morpholine	34
3.37	H	4-Me	-CH_2CO_2Me	Morpholine	27
3.38	5,6-di-OMe	4-Me	*tert*-Butyl	Morpholine	31

Table 3.2. In-house library of 2,3-diaminoindoles synthesised via the interrupted Ugi 3-CR.

The substrate scope was good, with either electron-withdrawing substituents (-R^1) or no substituents on the aromatic rings of *ortho*-sulfonylamino aryl aldehydes **3.15** affording the desired products after 16 hours, while longer reaction times (48-72 hours) were required in the presence of electron donating groups. Similarly, an

electron-withdrawing group (-R^2) on the benzenesulfonamide ring enabled a fast reaction (2 hours), while, in the presence of an electron-donating group, a satisfying formation of the desired product was achieved after 48-72 hours. This behaviour was probably due to the change in acidity of the sulfonamide group strongly affecting the formation rate of the iminium ion.

Biological evaluation of the NOD-antagonist activities of the in-house library of 2,3-diamoinoindoles

Biological studies were conducted by Prof. Z. Jacopin's group at the University of Ljubljana. While compounds **3.24**-**3.26**, **3.30**, **3.33**, **3.34**, **3.36**, and **3.38** were not included in the biological assays due to stability concerns, compounds **3.18**-**3.23**, **3.27**-**3.29**, **3.31**, **3.32**, **3.35**, and **3.37** were initially examined for their antagonist activities using the HEK-Blue NOD1/2 cell-based model, which stably overexpresses the human *CARD4* or *CARD15* genes, along with an NF-κB–inducible secreted embryonic alkaline phosphatase reporter (SEAP) gene. Recognition of a NOD1/2 agonist in these cell-based assays thus triggers a signalling pathway that leads to the activation of NF-κB and, in turn, to the production of SEAP. The HEK-Blue NOD1 cells were employed as a primary screening model, while an analogous assay with HEK-Blue NOD2 cells was used as the counter-screen to investigate the selectivity profile of the newly synthesised compounds. Specifically, the HEK-Blue NOD1/2 cells were preincubated for 1 hour with a 25 μM concentration of each compound (Noditinib-1 and the NOD2 antagonist SG84[53] were also employed as references) and then stimulated with 100 nM C12-iE-DAP or 2 μM MDP, respectively, followed by spectrophotometric determination of residual SEAP activity (RA) in the supernatant. As expected, the NOD1 agonist (C12-iE-DAP) and NOD2 agonist (MDP) significantly increased NF-κB transcriptional activities in their respective target cell lines; the latter were instead suppressed by both the NOD1 antagonist Noditinib-1 (RA = 9%) and the NOD2 antagonist SG84 (RA = 34%). As shown in Figure 3.11a, compounds **3.18**

(RA = 63%), **3.21** (RA = 52%), **3.23** (RA = 65%), **3.27** (RA = 50%), **3.28** (RA = 67%), **3.32** (RA = 51%), **3.35** (RA = 60%), and **3.37** (RA = 58%), emerged as the most pronounced NOD1 antagonists of the first series. Compounds **3.21** and **3.32**, featuring an *N*-methylpiperazine moiety, also exhibited modest NOD2 antagonistic activity, with RAs of 62% and 75%, respectively (Figure 3.11b).

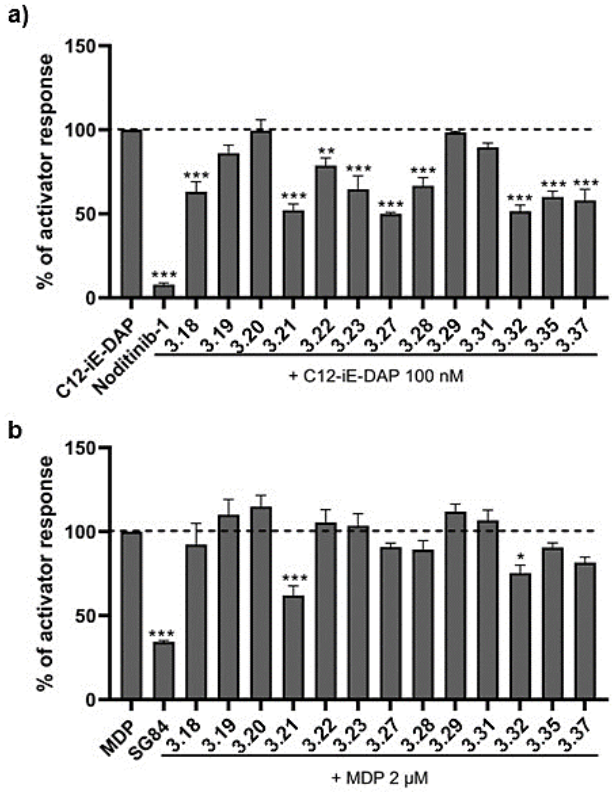

Figure 3.11. Suppressive effect of the synthesised NOD antagonists **3.18-3.23, 3.27-3.29, 3.31, 3.32, 3.35,** and **3.37** on NF-κB activation in HEK-Blue NOD1/2 cells. NF-κB transcriptional activity of (a) HEK-Blue NOD1 and (b) HEK-Blue NOD2 cells expressed as secreted embryonic alkaline phosphatase activity after 1 h treatment with the indicated synthesised compounds (25 µM) before stimulation for 18 h with 100 nM C12-iE-DAP and 2 µM MDP, respectively.

The other compounds did not show any significant antagonistic activity towards NOD1 or NOD2 (RA > 70%). In parallel, the compounds were also screened for cytotoxicity utilising the well-established MTS assay. The proliferation rates of

cells were determined in the presence of the synthesised compounds (25 μM) and compared to those of the untreated control. All tested compounds were well tolerated by the HEK-Blue NOD1 and NOD2 cells, as their residual metabolic activities did not drop below 80% of the control.

Albeit the single-point cell-based assays did not fully capture the complex SAR, several key features have been elucidated. First, it is evident that the most active compounds carry a cyclic secondary amine moiety (*e.g.*, morpholine, *N*-methylpiperazine or piperidine) at position 3 of the indole core, with the *N*-methylpiperazine moiety featured in compounds **3.21** and **3.32** leading to poorer NOD1/NOD2 selectivity. Second, the 2-position can accommodate bulky lipophilic amines (*n*-pentylamine, benzylamine, cyclohexylamine or *tert*-butylamine) and short amino acids (such as glycine featured in **3.37**). Third, the 4-methyl-, 4-methoxy- and 4-nitro- groups on the benzenesulfonyl ring do not have a decisive impact on the NOD antagonistic activity. In a direct comparison, however, the 4-nitrobenzenesulfonyl- substituent featured in **3.27** (RA = 50%) is superior to its 4-methoxybenzenesulfonyl- and 4-methylbenzenesulfonyl- counterparts present in **3.28** (RA = 67%) and **3.19** (RA = 86%), respectively. Fourth, compounds **3.22** (RA = 79%) and **3.31** (RA = 90%) do not show NOD1 antagonistic activity, which suggests the introduction of a chlorine to the 5/6-position of the indole core is detrimental for NOD antagonistic activity. The same still counts for the introduction of methyl- group to the 4-position, as observed for **3.29** (RA = 98%), compared to its unsubstituted counterpart **3.18** (RA = 63%). In general, the presence of a substituent at positions 4-7 of the indole scaffolds results in complete loss of activity, except for compounds **3.35** bearing a morpholino moiety at position 3. Lastly, the tricyclic indole ring-expanded analogue **3.32** (RA = 51%), retained the activity of its indole counterpart **3.21** (RA of 52%). This key information about the structural features required for a satisfactory NOD1 antagonism was then exploited to synthesise a second library of structurally optimised compounds with major focus on NOD1 inhibitory activity compared to NOD1/NOD2 selectivity.

Design and synthesis of a focused library of 2,3-diaminoindoles based on SAR studies from the in-house library

The most promising compounds **3.21**, **3.27**, and **3.32** were took as models to design a focused library of eight additional derivatives **3.39**-**3.46**, featuring a combination of key structural elements for NOD1 antagonistic activity (Figure 3.12 and Table 3.3).

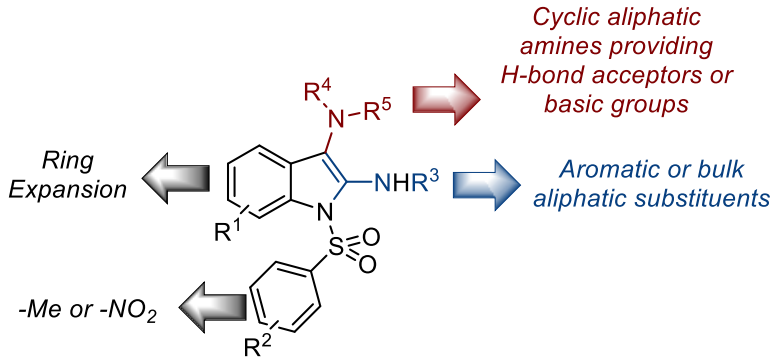

Figure 3.12. Key structural elements for the NOD1 antagonistic activity, derived from the screening of the first in-house library.

The new compounds were all obtained in good yields (51-74%) following the synthetic multicomponent approach already shown in Scheme 3.3.

More in detail, the 2-benzylamino moiety of **3.21** was replaced with a cyclohexyl amino and a *tert*-butyl amino group in **3.40** and **3.44**, respectively, so to explore the chemical space available around the 2-indole position. Similarly, the 2-cyclohexylamine of the tricyclic benzene-annulated indole derivative **3.32** was substituted with a *tert*-butyl amino or benzyl amino moiety to give compounds **3.45** and **3.46**, respectively. As a nitro substituent at the *para*-position of the benzenesulfonamide ring had proven to be superior to the *para*-methylated analogue (**3.27** and **3.19**, respectively) compounds **3.41**-**3.43** were included into the library. Finally, to confirm the importance of a cyclic amine moiety providing an H-bond acceptor or a basic group at the 3-position of the indole scaffold, compound **3.39** bearing a diethylamine moiety was synthesised.

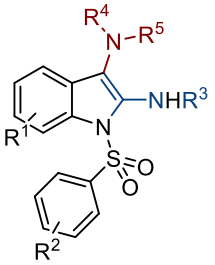

Compound	-R^1	-R^2	-R^3	-R^4R^5	Yield (%)
3.39	H	4-Me	*n*-Pentyl	$(Ethyl)_2$	52
3.40	H	4-Me	Cyclohexyl	*N*-Methyl-piperazine	60
3.41	H	4-Me	Benzyl	Morpholine	51
3.42	H	4-NO_2	*n*-Pentyl	Morpholine	59
3.43	H	4-NO_2	Benzyl	Morpholine	74
3.44	H	4-Me	*tert*-Butyl	*N*-Methyl-piperazine	53
3.45	Naphthyl	4-Me	*tert*-Butyl	*N*-Methyl-piperazine	54
3.46	Naphthyl	4-Me	Benzyl	*N*-Methyl-piperazine	57

Table 3.3. Focused library of compounds synthesised via the interrupted Ugi 3-CR.

Biological evaluation of the NOD-antagonist activities of the focused library of 2,3-diamoinoindoles

The new compounds **3.39-3.46** were tested for their suppressive effect on NOD1-dependent NF-κB activation in HEK Blue cells as previously reported for the in-house library. As shown in Figure 3.13, the replacement of the 2-benzylamino moiety of **3.21** (RA = 52%) with cyclohexylamine (**3.40** RA = 15%) and *tert*-butylamine (**3.44**, RA = 25%) counterparts significantly improved the NOD1 antagonistic activity. On the contrary, a ring expansion of **3.44** caused an important loss of the NOD antagonism, as evident from the benzene-annulated **3.45** (RA (NOD1) = 74%, RA (NOD2) = 94%). On the other hand, an analogous ring expansion of **3.21** as in compound **3.46** increased the antagonistic activities *versus* both NOD1 (RA = 18%) and NOD2 (RA = 19%). Once again, the presence of a 4-methylpiperazine moiety resulted in loss of selectivity (as seen with compounds

3.40, and **3.44-3.46**), while the diethylamino moiety introduced in compound **3.39** (and also featured in **3.18**) was able to provide greater NOD1 selectivity (RA (NOD2) = 90%) but still retained a moderate NOD1 antagonistic activity (RA = 47%).

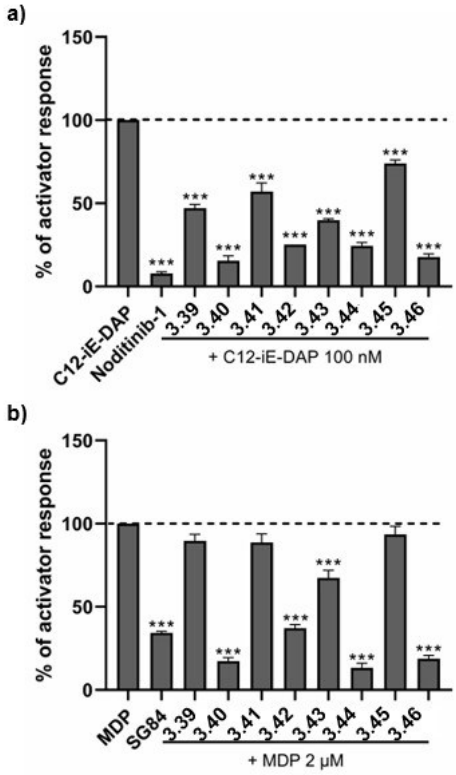

Figure 3.13. Suppressive effect of synthesised NOD antagonists **3.39-3.46** on NF-κB activation in HEK-Blue NOD1/2 cells. NF-κB transcriptional activity of HEK-Blue NOD1 (a) and HEK-Blue NOD2 (b) cells expressed as secreted embryonic alkaline phosphatase activity after 1 h treatment with the indicated synthesised compounds (25 µM) before stimulation for 18 h with 100 nM C12-iE-DAP and 2 µM MDP, respectively.

In sharp contrast to the findings from the first series, both compounds carrying the 4-nitrobenzenesulfonyl moiety (*i.e.*, **3.42** and **3.43**) exhibited weaker antagonistic activity than their 4-methylbenzenesulfonyl counterparts (particularly evident by comparing **3.41** and **3.43**).

The focused library was also tested for cytotoxicity utilising the MTS assay at 25 μM concentration of each compound, compared to untreated control. None of the newly synthesised derivatives was found to be cytotoxic, as the residual metabolic activities never fell below 80% of the control.

*NOD-antagonist IC_{50} values of selected compounds **3.40**, **3.42**, **3.44**, and **3.46***

Compounds **3.40**, **3.42**, **3.44**, and **3.46** exhibited the most pronounced NOD-antagonist activities in the preliminary screening and were, therefore, further evaluated for their dose dependence and IC_{50} values (Table 3.4). The NOD1- and NOD2 antagonist effects were dose dependent and followed a non-linear semi-logarithmic model. The NOD1 reference antagonist Noditinib-1 (**3.13**) showed submicromolar IC_{50} for NOD1 and 2 orders of magnitude weaker IC_{50} for NOD2 (0.771 *vs* 54.9 μM). As for the tested 2,3-diaminoindole derivatives, the collected results revealed a relatively nonselective nature of the indole scaffold in terms of NOD1 antagonism (*i.e.*, *vs* NOD2), with the introduced substitutions generally interfering with both pathways in similar manners, in agreement with previous reports.[54] The dose-dependence data did not completely reflect the antagonistic activities obtained for the single concentration of 25 μM. Nonetheless, three of the tested compounds (*i.e.*, **3.42**, **3.44**, and **3.46**) showed approximately twice lower IC_{50} values for NOD1 antagonism versus NOD2 antagonism indicating, a modest level of selectivity. Compound **3.44** was found to be the most potent NOD1 antagonist of the series, with inhibitory effects in the low micromolar range toward NOD1 and NOD2 (IC_{50} NOD1/NOD2 = 9.13 *vs* 20.8 μM). On the contrary, compound **3.40** emerged as the most balanced dual antagonist of the series, with similar potencies in the low micromolar range toward both NOD1 and NOD2 (IC_{50} NOD1/NOD2 = 18.5 *vs* 16.1 μM).

Compound	IC_{50} NOD1 (μM)	IC_{50} NOD2 (μM)
Noditinib-1 (3.13)	0.771	54.9
3.40	18.5	16.1
3.42	26.1	42.6
3.44	9.13	20.8
3.46	20.7	41.9

Table 3.4. NOD1 and NOD2 IC_{50} values emerged for the selected compounds.

Ligand-based NMR spectroscopy binding studies

To date, there is no experimental evidence of a direct binding between antagonist compounds and isolated NOD1. To fill this gap, a ligand-based NMR approach was employed to evaluate the interaction of NOD1 with both the newly discovered antagonist **3.44** and the reference compound Noditinib-1. The NMR studies were performed by the group of Prof. A. Carotenuto and Dott. D. Brancaccio, from University of Naples Federico II.

Ligand-based NMR has become highly popular in drug discovery thanks to several advantages, ranging from the use of low concentrations of the macromolecule, to not required isotopic labelling of the receptor and non-existent upper limits for its size. Furthermore, it is a very versatile approach, which has successfully been used as direct binding assay of ligands with different targets such as proteins in solution,[55,56] GPCRs,[57] and nucleic acids.[58] In our case, Saturation Transfer Difference[59] (STD-NMR) and WaterLOGSY[60] (WL-NMR) experiments were carried out for Noditinib-1 (Figure 3.14) and the most potent NOD1 antagonist of the focused library (*i.e.*, **3.44**, Figure 3.15), in the presence (left panel) and absence (right panel) of the protein (see Experimental Section for details).

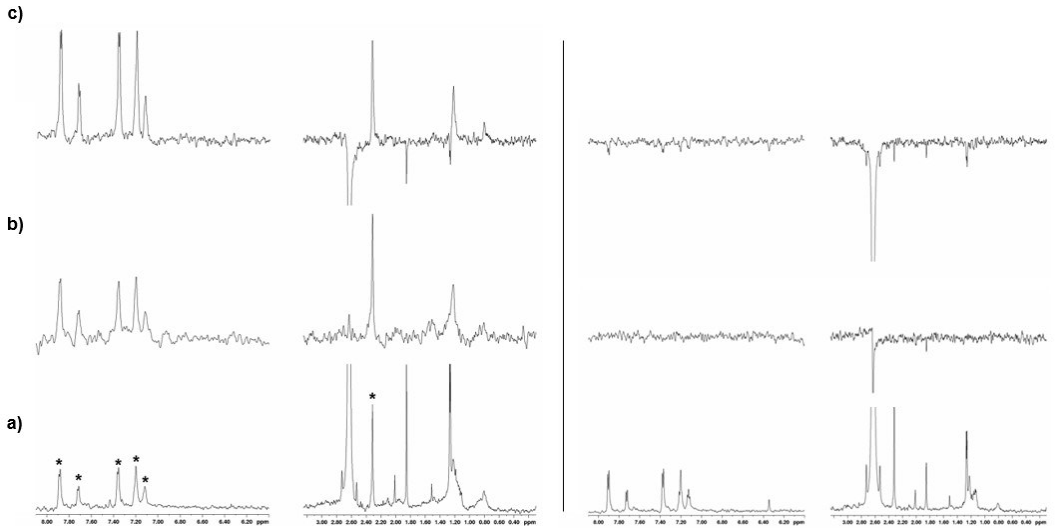

Figure 3.14. (a) ^{1}H NMR, (b) STD-NMR, and (c) WL-NMR spectra of Noditinib-1 (0.250 mM) in the presence (1 μM, left panel) and absence (right panel) of NOD1 protein. NMR signals of Noditinib-1 are marked with stars.

Since an STD-NMR spectrum only shows signals of the ligand that are in direct contact with the macromolecule, the presence of the NMR signals of Noditinib-1 after addition of NOD1 (Figure 3.14b, left panel) strongly suggested an actual interaction between the ligand and the protein. WL-NMR, showing positive peaks for the ligand (highlighted with asterisks) in the presence of the protein, provided further evidence of the specificity of the binding between Noditinib-1 and NOD1 (Figure 3.14c, left panel). To provide negative controls, STD-NMR and WL-NMR experiments were performed for Noditinib-1 in the absence of NOD1 protein. The non-appearance of proton signals in STD-NMR (Figure 13.4b, right panel) and the presence of negative signals in WL-NMR spectra (Figure 13.4c, right panel), respectively, confirmed that Noditinib-1 binds NOD1.

For the most potent NOD1 antagonist of the focused library, namely **3.44**, STD-NMR (Figure 3.15b) and WL-NMR (Figure 3.15c) spectra in the presence (left panel) and absence (right panel) of the protein, showed results very similar to those obtained for Noditinib-1, which is in good agreement with our rational design and with biological data.

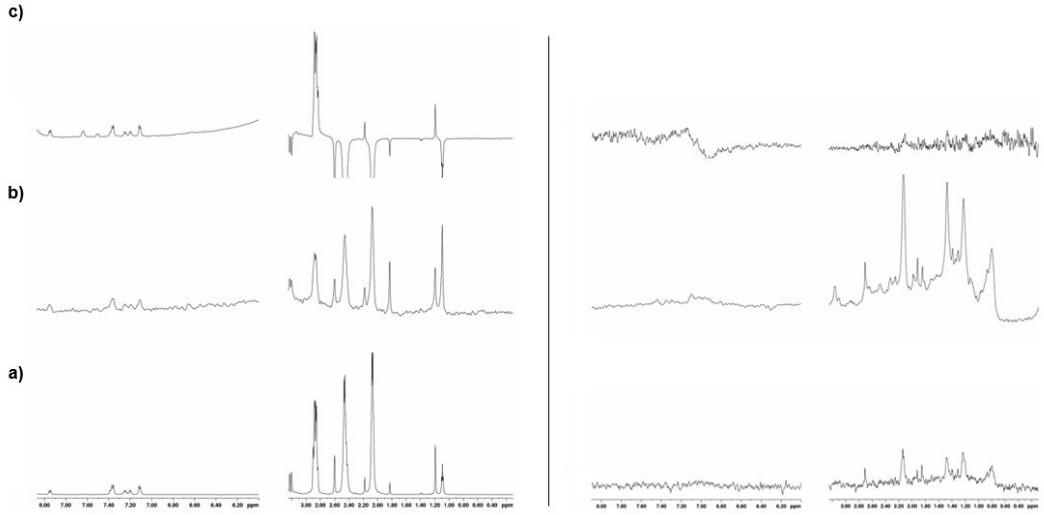

Figure 3.15. (a) ^{1}H NMR, (b) STD-NMR, and (c) WL-NMR spectra of compound **3.44** (0.250 mM) in the presence (1 μM, left panel) and absence (right panel) of NOD1 protein.

*Quantification of the binding affinity of **3.44** to NOD1*

The binding affinity of compound **3.44** for NOD1 was determined by the group of Prof. J. Amato and Prof. B. Pagano by means of fluorescence titration experiments, in which changes in the intrinsic fluorescence of a protein are monitored upon binding to a molecule. Fluorescence emission spectra of NOD1 were recorded upon addition of increasing amounts of compound **3.44**, which resulted in a significant decrease in the fluorescence intensity of the protein (Figure 3.16a). A titration curve was obtained by plotting the fraction of bound protein (α) *versus* the concentration of compound **3.44**, and then fitted by means of a nonlinear regression algorithm using an independent and equivalent binding sites model,[61] which gave an equilibrium dissociation constant (K_D) of 130 (±10) μM (Figure 3.16b). Fluorescence titration experiments were also attempted for Noditinib-1. However, its low solubility in the buffer used for the protein, in the millimolar concentration range, prevented the acquisition of reliable fluorescence spectra and, therefore, the determination of a K_D value for its interaction with NOD1.

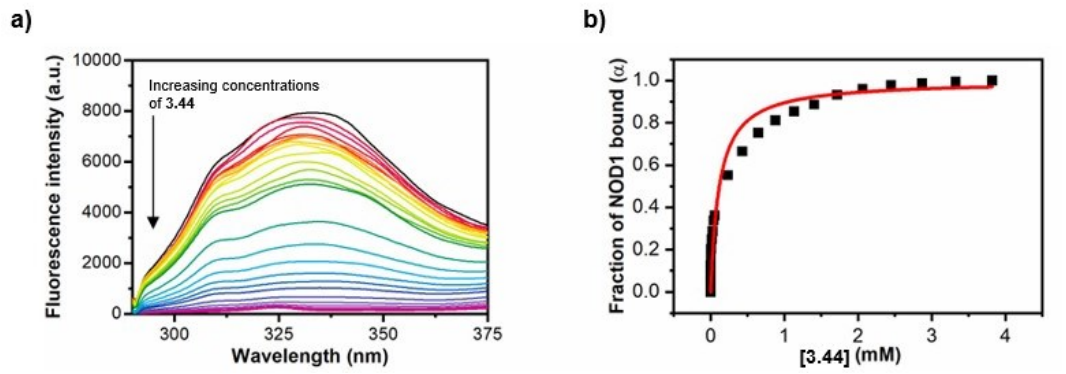

Figure 3.16. a) Fluorescence emission spectra of NOD1 (80 nM) in the absence (black line) and presence of increasing amounts of compound **3.44**; b) Titration curve obtained by plotting the fraction of bound protein (α) *versus* the concentration of compound **3.44**. The squares represent the experimental data, the red line is the best fit obtained with the theoretical model.

*Investigation of the binding mode of **3.44** to NOD1*

A combination of molecular modelling and NMR experimental studies was further employed to elucidate the binding mode of **3.44** to NOD1 (molecular modelling investigations were performed by the group of Prof. L. Marinelli and Dott. F. S. Di Leva, from University of Naples Federico II). Since no experimental structure of the full-length human protein is available yet, a 3D receptor homology model was initially built to perform computational studies. More in detail, NOD1 was modelled in its closed inactive conformation, which could in principle be competent for the binding of antagonist compounds like our newly synthesised derivative (see Experimental Section for details). Since no prior experimental knowledge of the binding region of **3.44** was available, all the possible "druggable" sites on the receptor were evaluated through a machine learning-based analysis performed with the *Prankweb* server.[62] These calculations identified two wide receptor areas, respectively located in the leucine-rich repeat (LRR) domain ("LRR site", Figure 3.17) and in the nucleotide binding domain (NBD) of the larger NACHT domain ("NBD" site, Figure 3.17).

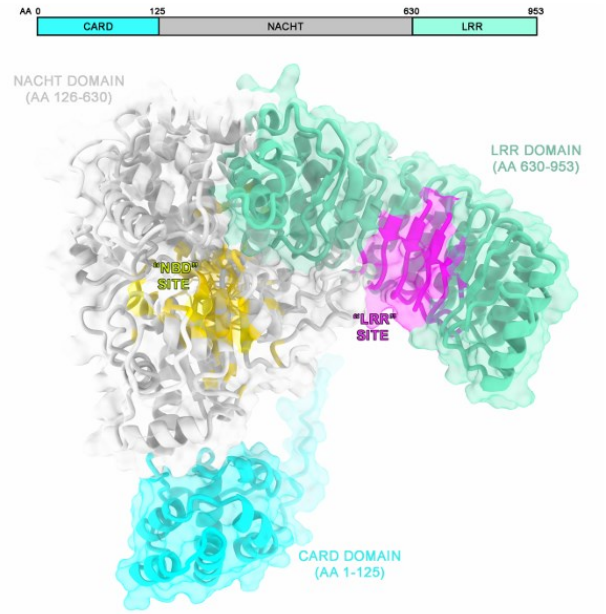

Figure 3.17. 3D Representation of the human NOD1 homology model. The two most probable ligand binding sites identified by *Prankweb* have been mapped onto the receptor surface in yellow and magenta, respectively.

The "LRR site" largely corresponds to a solvent-accessible pocket in the LRR domain, which is known to bind agonist compounds such as iE-DAP.[63] We thoroughly investigated the possible binding of **3.44** to this site by means of molecular docking, molecular dynamics (MD) simulations and advanced free energy calculations (data not shown). However, no reliable pose was found, suggesting that the ligand binding to "LRR" pocket could be unfavourable. Consequently, we explored the potential interaction of **3.44** with the "NBD site", which largely corresponds to the nucleotide (ATP/ADP) binding region in the NACHT domain.[64] Considering the plasticity of this pocket, we first performed induced fit docking (IFD) calculations, which identified three possible binding modes (Pose A, B, and C in Figure 3.18). Their reliability was assessed through extensive (2 μs long) MD simulations, taking into account explicit solvent effects and full protein flexibility. The analysis of the ligand's heavy atoms RMSD along the three MD trajectories allowed us to immediately discard pose A, since it was

unsteady during the whole simulation. Lower RMSD values were instead observed for **3.44** when starting from either the B or C pose. Interestingly, these two binding modes share the same initial orientation of the ligand's tosyl- and 4-methylpiperazinyl groups but differ in the arrangement of the *N*-(*tert*-butyl)-1*H* indol-2-amine scaffold, which is mutually flipped by 180°. However, while in pose B compound **3.44** displays progressively growing RMSD fluctuations (*i.e.*, after ≈ 0.8 μs) and does not show a conserved interaction pattern, in pose C it rapidly rearranges to assume a very stable binding conformation. As shown in Figure 3.19, according to this binding mode **3.44** would be located in a lipophilic cleft defined by the sidechains of M162, M212, F354, M366 and F518. Here, it forms van der Waals interactions with the side chains of M212, M366 and F518, while cation-π and T-shaped contacts are engaged by its 4-methylpiperazinyl- and indole moieties with F354 and Y362, respectively. Importantly, three tight and long-lasting H-bonds are established by the *N*-methyl-piperazine and the tosyl- (sulfonyl oxygen) substituents of **3.44** with T164 (side chain) and V208 (backbone), and Y366 (side chain) respectively, together with a transient interaction involving the phenol ring of Y149 and the other sulfonyl oxygen of the ligand tosyl- group.

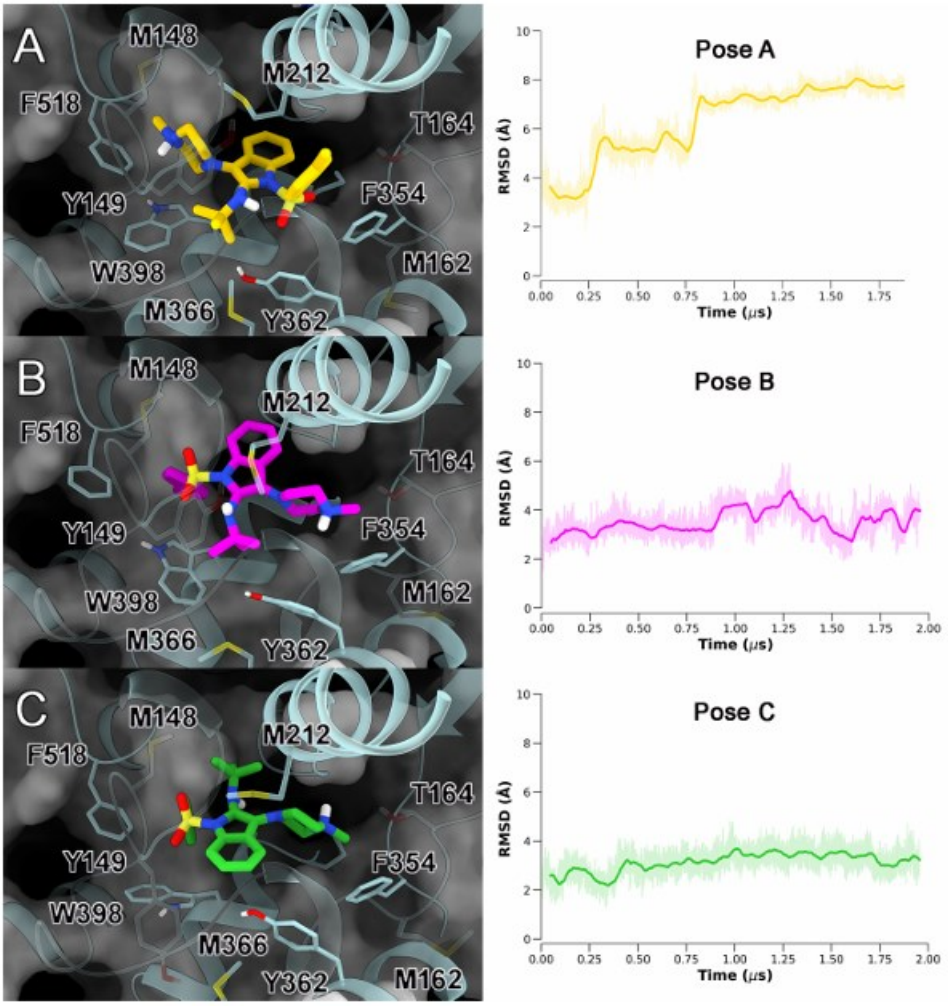

Figure 3.18. Left panels) The tree binding poses (A, B, and C) of **3.44** at the "NBD" site predicted by the induced fit docking calculations (NOD1 is depicted as grey surface and cyan cartoons; the ligand and the protein residues important for its binding are highlighted as sticks); Right panels) Ligand's heavy atoms RMSD (with respect to its initial conformation) along the MD simulations performed on each induced fit docking solution. The bold lines show a RMSD value smoothed with a rolling window of 2 ns, while the real fluctuations are shown with a slight transparency. Prior to RMSD calculation, the trajectory was aligned on the Cα atoms of the most stable secondary structure elements (helices and strands).

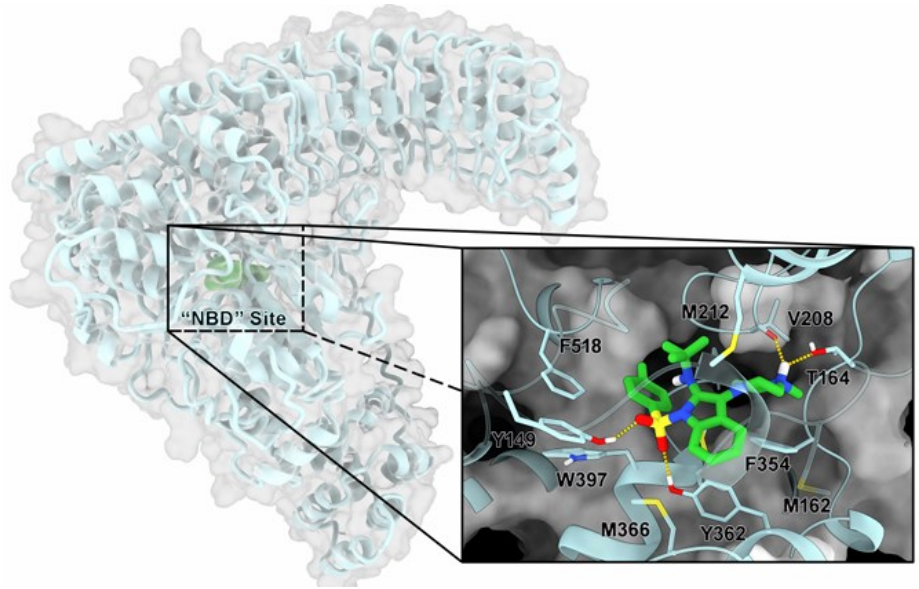

Figure 3.19. MD predicted binding pose of **3.44** at the "NBD" binding site of human NOD1. The protein is shown as grey surface and cyan cartoon. The ligand and the residues important for its binding are highlighted as green and cyan sticks, respectively. Hydrogen bonds are shown as yellow dashed lines, whereas non-polar hydrogens are omitted for sake of clarity.

Worthy of note, the volume occupied by **3.44** in the MD-predicted binding mode is widely superimposable with that of ADP (see Experimental Section). This prompted us to experimentally validate our computational model by performing competitive ligand-based NMR binding experiments between **3.44** and ADP. STD-NMR and WL-NMR spectra were thus acquired before and after the addition of ADP to the **3.44**/NOD1 complex. Notably, STD spectra (Figure 3.20a) showed a significant decrease in intensity of **3.44** proton resonances after the addition of ADP to the **3.44**/NOD1 complex, demonstrating that the two ligands compete for the same binding site. Additionally, **3.44** WaterLOGSY signals significantly decreased or inverted their phase after addition of ADP (Figure 3.20b), confirming that the two ligands occupy the same binding region, as suggested by computational studies.

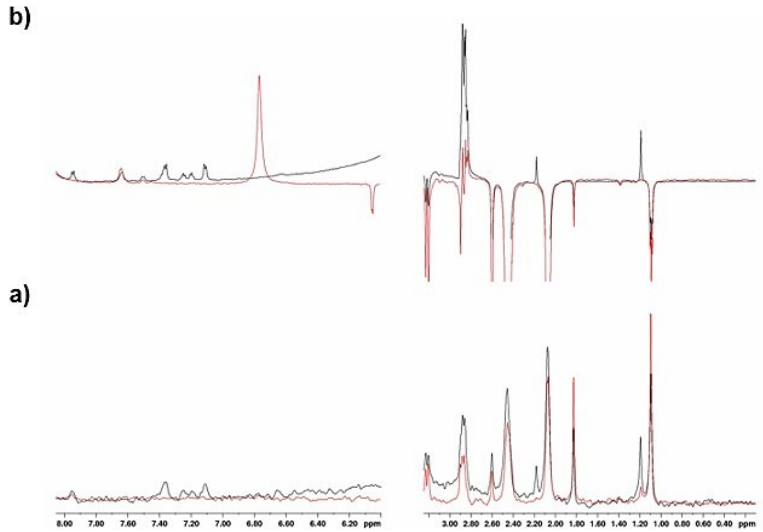

Figure 3.20. (a) STD-NMR and (b) WL-NMR spectra of **3.44** (0.250mM)/NOD1(1μM) in the absence (black) and presence (red) of ADP (0.250 mM).

Furthermore, to exclude the possibility that compound **3.44** would be hosted by the LRR domain, similar ligand-based WL-NMR competition experiments were performed before and after the addition of iE-DAP (Figure 3.21).

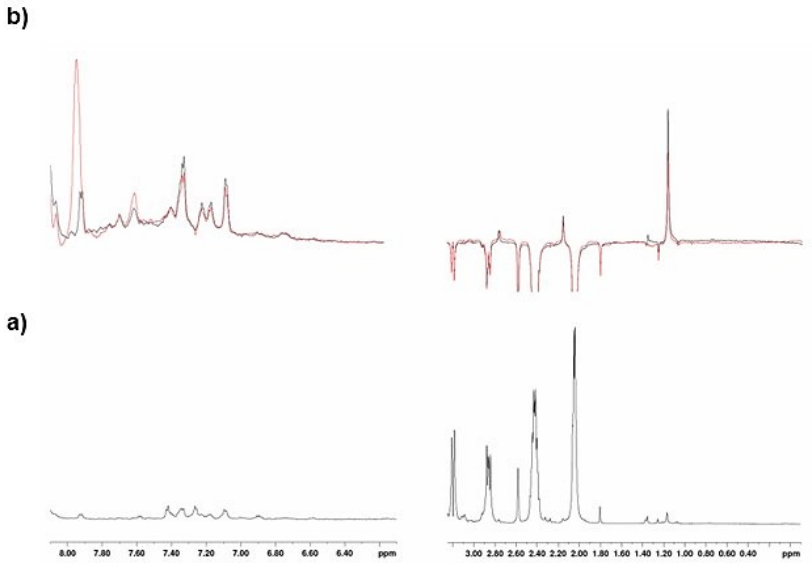

Figure 3.21. (a) ^{1}H NMR and (b) WL-NMR spectra of **3.44** (0.250 mM)/NOD1(1 μM) in the absence (black) and presence (red) of iE-DAP (0.250 mM).

The spectra did not exhibit a reduction in intensity or a phase inversion of the signals of **3.44** before (black spectrum) and after (red spectrum) the addition of iE-DAP to the **3.44**/NOD1 complex, thus confirming that the two ligands do not compete for the same binding site on the NOD1 protein. These data strongly suggest that compound **3.44** does not bind to the LRR domain, as predicted by molecular modelling.

Finally, to confirm the NBD as the binding site also for Notidinib-1 (**3.13**), NMR competition experiments were carried out on the **3.13**/NOD1 complex by using ADP as the displacement agent. As observed for **3.44**, the STD-NMR (Figure 3.22b) and WL-NMR (Figure 3.22c) spectra exhibited a decrease in intensity of the Noditinib-1 signals after the addition of ADP, thus proving that Noditinib-1 shares the same binding site as ADP.

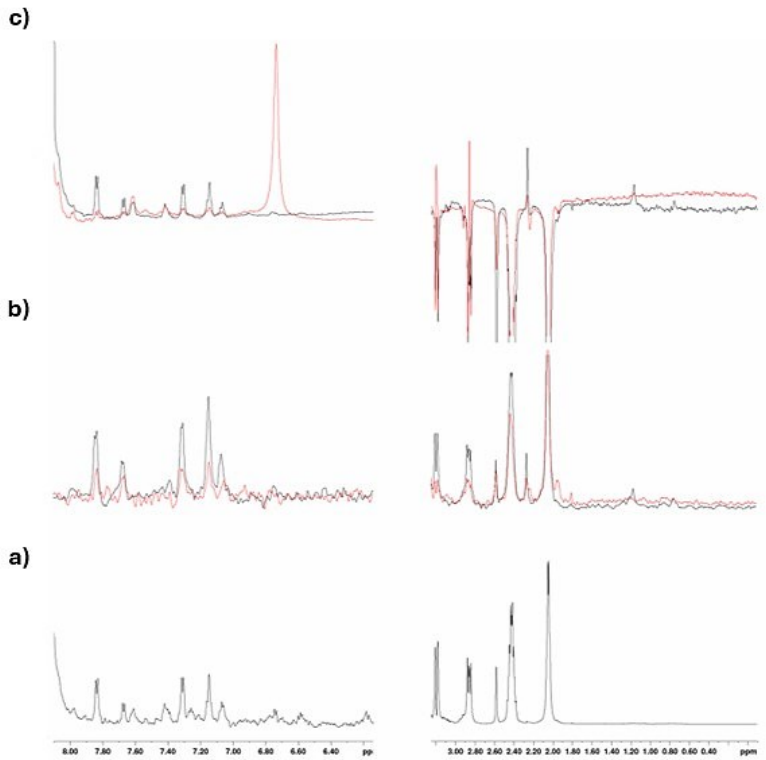

Figure 3.22. (a) ^{1}H NMR, (b) STD-NMR, and (c) WL-NMR spectra of **3.13** (0.250 mM)-NOD1(1 μM) in the absence (black) and presence (red) of ADP (0.250 mM).

To the best of our knowledge, the reported computational and NMR studies provided the first structural information regarding both the interaction site and the binding mode of small molecule inhibitors to NOD1. We are confident that the identification of the NOD1-NBD as the putative binding site, along with the unprecedented recognition of the key interactions occurring between our micromolar antagonist **3.44** and specific amino acid residues of the protein, will lay the ground for further *structure-based* design and discovery of NOD1 selective antagonists, pushing forward the druggability of NOD1-dependent diseases.

Bibliography

(1) *Worldwide cancer data;* from *the World Cancer Research Fund International.*
(2) Baudino, T.; *Current Drug Discovery Technologies,* **2015**, *12*, 3–20.
(3) Ke, X.; Shen, L.; *Frontiers in Laboratory Medicine,* **2017**, *1*, 69–75.
(4) Nam, N.-H.; Parang, K.; *Current Drug Targets,* **2003**, *4*, 159–179.
(5) Min, H.-Y.; Lee, H.-Y.; *Experimental and Molecular Medicine,* **2022**, *54*, 1670–1694.
(6) Zajac M.; Muszalska I.; Jelinska A.; *Current Medicinal Chemistry,* **2016**, *23*, 4176–4220.
(7) Vanoni, M. A.; *Archives of Biochemistry and Biophysics,* **2017**, *632*, 118–141.
(8) Motta, V.; Soares, F.; Sun, T.; Philpott, D. J.; *Physiological Reviews,* **2015**, *95*, 149–178.
(9) Terman, J. R.; Mao, T.; Pasterkamp, R. J.; Yu, H.-H.; Kolodkin, A. L.; *Cell,* **2002**, *109*, 887–900.
(10) Suzuki, T.; Nakamoto, T.; Ogawa, S.; Seo, S.; Matsumura, T.; Tachibana, K.; Morimoto, C.; Hirai, H.; *Journal of Biological Chemistry,* **2002**, *277*, 14933–14941.
(11) Lundquist, M. R.; Storaska, A. J.; Liu, T.-C.; Larsen, S. D.; Evans, T.; Neubig, R. R.; Jaffrey, S. R.; *Cell,* **2014**, *156*, 563–576.
(12) Ashida, S.; Furihata, M.; Katagiri, T.; Tamura, K.; Anazawa, Y.; Yoshioka, H.; Miki, T.; Fujioka, T.; Shuin, T.; Nakamura, Y.; Nakagawa, H.; *Clinical Cancer Research,* **2006**, *12*, 2767–2773.
(13) Mariotti, S.; Barravecchia, I.; Vindigni, C.; Pucci, A.; Balsamo, M.; Libro, R.; Senchenko, V.; Dmitriev, A.; Jacchetti, E.; Cecchini, M.; Roviello, F.; Lai, M.; Broccoli, V.; Andreazzoli, M.; Mazzanti, C. M.; Angeloni, D.; *Oncotarget,* **2016**, *7*, 1808–1825.
(14) Ho, J. R.; Chapeaublanc, E.; Kirkwood, L.; Nicolle, R.; Benhamou, S.; Lebret, T.; Allory, Y.; Southgate, J.; Radvanyi, F.; Goud, B.; *PLoS One,* **2012**, *7*, e39469.
(15) Wang, Y.; Deng, W.; Zhang, Y.; Sun, S.; Zhao, S.; Chen, Y.; Zhao, X.; Liu, L.; Du, J.; *Acta Physiologica,* **2018**, *222*, e12920.
(16) Hellweg, R.; Mooneyham, A.; Chang, Z.; Shetty, M.; Emmings, E.; Iizuka, Y.; Clark, C.; Starr, T.; Abrahante, J. H.; Schütz, F.; Konecny, G.; Argenta, P.; Bazzaro, M.; *Hormones and Cancer,* **2018**, *9*, 326–337.
(17) Gandalovičová, A.; Rosel, D.; Fernandes, M.; Veselý, P.; Heneberg, P.; Čermák, V.; Petruželka, L.; Kumar, S.; Sanz-Moreno, V.; Brábek, J.; *Trends Cancer,* **2017**, *3*, 391–406.
(18) Barravecchia, I.; Mariotti, S.; Pucci, A.; Scebba, F.; De Cesari, C.; Bicciato, S.; Tagliafico, E.; Tenedini, E.; Vindigni, C.; Cecchini, M.; Berti, G.; Vitiello, M.; Poliseno, L.; Mazzanti, C. M.; Angeloni, D.; *Biochimica et Biophysica Acta (BBA) - Molecular Basis of Disease,* **2019**, *9*, 2111–2124.
(19) Folkman, J.; Merler, E.; Abernathy, C.; Williams, G.; *Journal of Experimental Medicine,* **1971**, *133*, 275–288.

(20) Somchai, P.; Phongkitkarun, K.; Kueanjinda, P.; Jamnongsong, S.; Vaeteewoottacharn, K.; Luvira, V.; Okada, S.; Jirawatnotai, S.; Sampattavanich, S.; *Scientific Reports,* **2020**, *10*, 931.
(21) Pirali, T.; Mossetti, R.; Galli, S.; Tron, G. C.; *Organic Letters,* **2011**, *13*, 3734–3737.
(22) Watanabe, B.; Minami, S.; Ishida, H.; Yoshioka, R.; Nakagawa, Y.; Morita, T.; Hayashi, K.; *PLoS One,* **2015**, *10*, e0136242.
(23) Strober, W.; *Current Protocols in Immunology,* **2015**, *111,* A3-B.
(24) Geddes, K.; Magalhães, J. G.; Girardin, S. E.; *Nature Reviews Drug Discovery,* **2009**, *8*, 465–479.
(25) Uehara, A.; Fujimoto, Y.; Fukase, K.; Takada, H.; *Molecular Immunology,* **2007**, *44*, 3100–3111.
(26) Park, J.-H.; Kim, Y.-G.; Shaw, M.; Kanneganti, T.-D.; Fujimoto, Y.; Fukase, K.; Inohara, N.; Núñez, G.; *The Journal of Immunology,* **2007**, *179*, 514–521.
(27) Pashenkov, M. V.; Popilyuk, S. F.; Alkhazova, B. I.; L'vov, V. L.; Murugin, V. V.; Fedenko, E. S.; Khaitov, R. M.; Pinegin, B. V.; *International Immunopharmacology,* **2010**, *10*, 875–882.
(28) Petterson, T.; Jendholm, J.; Månsson, A.; Bjartell, A.; Riesbeck, K.; Cardell, L.-O.; *Journal of Leukocyte Biology,* **2010**, *89*, 177–187.
(29) Kerns, H. M. M.; Jutila, M. A.; Hedges, J. F.; *Cellular Immunology,* **2009**, *257*, 38–43.
(30) Martinon, F.; Mayor, A.; Tschopp, J.; *Annual Review of Immunology,* **2009**, *27*, 229–265.
(31) Platnich, J. M.; Muruve, D. A.; *Archives of Biochemistry and Biophysics,* **2019**, *670*, 4–14.
(32) Mukherjee, T.; Hovingh, E. S.; Foerster, E. G.; Abdel-Nour, M.; Philpott, D. J.; Girardin, S. E.; *Archives of Biochemistry and Biophysics,* **2019**, *670*, 69–81.
(33) Hysi, P.; Kabesch, M.; Moffatt, M. F.; Schedel, M.; Carr, D.; Zhang, Y.; Boardman, B.; von Mutius, E.; Weiland, S. K.; Leupold, W.; Fritzsch, C.; Klopp, N.; Musk, A. W.; James, A.; Nunez, G.; Inohara, N.; Cookson, W. O. C.; *Human Molecular Genetics,* **2005**, *14*, 935–941.
(34) McGovern, D. P. B.; Hysi, P.; Ahmad, T.; van Heel, D. A.; Moffatt, M. F.; Carey, A.; Cookson, W. O. C.; Jewell, D. P.; *Human Molecular Genetics,* **2005**, *14*, 1245–1250.
(35) Philpott, D. J.; Sorbara, M. T.; Robertson, S. J.; Croitoru, K.; Girardin, S. E.; *Nature Reviews Immunology,* **2014**, *14*, 9–23.
(36) Caso, F.; Costa, L.; Rigante, D.; Vitale, A.; Cimaz, R.; Lucherini, O. M.; Sfriso, P.; Verrecchia, E.; Tognon, S.; Bascherini, V.; Galeazzi, M.; Punzi, L.; Cantarini, L.; *Autoimmunity Reviews,* **2014**, *13*, 1220–1229.
(37) Zhou, Y.-J.; Zhou, H.; Li, Y.; Song, Y.-L.; *Diabetes and Metabolism,* **2012**, *38*, 538–543.
(38) Schertzer, J. D.; Tamrakar, A. K.; Magalhães, J. G.; Pereira, S.; Bilan, P. J.; Fullerton, M. D.; Liu, Z.; Steinberg, G. R.; Giacca, A.; Philpott, D. J.; Klip, A.; *Diabetes,* **2011**, *60*, 2206–2215.

(39) Nishio, H.; Kanno, S.; Onoyama, S.; Ikeda, K.; Tanaka, T.; Kusuhara, K.; Fujimoto, Y.; Fukase, K.; Sueishi, K.; Hara, T.; *Arteriosclerosis, Thrombosis, and Vascular Biology,* **2011**, *31*, 1093–1099.
(40) Shaw, P. J.; Barr, M. J.; Lukens, J. R.; McGargill, M. A.; Chi, H.; Mak, T. W.; Kanneganti, T.-D.; *Immunity,* **2011**, *34*, 75–84.
(41) Mertins, P.; Mani, D. R.; Ruggles, K. V.; Gillette, M. A.; Clauser, K. R.; Wang, P.; Wang, X.; Qiao, J. W.; Cao, S.; Petralia, F.; Kawaler, E.; Mundt, F.; Krug, K.; Tu, Z.; Lei, J. T.; Gatza, M. L.; Wilkerson, M.; Perou, C. M.; Yellapantula, V.; Huang, K.; Lin, C.; McLellan, M. D.; Yan, P.; Davies, S. R.; Townsend, R. R.; Skates, S. J.; Wang, J.; Zhang, B.; Kinsinger, C. R.; Mesri, M.; Rodriguez, H.; Ding, L.; Paulovich, A. G.; Fenyö, D.; Ellis, M. J.; Carr, S. A.; *Nature,* **2016**, *534*, 55–62.
(42) Jiang, H. Y.; Najmeh, S.; Martel, G.; MacFadden-Murphy, E.; Farias, R.; Savage, P.; Leone, A.; Roussel, L.; Cools-Lartigue, J.; Gowing, S.; Berube, J.; Giannias, B.; Bourdeau, F.; Chan, C. H. F.; Spicer, J. D.; McClure, R.; Park, M.; Rousseau, S.; Ferri, L. E.; *Protein Cell,* **2020**, *11*, 187–201.
(43) Groeger, S.; Wu, F.; Wagenlehner, F.; Dansranjav, T.; Ruf, S.; Denter, F.; Meyle, J.; *Frontiers in Cellular and Infection Microbiology,* **2022**, *12,* 12:935806.
(44) Khan, P. M.; Correa, R. G.; Divlianska, D. B.; Peddibhotla, S.; Sessions, E. H.; Magnuson, G.; Brown, B.; Suyama, E.; Yuan, H.; Mangravita-Novo, A.; Vicchiarelli, M.; Su, Y.; Vasile, S.; Smith, L. H.; Diaz, P. W.; Reed, J. C.; Roth, G. P.; *ACS Medicinal Chemistry Letters ,***2011**, *2*, 780–785.
(45) Magnuson, G.; Khan, P.; Yuan, H.; Brown, B.; Divlianska, D. B.; Stonich, D.; Peddibhotla, M.; Su, Y.; Dad, S.; Sergienko, E.; Chung, T. D.; Roth, G. P.; Wimer, C.; Diaz, P.; Correa, R. G.; Reed, J. C.; *Probe Reports from the NIH Molecular Libraries Program,* **2010**, National Centre for Biotechnology Information, Bethesda, MD.
(46) Rickard, D. J.; Sehon, C. A.; Kasparcova, V.; Kallal, L. A.; Zeng, X.; Montoute, M. N.; Chordia, T.; Poore, D. D.; Li, H.; Wu, Z.; Eidam, P. M.; Haile, P. A.; Yu, J.; Emery, J. G.; Marquis, R. W.; Gough, P. J.; Bertin, J.; *PLoS One,* **2013**, *8*, e69619.
(47) Ma, Y.; Li, X.; Pei, Y.; Ye, J.; Wei, X.; Yang, J.; Si, G.; Tian, J.; Dong, Y.; Liu, G.; *European Journal of Medicinal Chemistry,* **2020**, *204*, 112575.
(48) Wang, S.; Yang, J.; Li, X.; Liu, Z.; Wu, Y.; Si, G.; Tao, Y.; Zhao, N.; Hu, X.; Ma, Y.; Liu, G.; *Journal of Medicinal Chemistry,* **2017**, *60*, 5162–5192.
(49) Ma, Y.; Zhao, N.; Liu, G.; *Journal of Medicinal Chemistry,* **2011**, *54*, 2767–2777.
(50) Correa, R. G.; Khan, P. M.; Askari, N.; Zhai, D.; Gerlic, M.; Brown, B.; Magnuson, G.; Spreafico, R.; Albani, S.; Sergienko, E.; Diaz, P. W.; Roth, G. P.; Reed, J. C.; *Chemistry and Biology,* **2011**, *18*, 825–832.
(51) Mannes, P. Z.; Onyango, E. O.; Gribble, G. W.; *The Journal of Organic Chemistry,* **2016**, *81*, 12478–12481.
(52) Giustiniano, M.; Pelliccia, S.; Sangaletti, L.; Meneghetti, F.; Amato, J.; Novellino, E.; Tron, G. C.; *Tetrahedron Letters,* **2017**, *58*, 4264–4268.
(53) Guzelj, S.; Nabergoj, S.; Gobec, M.; Pajk, S.; Klančič, V.; Slütter, B.; Frkanec, R.; Štimac, A.; Šket, P.; Plavec, J.; Mlinarič-Raščan, I.; Jakopin, Ž.; *Journal of Medicinal Chemistry,* **2021**, *64*, 7809–7838.

(54) Keček Plešec, K.; Urbančič, D.; Gobec, M.; Pekošak, A.; Tomašič, T.; Anderluh, M.; Mlinarič-Raščan, I.; Jakopin, Ž.; *Bioorganic and Medicinal Chemistry* **2016**, *24*, 5221–5234.
(55) Giustiniano, M.; Daniele, S.; Pelliccia, S.; La Pietra, V.; Pietrobono, D.; Brancaccio, D.; Cosconati, S.; Messere, A.; Giuntini, S.; Cerofolini, L.; Fragai, M.; Luchinat, C.; Taliani, S.; La Regina, G.; Da Settimo, F.; Silvestri, R.; Martini, C.; Novellino, E.; Marinelli, L.; *Journal of Medicinal Chemistry,* **2017**, *60*, 8115–8130.
(56) Brancaccio, D.; Di Maro, S.; Cerofolini, L.; Giuntini, S.; Fragai, M.; Luchinat, C.; Tomassi, S.; Limatola, A.; Russomanno, P.; Merlino, F.; Novellino, E.; Carotenuto, A.; *ACS Medicinal Chemistry Letters,* **2020**, *11*, 1047–1053.
(57) Brancaccio, D.; Diana, D.; Di Maro, S.; Di Leva, F. S.; Tomassi, S.; Fattorusso, R.; Russo, L.; Scala, S.; Trotta, A. M.; Portella, L.; Novellino, E.; Marinelli, L.; Carotenuto, A.; *Journal of Medicinal Chemistry,* **2018**, *61*, 2910–2923.
(58) Gomez-Monterrey, I.; Campiglia, P.; Aquino, C.; Bertamino, A.; Granata, I.; Carotenuto, A.; Brancaccio, D.; Stiuso, P.; Scognamiglio, I.; Rusciano, M. R.; Maione, A. S.; Illario, M.; Grieco, P.; Maresca, B.; Novellino, E.; *Journal of Medicinal Chemistry,* **2011**, *54*, 4077–4091.
(59) Mayer, M.; Meyer, B.; *Angewandte Chemie International Edition* **1999**, *38*, 1784–1788.
(60) Dalvit, C.; Fogliatto, G.; Stewart, A.; Veronesi, M.; Stockman, B.; *Journal of Biomolecular NMR,* **2001**, *21*, 349–359.
(61) Cerofolini, L.; Amato, J.; Borsi, V.; Pagano, B.; Randazzo, A.; Fragai, M.; *Journal of Molecular Recognition,* **2015**, *28*, 376–384.
(62) Jendele, L.; Krivak, R.; Skoda, P.; Novotny, M.; Hoksza, D.; *Nucleic Acids Research,* **2019**, *47*, W345–W349.
(63) Laroui, H.; Yan, Y.; Narui, Y.; Ingersoll, S. A.; Ayyadurai, S.; Charania, M. A.; Zhou, F.; Wang, B.; Salaita, K.; Sitaraman, S. V.; Merlin, D.; *Journal of Biological Chemistry,* **2011**, *286*, 31003–31013.
(64) Jakopin, Ž.; *Journal of Medicinal Chemistry,* **2014**, *57*, 6897–6918.

Experimental Section

General methods

Commercially available reagents and solvents were used without further purification.

When necessary, reactions were performed in oven-dried glassware under a positive pressure of dry nitrogen.

All reactions were routinely checked by thin-layer chromatography (TLC) on 5x20 cm plates with a layer thickness of 0.25 mm (silica gel 60 F_{254}), and monitored by using UV, $KMnO_4$, and/or ninhydrin as the revelation method. Column chromatography purifications were carried out on silica gel 60 (70–230 mesh ASTM) using the reported eluents.

All NMR spectra were recorded on Bruker Avance NEO 400 or 700 MHz instruments. Experiments for structure elucidation were performed in the reported deuterated solvents, at 25° C, with a RT-DR-BF/1H-5-mm-OZ SmartProbe. Chemical shifts (δ) are reported in part per million (ppm) relative to the residual solvent peak; coupling constants (*J*), are reported in hertz (Hz).

High-resolution ESI-MS spectra were performed on a Thermo LTQ Orbitrap XL mass spectrometer. The spectra were recorded by infusion into the ESI source using MeOH as the solvent.

Compounds **3.18-3.46** were analysed by analytical reversed-phase Ultra High Performance Liquid Chromatography (RP-UHPLC) (Shimadzu Nexera liquid chromatograph LC-30AD) equipped with a C18-bonded column (Phenomenex Kinetex, 150 mm x 4.6 mm, 5 µm, 100 Å), using isocratic MeCN (0.1% TFA) in water (0.1% TFA) over 3 min, gradient 30% to 90% elution of MeCN (0.1% TFA) in water (0.1% TFA) over 7 min, isocratic 90% MeCN (0.1% TFA) in water (0.1% TFA) over 5 min, gradient 90% to 30% elution of MeCN (0.1% TFA) in water (0.1% TFA) over 3 min, and isocratic 30% MeCN (0.1% TFA) in water (0.1%

TFA) over 2 min, with a flow rate of 1 mL/min and UV detection at 254 nm by a diode array UV−Vis detector. The purity of all the compounds has been determined by HPLC analysis as ≥95% (except for compounds **3.34**, **3.36**, and **3.38**, which were found to be unstable to the conditions used for the HPLC analysis).

3.1.

General procedure for the synthesis of compounds 3.7 and 3.8

Commercially available (*R*)- and (*S*)-3-aminopyrrolidines **3.14** and **3.15** (Merck KGaA, Darmstadt, Germany) (0.5 mmol, 1.1 equiv.) were dissolved in DCM (2.0 mL, 0.25 M), the solution was chilled at 0° C, and a cold 0.5 M solution of 4-chlorobenzoyl chloride **3.13** (0.45 mmol, 1 equiv.) in DCM was added dropwise over 30 minutes. The reaction was stirred under a nitrogen atmosphere for additional 30 minutes, then the crude mixture was washed with a NaOH 5% aqueous solution, and the product was extracted with DCM (x4). The combined organic layers were dried over sodium sulfate, filtered, and concentrated under vacuum to give a crude mixture which was purified by column chromatography to afford intermediates **3.16** and **3.17** in 56% and 53% yields, respectively. The latter were then dissolved in DCM (0.15 M), the solution was cooled to 0° C, and HOBt (1 equiv.), EDC HCl (0.9 equiv.), and 3,5-bis(trifluoromethyl)benzoic acid **3.18** (0.9 equiv.) were added. The reaction mixture was stirred at room temperature overnight and then washed with a 1N HCl solution (x3), $NaHCO_3$ saturated solution (x3), and brine (x1). The organic phase was dried over sodium sulfate, filtered, and concentrated under vacuum to give a crude mixture which was purified via column chromatography (*n*-hexane/EtOAc) to afford **3.7** and **3.8** in 73% and 80% yield, respectively.

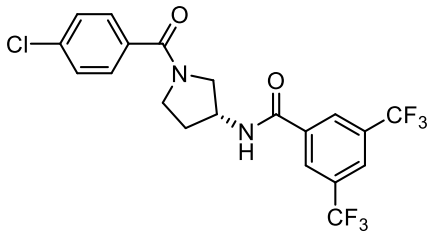

(*R*)-*N*-(1-(4-Chlorobenzoyl)pyrrolidin-3-yl)-3,5-bis(trifluoromethyl)benzamide (**3.7**). ^{1}H NMR (400 MHz, $CDCl_3$) δ 8.40 (s, 1H), 8.25 (s, 1H), 7.978–7.87 (m, 1H), 7.75–7.68 (m, 1H), 7.43–7.33 (m, 2H), 7.19–7.17 (s, 2H), 4.83–4.71 (m, 1H), 4.16–4.09 (m, 1H), 3.89–3.84 (m, 1H), 3.77–3.48 (m, 2H), 2.43–2.28 (m, 1H), 2.19–2.02 (m, 1H); HRMS (ESI) *m/z:* calcd $[M + H]^+$ for $C_{20}H_{16}ClF_6N_2O_2^+$ 465.0799; found $[M + H]^+$ 465.0800.

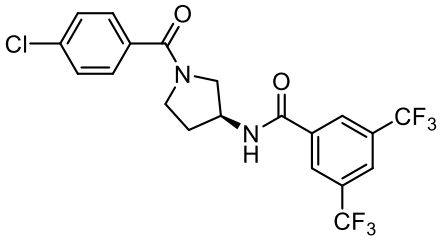

(*S*)-*N*-(1-(4-Chlorobenzoyl)pyrrolidin-3-yl)-3,5-bis(trifluoromethyl)benzamide (**3.8**). ^{1}H NMR (400 MHz, $CDCl_3$) δ 8.42 (s, 1H), 8.26 (s, 1H), 8.01–7.85 (m, 2H), 7.40–7.32 (m, 2H), 7.16–7.14 (m, 2H), 4.84–4.73 (m, 1H), 4.20–4.10 (m, 1H), 3.90–3.87 (m, 1H), 3.75–3.51 (m, 2H), 2.42–2.29 (m, 1H), 2.20–2.14 (m, 1H). HRMS (ESI) *m/z:* calcd $[M + H]^+$ for $C_{20}H_{16}ClF_6N_2O_2^+$ 465.0799; found $[M + H]^+$ 465.0799.

Procedure for the synthesis of compound 3.9

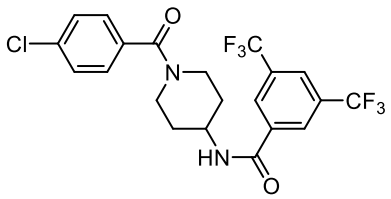

N-(1-(4-Chlorobenzoyl)piperidin-4-yl)-3,5-bis(trifluoromethyl)benzamide (**3.9**). 4-amino-1-Boc-pyrrolidine **3.19** (synthesised according to literature procedure,[1] 0.5 mmol, 1 equiv.) was dissolved in DCM (1.7 mL, 0.3 M); HOBt (0.6 mmol, 1.2 equiv.), EDC HCl (0.55 mmol 1.1 equiv.), and 3,5-bis(trifluoromethyl)benzoic acid **3.18** (0.5 mmol, 1 equiv.) were added, and the reaction was stirred at room temperature overnight. The crude mixture was washed with a citric acid solution (x2), $NaHCO_3$ saturated solution (x2), and brine (x1). The organic phase was dried over sodium sulfate, filtered, and concentrated under vacuum to give a crude mixture which was purified by column chromatography (*n*-hexane/EtOAc) to afford the intermediate *tert*-butyl 4-(3,5-bis(trifluoromethyl)benzamido)piperidine-1-carboxylate in 95% yield. The latter was dissolved in a 0.5 M 1:1 TFA/DCM solution at 0° C and stirred at room temperature for 30 min. Evaporation of the crude mixture gave deprotected **3.20** as TFA salt in quantitative yield. The latter was finally dissolved in DCM (0.2 M), cooled at 0° C, and Et_3N (3 equiv.) and 4-chlorobenzoyl chloride **3.13** (1.5 equiv.) were added dropwise. The crude mixture was stirred under nitrogen for 2 h, washed with 1N HCl solution (x2), $NaHCO_3$ saturated solution (x2), and brine (x1). The organic layer dried over sodium sulfate, filtered, and concentrated under vacuum to give a crude mixture which was purified by column chromatography (*n*-hexane/EtOAc) to afford **3.9** in 86% yield. ^{1}H NMR (400 MHz, $CDCl_3$) δ 8.32 (s, 2H), 7.90 (s, 1H), 7.81 (brd, -N*H*), 7.32 (d, J = 8.4 Hz, 2H), 7.25 (d, J = 8.4 Hz, 2H), 4.73–4.72 (m, 1H), 4.32–4.25 (m, 1H), 3.78–3.76 (m, 1H), 3.21–2.91 (m, 2H), 2.09–2.07 (m, 2H), 1.66–1.33 (m, 2H);

HRMS (ESI) *m/z:* calcd $[M + H]^+$ for $C_{21}H_{18}ClF_6N_2O_2^+$ 479.0956; found $[M + H]^+$ 479.0969.

Procedure for the synthesis of compound 3.10

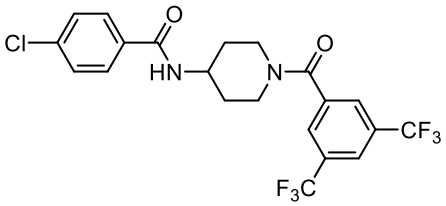

N-(1-(3,5-bis(Trifluoromethyl)benzoyl)piperidin-4-yl)-4-chlorobenzamide (**3.10**). 4-amino-1-Boc-pyrrolidine **3.19** (synthesised according to literature procedure,[1] 0.5 mmol, 1 equiv.) was dissolved in DCM (2.5 mL, 0.2 M), cooled at 0° C, and Et_3N (1.5 mmol, 3 equiv.) and 4-chlorobenzoyl chloride **3.13** (0.75 mmol, 1.5 equiv.) were added dropwise. The crude mixture was stirred under nitrogen for 2 h, then washed with a citric acid solution (x2), $NaHCO_3$ saturated solution (x2), and brine (x1). The organic phase was dried over sodium sulfate, filtered, and concentrated under vacuum to give a crude mixture which was purified by column chromatography (*n*-hexane/EtOAc) to afford the intermediate *tert*-butyl 4-(4-chlorobenzamido)piperidine-1-carboxylate in 97% yield. The latter was dissolved in a 0.5 M 1:1 TFA/DCM solution at 0° C and stirred at room temperature for 30 minutes. Evaporation of the crude mixture gave deprotected **3.21** as TFA salt in quantitative yield. Intermediate **3.21** was finally dissolved in in DCM (0.3 M); HOBt (1.2 equiv.), EDC HCl (1.1 equiv.), and 3,5-bis(trifluoromethyl)benzoic acid **3.18** (1 equiv.) were added, and the reaction was stirred at room temperature overnight. The reaction mixture was washed with 1N HCl solution (x2), $NaHCO_3$ saturated solution (x2), and brine (x1). The organic layer was dried over sodium sulfate, filtered, and concentrated under vacuum to give a crude mixture which was purified by column chromatography (*n*-hexane/EtOAc) to afford **3.10** in 62% yield. ^{1}H NMR (400MHz, $CDCl_3$) δ 7.92 (s, 1H), 7.82 (s, 2H), 7.66 (d, J = 7.6 Hz, 2H),

7.35 (d, *J* = 7.6 Hz, 2H), 6.28 (brd, -N*H*), 3.63–3.59 (m, 1H), 3.22–2.97 (m, 2H), 2.11–2.01 (m, 2H), 1.57–1.39 (m, 2H); HRMS (ESI) *m/z:* calcd $[M + H]^+$ for $C_{21}H_{18}ClF_6N_2O_2^+$ 479.0956; found $[M + H]^+$ 479.0957.

Procedure for the synthesis of compound 3.11

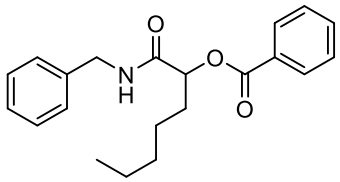

1-(Benzylamino)-1-oxoheptan-2-yl benzoate (**3.11**). *n*-Hexanal **3.22** (0.5 mmol, 1 equiv.), benzyl isocyanide **3.23** (0.5 mmol, 1 equiv.), and benzoic acid **3.24** (0.5 mmol, 1 equiv.) were one-pot mixed in DCM (1 mL, 0.5 M) and stirred at room temperature for 48 h. The crude mixture was purified via column chromatography (*n*-hexane/EtOAc) to afford 3.11 in 78% yield. ^{1}H NMR (400 MHz, $CDCl_3$) δ 8.05 (d, *J* = 7.6 Hz, 2H), 7.62–7.58 (m, 1H), 7.48–7.45 (m, 2H), 7.33–7.24 (m, 5H), 6.38–6.35 (m, -N*H*), 5.50–5.47 (m, 1H), 4.57–4.42 (m, 2H), 2.06–1.99 (m, 2H), 1.47–1.43 (m, 2H), 1.34–1.28 (m, 4H), 0.89–0.85 (m, 3H); HRMS (ESI) *m/z:* calcd $[M + H]^+$ for $C_{21}H_{26}NO_3^+$ 340.1908; found $[M + H]^+$ 340.1903.

Procedure for the synthesis of compound 3.12

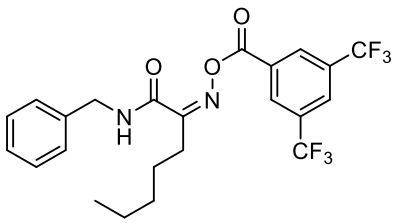

(*Z*)-*N*-Benzyl-2-(((3,5-bis(trifluoromethyl)benzoyl)oxy)imino)heptanamide (**3.12**). (*Z*)-*N*-hydroxyhexanimidoyl chloride **3.25** (synthesised according to literature procedure,[2] 1 mmol, 1 equiv.), benzyl isocyanide **3.23** (1 mmol, 1 equiv.), 3,5-

bis(trifluoromethyl)benzoic acid **3.18** (1 mmol, 1 equiv.), and Et_3N (2 mmol, 2 equiv.) were one-pot mixed in DMF (1 mL, 1M) and stirred at room temperature overnight. The crude mixture was washed with brine (x3), then dried over sodium sulfate, filtered, concentrated under vacuum, and purified via column chromatography (*n*-hexane/EtOAc) to afford **3.12** in 10% yield. ^{1}H NMR (400 MHz, $CDCl_3$) δ 8.37 (s, 2H), 8.10 (s, 1H), 7.22–7.18 (m, 5H), 6.16 (brt, -N*H*), 4.57 (d, J = 5.6 Hz, 1H), 2.68–2.64 (m, 2H), 1.68–1.63 (m, 2H), 1.39–1.31 (m, 4H), 0.89 (t, J = 6.8 Hz, 3H); HRMS (ESI) *m/z*: calcd $[M + Na]^+$ for $C_{23}H_{22}F_6N_2NaO_3^+$ 511.1432; found $[M + Na]^+$ 511.1430.

For details about biological assays, statistical analyses, and molecular modelling see: Barravecchia, I.; Barresi, E.; Russo, C.; Scebba, F.; De Cesari, C.; Mignucci, V.; De Luca, D.; Salerno, S.; La Pietra, V.; Giustiniano, M.; Pelliccia, S.; Brancaccio, D.; Donati, G.; Angeloni, D.; Marinelli, L.; Da Settimo, F.; Taliani, S.; *Molecules,* **2021**, *26*, 7519.

3.2.

Starting materials

General procedure for the synthesis of *N*-(2-formylphenyl)arylsulfonamides

N-(2-formylphenyl)arylsulfonamides were synthesised in three steps starting from commercially available anthranilic acids, except for *N*-(2-formylphenyl)-4-methylbenzenesulfonamide, *N*-(2-formylphenyl)-4-nitrobenzenesulfonamide, and *N*-(2-formylphenyl)-4-methoxybenzenesulfonamide, for which the corresponding 2-aminobenzylalcohols were commercially available.

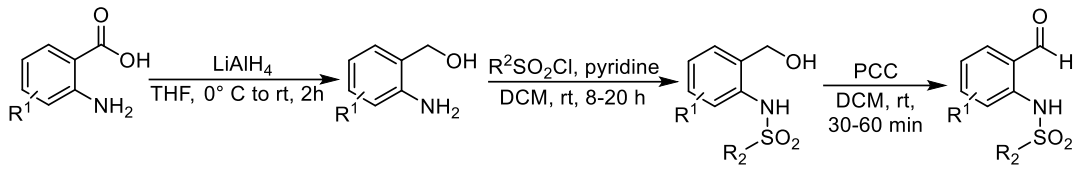

Step 1:[5] To a stirred solution of anthranilic acid (15 mmol, 1 equiv.) in THF (15 mL, 1 M,) lithium aluminum hydride (1 M in THF, 30 mmol, 2 equiv.) was slowly added at 0° C. Upon completion of the addition, the ice bath was removed, and stirring was continued for 2 hours at room temperature. Then the reaction was quenched with water and a 5% solution of NaOH in water. The inorganic solid residue was filtered under vacuum, washed with EtOAc and the filtrate was transferred to a separatory funnel. Water was added, the two layers were separated, and the aqueous phase was further extracted with EtOAc (x3). The combined organic extracts were washed with brine (x1), dried over sodium sulfate, concentrated under reduced pressure and the so-obtained 2-aminobenzylalcohols were used in the next step without further purification.

Step 2:[6] The corresponding 2-aminobenzylalcohol (10 mmol, 1 equiv.) was dissolved in DCM (8.5 mL, 1.2 M) and pyridine (10 mmol, 1 equiv.) and the desired benzenesulfonyl chloride (12 mmol, 1.2 equiv.) were added. The reaction mixture was stirred at room temperature until all the starting material was consumed, as judged by TLC (typically 8-20 hours). Then the reaction was concentrated under vacuum and triturated with *n*-hexane to give sufficiently pure *N*-(2-(hydroxymethyl)phenyl)benzenesulfonamides.

Step 3:[6] *N*-(2-(hydroxymethyl)phenyl)benzene-sulfonamide (5 mmol, 1 equiv.) was dissolved in DCM (20 mL, 0.25 M) and pyridinium chlorochromate (10 mmol, 2 equiv.) was added. The reaction was stirred at room temperature until all the starting material disappeared, as judged by TLC (typically 30-60 minutes). Then the reaction was filtered through a pad of Celite, concentrated under vacuum and purified by column chromatography (*n*-hexane/EtOAc) to give the desired *N*-(2-formylphenyl)arylsulfonamide.

Characterisation data of all synthesised *N*-(2-formylphenyl)arylsulfonamides were in agreement with literature reports.[7-9]

General procedure for the synthesis of compounds 3.18-3.46

The *N*-(2-formylphenyl)arylsulfonamide (0.7 mmol, 1 equiv.), the secondary amine (0.7 mmol, 1 equiv.), and the isocyanide (0.7 mmol, 1 equiv.) were one-pot mixed in DCM (1.4 mL, 0.5 M) at room temperature. The mixture was stirred under a nitrogen atmosphere until completion of the reaction, as monitored by TLC. Then the solvent was removed under vacuum and the crude material was purified by column chromatography or by crystallisation.

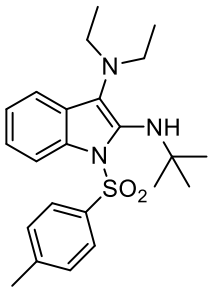

N^2-(*Tert*-butyl)-N^3,N^3-diethyl-1-tosyl-1*H*-indole-2,3-diamine (**3.18**). The crude material was purified by column chromatography (*n*-hexane/EtOAc 90:10) to give the product as a brownish solid (351.0 mg, 85% yield). ^{1}H NMR (400 MHz, $CDCl_3$) δ 8.09 (d, J = 8.0 Hz, 1H), 7.39 (d, J = 8.0 Hz, 2H), 7.30 (d, J = 8.0 Hz, 1H), 7.19–7.10 (m, 2H), 7.01 (d, J = 8.4 Hz, 2H), 3.91 (brs, -N*H*), 3.09 (q, J = 7.2 Hz, 4H), 2.25 (s, 3H), 1.27 (s, 9H), 0.84 (t, J = 7.2 Hz, 6H; HRMS (ESI) *m/z:* calcd $[M + H]^+$ for $C_{23}H_{32}N_3O_2S^+$ 414.2210; found $[M + H]^+$ 414.2203.

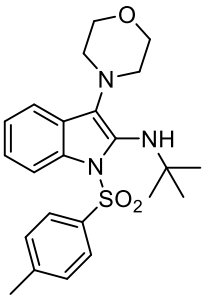

N-(*Tert*-butyl)-3-morpholino-1-tosyl-1*H*-indol-2-amine (**3.19**). The crude material was purified by column chromatography (*n*-hexane/EtOAc 80:20) to give the product as a yellow solid (393.1 mg, 92% yield). ^{1}H NMR (400 MHz, $CDCl_3$) δ 8.04 (d, J = 7.2 Hz, 1H), 7.40–7.35 (m, 3H), 7.19–7.11 (m, 2H), 7.05 (d, J = 8.0 Hz, 2H), 4.11 (brs, -N*H*), 3.79–3.76 (m, 4H), 3.20–3.18 (m, 4H), 2.27 (s, 3H), 1.29 (s, 9H); HRMS (ESI) *m/z:* calcd $[M + H]^+$ for $C_{23}H_{30}N_3O_3S^+$ 428.2003; found $[M + H]^+$ 428.2000.

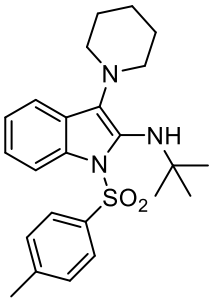

N-(*Tert*-butyl)-3-(piperidin-1-yl)-1-tosyl-1*H*-indol-2-amine (**3.20**). The crude material was purified by column chromatography (*n*-hexane/EtOAc 90:10) to give the product as a yellow solid (281.4 mg, 66% yield). ^{1}H NMR (400 MHz, $CDCl_3$) δ 8.02 (d, J = 8.0 Hz, 1H), 7.38 (d, J = 8.4 Hz, 2H), 7.34 (d, J = 7.6 Hz, 1H), 7.18–7.10 (m, 2H), 7.03 (d, J = 8.0 Hz, 2H), 4.01 (brs, -N*H*), 3.12–3.09 (m, 4H), 2.26 (s, 3H), 1.62–1.54 (m, 6H), 1.26 (s, 9H); HRMS (ESI) *m/z*: calcd $[M + H]^+$ for $C_{24}H_{32}N_3O_2S^+$ 426.2210; found $[M + H]^+$ 426.2209.

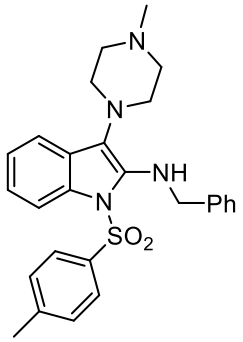

N-Benzyl-3-(4-methylpiperazin-1-yl)-1-tosyl-1*H*-indol-2-amine (**3.21**). The crude material was purified by column chromatography (*n*-hexane/EtOAc 50:50) to give the product as a yellowish solid (318.3 mg, 67% yield). 1H NMR (400 MHz, $CDCl_3$) δ 8.00 (d, J = 8.0 Hz, 1H), 7.57 (d, J = 8.4 Hz, 2H), 7.39–7.25 (m, 6H), 7.14 (d, J = 8.4 Hz, 2H), 7.09–7.02 (m, 2H), 5.65 (brt, -N*H*), 4.77 (s, 2H), 3.05–2.95 (m, 4H), 2.37–2.33 (m, 7H), 2.27 (s, 3H); HRMS (ESI) *m/z*: calcd $[M + H]^+$ for $C_{27}H_{31}N_4O_2S^+$ 475.2163; found $[M + H]^+$ 475.2199.

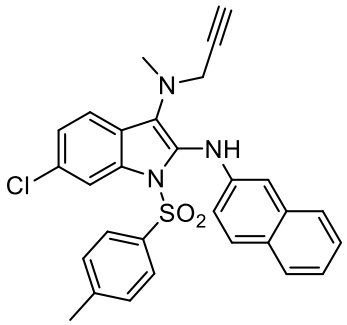

6-Chloro-N^3-methyl-N^2-(naphthalen-2-yl)-N^3-(prop-2-yn-1-yl)-1-tosyl-1*H*-indole-2,3-diamine (**3.22**). The crude material was purified by column chromatography (*n*-hexane/EtOAc 90:10) to give the product as a beige solid (257.2 mg, 50% yield). ^{1}H NMR (400 MHz, $CDCl_3$) δ 8.28 (brs, -N*H*), 7.69 (d, J = 8.0 Hz, 1H), 7.61–7.55 (m, 2H), 7.41–7.25 (m, 6H), 6.87 (dd, J_a= 8.4 Hz, J_b = 1.2 Hz, 1H), 6.73–6.71 (m, 2H), 6.47 (s, 1H), 6.15 (s, 1H), 3.75 (s, 2H), 2.86 (s, 3H), 2.13 (s, 1H), 1.96 (s, 3H); HRMS (ESI) *m/z:* calcd $[M + H]^+$ for $C_{29}H_{25}ClN_3O_2S^+$ 514.1351; found $[M + H]^+$ 514.1353.

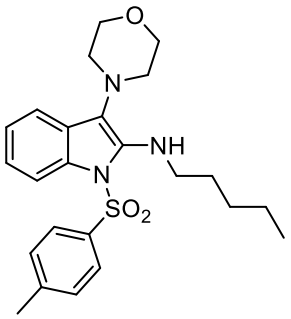

3-Morpholino-*N*-pentyl-1-tosyl-1*H*-indol-2-amine (**3.23**). The crude material was purified by crystallisation from MeOH to give the product as a yellow solid (180.1 mg, 72% yield). ^{1}H NMR (400 MHz, $CDCl_3$) δ 7.96 (d, J = 8.4 Hz, 1H), 7.59 (d, J = 8.4 Hz, 2H), 7.34 (d, J = 7.2 Hz, 1H), 7.15 (d, J = 8.0 Hz, 2H), 7.10–6.99 (m, 2H), 5.35 (brt, -N*H*), 3.76–3.74 (m, 4H), 3.53 (t, J = 8.0 Hz, 2H), 3.10–3.08 (m, 4H), 2.33 (s, 3H), 1.60–1.53 (m, 2H), 1.38–1.36 (m, 4H), 0.95–0.91 (m, 3H); HRMS (ESI) *m/z*: calcd $[M + H]^+$ for $C_{24}H_{32}N_3O_3S^+$ 442.2159; found $[M + H]^+$ 442.2151.

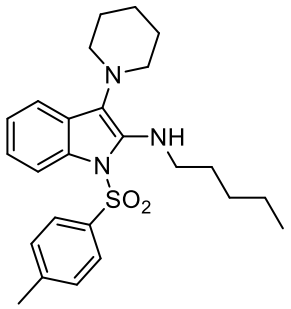

N-Pentyl-3-(piperidin-1-yl)-1-tosyl-1*H*-indol-2-amine (**3.24**). The crude material was purified by column chromatography (petroleum ether/EtOAc 99:1) to give the product as a yellow solid (79.3 mg, 51% yield). ^{1}H NMR (400 MHz, $CDCl_3$) δ 7.95 (d, J = 8.4 Hz, 1H), 7.58 (d, J = 8.0 Hz, 2H), 7.33 (d, J = 8.0 Hz, 1H), 7.14 (d, J = 8.0 Hz, 2H), 7.08–6.96 (m, 2H), 5.21 (brt, -N*H*), 3,51 (t, J = 7.2 Hz, 2H), 3.03–3.00 (m, 4H), 2.32 (s, 3H), 1.63–1.52 (m, 8H), 1.39–1.35 (m, 4H), 0.94–0.91 (m, 3H); HRMS (ESI) *m/z:* calcd $[M + H]^+$ for $C_{25}H_{34}N_3O_2S^+$ 440.2366; found $[M + H]^+$ 440.2359.

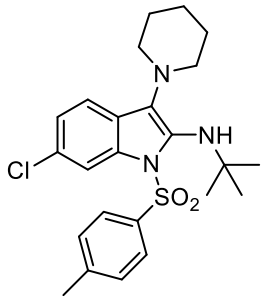

N-(*Tert*-butyl)-6-chloro-3-(piperidin-1-yl)-1-tosyl-1*H*-indol-2-amine (**3.25**). The crude material was purified by column chromatography (*n*-hexane/EtOAc 90:10) to give the product as a brownish solid (396.0 mg, 86% yield). ^{1}H NMR (400 MHz, $CDCl_3$) δ 8.05 (d, J = 2.0 Hz, 1H), 7.41 (d, J = 8.4 Hz, 2H), 7.24 (d, J = 8.4 Hz, 1H), 7.10–7.07 (m, 3H), 4.03 (brs, -N*H*), 3.07–3.05 (m, 4H), 2.29 (s, 3H), 1.61–1.55 (m, 6H), 1.26 (s, 9H); HRMS (ESI) *m/z*: calcd $[M + H]^+$ for $C_{24}H_{31}ClN_3O_2S^+$ 460.1821; found $[M + H]^+$ 460.1823.

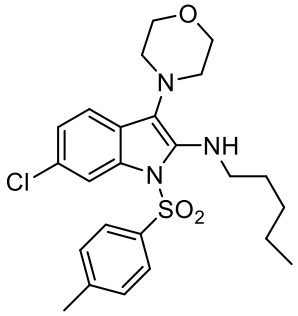

6-Chloro-3-morpholino-*N*-pentyl-1-tosyl-1*H*-indol-2-amine (**3.26**). The crude material was purified by column chromatography (*n*-hexane/EtOAc 90:10) to give the product as a brown solid (328 mg, 69% yield). ^{1}H NMR (400 MHz, $CDCl_3$) δ 7.98 (d, J = 1.6 Hz, 1H), 7.61 (d, J = 8.4 Hz, 2H), 7.24 (d, J = 8.0 Hz, 1H), 7.19 (d, J = 8.4 Hz, 2H), 7.05 (dd, J_a = 8.4 Hz, J_b = 1.6 Hz, 1H), 5.40 (brt, -N*H*), 3.75–3.73 (m, 4H), 3.54 (t, J = 7.2 Hz, 2H), 3.06–3.04 (m, 4H), 2.34 (s, 3H), 1.61–1.56 (m, 2H), 1.39–1.36 (m, 4H), 0.95–0.91 (m, 3H); HRMS (ESI) *m/z*: calcd $[M + H]^+$ for $C_{24}H_{31}ClN_3O_3S^+$ 476.1769; found $[M + H]^+$ 476.1796.

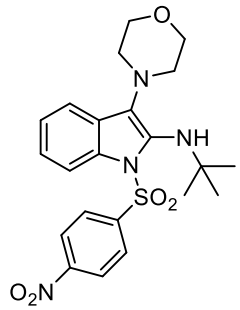

N-(*Tert*-butyl)-3-morpholino-1-((4-nitrophenyl)sulfonyl)-1*H*-indol-2-amine (**3.27**). The crude material was purified by column chromatography (*n*-hexane/EtOAc 80:20) to give the product as a yellow solid (235.6 mg, 85% yield). ^{1}H NMR (400 MHz, $CDCl_3$) δ 8.09 (d, J = 8.8 Hz, 2H), 8.03 (d, J = 8.4 Hz, 1H), 7.66 (d, J = 8.8 Hz, 2H), 7.36 (dd, J_a = 7.2 Hz, J_b = 1.2 Hz, 1H), 7.25–7.15 (m, 2H), 3.85 (brs, -N*H*), 3.78–3.76 (m, 4H), 3.16–3.13 (m, 4H), 1.29 (s, 9H); HRMS (ESI) *m/z*: calcd $[M + H]^+$ for $C_{22}H_{27}N_4O_5S^+$ 459.1697; found $[M + H]^+$ 459.1693.

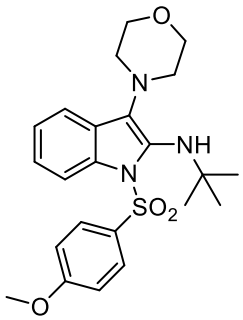

N-(*Tert*-butyl)-1-((4-methoxyphenyl)sulfonyl)-3-morpholino-1*H*-indol-2-amine (**3.28**). The crude material was purified by column chromatography (*n*-hexane/EtOAc 80:20) to give the product as a reddish sticky oil (204.5 mg, 46% yield). ^{1}H NMR (400 MHz, $CDCl_3$) δ 8.05 (d, J = 7.6 Hz, 1H), 7.45 (d, J = 9.2 Hz, 2H), 7.38–7.36 (m, 1H), 7.19–7.11 (m, 2H), 6.70 (d, J = 9.2 Hz, 2H), 4.13 (brs, -N*H*), 3.78–3.76 (m, 4H), 3.72 (s, 3H), 3.20–3.18 (m, 4H), 1.29 (s, 9H); HRMS (ESI) *m/z*: calcd $[M + H]^+$ for $C_{23}H_{30}N_3O_4S^+$ 444.1952; found $[M + H]^+$ 444.1945.

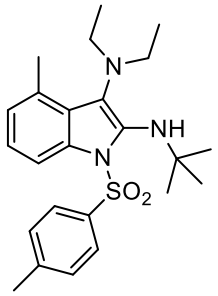

N^2-(*Tert*-butyl)-N^3,N^3-diethyl-4-methyl-1-tosyl-1*H*-indole-2,3-diamine (**3.29**). The crude material was purified by column chromatography (*n*-hexane/EtOAc 80:20) to give the product as a brownish solid (312.6 mg, 73% yield). ^{1}H NMR (400 MHz, $CDCl_3$) δ 7.98 (d, J = 8.0 Hz, 1H), 7.34 (d, J = 8.0 Hz, 2H), 7.07 (t, J = 8.0 Hz, 1H), 7.00–6.93 (m, 3H), 3.79 (brs, -N*H*), 3.03–2.89 (m, 4H), 2.45 (s, 3H), 2.25 (s, 3H), 1.32 (s, 9H), 0.82 (t, J = 8.0 Hz, 6H); HRMS (ESI) *m/z:* calcd $[M + H]^+$ for $C_{24}H_{34}N_3O_2S^+$ 428.2367; found $[M + H]^+$ 428.2361.

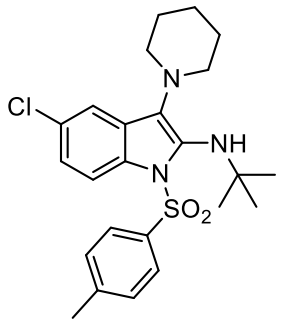

N-(*Tert*-butyl)-5-chloro-3-(piperidin-1-yl)-1-tosyl-1*H*-indol-2-amine (**3.30**). The crude material was purified by column chromatography (petroleum ether/EtOAc 99:1) to give the product as a white solid (280.3 mg, 61% yield). ^{1}H NMR (400 MHz, $CDCl_3$) δ 7.93 (d, J = 8.4 Hz, 1H), 7.38 (d, J = 8.4 Hz, 2H), 7.29 (d, J = 2.0 Hz, 1H), 7.10–.06 (m, 3H), 4.17 (brs, -N*H*), 3.05–3.03 (m, 4H), 2.29 (s, 3H), 1.64 1.53 (m, 6H), 1.27 (s, 9H); HRMS (ESI) *m/z*: calcd $[M + H]^+$ for $C_{24}H_{31}ClN_3O_2S^+$ 460.1820; found $[M + H]^+$ 460.1814.

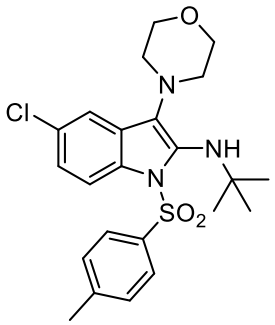

N-(*Tert*-butyl)-5-chloro-3-morpholino-1-tosyl-1*H*-indol-2-amine (**3.31**). The crude material was purified by column chromatography (petroleum ether/EtOAc 95:5) to give the product as white solid (323.6 mg, 70% yield). ^{1}H NMR (400 MHz, $CDCl_3$) δ 7.95 (d, J = 8.8 Hz, 1H), 7.39 (d, J = 8.0 Hz, 2H), 7.33 (d, J = 1.6 Hz, 1H), 7.12–7.08 (m, 3H), 4.31 (brs, -N*H*), 3.78–3.75 (m, 4H), 3.14–3.12 (m, 4H), 2.30 (s, 3H), 1.29 (s, 9H); HRMS (ESI) *m/z:* calcd $[M + H]^+$ for $C_{23}H_{29}ClN_3O_3S^+$ 462.1613; found $[M + H]^+$ 462.1608.

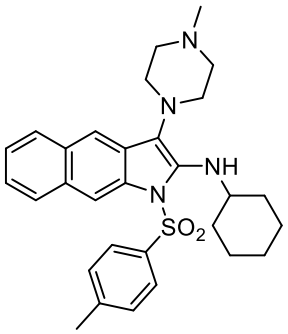

N-Cyclohexyl-3-(4-methylpiperazin-1-yl)-1-tosyl-1*H*-benzo[*f*]indol-2-amine (**3.32**). The crude material was purified by column chromatography (*n*-hexane/EtOAc 50:50) to give the product as a yellowish solid (222.7 mg, 43% yield). ^{1}H NMR (400 MHz, $CDCl_3$) δ 8.36 (s, 1H), 7.84 (d, J = 8.4 Hz, 1H), 7.67–7.64 (m, 2H), 7.59 (d, J = 8.0 Hz, 2H), 7.36–7.28 (m, 2H), 7.10 (d, J = 8.4 Hz, 2H), 5.60 (d, J = 8.8 Hz, NH), 4.19–4.11 (m, 1H), 3.24–3.17 (m, 4H), 2.52–2.48 (m, 4H), 2.38 (s, 3H), 2.28 (s, 3H), 2.06–2.01 (m, 2H), 1.82–1.77 (m, 2H), 1.71–1.65

(m, 1H), 1.46–1.35 (m, 2H), 1.31–1.18 (m, 3H); HRMS (ESI) *m/z:* calcd $[M + H]^+$ for $C_{30}H_{37}N_4O_2S^+$ 517.2632; found $[M + H]^+$ 517.2646.

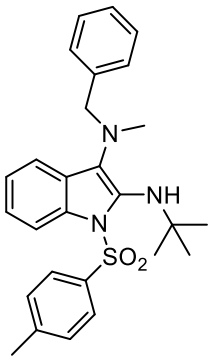

N^3-Benzyl-*N*^{2}-(*tert*-butyl)-*N*^{3}-methyl-1-tosyl-1*H*-indole-2,3-diamine (**3.33**). The crude material was purified by column chromatography (petroleum ether/EtOAc 98:2) to give the product as an off-white solid (161.1 mg, 82% yield). ^{1}H NMR (400 MHz, $CDCl_3$) δ 7.99 (d, J = 8.4 Hz, 1H), 7.32 (d, J = 7.6 Hz, 1H), 7.25–7.08 (m, 9H), 6.92 (d, J = 8.0 Hz, 2H), 4.36 (s, 2H), 3.92 (brs, -N*H*), 2.88 (s, 3H), 2.24 (s, 3H), 1.28 (s, 9H); HRMS (ESI) *m/z:* calcd $[M + H]^+$ for $C_{27}H_{32}N_3O_2S^+$ 462.2210; found $[M + H]^+$ 462.2203.

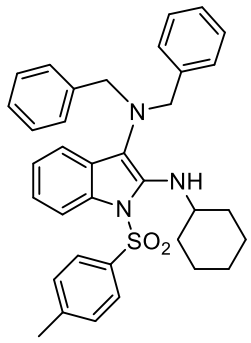

N^3,*N*^{3}-Dibenzyl-*N*^{2}-cyclohexyl-1-tosyl-1*H*-indole-2,3-diamine (**3.34**). The crude material was purified by column chromatography (petroleum ether/EtOAc 99:1) to give the product as a yellow solid (169.5 mg, 53% yield). ^{1}H NMR (400 MHz, $CDCl_3$) δ 7.97–7.95 (m, 1H), 7.37 (d, J = 8.0 Hz, 2H), 7.20–7.01 (m, 15H), 4.74–4.69 (m, -N*H*), 4.17 (s, 4H), 3.78–3.71 (m, 1H), 2.30 (s, 3H), 1.82–1.78 (m, 2H),

1.72–1.65 (m, 2H), 1.60–1.51 (m, 2H), 1.29–1.03 (m, 4H); HRMS (ESI) *m/z:* calcd $[M + H]^+$ for $C_{35}H_{38}N_3O_2S^+$ 564.2679; found $[M + H]^+$ 564.2675.

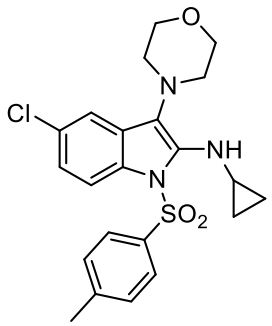

5-Chloro-*N*-cyclopropyl-3-morpholino-1-tosyl-1*H*-indol-2-amine (**3.35**). The crude material was purified by column chromatography (petroleum ether/EtOAc 95:5) to give the product as a yellow solid (311.2 mg, 70% yield). ^{1}H NMR (400 MHz, $CDCl_3$) δ 7.88 (d, J = 8.8 Hz, 1H), 7.52 (d, J = 8.4 Hz, 2H), 7.35 (d, J = 2.0, 1H), 7.19 (d, J = 8.4 Hz, 2H), 6.97 (dd, J_a = 8.8 Hz, J_b = 2.0 Hz, 1H), 5.58 (brd, -N*H*), 3.74–3.72 (m, 4H), 3.20–3.16 (m, 1H), 3.10–3.08 (m, 4H), 2.35 (s, 3H), 0.70–0.66 (m, 2H), 0.39–0.36 (m, 2H); HRMS (ESI) *m/z*: calcd $[M + H]^+$ for $C_{22}H_{25}ClN_3O_3S^+$ 446.1300; found $[M + H]^+$ 446.1292.

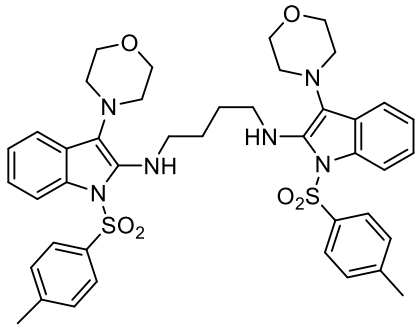

N^1,N^4-Bis(3-morpholino-1-tosyl-1*H*-indol-2-yl)butane-1,4-diamine (**3.36**). The crude material was purified by column chromatography (petroleum ether/EtOAc 7:3) to give the product as a beige solid (271.2 mg, 34% yield). ^{1}H NMR (400 MHz, $CDCl_3$) δ 7.97 (d, J = 8.4 Hz, 2H), 7.58 (d, J = 8.4 4H), 7.36 (d, J = 7.6 Hz,

2H), 7.14–7.00 (m, 8H), 5.37 (brt, -N*H*), 3.75–3.73 (m, 8H), 3.64–3.59 (m, 4H), 3.10–3.08 (m, 8H), 2.28 (s, 6H), 1.77–1.72 (m, 4H); HRMS (ESI) *m/z*: calcd $[M + H]^+$ for $C_{42}H_{49}N_6O_6S_2^+$ 797.3150; found $[M + H]^+$ 797.3136.

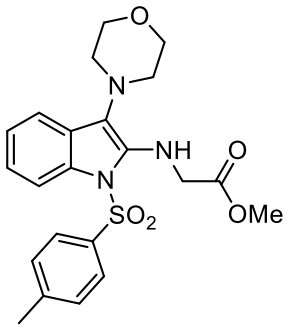

Methyl 2-((3-morpholino-1-tosyl-1*H*-indol-2-yl)amino)acetate (**3.37**). The crude material was purified by column chromatography (petroleum ether/EtOAc 7:3) to give the product as an orange solid (120.7 mg, 27% yield). ^{1}H NMR (400 MHz, $CDCl_3$) δ 7.94 (d, J = 8.0 Hz, 1H), 7.76 (d, J = 8.4 Hz, 2H), 7.36 (d, J = 7.6 Hz, 1H), 7.18 (d, J = 8.4 Hz, 2H), 7.10–6.99 (m, 2H), 6.12 (brt, -N*H*), 4.39 (d, J = 6.4 Hz, 2H), 3.78 (s, 3H), 3.73–3.70 (m, 4H), 3.06–3.04 (m, 4H), 2.33 (s, 3H); HRMS (ESI) *m/z*: calcd $[M + H]^+$ for $C_{22}H_{26}N_3O_5S^+$ 444.1588; found $[M + H]^+$ 444.1582.

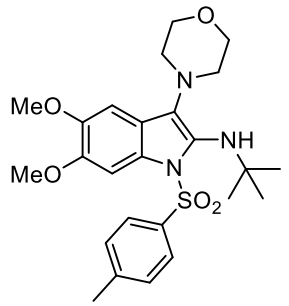

N-(*Tert*-butyl)-5,6-dimethoxy-3-morpholino-1-tosyl-1*H*-indol-2-amine (**3.38**). The crude material was purified by column chromatography (petroleum ether/EtOAc 7:3) to give the product as a yellow solid (151.9 mg, 31% yield). ^{1}H NMR (400 MHz, $CDCl_3$) δ 7.64 (s, 1H), 7.34 (d, J = 8.0 Hz, 2H), 7.03 (d, J = 8.4 Hz, 2H), 6.75 (s, 1H), 3.95 (s, 3H), 3.84 (s, 3H), 3.79–3.76 (m, 4H), 3.19–3.16 (m, 4H), 2.27

(s, 3H), 1.25 (s, 9H); HRMS (ESI) *m/z:* calcd $[M + H]^+$ for $C_{25}H_{34}N_3O_5S^+$ 488.2214; found $[M + H]^+$ 488.2208.

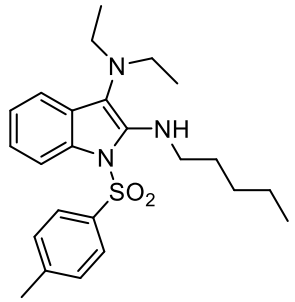

N^3,N^3-Diethyl-N^2-pentyl-1-tosyl-1*H*-indole-2,3-diamine (**3.39**). The crude material was purified by column chromatography (*n*-hexane/EtOAc 99:1) to give the product as a beige solid (157.7 mg, 52% yield). ^{1}H NMR (400 MHz, $CDCl_3$) δ 8.02 (d, J = 8.0 Hz, 1H), 7.56 (d, J = 7.2 Hz, 2H), 7.21–7.01 (m, 5H), 4.98 (brs, -N*H*), 3.54–3.51 (m, 2H), 3.01–2.97 (m, 4H), 2.29 (s, 3H), 1.62–1.60 (m, 2H), 1.40–1.39 (m, 4H), 0.96–0.94 (m, 3H), 0.81–0.78 (m, 6H); HRMS (ESI) *m/z:* calcd $[M + H]^+$ for $C_{24}H_{34}N_3O_2S^+$ 428.2367; found $[M + H]^+$ 428.2367.

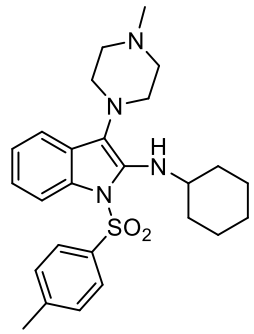

N-Cyclohexyl-3-(4-methylpiperazin-1-yl)-1-tosyl-1*H*-indol-2-amine (**3.40**). The crude material was purified by column chromatography (*n*-hexane/EtOAc 70:30) to give the product as a beige solid (197.2 mg, 60% yield). ^{1}H NMR (400 MHz, $CDCl_3$) δ 7.95 (d, J = 8.0 Hz, 1H), 7.58 (d, J = 8.0 Hz, 2H), 7.36 (d, J = 7.2 Hz, 1H), 7.12–6.95 (m, 4H), 5.21 (brt, -N*H*), 3.95–3.91 (m, 1H), 3.16–3.11 (m, 4H), 2.53–2.48 (m, 4H), 2.34 (s, 3H), 2.28 (s, 3H), 2.01–1.99 (m, 2H), 1.78–1.63 (m,

3H), 1.38–1.16 (m, 5H); HRMS (ESI) *m/z*: calcd $[M + H]^+$ for $C_{26}H_{35}N_4O_2S^+$ 467.2476; found $[M + H]^+$ 467.2483.

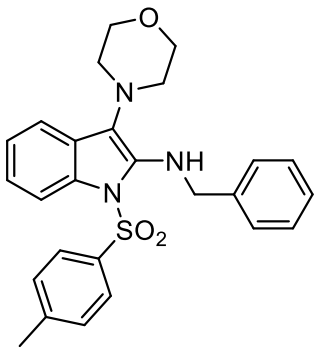

N-Benzyl-3-morpholino-1-tosyl-1*H*-indol-2-amine (**3.41**). The crude material was purified by column chromatography (*n*-hexane/EtOAc 95:5) to give the product as a reddish solid (164.3 mg, 51% yield). ^{1}H NMR (400 MHz, $CDCl_3$) δ 8.05 (d, J = 8.0 Hz, 1H), 7.62 (d, J = 8.0 Hz, 2H), 7.38–7.24 (m, 6H), 7.17–7.04 (m, 4H), 5.77 (brs, -N*H*), 4.82 (s, 2H), 3.57–3.55 (m, 4H), 2.96–2.94 (m, 4H), 2.35 (s, 3H). HRMS (ESI) *m/z:* calcd $[M + H]^+$ for $C_{26}H_{28}N_3O_3S^+$ 462.1846; found $[M + H]^+$ 462.1845.

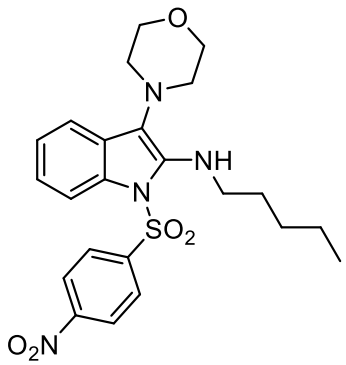

3-Morpholino-1-((4-nitrophenyl)sulfonyl)-*N*-pentyl-1*H*-indol-2-amine (**3.42**). The crude material was purified by column chromatography (*n*-hexane/EtOAc 99:1) to give the product as a reddish solid (195.8 mg, 59% yield). ^{1}H NMR (400 MHz, $CDCl_3$) δ 8.19 (d, J = 8.8 Hz, 2H), 7.96 (d, J = 8.0 Hz, 1H), 7.87 (d, J = 8.8 Hz,

2H), 7.35 (d, *J* = 7.6 Hz, 1H), 7.13 (t, *J* = 7.6 Hz, 1H), 7.06 (t, *J* = 7.06 Hz, 1H), 5.06 (brs, -N*H*), 3.76 19 3.74 (m, 4H), 3.54–3.50 (m, 2H), 3.06–3.04 (m, 4H), 1.62–1.59 (m, 2H), 1.38–1.37 (m, 4H), 0.95–0.92 (m, 3H); HRMS (ESI) *m/z*: calcd $[M + H]^+$ for $C_{23}H_{29}N_4O_5S^+$ 473.1854; found $[M + H]^+$ 473.1849.

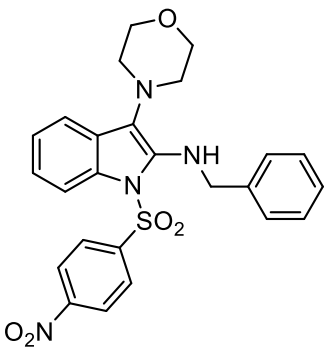

N-Benzyl-3-morpholino-1-((4-nitrophenyl)sulfonyl)-1*H*-indol-2-amine (**3.43**). The crude material was purified by column chromatography (*n*-hexane/EtOAc 99:1) to give the product as a reddish solid (255.6 mg, 74% yield). ^{1}H NMR (400 MHz, $CDCl_3$) δ 8.15 (d, *J* = 8.4 Hz, 2H), 8.02 (d, *J* = 8.0 Hz, 1H), 7.84 (d, *J* = 8.4 Hz, 2H), 7.37–7.27 (m, 6H), 7.16–7.08 (m, 2H), 5.39 (brs, -N*H*), 4.75 (s, 2H), 3.58–3.56 (m, 4H), 2.89–2.86 (m, 4H); HRMS (ESI) *m/z*: calcd $[M + H]^+$ for $C_{25}H_{25}N_4O_5S^+$ 493.1541; found $[M + H]^+$ 493.1541.

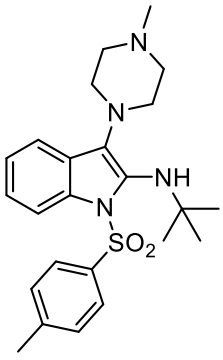

N-(*Tert*-butyl)-3-(4-methylpiperazin-1-yl)-1-tosyl-1*H*-indol-2-amine (**3.44**). The crude material was purified by column chromatography (*n*-hexane/EtOAc 60:40) to

give the product as a yellowish solid (163.3 mg, 53% yield). ^{1}H NMR (400 MHz, $CDCl_3$) δ 8.03 (d, J = 8.4 Hz, 1H), 7.40–.36 (m, 3H), 7.17–7.10 (m, 2H), 7.04 (d, J = 8.0 Hz, 2H), 3.23–3.22 (m, 4H), 2.54–2.51 (m, 4H), 2.37 (s, 3H), 2.27 (s, 3H), 1.27 (s, 9H). ^{13}C {^{1}H} NMR (175 MHz, $CDCl_3$) δ 144.2, 134.0, 133.5, 133.0, 129.4, 129.1, 127.7, 126.7, 123.8, 123.4, 118.7, 116.8, 55.7, 54.3, 50.3, 46.4, 30.3, 21.5; HRMS (ESI) *m/z*: calcd $[M + H]^+$ for $C_{24}H_{33}N_4O_2S^+$ 441.2319; found $[M + H]^+$ 441.2322.

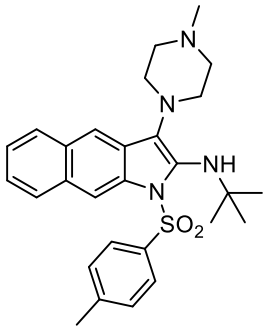

N-*Tert*-butyl)-3-(4-methylpiperazin-1-yl)-1-tosyl-1*H*-benzo[*f*]indol-2-amine (**3.45**). The crude material was purified by column chromatography (*n*-hexane/EtOAc 60:40) to give the product as a reddish-brown solid (185.1 mg, 54% yield). ^{1}H NMR (400 MHz, $CDCl_3$) δ 8.46 (s, 1H), 7.92–7.89 (m, 1H), 7.75–7.72 (m, 2H), 7.41–7.37 (m, 4H), 7.00 (d, J = 8.4 Hz, 2H), 3.28–3.26 (m, 4H), 2.58–2.56 (m, 4H), 2.39 (s, 3H), 2.23 (s, 3H), 1.33 (s, 9H); HRMS (ESI) *m/z*: calcd $[M + H]^+$ for $C_{28}H_{35}N_4O_2S^+$ 491.2476; found $[M + H]^+$ 491.2498.

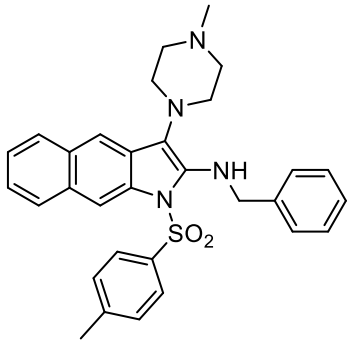

N-Benzyl-3-(4-methylpiperazin-1-yl)-1-tosyl-1*H*-benzo[*f*]indol-2-amine (**3.46**). The crude material was purified by column chromatography (*n*-hexane/EtOAc 60:40) to give the product as a yellowish solid (209.1 mg, 57% yield). ^{1}H NMR (400 MHz, $CDCl_3$) δ 8.43 (s, 1H), 7.87 (d, J = 8.0 Hz, 1H), 7.71 (s, 1H), 7.67 (d, J = 8.0 Hz, 1H), 7.57 (d, J = 8.0 Hz, 2H), 7.36–7.25 (m, 7H), 7.09 (d, J = 8.4 Hz, 2H), 6.00 (brt, -N*H*), 4.90 (d, J = 6.0 Hz, 2H), 3.11–3.08 (m, 4H), 2.36–2.33 (m, 4H), 2.29 (s, 3H); HRMS (ESI) *m/z*: calcd $[M + H]^+$ for $C_{31}H_{33}N_4O_2S^+$ 525.2319; found $[M + H]^+$ 525.2319.

For details about biological assays, statistical analyses, fluorescence titration experiments, NMR spectroscopy, and computational studies see: Russo, C.; Russomanno, P.; D'Amore, V. M.; Alfano, A. I., Santoro, F.; Guzelj, S.; Gobec, M.; Amato, J.; Pagano, B.; Marinelli, L.; Carotenuto, A.; Tron, G. C., Di Leva, F. S.; Jakopin, Z.; Brancaccio, D.; Giustiniano M.; *Journal of Medicinal Chemistry,* **2024**, accepted manuscript.

References

(1) Laduron, F.; Tamborowski, V.; Moens, L.; Horváth, A.; De Smaele, D.; Leurs, S. *Organic Process Research and Development,* **2005**, *9*, 102–104.

(2) Pirali, T.; Mossetti, R.; Galli, S.; Tron, G. C.; *Organic Letters,* **2011**, *13*, 3734–3737.

(3) Barravecchia, I.; Mariotti, S.; Pucci, A.; Scebba, F.; De Cesari, C.; Bicciato, S.; Tagliafico, E.; Tenedini, E.; Vindigni, C.; Cecchini, M.; Berti, G.; Vitiello, M.; Poliseno,

L.; Mazzanti, C. M.; Angeloni, D.; *Biochimica et Biophysica Acta (BBA) - Molecular Basis of Disease,* **2019**, *1865*, 2111–2124.
(4) Strober, W.; *Current Protocols in Immunology,* **2015**, *111*.
(5) Jia, M.-Q.; You, S.-L.; *ACS Catalysis,* **2013**, *3*, 622–624.
(6) Dhayalan, V.; Panchapakesan, G.; Mohanakrishnan, A. K.; *Synthetic Communications,* **2012**, *42*, 402–411.
(7) Li, Y.; Feng, Y.; Xu, L.; Wang, L.; Cui, X.; *Organic Letters,* **2016**, *18*, 4924–4927.
(8) Chwastek, M.; Pieczykolan, M.; Stecko, S.; *The Journal of Organic Chemistry,* **2016**, *81*, 9046–9074.
(9) Hechavarría Fonseca, M.; Eibler, E.; Zabel, M.; König, B.; *Tetrahedron Asymmetry,* **2003**, *14*, 1989–1994.
(10) Amato, J.; Cerofolini, L.; Brancaccio, D.; Giuntini, S.; Iaccarino, N.; Zizza, P.; Iachettini, S.; Biroccio, A.; Novellino, E.; Rosato, A.; Fragai, M.; Luchinat, C.; Randazzo, A.; Pagano, B.; *Nucleic Acids Research,* **2019**, *47*, 9950–9966.
(11) Amato, J.; Madanayake, T. W.; Iaccarino, N.; Novellino, E.; Randazzo, A.; Hurley, L. H.; Pagano, B.; *Chemical Communications,* **2018**, *54*, 9442–9445.
(12) Srimathi, T.; Robbins, S. L.; Dubas, R. L.; Hasegawa, M.; Inohara, N.; Park, Y. C.; *Biochemistry,* **2008**, *47*, 1319–1325.
(13) Maekawa, S.; Ohto, U.; Shibata, T.; Miyake, K.; Shimizu, T.; *Nature Communications,* **2016**, *7*, 11813.
(14) Jacobson, M. P.; Pincus, D. L.; Rapp, C. S.; Day, T. J. F.; Honig, B.; Shaw, D. E.; Friesner, R. A.; *Proteins: Structure, Function, and Bioinformatics,* **2004**, *55*, 351–367.
(15) Jacobson, M. P.; Friesner, R. A.; Xiang, Z.; Honig, B.; *Journal of Molecular Biology,* **2002**, *320*, 597–608.
(16) Charles University. *PrankWeb: Ligand Binding Site Prediction*, **2017-2023**.
(17) Krivák, R.; Hoksza, D.; *Journal of Cheminformatics,* **2018**, *10*, 39.
(18) Madhavi Sastry, G.; Adzhigirey, M.; Day, T.; Annabhimoju, R.; Sherman, W.; *Journal of Computer-Aided Molecular Design,* **2013**, *27*, 221–234.
(19) Greenwood, J. R.; Calkins, D.; Sullivan, A. P.; Shelley, J. C.; *Journal of Computer-Aided Molecular Design,* **2010**, *24,* 591–604.
(20) Shelley, J. C.; Cholleti, A.; Frye, L. L.; Greenwood, J. R.; Timlin, M. R.; Uchimaya, M.; *Journal of Computer-Aided Molecular Design,* **2007**, *21*, 681–691.
(21) LigPrep; *Schrödinger*, L. Schrödinger Release 2022-3, **2022** *New York*.
(22) Friesner, R. A.; Banks, J. L.; Murphy, R. B.; Halgren, T. A.; Klicic, J. J.; Mainz, D. T.; Repasky, M. P.; Knoll, E. H.; Shelley, M.; Perry, J. K.; Shaw, D. E.; Francis, P.; Shenkin, P. S.; *Journal of Medicinal Chemitry,* **2004**, *47*, 1739–1749.
(23) Halgren, T. A.; Murphy, R. B.; Friesner, R. A.; Beard, H. S.; Frye, L. L.; Pollard, W. T.; Banks, J. L.; *Journal of Medicinal Chemitry,* **2004**, *47*, 1750–1759.
(24) Jorgensen, W. L.; Chandrasekhar, J.; Madura, J. D.; Impey, R. W.; Klein, M. L.; *The Journal of Chemical Physics,* **1983**, *79*, 926–935.

(25) Tian, C.; Kasavajhala, K.; Belfon, K. A. A.; Raguette, L.; Huang, H.; Migues, A. N.; Bickel, J.; Wang, Y.; Pincay, J.; Wu, Q.; Simmerling, C.; *Journal of Chemical Theory and Computation,* **2020**, *16*, 528–552.
(26) Wang, J.; Wolf, R. M.; Caldwell, J. W.; Kollman, P. A.; Case, D. A.; *Journal of Computational Chemistry,* **2004**, *25*, 1157–1174.
(27) Bayly, C. I.; Cieplak, P.; Cornell, W.; Kollman, P. A.; *The Journal of Physical Chemistry,* **1993**, *97*, 10269–10280.
(28) Wang, J.; Wang, W.; Kollman, P. A.; Case, D. A.; *Journal of Molecular Graphics and Modelling,* **2006**, *25*, 247–260.
(29) *Gaussian 16: Revision C.01*; **2016**, Gaussian, Inc.: Wallingford.
(30) Case, D. A.; Cheatham, T. E.; Darden, T.; Gohlke, H.; Luo, R.; Merz, K. M.; Onufriev, A.; Simmerling, C.; Wang, B.; Woods, R. J.; *Journal of Computational Chemistry,* **2005**, *26*, 1668–1688.
(31) Darden, T.; Pearlman, D.; Pedersen, L. G.; *The Journal of Chemical Physics,* **1998**, *109*, 10921–10935.
(32) Ryckaert, J.-P.; Ciccotti, G.; Berendsen, H. J. C.; *Journal of Computational Physics,* **1977**, *23*, 327–341.
(33) Loncharich, R. J.; Brooks, B. R.; Pastor, R. W.; *Biopolymers,* **1992**, *32*, 523–535.
(34) Berendsen, H. J. C. 81, 3684.; Postma, J. P. M.; Van Gunsteren, W. F.; Dinola, A.; Haak, J. R.; *The Journal of Chemical Physics,* **1998**, *81*, 3684.

Chapter 4

A journey into Organic Electrosynthesis

As part of my PhD program, I had the opportunity to spend a six-month period in the Laboratory of Medicinal and Molecular Electrochemistry of Prof. Kevin Lam, at the Department of Pharmaceutical, Chemical, and Environmental Sciences of the University of Greenwich, UK. Prof. Lam's research focuses on the use of electrochemistry as a green activation method for the selective generation of highly reactive intermediates under otherwise unattainable mild conditions, with the aim to develop new and efficient electrochemical methodologies of general utility to the synthetic community. By approaching the basic concepts and the experimental set up of electrochemical reactions, I mainly worked on the investigation of the substrate scope and functional group tolerance of a new electrochemical hydrogenation protocol developed by the group, as well as on the extension of the strategy to the deuteration of unactivated alkenes and alkynes. The outcomes of these studies will be described in this chapter and are the result of an exceptional teamwork for which I want to thank Jamie Walsh and Dr. Matthew Leech, Cyrille Kiaku, Dr. Joe Higham, Lisa Giannessi, Emmanuelle Lambert, and, of course, Prof. Kevin Lam, for his inspiring ideas and invaluable advice.

4.1. Synthetic Organic Electrochemistry: a brief introduction

In recent decades Organic Electrosynthesis has been experiencing a renaissance as a mild, green, and innately atom efficient route to build up molecules.[1] By exploiting the cheapest and greenest source of electrons, electricity itself, it allows to achieve selective redox transformations while avoiding the harsh, hazardous, and often toxic oxidising and reducing agents required for traditional synthetic strategies.[2] Under exogenous oxidant/reductant-free conditions, electrochemical reactions usually display wide functional group compatibility, enabling new bonds to be forged with high levels of chemo- and regioselectivity, and take place at room temperature and atmospheric pressure, thus providing an energy-saving option.[3] Moreover, compared to conventional strategies often needing for quenching

procedures, electrochemical reactions can be easily stopped at any time by simply turning off the power supply.

The use of electricity in organic synthesis is far from being a recent invention: it was 1834 when Michael Faraday observed the formation of ethane gas while electrolysing a solution of sodium acetate.[4] This transformation was later investigated by Kolbe, whose eponymous reaction[5] (2 $RCOO^-$ → R–R + 2 CO_2 + 2 e^-) consists in the electrochemical decarboxylative dimerisation of organic carboxylates to alkanes.[6] Despite the initial success, organic electrosynthesis has later laid dormant until very recently, only being practiced as a niche technique, mostly due to a general lack of understanding of the process, along with the perceived endless number of reaction variables and complex reaction setup (potentiostats, divided/undivided cells, materials of the electrodes, supporting electrolytes, etc.).[1]

In its simplest configuration, an electrosynthetic reaction typically requires a power supply (1), a reaction solution (2) and two electrodes (anode 3 and cathode 4, respectively) connected to the power supply (Figure 4.1).[7]

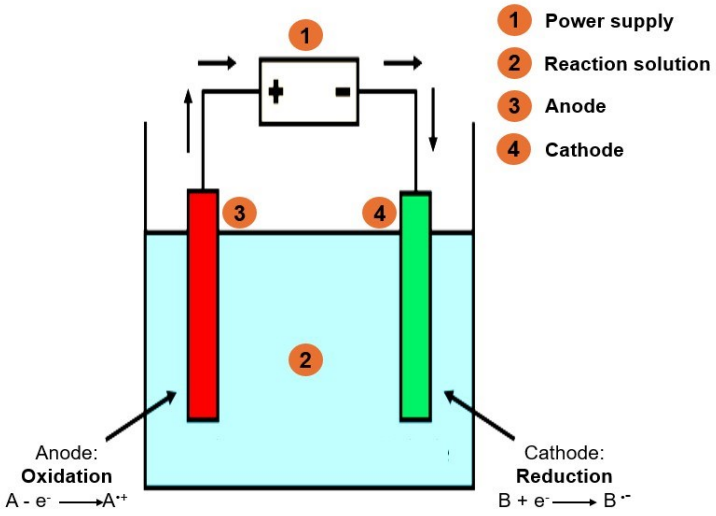

Figure 4.1. Simple electrochemical setup for synthesis.

A variety of external power sources can be employed, operating under constant current or constant potential conditions (galvanostats and potentiostats, respectively). At present, commercial power sources can usually perform both modes of electrolysis and are generally referred to as potentiostats.[8] The anode is connected to the positive pole of the potentiostat, while the cathode to the negative one, with electrons flowing from the anode, where the oxidative reaction take place, to the cathode, which is the reduction electrode. The potential (also referred to as voltage, V) describes the strength of the oxidative/reductive conditions, while the current (I) defines the rate of the electron movement. The oxidation and the reduction reactions are strictly coupled, and one cannot occur without the other. The electrode at which the desired reaction takes place is referred to as the working electrode, while the other one is the counter electrode. The electrical circuit is completed by the movement of charged species through the reaction solution, which consists of the substrate(s), an appropriate solvent, and, if necessary, a supporting electrolyte (usually ammonium and alkali metal-based salts[9]) enhancing the conductivity of the solution. When the products forming at one electrode may interfere with the reaction occurring at the other, it might be necessary to place the anode and the cathode in separate compartments (*i.e.*, a divided cell), which is usually achieved by means of an appropriate separator (*e.g.*, a porous material like a glass frit or a ceramic, or an ion exchange membrane). Such setups are often more complicated (due to the separative membranes and inherently higher resistance), and thus, for most applications, the use of undivided cells is preferred.

As for photoredox catalytic processes,[10] electrochemical reactions rely on SET events converting the substrates into radical species which then react further to finally afford the product. However, the electrochemical oxidation/reduction of the substrate are heterogeneous processes occurring at the electrode surface; the overall electrochemical reaction can, therefore, be seen as the combination of two basic events: the heterogeneous SET at the electrode surface, leading to the formation of a reactive intermediate, and a following chemical process occurring in solution.[2] As

such, both the electrode materials and the electrolyte additives can have a significant impact on the outcome of the reaction, importantly affecting its efficiency and selectivity.[11] Moreover, while the availability of a finite number of photocatalysts limits the range of redox potentials accessible via photoredox catalytic transformations, the window of potentials which can be achieved electrochemically is wider in both the oxidation and the reduction directions, and it is mainly limited by the choice of solvent and electrolytes.[12]

Operatively, two main electrolytic approaches can be performed:

- constant current (galvanostatic conditions), where the potential of the electrodes changes in response to the electrochemical reactions occurring on them, so to keep stable the current;

-constant potential (potentiostatic conditions), where the working electrode's potential is strictly controlled during the electrolysis, with the aid of a reference electrode.

Galvanostatic conditions usually ensure higher conversion, as the potential gradually increases until all redox-active species are consumed,[8] but sometimes they pose selectivity issues, as undesired redox-processes can occur at high potential. On the other hand, while providing exquisite selectivity, potentiostatic conditions are often affected by poor conversions and longer electrolysis times, due to the decreasing concentration of redox active species over time, which gradually reduces the current. In addition, a more sophisticated electrochemical setup is generally required for such an approach.[13]

The commercial availability of standardised electrosynthetic equipment[14] (*i.e.* ElectraSyn 2.0) has played a critical role in promoting the widespread adoption of synthetic electrochemistry in both academic and industrial laboratories.[15] Besides its inherently green features, which may be even magnified when electricity originating from renewable resources is employed,[16] electrochemistry has proven to offer new reaction pathways that are complementary to traditional synthetic procedures. Electron transfer in electrochemical transformations may actually

result in an inversion of the classic reactivities of functional groups (*umpolung*):[2] electron-rich compounds can be turned into electrophilic centres upon oxidation, while, once reduced, electron-deficient groups can act as nucleophilic reactive sites. This kind of reactivity is not easy to achieve by conventional organic methodologies and is one of the most powerful electrochemical approaches to the construction of complex molecular architectures. Unprecedent retrosynthetic disconnections and new reactivity paradigms can therefore become available by electrifying organic synthesis. To conclude, it is worth noting that most electrochemical reactions can be easily scaled up and have a great potential for industrial applications. For example, a variety of organic compounds (*e.g.,* acetoin, acetylene dicarboxylic acid, 2-aminomethyl pyridine, arabinose, and the fragrant molecule lysmeral) are efficiently synthesised on process scales ranging from kilograms to thousands of metric tons.[8]

4.2. eHydrogenation: Hydrogen-free Electrochemical Hydrogenation

Hydrogenations of unsaturated compounds are staple transformations widely employed in a variety of fields to synthesise pharmaceuticals, natural products, fine chemicals, and functional materials.[17,18] Nonetheless, the majority of conventional approaches to hydrogenation[19-24] are constrained by high-pressure dihydrogen, high temperatures, transition metal catalysts (*e.g*., palladium, cobalt, copper, iron, and iridium), and/or stoichiometric reducing agents. Recent advancements in the field include non-metal-mediated transfer hydrogenation strategies which are still limited by the use of toxic activating reagents, such as selenium, chlorosilanes, and boranes, activated in the form of frustrated Lewis pairs (FLPs), and H_2Se or HSe^-.[25-30] Diimide-mediated reductions have proven to be a viable complementary method to catalytic hydrogenations.[31-33] These reactions proceed via a cyclic transition state to facilitate the symmetrical transfer of hydrogen from *cis* diimide (HN=NH) to a double or triple bond, and are driven by the formation of dinitrogen

gas.[34,35] In contrast to catalytic hydrogenations, diimide-mediated reductions avoid the handling of explosive and flammable dihydrogen, can be carried out efficiently with readily available laboratory apparatus, and are milder, thereby avoiding the reductive cleavage of heteroatom bonds which is often a problem of catalytic hydrogenations. Diimide can be generated either from an explosive salt (KOOCNH=HNCOOK) or by oxidising hydrazine in the presence of pure oxygen, at temperatures above the flash point of many solvents. In addition, since diimide can disproportionate to hydrazine and dinitrogen, a large excess is needed, and hydrazine is often used as the solvent.

In recent years several electrochemical hydrogenation strategies have also been reported[36] and can serve as environmentally friendly and sustainable synthetic alternatives to traditional catalytic hydrogenations. Cheng and co-workers have demonstrated that the reduction of both terminal and internal olefins can be effectively performed in an undivided cell, under constant voltage electrolysis, by employing gaseous ammonia as the hydrogen source[37,38] (Figure 4.2a). However, the transformation was restricted to activated alkenes and posed health issues associated with the usage of gaseous ammonia. Subsequently, Huang *et al.* reported an electrochemical chemoselective 1,4-reduction of α,β-unsaturated carbonyl compounds using ammonium chloride and methanol as hydrogen donors[39] (Figure 4.2b). While powerful, this protocol lacked general applicability, being limited in scope to activated chalcone derivatives. In 2020, a simple method for the selective hydrogenation of α,β-unsaturated carboxylic acids, esters, and amides via electrochemical reduction with DMSO or H_2O as hydrogen donors was reported[40] (Figure 4.2c), followed by a parallel paired electrolysis strategy enabling the hydrogenation of electron-deficient internal alkenes and alkynes by means of KSCN or Ph_2S as anodising reagents, and MeOH as the proton donor (Figure 4.2d).[41]

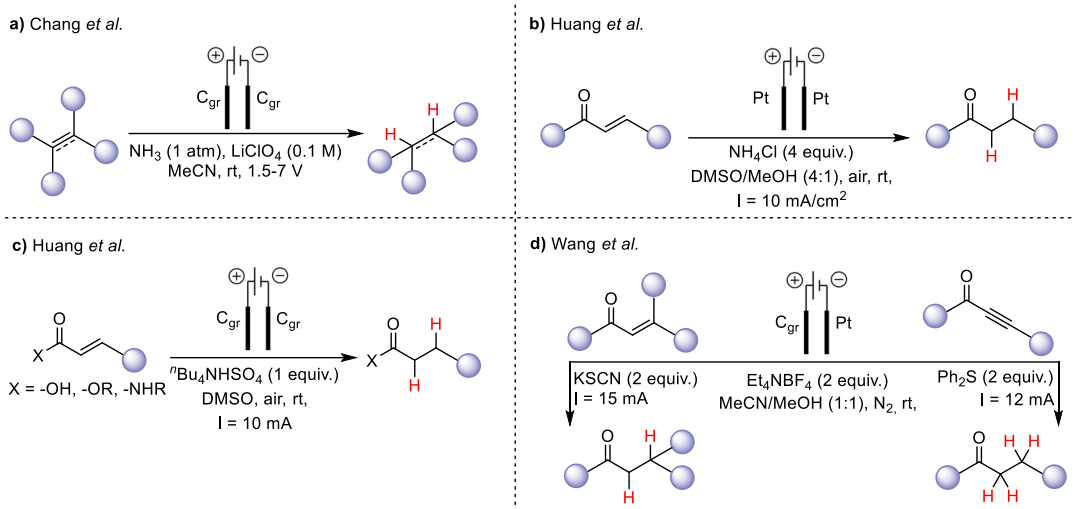

Figure 4.2. Previous electrochemical hydrogenation strategies.

Worthy of note, all of these strategies were not effective on unactivated alkenes and alkynes, whose hydrogenation under electrochemical conditions is known to be challenging, due to the susceptibility to oxidative functionalisation.[42,43] Just a few examples have been reported in the literature, mostly relying on the use of palladium either as a catalyst or as the cathodic material.[44,45] We therefore wondered if a more general, practical, and efficient electrochemical hydrogenation procedure could be accomplished by exploiting the partial anodic oxidation of hydrazine to diimide, followed by a diimide-mediated reduction of unsaturated substrates,[46] according to the mechanistic hypothesis depicted in Scheme 4.1. Indeed, a low anodic current would allow for a slow release of diimide in solution, favouring the hydrogenation of the desired substrate over disproportionation of the diimide. The electrochemical behaviour of hydrazine has been extensively studied due to its potential to replace the oxygen evolution reaction during water splitting for hydrogen production.[47] Under aqueous conditions, it is known that hydrazine is converted to dinitrogen. However, when the anodic oxidation of hydrazine is performed under non aqueous conditions, diimide has been postulated to be produced.[48,49]

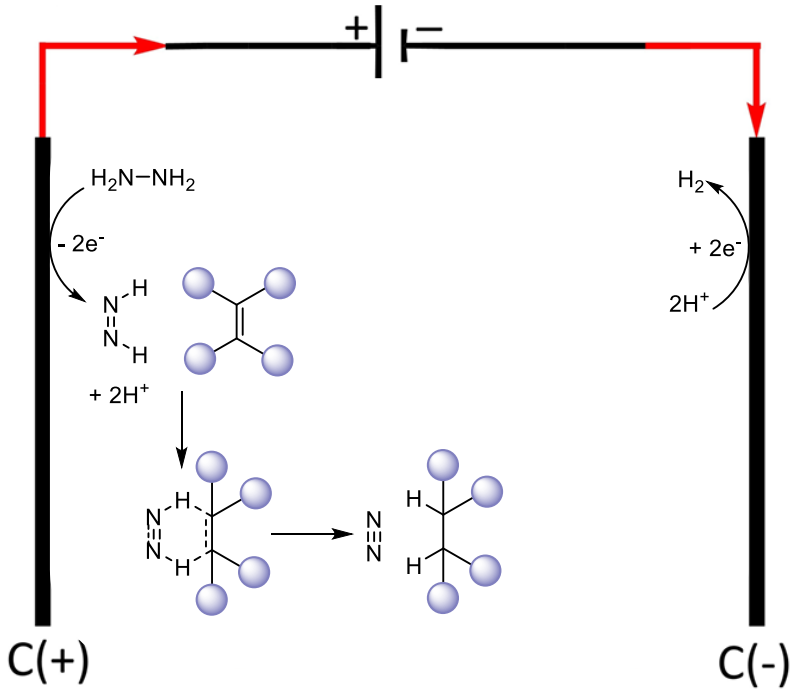

Scheme 4.1. Proposed reaction mechanism for the electrochemical diimide-mediated hydrogenation strategy.

We therefore started our investigation by electrolysing compound **4.1** in MeOH, in an undivided cell, at a constant current of 10 mA, in the presence of 8.5 equivalents of hydrazine monohydrate and inexpensive graphite electrodes, for 12 F/mol (Table 4.1, Entry 1). This gave the reduced derivative **4.2** in a modest 22% yield. We reasoned that, in the presence of a substrate bearing an easily reducible functionality, the addition of a Bronsted acid, besides increasing the conductivity of the medium, might furnish protons easily reduced to H_2, thus preventing the reduction of the substrate's labile functional group. Optimisation of the reaction conditions was therefore performed by changing the nature and the loading of the acid and the solvent (Entries 2-11), the amount of hydrazine (Entries 12-13), and the current intensity (Entries 14-16), to finally afford **4.2** in an excellent 97% yield when electrolysing compound **4.1** in MeOH, at a constant current of 10 mA, in the

presence of 8.5 equivalents of hydrazine monohydrate and 6.0 equivalents of TFA, for 12 F/mol (Entry 11).

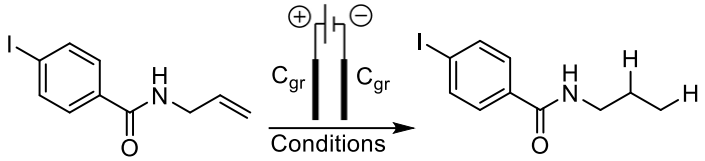

4.1 **4.2**

Entry	NH_2NH_2 (equiv.)	SE (equiv.)	Solvent (0.08 M)	Current (mA)	4.2 Yield (%)
1	8.5	None	MeOH	10	22
2	8.5	AcOH (7.5)	MeOH	10	33
3	8.5	AcOH (10)	MeOH	10	25
4	8.5	AcOH (4)	MeOH	10	40
5	8.5	AcOH (7.5)	MeCN	10	31
6	8.5	TsOH (7.5)	MeCN	10	13
7	8.5	MsOH (7.5)	MeCN	10	5
8	8.5	TFA (7.5)	MeCN	10	91
9	8.5	TFA (4)	MeCN	10	86
10	8.5	TFA (5)	MeCN	10	94
11	8.5	TFA (6)	MeOH	10	97 (71[b])
12	5	TFA (4)	MeCN	10	65
13	5	TFA (4)	MeCN	5	75
14	8.5	TFA (6)	MeCN	20	22
15	8.5	TFA (6)	MeCN	30	1
16	8.5	TFA (6)	MeCN	40	19

Conditions: reaction performed on a 0.4 mmol scale of **4.1**, employing an undivided cell and graphite electrodes, rt, 12 F/mol.
[a] GC yield (determined by using decane as internal standard)
[b] Isolated yield

Table 4.1. Optimisation of the reaction conditions for the electrochemical hydrogenation of unsaturated compounds.

Further control experiments have been summarised in Table 4.2 and show how both hydrazine and electricity are essential for the transformation.

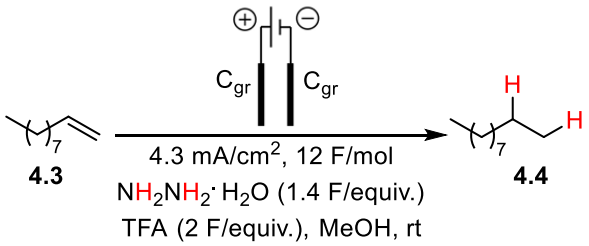

Entry	Deviation from standard conditions	4.4 Yield[a] (%)
1	None	81
2	No Hydrazine	0
3	*tert*-Butyl hydrazine	0
4	1-Aminopyrrolidine	0
5	No electricity	0

Conditions: reaction performed on a 0.4 mmol scale of **4.3** employing an undivided cell.
[a] Isolated yield

Table 4.2. Control experiments.

With the optimised conditions in hand, the generality of the protocol was initially evaluated by electrolysing a variety of terminal alkenes bearing a rich array of functional groups (Figure 4.3). In all cases, the reaction mixture was electrolysed until full disappearance of the starting material, leading to amounts of hydrazine and TFA, and total charge varying dependant on the substrate. The aryl sulfonamide **4.5** was obtained in 98% yield without reduction of the aryl bromide. A variety of allyl ethers bearing halogen (**4.6**-**4.9**) electron withdrawing (**4.10**, **4.13**), and electron donor (**4.11**, **4.12**, **4,14**) functional groups were smoothly reduced to the corresponding alkanes in moderate to excellent yield. Notably, the reaction tolerated the presence of a sulfide (**4.12**), and a pyridine (**4.15**), which could be challenging using palladium catalysis, due to catalyst poisoning. Alkenes bearing free alcohols and carboxylic acids were also found to be competent substrates for the transformation, affording alkanes **4.16**-**4.19** up to quantitative yield. Moreover, natural compounds isopulegol and sclareol were successfully reduced to **4.21** and **4.22** in 73% and 89% yields respectively. Protected alcohols (-OTBS, -OAc, **4.23** and **4.24**) and amines (-NHCbz, -NHAc, **4.25** and **4.26**) were reduced without any observed deprotection in high yields (for compound **4.23**, the

reaction required to be performed in the absence of TFA to avoid deprotection). The mildness of the protocol was further proved by obtaining **4.27** in a good 69% yield in the presence of an alkyl bromide functionality, which would have been challenging under conventional palladium catalysed approaches.

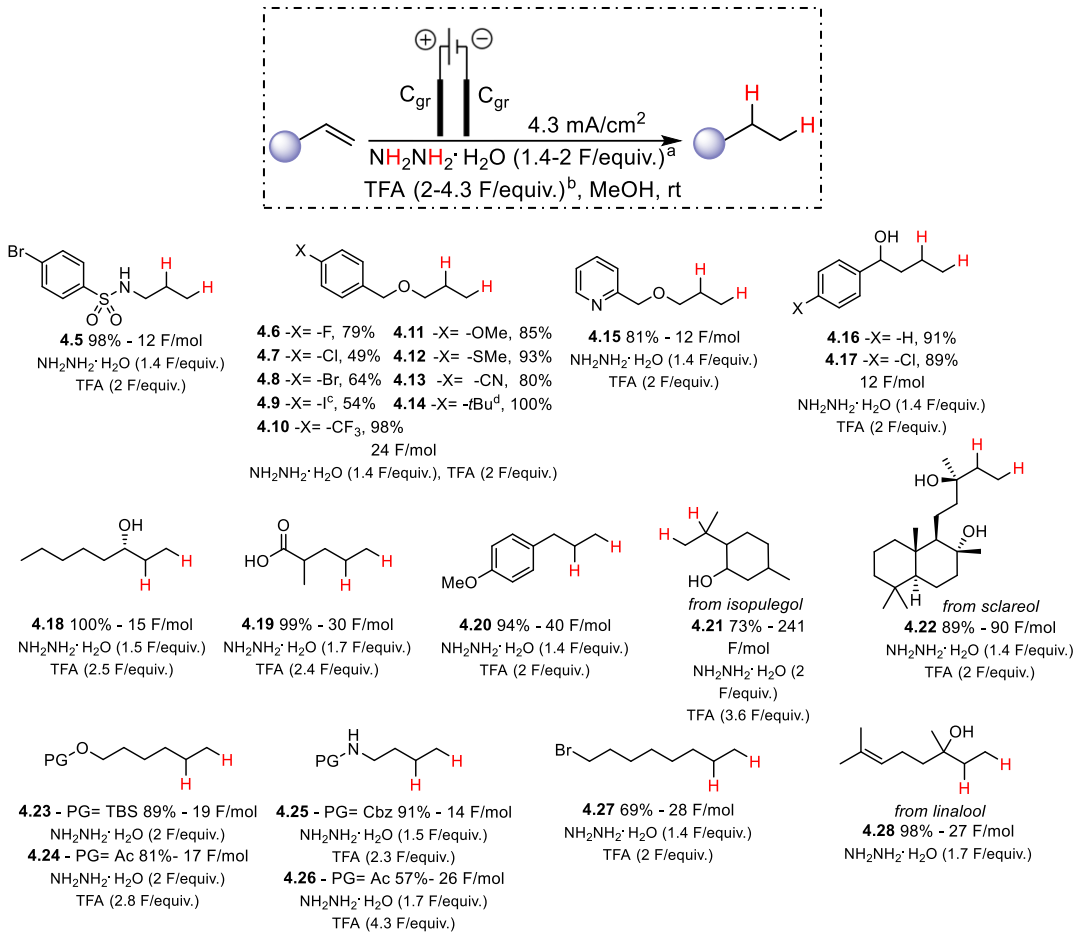

Figure 4.3. Substrate scope for the electrochemical hydrogenation of terminal alkenes. [a] Ratio of the charge required to complete the transformation per equivalent of hydrazine monohydrate; [b] Ratio of the charge required to complete the transformation per equivalent of trifluoroacetic acid; [c] **4.9** required a charge of 30 F/mol (1.8 F/equiv. NH_2NH_2 and 2.5 F/equiv. TFA were applied to complete the reaction); [d] **4.14** required a charge of 30 F/mol (1 F/equiv. NH_2NH_2 and 1.7 F/equiv. TFA were applied to complete the reaction).

The unique selectivity of the diimide-mediated reduction was also exploited to exclusively hydrogenate the more accessible, terminal double bond in linalool to

generate **4.28** in 98% yield. Finally, a scale-up reaction to 1 mmol gave the product **4.16** in 84% yield, which was comparable to the results obtained on a smaller scale. In addition to the reduction of terminal olefins, internal alkenes were also suitable substrates for the electrochemical hydrogenation (Figure 4.4).

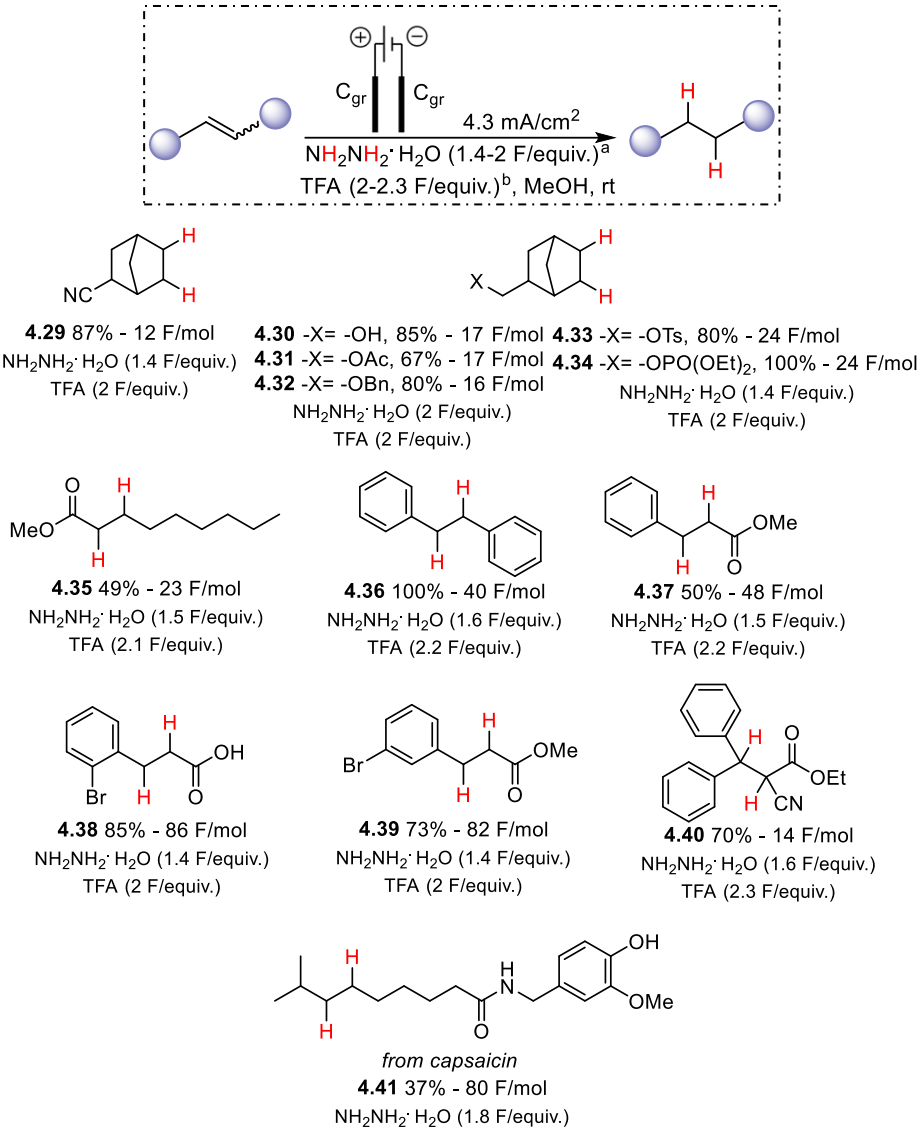

Figure 4.4. Substrate scope for the electrochemical hydrogenation of internal alkenes. [a] Ratio of the charge required to complete the transformation per equivalent of hydrazine monohydrate; [b] Ratio of the charge required to complete the transformation per equivalent of trifluoroacetic acid.

A range of norbornene derivatives were effectively hydrogenated up to quantitative yield (**4.29**-**4-34**). The reduction of activated internal alkenes also worked well, allowing conversion of acrylate, stilbene and cinnamic acid derivatives to the corresponding alkanes (**4.35**-**4.40**) in yields from good to excellent. The application of this mild methodology to the late-stage reduction of capsaicin successfully afforded the hydrogenated product **4.41**, demonstrating the efficacy of the protocol even on more challenging and less accessible double bonds.

The electrochemical hydrogenation protocol was further extended to alkyne substrates (Figure 4.5). By performing the reaction in the absence of TFA, *N*-Boc-propargylamine was fully reduced to **4.45** in 70% yield, without any observed deprotection. Primary and secondary alcohol functional groups were well tolerated, giving alkanes **4.46** and **4.47** in > 90% yields.

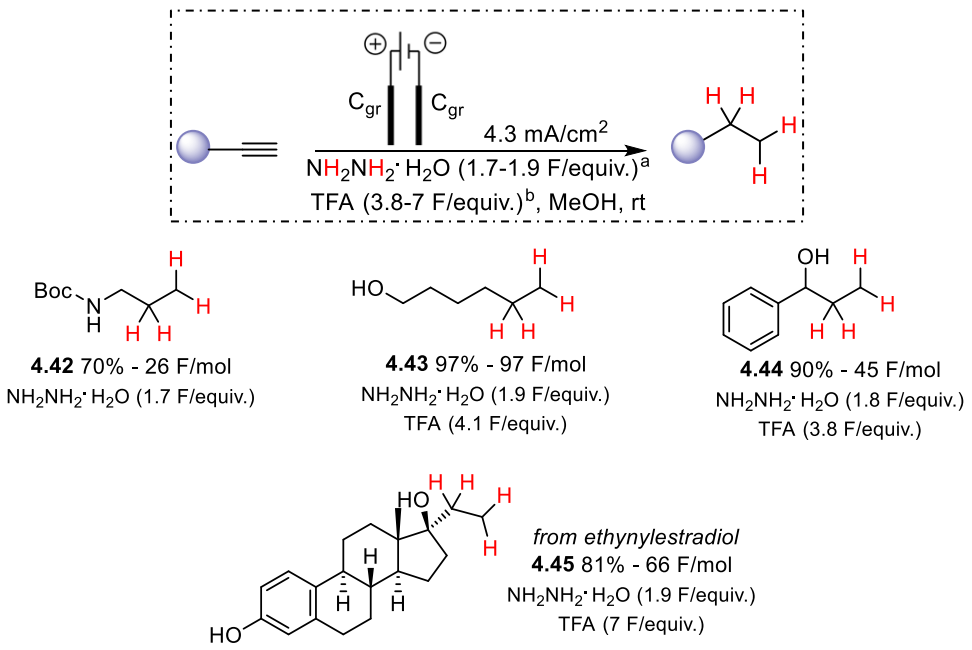

Figure 4.5. Substrate scope for the electrochemical hydrogenation of alkynes.
[a] Ratio of the charge required to complete the transformation per equivalent of hydrazine monohydrate; [b] Ratio of the charge required to complete the transformation per equivalent of trifluoroacetic acid.

In addition to alkenes and alkynes, the new e-hydrogenation strategy proved also to be effective for the reduction of nitro-[50-53] and azido- moieties to the corresponding free amines, which can be particularly interesting considering the wide use of amine compounds in the synthesis of pharmaceuticals and biologically active molecules. By slight modification of the reaction conditions (omitting TFA), many aromatic nitro- derivatives were successfully reduced to the corresponding anilines (Figure 4.6), while the direct reduction of nitro- compounds in the absence of hydrazine led to low yields of the amine along with complex mixtures of side-products. Notably, 2-amino-4-chloroaniline **4.46**, a key intermediate for the production of Tizanidine, was synthesised in 89% yield and obtained pure without further purification. Various other nitroarenes were also competent substrates, including those bearing halogen, piperazine, sulfone, pyridine, and indole functionalities (**4.47**-**4.52**). Similar conditions were applied to the reduction of azido- compounds, which gave a variety of amine derivatives with diverse functionalities (**4.53**-**4.58**), including a BPin group, up to 90% yield.

Prompted by the good yields and the wide functional group tolerance elicited by our new electrochemical hydrogenation protocol, we wondered if such a strategy could be extended to the obtainment of deuterium labelled organic molecules, exploiting the ability of hydrazine to rapidly exchange its protons in the presence of a suitable deuterium source. As discussed earlier (see Section 2.5), site selective deuteration of C-H bonds is becoming more and more a desirable transformation in the realm of analytical, pharmaceutical and synthetic chemistry. In recent years, a number of electrochemical deuteration methods have been developed[54] as attractive alternatives to conventional deuteration strategies requiring harsh reaction conditions (*e.g.*, high pressure of expensive and unrecoverable D_2 gas), transition metal catalysts, and/or stoichiometric reducing agents. Nevertheless, effective electrochemical approaches for the reductive deuteration of unactivated olefins remain underrepresented.

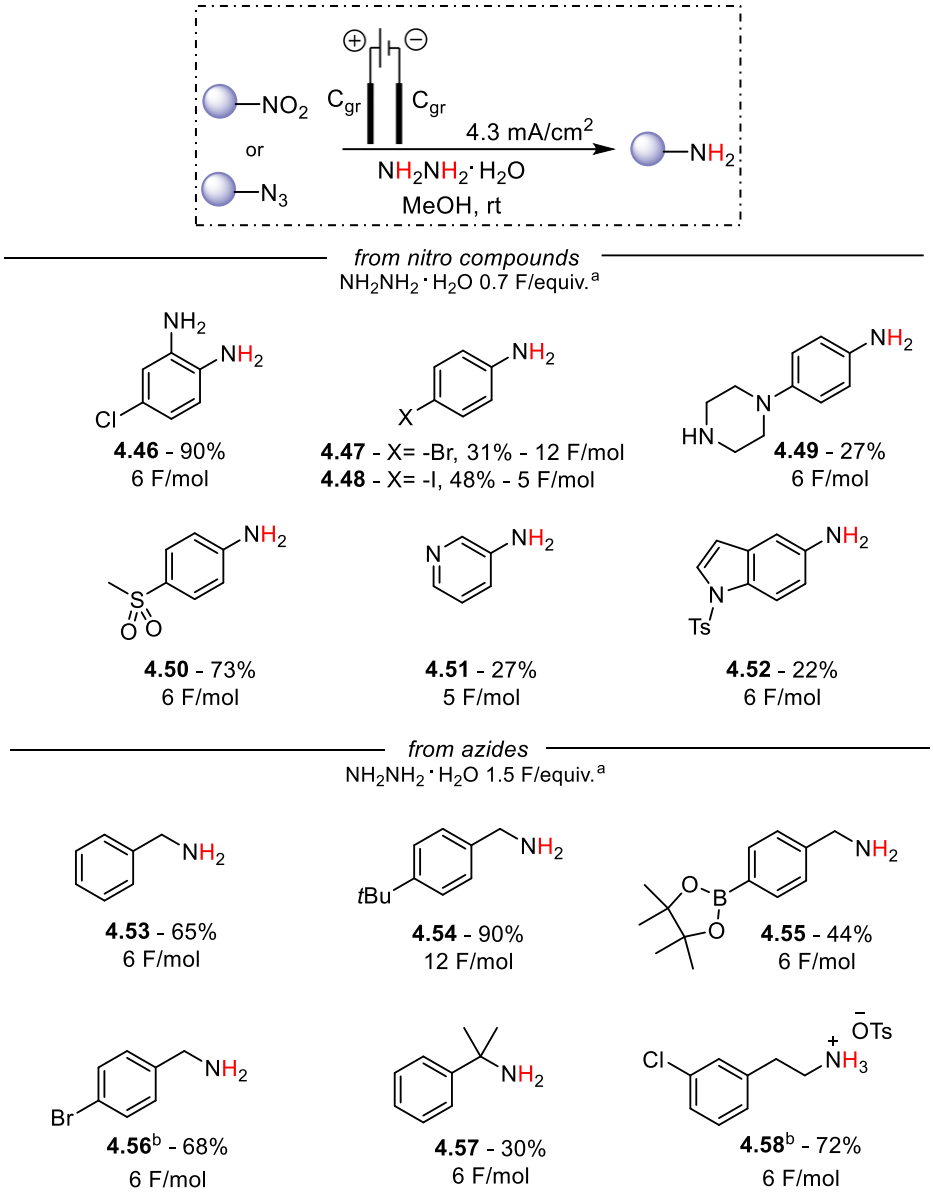

Figure 4.6. Substrate scope for the electrochemical reduction of nitro- and azido-compounds. [a] Ratio of the charge required to complete the transformation per equivalent of hydrazine monohydrate; [b] Reaction performed on 0.8 mmol scale.

F. Montanari had previously reported the deuteration of double bonds via the *in situ* formation of DN=ND from hydrazine and an inexpensive deuterium source.[55] Given this report, we hypothesised that the electrochemical deuteration of alkenes and alkynes would be feasible by modification of our reaction conditions. The

effectiveness of such an approach was initially evaluated by reacting compound **4.59** under standard conditions in a 9:1 MeCN/D_2O solvent system (Table 4.3, Entry 1). This led to the reduced derivative **4.60** with a 61:18 β/γ % of D incorporation. Avoiding TFA as competitive proton source (Entry 2) or replacing it with TFA-*d* (Entry 3) did not enable significant improvements, with the first attempt resulting in a dramatic drop of the system conductivity. While switching to a 9:1 MeCN/MeOD-d_1 mixture (Entry 4) solved this problem while lowering the **4.60** final content in deuterium, performing the reaction in pure MeOD-d_1 allowed a substantial increase in the percentage of D incorporation (Entry 5), with detrimental effect when adding 1 equivalent of TFA-*d* (Entry 6).

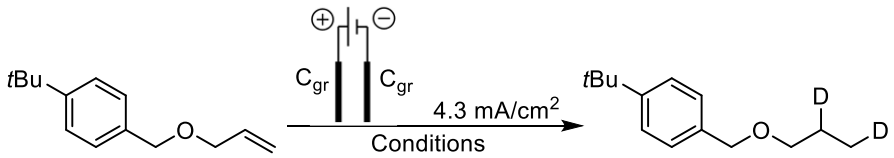

4.59 **4.60**

Entry	SE (equiv.)	Solvent (0.08 M)	β/γ % D incorporation[a]
1	TFA (6)	9:1 MeCN/D_2O	61/18
2	None	9:1 MeCN/D_2O	52/30
3	TFA-*d* (6)	9:1 MeCN/D_2O	50/0
4	None	9:1 MeCN/MeOD-d_1	38/34
5	None	MeOD-d_1	76/73
6	TFA-*d* (1)	MeOD-d_1	24/27
7	TFA-*d* (1)	9:1 MeCN/D_2O	68/74
8	TFA (1)	9:1 MeCN/D_2O	65/68
9	TFA (1)	3:1 MeCN/D_2O	75/68
10	TFA (1)	1:1 MeCN/D_2O	>99/>99

Conditions: reaction performed on a 0.4 mmol scale of **4.59**, employing an undivided cell and graphite electrodes, in the presence of 15 equiv. of NH_2NH_2, rt, 30 F/mol.
[a] Determined by ^1H NMR. Content of 100% indicates one D atom on one carbon of **4.59**.

Table 4.3. Optimisation of the reaction conditions for the electrochemical hydrogenation of unsaturated compounds.

On the other hand, the use of D_2O as the cheapest and most readily available deuterium source would have been highly desirable. We therefore tried to carry out

the transformation in the original 9:1 MeCN/D_2O mixture in the presence of 1 equivalent of supporting electrolyte, which resulted in a good percentage of D incorporation when using either TFA-*d* or TFA (68:74 β/γ % and 65:68 β/γ %, respectively, Entries 7 and 8). Finally, adjusting the MeCN/D_2O ratio from 9:1 to 3:1, and 1:1 (Entries 9 and 10) afforded **4.60** with a D content close to 100% for both the β and the γ position.

By applying the optimised reaction conditions, deuteration was achieved in high yields (73-87%) and with good percentages of deuterium incorporation from variously substituted alkenes and alkynes (**4.61**-**4.65**, Figure 4.7). Curiously, the extent of D incorporation was not uniform in several cases (e.g. **4.64** and **4.65**), probably due to incomplete exchange of protons and deuterons during the generation of the diimide, which led to the formation of a HN=ND species concurrently with the fully deuterated diimide.

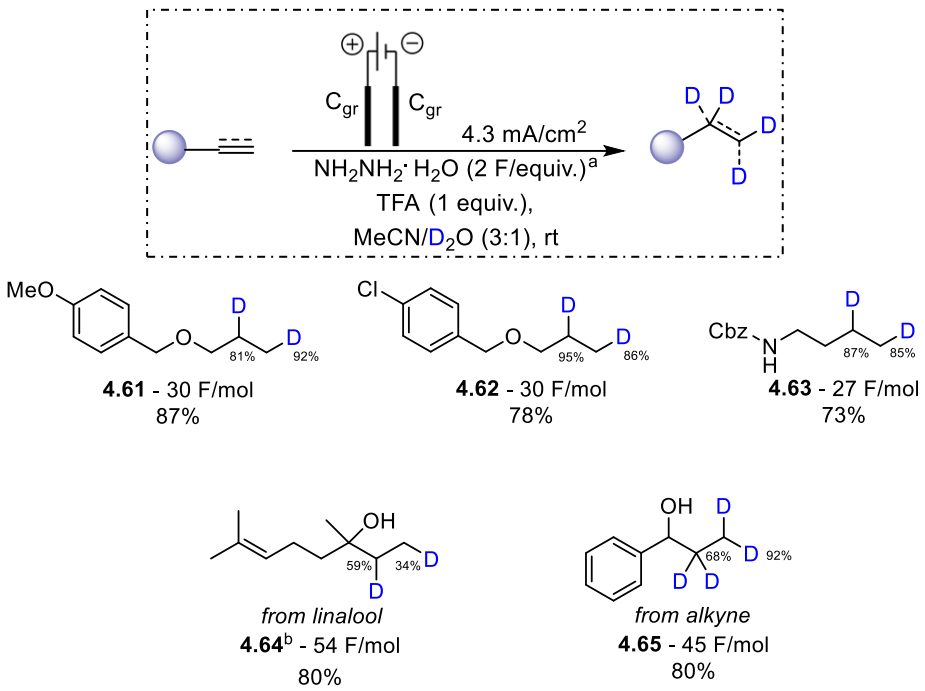

Figure 4.7. Substrate scope for the electrochemical deuteration of unsaturated compounds. [a] Ratio of the charge required to complete the transformation per equivalent of hydrazine monohydrate; [b] TFA was omitted.

Bibliography

(1) Horn, E. J.; Rosen, B. R.; Baran, P. S.; *ACS Central Science,* **2016**, *2*, 302–308.

(2) Frontana-Uribe, B. A.; Little, R. D.; Ibanez, J. G.; Palma, A.; Vasquez-Medrano, R.; *Green Chemistry,* **2010**, *12*, 2099–2119.

(3) Yuan, Y.; Lei, A.; *Nature Communications,* **2020**, *11*, 802.

(4) Faraday, M.; *Philosophical Transactions of the Royal Society of London,* **1832**, *122*, 125–162.

(5) Kolbe, H.; *Justus Liebigs Annalen der Chemie,* **1849**, *69*, 257–294.

(6) Leech, M. C.; Lam, K.; *Accounts of Chemical Research,* **2020**, *53*, 121–134.

(7) Schotten, C.; Nicholls, T. P.; Bourne, R. A.; Kapur, N.; Nguyen, B. N.; Willans, C. E.; *Green Chemistry,* **2020**, *22*, 3358–3375.

(8) Kingston, C.; Palkowitz, M. D.; Takahira, Y.; Vantourout, J. C.; Peters, B. K.; Kawamata, Y.; Baran, P. S.; *Accounts of Chemical Research,* **2020**, *53*, 72–83.

(9) Shono, T.; in *Comprehensive Organic Synthesis*; **1991**, Pergamon, Oxford, 1789–813.

(10) Verschueren, R. H.; De Borggraeve, W. M.; *Molecules,* **2019**, *24*, 2122.

(11) Heard, D. M.; Lennox, A. J. J.; *Angewandte Chemie International Edition,* **2020**, *59*, 18866–18884.

(12) Coppola, G. A.; Pillitteri, S.; Van der Eycken, E. V.; You, S.-L.; Sharma, U. K.; *Chemical Society Reviews,* **2022**, *51*, 2313–2382.

(13) Leech, M. C.; Lam, K.; *Nature Reviews Chemistry,* **2022**, *6*, 275–286.

(14) Yan, M.; Kawamata, Y.; Baran, P. S.; *Angewandte Chemie International Edition,* **2018**, *57*, 4149–4155.

(15) Zhu, C.; Ang, N. W. J.; Meyer, T. H.; Qiu, Y.; Ackermann, L.; *ACS Central Science,* **2021**, *7*, 415–431.

(16) Wiebe, A.; Gieshoff, T.; Möhle, S.; Rodrigo, E.; Zirbes, M.; Waldvogel, S. R.; *Angewandte Chemie International Edition,* **2018**, *57*, 5594–5619.

(17) J. G. de Vries; Elsevier, C. J.; *The Handbook of Homogeneous Hydrogenation*, **2007**, Wiley VCH: Weinheim.

(18) P. G. Andersson; I. J. Munslow.; *Modern Reduction Methods*; **2008** Wiley-VCH Verlag GmbH & Co. KGaA, Weinheim.

(19) Keinan, E..; Greenspoon, N.; *Journal of the American Chemical Society,* **1986**, *108*, 7314–7325.

(20) Czekelius, C.; Carreira, E. M.; *Organic Letters,* **2004**, *6*, 4575–4577.

(21) Mori, A.; Miyakawa, Y.; Ohashi, E.; Haga, T.; Maegawa, T.; Sajiki, H.; *Organic Letters,* **2006**, *8*, 3279–3281.

(22) Bennie, L. S.; Fraser, C. J.; Irvine, S.; Kerr, W. J.; Andersson, S.; Nilsson, G. N.; *Chemical Communications,* **2011**, *47*, 11653.

(23) Guo, N.; Hu, M.-Y.; Feng, Y.; Zhu, S.-F.; *Organic Chemistry Frontiers,* **2015**, *2*, 692–696.
(24) Tokmic, K.; Markus, C. R.; Zhu, L.; Fout, A. R.; *Journal of the American Chemical Society,* **2016**, *138*, 11907–11913.
(25) Sugiura, M.; Sato, N.; Kotani, S.; Nakajima, M.; *Chemical Communications,* **2008**, *36*, 4309.
(26) Kotani, S.; Osakama, K.; Sugiura, M.; Nakajima, M.; *Organic Letters,* **2011**, *13*, 3968–3971.
(27) Greb, L.; Oña-Burgos, P.; Schirmer, B.; Grimme, S.; Stephan, D. W.; Paradies, J.; *Angewandte Chemie International Edition,* **2012**, *51*, 10164–10168.
(28) Chernichenko, K.; Madarász, Á.; Pápai, I.; Nieger, M.; Leskelä, M.; Repo, T.; *Nature Chemistry,* **2013**, *5*, 718–723.
(29) Oestreich, M.; Hermeke, J.; Mohr, J.; *Chemical Society Reviews,* **2015**, *44*, 2202–2220.
(30) Li, H.-C.; An, C.; Wu, G.; Li, G.-X.; Huang, X.-B.; Gao, W.-X.; Ding, J.-C.; Zhou, Y.-B.; Liu, M.-C.; Wu, H.-Y.; *Organic Letters,* **2018**, *20*, 5573–5577.
(31) Pasto, D. J.; Taylor, R. T.; in *Organic Reactions*; **1991**, Wiley, 91–155.
(32) Imada, Y.; Iida, H.; Naota, T.; *Journal of the American Chemical Society,* **2005**, *127*, 14544–14545.
(33) Arakawa, Y.; Kohda, T.; Minagawa, K.; Imada, Y.; *SynOpen,* **2017**, *1*, 11–14.
(34) Ito, K.; Nagase, S.; *Chemical Physics Letters,* **1986**, *126*, 531–536.
(35) Corey, E. J.; Pasto, D. J.; Mock, W. L.; *Journal of the American Chemical Society* **1961**, *83*, 2957–2958.
(36) Yang, J.; Qin, H.; Yan, K.; Cheng, X.; Wen, J.; *Advanced Synthesis and Catalysis,* **2021**, *363*, 5407–5416.
(37) Li, J.; He, L.; Liu, X.; Cheng, X.; Li, G.; *Angewandte Chemie International Edition,* **2019**, *58*, 1759–1763.
(38) Zhang, X.; Jiang, R.; Cheng, X.; *The Journal of Organic Chemistry,* **2021**, *86*, 16016–16025.
(39) Huang, B.; Li, Y.; Yang, C.; Xia, W.; *Chemical Communications,* **2019**, *55*, 6731–6734.
(40) Qin, Y.; Lu, J.; Zou, Z.; Hong, H.; Li, Y.; Li, Y.; Chen, L.; Hu, J.; Huang, Y.; *Organic Chemistry Frontiers,* **2020**, *7*, 1817–1822.
(41) Qin, H.; Yang, J.; Yan, K.; Xue, Y.; Zhang, M.; Sun, X.; Wen, J.; Wang, H.; *Advanced Synthesis and Catalysis,* **2021**, *363*, 2104–2109.
(42) Siu, J. C.; Fu, N.; Lin, S.; *Accounts of Chemical Research,* **2020**, *53*, 547–560.
(43) Song, L.; Fu, N.; Ernst, B. G.; Lee, W. H.; Frederick, M. O.; Di Stasio, R. A.; Lin, S.; *Nature Chemistry,* **2020**, *12*, 747–754.
(44) Li, B.; Ge, H.; *Science Advances,* **2019**, *5,* eaaw2774.
(45) Wu, Y.; Liu, C.; Wang, C.; Lu, S.; Zhang, B.; *Angewandte Chemie International Edition,* **2020**, *59*, 21170–21175.

(46) Russo, C.; Leech, M. C.; Walsh, J. M.; Higham, J. I.; Giannessi, L.; Lambert, E.; Kiaku, C.; Poole, D. L.; Mason, J.; Goodall, C. A. I.; Devo, P.; Giustiniano, M.; Radi, M.; Lam, K.; *Angewandte Chemie International Edition* **2023**, *62*, e202309563.
(47) Chen, S.; Wang, C.; Liu, S.; Huang, M.; Lu, J.; Xu, P.; Tong, H.; Hu, L.; Chen, Q.; *The Journal of Physical Chemistry Letters* **2021**, *12*, 4849–4856.
(48) Miao, R.; Compton, R. G.; *The Journal of Physical Chemistry Letters,* **2021**, *12*, 1601–1605.
(49) Cao, X.; Wang, B.; Su, Q.; *Journal of Electroanalytical Chemistry,* **1993**, *361*, 211–214.
(50) Stergiou, A. D.; Symes, M. D.; *Cell Reports Physical Science,* **2022**, *3*, 100914.
(51) Waldvogel, S. R.; Streb, C.; *Chem,* **2022**, *8*, 2071–2073.
(52) Kisukuri, C. M.; Seidler, J.; Gärtner, T.; Rohrmann, D. F.; Waldvogel, S. R.; *Organic Process Research and Development,* **2023,** *in press*.
(53) Wirtanen, T.; Rodrigo, E.; Waldvogel, S. R.; *Advanced Synthesis and Catalysis,* **2020**, *362*, 2088–2101.
(54) Norcott, P. L.; *Chemical Communications,* **2022**, *58*, 2944–2953.
(55) Annunziata, R.; Fornasier, R.; Montanari, F.; *The Journal of Organic Chemistry,* **1974**, *39*, 3195–3197.

Experimental Section

General methods

All reactions were carried out under aerobic conditions unless otherwise stated. All solvents and commercially available reagents were purchased from standard vendors and used without further purification unless otherwise stated.

Electrolyses were performed using an IKA Electrasyn 2.0, with carbon graphite working and counter electrodes, and a variable stirring rate between 400 and 1500 rpm. Analytical thin-layer chromatography (TLC) was performed using silica gel plates (0.25 mm thickness) on aluminum support. Visualisation was accomplished by irradiation with a UV lamp and/or staining with either $KMnO_4$ or ninhydrin. Column chromatography was performed over Silica gel 60 Å (40-63μ mesh) using a CombiFlash Rf Lumen automatic flash chromatography system. Residual solvent was removed using a static oil pump (< 10 mbar).

NMR spectra were recorded on a JEOL ECZR 400 (^{1}H 399.78 MHz; ^{13}C 100.53 MHz; ^{19}F 376.17 MHz) or ECA 500 (^{1}H 500.16 MHz; ^{13}C 125.77 MHz) spectrometer and are reported relative to the residual solvent resonances. All heteronuclear NMR spectra were ^{1}H decoupled and recorded at room temperature unless otherwise stated. Chemical shifts (δ) are reported in part per million (ppm) relative to the residual solvent peak; coupling constants (*J*), are reported in hertz (Hz).

High Resolution Mass Spectrometry (HRMS) data were obtained by Dr. Iain Goodall and Dr. Perry Devo from the University of Greenwich Mass Spectrometry Service using a Waters Synapt G2 hybrid Quadrupole-orthogonal acceleration time-of-flight configuration (Waters, Manchester, UK) operating in Resolution Mode ($M/\Delta M \geq 18{,}000$), fitted with a Waters Acquity UPLC binary solvent chromatographic pump system. The column used was a reversed-phase Acquity BEH C18 2.1 x 50 mm, 1.7-micron bead, running a 3- minute separation with an

A:B eluent mixture comprising of either deionised water with 0.1% (v/v) formic acid and MeCN with 0.1% (v/v) formic acid (negative mode) or deionised water with 0.1% (v/v) ammonium hydroxide and MeCN with 0.1% (v/v) ammonium hydroxide (positive mode), respectively. Mass calibration of the instrument was performed using sodium formate cluster ions, and an orthogonal Lock-SprayTM ESI probe was used with a lock mass calibrant, leucine-enkephalin. The pseudomolecular leucine enkephalin ion at *m/z* = 554.2615 (Negative Ion Mode), and *m/z* = 556.2771 (Positive Ion Mode), was used as the internal mass correction calibrant. Additional samples were analysed on a Thermo LTQ Orbitrap XL coupled with a heated electrospray source (HESI). The capillary temperature was set to 275 °C and a voltage of 21 V. The sheath gas and auxiliary gas flow were set to 10 and 5 L h^{-1}, respectively, and the source current and voltage to 100 µA and 5 kV. A solution of analyte (0.1 mg/ml) and sodium formate (1% v/v) in MeCN was added by direct infusion (10 µL/min) into the mass spectrometer using a Hamilton syringe (250 µL).

Gas-Chromatography Mass Spectrometry (GC-MS) data were obtained using a Shimadzu Nexis GC-2030 gas chromatograph connected to a GCMS-QP2020 NX gas chromatograph mass spectrometer, equipped with an AOC-20i Plus auto injector. The column was a CD-5MS capillary column (30 m x 0.25 mm x 0.25 µm), with helium as the carrier gas. The sample injection volume was 1 µL, and separations run over a 5-minute period with an increasing oven temperature (gradient) between 40 – 280 °C. Results were visualised and processed using LabSolutions GCMS solution version 4.50.

High-Performance Liquid Chromatography-Mass Spectrometry (HPLC-MS) data were obtained using a Shimadzu LC-2050C 3D coupled with a Shimadzu LCMS-2020 FCV-20AH2. The column was an Ascentis Express 90Å AQ-C18, 2.7 µm. Results were visualised and processed using LabSolutions GCMS solution version 5.114.

Cyclic voltammetry studies were carried out using an Autolab 302N potentiostat interfaced through Nova 2.1 software to a personal computer. Electrochemical measurements were performed in a glovebox under an atmosphere of dinitrogen with oxygen and water levels of less than 5 ppm at 298 K, with solvents that had been thoroughly degassed and purified by passing through an alumina-based purification system. Sample concentrations of 1.0 mM were used, alongside 0.1 M [^{n}Bu$_4$N][PF$_6$] supporting electrolyte concentrations. Experiments were conducted using a standard three-electrode setup comprising of a glassy carbon disc working electrode, platinum wire counter electrode, and AgCl coated silver wire as a pseudo-reference electrode. Potentials are reported relative to the $[FeCp_2]^{+/0}$ redox couple, obtained through the addition of ferrocene to the analyte solution.

Starting materials

General procedure for the synthesis of allyl ethers from benzyl alcohols

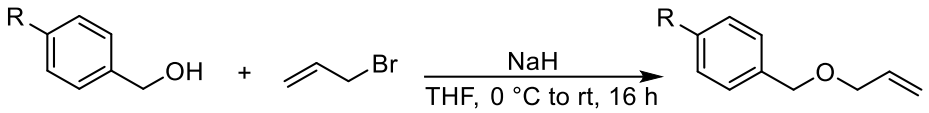

Under a dinitrogen atmosphere, a flame-dried 3-necked 100 mL round-bottomed flask was charged with THF (50 mL) and a benzyl alcohol (7.3 mmol), and then cooled to 0 °C with an ice bath. Sodium hydride (g and mmol. as specified for each substrate) was then added in one portion, and the grey suspension left to stir for 45 minutes. Then, allyl bromide (g and mmol. as specified for each substrate) was added in one portion, and the reaction mixture left to warm to room temperature and stir for 16 hours. The reaction mixture was then quenched with deionised water, before being extracted with EtOAc (3 x 50 mL). The extracts were combined, washed with brine (25 mL), dried over $MgSO_4$, filtered, and the solvent

removed under reduced pressure. Purification by flash chromatography (0 → 50% EtOAc in *n*-hexane) afforded the desired product.

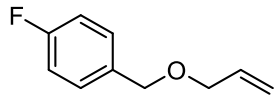

1-((Allyloxy)methyl)-4-fluorobenzene. Synthesised according to general procedure from 4-fluorobenzyl alcohol (0.79 mL, 7.3 mmol), NaH (0.349 g, 8.7 mmol, 60% dispersion in mineral oil), and allyl bromide (1.26 mL, 14.5 mmol). Extraction with EtOAc, purification by flash column chromatography (100% *n*-hexane → 50% EtOAc in *n*-hexane) and evaporation of the solvent afforded the alkene as a colourless liquid (0.55 g, 46% yield). Characterisation data are in agreement with literature reports.[1]

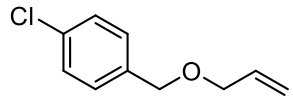

1-((Allyloxy)methyl)-4-chlorobenzene. Synthesised according to general procedure from 4-chlorobenzyl alcohol (1.04 g, 7.3 mmol), NaH (0.349 g, 8.7 mmol, 60% dispersion in mineral oil), and allyl bromide (1.26 mL, 14.5 mmol). Extraction with EtOAc, purification by flash column chromatography (100% *n*-hexane → 50% EtOAc in *n*-hexane) and evaporation of the solvent afforded the alkene as a colourless liquid (0.244 g, 17% yield). Characterisation data are in agreement with literature reports.[2]

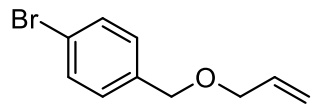

1-((Allyloxy)methyl)-4-bromobenzene. Synthesised according to general procedure from 4-bromobenzyl alcohol (1.36 g, 7.3 mmol), NaH (0.349g, 8.7 mmol, 60% dispersion in mineral oil), and allyl bromide (1.26 mL, 14.5 mmol). Extraction with

EtOAc, purification by flash column chromatography (100% *n*-hexane → 50% EtOAc in *n*-hexane) and evaporation of the solvent afforded the alkene as a colourless liquid (1.01 g, 61% yield). Characterisation data are in agreement with literature reports.[3]

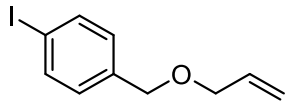

1-((Allyloxy)methyl)-4-iodobenzene. Synthesised according to general procedure from 4-iodobenzyl alcohol (1.70 g, 7.3 mmol), NaH (0.349 g, 8.7 mmol, 60% dispersion in mineral oil), and allyl bromide (1.26 mL, 14.5 mmol). Extraction with EtOAc, purification by flash column chromatography (100% *n*-hexane → 50% EtOAc in *n*-hexane) and evaporation of the solvent afforded the alkene as a colourless liquid (1.04 g, 52% yield). Characterisation data are in agreement with literature reports.[4]

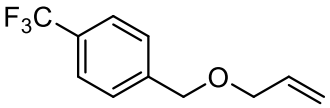

1-((Allyloxy)methyl)-4-(trifluoromethyl)benzene. Synthesised according to general procedure from 4-(trifluoromethyl)benzyl alcohol (1 mL, 7.3 mmol), NaH (0.349 g, 8.7 mmol, 60% dispersion in mineral oil), and allyl bromide (1.26 mL, 14.5 mmol). Extraction with EtOAc, purification by flash column chromatography (100% *n*-hexane → 50% EtOAc in *n*-hexane) and evaporation of solvent afforded the alkene as a colourless liquid (1.09 g, 69% yield). Characterisation data are in agreement with literature reports.[5]

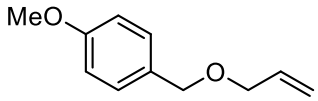

1-((Allyloxy)methyl)-4-methoxybenzene. Synthesised according to general procedure from 4-methoxybenzyl alcohol (1.00 g, 7.3 mmol), NaH (0.349 g, 8.7 mmol, 60% dispersion in mineral oil), and allyl bromide (1.26 mL, 14.5 mmol). Extraction with EtOAc, purification by flash column chromatography (100% *n*-hexane → 50% EtOAc in *n*-hexane) and evaporation of solvent afforded the alkene as a colourless liquid (1.13 g, 87% yield). Characterisation data are in agreement with literature reports.[6]

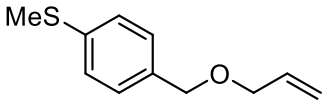

(4-((Allyloxy)methyl)phenyl)(methyl)sulfane. Synthesised according to general procedure from 4-(methylthio)benzyl alcohol (1.12 g, 7.3 mmol), NaH (0.349 g, 8.7 mmol, 60% dispersion in mineral oil), and allyl bromide (1.26 mL, 14.5 mmol). Extraction with EtOAc, purification by flash column chromatography (100% *n*-hexane → 50% EtOAc in *n*-hexane) and evaporation of solvent afforded the alkene as a colourless liquid (0.87 g, 62% yield). ^{1}H NMR (400 MHz, $CDCl_3$) δ 7.29–7.22 (m, 4H), 5.95 (m, 1H), 5.30 (dq, J_a = 17.2, J_b = 1.7 Hz, 1H), 5.21 (dq, J_a = 10.4, J_b = 1.7 Hz, 1H), 4.48 (s, 2H), 4.02 (dt, J_a = 5.6, J_b = 1.4 Hz, 2H), 2.48 (s, 3H) ; ^{13}C {^{1}H} NMR (101 MHz, $CDCl_3$) δ 137.8, 135.3, 134.8, 128.5, 126.8, 117.3, 71.8, 71.2, 16.1; HRMS (ESI) *m/z*: calcd $[M + H]^+$ for $C_{11}H_{15}OS^+$ 195.0838; found $[M + H]^+$ 195.0839.

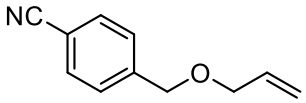

4-((Allyloxy)methyl)benzonitrile. Synthesised according to general procedure from 4-(hydroxymethyl)benzonitrile (0.97 g, 7.3 mmol), NaH (0.349 g, 8.7 mmol, 60%

dispersion in mineral oil), and allyl bromide (1.26 mL, 14.5 mmol). Extraction with EtOAc, purification by flash column chromatography (100% *n*-hexane → 50% EtOAc in *n*-hexane) and evaporation of solvent afforded the alkene as a colourless liquid (1.15 g, 91% yield Characterisation data are in agreement with literature reports.[6]

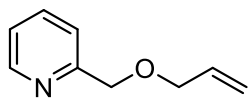

2-((Allyloxy)methyl)pyridine. Synthesised according to general procedure from pyridine-2-ylmethanol (0.79 g, 7.3 mmol), NaH (0.356 g, 8.9 mmol, 60% dispersion in mineral oil), and allyl bromide (1.26 mL, 14.5 mmol). Extraction with EtOAc, purification by flash column chromatography (100% *n*-hexane → 50% EtOAc in *n*-hexane) and evaporation of the solvent afforded the alkene as a pale-yellow liquid (0.65 g, 60% yield). Characterisation data are in agreement with literature reports.[1]

Procedure for the synthesis of 1-((allyloxy)methyl)-4-(*tert*-butyl)benzene

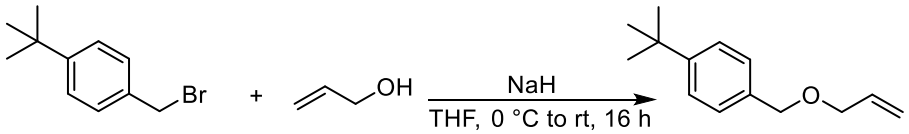

Under a dinitrogen atmosphere, a flame-dried 3-necked 100 mL round-bottomed flask was charged with THF (50 mL) and allyl alcohol (0.55 mL, 8.2 mmol), and then cooled to 0 °C with an ice bath. Sodium hydride (0.39 g, 0.98 mmol, 60% dispersion in mineral oil) was then added in one portion, and the grey suspension left to stir for 45 minutes. Then, 4-*tert*-butyl benzyl bromide (1.8 mL, 9.8 mmol) was added in one portion, and the reaction mixture left to warm to room temperature and stir for 16 hours. The reaction mixture was then quenched with deionised water, before being extracted with EtOAc (3 x 50 mL). The extracts were

combined, washed with brine (25 mL), dried over $MgSO_4$, filtered, and the solvent removed under reduced pressure. Purification by flash chromatography (0 → 50% EtOAc in *n*-hexane) afforded the alkene as a colourless liquid (1.44 g, 97% yield). Characterisation data are in agreement with literature reports.[7]

Procedure for the synthesis of *tert*-butyl(hex-5-en-1-yloxy)dimethylsilane

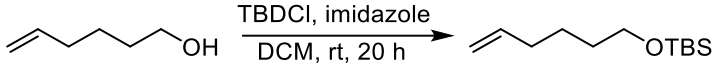

Synthesised according to literature procedure.[8] To a stirred solution of 5-hexen-1-ol (0.360 mL, 3.0 mmol) in DCM (10 mL) were added imidazole (0.211 g, 3.1 mmol, 1.03 equiv.) and *tert*-butyldimethylsilyl chloride (0.457 g, 3.03 mmol, 1.01 equiv.). The resultant mixture was allowed to stir at room temperature for 20 h, then the mixture was diluted with DCM (20 mL), washed with water (20 mL) and brine (20 mL), dried over anhydrous $MgSO_4$, filtered, and concentrated in vacuo. The crude was purified by flash column chromatography (100% *n*-hexane → 10% EtOAc in *n*-hexane) to give *tert*-butyl(hex-5-en-1-yloxy)dimethylsilane as a colorless oil (0.611 g, 2.9 mmol, 97% yield). Characterisation data are in agreement with literature reports.[8]

Procedure for the synthesis of benzyl but-3-en-1-ylcarbamate

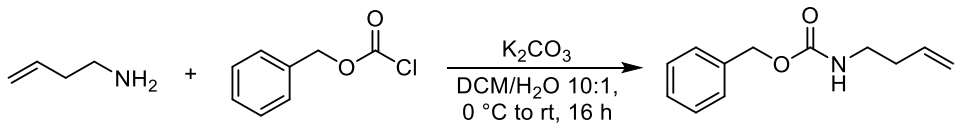

Synthesised according to literature procedure.[9] To a mixture of 3-butenylamine (0.260 mL, 2.8 mmol) and K_2CO_3 (1.16 g, 8.4 mmol, 3 equiv.) in a 10:1 DCM/H_2O mixture (17.0 mL DCM and 1.7 mL H_2O) at 0 °C, benzyl chloroformate (0.642 mL, 4.5 mmol, 1.6 equiv.) was slowly added. The reaction was warmed to room temperature and stirred for 16 h, then 15 mL of water were added, the layers were

separated, and the aqueous layer was extracted with DCM (2 x 20 mL). The combined organic extracts were dried over $MgSO_4$, filtered, concentrated in vacuo, and purified by flash column chromatography (100% *n*-hexane → 10% EtOAc in *n*-hexane) to afford benzyl but-3-en-1ylcarbamate as a colourless oil (0.517 g, 2.5 mmol, 90% yield). Characterisation data are in agreement with literature reports.[10]

Procedure for the synthesis of bicyclo[2.2.1]hept-5-en-2-yl)methyl acetate

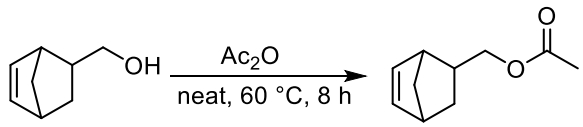

Synthesised according to literature procedure.[11] A 25 mL round-bottom flask was charged with 5-norbornene-2-methanol (0.243 mL, 2.0 mmol) followed by slow addition of acetic anhydride (0.284 mL, 3.0 mmol, 1.5 equiv.). The resulting mixture was stirred at 60 °C until completion of the reaction, as monitored by TLC. Then the mixture was diluted with Et_2O (30 mL) and washed with saturated $NaHCO_3$ aqueous solution (3 x 20 mL), the organic layer was dried over anhydrous $MgSO_4$, filtered, and concentrated in vacuo to afford bicyclo[2.2.1]hept-5-en-2-yl)methyl acetate as a colourless oil (0.319 g, 1.9 mmol, 96% yield) not requiring any further purification. Characterisation data are in agreement with literature reports.[12]

Procedure for the synthesis of 5-((benzyloxy)methyl)bicyclo[2.2.1]hept-2-ene

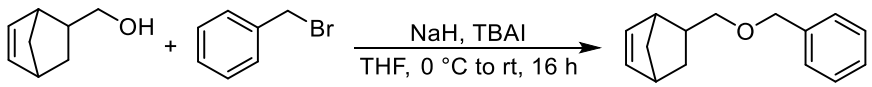

To a stirred solution of 5-norbornene-2-methanol (0.290 mL, 2.4 mmol) in THF (4 mL), at 0° C, were added TBAI (0.529 g, 1.4 mmol, 0.6 equiv.) and NaH (60% dispersion in mineral oil, 0.144 g, 3.6 mmol, 1.5 equiv.), followed by slow addition

of benzyl bromide (0.684 mL, 5.7 mmol, 2.4 equiv.). The reaction was warmed to room temperature and stirred for 16 h, then the mixture was quenched with a saturated NH_4Cl aqueous solution (20 mL) and extracted with EtOAc (3 x 20 mL). The combined organic extracts were dried over $MgSO_4$, filtered, concentrated in vacuo, and purified by flash column chromatography (100% *n*-hexane → 10% EtOAc in *n*-hexane) to afford 5 ((benzyloxy)methyl)bicyclo[2.2.1]hept-2-ene as a colourless liquid (0.298 g, 1.4 mmol, 58% yield). Characterisation data are in agreement with literature reports.[13]

Procedure for the synthesis of bicyclo[2.2.1]hept-5-en-2-ylmethyl diethyl phosphate

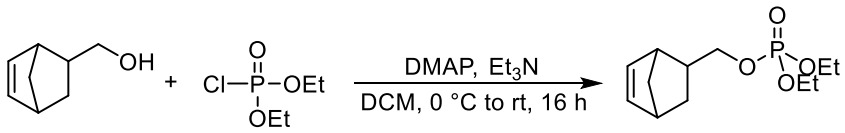

Under a dinitrogen atmosphere, a flame-dried 2-necked 50 mL round-bottomed flask was charged with DMAP (0.0507g, 0.4 mmol), DCM (10 mL), 5-norbornene-2-methanol (0.5 mL), and diethyl chlorophosphate (0.61 mL, 4.2 mmol). The mixture was cooled to 0 °C with an ice bath before triethylamine (0.87 mL) was added over a 5-minute period, and the reaction mixture left to warm to room temperature and stir for 16 hours. The reaction mixture was diluted with DCM (20 mL) and then quenched with a saturated aqueous solution of $NaHCO_3$. The organic layer was collected, and the aqueous layer extracted with DCM (3 x 20 mL). The organic extracts were combined, dried over $MgSO_4$, filtered, and the solvent removed under reduced pressure. Purification by flash chromatography (100% *n*-hexane → 100% EtOAc) afforded the alkene as a colourless liquid (0.684 g, 63% yield. ^{1}H NMR (500 MHz, $CDCl_3$) δ 6.14 (m, 0.5H), 6.08 (m, 1H), 5.96 (m, 0.5H), 4.11 (m, 4H), 3.90 (m, 0.5H), 3.78 (m, 0.5H), 3.59 (m, 0.5H), 2.93 (m, 0.5H), 2.82 (m, 0.5H), 2.77 (m, 1H), 2.44 (m, 0.5H), 1.80 (m, 1H), 1.44 (m, 0.5H), 1.33 (m,

6H), 1.29 (brs, 0.5H), 1.25 (m, 1H), 1.13 (m, 0.5H), 0.50 (m, 0.5H); $^{13}C\{^{1}H\}$ NMR (126 MHz, $CDCl_3$) δ 137.8, 137.1, 136.3, 132.2, 71.6 (d, J_{C-P} = 6 Hz), 70.9 (d, J_{C-P} = 6 Hz), 63.8 (d, J_{C-P} = 6 Hz), 63.7 (d, J_{C-P} = 6 Hz), 49.4, 45.0, 43.8, 43.4, 42.3, 41.7, 39.6 (d, J_{C-P} = 7 Hz), 39.5 (d, J_{C-P} = 7 Hz), 29.4, 28.7, 16.3 (d, J_{C-P} = 7 Hz); $^{31}P\{^{1}H\}$ NMR (162 MHz, $CDCl_3$) δ −0.7 (2P); HRMS (ESI) *m/z*: calcd $[M + H]^+$ for $C_{12}H_{22}O_4P^+$ 261.1256; found $[M + H]^+$ 261.1257.

Procedure for synthesis of 2-(4-(azidomethyl)phenyl)-4,4,5,5-tetramethyl-1,3,2-dioxaborolane

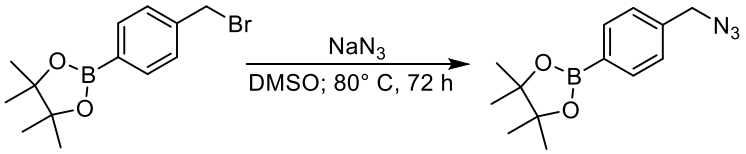

Sodium azide (0.390 g, 6 mmol, 1.5 equiv.) was added to a stirring solution of 2-(4-(bromomethyl)phenyl)-4,4,5,5-tetramethyl-1,3,2-dioxaborolane (1.188 g, 4 mmol) in DMSO (10 mL). The mixture was heated to 80 °C and stirred for 72 h. The reaction was quenched by the addition of brine (30 mL), and the aqueous phase extracted with EtOAc (3 x 50 mL). The combined organic phases were dried over $MgSO_4$, filtered, then concentrated in vacuo to afford the azide as a red oil (0.975 g, 94% yield). Characterisation data are in agreement with literature reports.[14]

Procedure for synthesis of *para*-bromobenzylazide

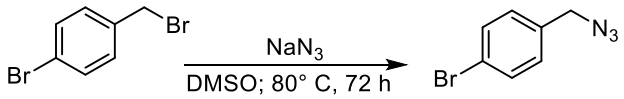

Sodium azide (0.780 g, 12 mmol, 3.6 equiv.) was added to a stirring solution of 4-bromobenzylbromide (0.839 g, 3.36 mmol) in DMSO(10 mL). The mixture was heated to 80 °C and stirred for 72 h. The reaction was quenched by the addition of brine (30 mL), and the aqueous phase extracted with EtOAc (3 x 50 mL). The

combined organic phases were dried over $MgSO_4$, filtered, then concentrated in vacuo to afford the azide as a colourless oil (0.556 g, 78% yield Characterisation data are in agreement with literature reports.[15]

Procedure for synthesis of cumyl azide

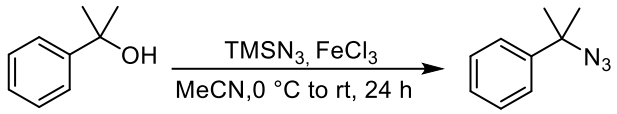

$FeCl_3$ (0.016 g, 0.5 mmol, 10 mol%) was added to a stirring solution of 2-phenylisopropanol (699 mL, 5 mmol) and $TMSN_3$ (795 mL, 6 mmol, 1.2 equiv.) in MeCN (25 mL) at 0 °C; the mixture was allowed to warm to room temperature overnight. Then the reaction was quenched with water (20 mL) and extracted with EtOAc (3 x 50 mL), the combined organic extracts were dried over $MgSO_4$, filtered and concentrated in vacuo to afford the azide as a red oil (0.587 mg, 73% yield). Characterisation data are in agreement with literature reports.[16]

Procedure for synthesis of 3-chlorophenethyl azide

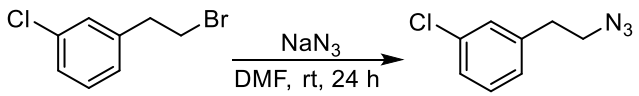

A solution of sodium azide in H_2O (0.780 g, 12 mmol, 3 equiv.) was added to a stirring solution of 1-(2-bromoethyl)-3-chlorobenzene (0.876 g, 4 mmol) in DMF (8 mL), and then stirred overnight at room temperature. The reaction was diluted with EtOAc (30 mL) and quenched by the addition of a saturated aqueous solution of LiCl (30 mL). The organic phase was washed with a saturated aqueous solution of LiCl (3 x 50 mL) then the organic phase were dried over $MgSO_4$, filtered, then concentrated in vacuo to afford the azide as a colourless oil (0.654 mg, 90% yield). Characterisation data are in agreement with literature reports.[17]

General procedure for the electrochemical hydrogenation of terminal and internal alkenes and alkynes

A 5 mL IKA Electrasyn electrochemical vial was charged with the alkene/alkyne (0.40 mmol), hydrazine monohydrate (mmol and equiv. as specified for each substrate), TFA (mmol and equiv. as specified for each substrate) and MeOH (5.0 mL). The resulting mixture was then electrolysed at a constant current of 10 mA until complete conversion of the starting material, as monitored by GC-MS or HPLC MS. Upon completion, the crude reaction mixture was poured into water (30 mL) and extracted with pentane or Et_2O (as specified for each compound, 3 x 20 mL). The combined organic extracts were dried over $MgSO_4$, filtered and the solvent was removed under vacuum to afford the desired hydrogenated product.

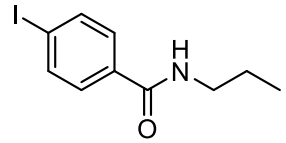

4-Iodo-*N*-propylbenzamide (**4.2**). Synthesised according to the general procedure from the corresponding alkene (0.1148 g, 0.40 mmol), hydrazine monohydrate (0.165 mL, 3.4 mmol, 8.5 equiv.), and TFA (0.184 mL, 2.4 mmol, 6 equiv.). After 12 F/mol, extraction with pentane and evaporation of solvent afforded the hydrogenated product as a pale yellow solid (0.0821 g, 71% yield). ^{1}H NMR (400 MHz, $CDCl_3$) δ 7.71–7.68 (m, 2H), 7.47–7.44 (m, 2H), 6.65 (s, 1H), 3.36–3.31 (m, 2H), 1.63–1.54 (m, 2H), 0.92 (t, J = 7.36 Hz, 3H); ^{13}C {^{1}H} NMR (101 MHz, $CDCl_3$) δ 167.0, 137.7, 134.3, 128.6, 98.2, 41.9, 22.9, 11.5.

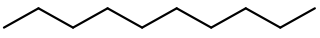

Decane (**4.4**). Synthesised according to the general procedure from the corresponding alkene (0.0561 g, 0.40 mmol), hydrazine monohydrate (0.165 mL, 3.4 mmol, 8.5 equiv.), and TFA (0.184 mL, 2.4 mmol, 6 equiv.). After 12 F/mol,

extraction with pentane and evaporation of solvent afforded the hydrogenated product as a colourless oil (0.0461 g, 81% yield). ^{1}H NMR (400 MHz, $CDCl_3$) δ 1.33–1.26 (m, 16H), 0.88 (t, J = 6.96 Hz, 6H); ^{13}C {^{1}H} NMR (101 MHz, $CDCl_3$) δ 32.1, 29.8, 29.5, 22.9, 14.3.

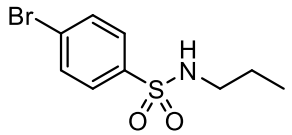

4-Bromo-*N*-propylbenzenesulfonamide (**4.5**). Synthesised according to the general procedure from the corresponding alkene (0.1105 g, 0.40 mmol), hydrazine monohydrate (0.165 mL, 3.4 mmol, 8.5 equiv.), and TFA (0.184 mL, 2.4 mmol, 6 equiv.). After 12 F/mol, extraction with pentane and evaporation of solvent afforded the hydrogenated product as a white solid (0.1090 g, 98% yield). ^{1}H NMR (400 MHz, $CDCl_3$) δ 7.75–7.72 (m, 2H), 7.66–7.63 (m, 2H), 4.84 (s, 1H), 2.93–2.88 (m, 2H), 1.53–1.44 (m, 2H), 0.86 (t, J = 7.24 Hz, 3H); ^{13}C {^{1}H} NMR (101 MHz, $CDCl_3$) δ 139.3, 132.5, 128.7, 127.6, 45.1, 23.0, 11.2.

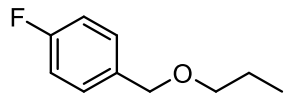

1-Fluoro-4-(propoxymethyl)benzene (**4.6**). Synthesised according to the general procedure from the corresponding alkene (0.0665 g, 0.40 mmol), hydrazine monohydrate (0.33 mL, 6.66 mmol, 16.65 equiv.), and TFA (0.37 mL, 4.83 mmol, 12.075 equiv.). After 24 F/mol, extraction with pentane and evaporation of solvent afforded the hydrogenated product as a colourless oil (0.0532 g, 79% yield). ^{1}H NMR (400 MHz, $CDCl_3$) δ 7.31 (m, 2H), 7.03 (m, 2H), 4.47 (s, 2H), 3.43 (t, J = 6.7 Hz, 2H), 1.64 (m, 2H), 0.94 (t, J = 7.4 Hz, 3H); ^{13}C{^{1}H} NMR (101 MHz, $CDCl_3$) δ 162.4 (d, $J_{C\text{-}F}$ = 245 Hz), 134.5 (d, $J_{C\text{-}F}$ = 3 Hz), 129.4 (d, $J_{C\text{-}F}$ = 3 Hz), 115.3 (d, $J_{C\text{-}F}$ = 21 Hz), 72.23, 72.20, 23.0, 10.7; ^{19}F NMR (376 MHz, $CDCl_3$) δ

−115.11 (m); Accurate Mass (EI) *m/z:* calcd M^+ for $C_{10}H_{13}FO^+$ 168.0945; found M^+ 168.0695 (spectral accuracy: 99.2%).

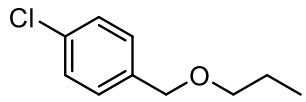

1-Chloro-4-(propoxymethyl)benzene (**4.7**). Synthesised according to the general procedure from the corresponding alkene (0.0731 g, 0.40 mmol), hydrazine monohydrate (0.33 mL, 6.66 mmol, 16.65 equiv.), and TFA (0.37 mL, 4.83 mmol, 12.075 equiv.). After 24 F/mol, extraction with pentane and evaporation of solvent afforded the hydrogenated product as a pale-yellow oil (0.0362 g, 49% yield). ^{1}H NMR (400 MHz, $CDCl_3$) δ 7.25–7.16 (m, 4H), 4.38 (s, 2H), 3.34 (t, J = 6.7 Hz, 2H)), 1.55 (m, 2H), 0.86 (t, J = 7.4 Hz, 3H); ^{13}C{^{1}H} NMR (101 MHz, $CDCl_3$) δ 137.3, 133.3, 129.0, 128.6, 72.3, 72.1, 23.0, 10.7.

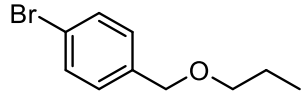

1-Bromo-4-(propoxymethyl)benzene (**4.8**). Synthesised according to the general procedure from the corresponding alkene (0.0908 g, 0.40 mmol), hydrazine monohydrate (0.33 mL, 6.66 mmol, 16.65 equiv.), and TFA (0.37 mL, 4.83 mmol, 12.075 equiv.). After 24 F/mol, extraction with pentane and evaporation of solvent afforded the hydrogenated product as a colourless oil (0.0587 g, 64% yield). ^{1}H NMR (400 MHz, $CDCl_3$) δ 7.46 (m, 2H), 7.22 (m, 2H), 4.45 (s, 2H), 3.42 (t, J = 6.7 Hz, 2H), 1.63 (m, 2H), 0.94 (t, J = 7.4 Hz, 3H); ^{13}C{^{1}H} NMR (101 MHz, $CDCl_3$) δ 137.9, 131.5, 129.3, 121.4, 72.3, 72.1, 23.0, 10.7.

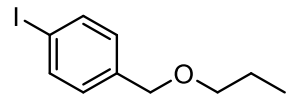

1-Iodo-4-(propoxymethyl)benzene (**4.9**). Synthesised according to the general procedure from the corresponding alkene (0.1096 g, 0.40 mmol), hydrazine monohydrate (0.33 mL, 6.66 mmol, 16.65 equiv.), and TFA (0.37 mL, 4.83 mmol, 12.075 equiv.). After 24 F/mol, extraction with pentane and evaporation of solvent afforded the hydrogenated product as a pale-yellow oil (0.0602 g, 54% yield). ^{1}H NMR (400 MHz, $CDCl_3$) δ 7.67 (m, 2H), 7.09 (m, 2H), 4.45 (s, 2H), 3.42 (t, J = 6.7 Hz, 2H), 1.63 (m, 2H), 0.94 (t, J = 7.4 Hz, 3H); ^{13}C{^{1}H} NMR (101 MHz, $CDCl_3$) δ 138.5, 137.5, 129.6, 92.9, 72.3, 72.2, 23.0, 10.7.

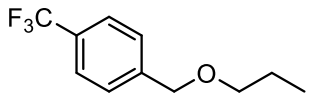

1-(Propoxymethyl)-4-(trifluoromethyl)benzene (**4.10**). Synthesised according to the general procedure from the corresponding alkene (0.0865 g, 0.40 mmol), hydrazine monohydrate (0.33 mL, 6.66 mmol, 16.65 equiv.), and TFA (0.37 mL, 4.83 mmol, 12.075 equiv.). After 4 F/mol, extraction with pentane and evaporation of solvent afforded the hydrogenated product as a pale-yellow oil (0.0852 g, 98% yield). ^{1}H NMR (400 MHz, $CDCl_3$) δ 7.60 (m, 2H), 7.46 (m, 2H), 4.56 (s, 2H), 3.46 (t, J = 6.7 Hz, 2H), 1.66 (m, 2H), 0.96 (t, J = 7.4 Hz. 3H); ^{13}C{^{1}H} NMR (101 MHz, $CDCl_3$) δ 143.0, 129.8 (q, $J_{C\text{-}F}$ = 33 Hz), 127.6, 125.4 (q, $J_{C\text{-}F}$ = 3.8 Hz), 124.4 (q, $J_{C\text{-}F}$ = 272 Hz), 72.6, 72.1, 23.1, 10.7; ^{19}F NMR (376 MHz, $CDCl_3$) δ −62.38; Accurate Mass (EI) m/z: calcd M^+ for $C_{11}H_{13}F_3O^+$ 218.0913; found M^+ 218.0904 (spectral accuracy: 99.2%).

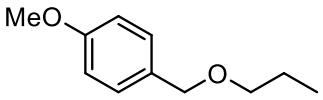

1-Methoxy-4-(propoxymethyl)benzene (**4.11**). Synthesised according to the general procedure from the corresponding alkene (0.0713 g, 0.40 mmol), hydrazine monohydrate (0.33 mL, 6.66 mmol, 16.65 equiv.), and TFA (0.37 mL, 4.83 mmol, 12.075 equiv.). After 24 F/mol, extraction with pentane and evaporation of solvent afforded the hydrogenated product as a pale-yellow oil (0.0613 g, 85% yield). ^{1}H NMR (400 MHz, $CDCl_3$) δ 7.18 (m, 2H), 6.79 (m, 2H), 4.35 (s, 2H), 3.71 (s, 3H), 3.32 (t, J = 6.7 Hz, 2H), 1.54 (m, 2H), 0.85 (t, J = 7.4 Hz, 3H); ^{13}C{^{1}H} NMR (101 MHz, $CDCl_3$) δ 159.2, 130.9, 129.3, 113.8, 72.6, 71.9, 55.3, 23.0, 10.7.

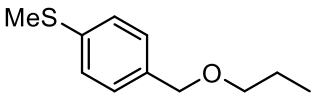

Methyl(4-(propoxymethyl)phenyl)sulfane (**4.12**). Synthesised according to the general procedure from the corresponding alkene (0.0777 g, 0.40 mmol), hydrazine monohydrate (0.33 mL, 6.66 mmol, 16.65 equiv.), and TFA (0.37 mL, 4.83 mmol, 12.075 equiv.). After 24 F/mol, extraction with pentane and evaporation of solvent afforded the hydrogenated product as a pale-yellow oil (0.0730 g, 93% yield). ^{1}H NMR (400 MHz, $CDCl_3$) δ 7.16 (m, 4H), 3.33 (s, 2H), 2.38 (t, J = 6.7 Hz, 2H), 1.54 (m, 2H), 0.85 (t, J = 7.4 Hz, 3H); ^{13}C{^{1}H} NMR (101 MHz, $CDCl_3$) δ 137.6, 135.8, 128.4, 126.8, 72.5, 72.1, 23.1, 16.1, 10.7; Accurate Mass (EI) *m/z*: calcd M^+ for $C_{11}H_{16}OS^+$: 196.0916; found M^+196.0757 (spectral accuracy: 99.4%).

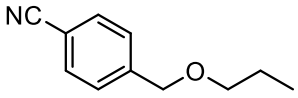

4-(Propoxymethyl)benzonitrile (**4.13**). Synthesised according to the general procedure from the corresponding alkene (0.0693 g, 0.40 mmol), hydrazine monohydrate (0.33 mL, 6.66 mmol, 16.65 equiv.), and TFA (0.37 mL, 4.83 mmol, 12.075 equiv.) After 24 F/mol, extraction with pentane and evaporation of solvent

afforded the hydrogenated product as a pale-yellow oil (0.0561 g, 80% yield). ^{1}H NMR (400 MHz, $CDCl_3$) δ 7.55 (m, 2H), 7.37 (m, 2H), 4.48 (s, 2H), 3.39 (t, J = 6.7 Hz, 2H), 1.57 (m, 2H), 0.88 (t, J = 7.4 Hz, 3H); ^{13}C{^{1}H} NMR (101 MHz, $CDCl_3$) δ 144.5, 132.3, 127.7, 119.0, 111.2, 72.8, 71.9, 23.0, 10.7.

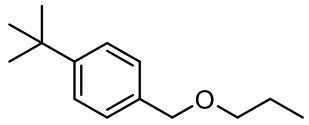

1-(*Tert*-butyl)-4-(propoxymethyl)benzene (**4.14**). Synthesised according to the general procedure from the corresponding alkene (0.0817 g, 0.40 mmol), hydrazine monohydrate (0.6 mL, 12.1 mmol, 30.25 equiv.), and TFA (0.55 mL, 7.18 mmol, 17.95 equiv.). After 30 F/mol, extraction with pentane and evaporation of solvent afforded the hydrogenated product as a colourless oil (0.0823 g, 100% yield). ^{1}H NMR (400 MHz, $CDCl_3$) δ 7.41 (m, 2H), 7.32 (m, 2H), 4.52 (s, 2H), 3.48 (t, J = 6.7 Hz, 2H), 1.68 (m, 2H), 1.36 (s, 9H), 0.99 (t, J = 7.4 Hz, 3H); ^{13}C{^{1}H} NMR (101 MHz, $CDCl_3$) δ 149.9, 135.2, 127.0, 124.8, 72.2, 17.7, 34.0, 30.9, 22.5, 10.2.

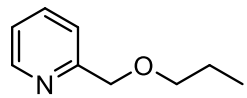

2-(Propoxymethyl)pyridine (**4.15**). Synthesised according to the general procedure from the corresponding alkene (0.0597 g, 0.40 mmol), hydrazine monohydrate (0.33 mL, 6.66 mmol, 16.65 equiv.), and TFA (0.37 mL, 4.83 mmol, 12.075 equiv.). After 24 F/mol, extraction with pentane and evaporation of solvent afforded the hydrogenated product as a yellow oil (0.0490 g, 81%). ^{1}H NMR (400 MHz, $CDCl_3$) δ 8.51 (brd, J = Hz, 1H), 7.68 (td, J = 7.7, 1.8 Hz, 1H), 7.44 (m, 1H), 7.16 (m, 1H), 4.61 (s, 2H), 3.50 (t, J = 6.7 Hz, 2H), 1.65 (m, 2H), 0.94 (t, J = 7.4 Hz, 3H); ^{13}C{^{1}H} NMR (101 MHz, $CDCl_3$) δ 158.9, 148.9, 136.9, 122.4, 121.5, 73.6, 72.9, 23.0, 10.7; HRMS (ESI) *m/z*: calcd $[M + H]^+$ for $C_9H_{14}NO^+$ 152.1070; found $[M + H]^+$ 152.1082.

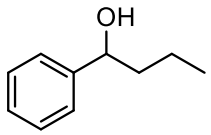

1-Phenylbutan-1-ol (**4.16**). Synthesised according to the general procedure from the corresponding alkene (0.0593 g, 0.40 mmol), hydrazine monohydrate (0.165 mL, 3.4 mmol, 8.5 equiv.), and TFA (0.184 mL, 2.4 mmol, 6 equiv.). After 12 F/mol, extraction with pentane and evaporation of solvent afforded the hydrogenated product as a colourless oil (0.0547 g, 91% yield). ^{1}H NMR (400 MHz, $CDCl_3$) δ 7.27–7.18 (m, 5H), 4.60–4.56 (m, 1H), 2.02 (s, 1H), 1.76–1.55 (m, 2H), 1.40–1.20 (m, 2H), 0.86 (t, J = 7.41 Hz, 3H); ^{13}C {^{1}H} NMR (101 MHz, $CDCl_3$) δ 145.0, 128.5, 127.6, 126.0, 74.5, 41.3, 19.1, 14.1.

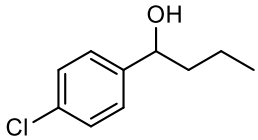

1-(4-Chlorophenyl)butan-1-ol (**4.17**). Synthesised according to the general procedure from the corresponding alkene (0.0731 g, 0.40 mmol), hydrazine monohydrate (0.165 mL, 3.4 mmol, 8.5 equiv.), and TFA (0.184 mL, 2.4 mmol, 6 equiv.). After 12 F/mol, extraction with pentane and evaporation of solvent afforded the hydrogenated product as a colourless oil (0.0657 g, 89% yield). ^{1}H NMR (400 MHz, $CDCl_3$) δ 7.28–7.25 (m, 2H), 7.24–7.21 (m, 2H), 4.62–4.58 (m, 1H), 2.13 (s, 1H), 1.75–1.55 (m, 2H), 1.42–1.20 (m, 2H), 0.89 (t, J = 7.36 Hz, 3H); ^{13}C {^{1}H} NMR (101 MHz, $CDCl_3$) δ 143.5, 133.1, 128.6, 127.4, 73.8, 41.3, 19.0, 14.0.

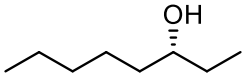

(*R*)-Octan-3-ol (**4.18**). Synthesised according to the general procedure from the corresponding alkene (0.0513 g, 0.40 mmol), hydrazine monohydrate (0.194 mL,

4.0 mmol, 10 equiv.), and TFA (0.184 mL, 3.4 mmol, 6 equiv.). After 15 F/mol, extraction with pentane and evaporation of solvent afforded the hydrogenated product as a colourless liquid (0.0509 g, 100% yield). ^{1}H NMR (400 MHz, $CDCl_3$) δ 3.52 (m, 1H), 1.55–1.26 (m, 11H), 0.95–0.87 (m, 6H); $^{13}C\{^{1}H\}$ NMR (101 MHz, $CDCl_3$) δ 73.4, 37.0, 32.0, 30.2, 25.4, 22.7, 14.1, 10.0.

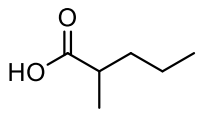

2-Methylpentanoic acid (**4.19**). Synthesised according to the general procedure from the corresponding alkene (0.0457 g, 0.40 mmol), hydrazine monohydrate (0.340 mL, 7.0 mmol, 17.5 equiv.), and TFA (0.387 mL, 5.0 mmol, 12.4 equiv.). After 30 F/mol, extraction with Et_2O and evaporation of solvent afforded the hydrogenated product as a pale-yellow liquid (0.0460 g, 99%). ^{1}H NMR (400 MHz, $CDCl_3$) δ 11.32 (brs, -COO*H*), 2.51–2.43 (m, 1H), 1.71–1.63 (m, 1H), 1.46–1.32 (m, 3H), 1.17 (d, J = 7.0 Hz, 3H), 0.91 (t, J = 7.2 Hz, 3H); $^{13}C\{^{1}H\}$ NMR (101 MHz, $CDCl_3$) δ 183.9, 39.3, 35.7, 20.4, 16.8, 13.9.

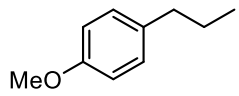

1-Methoxy-4-propylbenzene (**4.20**). Synthesised according to the general procedure from the corresponding alkene (0.0593 g, 0.40 mmol), hydrazine monohydrate (0.536 mL, 11 mmol, 27.5 equiv.), and TFA (0.594 mL, 7.76 mmol, 19.4 equiv.). After 40 F/mol, extraction with pentane and evaporation of solvent afforded the hydrogenated product as a colourless liquid (0.0565 g, 94% yield). ^{1}H NMR (400 MHz, $CDCl_3$) δ 7.11–7.09 (m, 2H), 6.85–6.82 (m, 2H), 3.79 (s, 3H), 2.55–2.52 (m, 2H), 1.66–1.57 (m, 2H), 0.94 (t, J = 7.18 Hz, 3H); $^{13}C\{^{1}H\}$ NMR (101 MHz, $CDCl_3$) δ 157.7, 134.9, 129.4, 113.7, 55.4, 37.3, 24.9, 13.9.

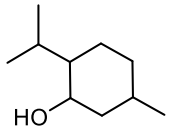

2-isopropyl-5-methylcyclohexan-1-ol (**4.21**). Synthesised according to the general procedure from the corresponding alkene (0.0617 g, 0.40 mmol, mixture of isomers), hydrazine monohydrate (2.40 mL, 49.2 mmol, 123 equiv.), and TFA (2.03 mL, 26.5 mmol, 66.3 equiv.). After 241 F/mol, extraction with pentane and evaporation of solvent afforded the hydrogenated product as a white solid (0.0456 g, 73% yield). Characterisation data are in agreement with literature reports.[18]

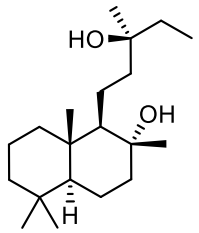

(1*R*,2*R*,4*aS*,8*aS*)-1-((*S*)-3-Hydroxy-3-methylpentyl)-2,5,5,8a-tetramethyldecahydro naphthalen-2-ol (**4.22**). Synthesised according to the general procedure from the corresponding alkene (0.1234 g, 0.40 mmol), hydrazine monohydrate (1.116 mL, 22.9 mmol, 57.25 equiv.), and TFA (1.237 mL, 16.16 mmol, 40.4 equiv.). After 82 F/mol, extraction with pentane and evaporation of solvent afforded the hydrogenated product as a colourless liquid (0.1105 g, 89% yield). ^{1}H NMR (400 MHz, $CDCl_3$) δ 1.86–1.82 (m, 1H), 1.67–1.57 (m, 4H), 1.54–1.41 (m, 6H), 1.38–1.31 (m, 2H), 1.27–1.25 (m, 1H), 1.17 (s, 3H), 1.15 (s, 3H), 1.14–1.11 (m, 2H), 1.00–0.92 (m, 2H), 0.89 (t, J = 7.72 Hz, 3H), 0.86 (s, 3H), 0.78 (d, J = 3.93 Hz, 6H); ^{13}C {^{1}H} NMR (101 MHz, $CDCl_3$) δ 74.9, 73.6, 62.1, 56.2, 44.5, 44.3, 42.1, 39.8, 39.4, 35.4, 33.5, 33.4, 25.8, 24.5, 21.6, 20.7, 19.0, 18.6, 15.5, 8.4; HRMS (ESI) *m/z*: calcd $[M + H]^+$ for $C_{20}H_{39}O_2^+$ 311.2945; found $[M + H]^+$ 311.2948.

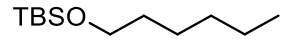

Tert-butyl(hexyloxy)dimethylsilane (**4.23**). Synthesised according to the general procedure from the corresponding alkene (0.0858 g, 0.40 mmol) and hydrazine monohydrate (0.184 mL, 3.8 mmol, 9.5 equiv.). After 19 F/mol, extraction with pentane and evaporation of solvent afforded the hydrogenated product as a colourless liquid (0.0771 g, 89% yield). ^{1}H NMR (500 MHz, $CDCl_3$) δ 3.60 (t, J = 6.7 Hz, 2H), 1.54–1.48 (m, 2H), 1.35–1.24 (m, 6H), 0.90–0.87 (m, 12H), 0.05 (s, 6H); ^{13}C{^{1}H} NMR (126 MHz, $CDCl_3$) δ 63.5, 33.0, 31.8, 26.1, 25.6, 22.8, 18.5, 14.2, -5.2.

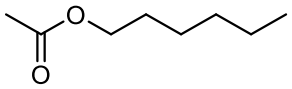

Hexyl acetate (**4.24**). Synthesised according to the general procedure from the corresponding alkene (0.0569 g, 0.40 mmol), hydrazine monohydrate (0.165 mL, 3.4 mmol, 8.5 equiv.), and TFA (0.184 mL, 3.4 mmol, 6 equiv.). After 17 F/mol, extraction with pentane and evaporation of solvent afforded the hydrogenated product as a colourless liquid (0.0467 g, 81% yield). ^{1}H NMR (400 MHz, $CDCl_3$) δ 4.04 (t, J = 6.8 Hz, 2H), 2.03 (s, 3H), 1.64–1.57 (m, 2H), 1.37–1.24 (m, 6H), 0.88 (t, J = 6.8 Hz, 3H); ^{13}C{^{1}H} NMR (101 MHz, $CDCl_3$) δ 171.4, 64.7, 31.5, 28.6, 25.7, 22.6, 21.1, 14.1.

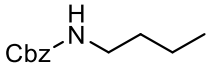

Benzyl butylcarbamate (**4.25**). Synthesised according to the general procedure from the corresponding alkene (0.0821 g, 0.40 mmol), hydrazine monohydrate (0.185 mL, 3.8 mmol, 9.5 equiv.), and TFA (0.184 mL, 3.4 mmol, 6 equiv.). After 14 F/mol, extraction with Et_2O and evaporation of solvent afforded the hydrogenated product as a colourless liquid (0.0754 g, 91% yield). ^{1}H NMR (400 MHz, $CDCl_3$) δ 7.42–7.29 (m, 5H), 5.09 (s, 2H), 4.78 (brs, -N*H*), 3.19 (q, J = 6.7 Hz, 2H), 1.52–

1.44 (m, 2H), 1.39–1.29 (m, 2H), 0.92 (t, J = 7.3 Hz, 3H); $^{13}C\{^{1}H\}$ NMR (101 MHz, $CDCl_3$) δ 156.5, 136.8, 128.6, 128.2, 128.2, 66.7, 40.9, 32.1, 20.0, 13.8.

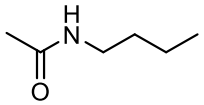

N-Butylacetamide (**4.26**). Synthesised according to the general procedure from the corresponding alkene (0.0453 g, 0.40 mmol), hydrazine monohydrate (0.300 mL, 6.2 mmol, 15.5 equiv.), and TFA (0.184 mL, 3.4 mmol, 6 equiv.). After 26 F/mol, extraction with Et_2O, purification by flash column chromatography (40% EtOAc in *n*-hexane → 90% EtOAc in *n*-hexane) and evaporation of solvent afforded the hydrogenated product as a colourless liquid (0.0263 g, 57% yield). ^{1}H NMR (400 MHz, $CDCl_3$) δ 5.65 (brs, -N*H*), 3.24–3.19 (m, 2H), 1.96 (s, 3H), 1.50–1.43 (m, 2H), 1.37–1.28 (m, 2H), 0.90 (t, J = 7.3 Hz, 3H); $^{13}C\{^{1}H\}$ NMR (101 MHz, $CDCl_3$) δ 170.2, 39.5, 31.7, 23.4, 20.1, 13.8.

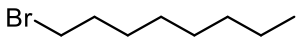

1-Bromooctane (**4.27**). Synthesised according to the general procedure from the corresponding alkene (0.0764 g, 0.40 mmol), hydrazine monohydrate (0.387 mL, 7.93 mmol, 19.83 equiv.), and TFA (0.429 mL, 5.6 mmol, 14 equiv.). After 28 F/mol, extraction with pentane and evaporation of solvent afforded the hydrogenated product as a colourless oil (0.0533 g, 69% yield). ^{1}H NMR (400 MHz, $CDCl_3$) δ 3.40 (t, J = 6.86 Hz, 2H), 1.88–1.82 (m, 2H). 1.45–1.39 (m, 2H), 1.31–1.24 (m, 8H), 0.88 (t, J = 6.94 Hz, 3H); ^{13}C $\{^{1}H\}$ NMR (101 MHz, $CDCl_3$) δ 34.2, 33.0, 31.9, 29.2, 28.9, 28.3, 22.8, 14.2.

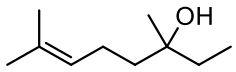

3,7-Dimethyloct-6-en-3-ol (**4.28**). Synthesised according to the general procedure from the corresponding alkene (0.0617 g, 0.40 mmol) and hydrazine monohydrate

(0.311 mL, 6.4 mmol, 16.0 equiv.). After 27 F/mol, extraction with Et_2O and evaporation of solvent afforded the hydrogenated product as a colourless liquid (0.0613 g, 98% yield). ^{1}H NMR (500 MHz, $CDCl_3$) δ 5.11 (m, 1H), 2.04–1.99 (m, 2H), 1.67 (d, J = 1.4 Hz, 3H), 1.61 (s, 3H), 1.51–1.44 (m, 4H), 1.34 (brs, -O*H*), 1.14 (s, 3H), 0.88 (t, J = 7.5 Hz, 3H); ^{13}C{^{1}H} NMR (126 MHz, $CDCl_3$) δ 131.7, 124.6, 73.0, 41.2, 34.4, 26.3, 25.8, 22.7, 17.7, 8.3.

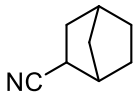

Bicyclo[2.2.1]heptane-2-carbonitrile (**4.29**). Synthesised according to the general procedure from the corresponding alkene (0.0477 g, 0.40 mmol, mixture of isomers), hydrazine monohydrate (0.165 mL, 3.4 mmol, 8.5 equiv.), and TFA (0.184 mL, 2.4 mmol, 6 equiv.). After 12 F/mol, extraction with pentane and evaporation of solvent afforded the hydrogenated product as a colourless oil (0.0422 g, 87% yield). Characterisation data are in agreement with literature reports.[19]

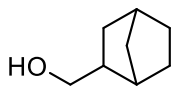

Bicyclo[2.2.1]heptan-2-ylmethanol (**4.30**). Synthesised according to the general procedure from the corresponding alkene (0.0497 g, 0.40 mmol, mixture of isomers), hydrazine monohydrate (0.165 mL, 3.4 mmol, 8.5 equiv.), and TFA (0.184 mL, 3.4 mmol, 6 equiv.). After 17 F/mol, extraction with pentane and evaporation of solvent afforded the hydrogenated product as a colourless liquid (0.0429 g, 85% yield). ^{1}H NMR (400 MHz, $CDCl_3$, mixture of *endo* and *exo* isomers) δ 3.63–3.30 (m, 2H), 2.26–1.99 (m, 2.2H), 1.71–1.44 (m, 3.7H), 1.37–0.90 (m, 5.7H), 0.63–0.57 (m, 0.5H); ^{13}C{^{1}H} NMR (101 MHz, $CDCl_3$, mixture of *endo* and *exo* isomers) δ 67.0, 65.2, 44.9, 42.5, 39.9, 38.1, 37.8, 36.7, 36.2, 35.2, 34.1, 33.7, 30.0, 29.9, 29.0, 22.6.

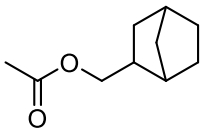

Bicyclo[2.2.1]heptan-2-ylmethyl acetate (**4.31**). Synthesised according to the general procedure from the corresponding alkene (0.0665 g, 0.40 mmol, mixture of isomers), hydrazine monohydrate (0.165 mL, 3.4 mmol, 8.5 equiv.), and TFA (0.184 mL, 3.4 mmol, 6 equiv.). After 17 F/mol, extraction with pentane and evaporation of solvent afforded the hydrogenated product as a colourless liquid (0.0451 g, 67% yield). ^{1}H NMR (400 MHz, $CDCl_3$, mixture of *endo* and *exo* isomers) δ 4.12–3.78 (m, 2H), 2.23–2.10 (m, 2.5H), 2.05–2.04 (m, 3H), 1.81–1.67 (m, 1.3H), 1.58–0.99 (m, 7.7H), 0.71–0.65 (m, 0.6H); ^{13}C{^{1}H} NMR (101 MHz, $CDCl_3$, mixture of *endo* and *exo* isomers) δ 170.7, 170.7, 67.3, 65.9, 40.3, 39.1, 38.0, 37.8, 37.7, 36.0, 35.5, 34.5, 33.40, 33.0, 29.2, 29.0, 28.2, 22.0, 20.4.

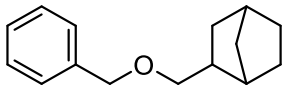

2-((Benzyloxy)methyl)bicyclo[2.2.1]heptane (**4.32**). Synthesised according to the general procedure from the corresponding alkene (0.0857 g, 0.40 mmol, mixture of isomers), hydrazine monohydrate (0.165 mL, 3.4 mmol, 8.5 equiv.), and TFA (0.184 mL, 3.4 mmol, 6 equiv.). After 16 F/mol, extraction with pentane and evaporation of solvent afforded the hydrogenated product as a colourless liquid (0.0692 g, 80% yield). ^{1}H NMR (400 MHz, $CDCl_3$, mixture of *endo* and *exo* isomers) δ 7.39–7.26 (m, 5H), 4.58–4.50 (m, 2H), 3.47–3.17 (m, 2H), 2.32–2.28 (m, 0.5H), 2.23–2.13 (m, 1.8H), 1.84–1.67 (m, 1H), 1.57–0.98 (m, 7.3H), 0.67–0.62 (m, 0.5H); ^{13}C{^{1}H} NMR (101 MHz, $CDCl_3$, mixture of *endo* and *exo* isomers) δ 138.5, 138.5, 128.0, 127.3, 127.2, 74.3, 72.7, 72.6, 72.3, 41.7, 39.5, 39.5, 38.3, 38.2, 36.4, 35.9, 34.9, 34.1, 33.7, 29.6, 29.5, 28.7, 22.4.

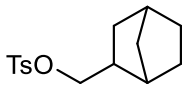

Bicyclo[2.2.1]heptan-2-ylmethyl 4-methylbenzenesulfonate (**4.33**). Synthesised according to the general procedure from the corresponding alkene (0.1113 g, 0.40 mmol, mixture of isomers), hydrazine monohydrate (0.330 mL, 6.80 mmol, 17 equiv.), and TFA (0.368 mL, 4.80 mmol, 12 equiv.). After 24 F/mol, extraction with pentane and evaporation of solvent afforded the hydrogenated product as a colourless oil (0.0897 g, 80% yield). ^{1}H NMR (400 MHz, $CDCl_3$, mixture of *endo* and *exo* isomers) δ 7.80 (dd, J_a = 8.3, J_b = 3.3 Hz, 2H), 7.35 (d, J = 8.4 Hz, 2H), 4.03 (dd, J_a = 9.5, J_b = 6.8 Hz, 0.5H), 3.90 (t, J = 9.5 Hz, 0.5H), 3.79–3.65 (m, 1H), 2.45 (s, 3H), 2.24 (s, 0.5H), 2.20–2.15 (m, 1.5H), 2.10 (s, 0.5H), 1.82–1.74 (m, 0.5H), 1.70–1.62 (m, 0.5H), 1.54–1.43 (m, 1.5H), 1.39–1,21 (m, 3.5H), 1.18–1.05 (m, 2H), 1.03–0.90 (m, 1H), 0.57 (ddd, J_a = 12.5, J_b = 5.32, J_c = 2.2 Hz, 0.5H); ^{13}C{^{1}H} NMR (101 MHz, $CDCl_3$, mixture of *endo* and *exo* isomers) δ 144.0, 132.6, 129.2, 127.3, 127.2, 72.8, 71.8, 40.4, 39.0, 38.2, 37.5, 37.4, 35.9, 35.5, 34.4, 33.0, 32.6, 29.0, 28.8, 28.0, 21.7, 21.0; HRMS (ESI) *m/z*: calcd $[M + NH_4]^+$ for $C_{15}H_{24}NO_3S^+$ 298.1471; found $[M + NH_4]^+$ 298.1479.

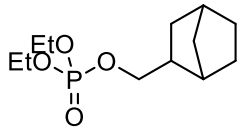

Bicyclo[2.2.1]heptan-2-ylmethyl diethyl phosphate (**4.34**). Synthesised according to the general procedure from the corresponding alkene (0.1041 g, 0.40 mmol, mixture of isomers), hydrazine monohydrate (0.33 mL, 6.66 mmol, 16.6 equiv.), and TFA (0.37 mL, 4.83 mmol, 12.08 equiv.). After 24 F/mol, extraction with pentane and evaporation of solvent afforded the hydrogenated product as a pale-yellow oil (0.0866 g, 83% yield). ^{1}H NMR (400 MHz, $CDCl_3$, mixture of *endo* and *exo* isomers) δ 4.07 (m, 4H), 4.00 (m, 0.5H), 3.88 (m, 0.5H), 3.70 (m, 1H), 2.25 (m, 0.5H), 2.17 (m, 2H), 1.78 (m, 0.5H), 1.66 (m, 0.5H), 1.53–1.41 (m, 2H), 1.29

(dt, J_a = 7.1, J_b = 0.94 Hz, 6H), 1.25–0.93 (m, 3H), 0.62 (ddd, J_a = 12.4, J_b = 5.4, J_c = 2.2 Hz, 0.5H); $^{13}C\{^1H\}$ NMR (101 MHz, $CDCl_3$, mixture of *endo* and *exo* isomers) δ 70.8 (d, J_{C-P} = 6 Hz), 69.7 (d, J_{C-P} = 6 Hz), 64.0 (d, J_{C-P} = 6 Hz), 42.4 (d, J_{C-P} = 6 Hz), 40.2 (d, J_{C-P} = 7 Hz), 39.7, 38.1, 38.1, 36.7, 36.2, 35.1, 33.6, 33.2, 29.8, 29.6, 28.8, 22.5, 16.1 (d, J_{C-P} = 7 Hz); $^{31}P\{^1H\}$ NMR (162 MHz, $CDCl_3$) δ −0.99 (s); HRMS (ESI) *m/z:* calcd $[M + H]^+$ for $C_{12}H_{24}O_4P^+$ 263.1407; found $[M + H]^+$ 263.1404.

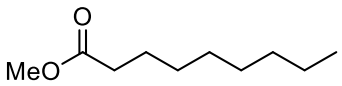

Methyl nonanoate (**4.35**). Synthesised according to the general procedure from the corresponding alkene (0.0681 g, 0.40 mmol), hydrazine monohydrate (0.302 mL, 6.2 mmol, 15.5 equiv.), and TFA (0.334 mL, 4.36 mmol, 10.9 equiv.). After 23 F/mol, extraction with pentane and evaporation of solvent afforded the hydrogenated product as a colourless liquid (0.0338 g, 49% yield). ^1H NMR (400 MHz, $CDCl_3$) δ 3.66 (s, 3H), 2.29 (t, J = 7.41 Hz, 2H), 1.65–1.57 (m, 2H), 1.29–1.24 (m, 10H), 0.87 (t, J = 6.96 Hz, 3H); $^{13}C\{^1H\}$ NMR (101 MHz, $CDCl_3$) δ 174.6, 51.6, 34.2, 31.9, 29.3, 29.2, 25.1, 22.8, 14.2.

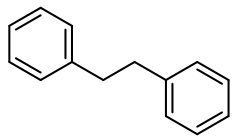

1,2-Diphenylethane (**4.36**). Synthesised according to the general procedure from the corresponding alkene (0.0721 g, 0.40 mmol), hydrazine monohydrate (0.497 mL, 10.2 mmol, 25.5 equiv.), and TFA (0.551 mL, 7.2 mmol, 18 equiv.). After 40 F/mol, extraction with pentane and evaporation of solvent afforded the hydrogenated product as a colourless liquid (0.0728 g, 100% yield). ^1H NMR (400 MHz, $CDCl_3$) δ 7.31–7.26 (m, 5H), 7.22–7.18 (m, 5H), 2.92 (s, 4H); $^{13}C\{^1H\}$ NMR (101 MHz, $CDCl_3$) δ 141.9, 128.6, 128.5, 126.1, 38.1.

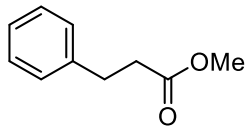

Methyl 3-phenylpropanoate (**4.37**). Synthesised according to the general procedure from the corresponding alkene (0.0649 g, 0.40 mmol), hydrazine monohydrate (0.604 mL, 12.4 mmol, 31 equiv.), and TFA (0.673 mL, 8.8 mmol, 22 equiv.). After 48 F/mol, extraction with pentane and evaporation of solvent afforded the hydrogenated product as a colourless liquid (0.0328 g, 50% yield). ^{1}H NMR (400 MHz, $CDCl_3$) δ 7.31–7.28 (m, 2H), 7.23–7.19 (m, 2H), 3.68 (s, 3H), 2.96 (t, J = 7.44 Hz, 2H), 2.64 (t, J = 8.03 Hz, 2H); ^{13}C {^{1}H} NMR (101 MHz, $CDCl_3$) δ 173.5, 140.7, 128.7, 128.4, 126.4, 51.8, 35.8, 31.1.

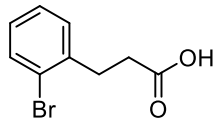

3-(2-Bromophenyl)propanoic acid (**4.38**). Synthesised according to the general procedure from the corresponding alkene (0.0908 g, 0.40 mmol), hydrazine monohydrate (1.184 mL, 24.4 mmol, 61 equiv.), and TFA (1.318 mL, 17.2 mmol, 43 equiv.). After 86 F/mol, extraction with pentane and evaporation of solvent afforded the hydrogenated product as a colourless liquid (0.0779 g, 85% yield). ^{1}H NMR (400 MHz, $CDCl_3$) δ 7.55–7.52 (m, 1H), 7.25–7.21 (m, 2H), 7.09–7.06 (m, 1H), 3.07 (t, J = 7.57 Hz, 2H), 2.66 (t, J = 8.13 Hz, 2H); ^{13}C {^{1}H} NMR (101 MHz, $CDCl_3$) δ 173.2, 139.9, 133.1, 130.6, 128.3, 127.7, 124.5, 34.1, 31.6.

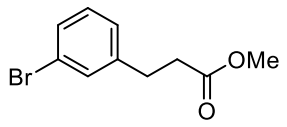

Methyl 3-(3-bromophenyl)propanoate (**4.39**). Synthesised according to the general procedure from the corresponding alkene (0.0964 g, 0.40 mmol), hydrazine monohydrate (1.116 mL, 22.9 mmol, 57.3 equiv.), and TFA (1.237 mL, 16.16

mmol, 40.4 equiv.). After 82 F/mol, extraction with pentane and evaporation of solvent afforded the hydrogenated product as a colourless liquid (0.0710 g, 73% yield). ^{1}H NMR (400 MHz, $CDCl_3$) δ 7.35–7.31 (m, 2H), 7.17–7.10 (m, 2H), 3.66 (s, 3H), 2.91 (t, J = 7.42 Hz, 2H), 2.63–2.59 (m, 2H); ^{13}C {^{1}H} NMR (101 MHz, $CDCl_3$) δ 173.1, 142.9, 131.5, 130.2, 129.6, 127.1, 122.7, 51.9, 35.5, 30.6.

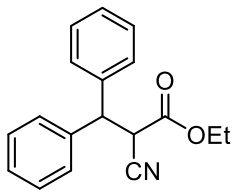

Ethyl 2-cyano-3,3-diphenylpropanoate (**4.40**). Synthesised according to the general procedure from the corresponding alkene (0.1109 g, 0.40 mmol), hydrazine monohydrate (0.166 mL, 3.4 mmol, 8.5 equiv.), and TFA (0.184 mL, 2.4 mmol, 6 equiv.). After 14 F/mol, extraction with pentane and evaporation of solvent afforded the hydrogenated product as a colourless liquid (0.0782 g, 70% yield). ^{1}H NMR (400 MHz, $CDCl_3$) δ 7.32–7.16 (m, 10H), 4.65 (d, J = 8.68 Hz, 1H), 4.15 (d, J = 8.55 Hz, 1H), 4.05–3.99 (m, 2H), 1.01 (t, J = 7.16 Hz, 3H); ^{13}C {^{1}H} NMR (101 MHz, $CDCl_3$) δ 165.2, 139.4, 138.8, 129.0, 129.0, 128.3, 128.0, 127.9, 127.8, 115.9, 63.0, 51.2, 43.7, 13.8.

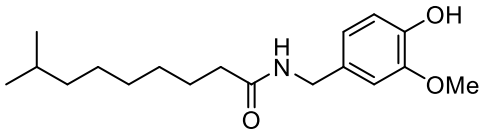

N-(4-hydroxy-3-methoxybenzyl)-8-methylnonanamide (**4.41**). Synthesised according to the general procedure from the corresponding alkene (0.1222 g, 0.40 mmol) and hydrazine monohydrate (0.826 mL, 17.0 mmol, 42.5 equiv.). After 80 F/mol, extraction with Et_2O, purification by flash column chromatography (100% DCM → 10% MeOH in DCM) and evaporation of solvent afforded the hydrogenated product as a yellow solid (0.0455 g, 37% yield). ^{1}H NMR (400 MHz,

$CDCl_3$) δ 6.79 (d, J = 8.0 Hz, 1H), 6.74 (d, J = 2.0 Hz, 1H), 6.70 (dd, J_a = 8.0 Hz, J_b = 2.0 Hz, 1H), 5.62 (brs, -N*H*), 4.29 (d, J = 5.6 Hz, 2H), 3.81 (s, 3H), 2.13 (t, J = 7.6 Hz, 2H), 1.62–1.54 (m, 2H), 1.49–1.39 (m, 1H), 1.29–1.18 (m, 6H), 1.10–1.04 (m, 2H), 0.79 (d, J = 6.6 Hz, 6H); $^{13}C\{^1H\}$ NMR (101 MHz, $CDCl_3$) δ 173.0, 146.8, 145.2, 130.5, 120.89, 114.5, 110.8, 56.0, 43.6, 39.0, 37.0, 29.7, 29.4, 28.0, 27.3, 25.9, 22.7.

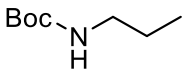

Tert-butyl propylcarbamate (**4.42**). Synthesised according to the general procedure from the corresponding alkyne (0.0621 g, 0.40 mmol) and hydrazine monohydrate (0.300 mL, 6.2 mmol, 15.5 equiv.). After 26 F/mol, extraction with Et_2O and evaporation of solvent afforded the hydrogenated product as a colourless liquid (0.0446 g, 70% yield). ^1H NMR (400 MHz, $CDCl_3$) δ 4.54 (brs, -N*H*), 3.06 (t, J = 7.1 Hz, 2H), 1.52–1.43 (m, 12H), 0.89 (t, J = 7.4 Hz, 3H); $^{13}C\{^1H\}$ NMR (101 MHz, $CDCl_3$) δ 156.1, 79.1, 42.4, 28.5, 23.4, 11.3.

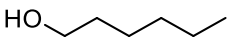

Hexan-1-ol (**4.43**). Synthesised according to the general procedure from the corresponding alkyne (0.0393 g, 0.40 mmol), hydrazine monohydrate (0.991 mL, 20.4 mmol, 51 equiv.), and TFA (0.740 mL, 9.4 mmol, 23.6 equiv.). After 97 F/mol, extraction with pentane and evaporation of solvent afforded the hydrogenated product as a colourless liquid (0.0396 g, 97% yield). ^1H NMR (500 MHz, $CDCl_3$) δ 3.58 (t, J = 6.7 Hz, 2H), 2.34–2.29 (m, -O*H*), 1.55–1.49 (m, 2H), 1.34–1.22 (m, 6H), 0.96–0.76 (m, 3H); $^{13}C\{^1H\}$ NMR (126 MHz, $CDCl_3$) δ 63.0, 32.8, 31.7, 25.5, 22.7, 14.1.

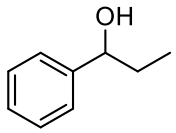

1-Phenylpropan-1-ol (**4.44**). Synthesised according to the general procedure from the corresponding alkyne (0.0529 g, 0.40 mmol), hydrazine monohydrate (0.486 mL, 10.0 mmol, 25 equiv.), and TFA (0.355 mL, 4.6 mmol, 11.6 equiv.). After 45 F/mol, extraction with Et_2O and evaporation of solvent afforded the hydrogenated product as a colourless liquid (0.0490 g, 90% yield). ^{1}H NMR (400 MHz, $CDCl_3$) δ 7.38–7.21(m, 5H), 4.60 (t, J = 6.6 Hz, 1H), 1.94 (brs, -O*H*), 1.89–1.70 (m, 2H), 0.92 (t, J = 7.4 Hz, 3H); ^{13}C{^{1}H} NMR (101 MHz, $CDCl_3$) δ 144.7, 128.5, 127.6, 126.1, 76.1, 32.0, 10.3.

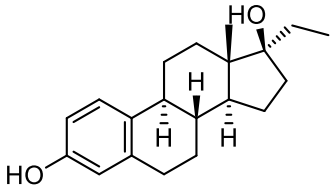

(8*R*,9*S*,13*S*,14*S*,17*S*)-17-Ethyl-13-methyl-7,8,9,11,12,13,14,15,16,17-decahydro-6*H*-cyclopenta[*a*]phenanthrene-3,17-diol (**4.45**). Synthesised according to the general procedure from the corresponding alkyne (0.1186 g, 0.40 mmol), hydrazine monohydrate (0.690 mL, 14.2 mmol, 35.5 equiv.), and TFA (0. 285 mL, 3.7 mmol, 9.3 equiv.). After 66 F/mol, extraction with Et_2O and evaporation of solvent afforded the hydrogenated product as a white solid (0.0973 g, 81% yield). ^{1}H NMR (400 MHz, DMSO-d_6,) δ 8.96 (s, -O*H* phenol), 7.03 (d, J = 8.4 Hz, 1H), 6.49 (dd, J_a = 8.4, J_b = 2.7 Hz, 1H), 6.42 (d, J = 2.7 Hz, 1H), 3.78 (brs, -O*H*), 2.77–2.63 (m, 2H), 2.26–2.19 (m, 1H), 2.07–1.99 (m, 1H), 1.82–1.73 (m, 2H), 1.55–1.16 (m, 11H), 0.90 (t, J = 7.2 Hz, 3H), 0.79 (s, 3H); ^{13}C{^{1}H} NMR (101 MHz, DMSO-d_6) δ 155.6, 137.9, 131.2, 126.7, 115.6, 113.4, 82.5, 49.8, 47.1, 44.1, 33.2, 32.0, 29.9, 29.1, 27.9, 26.9, 23.8, 15.4, 8.8.

General procedure for the electrochemical hydrogenation of nitro compounds

A 5 mL IKA Electrasyn electrochemical vial was charged with the nitro-compound (0.40 mmol), hydrazine monohydrate (mmol and equiv. as specified for each substrate), and MeOH (5 mL). The resulting mixture was electrolysed at a constant current of 10 mA until complete conversion of the starting material, as monitored by GC-MS or HPLC-MS. Upon completion, the crude reaction mixture was poured into water (30 mL) and extracted with EtOAc (3 x 20 mL). The combined organic extracts were dried over $MgSO_4$, filtered and the solvent was removed under vacuum to afford the desired amine product.

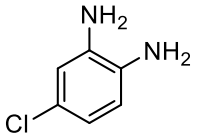

4-Chlorobenzene-1,2-diamine (**4.46**). Synthesised according to the general procedure from 5-chloro-2-nitroaniline (0.0690 mg, 0.40 mmol) and hydrazine monohydrate (0.165 mL, 3.4 mmol, 8.5 equiv.). After 6 F/mol, extraction with EtOAc and evaporation of solvent afforded the reduced product as a yellow solid (0.051 g, 90% yield). ^{1}H NMR (400 MHz, DMSO-d_6) δ 6.51 (d, J = 2.4 Hz, 1H), 6.46 (d, J = 8.2 Hz, 1H), 6.35 (dd, J_a = 8.2 Hz, J_b = 2.4 Hz, 1H), 4.73 (s, 2H), 4.54 (s, 2H); ^{13}C {^{1}H} NMR (101 MHz, DMSO-d_6) δ 137.2, 134.4, 120.8, 128.1, 116.6, 115.5, 113.8.

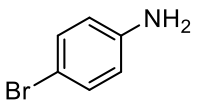

4-Bromoaniline (**4.47**). Synthesised according to the general procedure from 1-bromo-4-nitrobenzene (0.0808 g, 0.40 mmol) and hydrazine monohydrate (0.330 mL, 6.8 mmol, 17.0 equiv.). After 12 F/mol, extraction with EtOAc, purification by flash column chromatography (100% *n*-hexane → 30% EtOAc in *n*-hexane), and

evaporation of solvent afforded the reduced product as a brown solid (0.021 g, 31% yield). ^{1}H NMR (400 MHz, $CDCl_3$) δ 7.23 (d, J = 7.0 Hz, 2H), 7.56 (d, J = 7.0 Hz, 2H), 3.61 (brs, 2H); $^{13}C\{^{1}H\}$ NMR (101 MHz, $CDCl_3$) δ 145.5, 132.1, 116.81, 110.3.

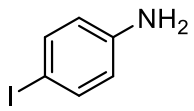

4-Iodoaniline (**4.48**). Synthesised according to the general procedure from 1-iodo-4-nitrobenzene (0.0996 g, 0.40 mmol) and hydrazine monohydrate (0.165 mL, 3.4 mmol, 8.5 equiv.). After 5 F/mol, extraction with EtOAc, purification by flash column chromatography (100% *n*-hexane → 30% EtOAc in *n*-hexane), and evaporation of solvent afforded the reduced product as a brown solid (0.0420 g, 48% yield). ^{1}H NMR (400 MHz, $CDCl_3$) δ 7.41 (d, J = 8.63 Hz, 2H), 6.47 (d, J = 8.63 Hz, 2H), 3.67 (brs, 2H); $^{13}C\{^{1}H\}$ NMR (101 MHz, $CDCl_3$) δ 146.2, 138.1, 117.4, 79.5.

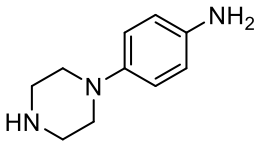

4-(Piperazin-1-yl)aniline (**4.49**). Synthesised according to the general procedure from 1-(4-nitrophenyl)piperazine (0.0831 g, 0.40 mmol) and hydrazine monohydrate (0.165 mL, 3.4 mmol, 8.5 equiv.). After 6 F/mol, extraction with EtOAc and evaporation of solvent afforded the reduced product as a brown solid (0.0710 g, 100% yield). ^{1}H NMR (400 MHz, DMSO-d_6) δ 6.67 (d, J = 8.8 Hz, 2H), 6.50 (d, J = 8.8 Hz, 2H), 4.49 (brs, 2H), 3.29 (brs, 1H), 2.81 (s, 8H); $^{13}C\{^{1}H\}$ NMR (101 MHz, DMSO-d_6) δ 143.8, 142.5, 118.5, 115.3, 52.2, 46.4.

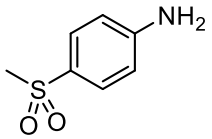

4-(Methylsulfonyl)aniline (**4.50**). Synthesised according to the general procedure from 1-(methylsulfonyl)-4-nitrobenzene (0.0805 mg, 0.40 mmol) and hydrazine monohydrate (0.165 mL, 3.4 mmol, 8.5 equiv.). After 6 F/mol, extraction with EtOAc, purification by flash column chromatography (100% EtOAc), and evaporation of solvent afforded the reduced product as a white solid (0.0500 g, 73% yield). ^{1}H NMR (400 MHz, $CDCl_3$) δ 7.67 (d, J = 8.7 Hz, 2H), 6.70 (d, J = 8.7 Hz, 2H), 4.29 (s, 2H), 3.00 (s, 3H); ^{13}C {^{1}H} NMR (101 MHz, $CDCl_3$) δ 151.6, 129.5, 128.7, 114.2, 45.1.

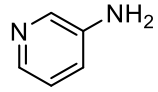

Pyridin-3-amine (**4.51**). Synthesised according to the general procedure from 3-nitropyridine (0.0496 g, 0.40 mmol) and hydrazine monohydrate (0.165 mL, 3.4 mmol, 8.5 equiv.). After 5 F/mol, extraction with EtOAc, purification by flash column chromatography (100% EtOAc) and evaporation of solvent afforded the reduced product as a colourless oil (0.0100 mg, 27% yield). ^{1}H NMR (400 MHz, DMSO-d_6) δ 7.94 (d, J = 2.5 Hz, 1H), 7.74 (dd, J_a = 4.7 Hz, J_b = 1.5 Hz, 1H), 7.02 (dd, J_a =4.6 Hz, J_b = = 8.1 Hz, 1H), 6.9 (ddd, J_a = 8.2 Hz, J_b = 2.8 Hz, J_c = 1.5 Hz, 1H), 5.27 (s, 2H); ^{13}C{^{1}H} NMR (101 MHz, DMSO- d_6) δ 145.4, 137.5, 136.9, 124.1, 120.2.

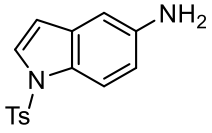

1-Tosyl-1*H*-indol-5-amine (**4.52**). Synthesised according to the general procedure from 5-nitro-1-tosyl-1H-indole (0.1265 g, 0.40 mmol) and hydrazine monohydrate

(0.165 mL, 3.4 mmol, 8.5 equiv.). After 6 F/mol, extraction with EtOAc, purification by flash column chromatography (100% DCM) and evaporation of solvent afforded the reduced product as a yellow/orange oil (0.0250 g, 22% yield). ^{1}H NMR (400 MHz, $CDCl_3$) δ 7.78 (d, J = 8.6 Hz, 1H), 7.71 (d, J = 8.6 Hz, 2H), 7.45 (d, J = 3.6 Hz, 1H), 7.19 (d, J = 7.4 Hz, 2H), 6.76 (d, J = 2.2 Hz, 1H), 6.70 (dd, J_a = 8.8 Hz, J_b = 2.3 Hz, 1H), 6.47 (dd, J_a = 3.7, J_b = 0.8 Hz, 1H), 3.61 (s, 2H), 2.32 (s, 3H); ^{13}C {^{1}H} NMR (101 MHz, $CDCl_3$) δ 144.7, 142.8, 135.4, 132.2, 129.8, 129.0, 127.1, 126.8, 114.5, 114.2, 109.0, 106.1, 21.6; HRMS (ESI) *m/z:* calcd $[M + H]^+$ for $C_{15}H_{15}N_2O_2S^+$ 287.0849; found $[M + H]^+$ 287.0864 .

General procedure for the electrochemical hydrogenation of azido compounds

A 5 mL IKA Electrasyn electrochemical vial was charged with the azido compound (0.40 mmol), hydrazine monohydrate (mmol and equiv. as specified for each substrate), and MeOH (5 mL). The resulting mixture was electrolysed at a constant current of 10 mA until complete conversion of the starting material, as monitored by GC-MS or HPLC-MS. Upon completion, the crude material was purified as described for each compound.

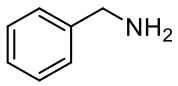

Phenylmethanamine (**4.53**). Synthesised according to the general procedure from the corresponding azide (0.5 M in DCM, 0.800 mL, 0.4 mmol) and hydrazine monohydrate (0.078 mL, 1.6 mmol, 4 equiv.). Upon completion of the reaction, after 6 F/mol, MeOH was removed under reduced pressure and the resultant yellowish oil was diluted with DCM (20 mL); 1.0 M aqueous HCl was added (20 mL) and the two phases separated; the organic layer was further washed with aqueous 1.0 M HCl (2 x 15 mL) before the combined aqueous phases were extracted with DCM (2 x 20 mL). The aqueous layer was then basified by slow

addition of 1.0 M aqueous NaOH (until pH ~ 12) and further extracted with DCM (3 x 30 mL). The combined organic extracts were dried over anhydrous $MgSO_4$, filtered, and concentrated in vacuo to afford the reduced product as a colourless liquid (0.027 g, 63% yield). ^{1}H NMR (400 MHz, $CDCl_3$) δ 7.36–7.23 (m, 5H), 3.87 (s, 2H), 1.52 (s, 2H); ^{13}C {^{1}H} NMR (101 MHz, $CDCl_3$) δ 142.9, 128.1, 126.6, 126.3, 46.0.

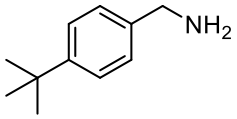

(4-(*Tert*-butyl)phenyl)methanamine (**4.54**). Synthesised according to the general procedure from the corresponding azide (0.0757 g, 0.4 mmol) and hydrazine monohydrate (0.165 mL, 3.4 mmol, 8.5 equiv.). Upon completion of the reaction, after 12 F/mol, the crude mixture was diluted with DCM (10 mL) and poured into H_2O (20 mL) followed by an extraction with DCM (3 x 10 mL). The combined organic extracts were dried over $MgSO_4$, filtered, then concentrated under reduced pressure to afford reduced product as a yellow oil (0.0590 g, 90% yield). ^{1}H NMR (400 MHz, $CDCl_3$) δ 7.40–7.34 (m, 2H), 7.28–7.23 (m, 2H), 3.84 (s, 2H), 1.70 (s, 2H), 1.32 (s, 9H); ^{13}C {^{1}H} NMR (101 MHz, $CDCl_3$) δ 149.7, 140.2, 126.8, 125.4, 46.1, 34.4, 31.4.

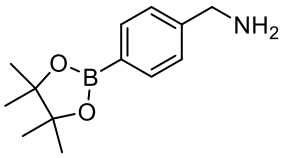

(4-(4,4,5,5-Tetramethyl-1,3,2-dioxaborolan-2-yl)phenyl)methanamine (**4.55**). Synthesised according to the general procedure from the corresponding azide (0.1040 mg, 0.4 mmol) and hydrazine monohydrate (0.120 mL, 2.4 mmol, 6 equiv.). Upon completion of the reaction, after 6 F/mol, the crude mixture was diluted with DCM (10 mL) and poured into H_2O (20 mL) followed by an extraction

with DCM (3 x 10 mL). The combined organic extracts were dried over $MgSO_4$, filtered, then concentrated under reduced pressure to afford reduced product as a yellow oil (0.0406 g, 44% yield). ^{1}H NMR (400 MHz, $CDCl_3$) δ 7.78 (d, J = 8.2 Hz, 2H), 7.32 (dd, J_a = 7.5, J_b = 0.7 Hz, 2H), 3.88 (s, 2H), 1.72 (s, 2H), 1.34 (s, 12H); ^{13}C {^{1}H} NMR (101 MHz, $CDCl_3$) δ 146.5, 135.1, 126.4, 83.7, 46.5, 24.8. [quaternary signal adjacent to B was not observed]; ^{11}B NMR (160 MHz, $CDCl_3$) δ 29.9.

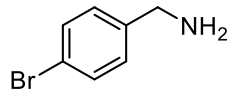

(4-Bromophenyl)methanamine (**4.56**). Synthesised according to the general procedure from the corresponding azide (0.1690 g, 0.8 mmol) and hydrazine monohydrate (0.160 mL, 3.2 mmol. 4 equiv.). Upon completion of the reaction, after 6 F/mol, the crude mixture was concentrated under reduced pressure, then redissolved in Et_2O (20 mL) and the product extracted into the aqueous phase with an aqueous solution of 1 M HCl (10 mL). The aqueous phase was basified with a 1 M aqueous solution of NaOH (20 mL, pH ≈ 14) and the product extracted with DCM (3 x 10 mL). The combined organic extracts were dried over $MgSO_4$, filtered, then concentrated under reduced pressure to afford the reduced product as a yellow oil (0.1010 g, 68% yield). ^{1}H NMR (400 MHz, $CDCl_3$) δ 7.44 (d, J = 8.4 Hz, 2H), 7.19 (d, J = 8.4 Hz, 2H), 3.82 (s, 2H), 1.51 (s, 2H); ^{13}C {^{1}H} NMR (101 MHz, $CDCl_3$) δ 142.1, 131.5, 128.8, 120.5, 45.8.

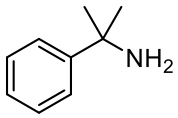

2-Phenylpropan-2-amine (**4.57**). Synthesised according to the general procedure from the corresponding azide (0.0645 g, 0.4 mmol) and hydrazine monohydrate (0.08 mL, 1.6 mmol, 4 equiv.). Upon completion of the reaction, after 6 F/mol, the

crude mixture was diluted with DCM (10 mL) and poured into H_2O (20 mL), followed by an extraction with DCM (3 x 10 mL). The combined organic extracts were dried over $MgSO_4$, filtered, then concentrated under reduced pressure to afford the reduced product as a yellow oil (0.0162 g, 30% yield). ^{1}H NMR (500 MHz, $CDCl_3$) δ 7.53–7.48 (m, 2H), 7.38–7.29 (m, 2H), 7.25–7.20 (m, 1H), 1.85 (s, 2H), 1.51 (s, 6H); ^{13}C {^{1}H} NMR (126 MHz, $CDCl_3$) δ 150.1, 128.2, 126.2, 124.6, 52.5, 32.7.

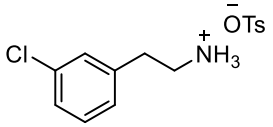

2-(3-Chlorophenyl)ethan-1-aminium tosylate (**4.58**). Synthesised according to the general procedure from the corresponding azide (0.1450 mg, 0.8 mmol) and hydrazine monohydrate (0.160 mL, 3.2 mmol, 4 equiv.). Upon completion of the reaction, after 6 F/mol, the crude reaction mixture was concentrated under reduced pressure and redissolved in a mixture of EtOAc (5 mL), Et_2O (1 mL) and DCM (1 mL); then TsOH • H_2O (152 mg, 0.8 mmol) in EtOAc (5 mL) was added. The resultant white precipitate was filtered and washed with Et_2O to afford ammonium salt as a white powder (0.190 g, 72%). ^{1}H NMR (500 MHz, DMSO-d_6) δ 7.82 (brs, 3H), 7.50 (d, J = 8.2 Hz, 2H), 7.39–7.28 (m, 3H), 7.22 (dt, J_a = 7.2, J_b = 1.6 Hz, 1H), 7.15–7.08 (m, 2H), 3.12–2.98 (m, 2H), 2.86 (dd, J_a = 8.9, J_b = 6.7 Hz, 2H), 2.29 (s, 3H); ^{13}C {^{1}H} NMR (126 MHz, DMSO-d_6) δ 144.9, 139.3, 137.4, 132.7, 129.9, 128.1, 127.6, 127.0, 126.3, 125.0, 32.0, 32.0, 20.3;; HRMS (ESI) *m/z*: calcd $[M + H]^+$ for $C_8H_{11}ClN^+$ 156.0580 found $[M + H]^+$ 156.0582.

General procedure for the electrochemical deuteration of alkenes and alkynes

A 5 mL IKA Electrasyn electrochemical vial was charged with the alkene/alkyne (0.40 mmol), hydrazine monohydrate (mmol and equiv. as specified for each

substrate), TFA (0.031 mL, 0.4 mmol, 1 equiv.), and a 1:1 MeCN/D_2O mixture (2.5 mL MeCN and 2.5 mL D_2O). The resulting mixture was electrolysed at a constant current of 10 mA until complete conversion of the starting material, as monitored by GC-MS or HPLC-MS. Upon completion, the crude reaction mixture was poured into water (30 mL) and extracted with pentane or Et_2O (as specified for each compound, 3 x 20 mL). The combined organic extracts were dried over $MgSO_4$, filtered and the solvent was removed under vacuum to afford the desired deuterated product.

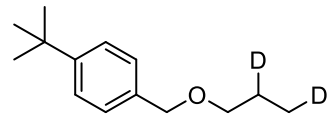

1-(*Tert*-butyl)-4-((propoxy-2,3-d_2)methyl)benzene (**4.60**). Synthesised according to the general procedure from the corresponding alkene (0.0817 g, 0.40 mmol), hydrazine monohydrate (0.450 mL, 9.0 mmol, 22.5 equiv.), and TFA (0.031 mL, 0.4 mmol, 1 equiv.). After 45 F/mol, extraction with Et_2O and evaporation of solvent afforded the deuterated product as a yellow oil (0.061 g, 73% yield). ^{1}H NMR (400 MHz, $CDCl_3$) δ 7.38 (d, J = 8.3 Hz, 2H), 7.29 (d, J = 8.0 Hz, 2H), 4.49 (s, 2H), 3.44 (d, J = 6.8 Hz, 2H), 1.7–1.57 (m, 1H), 1.34 (s, 1H, 100% deuterium incorporation), 1.01–0.89 (m, 2H, 100% deuterium incorporation); ^{13}C {^{1}H} NMR (101 MHz, $CDCl_3$) δ 150.5, 135.8, 127.6, 125.4, 72.8, 72.2, 34.6, 31.5, 22.9–22.4 (m), 11.8-6.0 (m); Accurate Mass (EI) *m/z*: calcd M^+ for $C_{14}H_{20}OD_2^+$ 208.1791; found M^+ 208.1746 (Spectral Accuracy: 99.4%).

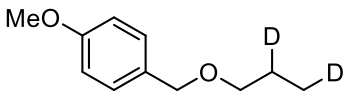

1-Methoxy-4-((propoxy-2,3-d_2)methyl)benzene (**4.61**). Synthesised according to the general procedure from 1the corresponding alkene (0.0712 g, 0.40 mmol), hydrazine monohydrate (0.3 mL, 6.00 mmol, 15 equiv.), and TFA (0.031 mL, 0.4

mmol, 1 equiv.). After 30 F/mol, extraction with Et_2O and evaporation of solvent afforded the deuterated product as a yellow oil (0.0635 g, 87% yield). ^{1}H NMR (400 MHz, $CDCl_3$) δ 7.26 (d, J = 7.5 Hz, 2H), 6.87 (d, J = 8.8 Hz, 2H), 4.43 (s, 2H), 3.79 (s, 3H), 3.46–3.28 (m, 2H), 1.69–1.51 (m, 1.19 H, 81% deuterium incorporation), 0.94–0.88 (m, 2.08 H, 92% deuterium incorporation); ^{13}C {^{1}H} NMR (101 MHz, $CDCl_3$) δ 159.2, 130.9, 129.3, 113.8, 72.6, 71.9, 55.4, 22.9–22.4 (m), 12.3-7.7 (m). Accurate Mass (EI) *m/z*: calcd M^+ for $C_{10}H_{14}O_2D_2^+$ 182.1270; found M^+ 182.1299 (Spectral Accuracy: 98.7%).

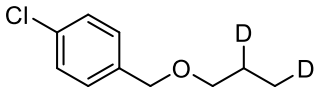

1-Chloro-4-((propoxy-2,3-*d*$_2$)methyl)benzene (**4.62**). Synthesised according to the general procedure from the corresponding alkene (0.0731 g, 0.40 mmol), hydrazine monohydrate (0.3 mL, 6.00 mmol, 15 equiv.), and TFA (0.031 mL, 0.4 mmol, 1 equiv.). After 30 F/mol, extraction with Et_2O and evaporation of solvent afforded the deuterated product as a yellow oil (0.058 g, 0.31 mmol, 78% yield). ^{1}H NMR (400 MHz, $CDCl_3$) δ 7.32–7.26 (m, 4H), 4.46 (s, 2H), 3.43–3.41 (m, 2H), 1.85–1.44 (m, 1.05 H, 95% deuterium incorporation), 0.94–0.90 (m, 2.14 H, 86% deuterium incorporation); ^{13}C {^{1}H} NMR (101 MHz, $CDCl_3$) δ 137.3, 133.3, 128.9, 128.6, 72.3, 72.1, 22.9–22.4 (m), 10.6–10.1 (m); Accurate Mass (EI) *m/z*: calcd M^+ for $C_{10}H_{11}ClOD_2^+$ 186.0677; found M^+ 186.0775 (Spectral Accuracy: 98.9%).

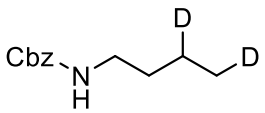

Benzyl (butyl-3,4-*d*$_2$)carbamate (**4.63**). Synthesised according to the general procedure from the corresponding alkene (0.082 g, 0.4 mmol), hydrazine monohydrate (0.262 mL, 5.4 mmol, 13.5 equiv.) and TFA (0.031 mL, 0.4 mmol, 1 equiv.). After 27 F/mol, extraction with Et_2O, purification by flash column

chromatography (100% *n*-hexane → 20% EtOAc in *n*-hexane), and evaporation of solvent afforded the deuterated product as a colourless liquid (0.061 g, 73% yield). ^{1}H NMR (400 MHz, $CDCl_3$) δ 7.36–7.29 (m, 5H), 5.10 (s, 2H), 4.73 (brs, -N*H*), 3.20 (q, J = 6.7 Hz, 2H), 1.47 (q, J = 7.3 Hz, 2H), 1.37–1.28 (m, 1.13H, 87% deuterium incorporation), 0.95–0.86 (m, 2.15H, 85% deuterium incorporation); ^{13}C {^{1}H} NMR (101 MHz, $CDCl_3$) δ 156.5, 136.8, 128.6, 128.2, 128.2, 66.7, 40.9, 32.0, 20.1–19.3 (m), 13.8–13.2 (m); HRMS (ESI) *m/z*: calcd $[M + H]^+$ for $C_{12}H_{16}D_2NO_2^+$ 210.1458; found $[M + H]^+$ 210.1458.

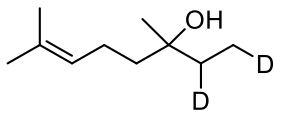

3,7-Dimethyloct-6-en-1,2-*d*$_2$-3-ol (**4.64**). Synthesised according to the general procedure from the corresponding alkene (0.072 mL, 0.4 mmol) and hydrazine monohydrate (0.137 mL, 23.4 mmol, 27.0 equiv.). After 54 F/mol, extraction with Et_2O and evaporation of solvent afforded the deuterated product as a colourless liquid (0.051 g, 80% yield). ^{1}H NMR (400 MHz, $CDCl_3$) δ 5.16–5.10 (m, 1H), 2.06–2.00 (m, 2H), 1.69 (d, J = 1.3 Hz, 3H), 1.62 (s, 3H), 1.50–1.43 (m, 3.41H, 59% deuterium incorporation), 1.25 (brs, -O*H*), 1.15 (s, 3H), 0.90–0.86 (m, 2.66H, 34% deuterium incorporation); ^{13}C {^{1}H} NMR (101 MHz, $CDCl_3$) δ 131.8, 124.6, 73.0, 41.1, 34.4–33.7 (m), 8.3–7.7 (m); HRMS (ESI) *m/z*: calcd $[M - H]^-$ for $C_{10}H_{17}D_2O^-$ 157.1567; found $[M - H]^-$ 157.1561.

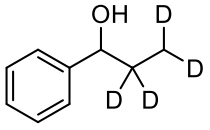

1-Phenylpropan-2,2,3,3-*d*$_4$-1-ol (**4.65**). Synthesised according to representative procedure from the corresponding alkyne (0.049 mL, 0.4 mmol), hydrazine monohydrate (0.437 mL, 9.0 mmol, 22.5 equiv.) and TFA (0.031 mL, 0.4 mmol, 1 equiv.). After 45 F/mol, extraction with Et_2O and evaporation of solvent afforded

the deuterated product as a colourless liquid (0.054 g, 99% yield). ^{1}H NMR (400 MHz, $CDCl_3$) δ 7.38–7.25 (m, 5H), 4.61–4.59 (m, 1H), 2.02 (brs, -O*H*), 1.85–1.71 (m, 0.64H, 68% deuterium incorporation), 0.92–0.87 (m, 1.16H, 92% deuterium incorporation); ^{13}C {^{1}H} NMR (101 MHz, $CDCl_3$) δ 144.7, 128.5, 127.6, 126.1, 76.0, 32.0–31.0 (m), 10.1–9.1 (m); HRMS (ESI) *m/z*: calcd $[M - H]^-$ for $C_9H_7D_4O^-$ 139.1066; found: 139.1070.

References

(1) Doobary, S.; Sedikides, A. T.; Caldora, H. P.; Poole, D. L.; Lennox, A. J. J.; *Angewandte Chemie International Edition,* **2020**, *59*, 1155–1160.

(2) Ringom, R.; Benneche, T.; *ChemInform,* **1999**, *30,* 41–47.

(3) Molnár, I. G.; Gilmour, R.; *Journal of the American Chemical Society,* **2016**, *138*, 5004–5007.

(4) Vibert, F.; Marque, S. R. A.; Bloch, E.; Queyroy, S.; Bertrand, M. P.; Gastaldi, S.; Besson, E.; *The Journal of Physical Chemistry C,* **2015**, *119*, 5434–5439.

(5) Yokoyama, T.; Kutsumura, N.; Ohgiya, T.; Nishiyama, S.; *Bulletin of the Chemical Society of Japan,* **2007**, *80*, 578–582.

(6) Bag, S.; Jayarajan, R.; Mondal, R.; Maiti, D.; *Angewandte Chemie* **2017**, *129*, 3230–3234.

(7) Abecassis, K.; Gibson, S. E.; Martin-Fontecha, M.; *European Journal of Organic Chemistry,* **2009**, *10*, 1606–1611.

(8) Lu, B. L.; Williams, G. M.; Verdon, D. J.; Dunbar, P. R.; Brimble, M. A.; *Journal of Medicinal Chemistry,* **2020**, *63*, 2282–2291.

(9) Patterson, J. R.; Terrell, L. R.; Donatelli, C. A.; Holt, D. A.; Jolivette, L. J.; Rivero, R. A.; Roethke, T. J.; Shu, A.; Stoy, P.; Ye, G.; Youngman, M.; Lawhorn, B. G.; *Journal of Medicinal Chemistry,* **2020**, *63*, 14867–14884.

(10) Karageorgis, G.; Warriner, S.; Nelson, A.; *Nature Chemistry,* **2014**, *6*, 872–876.

(11) Anbu, N.; Nagajurn, N.; Jacob, M.; Kalaiarasi, J. M. V. K., Dhakshinamoorthy, A.; *Chemistry,* **2019**, *1*, 69–79.

(12) Suzuki, H.; Matsumura, S.; Satoh, Y.; Sogoh, K.; Yasuda, H.; *Reactive and Functional Polymers,* **2004**, *58*, 77–91.

(13) Ho Kim, S.; Worsley, M. A.; Valdez, C. A.; Shin, S. J.; Dawedeit, C.; Braun, T.; Baumann, T. F.; Letts, S. A.; Kucheyev, S. O.; Jen J. Wu, K.; Biener, J.; Satcher, J. H.; Hamza, A. V.; *RSC Advances,* **2012**, *2*, 8672.

(14) Zhai, W.; Chapin, B. M.; Yoshizawa, A.; Wang, H.-C.; Hodge, S. A.; James, T. D.; Anslyn, E. V.; Fossey, J. S.; *Organic Chemistry Frontiers,* **2016**, *3*, 918–928.

(15) Tummatorn, J.; Thongsornkleeb, C.; Ruchirawat, S.; Gettongsong, T.; *Organic and Biomolecular Chemistry,* **2013**, *11*, 1463.
(16) Sawama, Y.; Nagata, S.; Yabe, Y.; Morita, K.; Monguchi, Y.; Sajiki, H.; C*hemistry – A European Journal,* **2012**, *18*, 16608–16611.
(17) Lenstra, D. C.; Lenting, P. E.; Mecinović, J.; *Green Chemistry,* **2018**, *20*, 4418–4422.
(18) Toogood, H. S.; Cheallaigh, A. N.; Tait, S.; Mansell, D. J.; Jervis, A.; Lygidakis, A.; Humphreys, L.; Takano, E.; Gardiner, J. M.; Scrutton, N. S.; *ACS Synthetic Biology,* **2015**, *4*, 1112–1123.
(19) Morton, C. J. H.; Gilmour, R.; Smith, D. M.; Lightfoot, P.; Slawin, A. M. Z.; MacLean, E. J.; *Tetrahedron,* **2002**, *58*, 5547–5565.

General Conclusions

In pursuing the Green Chemistry ideals for more sustainable chemical processes, this Doctoral Thesis reports our efforts to contribute to the field by developing innovative synthetic approaches for both organic and medicinal chemistry applications. Isocyanide manifold reactivity has been an invaluable ally along this journey, providing versatile chemical behaviours and unique reactivity paradigms which are not shared by any other class of organic compounds.

- By combining the inherently green properties of multicomponent reactions with the unprecedent synthetic opportunities enabled by visible light photoredox catalysis, we showed how an extension of the accessible chemical space can be easily achieved under otherwise unattainable mild conditions, as for the synthesis of 2-aminomethyl-1,3,4-oxadiazole derivatives.
- The feasibility of performing in water photochemical reactions, overcoming solubility issues of most organic compounds by means of micellar solvent systems, was demonstrated by developing a photomicellar catalysed synthesis of amides from isocyanides and tertiary aromatic amines. Additional experimental data were collected to establish general criteria to drive the selection of the optimum photocatalyst/surfactant pairs.
- The disclosure of a previously unknown photoreactivity of both aromatic and aliphatic isocyanides under visible light irradiation (via direct photoexcitation the former, via EDA complex formation with tertiary aromatic amines the latter) was exploited to perform a wide collection of metal-free Ugi and Ugi-like multicomponent reactions leading to multifunctional molecular architectures not always accessible via classic MCRs.
- Moreover, the possibility to finely tune the optical and redox properties of aryl isocyanides by proper modifications of their aromatic moieties was evaluated through a combination of synthetic, optical, electrochemical, and computational studies with the aim to verify the viability of designing a new class of isocyanide-

based organic visible-light photocatalysts. Interestingly, these studies gave easy access to site-selective deuterium labelled compounds, which would be difficult to synthesise by traditional methods.

- The opportunity to access elusive class of compounds and overcome limitations of existing synthetic strategies was highlighted by exploiting isocyanides' unconventional reactivity as polarised triple bonds, elicited by ligation to metals, to develop an alternative route to pharmaceutically relevant 4-substituted-5-aminoimidazole derivatives.
- The use of isocyanide-based multicomponent reactions as incomparable tools in medicinal chemistry research was encouraged by emphasising their extraordinary synthetic efficiency and high exploratory power in affording large libraries of complex and diverse compounds for biological evaluations. By dramatically shortening the time required for SARs investigations, this can have significant impact on drug discovery campaigns. We harnessed such an approach in the identification of novel MICAL2 and NOD1 small molecules inhibitors, with potential application as new anticancer agents.
- Finally, the potentialities of organic electrochemistry in providing innovative solutions for modern green syntheses were well exemplified by the development of an electrochemical hydrogen-free hydrogenation and deuteration strategy, featuring operational simplicity, general applicability, high yields, and mild reaction conditions.

We hope that our findings can provide new insights and practical tools to further foster future advancements in the field.

Acknowledgments

Innanzitutto, un enorme grazie alla mia Tutor, la Prof.ssa Mariateresa Giustiniano: un incredibile esempio di curiosità, dedizione e passione per il proprio lavoro, oltre che fonte inesauribile di ispirazione, idee e consigli preziosi. Indubbiamente la mente più brillante che conosca: grazie per essere stata come un faro ad illuminare il mio intero cammino dottorale.

Grazie ad Ilenia, la primissima persona ad avermi accolta in laboratorio ai tempi della tesi e, da allora, guida insostituibile. Abbiamo condiviso stress, ansie e, soprattutto, tante risate: grazie per avermi sempre capita, appoggiata e risollevata con il tuo buon umore contagioso, e per essere un'amica sincera su cui poter contare in ogni momento.

Il mio ringraziamento a tutti i docenti e ricercatori che in svariati modi hanno contribuito a questo lavoro di tesi, offrendomi occasioni di confronto e di crescita: la mia co-tutor Prof.ssa Valeria La Pietra, Prof.ssa Jussara Amato, Prof. Bruno Pagano, Dott. Rolando Cannalire, Dott. Diego Brancaccio, Dott.ssa Federica Santoro, Dott.ssa Greta Donati, Dott. Francesco di Leva, Dott. Francesco Merlino.

Un grazie anche a tutti i tesisti che si sono avvicendati in laboratorio durante questo percorso: una piacevole compagnia ed un aiuto prezioso nelle lunghe giornate di lavoro, oltre ad un utile esercizio per migliorare le mie capacità di insegnamento.

My sincere gratitude to Prof. Laurence Grimaud and Prof. Alexander Dömling for reviewing my thesis: thank you for your expert opinions and helpful advice to improve it. It has been a real honour.

I would also like to deeply thank Prof. Kevin Lam for giving me the opportunity to join his group: it was really an electrifying experience. Thank you for the amazing chemistry, for all the discussions during the lab group meetings, for the inspiring ideas, and for the trust you gave me. You made me a more confident chemist: I will always be grateful for this.

A huge thanks to the whole “English team”: Cyrille, Jamie, Marylise, Annie, Joe, Matthew, Lisa, Emmanuelle. It has been a pleasure to share the lab with you in Gillingham and to hang out with you outside the lab, having the privilege to know the wonderful people you are. Thanks for all the fun and the laughs: you gave me some of the best times of my PhD, I will never forget them.

A Maria Giovanna e Jolanda, le mie amiche di sempre: grazie per la pazienza, l’ascolto e la comprensione, e per esserci state costantemente anche durante i miei silenzi.

Infine, grazie alla mia famiglia per avermi sempre supportata e sopportata: parte di questo traguardo è anche vostra, ve la dedico con tutto il cuore.